P. Déjardin (Ed.)

PRINCIPLES AND PRACTICE

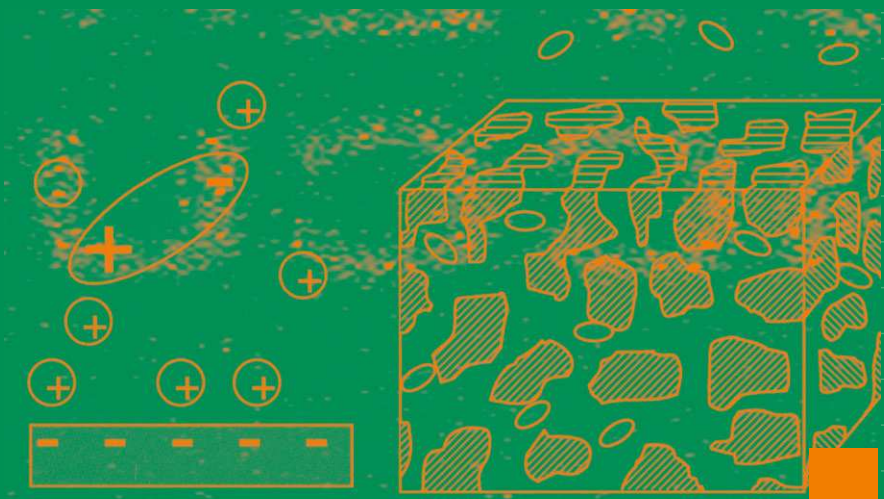

Proteins at Solid–Liquid Interfaces

Springer

PRINCIPLES AND PRACTICE

Philippe Déjardin (Ed.)

Proteins at Solid–Liquid Interfaces

With 165 Figures and 32 Tables

Springer

Dr. Philippe Déjardin
Directeur de Recherche CNRS
IEM – Université Montpellier 2
CC 047
2 Place Eugène Bataillon
34095 Montpellier Cedex 5
France
e-mail: Philippe.Dejardin@iemm.univ-montp2.fr

Library of Congress Control Number: 2006927284

ISBN-10 3-540-32657-X Springer Berlin Heidelberg New York
ISBN-13 978-3-540-32657-1 Springer Berlin Heidelberg New York

This work is subject to copyright. All rights reserved, whether the whole or part of the material is concerned, specifically the rights of translation, reprinting, reuse of illustrations, recitation, broadcasting, reproduction on microfilm or in any other way, and storage in data banks. Duplication of this publication or parts thereof is permitted only under the provisions of the German Copyright Law of September 9, 1965, in its current version, and permission for use must always be obtained from Springer. Violations are liable for prosecution under the German Copyright Law.

Springer is a part of Springer Science+Business Media
springer.com

© Springer-Verlag Berlin Heidelberg 2006

The use of general descriptive names, registered names, trademarks, etc. in this publication does not imply, even in the absence of a specific statement, that such names are exempt from the relevant protective laws and regulations and therefore free for general use.

Editor: Dr. Sabine Schreck, Heidelberg, Germany
Desk Editor: Dr. Jutta Lindenborn, Heidelberg, Germany
Cover design: *design&production*, Heidelberg, Germany
Typesetting and production: LE-TEX Jelonek, Schmidt & Vöckler GbR, Leipzig, Germany
31/3100-YL - 5 4 3 2 1 0 - Printed on acid-free paper

Preface

The adsorption of proteins at interfaces plays a role in many fields, such as health, food, environment and analysis. Fundamental aspects are useful when considering applications. We focus here especially on solid–liquid interfaces and present a few fundamental studies regarding adsorption kinetics and conformational changes, and examples of applications to sensors and membranes.

The first part is dedicated to fundamental studies performed using optical waveguide lightmode spectroscopy, as an example of a technique that has the advantage of not requiring labelled proteins, but is limited to specific supports. Conversely, the radiolabelling of proteins, which has the disadvantage of any labelling process, allows application to any kind of surfaces. As proteins bear both positive and negative charges, we can expect the influence of an electric field normal to the interface on the packaging order at interfaces. The refining of data treatment may also lead to the determination of useful structural parameters. The balance between protein–surface and protein–protein interactions is a key point for the description of the structure at high coverage of the surface. Electrokinetic methods, like measurement of the streaming potential, may be helpful in the electrical characterisation of the interfacial layer facing the solution.

The second part includes different bench techniques that were developed to improve the sensitivity of the characterisation of the orientation and structure of the proteins at interfaces: dual polarisation interferometry and total internal reflection ellipsometry are such recent examples. Concerning the determination of the secondary structure at interfaces, Fourier transform infrared (FTIR) spectroscopy and circular dichroism are very well adapted. Application to flat model surfaces can be performed by using the attenuated total reflectance-FTIR technique. The accessibility to the internal part of globular proteins is measured by the hydrogen–deuterium exchange rate. The evaluation of proteins on biodevices by time of flight – secondary ion mass spectroscopy is certainly a challenge given the size of the molecules. Data treatment according to mutual information theory, however, might be very helpful.

The third part considers studies more closely linked to applications. Determination of the conformation and orientation of the proteins at in-

terfaces is of particular importance for the understanding of the behaviour of cells at interfaces. A model study is presented with fibronectin at polymer surfaces with graded characteristics such as hydrophilicity, charge density and swelling. In addition to sensors, materials with a large area of contact with solutions containing proteins can be used in large-scale applications. Microporous membranes and textiles are typically representative of this category. They can act as concentrators of enzymes for the high-yield transformation of substrates. The biocompatibility of these materials, however, with the specific significance of anti-fouling properties and/or retaining enzyme activity, is a key parameter for satisfactory functioning. Different approaches for obtaining protein-resistant surfaces from polyacrylonitrile membranes are presented. The modulation of the adsorption and activity of biomolecules can also be performed by surface modification of polypropylene membranes. One important "bio-inspired" route to surface modification is the introduction of phosphorylcholine moieties, since the zwitterionic group of the phospatidylcholine and sphingomyelin polar head covers a large fraction of the external surface of the erythrocyte and platelet membranes.

I would like to thank the authors for their contributions and the editorial staff of Springer for their assistance. I hope that this book may stimulate initiatives of work in the constantly renewing and fascinating field of interfacial phenomena.

Montpellier, February 2006 *Philippe Déjardin*

Contents

Part I Analysis of the Adsorption Kinetics

Contributors

Aoyagi, Satoka
Faculty of Life and Environmental Science, Department of Regional Development, Shimane University 1060 Nishikawatsu-cho, Matsue-shi, Shimane, 690-8504, Japan, Shimane University, Japan

Arwin, Hans
Laboratory of Applied Optics, Department of Physics, Chemistry and Biology, Linköping University, SE-581-83 Linköping, Sweden

Déjardin, Philippe
European Membrane Institute, UMR 5635 (ENSCM-UMII-CNRS), Université Montpellier 2, CC 047, 34095 Montpellier Cedex 5, France

Dai, Zheng-Wei
Institute of Polymer Science, Zhejiang University, Hangzhou 310027, People's Republic of China

Freeman, Neville
Farfield Scientific Ltd, Farfield House, Southmere Court, Electra Way, Crewe Business Park, Crewe, Cheshire, CW1 6GU, UK

Huang, Xiao-Jun
Institute of Polymer Science, Zhejiang University, Hangzhou 310027, People's Republic of China

Innocent, Christophe
European Membrane Institute, UMR 5635 (ENSCM-UMII-CNRS), Université Montpellier 2, CC 047, 34095 Montpellier Cedex 5, France

Ishihara, Kazuhiko
Department of Materials Engineering, School of Engineering, The University of Tokyo, 7-3-1 Hongo, Bunkyo-ku, Tokyo 113-8656, Japan

Iwasaki, Yasuhiko
Institute of Biomaterials and Bioengineering, Tokyo Medical and Dental University, 2-3-10 Kanda-surugadai, Chiyoda-ku, Tokyo 101-0062, Japan

Kudo, Masahiro
Department of Materials and Life Science, Seikei University, Japan

Nakabayashi, Nobuo
Institute of Biomaterials and Bioengineering, Tokyo Medical and Dental University, 2-3-10 Kanda-surugadai, Chiyoda-ku, Tokyo 101-0062, Japan

Noinville, Sylvie
Laboratoire de Dynamique, Interactions et Réactivité, CNRS-Université Pierre et Marie Curie, UMR 7075, 2 rue Henri Dunant, 94320 Thiais, France

Poksinski, Michal
Laboratory of Applied Optics, Department of Physics, Chemistry and Biology, Linköping University, SE-581-83 Linköping, Sweden

Pompe, Tilo
Leibniz Institute of Polymer Research Dresden, Max Bergmann Center of Biomaterials Dresden, Hohe Str. 6, 01069 Dresden, Germany

Ramsden, Jeremy J.
Department of Materials, Cranfield University, MK43 0AL, UK

Renner, Lars
Leibniz Institute of Polymer Research Dresden, Max Bergmann Center of Biomaterials Dresden, Hohe Str. 6, 01069 Dresden, Germany

Revault, Madeleine
Laboratoire de Dynamique, Interactions et Réactivité, CNRS-Université Pierre et Marie Curie, UMR 7075, 2 rue Henri Dunant, 94320 Thiais, France

Seta, Patrick
European Membrane Institute, UMR 5635 (ENSCM-UMII-CNRS), Université Montpellier 2, CC 047, 34095 Montpellier Cedex 5, France

Van Tassel, Paul R.
Department of Chemical Engineering, Yale University, New Haven, CT 06520-8286, USA

Vasina, Elena N.
European Membrane Institute, UMR 5635 (ENSCM-UMII-CNRS), Université Montpellier 2, CC 047, 34095 Montpellier Cedex 5, France

Wan, Ling-Shu
Institute of Polymer Science, Zhejiang University, Hangzhou 310027, People's Republic of China

Werner, Carsten
Leibniz Institute of Polymer Research Dresden, Max Bergmann Center of Biomaterials Dresden, Hohe Str. 6, 01069 Dresden, Germany

Xu, Zhi-Kang
Institute of Polymer Science, Zhejiang University, Hangzhou 310027, People's Republic of China

Yang, Qian
Institute of Polymer Science, Zhejiang University, Hangzhou 310027, People's Republic of China

1 Protein Adsorption Kinetics: Influence of Substrate Electric Potential

Paul R. Van Tassel

Abstract. Substrate electric potential plays an important role in determining the adsorptive behavior of proteins and other macromolecules. In this chapter we describe the measurement of protein adsorption kinetics in the presence of an applied potential using optical waveguide lightmode spectroscopy. We analyze the resulting kinetics in terms of transport- and surface-limited models and show that while substrate potential is an important influencing factor, transport limited by convective diffusion and adsorption in seeming violation of electrostatic principles are prevalent in simple protein systems.

1.1 Introduction

Protein molecules immobilized at a material surface play a key role in many biosensing, tissue engineering, enzymatic catalysis, bioseparation, and bioelectronics applications. The tendency of proteins to attach to interfacial regions is well documented (Haynes and Norde 1994; Malmsten 1998a, b; Van Tassel 2003). Ionic, van der Waals, solvation, and donor–acceptor interactions all play important roles in rendering the interfacially adsorbed state to be thermodynamically favored over the solution state (Haynes and Norde 1994). Proteins are colloidal objects that possess a distribution of surface charge and, in an electrolytic solution, a distribution of weakly associated counterions. Their interaction with a solid substrate is thus sensitive to the substrate's charge distribution. By controlling the electric potential of an adsorbing surface, one alters this charge distribution and, therefore, the surface–protein interaction. In principle, the adsorption process may be controlled in this way, perhaps leading to adsorbed layers of enhanced density or preferred orientation or spatial distribution. However, the interaction between a protein and an adsorbing surface is complex, and predicting adsorbed layer properties by considering the contributions from

Paul R. Van Tassel: Department of Chemical Engineering, Yale University, New Haven, CT 06520-8286, USA, E-mail: paul.vantassel@yale.edu

Principles and Practice
Proteins at Solid–Liquid Interfaces
Philippe Déjardin (Ed.)
© Springer-Verlag Berlin Heidelberg 2006

the interaction modes given above remains a significant challenge. Thus, while influencing an adsorbed protein layer through the substrate's electric potential is both possible and desirable (Asanov et al. 1997, 1998; Bernabeu and Caprani 1990; Bos et al. 1994; Brusatori et al. 2003; Brusatori and Van Tassel 2003; Feng and Andrade 1994; Fievet et al. 1998; Fraaije et al. 1990; Khan and Wernet 1997), the process is as yet poorly understood.

In this contribution, we review our recent work investigating the influence of substrate electric potential on protein adsorption kinetics (Brusatori et al. 2003; Brusatori and Van Tassel 2003). We begin with a brief presentation of certain basic theoretical considerations. We then introduce the method by which we measure protein adsorption kinetics under electric potential control: optical waveguide lightmode spectroscopy (OWLS). Next, we introduce some key results and discuss them in the context of findings by other groups. By summarizing several important results and open questions, we hope to guide future efforts to produce controlled layers of adsorbed protein through the control of substrate electric potential.

1.2 Theoretical Prediction

Proteins are composed of amino acids, some of which contain acidic/basic sites. Thus, at all but the isoelectric pH, a protein molecule possesses a net charge and therefore migrates in response to an electric field. Since the charge distribution is generally not spherically symmetrical, the electric field also imposes a torque on the molecule, causing it to rotate. Of course, electric-field-induced migration and rotation must compete against the molecule's thermal diffusive motion, so these influences are only observed in excess of some threshold field strength. Due to screening by solution ions, electric field effects become appreciable only within a few Debye lengths of a charged surface and are most important at or near direct contact, where properties such as the rate of attachment, mean protein orientation, and the rate and extent of subsequent postadsorption changes in orientation and conformation may be profoundly affected.

The transport of protein in a flowing solution is described by

$$\frac{\partial c}{\partial t} + \vec{v} \bullet \vec{\nabla} c = \vec{\nabla} \bullet \left(D \vec{\nabla} c + \frac{cq\vec{E}}{\zeta} \right) \tag{1}$$

where c is the protein concentration, t is the time, $\vec{v}$ is the fluid flow velocity vector, D is the diffusivity, q is the effective protein charge, $\vec{E}$ is the electric field vector, and ζ is the friction coefficient (a measure of the viscous drag

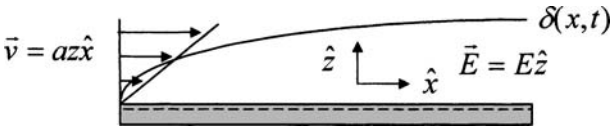

Fig. 1. A schematic of a typical protein adsorption scenario, where adsorption occurs from a flowing solution over a flat, charged surface. Near the surface, simple shear flow occurs resulting in a velocity profile $\vec{v} = az\hat{x}$, where a is the shear rate, z is the distance from the surface, and $\hat{x}$ is a unit vector parallel to the surface. A convective-diffusion boundary layer develops $\delta(x,t)$, of thickness δ, above (below) which convection is more (less) rapid than diffusion. An applied electric field is expressed as $\vec{E} = E\hat{z}$, where $\vec{E}$ is the electric field vector, E is the magnitude and $\hat{z}$ is a unit vector normal to the surface

on the protein). The flow field must be known in advance to solve Eq. 1. So long as the concentration is quite low, one may neglect the influence of the migrating proteins on the fluid and solve for the flow field using the standard Navier-Stokes equation. A typical configuration involves flow past a flat, charged surface, as depicted in Fig. 1.

The two terms on the right side of Eq. 1 represent, respectively, the contributions from thermal diffusion and electric-field-induced migration. It is interesting to consider the limiting cases where one is much larger than the other. Neglecting the second term gives pure convective diffusion. In this case, one may approximate the flux (J) to the surface by assuming steady shear flow over a flat surface acting as a perfect adsorptive sink, $J(x,t) = Dc_\mathrm{b}/\delta(x,t)$, where c_b is the bulk protein concentration, and

$$\delta(x,t) = \frac{(45Dx/2a)^{1/3}}{f\left(\dfrac{4Dt}{(45Dx/2a)^{2/3}}\right)} \tag{2}$$

is the convective diffusion boundary layer, a function of the diffusivity (D), the distance along the surface in the direction of the flow (x), the shear rate (a), and the time (t) (Brusatori et al. 2003; Calonder and Van Tassel 2001). The function $f(\tau)$ is the inverse of $\tau(f) = [1-(1-f^3)^{2/3}]/2f^2$ for $\tau < 1/2$ and $f(\tau) = 1$ for $\tau > 1/2$. Pure convective diffusion is therefore characterized by an initially zero flux that increases to a steady-state value at dimensionless time, $\tau = 1/2$.

Inclusion of the second term on the right of Eq. 1 requires knowledge of the electric field as a function of position. A starting point toward its approximation is the Poisson-Boltzmann equation describing the distribution of electric potential in an ionic solution:

$$\nabla^2\Psi = -\frac{e}{\varepsilon}\sum_i z_i c_i^0 \mathrm{e}^{-z_i e\Psi/kT} \tag{3}$$

In Eq. 3, Ψ is the electric potential, e is the elementary charge, ε is the dielectric constant, z_i is the valance of the ith ionic species, c_i^0 is the bulk concentration of the ith species, k is the Boltzmann constant, and T is the absolute temperature. An important assumption leading to Eq. 3 is the complete neglect of spatial correlations among the ions in solution. Clearly, the validity of this assumption is suspect for higher ionic concentrations. When the electric potential energy is weaker than the thermal energy, the exponential in Eq. 3 may be linearized. The result is the linear Poisson-Boltzmann equation, $\nabla^2\Psi = \kappa^2\Psi$, where κ is the inverse of the Debye length,

$$\kappa = \left[\frac{e^2 \sum_i z_i^2 c_i^0}{\varepsilon k T}\right]^{1/2} \tag{4}$$

The linearized version of Eq. 3 may be solved over the region extending away from a flat surface to yield

$$\Psi(x) = \Psi_0 \mathrm{e}^{-\kappa z} = \frac{\sigma}{\varepsilon\kappa}\mathrm{e}^{-\kappa z} \tag{5}$$

where Ψ_0 is the surface potential, z is the distance from the surface, and σ is the surface charge density (the second equality follows from integrating the charge density as given by the Poisson equation). The electric field is then given by

$$\vec{E}(x) = -\frac{\mathrm{d}\Psi}{\mathrm{d}z}\hat{z} = \frac{\sigma}{\varepsilon}\mathrm{e}^{-\kappa z}\hat{z} \tag{6}$$

where $\hat{x}$ is the unit vector normal to the flat surface.

Neglecting the first term on the right side of Eq. 1 is equivalent to ignoring diffusive motion. Assuming fully developed shear flow, a no-slip, perfect sink boundary condition, and an electric field given by Eq. 6, the z component velocity and the z position of a protein are given by:

$$v_z = \frac{qE(z)}{\zeta} = \frac{q\sigma}{\varepsilon\zeta}\mathrm{e}^{-\kappa z} = \frac{\mathrm{d}z}{\mathrm{d}t} \quad \Rightarrow \quad z(t) = z_0 + \kappa^{-1}\ln\left(1 + \frac{q\sigma\kappa t}{\varepsilon\zeta}\mathrm{e}^{-\kappa z_0}\right) \tag{7}$$

The velocity in the x direction is $v_x(t) = az(t)$, so the distance traveled in the x direction ($x = 0$ corresponds to the leading edge of the surface, as shown in Fig. 1) is:

$$\begin{aligned} x(t) &= \int_0^t v_x\left(t'\right)\mathrm{d}t' \\ &= az_0 t + a\kappa^{-1}\left[\left(t + \frac{\varepsilon\zeta}{q\sigma\kappa}\mathrm{e}^{\kappa z_0}\right)\ln\left(1 + \frac{q\sigma\kappa t}{\varepsilon\zeta}\mathrm{e}^{-\kappa z_0}\right) - t\right] \end{aligned} \tag{8}$$

The concentration profile is thus given by:

$$c(x,z,t) = c_\mathrm{b} H\left(az_0 t + a\kappa^{-1}\left[\left(t + \frac{\varepsilon\zeta}{q\sigma\kappa}\mathrm{e}^{\kappa z_0}\right)\ln\left(1 + \frac{q\sigma\kappa t}{\varepsilon\zeta}\mathrm{e}^{-\kappa z_0}\right) - t\right] - x\right) \tag{9}$$

where z_0 is the implicit solution to Eq. 7, in terms of $z(t)$ and t, and H is the Heaviside function (i. e., $H(\lambda) = 1$ for $\lambda > 0$ and $H(\lambda) = 0$ for $\lambda < 0$). The flux to the surface is thus:

$$J(x,t) = \frac{q\sigma}{\varepsilon\zeta} c(x, z = 0, t) \tag{10}$$

Pure electrophoretic migration is therefore characterized by an initial period of zero flux, during a time needed for the argument of the Heaviside function in Eq. 9 to vanish, followed by a steady-state flux. Both of these flux predictions hold only in the limit where surface adsorption is rapid compared to transport to the surface (i. e., where the surface may be considered to be a perfect sink). This is usually the case during the initial stages of surface filling. Subsequently, the kinetics are limited by surface effects. The surface-limited rate of adsorption may be expressed as:

$$\frac{\mathrm{d}\Gamma}{\mathrm{d}t} = k_\mathrm{a} c_\mathrm{b} \Phi - \sum_i k_{\mathrm{d},i} \Gamma_i \tag{11}$$

where Γ is the density of adsorbed protein (mass per area), k_a is the adsorption rate constant, Φ is the one-body cavity function, and $k_{\mathrm{d},i}$ and Γ_i are the desorption rate constant and the density of protein in the ith structural state, respectively (these states may denote various conformations, orientations, or states of aggregation; Tie et al. 2003). The cavity function is defined as $\Phi = \langle \mathrm{e}^{-u/kT} \rangle_{\Gamma,T}$, where u is the potential energy of a single molecule interacting with the surface and with all of the previously adsorbed molecules (u depends on position and orientation), k is the Boltzmann constant, T is the absolute temperature, and the brackets represent an averaged quantity, over all representations of the adsorbed layer at density Γ and temperature T, according to their appropriate weights, and over all orientations and positions of the single "reference" molecule. All of the quantities on the right of Eq. 11 (except c_b) may be altered by application of an electric field.

To make quantitative predictions, the potential energy of interactions between protein molecules and the charged surface must be calculated. The electrostatic contribution to this energy may be determined using the Derjaguin-Landau-Verwey-Overbeek (DLVO; Asthagiri and Lenhoff 1997; Oberholzer and Lenhoff 1999; Ravichandran and Talbot 2000; Roth and Lenhoff 1993, 1995) or density functional (Carignano and Szleifer 2002; Fang and Szleifer 2003) approaches.

1.3 Experimental Measure

1.3.1 OWLS Principles

OWLS is a method for detecting interfacial adsorption based on the guided light modes excited in a planar, dielectric waveguide sandwiched between media of lower refractive index (Ramsden 1993; Voros et al. 2002). The OWLS detection mechanism may be understood through a four-layer model, consisting of a glass support (S), a waveguiding film (F), a second film (F′), and a cover solution (C)(Brusatori and Van Tassel 2003; Tiefenthaler and Lukosz 1989). In what follows, the F′ layer may represent an adsorbed layer or a second layer to a two-layer waveguiding film. A polarized laser beam of wavelength λ is directed through the glass support toward an optical grating at the FF′C interface at an angle α. The corresponding effective refractive index (N) is:

$$N \equiv n_{\mathrm{F}} \sin \phi_{\mathrm{F}} = n_{\mathrm{air}} \sin \alpha + \frac{\ell \lambda}{\Lambda} \tag{12}$$

where n_{F} is the film's refractive index, ϕ_{F} is the propagation angle within the film, n_{air} is the refractive index of air, ℓ is the diffraction order of the grating, and Λ is the grating period. The condition under which coherent propagation occurs in the direction parallel to the film is:

$$2k_{z,\mathrm{F}} d_{\mathrm{F}} + \varphi_{\mathrm{F,S}} + \varphi_{\mathrm{F,F',C}} = 2\pi m \tag{13}$$

where $k_{z,\mathrm{F}}$ is the component of the wave vector normal to the waveguiding film, d_{F} is the thickness of the waveguiding film, $\varphi_{\mathrm{F,S}}$ and $\varphi'_{\mathrm{F,F}}$, C are the phase shifts associated with the reflections at the F,S and the F,F′,C interfaces, respectively, and the integer m is the mode number.

The phase shift at a given interface is related to its reflection coefficient via $r = |r|\mathrm{e}^{i\varphi}$. For a simple interface between films α and β,

$$r_{\alpha,\beta} = \frac{\dfrac{k_{z,\alpha}}{n_\alpha^{2\varrho}} - \dfrac{k_{z,\beta}}{n_\beta^{2\varrho}}}{\dfrac{k_{z,\alpha}}{n_\alpha^{2\varrho}} + \dfrac{k_{z,\beta}}{n_\beta^{2\varrho}}} \tag{14}$$

where α, β = F, F′, or C, n_α is the refractive index of film α, and $k_{z,\alpha}$ is the component of the wave vector normal to the film α:

$$k_{z,\alpha} = \frac{2\pi}{\lambda} n_\alpha \cos \phi_\alpha \tag{15}$$

where ϕ_α is the propagation angle in the α film (by Snell's law, $\cos\phi_\alpha = [1-N^2/\mathrm{Re}(n_\alpha)^2]^{1/2}$ is the real part of n_α. In Eq. 14, $\varrho = 0$ or 1 for electric field vectors oriented normal (transverse electric, or TE) or parallel (transverse magnetic, or TM) to the plane of incidence, respectively. The reflection coefficient across the F,F′,C interface is:

$$r_{\mathrm{F,F'C}} = \frac{r_{\mathrm{F,F'}} + r_{\mathrm{F',C}}\mathrm{e}^{i\delta}}{1 + r_{\mathrm{F,F'}}r_{\mathrm{F',C}}\mathrm{e}^{i\delta}} \tag{16}$$

where

$$\delta = 2k_{z,\mathrm{F'}}d_{\mathrm{F'}} + \frac{4\pi i}{\lambda}\mathrm{Im}(n_{\mathrm{F'}})d_{\mathrm{F'}}\tan\phi_{\mathrm{F'}}\sin\phi_{\mathrm{F'}} \tag{17}$$

and $\mathrm{Im}(n_{\mathrm{F'}})$ is the imaginary component of the refractive index. The phase shifts $\varphi_{\mathrm{F,S}}$ and $\varphi_{\mathrm{F,F',C}}$ are expressed in terms of the associated reflection coefficients by $\varphi = \arcsin[\mathrm{Im}(r)/|r|]$.

In the absence of an F′ layer, the above approach allows for the solution of the refractive index and thickness of the waveguiding film, n_{F} and d_{F} from the effective refractive indices of the transverse electric (N_{TE}) and transverse magnetic (N_{TM}) modes and from the known refractive indices of the support (n_{S}) and cover (n_C) solutions. Once known, these quantities may be used to calculate $n_{\mathrm{F'}}$ and $d_{\mathrm{F'}}$ during an adsorption experiment. From these values, the mass density of an adsorbed layer is determined via de Feijter's formula (de Feijter et al. 1978):

$$\Gamma = \frac{\left(n_{\mathrm{F'}} - n_{\mathrm{C}}\right)d_{\mathrm{F'}}}{\frac{\mathrm{d}n_{\mathrm{C}}}{\mathrm{d}c_{\mathrm{b}}}} \tag{18}$$

where the refractive index increase with bulk protein concentration, $\mathrm{d}n_{\mathrm{C}}/\mathrm{d}c_{\mathrm{b}}$, has the nearly universal value of 0.182 cm^3/g. Alternatively, the mass density may be determined via a single effective refractive index by:

$$\begin{aligned}\Gamma &= \left(n_{\mathrm{F'}} - n_{\mathrm{C}}\right)d_{\mathrm{F'}}\left(\frac{\partial n_{\mathrm{C}}}{\partial c_{\mathrm{b}}}\right)^{-1} \\ &= \frac{n_{\mathrm{F}}^2 - n_{\mathrm{C}}^2}{n_{\mathrm{F'}} + n_{\mathrm{C}}}\left(\frac{\partial N_{\mathrm{TE}}}{\partial d_{\mathrm{F}}}\right)^{-1}\left(\frac{\partial n_{\mathrm{C}}}{\partial c_{\mathrm{b}}}\right)^{-1}\Delta N_{\mathrm{TE}}\end{aligned} \tag{19}$$

where the refractive index $n_{\mathrm{F'}}$ and the term $\partial N_{\mathrm{TE}}/\partial d_{\mathrm{F}}$ are determined by a separate double mode experiment. The angular scan required for a single-mode measurement is much narrower, so the rate at which measurements may be taken (approximately 3 s) greatly exceeds that of a double-mode experiment (approximately 20 s).

1.3.2 OWLS Experiments

A schematic of our OWLS system (BIOS-1, MicroVacuum, Budapest, Hungary), as modified to allow for detection in the presence of an applied potential difference, appears in Fig. 2. The adsorbing surface is an indium tin oxide (ITO, or $In_{2-2x}Sn_xO_{3-x}$ with $x = 0.50 \pm 0.02$)-coated optical waveguide 2400 sensor chip (MicroVacuum). The ITO layer has a thickness of approximately 10 nm and complex refractive index 1.80−0.03i and rests on a silicon titanium oxide layer (STO, or $Si_{1-x}Ti_xO_2$ with $x = 0.25 \pm 0,05$) of thickness ca. 200 nm and refractive index 1.77 ± 0.03. The water contact angle of the ITO coating is $48.1 \pm 0.1°$; this value does not change within the range of applied potential investigated here. The sensor chip serves as the base of a temperature-controlled flow cell of volume 70 µl. A flat platinum counterelectrode is situated at the top of the flow cell 1.0 mm from the ITO surface. The sensor chip/flow cell assembly rests on the head of a precision goniometer.

An electric circuit schematic appears in Fig. 3. A potential difference between the ITO working electrode and the platinum counter is applied via an external power supply. The current is measured across a 100-kW resistor via a voltmeter, and the magnitude of the potential difference is determined using a second voltmeter. The potential of the ITO surface relative to a reference electrode (situated in the inlet solution) is measured using an electrometer.

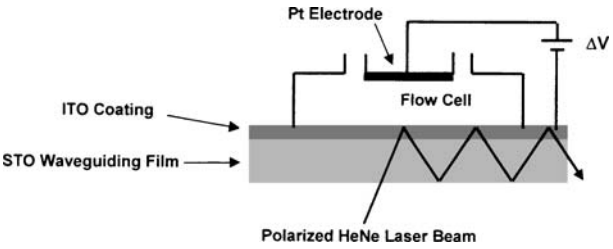

Fig. 2. A schematic of our modified optical waveguide lightmode spectroscopy (OWLS) system for the continuous measurement of macromolecular adsorption under an applied potential. The adsorbing substrate is an approximately 10-nm indium tin oxide (*ITO*) layer on a silicon titanium oxide (*STO*) waveguiding film of approximately 200 nm, itself supported on a glass substrate (not shown). A potential difference (ΔV) is applied between the ITO layer and a flat platinum (*Pt*) counterelectrode, situated 1 mm above at the top of the flow cell. A polarized HeNe laser beam directed toward a grating coupler at the STO/ITO interface (not shown) from below excites a guided mode at a resonant angle, from which adsorbed layer mass and thickness may be determined

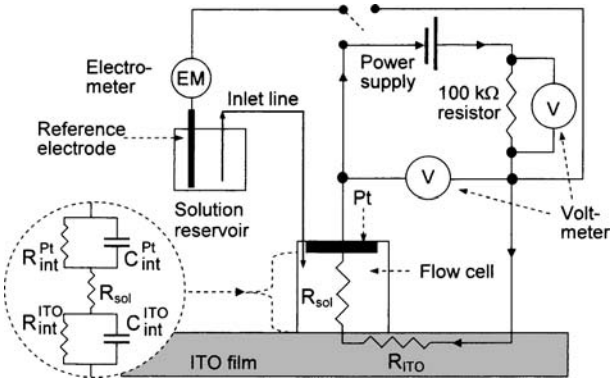

Fig. 3. A schematic of the electric circuit of our OWLS system. The ITO– and Pt–solution interfaces may be considered as resistors ($R_{\text{int}}^{\text{ITO}}$ and $R_{\text{int}}^{\text{Pt}}$, respectively) and capacitors ($C_{\text{int}}^{\text{ITO}}$ and $C_{\text{int}}^{\text{Pt}}$, respectively) in parallel. The ITO film and the solution within the flow cell act as resistors (R_{ITO} and R_{sol}, respectively). A potential difference is applied through a power supply (V) and the current is measured via the voltage drop across a 100-kΩ resistor. A second voltmeter is used to measure the potential difference between the ITO and Pt electrodes. The potentials of the ITO and Pt electrodes versus a reference electrode (e.g., Ag/AgCl) are measured using an electrometer (*EM*)

Prior to each experiment, the flow cell, tubing, and sensor chip are cleaned by exposure to a 2% Hellmanex (Hellma, Mulheim, Germany) solution in ultrapure water, followed by an intensive rinse with ultrapure water. An experiment begins with the introduction of a pure buffer to the flow cell via a peristaltic pump. An angular scan is performed, resulting in a mode spectrum from which N_{TE} and N_{TM} are obtained at approximately 20-s intervals. During an open-circuit potential (OCP) experiment, a flowing protein solution then replaces the flowing buffer solution once stable values of N_{TE} and N_{TM} are achieved. In other experiments, a voltage difference ΔV is applied ($\Delta V = V_{\text{ITO}} - V_{\text{Pt}}$), resulting in further changes to N_{TE} and N_{TM}. Once steady values are recovered, a protein solution is introduced.

1.4 Results

We begin by discussing certain important optoelectronic properties of the ITO-coated sensor chip. In Fig. 4, we present the effective refractive index, the current, and the ITO and platinum electrode potentials versus applied voltage in the presence of deionized water (of pH 5.5–6 and conductivity 1.30 ± 0.05 µS at 25 °C) and HEPES buffer [10 mM N-(2-hydroxyethyl)

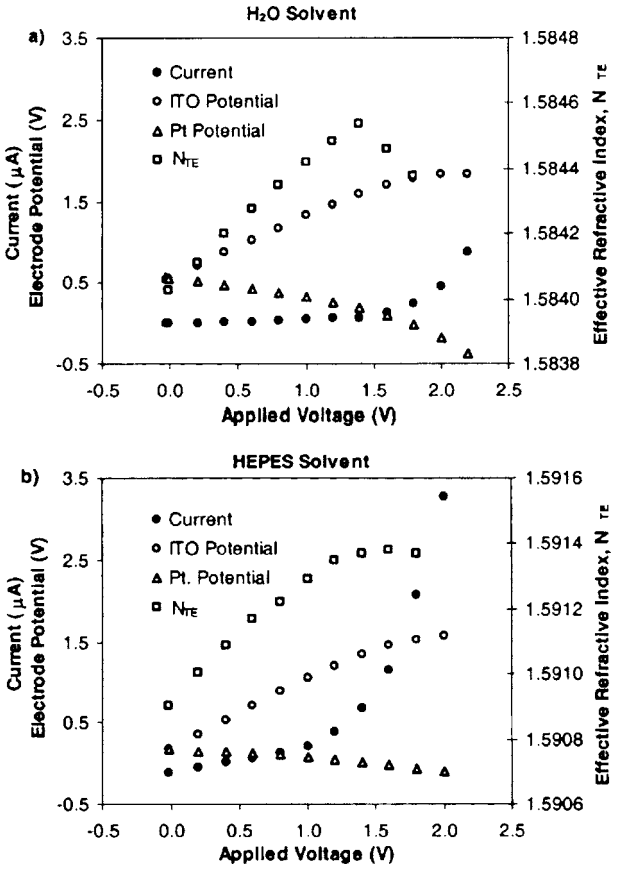

Fig. 4. The asymptotic current, the electric potential of the ITO and Pt electrodes, and the effective refractive index of the ITO-coated sensor chip as a function of applied voltage for **a** water and **b** HEPES buffer [10 mM N-(2-hydroxyethyl) piperazine-N′-(ethanesulfonic acid) in 100 mM NaCl, adjusted to pH 7.4 by addition of 6 N NaOH] solvents. The increases in current at 1.5 V and 1.0 V, respectively, indicate the onset of water electrolysis. N_{TE} Effective refractive index of the transverse electric mode. Reproduced with permission from Brusatori et al. (2003)

piperazine-N′-(ethanesulfonic acid) in 100 mM NaCl, adjusted to pH 7.4 by addition of 6 N NaOH]. We observe the effective refractive index to increase with applied potential up to $\Delta V = V_{ITO} - V_{Pt} > 1.4$ V. Upon further voltage increase, N_{TE} decreases in the water system and plateaus in the HEPES system. These changes suggest an alteration in optical density of the ITO-coated waveguiding film due to accumulation of charged species at the interface and/or within the film, and possibly also to mild oxidative reactions. A voltage-induced orientation of water in the porous ITO

film is also a possible explanation, as suggested elsewhere (Stankowski and Ramsden 2002). The somewhat sharp increase in current above an applied voltage of 1.5 V (water) and 1.0 V (HEPES) is due to the onset of water electrolysis. However, we observe no H_2 or O_2 gas formation and attribute this absence to the low overall current density.* Increasing the applied voltage increases V_{ITO} and decreases V_{Pt}; the latter becomes negative relative to a standard hydrogen electrode (SHE) when ΔV exceeds 1.7 V and 1.5 V for water and HEPES, respectively. We find prolonged cathodic polarization (i. e., $\Delta V < 0$) to result in increased opacity of the ITO film. This is probably due to electrochemical reduction and renders the sensor chip unusable in an OWLS experiment.

We wish to use the measured effective refractive index to calculate the adsorbed protein density, but doing so brings forth two important questions: (1) Must the ITO layer be considered explicitly, and if so, must the imaginary portion of its complex refractive index be considered? (2) Do the model Eqs. 12–19 hold under an applied voltage? To answer these questions, we measure the refractive index of a (non-adsorbing) 5.0 mg/ml glucose solution in water, with and without an applied potential, using three different waveguide models: (1) a three-layer model in which the STO and ITO films are considered to be a single layer (i. e., both reflection coefficients are determined via Eq. 12), (2) a four-layer model in which $n_{F'}$ is real (i. e., the F′ layer is a dielectric), and (3) a four-layer model in which $n_{F'}$ is complex (i. e., the F′ layer is a conductor). The glucose solution has a known refractive index of $1.33173 \pm 1\times10^{-5}$ at 25 °C. In Table 1, we show refractive index values measured using OWLS within each of the three waveguide models for cases of OCP and an applied voltage of $\Delta V = 5$ V. We observe all values to be within 3×10^{-5} of one another. Since the difference $(n_F - n_C)$ appearing in Eq. 18 is typically around 0.5, uncertainty of this magnitude has no appreciable effect on a measured adsorbed density. Thus, we conclude that an applied potential difference has only a negligible effect on the instrument's detection and that one may consider the STO and ITO films as a single effective film.

Using OWLS and employing a four-layer waveguide model – in which the STO and ITO layers are treated as a single layer, as justified above – we measure the adsorption kinetics of human serum albumin and horse heart cytochrome c, in flowing water or HEPES solutions at a surface shear rate of 1.5/s, onto ITO as a function of applied potential (Brusatori et al. 2003; Brusatori and Van Tassel 2003). The raw data of a typical experiment are shown in Fig. 5. Following a baseline measured under flowing solvent (deionized water in this case), application of a potential difference (1.0 V)

* A current of 1 μA results in the production of approx. 0.5×10^{-7} M/s of H_2 in our flow cell. The time needed to achieve the solubility limit of approx. 10^{-3} M is thus approximately 2×10^4 s; this is much greater than the space time of the flow cell, which is about 50 s.

Table 1. The refractive index, n_C, of a 5.0 mg/ml glucose solution – for an open circuit potential (*OCP*) and an applied voltage of 5 V – as determined using (1) a three-layer waveguide model where the silicon titanium oxide (*STO*) and indium tin oxide (*ITO*) layers are treated as a single layer, (2) a four-layer waveguide model where the ITO film is treated as a separate dielectric layer (i. e., of real refractive index), and (3) a four-layer waveguide model where the ITO film is treated as a separate conducting layer (i. e., of complex refractive index). The closeness of the values demonstrates both the validity of treating the STO and ITO films as a single optical layer and the accuracy of detection in the presence of an applied voltage

OCP	Three-layer waveguide model with composite STO-ITO layer	$n_C = 1.33177 \pm 1\times10^{-5}$
OCP	Four-layer waveguide model with dielectric ITO layer	$n_C = 1.33178 \pm 1\times10^{-5}$
OCP	Four-layer waveguide model with conducting ITO layer	$n_C = 1.33177 \pm 1\times10^{-5}$
$\Delta V = 5$ V	Three-layer waveguide model with composite STO-ITO layer	$n_C = 1.33175 \pm 2\times10^{-5}$
$\Delta V = 5$ V	Four-layer waveguide model with dielectric ITO layer	$n_C = 1.33175 \pm 2\times10^{-5}$
$\Delta V = 5$ V	Four-layer waveguide model with conducting ITO layer	$n_C = 1.33175 \pm 2\times10^{-5}$

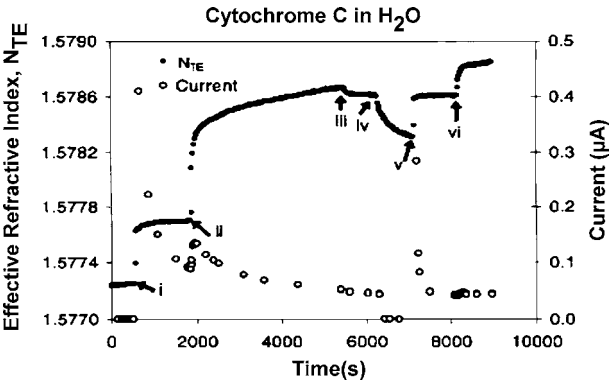

Fig. 5. The effective refractive index (the raw output signal during an OWLS measurement) and the current during cytochrome c adsorption from water onto ITO as a function of time. At point i, a voltage difference of 1.0 V is applied. At point ii, the protein solution is introduced. At point iii, the protein solution is replaced by a buffer solution. At point iv, the system is returned to an open-circuit potential (OCP), and at point v, the 1.0 V voltage difference is reapplied. At point vi, the protein solution is reintroduced. Reproduced with permission from Brusatori et al. (2003)

between the adsorbing substrate and a platinum counterelectrode (i) yields an increase in the measured effective refractive index, the fundamental output signal of OWLS (see Eq. 10). This increase is not fully understood, but is likely to be due to penetration of small ions into the ITO and/or the

underlying silicon titanium oxide films (even in deionized water, carbonate and other ionic impurities are present), or to mild oxidation of the ITO. The current increases initially but then decreases, as would occur for a resistor and capacitor in series (see Fig. 3). Upon the addition of cytochrome c in water (ii), the signal greatly increases due to optical changes at the interface brought about by adsorption. A return to the deionized water (iii) causes only a small signal reduction, indicating that only a small quantity of protein desorbs. When the electric field is removed (iv), a decreased signal results; however, this is not due to further desorption as a re-application of the field (v) returns the signal to its previous level. Finally, a re-introduction of the protein (vi) yields an additional signal increase. This additional adsorption is likely to be due to an increased amount of area on the surface open for adsorption. The cause of this increased available area is probably aggregation among the adsorbed molecules.

In Figs. 6 and 7, we show the adsorbed density versus time for albumin and cytochrome c in both water and HEPES solvents. In all cases, we observe the total amount adsorbed to increase with increasing applied potential. For water systems, adsorption curves reach a virtual plateau during OCP ($\Delta V_{\mathrm{OCP}} = -0.02 \pm 0.01$ V) but fail to do so in the presence of an applied voltage. The amount adsorbed during 1 h is greatly increased (by up to a factor of 4) by an applied potential difference. We observe a similar, but less pronounced voltage dependence in the HEPES systems (where $\Delta V_{\mathrm{OCP}} = +0.02 \pm 0.01$ V). Variability is approximately 20% for runs using different ITO-coated sensor chips (most likely due to subtle variations in surface microstructure) and approximately 8% for runs on the same sensor chip.

The principal advantage of OWLS over other detection methods is the precision of the output signal. We exploit this advantage in Fig. 8 by plotting the discrete time derivative of the adsorbed density, $\mathrm{d}\Gamma/\mathrm{d}t$, as a function of surface density, Γ. These derivative data are themselves sufficiently precise so as to allow for a clear delineation of transport- and adsorption-limited regimes. Adsorption is initially limited by the rate of transport to the surface; this occurs by a combination of diffusion and electrophoretic migration in the presence of a flow field. We observe the adsorption rate to continuously increase during this regime, as would occur initially for convective diffusion in laminar flow (see Theoretical Prediction). If the surface were a perfect sink, a plateau would eventually be reached upon achievement of a steady-state concentration profile above the surface. In the example shown here, surface availability begins to reduce the rate of adsorption before such a steady, transport-limited rate is achieved. Theoretical treatments of the surface-limited regime (Eq. 11) predict an initial linear decrease in adsorption rate with increasing surface coverage, followed by a nonlinear asymptotic dependence; our observations are consistent with

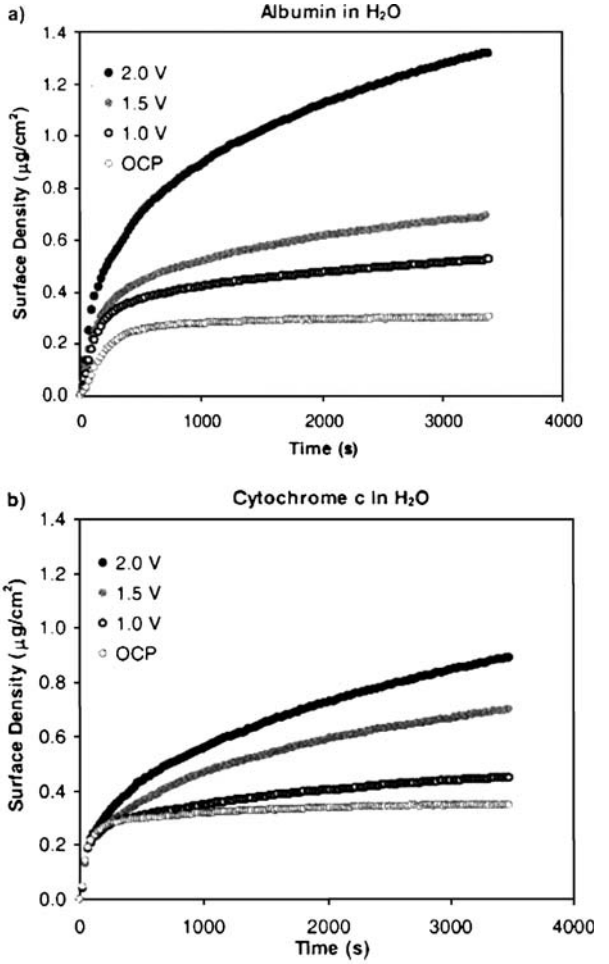

Fig. 6. The density of adsorbed protein versus time for **a** albumin and **b** cytochrome c in water onto ITO at OCP and under various applied potentials (1.0, 1.5, and 2.0 V). Since monolayer densities are approximately 0.46 and 0.33 μg/cm^2 for albumin and cytochrome c, respectively, multilayer adsorption is occurring under an applied potential

these predictions. Extrapolation of data in the linear portion of the surface-limited regime to zero density yields an estimate of the apparent adsorption rate constant, $k_{a'}$ (Calonder et al. 2001; Calonder and Van Tassel 2001). Rate curves such as these also allow for an estimate of the free protein concentration at the surface, and thus of the perfect sink approximation employed in the analysis shown in "Theoretical Prediction". For a given adsorbed density, this is just the ratio of the adsorption rate to the corresponding value of the extrapolated linear region.

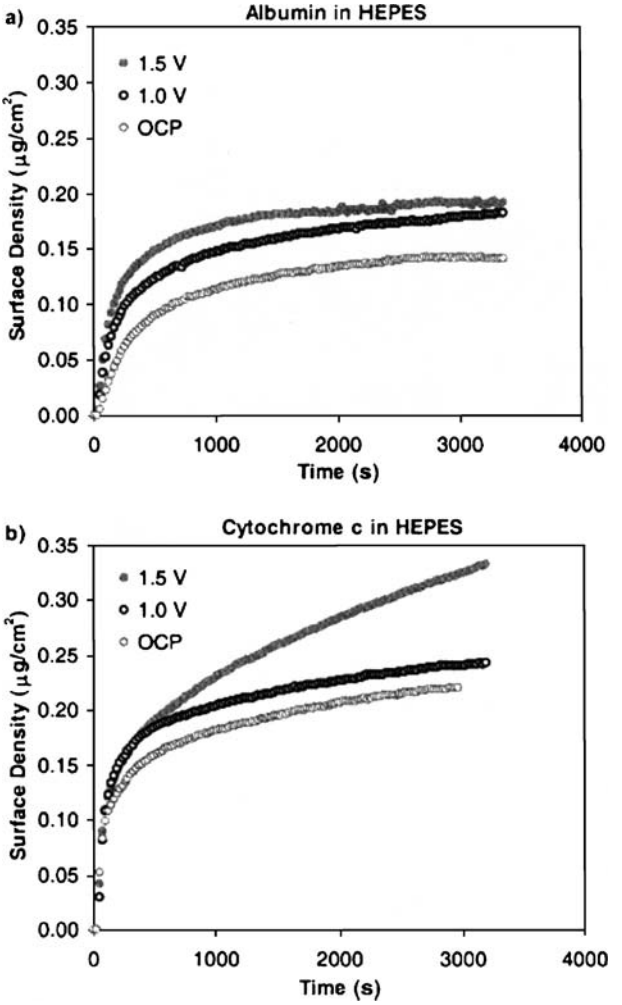

Fig. 7. The density of adsorbed protein versus time for **a** albumin and **b** cytochrome c in HEPES buffer onto ITO at OCP and under various applied potentials (1.0 and 1.5 V)

In Fig. 8, we show the adsorption rate as a function of the adsorbed amount (and, in the insets, as a function of time) for albumin and cytochrome c in water. In the insets, we also show predictions based upon purely convective diffusion (Eq. 2). For albumin, we observe the adsorption rate to increase with applied voltage over the entire range of surface coverage. As shown by the inset, the initial rate is increased significantly by the presence of an applied potential, indicating a transport mechanism to which both convective diffusion and electrophoretic migration contribute. It should be noted that the observed behavior is far from the limit of

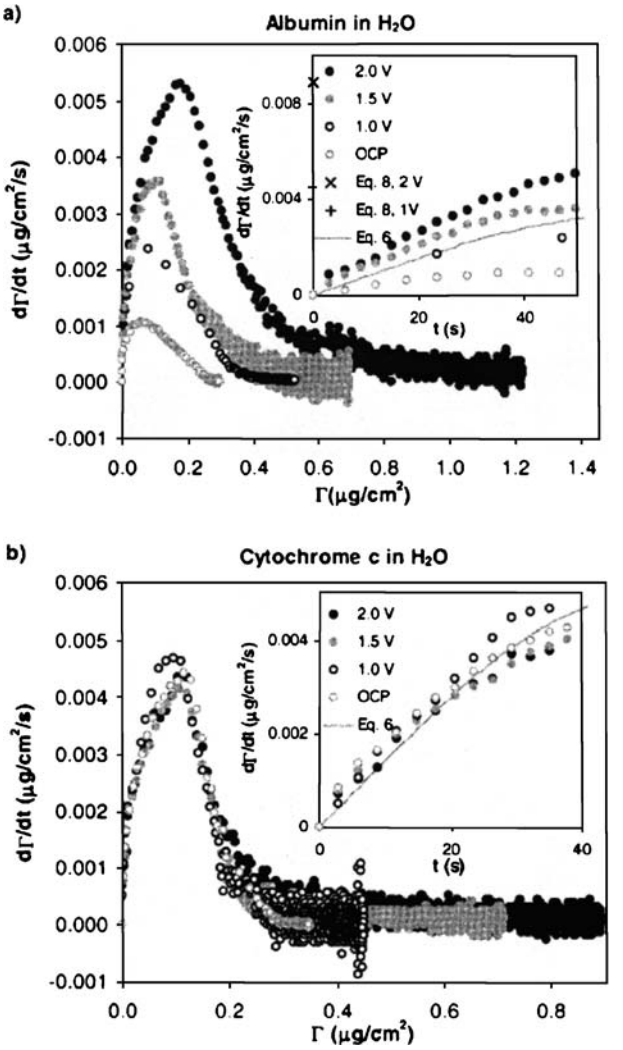

Fig. 8. The rate of adsorption versus adsorbed density (and in the inset, versus time) for **a** albumin and **b** cytochrome c in water onto ITO at OCP and under various applied voltages (1.0, 1.5, and 2.0 V). Also shown are predictions (*solid lines*) for pure convective diffusion given by Eq. 2. Both convective diffusion and electromigration influence transport of the negatively charged albumin, but only convective diffusion influences the transport of the positively charged cytochrome c. If electromigration were the dominant transport mechanism, an initial nonzero adsorption rate would result, as predicted by Eq. 10. Γ Surface density, $d\Gamma/dt$ time derivative of the adsorbed density, t time

pure electrophoretic migration characterized by an initially nonzero, time-independent adsorption rate, as predicted by Eq. 10. For cytochrome c, we observe the transport-limited rates to be essentially independent of ap-

Table 2. The apparent adsorption rate constant $k_{a'}$ determined by extrapolating the linear region of a time derivative of the adsorbed density ($d\Gamma/dt$) versus surface density (Γ) curve (see Fig. 8), and the first-order density expansion coefficient to the cavity function C_1 (Eq. 11), for human serum albumin and horse heart cytochrome c (*Cyt c*) in water and HEPES [10 mM N-(2-hydroxyethyl) piperazine-N′-(ethanesulfonic acid) in 100 mM NaCl, adjusted to pH 7.4 by addition of 6 N NaOH] buffer onto ITO at an OCP and under an applied voltage (1.0, 1.5, or 2.0 V)

Protein	Applied potential (V)	H_2O solvent		HEPES solvent	
		$k_{a'}$ (10^{-5} cm/s)	C_1 ($cm^2/\mu g$)	$k_{a'}$ (10^{-5} cm/s)	C_1 ($cm^2/\mu g$)
Albumin	OCP	1.5 ± 0.1	−3.6 ± 0.1	0.4 ± 0.01	−9.2 ± 0.6
	1.0	3.4 ± 0.1	−2.8 ± 0.1	1.1 ± 0.1	−8.2 ± 1.0
	1.5	5.2 ± 0.2	−3.2 ± 0.3	1.5 ± 0.1	−7.1 ± 0.7
	2.0	9.1 ± 0.2	−2.1 ± 0.1	–	–
Cyt c	OCP	9.9 ± 0.3	−4.5 ± 0.4	3.8 ± 0.2	−8.1 ± 0.7
	1.0	9.5 ± 0.2	−4.7 ± 0.1	4.5 ± 0.3	−6.7 ± 0.8
	1.5	9.0 ± 0.3	−4.5 ± 0.3	4.3 ± 0.6	−6.7 ± 2.0
	2.0	8.3 ± 0.3	−4.3 ± 0.4	–	–

plied potential and the surface-limited rates to be enhanced only at higher coverage (i. e., in the asymptotic region). In Table 2, we show the apparent adsorption rate constant, $k_{a'}$, versus voltage obtained by extrapolating data in the linear regions. For albumin in both water and HEPES solvents, we find $k_{a'}$ to increase significantly with voltage. For cytochrome c, the effect is solvent dependent: we find a decrease in $k_{a'}$ with voltage for water but no appreciable change for HEPES. We also observe the linear coefficient to the density expansion of the cavity function (as introduced in Eq. 11), obtained from the slope of the linear region, to decrease (in magnitude) with voltage for albumin in both solvents but to remain roughly unchanged for cytochrome c.

1.5 Discussion

We observe an applied potential to have a significant effect on adsorption beyond the transport-limited regime. The apparent adsorption rate constant introduced in and around Eq. 11 – a measure of the rate of adsorption to an empty surface and a physical property depending on protein/surface/solvent characteristics – increases with applied voltage for the negatively charged albumin, decreases somewhat for the positively charged cytochrome c in water, and remains roughly constant for cytochrome c in HEPES. Interestingly, we observe the rate of adsorption onto

surfaces of higher coverage to increase significantly with voltage in all systems investigated. Since these measurements occur well beyond the transport-limited regime, this reflects an increased rate of attachment among protein molecules at or near the surface. Since direct alteration of the apparent rate constant by interactions with previously adsorbed proteins is unlikely, the increase in overall adsorption rate is probably due to an increased amount of surface available for adsorption and, at higher coverage, a formation of multilayers. A measure of the available surface is given by the cavity function Φ (as introduced in Eq. 11), and contributing factors to its increase are: (1) the adsorption of protein molecules with smaller projected areas, as would occur in an end-on orientation of a nonspherical protein, and (2) the formation of protein clusters on the surface. We quantify changes in Φ with voltage by considering its first-order density expansion coefficient, C_1, obtained from the slopes of the linear regions of $\mathrm{d}\Gamma/\mathrm{d}t$ versus Γ curves. As reported in Table 2, we observe C_1 to decrease with voltage for albumin, but to be roughly independent of voltage for cytochrome c (see Table 2). A smaller adsorbed molecule projected area, or adsorption directly to the edge of growing clusters, are physical explanations consistent with this observation. Both of these features are engendered by adsorption of protein oriented such that a complementary (in this case negative) charge faces the adsorbing substrate. In this way, even the positively charged cytochrome c may adsorb more rapidly with applied voltage.

Assuming a rectangular array of adsorbed proteins, the dimensions of which are the same as those previously reported [$8 \times 8 \times 3$ nm for albumin (He and Carter 1992), $3.7 \times 2.5 \times 2.5$ nm for cytochrome c (Lvov et al. 1995)], the maximal densities are approximately 0.46 and 0.33 $\mu g/cm^2$ for albumin and cytochrome c, respectively. Clearly, multilayer adsorption under applied voltage is occurring for both proteins in water and possibly, following sufficient time, for cytochrome c in HEPES. As mentioned above, adsorption in the first layer probably involves attachment at a region of complementary charge. This in turn may expose regions of opposite charge, to which charged patches of incoming proteins may be attracted. A plausible cause of multilayer adsorption is therefore the axial interaction between aligned dipoles. One expects this interaction to become weaker with each layer, however, due to incomplete charge reversal. Thus, even systems exhibiting multilayers possess kinetic curves with negative curvature, if not true plateaus.

We observe the overall extent of adsorption and the influence on adsorption by an applied voltage to be greatest when employing a water solvent. One issue here is solvent quality: HEPES is a better solvent, as evidenced by higher protein solubility. Another issue is the higher pH of HEPES (7.4) compared to deionized water (5.5–6.0). For a given potential difference, this

works to lower both ITO and platinum potentials (as shown in Fig. 4a,b). However, when comparing adsorption at roughly equal electrode potentials (e. g., water at $\Delta V = 1.0\,\mathrm{V}$ and HEPES at $\Delta V = 1.5\,\mathrm{V}$), we continue to observe a greater degree of adsorption in the water system. A third issue is ionic strength: the ability of charged species in solution to screen electrostatic interactions is well established and this is clearly serving to reduce in magnitude the effective (or "zeta") potential of the proteins and surfaces investigated here. For example, screening of dipolar interactions by ionic species in the HEPES solvent seems to suppress multilayer formation.

An applied potential clearly offers an opportunity to influence the structure and formation kinetics of an adsorbed protein layer. Interestingly, our work, and that of others (Asanov et al. 1997, 1998; Bernabeu and Caprani 1990; Bos et al. 1994; Feng and Andrade 1994; Fievet et al. 1998; Fraaije et al. 1990; Khan and Wernet 1997) shows that observed behavior does not always follow that expected from basic electrostatic considerations. There is little agreement on the cause of such behavior and, therefore, on the very nature of an applied potential's influence on protein adsorption. Proposed explanations invoke surface-bound counterions, local pH effects, interfacial solvent structure, and protein charge heterogeneity. We will now comment upon each of these effects:

1.5.1 Surface-Bound Counterions

Could similarly charged surfaces be attracted to one another given the presence of a third, oppositely charged species? At first glance this would seem unlikely since counterions would at most completely compensate the charge, leaving two neutral surfaces. The classic Poisson-Boltzmann approach, in which solvated electrolytic species are assumed uncorrelated, predicts only repulsion between like charged objects in an electrolytic solution. However, there are examples where charge overcompensation may occur. A spectacular recent example of this is the layer-by-layer method of growing thin films by exposing a substrate alternatively to solutions of polyanions and polycations (Decher and Schlenoff 2003). Although not fully understood theoretically, the idea is that for entropic reasons, charged sites on the polyions exchange nearly completely with smaller ions at the surface. However, in addition to sites contacting the surface, the polyions generally contain additional charged sites that extend away from the surface, thus resulting in charge overcompensation. However, this type of charge overcompensation would not be expected from the relatively small ionic species present in most protein adsorption systems.

1.5.2 Local pH Effects

Proteins are amphoteric, that is, they possess a number of acid/base sites whose charge is pH dependent. Since a positively (negatively) charged surface will repel solvated protons (hydroxide ions) and thus raise (lower) the pH near to the surface, the sign of a protein's overall change could change upon approach to the surface. In this case, attraction that is indeed electrostatic in origin may follow. Could this effect explain the antielectrostatic behavior reported in the literature? Evidence to suggest otherwise lies in the following observation: the degree of buffering has been shown to have little effect on these antielectrostatic adsorption trends (Brusatori and Van Tassel 2003).

1.5.3 Solvent Interfacial Structure

Solvent molecules (typically water) at or near a solid substrate often experience a hindered rotation relative to those far from the interfacial region. If liberated from the surface via, for example, displacement by an adsorbed protein, a net entropy gain results. An estimation of the rotational contribution to the entropy is given by the statistical mechanical result for an ideal gas rigid rotor, $S_{\mathrm{rot}} = Nk \ln q_{\mathrm{rot}}$ where N is the number of molecules, k is the Boltzmann constant, and q_{rot} is the rotational partition function. For water at 300 K, $q_{\mathrm{rot}} \approx 30$, so the contribution per mole of water liberated from the surface is about 28 J/Kmol. An average-sized protein might result in the liberation of 50 water molecules, so the contribution to the overall free energy of adsorption at 300 K from the solvent rotation would be about –420 kJ/mol. Of course, this is an upper limit since the molecules at the surface do possess some rotational freedom. This estimate would most accurately apply to water at a neutral, hydrophobic surface, where the molecules are expected to be very ordered. As the magnitude of surface charge is increased, the water becomes more disordered (i. e., they may experience enhanced rotation), and the free energy gain from its liberation is thus diminished. As several of the aforementioned studies show trends consistent with these thoughts, the role of solvent structure in the overall influence of an applied electric field cannot be discounted.

1.5.4 Protein Charge Heterogeneity

Based on electrostatics, can a positively (negatively) charged protein be attracted to a positively (negatively) charged surface? Within the Poisson-

Boltzmann approach, the answer is yes, according to Asthagiri and Lenhoff (1997), so long as both protein and surface contain charge heterogeneity. The idea is that regions of complementary charge may come into close contact, while overall repulsion is sufficiently screened by counterions so that a net attraction occurs. This explanation appears to most plausibly explain our observed increase in cytochrome c adsorption with increasing adsorbent potential.

1.6 Conclusions

An electric potential applied to an adsorbing substrate offers the possibility of controlling the structure of an adsorbed protein layer. This represents a powerful method of producing nanostructured coatings for biosensing, tissue engineering, enzymatic catalysis, bioseparation, and bioelectronics applications. Only in the past few years have techniques become available to measure the adsorbed layer properties *in situ* during formation. While several puzzling observations remain to be resolved, and while quantitative prediction of the effects of the applied potential, such as counterion binding, local pH enhancement, solvent structure, and charge heterogeneity remains sparse, the prospects are strong for a general understanding, in the not-to-distant future, of the influence of substrate electric potential on protein adsorption, and the engineering of protein coatings to near-exact specifications using voltage-based methods is certainly a realistic and laudable goal.

References

Asanov AN, DeLucas LJ, Oldham PB, Wilson WW (1997) Heteroenergetics of bovine serum albumin adsorption from good solvents related to crystallization conditions. J Colloid Interface Sci 191:222–235

Asanov AN, Wilson WW, Odham PB (1998) Regenerable biosensor platform: a total internal reflection fluorescence cell with electrochemical control. Anal Chem 70:1156–1163

Asthagiri D, Lenhoff AM (1997) Influence of structural details in modeling electrostatically driven protein adsorption. Langmuir 13:6761–6768

Bernabeu P, Caprani A (1990) Influence of surface charge on adsorption of fibrinogen and or albumin on a rotating disk electrode of platinum and carbon. Biomaterials 11:258–264

Bos MA, Shervani Z, Anusiem ACI, Giesbers M, Norde W, Kleijn JM (1994) Influence of the electric potential of the interface on the adsorption of proteins. Colloids Surf B 3:91–100

Brusatori MA, Tie Y, Van Tassel PR (2003) Protein adsorption kinetics under an applied electric field: an optical waveguide lightmode spectroscopy study. Langmuir 19:5089–5097

Brusatori MA, Van Tassel PR (2003) Biosensing under an applied voltage using optical waveguide lightmode spectroscopy. Biosens Bioelectron 18:1269–1277

Calonder C, Tie Y, Van Tassel PR (2001) History dependence of protein adsorption kinetics. Proc Natl Acad Sci U S A 98:10664–10669
Calonder C, Van Tassel PR (2001) Kinetic regimes of protein adsorption. Langmuir 17:4392–4395
Carignano MA, Szleifer I (2002) Adsorption of model charged proteins on charged surfaces with grafted polymers. Mol Phys 100:2993–3003
de Feijter JA, Benjamins J, Veer FA (1978) Ellipsometry as a tool to study the adsorption of synthetic and biopolymers at the air–water interface. Biopolymers 17:1759–1772
Decher G, Schlenoff JB (eds) (2003). Multilayer Thin Films. Weinheim, Wiley-VCH
Fang F, Szleifer I (2003) Competitive adsorption in model charged protein mixtures: equilibrium isotherms and kinetics behavior. J Chem Phys 119:1053–1065
Feng L, Andrade JD (1994) Protein adsorption on low-temperature isotropic carbon 2. Effects of surface charge of solids. J Colloid Interface Sci 166:419–426
Fievet P, Mullet M, Reggiani JC, Pagetti J (1998) Influence of surface charge on adsorption of a hydrophobic peptide onto a carbon surface by capacitance measurements. Colloids Surf A 144:35–42
Fraaije J, Kleijn JM, Vandergraaf M, Dijt JC (1990) Orientation of adsorbed cytochrome-c as a function of the electrical potential of the interface studied by total internal reflection fluorescence. Biophys J 57:965–975
Haynes CA, Norde W (1994) Globular proteins at solid/liquid interfaces. Colloids Surf B 2:517–566
He XM, Carter DC (1992) Atomic structure and chemistry of human serum albumin. Nature 358:209–215
Khan GF, Wernet W (1997) Adsorption of proteins on electro-conductive polymer films. Thin Solid Films 300:265–271
Lvov Y, Ariga K, Ichinose I, Kunitake T (1995) Assembly of multicomponent protein films by means of electrostatic layer-by-layer adsorption. J Am Chem Soc 117:6117–6123
Malmsten M (ed) (1998a) Biopolymers at Interfaces. Surfactant Science Series. New York, Marcel Dekker
Malmsten M (1998b) Formation of adsorbed protein layers. J Colloid Interface Sci 207:186–199
Oberholzer MR, Lenhoff AM (1999) Protein adsorption isotherms through colloidal energetics. Langmuir 15:3905–3914
Ramsden JJ (1993) Review of new experimental techniques for investigating random sequential adsorption. J Stat Phys 73:853–877
Ravichandran S, Talbot J (2000) Mobility of adsorbed proteins: a Brownian dynamics study. Biophys J 78:110–120
Roth CM, Lenhoff AM (1993) Electrostatic and Vanderwaals contributions to protein adsorption – computation of equilibrium constants. Langmuir 9:962–972
Roth CM, Lenhoff AM (1995) Electrostatic and Van-Der-Waals contributions to protein adsorption – comparison of theory and experiment. Langmuir 11:3500–3509
Stankowski S, Ramsden JJ (2002) Voltage-dependent coupling of light into ITO-covered waveguides. J Phys D Appl Phys 35:299–302
Tie Y, Calonder C, Van Tassel PR (2003) Protein adsorption: kinetics and history dependence. J Colloid Interface Sci 268:1–11
Tiefenthaler K, Lukosz W (1989) Sensitivity of grating couplers as integrated optical chemical sensors. J Opt Soc Am B Opt Phys 6:209–220
Van Tassel PR (2003) Biomolecules at interfaces. In: Mark HF (ed) Encyclopedia of Polymer Science and Technology, 3rd edn. Wiley Interscience, New York, pp 285–305
Voros J, Ramsden JJ, Csucs G, Szendro I, De Paul SM, Textor M, Spencer ND (2002) Optical grating coupler biosensors. Biomaterials 23:3699–3710

2 From Kinetics to Structure: High Resolution Molecular Microscopy

Jeremy J. Ramsden

Abstract. Existing methods of protein structural determination either present a static picture under unnatural conditions or impose a considerable perturbation on the molecule during measurement. This chapter introduces high resolution optical waveguide lightmode spectroscopy (OWLS) as an alternative non-imaging technique of great power and versatility enabling the structure and dynamics of proteins at interfaces to be characterized with unprecedented richness and precision.

2.1 Introduction

Our knowledge of the extraordinary versatility of proteins has been greatly enhanced by the combination of new experimental techniques capable of revealing structural and dynamical details with ever deeper understanding of the molecular mechanisms of processes within living organisms. Hence, "structure" can often now be correlated with "function". While these two terms are not very easy to define in a fully satisfactory way, it can be done ostensively, an excellent example being provided by the story of haemoglobin. The peculiar features of its function, most notably its sigmoidal binding affinity for oxygen, were already known and molecular models inferred well before the details of its structure were discovered through X-ray diffraction (XRD) (e. g. Perutz 1993).

Although XRD has since become the workhorse of protein structure determination, it suffers from two significant weaknesses:

1. It presents an essentially static picture of a single structure[1]
2. Proteins must be present as crystals, and the exigencies of crystallization require that the proteins be placed in unusual salt conditions (good "salting out" salts (Cacace et al. 1997)).

Jeremy J. Ramsden: Department of Materials, Cranfield University, MK43 0AL, UK, E-mail: j.ramsden@cranfield.ac.uk

[1] Partly mitigated by analysing the Debye–Waller factors of the diffraction pattern.

Principles and Practice
Proteins at Solid–Liquid Interfaces
Philippe Déjardin (Ed.)
© Springer-Verlag Berlin Heidelberg 2006

Only very recently has the availability of intense synchrotron sources enabled smaller and less perfect crystals, hence growable under less exigent conditions, to be measured, and has also permitted snapshots and rapid sequences of snapshots to be taken, providing time-resolved structural information. But this work is still quite preliminary.

Alternative approaches have, therefore, been tirelessly sought, in which proteins could be observed in their native environments and sequences of structural changes resolved temporally.

One of the most promising of the new approaches has been single-molecule observation techniques developed in a number of laboratories, mainly in Japan, in which a label (e.g. a fluorophore) is attached to the protein, and high resolution optical microscopy used to observe its motions. This impressive work has led to very significant new insights into the working mechanism of molecular motors being obtained (Yanagida et al. 1993, Funatsu et al. 1995, Ishijima et al. 1998). Note that many of the problems investigated in this field are connected with proteins at some kind of interface, most typically the solid/liquid interface, where the solid part may be a bilayer liquid membrane, and the liquid an aqueous fluid mimicking the cytoplasm.

Much interest has also been shown in the atomic force microscope (AFM), but it seems fair to say that its most successful application has been for the imaging of regular arrays, to which averaging and refinement can be applied to achieve truly molecular resolution (as it is of course with XRD). Although there are examples showing how AFM of individual proteins can provide important corroborative information, there is not the same strong line of inference from the raw measured data to the desired molecularly resolved information as exists for XRD; analysis often boils down to the subjective assessment of images, and high resolution kinetics is problematic.

With both these techniques (single-molecule observation and AFM), although the protein is measured in a native environment, the molecule is severely perturbed. Although the label required in the fluorescent technique may be small relative to the entire protein molecule (and even this is often not the case), it is likely to be large relative to some functionally important part. With AFM, the contact between the cantilever-mounted tip and the protein is akin to using an elephant to move a football—irreparable damage to the latter is likely to result.

Hence the search for non-invasive, native-compatible and dynamically sensitive techniques continues. Note that both the single-molecule observation and AFM techniques require that the protein under investigation is present at a solid/liquid interface. Since the majority of proteins in their native state operate at such an interface, most commonly the surface of a bilayer lipid membrane, this is not a restricting condition.

The purpose of this chapter is to show that another new technique, well adapted to the study of proteins at or near interfaces, namely high resolution optical waveguide lightmode spectroscopy (OWLS), is capable of providing structural information superior to that obtainable from AFM, with excellent time resolution, in native environments, and without the need for labels. It is well known that even though the "ruler" of optical methods is of the order of a wavelength, i.e. hundreds of nanometres for visible radiation, interferometry can resolve structural changes with subnanometre resolution and nanosecond time resolution (Rembe et al. 2005). In the same way, OWLS, also known as high resolution molecular microscopy (HRMM), can also achieve subnanometre resolution of key average characteristic lengths of molecular systems.

The basic experimental arrangement is to place the interfacial region under examination on a planar optical waveguide. For example, if the interaction of a protein with lipid bilayers is being studied, the waveguide is coated with the bilayer, which is placed in contact with a dilute solution of the protein.

The structure of the remainder of this chapter is as follows: The second section focuses on OWLS, describing the fundamentals of reflectance-based methods for interrogating objects at an interface in general and OWLS in particular (briefly contrasting it with other optical methods); the next section outlines the practical determination of the lightmode spectrum; the section on static structures examines how static structural parameters of adlayers are obtained; the following section discusses kinetic analysis and dynamic structural inference; and the last section discusses advanced topic in kinetic analysis and dynamic structural inference.

2.2 Optical Waveguide Lightmode Spectroscopy

In the latter half of the 17th century Newton (1730) demonstrated the existence of an evanescent field when light falls on the interface between dense and rare optical media and is totally reflected back into the dense medium. During the intervening years the phenomenon has been extensively studied, and has given rise to important measurement techniques for investigating interfacial phenomena (cf. Table 1). The overall approach is for the optically dense medium (typically a transparent dielectric) to form the substrate in contact with the optically rare medium (typically an aqueous solution) from which particles accumulate at the interface between the two media. Any change of electronic polarizability within the evanescent field, which decays exponentially into the rare medium, gives rise to a change of phase of the totally internally reflected light, which is essentially

Table 1. Theoretical foundations of different optical techniques for investigating interfacial phenomena and their experimental development, with the names of the pioneering contributors and of the instrument makers. Acronyms: SAR, Scanning Angle Reflectometry; SPR, Surface Plasmon Resonance. SAR does not make use of the evanescent field as such. In SPR, the field is generated by the collective vibrations of electrons in a thin metal film deposited at the interface

Technique	Theoretical basis	Experimental demonstration	Laboratory instruments	Large-scale commercialization
SAR	Fresnel (1818) Bousquet (1957)	Schaaf et al. (1985)	–	Not anticipated
Ellipsometry	Fresnel (1818) van Ryn van Alkemade (1883)	Jamin (1850)	Rudolf (1976)	Not anticipated
SPR	Maxwell-Garnett (1906)	Turbadar (1959)	Biacore (1990)	Anticipated?
OWLS	Tien (1977)	Ramsden (1993a)	MicroVacuum (2001)	Corning (2006)

the parameter measured. Table 1 provides a brief historical survey of the relevant developments up to the present.

Ample comparison of these different techniques has been made elsewhere (e.g. Ramsden 1994, 1997); the next table summarizes some advantages and disadvantages. We shall take a further comparative look in Sect. 2.4.

Table 2. Brief summary of some of the pertinent advantages and disadvantages of different optical techniques. Regarding the sensitivity, OWLS is intrinsically about 10 times more sensitive than SPR (for the determination of a single parameter) (Lukosz 1991). SPR only occurs with the p polarization; practically, SAR also has that restriction. See the chapter in this volume by Poksinski and Arwin concerning ellipsometry

Technique	Advantages	Disadvantages
SAR	Comprehensive theoretical analysis	Slow Not very sensitive
Ellipsometry	Very versatile Extensive literature	No closed form solutions of equations Not very sensitive
SPR	Strong commercial development Not very sensitive Requires a metal substrate	No closed form solutions of equations
OWLS	Highly informative closed form solutions of equations Very sensitive; versatile	Cannot be used with opaque substrates Compatible with other photonics devices

2.2.1 Principles of Optical Biosensing

Fresnel's coefficients of reflection give the ratio of reflected to incident amplitude for beams incident from the high refractive index side (labelled F) onto an interface between two transparent dielectrics F and J. Their refractive indices are n_F and n_J respectively, with $n_F > n_J$[2,3]. The coefficients are:

$$R_\varrho = \frac{k_F/n_F^{2\varrho} - k_J/n_J^{2\varrho}}{k_F/n_F^{2\varrho} + k_J/n_J^{2\varrho}} \tag{1}$$

for the perpendicular (s, $\varrho = 0$) and parallel (p, $\varrho = 1$) polarizations, with

$$k_F = k n_F \cos\theta \tag{2}$$

where $k = 2\pi/\lambda$, the wavenumber for the light in vacuo, θ is the angle of incidence measured from the normal to the interface, and

$$k_J = k\sqrt{n_J^2 - n_F^2 \sin^2\theta}\,. \tag{3}$$

For a thin film A of thickness d_A interposed at the interface, these expressions are modified by summing the reflections and transmissions at the two interfaces, yielding (Bousquet 1957):

$$R_{F,A,C} = \frac{R_{F,A} + R_{A,C}\,e^{-2i\beta_A}}{1 + R_{F,A}R_{A,C}\,e^{-2i\beta_A}} \tag{4}$$

where β_A is the phase thickness of A, defined by

$$\beta_A = d_A \mid k_A \mid \tag{5}$$

with k_A defined by Eq. 3 with J = A. These expressions may be straightforwardly extended to multiple thin layers in an interfacial stack (Ramsden 1993a).

Careful measurement of the amplitude of reflected light as a function of incident angle can, in principle, yield enough data to enable Eq. 1 to be fitted to the data with the unknown parameters (which are typically the opto-geometric parameters of the thin interfacial film) as fitting variables. Often the measurement is carried out with p-polarized light in the vicinity

[2] In general the media may also absorb some light, i. e. n_F and n_J are actually complex numbers, but typically the imaginary part is very small compared to the real part, and for the convenience of writing we shall suppose it to vanish.

[3] Horváth et al. (2002) have demonstrated reverse symmetry waveguide sensing with $n_F < n_J$.

of the Brewster angle for the F,S interface (at which the reflected component vanishes).

In ellipsometry, it is the change in polarization upon reflection or transmission which is measured.

The phenomenon of *total internal reflection*, which occurs when θ exceeds a critical angle (such that the angle of transmission would become imaginary) was known to Newton (1730), and may indeed have been discovered by him (at any rate he gives the first account published in writing). In effect, light propagating in a planar optical waveguide, i. e. a thin slab of high refractive index material sandwiched between slabs of low index material, does so via alternate total internal reflections at the two boundaries in a zig-zag path, which of course implies penetration of the light into the optically rarer medium beyond the waveguide, and is equivalent to a phase shift Φ (Eq. 8). The guided mode within the waveguide is a stationary wave, and beyond the waveguide an exponentially decaying evanescent field (Ramsden 1993a). The point at which the light turns back toward the waveguide exactly equals the characteristic decay length of the evanescent field.

2.2.2 Mode Equations for OWLS

The mode equations, which govern the relation between the effective refractive indices N and the optogeometric parameters of the waveguide, can be easily derived from Eqs. (1–3), bearing in mind that R, being in general complex, can be written as the product of its modulus and argument:

$$\hat{R} = \mid \hat{R} \mid \, e^{i\Phi} \tag{6}$$

and by noting that the existence criterion for a guided mode is that the sum of the phase shifts occurring at the two reflections and upon twice traversing the width of the waveguide must sum to an integral multiple of 2π, otherwise destructive interference occurs (Tiefenthaler and Lukosz):

$$\Phi_{S,F} + 2\beta_F + \Phi_{F,A,C} = 2\pi m \,, \quad m = 0, 1, 2, \ldots \tag{7}$$

where m is the mode number, and the phase changes upon reflectance are derived from Eqs. 1 and 6:

$$\Phi_{F,S} = -2 \arctan \left[\left(\frac{n_F}{n_S} \right)^{\varrho} \left(\frac{N^2 - n_S^2}{n_F^2 - N^2} \right)^{1/2} \right] . \tag{8}$$

This assumes that the F,S interface is flat and abrupt.

Introducing the normalized propagation constant b (Ghatak and Thyagarajan 1989):

$$b = (N^2 - n_S^2)/(n_F^2 - n_S^2) \,, \tag{9}$$

the asymmetry parameter a

$$a = (n_S^2 - n_C^2)/(n_F^2 - n_S^2) \,, \tag{10}$$

and the dimensionless waveguide parameter W:

$$W = k d_F (n_F^2 - n_S^2) \,, \tag{11}$$

where $k = 2\pi/\lambda$ is the wavenumber of the light in vacuo with wavelength λ, the mode equations for a three layer waveguide (S,F,C) are then

$$\tan[W(1-b)^{1/2}] = \left(\frac{n_F}{n_S}\right)^{2\varrho} \frac{\left(\frac{b}{1-b}\right)^{1/2} + \left(\frac{n_F}{n_C}\right)^{2\varrho} \left(\frac{b+a}{1-b}\right)^{1/2}}{1 - [b(b+a)]^{1/2} (n_S n_C / n_F^2)^{-2\varrho(1-b)}} \tag{12}$$

with $\varrho = 0$ and 1 for the TE (transverse electric, i.e. s-polarized) and TM (transverse magnetic, i.e. p-polarized) modes, respectively. The lower cutoff is given by

$$W_c^{(\varrho)} = \arctan\left[\left(\frac{n_F}{n_C}\right)^{2\varrho} a^{1/2}\right] + m\pi \tag{13}$$

and the penetration depth by

$$\Delta z = 1/[k(N^2 - n_C^2)]^{1/2} \,. \tag{14}$$

$\Phi_{F,A,C}$ can be calculated if the adlayer A is assumed to be a uniform, homogeneous film (Tiefenthaler and Lukosz 1989). Measurement of two modes (typically the zeroth order TM and TE) and the simultaneous solution of the corresponding two mode equations enables the thickness and refractive index of the adlayer to be calculated. The explicit solutions for n_A and d_A are given by Guemouri et al. (2000). As discussed in the next subsection, these two parameters can then be combined to yield the number of particles ν captured at unit area of interface according to

$$\nu = d_A \frac{n_A - n_C}{\mathrm{d}n/\mathrm{d}c} \tag{15}$$

where $\mathrm{d}n/\mathrm{d}c$ is the refractive index increment of the particle, dependent on its polarizability and the medium in which it is dissolved or suspended (Ball and Ramsden 1998)

If the adlayer is not isotropic, then it must be characterized by two or more refractive indices. A fairly common case is for the adlayer to be uniaxial, and hence characterized by two refractive indices, n_o and n_e (ordinary and extraordinary). They are related to the measured effective refractive indices by

$$n_o = n_{A,TE} \tag{16}$$

where $n_{A,TE}$ is the adlayer refractive index in the TE mode equation (Eq. 7), and

$$n_e = \left[\frac{1}{n_o^2} + \left(\frac{n_F}{N_{TM}} \right)^2 \left(\frac{1}{n_{A,TM}^2} - \frac{1}{n_o^2} \right) \right]^{-1/2} . \tag{17}$$

In solving the mode equations, if there are only two of them (e.g. corresponding to the TE_0 and TM_0 modes), then d_A must be measured independently in order to proceed. On the other hand, if thicker waveguides are used, supporting higher modes, then all the parameters may be determined independently (albeit at lower sensitivity (Tiefenthaler and Lukosz 1989, Mann 2001).

2.2.3 The Uniform Thin Film Approximation (UTFA)

For many of the applications relevant to this volume, nanoscale particles such as proteins are added to the interface, and the question arises whether the resulting monolayer deposit, which is inherently heterogeneous, can be modelled as a homogeneous, uniform thin film. Were that to be the case the analysis of the raw data would be much easier than otherwise. Careful comparison of results assuming such a film with explicit consideration (using Mie theory) of the actual heterogeneity of such layers has revealed that the UTFA is an excellent approximation up to particle diameters of around 50 nm (Mann et al. 1997). These films are often isotropic, or anisotropic to a negligible degree, which means that they are fully characterized by just two parameters, refractive index n_A and geometrical thickness d_A[4].

In OWLS, these two parameters can be obtained by a straightforward analytical solution of two simultaneous mode equations using the effective refractive indices of two independent modes as the input. A disadvantage of

[4] One way in which the assumptions of the UTFA could be invalidated even though minute nanoparticles are being adsorbed as a monolayer is if those particles cluster together to create large islands. Such behaviour is evidenced by a broadening of the TM incoupling peak but not the TE one (J.J. Ramsden and T. Jaworek, unpublished observations), and has a definite kinetic signature as discussed in Sect. 2.6.1.

the other optical methods (viz., SAR, ellipsometry and SPR) is that tedious fitting calculations are required to extract n_A and d_A. While the general availability of powerful personal computers makes this less of a problem than formerly, the fitting procedure is itself not robust insofar as a large family of possible solutions satisfy the equations.

In many applications, however, only the number ν of particles per unit area of interface (or the amount M of protein deposited on a membrane) is required, and this can be straightforwardly obtained from any n_A and d_A pair yielding a solution[5] by

$$\nu = M/m = d_A(n_A - n_C)/(m\ \mathrm{d}n/\mathrm{d}c) \tag{18}$$

where m is the mass of one adsorbate particle (e.g. a single protein molecule) and $\mathrm{d}n/\mathrm{d}c$ is the refractive index increment (rii) of the adsorbate solution. The rii simply expresses the slope of a plot of solution refractive index versus the concentration of protein which it contains. For a given protein dissolved in a given solvent, this has been shown to be linear up to concentrations of around 0.5 g/ml, in which range even dense monolayers comfortably fall (de Feijter et al. 1978). Some common and other blood proteins dissolved in common buffers used in biological research all have a value of about 0.18 cm^3/g (de Feijter et al. 1978, Ball and Ramsden 1998).

2.2.4 Optical Invariants

A weakness of the method outlined in Sect. 2.2 for evaluating OWLS data is that the results depend in an ill-defined fashion on the model chosen to describe the adlayer A. For many adlayers encountered in practice, especially those formed from macromolecules captured at the solid–liquid interface, the assumption of a uniform, homogeneous film is unrealistic.

The use of optical invariants enables key parameters characterizing the adlayer to be calculated without the need for possibly unwarranted assumptions. The difference between the optical responses of the idealized Fresnel interface and the real interface is given in terms of surface excess polarization densities (Mann 2001) (cf. Gibbs' surface excess quantities in his treatment of the thermodynamics of thin films). Any measurable quantities should be independent of the position of the (fictitious) Fresnel interface: such optical invariants are obtained by combining the polarizabilities obtained by a multipole expansion of the surface excess polarization densities

[5] More rigorously, this implies that n_A and d_A are not *optical invariants* of the system. The optical invariants arise analogously to the Gibbs formulation of interfacial thermodynamic properties: they are such quantities that are invariant under small movements of the interfacial boundary (see Sect. 2.2.4).

such that the combinations are invariant with respect to displacement of the idealized Fresnel interface. These optical invariants allow determination of the maximum information available from the data with the minimum of ambiguity.

Mann (2001) has derived the optical invariants for OWLS and given analytic equations relating the parameters obtained from OWLS measurements to the optogeometric parameters of uniaxially anisotropic adlayers. The first order non-invariant excess polarization density parallel to the interface is

$$\tilde{\gamma}_e = kd_A\tilde{n}^2 \tag{19}$$

where $\tilde{n}$ is the excess parallel refractive index, i. e.

$$\tilde{n}^2 = n_\parallel^2 - n_C^2 \tag{20}$$

where $n_\parallel$ is the refractive index parallel to the interface, i. e. the ordinary refractive index, and we can call $\tilde{n}^2/n_C^2$ the increment of the relative dielectric constant of the adlayer.

The first and second order (in d_A/λ) invariants are J_1, J_{21}, J_{22} and J_{23}:

$$J_1 = \frac{n_\parallel^2 - n_F^2 - (n_F^2 - \tilde{n}^2)\alpha}{n_C^2/\tilde{n}^2 + 1 + \alpha} kd_A \tag{21}$$

where the optical anisotropy of the adlayer is

$$\alpha = \frac{n_\perp^2 - n_\parallel^2}{\tilde{n}^2}\,, \tag{22}$$

where $n_\perp$ is the refractive index perpendicular to the interface, i. e. the extraordinary refractive index;

$$J_{21} = \frac{n_C^2}{2}\left(\frac{\tilde{n}^2}{\mathcal{N}_{FC}} - 1\right)(kd_A)^2\,, \tag{23}$$

where

$$\mathcal{N}_{FC} = n_F^2 - n_C^2\,, \tag{24}$$

i. e. depending only on polarization density parallel to the interface;

$$J_{22} = -\frac{1 - \tilde{n}^2(1+\alpha)/\mathcal{N}_{FC} + \alpha/2}{n_C^2/\tilde{n}^2 + 1 + \alpha}(kd_A)^2\,; \tag{25}$$

and

$$J_{23} = J_{21} - J_{22}\frac{n_F^2 n_C^2}{n_F^2 + n_C^2}\,. \tag{26}$$

Table 3. Comparison of different techniques in terms of obtainable quantities

Technique	Non-invariant	Optical invariants 1st order[a]	2nd order[a]
OWLS	$\tilde{\gamma}_e$	J_1	J_{22}, J_{23}
Ellipsometry		J_1	J_{23}
SAR		J_1	J_{22}, J_{23}

[a] in d_A/λ

The power of the optical waveguide technique is that four opto-geometric parameters characterizing an (anisotropic) adlayer can be extracted. Table 3 compares the available parameters with those from other optical techniques.

If d_A/λ is small (< 0.01), then $\tilde{\gamma}_e$ and J_1 dominate the waveguide optical response, and (Mann 2001)

$$\tilde{\gamma}_e = -\frac{\mathcal{N}_{FC}}{\mathcal{N}_{FE}^{1/2}} \left(\pi m - k d_F \mathcal{N}_{FE}^{1/2} + 2 \arctan \left(\frac{N_{TE}^2 - n_C^2}{\mathcal{N}_{FE}} \right)^{1/2} \right) \tag{27}$$

where

$$\mathcal{N}_{FE} = n_F^2 - N_{TE}^2 \tag{28}$$

and

$$J_1 = \frac{N_{TM}^2 - \mathcal{N}_{CF}}{N_{TM}^2 \mathcal{N}_{CF}/n_F^2} \left\{ \tilde{\gamma}_e - \frac{\mathcal{N}_{FC}}{\mathcal{N}_{FM}^{1/2}} \left[\pi m - k d_F \mathcal{N}_{FM}^{1/2} + 2 \arctan \left(\frac{n_F^2}{n_C^2} \left(\frac{N_{TM}^2 - n_C^2}{\mathcal{N}_{FM}} \right)^{1/2} \right) \right] \right\} , \tag{29}$$

where

$$\mathcal{N}_{CF} = \frac{n_F^2 n_C^2}{n_F^2 + n_C^2} \tag{30}$$

and

$$\mathcal{N}_{FM} = n_F^2 - N_{TM}^2 \, . \tag{31}$$

The adlayer mass M per unit area, for thin films, i. e. $d_A/\lambda < 0.01$, is given by

$$M \approx -\tilde{\gamma}_e (\mathrm{d}c/\mathrm{d}n^2)/k \, , \tag{32}$$

i. e. depending only on the TE modes.

2.3 The Practical Determination of Waveguide Parameters

The fundamental parameter of the optical waveguide is the effective refractive index N. Equivalently, one may refer to the phase velocity, propagation constant, reflection phase change, etc.—all are equivalent (Ramsden 1993a). N characterizes a guided mode. Modes are discrete, and for the thinnest waveguides, which are the most sensitive to changes in the interfacial region, are well separated. It is important to realize that even though the overall waveguiding structure through which light is propagating comprises several layers, each with a distinct refractive index, the light propagates through all of them with a common phase velocity.

The two main methods for determining the lightmode spectrum are (i) coupling, and (ii) interferometry. In this chapter we shall only deal with the former, for it most readily and directly allows the precise and accurate determination of the absolute values of the effective refractive indices of two or more modes, which are required for the structural analysis that is our ultimate goal. Interferometry is covered in the references cited earlier (Ramsden 1994, 1997), and see also the chapter by Freeman in this volume.

Coupling requires a grating (or, less conveniently, a prism). Consider a slab structure consisting of a support layer S (typically made from optical glass about a few tenths of a mm thick), a thin high refractive index transparent film F (typically a metal oxide $\sim$ 100 nm thick), and the cover medium C (typically air or water). An optical grating is incorporated into the waveguide at the F,S or F,C interface. A shallow grating, a few nm deep, is sufficient for coupling the few percent of light needed for measurement purposes. In a typical incoupling configuration, an external beam impinges onto the grating, making an angle α with the grating normal. The wavenumber component in the direction of guided propagation is then $n_{\text{air}} \sin\alpha + 2\pi\ell/\Lambda$, where $\ell = 0, \pm1, \pm2, \ldots$ is the diffraction order and Λ the grating constant. If this matches a guided mode with wavenumber kN, incoupling will occur according to the coupling condition

$$N = n_{\text{air}} \sin\alpha + \lambda\ell/\Lambda \ . \tag{33}$$

The procedure is, therefore, to measure the light emerging from the end of the waveguide while varying α. The emerging light will appear as a series of sharp peaks, successively $\text{TM}_{m=0,\ell=1}$,$\text{TE}_{m=0,\ell=1}$, etc., called the mode spectrum. At the time of writing, the highest precision in the determination of N is achievable by mechanical goniometry in a temperature-controlled environment, with which α can typically be determined to microradian precision.

The refractive index of most substances varies significantly with temperature. The variation is directly related to the coefficient of thermal

Table 4. Contributions to the uncertainty of N in an input grating coupler. It should also be noted that since $\partial N/\partial n_C \sim 0.1$ and $\partial n_C/\partial T \sim 10^{-4}\mathrm{K}^{-1}$ for water, aqueous solutions should be thermostated to ±0.1 °C to keep within the bounds of uncertainty imposed by the other terms

Parameter	Typical value	Uncertainty	Physical origin
n_{air}	1.0002673	10^{-7}	Temperature fluctuations ($T \pm 1$ °C)
Λ	416.147 nm	0.001	Grating lateral thermal movement
α	0.09 rad	1.25×10^{-6} rad	Goniometer mechanical instability
λ	632.816 nm	0.001 nm	Laser mode jumping

expansion of the substance, as can be seen from the Lorentz-Lorenz equation, which connects the macroscopic index of refraction with various atomic or molecular parameters, i. e. molecular mass M_r, density ϱ and molar refractivity R_M:

$$n^2 = (M_r + 2\varrho R_M)/(M_r - \varrho R_M) \; . \tag{34}$$

Of these, only the density varies with temperature. Therefore, it is obviously important to record the temperature of the sample under investigation when making optical measurements. Table 4 lists the various sources of uncertainty in the determination of the mode spectrum peaks. After applying the usual combining laws it can be seen that all factors contribute roughly equally to the overall uncertainty in N, typically $\pm 1 - 2 \times 10^{-6}$.

2.3.1 Device Fabrication

The optical waveguides and grating couplers can be made by a variety of routes. For fabricating the thin layers of high refractive index transparent oxides, either physical vapour deposition (e. g. evaporation or sputtering) or sol-gel pyrolysis are used. The optical quality requirements are extremely stringent: the absorption coefficient should generally be less than 10^{-5} cm^{-1}, otherwise insufficient light will reach the end of the waveguide and the signal:noise ratio will be degraded. The gratings required for coupling can be made by either topographical or refractive index modulation. The former can be achieved by structuring the optical glass support (the S layer) using the conventional methods of photolithography; to obtain the fine gratings required (Λ of the order of 400 nm or less) for working with $\ell = 1$, holographic exposure of photoresist is required. Coarser gratings can be used with higher order diffraction peaks but the signal:noise ratio is lower. It is also possible to modulate the surface of the F layer: however, this is less desirable since the surface (that will interact with the proteins) may

then become chemically contaminated. Shallow gratings (5–10 nm deep) are sufficient and have the great advantage that the F layer is thereby so slightly modulated in the grating region that the mode equations derived above retain their validity. A further advantage is that, from the hydrodynamic viewpoint, the surface may still be considered planar.

Perfect planarity is, however, only achievable with refractive index modulation. This can be achieved by exposing the substrate to a beam of energetic nitrogen through a mask (created, as above, by photolithography via holographic exposure of photoresist). Nitrogen atoms implanted in the silica modify its refractive index. The technology is non-trivial to perfect, however, mainly because of the difficulty of removing photoresist residues hardened by exposure to the energetic nitrogen beam.

Further fabrication steps concern the coating of the waveguide with whatever material is serving as adsorbent for the proteins under investigation. Lipid bilayers are conveniently deposited on the surface using the Langmuir-Blodgett technique (Ramsden 1999); alternatively a suspension of lipid vesicles can be used, which fuse with the surface to create the bilayer (Csúcs and Ramsden 1998a). In both cases, a few molecular layers of water between the inner leaflet of the bilayer and the solid support ensure that the membrane (in its liquid crystalline state) has native fluidity, i. e. the lateral diffusivity of the lipid molecules is approximately the same as in the membrane of a living cell.

Polymer layers, including polyelectrolytes, can be deposited by spontaneous attachment from solution (e. g. Ramsden et al. 1995); the large number of contacts per molecule ensures irreversible attachment. Other materials can be deposited by physical or chemical vapour deposition. A layer 10 nm thick will generally be found to completely mask the underlying F layer (Kurrat et al. 1997). The only restriction is that the layer should not absorb the guided light; hence metals can only be deposited to a thickness of about 2 nm, which is often insufficient for a continuous layer to be formed; and materials (dyestuffs) with intensive absorption bands coinciding with the wavelength of the guided light should be avoided.

2.3.2 Fluid Handling Arrangements

The overwhelming majority of in situ investigations into protein structure involve aqueous solutions of proteins. Hence, a way must be found to bring the solutions in contact with the adsorbing surface. A convenient way of doing this is to clamp a cuvette to the surface of the waveguide, such that it forms the bottom of the cuvette.

2.4 Static Structure

The procedures to be followed are implicit in the treatment given in Sect. 2.2. The parameters emerging are (for waveguides supporting zeroth and first order TM and TE modes) d_A, n_o, n_e and one other (e.g. n_C); if the adlayer is isotropic a single refractive index n_A suffices. Examples of an isotropic adlayer constituted from small spheroidal proteins is given by Guemouri et al. (1998); and of a continuous anistropic layer by Ramsden (1999) and Ramsden et al. (1995).

2.5 Kinetic Analysis and Dynamic Structural Inference

The canonical expression for the accumulation of particles at the solid/liquid (and indeed the solid/gas) interface is

$$\mathrm{d}M/\mathrm{d}t = k_a\, c^* \phi(M) - k_d(t, M)M \tag{35}$$

where M is the mass (per unit area) of accumulated material (sometimes we shall use ν to denote the number of adsorbed particles per unit area), k_a is the chemical adsorption coefficient (which may depend on ν); c^*, the effective bulk solution concentration of the particles; ϕ, the available area function; and k_d, the chemical desorption "coefficient" (which may depend on both M and t). In the following subsections, each of these factors will be analysed.

2.5.1 Particle Transport

We first suppose that our particles are smooth, rigid and spherical and totally buoyant, i.e. their movement is not influenced by terrestrial gravity.

A particle suspended in a fluid can be transported by convection (i.e. entrained by the motion of the fluid) or by diffusion. The key parameter is the relative motion of the fluid with respect to the adsorbent. Far from the surface, the flow is uninfluenced by the surface; at the surface, on the other hand, friction dictates that the fluid is stationary (ignoring the possibility of slip); and the velocity in between is constantly diminishing. Hence near a surface, a particle will move by diffusion, and far from the surface by convection. At a certain intermediate distance, typically of the order of tens of micrometres, the transport régime will cross over from convection to

diffusion. This distance is known as the diffusion boundary distance (δ). A comprehensive treatment is given by Levich (1962). The flow in certain geometries, such as the tube or plate, can be solved analytically. These geometries are therefore particularly favourable for kinetic evaluation, a factor which should be borne in mind when designing flow cuvettes. For flow in a tube,

$$\delta = \left(\frac{3}{2}\right)^{2/3} \left(\frac{DC}{F}\right)^{1/3} \tag{36}$$

where D is the diffusivity of the protein, F the volumetric flow rate, and C a constant depending on the dimensions of the tube.

When choosing flow rates, it should be remembered that only laminar flow régimes can be analysed conveniently, i. e. up to Reynolds numbers of at most around 1000. In principle a diffusion boundary still exists in the case of turbulent flow, but the motion is much more complicated than in the case of laminar flow.

Hence, a protein-sized particle will be moving diffusively already at a distance of the order of a thousand times its own dimensions (a few nm in diameter) from the adsorbing surface.

At a distance of the order of ten times its own dimensions from the adsorbing surface, the particle may begin to be influenced by the long range hydrophilic repulsion (see Cacace et al. (1997) for a discussion of intermolecular forces), which will considerably retard its rate of arrival at the surface. When designing the flow conditions for an experiment, it is only necessary to ensure that convective-diffusion is rapid enough to replenish the particles lost from the solution in the vicinity of the surface by attachment to it. This is of practical importance given that many biological samples of carefully purified macromolecules are available only in extremely small quantities.

Good quantitative approximations for analysing the flow régimes can be derived from the equations of Fick and Smoluchowski (see Ramsden (1998) for a more complete discussion). If the surface (at $z = 0$, where z is the coordinate normal to the surface) is a perfect sink for the adsorbate, then the bulk (solution) concentration c_b is zero at $z = 0$, the concentration gradient will be approximately linear, and the rate of accumulation is

$$\mathrm{d}\nu/\mathrm{d}t = c_b D/\delta \; . \tag{37}$$

It is a good idea to compare the experimentally observed rate with this maximum upper limit (which may, however, be exceeded if there is a long range attractive force, e. g. electrostatic, between particle and surface).

The effect of any energy barrier is to retard accumulation. In the immediate vicinity of the surface, the local bulk concentration c_v will be much

higher than zero (although still less than c_b). It is convenient to consider that the rate of accumulation at the surface is given by the product of c_v and a chemical rate coefficient k_a, which is directly related to the repulsive energy barrier (Spielman and Friedlander 1974):

$$dM/dt = k_a\, c_v \tag{38}$$

and the Fick-Smoluchowski régime (linear concentration gradient) applies to the zone above this vicinal region. Hence

$$V\frac{dc_v}{dt} = \gamma S\left[D\frac{(c_b - c_v)}{\delta} - k_a c_v\right], \tag{39}$$

where V and S are unit volume and surface respectively. Strictly speaking the distance of the vicinal layer from the surface should be subtracted from δ in the denominator, but since that distance is of the order of molecular dimensions, i.e. only a few nm, whereas δ is of the order of a few or a few tens of microns, this correction can be neglected. If desorption of the material also has to be taken into account a term with a chemical desorption coefficient k_d can be included:

$$V\frac{dc_v}{dt} = S\left[D\frac{(c_b - c_v)}{\delta} + k_d(t)\nu - k_a c_v\right]. \tag{40}$$

In a great many cases accumulation of material is limited to a monolayer, or to occupying a monolayer of receptors, in which case a function ϕ must be introduced, which gives the fraction of the surface still available for adsorption or binding (i.e. the probability that space is available). Our kinetic equation then becomes:

$$V\frac{dc_v}{dt} = S\left[D\frac{(c_b - c_v)}{\delta} + k_d(t)\nu - k_a c_v\phi(\nu)\right]. \tag{41}$$

We shall discuss ϕ—which obviously depends on M or ν—below. One important implication is that as the surface fills up, i.e. as $\phi \to 0$, c_v will tend to approach c_b, and dM/dt will asymptotically approach zero regardless of the flow régime. This can be immediately seen by letting the left hand side of whichever of the previous three equations is appropriate go to zero, yielding an explicit expression for c_v, e.g.

$$c_v = c_b/(1 + \delta\phi/D) \tag{42}$$

if $k_a = 1$ and $k_d = 0$, which can then be substituted into Eq. 35, in which $c^* = c_v$.

The pure diffusion régime

If there is no flow at all then the vicinal layer is replenished by diffusion only, i. e. there is no distance at which concentration is maintained constant by effectively an infinite reservoir as in convective diffusion. This leads to the well-known result of Smoluchowski, according to which the flux to the surface constantly diminishes as $t^{-\beta}$, where $\beta = 0.5$ for standard diffusion (other exponents have been found for the diffusion of highly non-spherical, non-compact proteins such as tenascin (Ramsden 1992).

If the flow rate is slow enough for the rate of adsorption to be limited by transport alone, or, more quantitatively, if the dimensionless parameter.

$$\varepsilon = k_a \delta^2 / D \tag{43}$$

becomes large relative to unity, then the initial rate of adsorption is given by Eq. 37, from which D may be obtained. This is a useful way to determine the diffusion coefficient in solution.

2.5.2 The Chemical Adsorption Coefficient

If a repulsive potential barrier $U(z)$ exists between protein and surface, where z is the distance between them, not every arriving protein will adsorb, even if there is space for it to do so, and $\dot{\nu}$ will be diminished by a rate coefficient k_a, which can be found by integrating $U(z)$:

$$k_a = D \Big/ \left[\int_0^\infty [\exp(\Delta U(z)/kT) - 1] \mathrm{d}z \right] . \tag{44}$$

Sometimes the denominator of the right hand term is called the "adsorption length", δ_a. The interaction potential U can be approximated by the sum of the particle-surface interaction free energies, corresponding to the Lifschitz-van der Waals (LW), electrostatic (el) and electron donor-acceptor (da) interactions:

$$U(z) = \Delta G^{(\mathrm{LW})} + \Delta G^{(\mathrm{el})} + \Delta G^{(\mathrm{da})} , \tag{45}$$

with each of the terms given by

$$\Delta G^{(\mathrm{LW})} = -A_H r/(6z) , \tag{46}$$

where r is the particle radius and A_H the mean Hamaker constant;

$$\Delta G^{(\mathrm{el})} = 4\pi\varepsilon_0\varepsilon\psi_1\psi_3 \ln[1 + \exp(-\kappa z)]r , \tag{47}$$

where the ψ are the electrostatic surface potentials of adsorbent (particle) and adsorbate, and $1/\kappa$ is the well known Debye length; and

$$\Delta G^{(\mathrm{da})} = 2\pi\chi\Delta G^{(\mathrm{da})\parallel} \exp[(\ell_0 - z)/\chi]r \,, \tag{48}$$

where χ is the decay length for the da interactions, and $\Delta G^{(\mathrm{da})\parallel}$ the da interaction energy for two infinite planar surfaces of the materials of adsorbent and adsorbate at "contact" (i. e. separated by a distance of approximately 0.15 nm).

2.5.3 The Analysis of The Available Area Function

If we assume that the potential barrier determining k_a does not change with the accumulation of material, then k_a merely acts as a linear scaling factor on the adsorption rate (Eq. 35), and does not affect the *form* of the rate law. In contrast, the function ϕ affects its shape, and the main goal of many quantitative adsorption studies is to identify the function ϕ and correlate it with the molecular properties of the system under study.

General properties of ϕ

It is obvious that $\phi = 1$ for a totally empty surface with $\theta = 0$. θ is the fraction of the surface covered by adsorbed particles, and is related to ν and total adsorbed mass M by

$$\theta = \nu a = Ma/m \tag{49}$$

where a is the occupied area per particle and m its mass. The analysis of high-resolution kinetics (such as those obtainable with OWLS) allows a to be determined with an accuracy equal to or better than with atomic force microscopy. A totally full surface ($\theta = 1$) will have $\phi = 0$. What is less obvious is that a surface may be less than fully occupied ($\theta < 1$) but nevertheless may not be able to offer any free place to an incoming particle. Even polygons that can tile the plane will only reach $\theta = 1$ if they are perfectly aligned. If they are placed randomly, ϕ will already approach zero for θ as little as 0.5.

Given that ϕ is a function of θ, we can quite generally expand it in powers of θ:

$$\phi = 1 - b_1\theta + b_2\theta^2 + b_3\theta^3 + \ldots \tag{50}$$

The so-called random sequential adsorption (RSA) has been analysed extensively in two dimensions (e. g. Evans 1993) from purely geometrical considerations. The coefficients b_1, b_2, and b_3 have been determined for

Table 5. Coefficients for the available area function

Mode	b_1	b_2	b_3	Application
Langmuir	1	0	0	Clustering, large receptors
RSA (spheres)	4	3.808	1.407	Irreversible adsorption
GBD[a]	$4(1-j)$	$3.808 - 0.180j - 3.128j^2$	$1.407 + 4.679j - 25.58j^2 + 8.550j^3$	Nucleation and growth

[a] j is the ratio of probabilities p/p', p' being the probability of a particle adsorbing on a hitherto unoccupied patch of the absorbent at which it arrives, and p the probability that it adsorbs after having reached a space large enough to accommodate it by a path of correlated lateral diffusion in the immediate vicinity of previously adsorbed particles. In the former case a protein arrives at an empty patch of surface, whereas in the latter case it arrives at a region where previously arrived particles are already adsorbed, and migrates to the edge of the cluster before becoming attached to the surface. $j = 0$, the lowest possible value, would correspond to pure random sequential adsorption (i.e. binding takes place solely independently of preadsorbed particles at empty patches of surface), and higher values correspond to increasingly favoured particle clustering.

spheres and ellipsoids (ellipsoids with an aspect ratio of 1:4 have virtually identical coefficients to those of spheres (Viot et al. 1992), for irreversible and reversible deposition, and deposition of laterally mobile particles (reversibility and mobility only affect b_3), etc. Experimental limitations make it unnecessary to expand ϕ beyond the third power of θ. Table 5 gives some values of the coefficients.

Practically, by plotting the rate of adsorption against the amount adsorbed, i.e. in direct accordance with Eq. 35, it is often possible to identify the adsorption mechanism merely by visual inspection. Four principle types of behaviour are observed:

1. $d\nu/dt \sim$ constant implies that $\phi = 1$. This is characteristic of the formation of isolated aligned chains of adsorbate (e.g. lysozyme dissolved at low ionic strength (Ball and Ramsden (1997), with images given in Ramsden (1998));
2. $d\nu/dt$ concave (i.e. progressively slower) implies that $\phi(\theta)$ is a characteristic polynomial function of θ, implying that the proteins interact via excluded volume only, i.e. "pure" random sequential adsorption (e.g. common blood proteins such as transferrin and serum albumin (Ramsden 1993c, Kurrat et al. 1994));
3. $d\nu/dt \sim$ linear, implying that $\phi = 1 - \theta$ (Langmuir adsorption): for adsorption onto a continuum, however, the annihilation of exclusion zones implied by this linear relation between ϕ and θ can only occur upon 2D clustering or crystallization (e.g. cytochrome P450 added to a membrane (Ramsden et al. 1994));

4. $d\nu/dt$ concave/convex implies generalized ballistic deposition (GBD) (e. g. phospholipase A_2 (Csúcs and Ramsden 1998b));
5. $d\nu/dt$ bell-shaped implies nucleation and growth of deposits (e. g. lysozyme on silica in the presence of thiocyanate ions (SCN^-) (Ball et al. 1999).

Equation 35 with the appropriate expression for ϕ can be fitted to numerically differentiated data, or the numerically integrated version of Eq. 35 fitted to the (M, t) data, by a least-squares optimization procedure, with free parameters a, k_a (and j for a GBD process, see Table 5), and k_d for reversible adsorption. If there is a desorption phase, it is more robust to globally fit both adsorption and desorption to Eq. 35 with an appropriate change of boundary conditions at the moment of flooding.[6]

Asymptotic behaviour and jamming limit

Experimental values of the jamming limit θ_J (i. e. the value of θ when $\phi = 1$) can be compared with theoretical values for spheres (Schaaf and Talbot 1989), and spherocylinders and ellipsoids (Viot et al. 1992) in order to deduce the shape of the molecule. When θ is very close to θ_J, the final approach to jamming follows a power law whose exponent depends on the number of degrees of freedom of the adsorbing particle. Ellipsoids are specified by both position and orientation, i. e. they have one more degree of freedom than spheres, but the experimental data is usually too noisy to permit determination of the exponent sufficiently precisely to enable the number of degrees of freedom to be unambiguously established.

2.6 Behaviour of Real Proteins

Unlike rigid colloidal particles, proteins have only limited conformational stability and any perturbation, such as adsorption to a surface, may involve energies comparable to the cohesive energy of the molecule and hence may engender conformational changes. Suppose that the enthalpy of protein adhesion to a surface equals or exceeds the enthalpy of the intramolecular contacts in the native protein conformation. Then unfolding (denaturation), which implies a gain of entropy, since many denatured conformations are possible, inevitably implies a loss of free energy, which drives the process towards adsorption with denaturation (Fernández and

[6] If the particle-free solution (PFS) is introduced rapidly, then the entire diffusion boundary region will be rapidly swept clear, i. e. $c(z) = 0$ for all $z > 0$. On the other hand, if the PFS is introduced slowly, then $c(z) = 0$ for only $z \geq \delta$ initially.

Ramsden 2001). In general, it can only be prevented if the surface interacts less with the protein than the protein interacts with itself, i. e. if the molecule would lose less enthalpy upon binding than upon folding into its native conformation.

In considering the energy balance, it should be borne in mind that many surfaces engender changes in the solvent structure, especially of extensively hydrogen bonded solvents such as water (Wiggins 2002), and these changes may perturb the protein even before it arrives at the surface.

Evidence for conformational rearrangement, including simple reorientation, can be obtained from a series of adsorption measurements carried out at different bulk concentrations. If the usual method of analysis (e. g. Ramsden 1993a) yields decreasing a with increasing c_b, rearrangement can be inferred, and its characteristic time $\tau_s = 1/k_s$ can be obtained by equating it to the characteristic time for adsorption, $\tau_a = 1/(Jc_b\phi a)$, at the bulk concentration corresponding to the mid-point between the limiting lower and higher areas, where J is the protein flux to the empty surface normalized to unit adsorbent area and unit bulk concentration. A more sophisticated approach involves simultaneously fitting the adsorption data to equations explicitly taking rearrangement into account (Van Tassel et al. 1998):

$$\dot{\nu}_\alpha = k_a\, c_b\phi - k_s \nu_\alpha \Psi \tag{51}$$

and

$$\dot{\nu}_\beta = k_s \nu_\alpha \Psi\,, \tag{52}$$

where subscripts α and β refer respectively to the lower and higher areas, and Ψ is a function analogous to ϕ giving the probability that space to rearrange (taking up more space) is available.

2.6.1 Evaluation of Lateral Diffusivity and 2D Crystal Unit Cell Size

Extremely valuable information may be obtained by repeating adsorption measurements at different bulk concentrations. We consider three cases, A, B and C:

A. In this, the simplest case, the same behaviour is obtained at all c_b and the (M, t) curves may be superimposed upon each other by rescaling time as the product $c_b t$.

B. The shape of the $\dot{\nu}$ vs ν plot is the same for all c_b, but a varies (usually increasing with decreasing c_b) (Ramsden 1993c). This implies that

adsorbed proteins are occupying more area after initial attachment, via orientational or conformational rearrangement. Let k_r be the rate of rearrangement. The characteristic time for rearrangement $\tau_r = 1/k_r$ may be supposed equal to the characteristic time for adsorption $\tau_a = 1/(Jc_b\phi a)$ at the bulk concentration corresponding to the mid-point between the limiting lower and higher areas a, where J is the protein flux to the empty surface normalized to unit adsorbent area and unit bulk concentration. A more sophisticated approach involves simultaneously fitting the adsorption data to the equations explicitly taking rearrangement into account (Van Tassel et al. 1998), see Eqs. 51 and 52.

C. The adsorption changes from RSA at high c_b to Langmuir at low c_b (Ramsden et al. 1994). At low bulk concentration, τ_a is long and adsorbed proteins have time to diffuse laterally, for which the characteristic time $\tau_2 = 1/(D_2\nu)$, and crystallize. τ_2 can be obtained from the value of c_b at the crossover point when the series of $\dot{\nu}$ vs ν curves changes from RSA to Langmuir, at which point it may be supposed that $\tau_2 = \tau_a$. The next step is to compare a obtained at high c_b with that obtained at low c_b. Near equivalence means that the proteins are forming a random cluster. If the value at low c_b is much greater than at high c_b, two dimensional crystallization may be inferred and the value of a at low c_b corresponds to unit cell size.

2.6.2 Desorption

A further extremely important extension of the basic experiment of allowing one protein to adsorb from solution at a single bulk concentration is to suddenly flood the system with protein-free solvent, which in practice generally means replacing flow of the protein solution by flow of protein-free solvent. In that case Eq. 35 becomes simply

$$\mathrm{d}M/\mathrm{d}t = -k_d M \,. \tag{53}$$

As already pointed out, in general, k_d is not a true constant. Only in the case of pure exponential decay of M can ideal, memory-free desorption be inferred, and another characteristic time, $\tau_d = 1/k_d$, be defined. Usually $M(t)_{c_b=0}$ is strongly non-exponential. In this case it is convenient to use a memory function to characterize the adsorption behaviour. The amount of protein bound, $\nu(t)$, can be represented by the integral (Talbot 1996)

$$\nu(t) = k_a c \int_0^t \phi(t_1) Q(t, t_1) \mathrm{d}t_1 \,. \tag{54}$$

The memory kernel Q denotes the fraction of protein bound at epoch t_1 that remains adsorbed at epoch t (if dissociation is indeed a first order (Poisson) process then $Q(t) = \exp(-k_d t)$). A necessary condition for the system to reach equilibrium is

$$\lim_{t\to\infty} Q(t) = 0 \,. \tag{55}$$

The dissociation coefficient is time dependent and is given by the quotient

$$k_d(t) = \frac{\int_0^t \phi(t_1) Q'(t, t_1) \mathrm{d}t_1}{\int_0^t \phi(t_1) Q(t, t_1) \mathrm{d}t_1} \,. \tag{56}$$

Cooperative effects are not uncommon in densely packed protein monolayers. An example in which the desorption of an individual particle is influenced by its adsorbed neighbours is described by Kurrat et al. (1994).

2.6.3 Multilayers

Many of the pure solutions of globular and fibrous proteins investigated hitherto have shown only monolayer adsorption. An exception is laminin allowed to adsorb in the presence of calcium ions (Ramsden 1993b), in which case adsorption switches from monolayer in the absence of Ca^{2+} to multilayer. The canonical behaviour, which is supposed to also describe the formation of amyloid plaques in higher organisms, is the sequence (starting from a dilute solution of A suddenly placed in contact with a surface): (i) adsorption of A at the solid/liquid interface; either (ii) polymerization of A (facilitated by the juxtaposition of the individual A on the surface) and conformational change of A ($\rightarrow$ A′ due to polymerization) or (iii) conformational change of A ($\rightarrow$ A′ due to adsorption) and polymerization of A′; (iv) adhesion of A to A′.

Multilayers have also been observed in the case of adsorption of complex mixtures of proteins, e. g. blood serum (Kurrat et al. 1998). The behaviour is extremely complex and not well understood. An approach starting with a mixture of the two most abundant proteins, followed by the three most abundant, etc., would doubtless help to elucidate the process, but given that there are about 1000 different proteins in blood serum, the development of high throughput screening methods capable of yielding the level of physico–chemical information currently obtainable from OWLS is required for seriously advancing towards understanding the mechanisms involved.

2.7 Conclusions

High resolution optical waveguide lightmode spectroscopy (HR-OWLS), also known as high resolution molecular microscopy (HRMM) is able to yield detailed physico–chemical characterization of proteins, other biopolymers, polymers and other particles (even living cells (Ramsden et al. 1995)) adsorbing at and desorbing from buried surfaces such as the solid/liquid interface.

The high precision of OWLS—in essence due to its very high signal/noise ratio, traceable to the very large number of multiple reflections per unit area of observed interface—enables the opto-geometric parameters of even monomolecular layers to be determined, such as the thickness (to a precision of $\pm 10^{-1}$ nm) and the refractive indices (to a precision of about $\pm 3 \times 10^{-4}$), from which a robust determination of the predominant orientation of the molecular components of the layer can be deduced. Small conformational changes resulting from a change of conditions can be detected in this way.

Much more information is obtainable if the kinetics of addition and spontaneous removal of particles to and from the surface is followed with good time resolution: the mean projected area and shape of the adsorbing particles, their lateral diffusion and sticking coefficients if they tend to cluster on the surface, the lattice parameters of two dimensional crystals if they form regular arrays, their expansion coefficient and the kinetics of expansion if they undergo area-changing reorientation or conformational change, the adsorption free energy barrier, etc. If a series of experiments under different conditions is carried out, the different contributions to the adsorption free energy barrier may be resolvable. If the memory function can be characterized, a wealth of detail concerning the dynamics of the adsorbed protein may be inferred, including cooperative effects. Additional experiments involving repeated pulses of protein solutions of different concentrations may further illuminate these processes.

The HRMM approach is fundamentally different from that of scanning probe or single molecule fluorescence microscopies, its main rivals in examining the behaviour of complex nanoparticles such as proteins, in that individual objects or their locations are not imaged. Hence the radial distribution function of the deposited objects cannot be measured directly. Nevertheless, all the information obtainable from the imaging techniques can be inferred from OWLS measurements, as well as a great many essential parameters characterizing all aspects of the adsorption process in a totally non-destructive, non-invasive fashion.

Acknowledgements. The author sincerely thanks the other members of the MEMbrane-coated Optical-grating Coupler Sensors (MEMOCS) consortium for numerous valuable discussions on the subject of this Chapter during the past few years.

References

Ball V, Ramsden JJ (1997) Absence of surface exclusion in the first stage of lysozyme adsorption is driven through electrostatic self-assembly. J phys Chem B 101:5465–5469

Ball V, Ramsden JJ (1998) Buffer dependence of refractive index increments of protein solutions. Biopolymers 46:489–492

Ball V, Lustig A, Ramsden JJ (1999) Lag phases in the adsorption of lysozyme to $Si(Ti)O_2$ surfaces in the presence of sodium thiocyanate. Part I. Phenomenology. Phys Chem Chem Phys (PCCP) 1:3667–3671

Bousquet P (1957) Étude théorique des propriétés optiques des couches minces transparentes. Ann Phys Sér 13, 2:5–15

Cacace MG, Landau EM, Ramsden JJ (1997) The Hofmeister series: salt and solvent effects on interfacial phenomena. Q Rev Biophys 30:241–278

Csúcs G, Ramsden JJ (1998a) Interaction of phospholipid vesicles with smooth metal oxide surfaces. Biophys Biochim Acta 1369:61–70

Csúcs G, Ramsden JJ (1998b) Generalized ballistic deposition of small buoyant particles. J chem Phys 109:779–781

de Feijter JA, Benjamins J, Veer FA (1978) Ellipsometry as a tool to study the adsorption behaviour of polymers at the air-water interface. Biopolymers 17:1759–1772

Evans JW (1993) Random and cooperative sequential adsorption. Rev mod Phys 65:1281–1329

Fernández A, Ramsden JJ (2001) On adsorption-induced denaturation of folded proteins. J Biol Phys Chem 1:81–84

Funatsu T, Harada Y, Tokunaga M, Saito K, Yanagida T (1995) Imaging of single fluorescent molecules and individual ATP turnovers by single myosin molecules in aqueous solution. Nature (Lond.) 374:555–559

Ghatak A, Thyagarajan K (1989) Optical Electronics. Cambridge University Press

Guemouri L, Ogier J, Ramsden JJ (1998) Optical properties of protein monolayers during assembly. J chem Phys 109:3265–3268

Guemouri L, Ogier J, Zekhnini Z, Ramsden JJ (2000) The architecture of fibronectin at surfaces. J chem Phys 113; 8183–8186

Horváth R, Pedersen HC (2002) Demonstration of reverse symmetry waveguide sensing in aqueous solutions. Appl Phys Lett 81:2166-2168

Ishijima A, Kojima H, Funatsu T, Tokunaga M, Higuchi H, Tanaka H, Yanagida T (1998) Simultaneous observation of individual ATPase and mechanical events by a single myosin molecule during interaction with actin. Cell 92:161–171

Kurrat R, Ramsden JJ, Prenosil JE (1994) Kinetic model for serum albumin adsorption: experimental verification. J chem Soc Faraday Trans 90:587–590

Kurrat R, Textor M, Ramsden JJ, Boni P, Spencer ND (1997) Instrumental improvements in optical waveguide lightmode spectroscopy for the study of biomolecule adsorption. Rev Sci Instrum 68:2172–2176

Kurrat R, Wälivaara B, Marti A, Textor M, Tengvall P, Ramsden JJ, Spencer ND (1998) Plasma protein adsorption on titanium. Colloids Surfaces B 11:187–201

Levich VG (1962) Physicochemical Hydrodynamics. Prentice Hall, Englewood Cliffs, New Jersey

Lukosz W (1991) Principles and sensitivities of integrated optical and surface plasmon sensors for direct affinity sensing and immunosensing. Biosensors Bioelectronics 6:215–225

Mann EK (2001) Evaluating optical techniques for determining film structure:optical invariants for anisotropic dielectric thin films. Langmuir 17:5872–5881

Newton I (1730) Opticks, 4th edn. William Innys, London, Book 3, Qu. 29

Nishizaka T, Miyata H, Yoshikawa H, Ishiwata S, Kinosita K (1995) Unbinding force of a single motor molecule of muscle measured using optical tweezers. Nature (Lond.) 377:251–254

Mann EK, Heinrich L, Schaaf P (1997) Validation of the uniform thin-film approximation for the optical analysis of particulate films. Langmuir 13:4906–4909

Perutz M (1993) Protein Structure. W. Freeman, Oxford

Ramsden JJ (1992) Observation of anomalous diffusion of proteins near surfaces. J phys Chem 96:3388–3391

Ramsden JJ (1993a) Review of new experimental methods for investigating random sequential adsorption. J statist Phys 73:853–877

Ramsden JJ (1993b) Calcium-dependence of laminin binding to phospholipid membranes. Biopolymers 33:475–477

Ramsden JJ (1993c) Concentration scaling of protein deposition kinetics. Phys Rev Lett 71:295–298

Ramsden JJ (1994) Experimental methods for investigating protein adsorption kinetics at surfaces. Q Rev Biophys 27:41–105

Ramsden JJ (1997) Optical biosensors. J molec Recog 10:109–120

Ramsden JJ (1998) Kinetics of protein adsorption. In: Malmsten M (ed) Biopolymers at Interfaces. Dekker, New York, Ch. 10 (pp 321–361)

Ramsden JJ (1999) Molecular orientation in lipid bilayers. Phil Mag B 79:381–386

Ramsden JJ, Bachmanova GI, Archakov AI (1994) Kinetic evidence for protein clustering at a surface. Phys Rev E 50:5072–5076

Ramsden JJ, Li S-Y, Heinzle E and Prenosil JE (1995) An optical method for the measurement of number and shape of attached cells in real time. Cytometry 19:97–102

Ramsden JJ, Lvov YuA, Decher G. (1995) Optical and X-ray structural monitoring of molecular films assembled via alternate polyion adsorption. Thin solid Films 254:246–251; *ibid.* (erratum) 261:343–344

Rembe C, Dräbenstedt A, Heimes F (2005) An accurate new 3D-motion analyser for MEMS and bioMEMS. J Biol Phys Chem 5:37–40

Schaaf P, Talbot J. (1989) Surface exclusion effects in adsorption processes. J chem Phys 91:4401–4409

Spielman LA, Friedlander SK (1974) Role of the electrical double layer in particle deposition by convective diffusion. J Colloid Interface Sci 46:22–31

Talbot J (1996) Time dependent desorption: a memory function approach. Adsorption 2:89–94

Tiefenthaler K, Lukosz W (1989) Sensitivity of grating couplers as integrated-optical chemical sensors. J. opt. Soc. Am. B 6:209–220

Van Tassel PR, Guemouri L, Ramsden JJ, Tarjus G, Viot P, Talbot J (1998) A particle-level model of irreversible protein adsorption with a postadsorption transition. J Colloid Interface Sci 207:317–323

Viot P, Tarjus G, Ricci SM, Talbot J (1992) Random sequential adsorption of anisotropic particles. I. Jamming limit and asymptotic behavior. J chem Phys 97:5212–5218

Wiggins PM (2002) Enzyme reactions and two state water. J Biol Phys Chem 2:25–37

Yanagida T, Harada Y, Ishijima A. (1993) Nanomanipulation of actomyosin molecular motors in vitro: a new working principle. TIBS 18:319–323

3 Initial Adsorption Kinetics in a Rectangular Thin Channel, and Coverage-Dependent Structural Transition Observed by Streaming Potential

Philippe Déjardin, Elena N. Vasina

Abstract. One fundamental parameter contributing to the analysis of protein–solid surface interactions is the adsorption kinetic constant k_a. For a rectangular channel we give a global representation of the initial experimental adsorption constant k at distance x from the entrance channel, as a function of wall shear rate γ, through the variable $1.86\ k(x/\gamma)^{1/3}$. It is possible to visualize on a single graph the adsorption kinetic constant, the diffusion coefficient, depletion magnitude at the interface, and its thickness relative to that of the transport-limited Lévêque limit. With radiolabeled molecules (with a γ emitter like ^{125}I) and well-defined geometries, calibration does not require a known solute diffusion coefficient and is obtained from the abrupt variation of radioactivity at the buffer–protein solution change and vice-versa. Experimental data obtained for the system α-chymotrypsin/mica show that when surface coverage reaches some critical level, the streaming potential becomes almost independent of further interfacial concentration increase; this suggests an interfacial structural transition induced by interactions between adsorbed molecules. Several models based on protein–protein dipolar interactions are proposed.

3.1 Introduction

Protein adsorption at solid–liquid interfaces (Andrade 1985; Brash and Horbett 1995) is important in many fields such as hemocompatible materials (Leonard et al. 1987), diagnostic kits (Malmsten et al. 1996), enzymatic activity (Quiquampoix and Ratcliffe 1992; Servagent-Noinville et al. 2000) and environmental hazards in mineral soils (Vasina et al. 2005). Natural and artificial vessels adsorb proteins from blood. Conformational changes or reactions at interfaces can induce series of biochemical reactions. In general, this type of phenomenon must be avoided as coagulation and complement

Philippe Déjardin, Elena N. Vasina: European Membrane Institute, UMR 5635 (ENSCM-UMII-CNRS), Université Montpellier 2, CC 047, 34095 Montpellier Cedex 5, France, E-mail: philippe.dejardin@iemm.univ-montp2.fr, e.n.vasina@lboro.ac.uk

Principles and Practice
Proteins at Solid–Liquid Interfaces
Philippe Déjardin (Ed.)
© Springer-Verlag Berlin Heidelberg 2006

systems can be activated. Application to biosensors has been proposed (Mar et al. 1999). Surface hydrophilization via polymer pretreatment can inhibit or limit these phenomena in solid-phase diagnostics (Malmsten et al. 1996), in hemodialysis hollow fibers (Yan et al. 1992) or on polymer surfaces (Lee et al. 1990). Such polymer pretreatment is generally based on copolymers that contain poly (ethylene oxide) chains (Holmberg et al. 1997; Lee et al. 1989; Nitschke et al. 2000; Price et al. 2001; Tirelli et al. 2002; Wu et al. 2000; Xu and Marchant 2000) or phosphorylcholine moeities (Huang et al. 2005; Ishihara et al. 1999a, b; Iwasaki et al. 2003; Kojima et al. 1991; Nakabayashi and Williams 2003; Nakabayashi and Iwasaki 2004; Ueda et al. 1991; Ye et al. 2005; see Chaps. 10–12). In addition, protein adsorption modifies the interfacial charge density, or the electrokinetic potential at the interface, which can be deduced from streaming potential measurements. This technique was used also to study adsorption kinetics (Ethève and Déjardin 2002; Norde and Rouwendal 1990; Zembala and Déjardin 1994).

One fundamental parameter contributing to the analysis of protein–solid surface interactions is the adsorption kinetic constant k_a, which is related to the energy barrier the protein molecule has to overcome during adsorption mechanism. Determination of the adsorption constant, however, is not straightforward: The initial adsorption process can be controlled by transport or interfacial reaction as the two extreme limits; in addition, any intermediate case can exist where both the transport and the interfacial reaction have to be taken into account and their interplay accurately described. Under well-controlled laminar flow conditions, for instance, in a channel (Fig. 1) or tube with a radius much larger than the diffusion layer thickness, the experimental adsorption kinetic constant $k(x)$ is compared to the Lévêque constant $k_{Lev}(x)$ corresponding to a fully transport-controlled process in a rectangular channel, where x is the distance from the channel entrance to the observation point. Such comparison gives a qualitative estimation of the role of transport in the overall adsorption process.

The rate of adsorption in the presence of low-concentration solutions, when the steady-state of the concentration profile $C(x, y)$ has been established, can be written as:

$$\frac{\partial \Gamma(x,t)}{\partial t} = D\left(\frac{\partial C(x,y)}{\partial y}\right)_{y=0} = k(x)\,C_b = k_a C(x,0) \tag{1}$$

where Γ is the interfacial concentration, t is the time, D is the diffusion coefficient, C_b is the bulk solution concentration; k_a is the adsorption kinetic constant at the interface, $C(x, 0)$ is the solution concentration at distance x from the channel entrance and at $y = 0$, and $k(x)$ is the kinetic constant of the overall process at x.

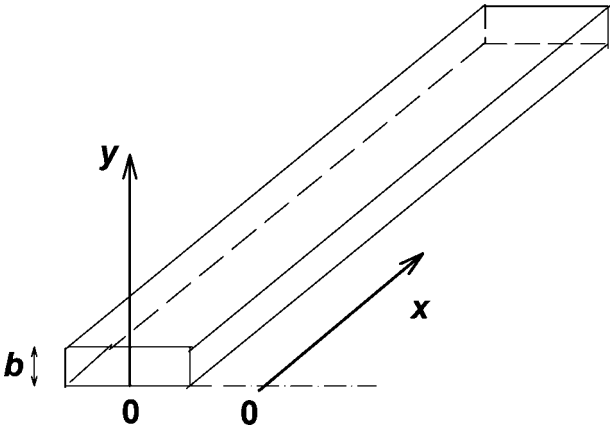

Fig. 1. Channel with rectangular section. Flow occurs in the x direction. The distance to the wall is given by y, channel height by b, and fluid velocity profile by $v(y) = \gamma y(1 - y/b)$, where γ is the wall shear rate

In case of the fully transport-controlled process ($C(x, 0) = 0$), the kinetic constant k at distance x from the entrance of the channel depends only on diffusion through the solute diffusion coefficient D and convection through the wall shear rate γ. According to Lévêque (1928) its expression is $k_{\mathrm{Lev}}(x) = 0.538\,(\mathrm{D}^2\gamma/x)^{1/3}$, a relationship that was also derived later (Levich 1962). When adsorption is controlled only by the interfacial reaction $k \approx k_{\mathrm{a}}$ and practically does not depend on x.

Figure 2 illustrates the interfacial region of depletion in solution obtained by numerical simulations. For a given solute diffusion coefficient, the higher the adsorption kinetic constant, k_{a}, the larger the interfacial depletion, and the larger the distance from the channel entrance, the larger the thickness, δ, of the depletion layer and the depletion magnitude at the surface. Hence the crossover length L_{co} (Eq. 5c) was introduced in the complete treatment (Déjardin et al. 1994), contrary to the simpler case of the rotating disk where δ is constant (Coltrin and Mitchell 2003; Levich 1962). We define the depletion $d(x)$ at the interface:

$$d(x) = 1 - \frac{C(x, 0)}{C_{\mathrm{b}}} \tag{2}$$

As the steady-state adsorption rate is related to the slope of $C(x, y)$ at the wall (Eq. 1):

$$\frac{\partial \Gamma(x, t)}{\partial t} = D\frac{C_{\mathrm{b}} - C(x, 0)}{\delta(x)} = k(x)\, C_{\mathrm{b}} = k_{\mathrm{a}}\, C(x, 0) \tag{3}$$

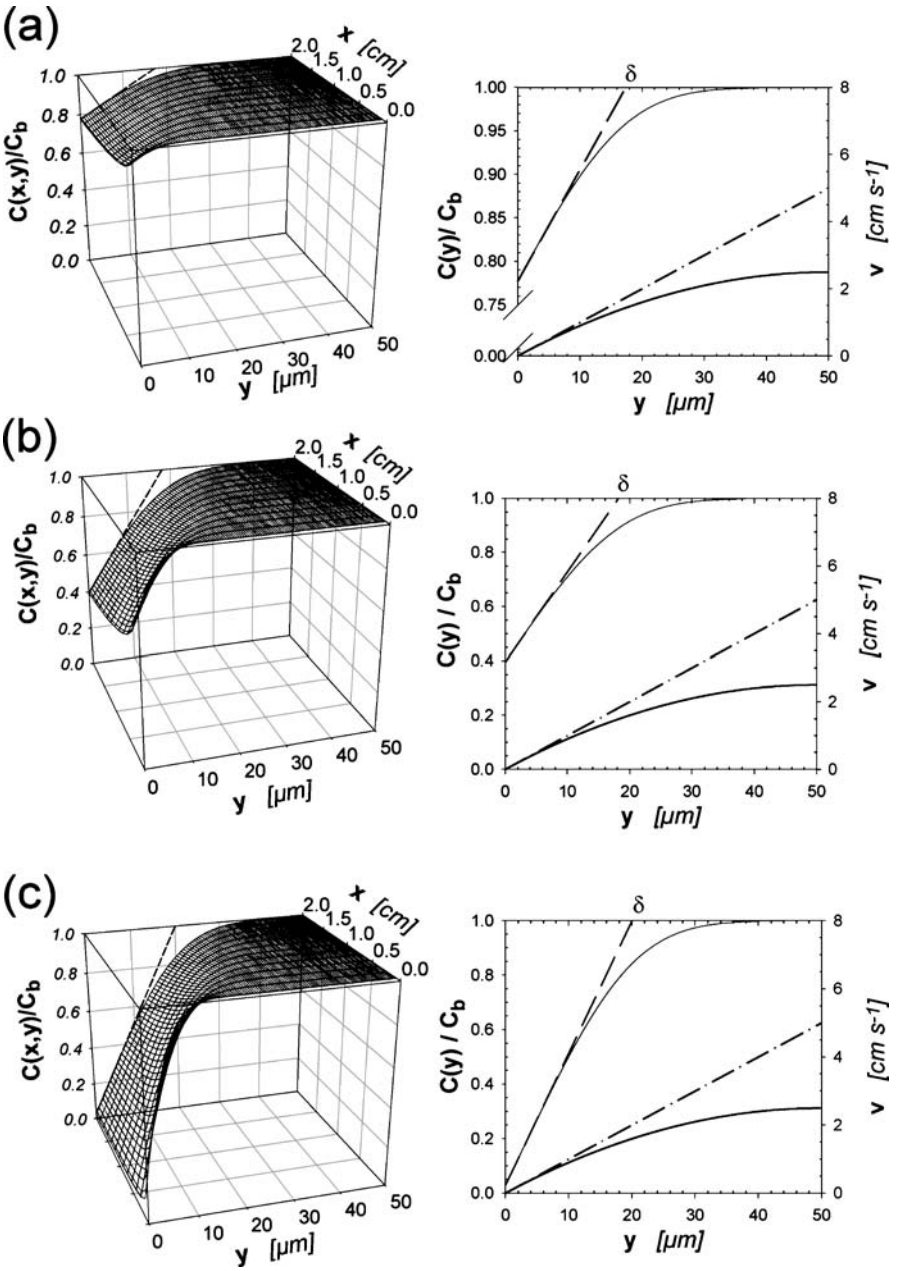

Fig. 2. Stationary concentration profiles normalized to the bulk concentration C_b, for $D = 6.0\times10^{-7}$ cm^2 s^{-1}, and wall shear rate 1,000 s^{-1}. Channel height is 100 μm. *Left* Three-dimensional graph $C(x, y)$ from the entrance to distance $x = 2$ cm. *Right* Concentration profile at $x = 2$ cm, with the tangent to the profile at the wall (*dashed line*, left scale), and parabolic velocity profile with the tangent at the wall (*dash-dotted line*, right axis). **a** $k_a = 1.0\times10^{-4}$ cm s^{-1}; **b** $k_a = 5.0\times10^{-4}$ cm s^{-1}; **c** $k_a = 1.0\times10^{-2}$ cm s^{-1}

we obtain:

$$k(x) = k_a\,[1 - d(x)] = D\frac{d(x)}{\delta(x)}\,. \tag{4}$$

The Lévêque limit where depletion is complete corresponds to $d \to 1$, $k_{Lev}(x) = D/\delta_{Lev}(x)$ and $\delta_{Lev}(x) = 1.859(Dx/\gamma)^{1/3}$. When approaching this limit, $k(x) \ll k_a$, while for the opposite one of a negligible depletion $k(x) \to k_a$.

The Damköhler number, $Da = k_a/<v>$, where $<v>$ is the average velocity of the fluid, is often used as a criterion to separate the domains of control by the interfacial reaction ($Da \ll 1$) and by transport ($Da \gg 1$), especially in studies concerning porous media (Adler and Thovert 1998). There is a direct connection between the ratio k_a/k_{Lev} and this number. The difference originates from the introduction of the diffusion coefficient. Other expressions of Da are used that also take it into account (Bizzi et al. 2002; Coltrin and Mitchell 2003) for gas phases: $Da = k_a/(D/\delta)$, where δ is the diffusion layer thickness. In the present problem, we can define a Damköhler number $Da(x) = k_a/k_{Lev}(x)$, with $k_{Lev}(x) = D/\delta_{Lev}(x)$.

As summarized earlier (Docoslis et al. 1999), the experimental determination of the adsorption kinetic constant k_a has three major sources of difficulties: (1) mass transport, easier to take into account with the simple geometries of rectangular channels or circular tubes, (2) steric hindrance at the interface, which can be limited by using low-concentration solutions, and (3) determination of low interfacial concentration, which requires very sensitive techniques, usually using radioactive or fluorescently labeled molecules like in the total internal reflection fluorescence (TIRF) technique (Britt et al. 1998; Buijs et al. 1998; Kelly and Santore 1995; Malmsten et al. 1996; Rebar and Santore 1996; Robeson and Tilton 1996; Wertz and Santore 2002). Sophisticated optical methods such as surface plasmon resonance (SPR; Mar et al. 1999) and optical waveguide lightmode spectroscopy (OWLS; Calonder and Van Tassel 2001; Hook et al. 2002; Ramsden et al. 1995; Chaps. 1–2) provide the means to measure low interfacial concentrations without labeled molecules.

The following data treatment can be useful for the SPR, reflectometry, ellipsometry, and OWLS techniques if the experimental flow cells have rectangular channel geometries. For instance, in OWLS experiments, a chamber tightened with an O-ring joint is not adapted to the present formulation as the channel width varies continuously and strongly near the inlet, which leads to a nonconstant wall shear rate. In this case the Lévêque limit formula is no longer applicable. The cell has to be adapted (Chap. 1) to achieve a constant width. Moreover, the height of the channel should be large enough to provide a linear velocity profile in the depletion layer, which is assumed in the Lévêque derivation, and its extension to finite k_a (Déjardin et al. 1994).

For example, in Fig. 2 the channel height of 100 μm is too small to fulfill the criterion when $D = 6.0\times10^{-7}$ cm^2 s^{-1} and $\gamma = 1{,}000$ s^{-1}. Another technique is the impinging jet on a flat substrate, which was also used in combination with TIRF to study the deposition of latex particles (Göransson and Trägardh 2000). Here we do not consider this kind of geometry.

In the first part of the present work we recall derivation of the simple accurate approximations, providing an easy way to treat quantitative data; thus, one can deduce the protein diffusion coefficient D and protein interfacial adsorption kinetic constant k_a from experimental initial constant k as a function of the variable $(k/k_{Lev})D^{2/3}$, where $k_{Lev}/D^{2/3}$ does not depend on D.

In the second part, we present the variation of the interfacial potential as a function of surface coverage and suggest the possible importance of protein–protein dipolar attractive interactions to create domains with an antiferroelectric order at high coverage.

3.2 The Initial Adsorption Constant and its Limit Expressions

3.2.1 The Local Initial Adsorption Constant $k(x)$, its Limit Expressions and Approximation

Full Solution and Limit Expressions

Let us recall that the general expression (Dejardin et al. 1994) for the constant $k(x)$ at distance x from the channel entrance as a function of k_a and k_{Lev} is not easily accessible for the determination of k_a.

$$k(x) = k_a g(X)\ , \tag{5a}$$

with

$$X = \frac{x}{L_{co}} \tag{5b}$$

where

$$L_{co} = 3\left(\frac{\Gamma'(2/3)}{\Gamma'(1/3)}\right)^3 \frac{D^2\gamma}{k_a^3} \tag{5c}$$

and

$$g(X) = e^{-X} + G(2/3, X) - G(1/3, X) \tag{5d}$$

with

$$G(n,x) = \frac{1}{\Gamma'(n)} e^{-X} \int_0^X z^{n-1} e^z dz \tag{5e}$$

$\Gamma'(n)$ is the usual gamma function (Abramovitz and Stegun 1972). The prime is added to avoid confusion with Γ used for the interfacial concentration.

It is preferable to have k_a as a function of experimental $k(x)$. It has been shown that rather good approximations of the general solution can be obtained at the two limits of the controls by transport and the interfacial reaction (Dejardin et al. 1994). These involve the inverse of the kinetic constants and, in fact, lead directly to the interpretation of the total resistance (time) of the adsorption process as being the sum of one resistance due to the transport and the other resistance due to the interfacial reaction. Close to the conditions of the transport-controlled process,

$$k^{-1} = k_{Lev}^{-1} + 0.684 k_a^{-1} , \tag{6a}$$

while close to the conditions of the control by interfacial reaction

$$k^{-1} = 0.827 k_{Lev}^{-1} + k_a^{-1} \tag{6b}$$

Both expressions are similar to the simplest approximation, which considers no coupling between transport and the interfacial reaction:

$$k^{-1} = k_a^{-1} + k_{Lev}^{-1} \tag{7}$$

Equation 7 can be also obtained by assuming that the thickness of the diffusion layer (when $C(x, y = 0) = 0$, Lévêque model) is unaltered whatever the finite value of k_a, say whatever the nonzero steady-state value of the volume concentration near the interface. Equation 7 corresponds to the work (Bowen and Epstein 1979) and matches Eq. 2.45 of Bowen et al. (1976).

Approximation of $k(x)/k_a$ as a function of $k(x)/k_{Lev}(x)$

If the linear approximations given in Eq. 6a and b are valid at to the two limits can be useful in practice, as it is easy to deduce k_a from $k(x)$ and $k_{Lev}(x)$, they do not describe the entire domain as does the general expression (which writes k as a function of k_a, not the reverse). Recently we have proposed (Déjardin and Vasina 2004) to approximate the general expression in Eq. 5a by the function $y = f(u)$, where $y = k/k_a$ and $u = k/k_{Lev}$:

$$f(u) = \frac{(u-1)(au-1)}{(bu+1)} \tag{8}$$

with $a = 0.451707$ and $b = -0.624713$, to satisfy the two limits of Eq. 6a,b. The greatest relative variation between Eq. 8 and the complete calculation

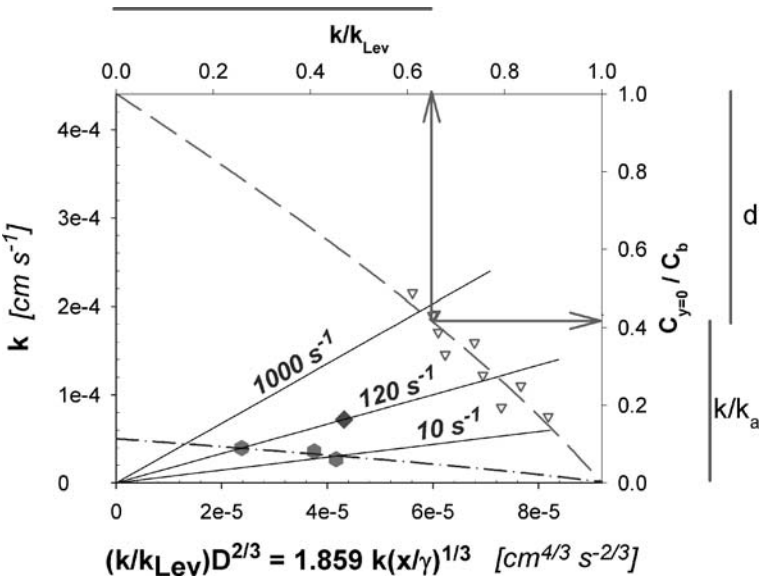

Fig. 3. Adsorption of α-chymotrypsin (∇, *dashed line*, 10^{-2} M Tris; pH 8.6) onto mica. The normalization of the scales to the intercepts k_a and $D^{2/3}$ illustrates the magnitude of the depletion at the interface ($C_{y=0}/C_b$; right axis), where y is the distance to the interface, and the departure from the fully transport-limited process (k/k_{Lev}; top axis). For measurements performed at the same distance x, the experimental points corresponding to one given wall shear rate are positioned on a *straight line* passing through the origin. An example is provided with the points corresponding to experiments in 10^{-2} M (∇), 0.2 M ($\blacklozenge$) and 0.5 M ($\hexagon$ *dash-dotted line*) Tris, pH 8.6

is 1% around $u = 0.8$. Let us note that $k(x)/k_a = C(x,0)/C_b$, so the ordinate illustrates the depletion in solution at the interface, while $u = k/k_{Lev}$ estimates contribution of the transport. Figure 3 shows an example of these two items.

Equation 8 can be transformed into a two-parameter fit (D and k_a) to experimental $k(x,\gamma)$ as a function of $u' = k(x/\gamma)^{1/3}/0.538 = uD^{2/3}$, which does not require the knowledge of D.

$$k = \frac{k_a}{D^{2/3}} \frac{(u' - D^{2/3})(au' - D^{2/3})}{bu' + D^{2/3}} \tag{9}$$

In such a representation, the intercept of the fit with the ordinate axis gives k_a, while the intercept with the abscissa axis gives $D^{2/3}$ (see Fig. 3). Figure 4 illustrates the magnitude of error in the adsorption kinetic constant k_a and diffusion coefficient D that can occur when using Eq. 7. Equation 7 corresponds there to the straight line $k = k_a(1 - u'/D^{2/3})$.

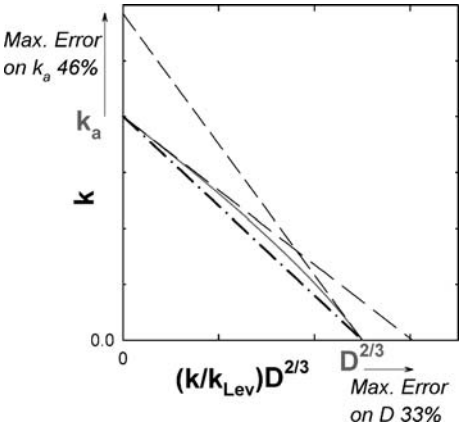

Fig. 4. Illustration of the maximum (*Max.*) error on adsorption constant k_a and diffusion coefficient D when neglecting any coupling between transport and interfacial reaction (*straight dash-dotted line*; Eq. 7 in text), compared to exact solution (*full curved line*). The *dashed lines* demonstrate linear approximations at the two extreme limits

3.2.2 The Mean Adsorption Constant, its Limit Expressions and Approximation

Mean <*k*> Over the Full Length of the Channel

In some cases it is necessary to find the average adsorption constant over the full sample length where laminar convection occurs. When the process is fully transport-controlled, the integration of the local Lévêque equation over the channel length L leads to $<k_{Lev}> = 0.808(D^2\gamma/L)^{1/3}$. When the contribution of the interfacial reaction is taken into account, the mean kinetic constant $<k>$ over the channel length L is given by (Valette et al. 1999):

$$<k> = \frac{k_a}{\Lambda}\int_0^{\Lambda} g(X)\mathrm{d}X \tag{10a}$$

where:

$$\Lambda = \frac{L}{L_{co}} = \left[\frac{3}{2\Gamma'(2/3)}\frac{k_a}{<k_{Lev}>}\right]^3 \tag{10b}$$

Hence:

$$<k> = \frac{k_a}{\Lambda}\left(1 + \frac{3\Lambda^{2/3}}{2\Gamma'(2/3)} - \frac{3\Lambda^{1/3}}{\Gamma'(1/3)} - g(\Lambda)\right) \tag{10c}$$

Close to the conditions of transport-controlled process, we have:

$$<k>^{-1} \approx <k_{\mathrm{Lev}}>^{-1} + 0.913 k_{\mathrm{a}}^{-1} \tag{10d}$$

while close to the conditions of control by the interfacial reaction

$$<k>^{-1} \approx k_{\mathrm{a}}^{-1} + 0.930 <k_{\mathrm{Lev}}>^{-1} \tag{10e}$$

with the total resistance being the sum of the two resistances (one due to the transport and the other one due to the interfacial reaction).

As the numerical coefficients in both linear approximations are close to 1, the simple approximation

$$<k>^{-1} \approx k_{\mathrm{a}}^{-1} + <k_{\mathrm{Lev}}>^{-1} \tag{11}$$

is rather good for the whole range of k_{a}. The same route as that for the local adsorption constant led to the following approximation of $<k>/k_{\mathrm{a}}$ as a function of $U = <k>/< k_{\mathrm{Lev}}>$:

$$F(U) = \frac{(U-1)(AU-1)}{(BU+1)} \tag{12}$$

where $A = 0.203127$ and $B = -0.272759$, to satisfy Eqs. 10d–e. The greatest relative variation between Eq. 12 and the complete calculation is 0.03% around $U = 0.8$. It can be used in the form $<k> = k_{\mathrm{a}} F(U)$ for a two-parameter fit (D and k_{a}) to the experimental value of $<k>$ as a function of $U' = <k>(L/\gamma)^{1/3}/0.808 = UD^{2/3}$.

$$\langle k \rangle = \frac{k_{\mathrm{a}}}{D^{2/3}} \frac{(U' - D^{2/3})(AU' - D^{2/3})}{BU' + D^{2/3}} \tag{13}$$

Mean [*k*] Over a Restricted Length

In experiments, the adsorption kinetics is always integrated over some length Δx of the channel, between $x - \Delta x/2$ and $x + \Delta x/2$. We shall estimate the influence of Δx on the numerical coefficients a and b in Eqs. 8 or 9.

Referring to Eq. 8, the variable $u = k(x)/k_{\mathrm{Lev}}(x)$ becomes $u^* = [k]/[k_{\mathrm{Lev}}]$, where the star superscript and the brackets mean that the average is taken between $x_1 = x - \Delta x/2$ and $x_2 = x + \Delta x/2$. $[k]$ is the actual measured average kinetic constant, which was assumed to be $k(x)$ in Eq. 8, and $[k_{\mathrm{Lev}}] = \Delta x^{-1}(x_2 <k_{\mathrm{Lev}}>_2 - x_1 <k_{\mathrm{Lev}}>_1)$. $<k_{\mathrm{Lev}}>_i$ is the mean value of the Lévêque constant between $x = 0$ and $x = x_i$.

We adopt the same procedure looking for two limit expressions for a transport-limited process and interfacial reaction control (see Appendix). For small values of $\varepsilon = \Delta x/x$ we obtain:

$$a \approx a_0 \left(1 + 0.078\,\varepsilon^2\right) \; ; \quad b \approx b_0 \left(1 + 0.044\,\varepsilon^2\right) \tag{14}$$

where a_0 and b_0 are the values of the numerical coefficients determined in Eq. 8, which corresponds to $\Delta x \to 0$.

3.2.3 Experimental Results and Discussion

A flow cell of adequate dimensions $4 \times 11 \times 1$ cm (to be inserted in a detector of gamma radioactivity) consisted of two polymethylmethacrylate plates, between which were pressed two mica plates separated by a spacer. A top view of the cell is provided in Fig. 5. The data acquisition was performed using the same kind of procedure as for capillary geometry (Boumaza et al. 1992; Le and Déjardin 1998). For a detection window of width w and a channel height h, the radioactivity jump at the arrival of radiolabeled protein solution is $A_v \sim whC_b$, while the surface radioactivity on the two faces (mica plates) is $A_s \sim 2w\Gamma$. Therefore $\Gamma(t) = (h/2)C_bA_s(t)/A_v$ and $k(t) = (h/2)(dA_s/dt)/A_v$.

Recently we studied (Vasina and Déjardin 2004) the adsorption of α-chymotrypsin onto mica at different concentrations of Tris buffer at pH 8.6. Examples of the adsorption kinetics data are given in Fig. 6. The initial adsorption rate is linear with a protein solution concentration in the range considered (Fig. 7).

In Fig. 3 some of our results emphasizing the peculiarities of the representation given by Eq. 9 are plotted. The scanning of adsorption with

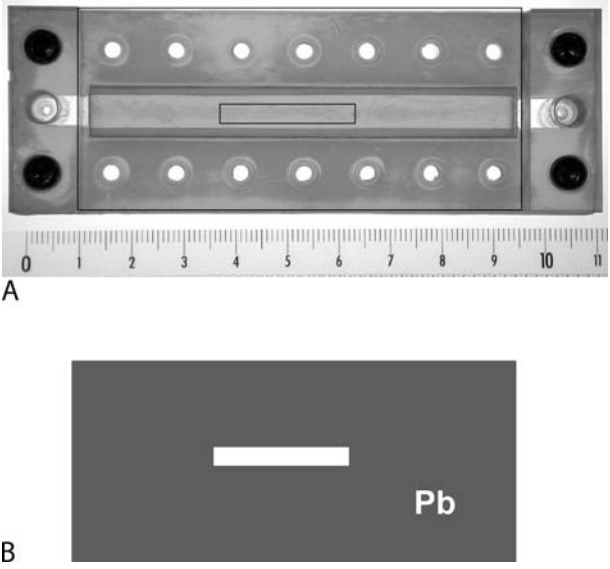

Fig. 5. (**A**) Top view of the experimental cell showing the mica sheets constituting the two faces of the channel (scale in centimeters). Measurement of adsorption concerns only the central part of the cell, using appropriate lead shields (**B**). The cell is inserted in a γ-radioactivity detector

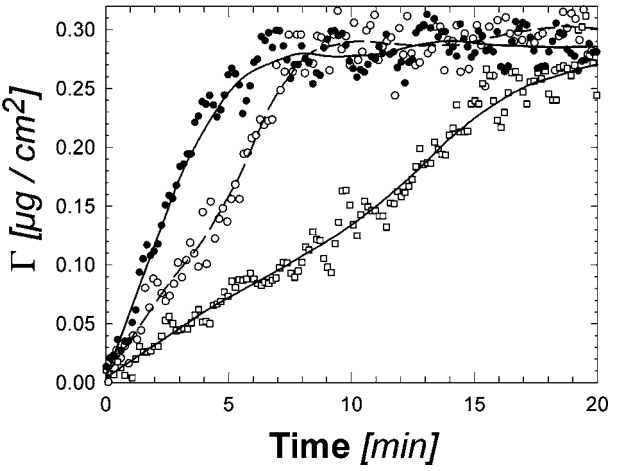

Fig. 6. Experimental data of adsorption kinetics of α-chymotrypsin on mica recorded for wall shear rate 120 s^{-1} and different bulk α-chymotrypsin concentrations, C_b: 10 μg ml^{-1} (●); 5 μg ml^{-1} (○); 2.5 μg ml^{-1} (□)

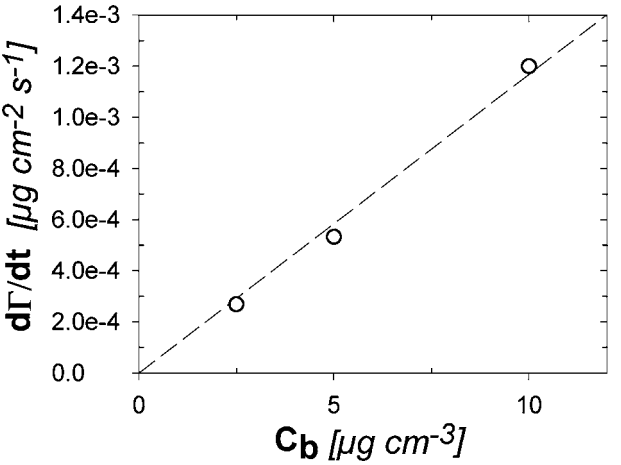

Fig. 7. Initial adsorption rate of α-chymotrypsin on mica as a function of solution concentration C_b at pH 8.6, Tris buffer (concentration 10^{-2} M). Mean slope (*dashed line*) $k \approx 1.2 \times 10^{-4}$ cm s^{-1}

convection is viewed as straight lines passing through the origin with their slope increasing with wall shear rate γ as 0.538 $(\gamma/x)^{1/3}$. The application of Eq. 9 to the adsorption of α-chymotrypsin onto mica in the rectangular channel provides two parameters: the diffusion coefficient D and the adsorption kinetic constant k_a (for instance, in 10^{-2} M Tris buffer, pH 8.6: $D = 8.8 \pm 0.7 \times 10^{-7}$ cm^2 s^{-1} and $k_a = 4.4 \pm 0.5 \times 10^{-4}$ cm s^{-1}). The two-parameter fit was performed using SigmaPlot®.

The depletion (Eq. 2) with its complement to unity, say $k(x, \gamma)/k_a$ or $C(x, 0, \gamma)/C_b$, is directly visualized in Fig. 3. Moreover, given the curvature of the function $k(u')$, the thickness of the depletion layer is always smaller than that of the Lévêque model, as $k(x, \gamma) = Dd(x, \gamma)/\delta(x, \gamma)$ with $d(x, \gamma) = 1$ in the Lévêque limit, therefore $\delta(x, \gamma)/\delta_{Lev}(x, \gamma) = d(x, \gamma)/[k(x, \gamma)/k_{Lev}(x, \gamma)]$. Both terms of the ratio are noted in Fig. 3.

In our experiments, the detection occurs between 2.5 and 5.5 cm from the channel entrance, therefore $\varepsilon = 0.75$. Taking into account this range of integration (Eqs. 9 and 14), we obtain for Tris buffer 10^{-2} M at pH 8.6, corrections of –1% for the protein diffusion coefficient D and +6% for its adsorption kinetic constant k_a.

When comparing the present treatment to other works in the literature, we should mention that we do not assume any value for the protein diffusion coefficient. The calibration is provided by the increase in radioactivity when the radiolabeled protein solution arrives in a channel of known geometry or by its drop when the radiolabeled solution is replaced by buffer. We do not assume any Lévêque regime with a known diffusion coefficient, as is sometimes assumed in fluorescence (TIRF) experiments (Wertz and Santore 1999, 2002).

3.3 The Structural Transition with Increasing Interfacial Concentration

As can be seen in Fig. 6, the adsorption rate slightly increases at about half the maximum interfacial concentration. Such an increase could be the signature of a structural change at the interface. It was recognized for many years that protein crowding at the interface leads to profound changes there because of the increasing probability of the protein–protein interactions (Andrade 1985). In the present case, such a change in the adsorption rate could also be caused by the conditions of flow in the channel, associated with the early saturation of the surface upward of the point of examination. Simulations suggest, however, that this hypothesis should be rejected, as it would require an adsorption constant much higher than that deduced from the previous analysis (Vasina and Dejardin 2004). To describe the conformational changes (see Chap. 6) and/or orientation, many models can be proposed, among them the side-on/end-on process, the reverse process, and the spreading of the (soft) protein on the surface. Techniques like neutron reflectivity (Su et al. 1998), ellipsometry (Bae et al. 2005; Cuypers et al. 1978; McClellan and Franses 2005; Poksinski and Arwin 2004; Seitz et al. 2005; Werner et al. 1999), and scanning angle reflectometry (Ladam et al. 2002; Schaaf and Déjardin 1988) are able to provide information about

the orientation of an ellipsoid-modeled molecule. Circular dichroism and differential scanning calorimetry are also useful in the study of the protein conformations (Giacomelli and Norde 2001; Norde and Zoungrana 1998; Vermeer and Norde 2000; Vermeer et al. 2001; Voegel et al. 1987; Zoungrana et al. 1997). Infrared attenuated total reflection (Noinville et al. 2002a,b, 2003) provides data about possible changes in the tertiary structure (see Chap. 6).

The TIRF technique was refined to take into account the dependence on the emission properties of the fluorophore with its ionization state or with the electric potential (Daly et al. 2003; Robeson and Tilton 1996). If the ionic strength is chosen in such a way that the interfacial electric potential varies over a distance comparable to the protein size, then the signal will be dependent upon the orientation of the molecule. Indeed the interfacial transition is easily observed and is concomitant with the change in kinetic regime.

3.3.1 Observation by Streaming Potential

Measurement of streaming current (Daly et al. 2003) and streaming potential (Ethève and Dejardin 2002; Vasina and Dejardin 2004) during adsorption can be useful to obtain information on the orientation of molecules at interfaces. The variation of streaming potential with protein interfacial concentration exhibits a change at some critical concentration for the α-chymotrypsin/mica system at pH 8.6 in 10^{-2} M Tris (Fig. 8). The variation in zeta potential was deduced from the streaming potential, E_s, as a function of time at a defined pressure differential, ΔP, via the classical Smoluchowski relationship (Hunter 1981), with $\Delta E_s = E_s - E_{s0}$, where E_{s0} is the asymmetry potential,

$$\varsigma = \frac{\Delta E_s}{\Delta P} \frac{\eta \lambda_0}{\varepsilon_0 \varepsilon_r} \tag{15}$$

where λ_0 is the electrolyte solution conductivity, η is the solution viscosity, ε_0 is the vacuum dielectric permittivity and ε_r is the relative permittivity.

The quantitative analysis of the data, however, is not simple as initially, when transport is important, the interfacial concentration is not uniform. Indeed, the Smoluchowski relationship assumes a uniform charge density along the channel walls. For another system – lysozyme/silica capillary; pH 7.4, 10^{-2} M phosphate buffer (Ethève and Dejardin 2002) – we observed the same kind of variation and assumed that the streaming potential resulted from the mean charge density along the capillary and estimated by numerical simulations the average interfacial concentration. This did not

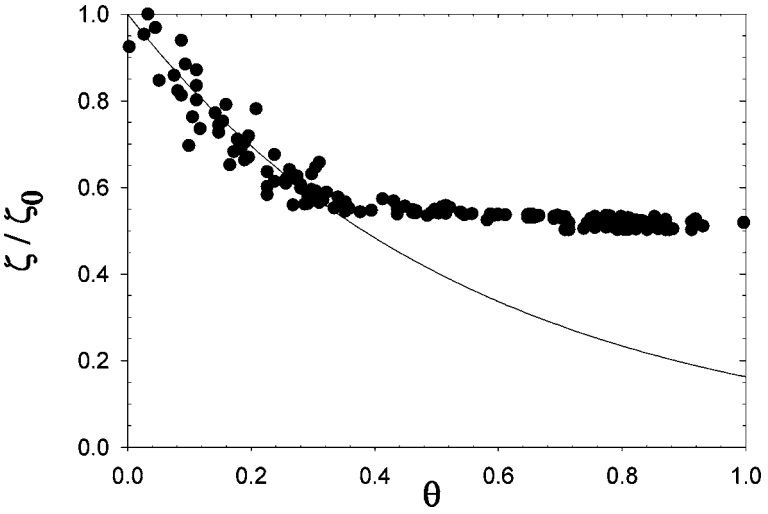

Fig. 8. Variation of the ζ potential, relative to the initial ζ_0 potential (–95 mV) of the bare mica, as a function of α-chymotrypsin interfacial concentration. Solution concentration $C_b = 2.5$ μg ml^{-1} in Tris 10^{-2} M, pH 8.6. Wall shear rate 120 s^{-1}. The *full line* represents the expected variation, based on the behavior at small θ, for particles bearing only one type of charge

lead to any dramatic changes in the observation of the transition. After the transition, local and average concentrations become much closer.

When comparing to similar works with random deposition of uniformly charged particles (Zembala and Adamczyk 2000) where such transition was not observed, it was concluded that the transition could be the result of the peculiar nature of the proteins. Contrary to the particles, proteins bear the two types of charge, positive and negative. Moreover, the charge distribution on the protein surface is not uniform. Let us analyze the present system along the same lines as the ones used for particles. As a first approximation, α-chymotrypsin can be assumed globally neutral because its isoelectric point is 8.2. For particles, the variation of ζ/ζ_0 with coverage was described as obeying a sum of an exponential function and a linear one (Zembala and Adamczyk 2000).

$$\frac{\zeta}{\zeta_0} = e(C_i^0\vartheta) + \frac{\zeta_p}{\zeta_0} C_p^0 \vartheta \tag{16a}$$

where ζ_0 and ζ_p are the potentials of the bare surface and uniformly charged particle, respectively, in the presence of buffer. After additional control experiments, another expression was proposed (Zembala 2004):

$$\frac{\zeta}{\zeta_0} = e(C_i^0\vartheta) + \frac{\zeta_p}{\zeta_0}\left[1 - e(-C_p^0\vartheta)\right] \tag{16b}$$

When the particle radius r is much larger than the Debye length κ^{-1}, then $C_i^0 = -10.21$ and $C_p^0 = 6.51$. The dependence of those coefficients on rκ has been established (Zembala et al. 2001). As the dimensions of α-chymotrypsin are $5.1 \times 4 \times 4\,\mathrm{nm}^3$, with $r = 2{-}2.5\,\mathrm{nm}$ and $\kappa^{-1} = 6.3\,\mathrm{nm}$, we have $r\kappa = 0.3 - 0.4$, thus $C_i^0 \approx -4.5{-}5$. As the net protein charge is almost zero, according to the model, the variation of ζ/ζ_0 should follow an exponential decay, $\exp(-C_i^0\theta)$, corresponding to the flow attenuation or substrate charge screening by the deposited neutral protein particles. We found the constant 1.8 instead of 4.5 (Fig. 8). The passage from local to mean coverage by simulations leads to the slightly lower value of 1.7. The smaller decrease in ζ/ζ_0 with coverage, compared to what should be expected from the model, may have two explanations: the distribution of charges on the protein surface and/or the nonrandom adsorption (Dabros and van de Ven 1993). It is clear, however, that whatever the mechanism, proteins and homogeneously charged particles have different qualitative behaviors at high coverage. The reason is probably the protein–protein interaction associated with the mobility of proteins on the surface. As α-chymotrypsin possesses a high dipole moment (483 D; Antosiewicz and Porschke 1989), the reasonable model of parallel dipoles at low ionic strength and low coverage, based on the ionic interaction between the mica and the protein, would lead at high coverage to a strong repulsion component between parallel dipoles, when the distance between like charges become shorter. As experiments show that the maximum interfacial concentration for proteins, and especially here for α-chymotrypsin, is generally near the full close-packed monolayer, some specific mechanism should occur.

3.3.2 Different Models

Figure 9 illustrates the two models of rearrangements of the dipoles roughly normal or parallel to the surface to obtain an attractive component between adsorbed proteins. We proposed the model of the ferroelectric-antiferroelectric arrangement normal to the surface to explain the change in variation of the ζ potential (Vasina and Dejardin 2004; Fig. 9, left). Saving almost the same orientation of the proteins with respect to the surface (Robeson and Tilton 1996), cooperative clustering could appear also by dipolar interactions in the direction parallel to the surface (Fig. 9, right). The complete analysis would, however, require a careful description of the balance between attractive and repulsive electrostatic components, probably in connection with the local concentration of small ions. Such ferroelectric to antiferroelectric order transition was already considered for

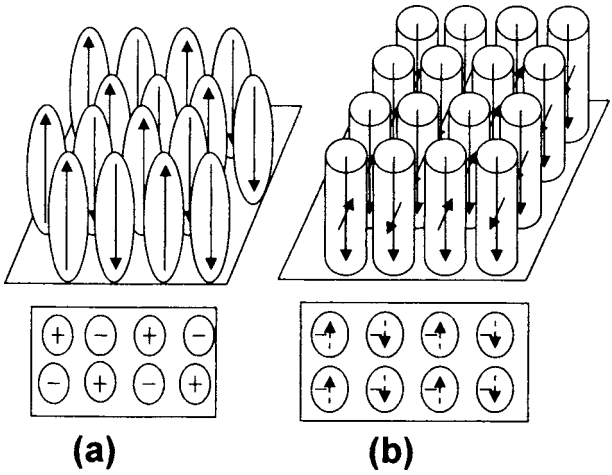

Fig. 9. Schematic representation of possible ordered domains at the interface, with a top view of the charge repartitions. **a** Alternate orientation of the dipoles normal to the surface for intermolecular attraction, but with a repulsive component in front of the surface. **b** Alternate orientation of the dipoles parallel to the surface for intermolecular attraction, but with a repulsive intermolecular component between the likely oriented dipoles normal to the surface. Ellipsoid or cylinder representation is arbitrary

small dipolar molecules like carbon monoxide and halogenated methane (Burns and Dennison 1998; Burns et al. 2004).

Recently, it was shown by TIRF and streaming-current measurements on the lysozyme/silica system at high wall shear rates that the TIRF overshoot did not correspond to any particular event in the interfacial potential (Daly et al. 2003). Therefore, it appears that the concomitance of the changes in kinetic regime and interfacial potential is not always the rule. One important phenomenon behind the process is surface diffusion, which has to be taken into account. Different kinds of behavior are probably linked to the relative rate of arrival of molecules compared to their surface diffusion rate (see Chap. 2).

3.4 Conclusion

We proposed simple relationships in the channel geometry to describe the passage from a fully transport-controlled process to an interface-controlled one when increasing convection (say wall shear rate γ) for a study at some distance x from the entrance, as well as for the average value over the full or partial length of the channel (or wall). The experimental data of the initial experimental kinetic constant $k(x, \gamma)$ are plotted as a function of

$(k/k_{\mathrm{Lev}})D^{2/3}$, where k_{Lev} is the Lévêque limit and D the diffusion coefficient. The adsorption kinetic constant k_{a} and the protein diffusion coefficient to power 2/3 can be easily determined as the intercepts of the fit curve with the ordinate and abscissa axes, respectively. The normalizations of ordinates and abscissae to the intercepts provide directly the magnitude of the depletion in the liquid phase at the interface, and the relative evaluation to the transport-limited process. An example is given for the system α-chymotrypsin/mica at pH 8.6.

The variation of ζ potential as a function of surface coverage exhibits a change of regime, this suggests a new arrangement of adsorbed protein molecules above a threshold of surface occupation. The possibility of dipolar attractive interactions between the proteins is considered to create domains with an antiferroelectric order at high coverage.

Acknowledgements. We are grateful to R. Souard and P. Montels (EMI) for manufacturing the flow cell, and to D. Cot (EMI) for the photo. This work was supported by "Programme Ecologie Quantitative" of the French Ministry of Research, and performed within the framework of collaboration between Centre National de la Recherché Scientifique (France) and Kazan State University (Russia), project 12889.

Appendix

We study the influence of the length of examination Δx around the average mean distance to the channel entrance x, through the parameter $\varepsilon = \Delta x/x$, on the numerical parameters a and b determined in Eq. 8. The two local limit expressions, valid near the control by the interfacial reaction (Eq. 6b) or by transport (Eq. 6a), can be written as $k^{-1}(x) = c_{\mathrm{a}}k_{\mathrm{a}}^{-1} + c_{\mathrm{L}}k_{\mathrm{Lev}}^{-1}(x)$, where c_{a} and c_{L} are numerical coefficients (Dejardin et al. 1994; Dejardin and Vasina 2004). In what follows, the average between $x_1 = x - \Delta x/2$ and $x_2 = x + \Delta x/2$, is indicated by the use of brackets [].

1. $k \approx k_{\mathrm{a}} \ll k_{\mathrm{Lev}}$; $c_{\mathrm{a}} = 1.0$; $c_{\mathrm{L}} = 0.827$

$$k(x) \approx k_{\mathrm{a}}\left(1 - c_{\mathrm{L}}\frac{k_{\mathrm{a}}}{k_{\mathrm{Lev}}}\right) \tag{A1a}$$

or

$$[k(x)]^{-1} = k_{\mathrm{a}}^{-1} + c_{\mathrm{L}}\left[k_{\mathrm{Lev}}^{-1}(x)\right] \tag{A1b}$$

2. $k \approx k_{\mathrm{Lev}} \ll k_{\mathrm{a}}$; $c_{\mathrm{L}} = 1.0$; $c_{\mathrm{a}} = 0.684$

$$k(x) \approx k_{\mathrm{Lev}}(x)\left(1 - c_{\mathrm{a}}\frac{k_{\mathrm{Lev}}(x)}{k_{\mathrm{a}}}\right) \tag{A2a}$$

or

$$[k(x)]^{-1} \approx [k_{\mathrm{Lev}}(x)]^{-1} + c_a\, k_{\mathrm{a}}^{-1} \frac{\left[k_{\mathrm{Lev}}^2(x)\right]}{[k_{\mathrm{Lev}}(x)]^2} \tag{A2b}$$

We are looking for an expression of $[k\ (x)]/k_{\mathrm{a}}$ as a function of $u^* = [k(x)]/[k_{\mathrm{Lev}}(x)]$. The relationships A1 and A2 are written as:

$$[k(x)]/k_{\mathrm{a}} = 1 - c_{\mathrm{L}}[k(x)][k_{\mathrm{Lev}}^{-1}] \tag{A3}$$

$$[k(x)]/k_{\mathrm{a}} = c_{\mathrm{a}}^{-1}([k_{\mathrm{Lev}}(x)]^2/[k_{\mathrm{Lev}}^2(x)])(1 - u^*) \tag{A4}$$

with

$$[k_{\mathrm{Lev}}^{-1}(x)] \approx [k_{\mathrm{Lev}}(x)]^{-1}\left(1 + \frac{1}{108}\varepsilon^2\right) \tag{A5}$$

and

$$\frac{[k_{\mathrm{Lev}}^2(x)]}{[k_{\mathrm{Lev}}(x)]^2} \approx 1 + \frac{1}{108}\varepsilon^2 \tag{A6}$$

The final relationship:

$$[k(x)]/k_{\mathrm{a}} = 1 - c_{\mathrm{L}}(1 + \varepsilon^2/108)u^* \tag{A7}$$

$$[k(x)]/k_{\mathrm{a}} = c_{\mathrm{a}}^{-1}(1 + \varepsilon^2/108)(1 - u^*) \tag{A8}$$

must be the limits of the function $\phi_\varepsilon(u^*)$ as $u^* \to 0$ and $u^* \to 1$, respectively:

$$\phi_\varepsilon(u^*) = \frac{\left(u^* - 1\right)\left(a_\varepsilon\, u^* - 1\right)}{\left(b_\varepsilon\, u^* + 1\right)} \tag{A9}$$

We found for the first terms in powers of ε (for $\varepsilon < 1$) $a_\varepsilon = a_0(1 + 0.078\varepsilon^2)$ and $b_\varepsilon = b_0(1 + 0.044\varepsilon^2)$

References

Abramovitz M, Stegun IA (1972) Handbook of Mathematical Functions. Dover Publications, New York, p 255

Adler PM, Thovert J-F (1998) Real porous media: local geometry and macroscopic properties. Appl Mech Rev 51:537–585

Andrade J (1985) Surface and Interfacial Aspects of Biomedical Polymers. Plenum Press, New York
Antosiewicz J, Porschke D (1989) The nature of protein dipole moments: experimental and calculated permanent dipole of α-chymotrypsin. Biochemistry 28:10072–10078
Bae YM, Oh B-K, Lee W, Lee WH, Choi J-W (2005) Study on orientation of immunoglobulin G on protein G layer. Biosens Bioelectron 21:103–110
Bizzi M, Basini L, Saracco G, Specchia V (2002) Short contact time catalytic partial oxidation of methane: analysis of transport phenomena effects. Chem Eng J 90:97–106
Boumaza F, Dejardin P, Yan F, Bauduin F, Holl Y (1992) Fibrinogen adsorption on Pyrex glass tubes – a continuous kinetic study. Biophys Chem 42:87–92
Bowen BD, Levine S, Epstein N (1976) Fine particle deposition in laminar flow through parallel-plate and cylindrical channels. J Colloid Interface Sci 54:375–390
Bowen BD, Epstein N (1979) Fine particle deposition in smooth parallel-plate channels. J Colloid Interface Sci 72:81–97
Brash J, Horbett TA (1995) Proteins at Interfaces II: Fundamentals and Applications. American Chemical Society, Washington DC, USA
Britt DW, Buijs J, Hlady V (1998) Tobacco mosaic virus adsorption on self-assembled and Langmuir-Blodgett monolayers studied by TIRF and SFM. Thin Solid Films 329:824–828
Buijs J, Britt DW, Hlady V (1998) Human growth hormone adsorption kinetics and conformation on self-assembled monolayers. Langmuir 14:335–341
Burns TE, Dennison JR (1998) Physisorbed CO on ionic crystals: an extended BEG spin-lattice model of adsorbed dipolar molecules. Surf Sci 395:46–59
Burns TE, Dennison JR, Kite J (2004) Extended BEG model of monhalogenated methanes physisorbed on ionic crystals. Surf Sci 554:211–221
Calonder C, Van Tassel PR (2001) Kinetic regimes of protein adsorption. Langmuir 17:4392–4395
Coltrin ME, Mitchell CC (2003) Mass transport and kinetic limitations in MOCVD-selective area growth. J Cryst Growth 254:35–45
Cuypers PA, Hermens WT, Hemker HC (1978) Ellipsometry as a tool to study protein films at liquid–solid interfaces. Anal Biochem 84:56–67
Dabros T, van de Ven TGM (1993) Particle deposition on partially coated surfaces. Colloids Surf A 75:95–104
Daly SM, Przybycien TM, Tilton RD (2003) Coverage-dependent orientation of lysozyme adsorbed on silica. Langmuir 19:3848–3857
Dejardin P, Le MT, Wittmer J, Johner A (1994) Adsorption rate in the convection-diffusion model. Langmuir 10:3898–3901
Dejardin P, Vasina EN (2004) An accurate simplified data treatment for the initial adsorption kinetics in conditions of laminar convection in a slit: application to protein adsorption. Colloids Surf B 33:121–127
Docoslis A, Wu W, Giese RF, van Oss CJ (1999) Measurements of kinetic constants of protein adsorption onto silica particles. Colloids Surf B 13:83–104
Ethève J, Dejardin P (2002) Adsorption kinetics of lysozyme on silica at pH 7.4: correlation between streaming potential and adsorbed amount. Langmuir 18:1777–1785
Giacomelli CE, Norde W (2001) The adsorption-desorption cycle. Reversibility of the BSA-silica system. J Colloid Interface Sci 233:234–240
Göransson A, Trägardh C (2000) An experimental study of the kinetics of particle deposition in a wall-jet cell using total internal reflection fluorescence. J Colloid Interface Sci 231:228–237
Holmberg K, Tiberg F, Malmsten M, Brink C (1997) Grafting with hydrophilic polymer chains to prepare protein-resistant surfaces. Colloids Surf A 123–124:297–306

Hook F, Voros J, Rodahl M, Kurrat R, Boni P, Ramsden JJ, Textor M, Spencer ND, Tengvall P, Gold J, Kasemo B (2002) A comparative study of protein adsorption on titanium oxide surfaces using in situ ellipsometry, optical waveguide lightmode spectroscopy, and quartz crystal microbalance/dissipation. Colloids Surf B 24:155–170

Huang XJ, Xu ZK, Wan LS, Wang ZG, Wang JL (2005) Surface modification of polyacrylonitrile-based membranes by chemical reactions to generate phospholipid moieties. Langmuir 21:2941–2947

Hunter RJ (1981) Zeta potential in colloid science. Principles and applications. In: Ottewill RH, Rowell RL (eds) Colloid Science. Academic Press, London, p 81

Ishihara K, Fukumoto K, Iwasaki Y, Nakabayashi N (1999a) Modification of polysulfone with phospholipid polymer for improvement of the blood compatibility. Part 1. Surface characterization. Biomaterials 20:1545–1551

Ishihara K, Fukumoto K, Iwasaki Y, Nakabayashi N (1999b) Modification of polysulfone with phospholipid polymer for improvement of the blood compatibility. Part 2. Protein adsorption and platelet adhesion. Biomaterials 20:1553–1559

Iwasaki Y, Tojo Y, Kurosaki T, Nakabayashi N (2003) Reduced adhesion of blood cells to biodegradable polymers by introducing phosphorylcholine moieties. J Biomed Mater Res A 65:164–169

Kelly MS, Santore MM (1995) The role of a single end group in poly(ethylene oxide) adsorption on colloidal and film polystyrene: complimentary sedimentation and total internal reflectance fluorescence studies. Colloids Surf A 96:199–215

Kojima M, Ishihara K, Watanabe A, Nakabayashi N (1991) Interaction between phospholipids and biocompatible polymers containing a phosphorylcholine moiety. Biomaterials 12:121–124

Ladam G, Schaaf P, Decher G, Voegel J-C, Cuisinier FJG (2002) Protein adsorption onto auto-assembled polyelectrolyte films. Biomol Eng 19:273–280

Le MT, Dejardin P (1998) Simultaneous adsorption of fibrinogen and kininogen at a silica/solution interface. Langmuir 14:3356–3364

Lee J, Kopecek J, Andrade J (1989) Protein-resistant surfaces prepared by PEO-containing block copolymer surfactants. J Biomed Mater Res 23:351–368

Lee J, Kopeckova P, Kopecek J, Andrade J (1990) Surface properties of copolymers of alkyl methacrylates with methoxy(polyethyleneoxyde) methacrylates and their application as protein-resistant coatings. Biomaterials 11:455

Leonard E, Turitto V, Vroman L (1987) Blood in Contact with Natural and Artificial Surfaces. New York Academy of Sciences, New York

Lévêque M (1928) Les lois de transmission de la chaleur par convection. Faculté des Sciences, Paris

Levich VG (1962) Physical Hydrodynamics. Prentice-Hall, Englewood Cliffs, NJ, USA

Malmsten M, Lassen B, Holmberg K, Thomas V, Quash G (1996) Effects of hydrophilization and immobilization on the interfacial behavior of immunoglobulins. J Colloid Interface Sci 177:70–78

Mar MN, Ratner BD, Yee SS (1999) An intrinsically protein-resistant surface plasmon resonance biosensor based upon a RF-plasma-deposited thin film. Sens Actuators B 54:125–131

McClellan SJ, Franses EI (2005) Adsorption of bovine serum albumin at solid/aqueous interfaces. Colloids Surf 260:265–275

Nakabayashi N, Williams DF (2003) Preparation of non-thrombogenic materials using 2-methacryloyloxyethyl phosphorylcholine. Biomaterials 24:2431–2435

Nakabayashi N, Iwasaki Y (2004) Copolymers of 2-methacryloyloxyethyl phosphorylcholine (MPC) as biomaterials. Bio-Med Mater Eng 14:345–354

Nitschke M, Menning A, Werner C (2000) Immobilization of PEO-PPO-PEO triblock copolymers on PTFE-like fluorocarbon surfaces. J Biomed Mater Res 50:340–343

Noinville S, Revault M, Baron M-H (2002a) Conformational changes of enzymes adsorbed at liquid–solid interface: relevance to enzymatic activity. Biopolymers 67:323–326

Noinville S, Revault M, Baron M-H, Tiss A, Yapoudjian S, Ivanova M, Verger R (2002b) Conformational changes and orientation of Humicola lanuginosa lipase on a solid hydrophobic surface: an in situ interface Fourier transform infrared–attenuated total reflection study. Biophys J 82:2709–2719

Noinville S, Bruston F, El Amri C, Baron D, Nicolas P (2003) Conformation, orientation, and adsorption kinetics of dermaseptin B2 onto synthetic supports at aqueous/solid interface. Biophys J 85:1196–1206

Norde W, Rouwendal E (1990) Streaming potential measurements as a tool to study protein adsorption kinetics. J Colloid Interface Sci 139:169–176

Norde W, Zoungrana T (1998) Surface-induced changes in the structure and activity of enzymes physically immobilized at solid/liquid interfaces. Biotechnol Appl Biochem 28:133–143

Poksinski M, Arwin H (2004) Protein monolayers monitored by internal reflection ellipsometry. Thin Solid Films 455–456:716–721

Price ME, Cornelius RM, Brash JL (2001) Protein adsorption to polyethylene glycol modified liposomes from fibrinogen solution and from plasma. Biochim Biophys Acta 1512:191–205

Quiquampoix H, Ratcliffe RG (1992) A P-31 NMR Study of the adsorption of bovine serum albumin on montmorillonite using phosphate and the paramagnetic cation Mn^{2+}-modification of conformation with pH. J Colloid Interface Sci 148:343–352

Ramsden JJ, Lvov YM, Decher G (1995) Determination of optical constants of molecular films assembled via alternate polyion adsorption. Thin Solid Films 254:246–251

Rebar VA, Santore MM (1996) History-dependent isotherms and TIRF calibrations for homopolymer adsorption. Macromolecules 29:6262–6272

Robeson JL, Tilton RD (1996) Spontaneous reconfiguration of adsorbed lysozyme layers observed by total internal reflection fluorescence with a pH-sensitive fluorophore. Langmuir 12:6104–6113

Schaaf P, Dejardin P (1988) Structural changes within an adsorbed fibrinogen layer during the adsorption process: a study by scanning angle reflectometry. Colloids Surf 31:89–103

Seitz R, Brings R, Geiger R (2005) Protein adsorption on solid–liquid interfaces monitored by laser ellipsometry. Appl Surf Sci 252:154–157

Servagent-Noinville S, Revault M, Quiquampoix H, Baron MH (2000) Conformational changes of bovine serum albumin induced by adsorption on different clay surfaces: FTIR analysis. J Colloid Interface Sci 221:273–283

Su TJ, Lu JR, Thomas RK, Cui ZF, Penfold J (1998) The effect of solution pH on the structure of lysozyme layers adsorbed at the silica–water interface studied by neutron reflection. Langmuir 14:438–445

Tirelli N, Lutolf MP, Napoli A, Hubbell JA (2002) Poly(ethylene glycol) block copolymers. Rev Mol Biotechnol 90:3–15

Ueda T, Watanabe A, Ishihara K, Nakabayashi N (1991) Protein adsorption on biomedical polymers with a phosphorylcholine moiety adsorbed with phospholipid. J Biomater Sci Polym Ed 3:185–194

Valette P, Thomas M, Dejardin P (1999) Adsorption of low molecular weight proteins to hemodialysis membranes: experimental results and simulations. Biomaterials 20:1621–1634

Vasina EN, Dejardin P (2004) Adsorption of alpha-chymotrypsin onto mica in laminar flow conditions. Adsorption kinetic constant as a function of tris buffer concentration at pH 8.6. Langmuir 20:8699–8706

Vasina EN, Dejardin P, Rezaei H, Grosclaude J, Quiquampoix H (2005) Fate of prions in soil: adsorption kinetics of recombinant unglycosylated ovine prion protein onto mica in laminar flow conditions and subsequent desorption. Biomacromolecules 6:3425–3432

Vermeer AWP, Norde W (2000) The influence of the binding of low molecular weight surfactants on the thermal stability and secondary structure of IgG. Colloids Surf A 161:139–150

Vermeer AWP, Giacomelli CE, Norde W (2001) Adsorption of IgG onto hydrophobic Teflon. Differences between the Fab and Fc domains. Biochim Biophys Acta 1526:61–69

Voegel JC, Dejardin P, Strasser C, de Baillou N, Schmitt A (1987) Thermal desorption spectrometry of fibrinogen. Colloids Surf 25:139–144

Werner C, Eichhorn KJ, Grundke K, Simon F, Grahlert W, Jacobasch HJ (1999) Insights on structural variations of protein adsorption layers on hydrophobic fluorohydrocarbon polymers gained by spectroscopic ellipsometry (part I). Colloid Surf A 156:3–17

Wertz CF, Santore MM (1999) Adsorption and relaxation kinetics of albumin and fibrinogen on hydrophobic surfaces: single species and competitive behavior. Langmuir 15:8884–8894

Wertz CF, Santore MM (2002) Adsorption and reorientation kinetics of lysozyme on hydrophobic surfaces. Langmuir 18:1190–1199

Wu YJ, Timmons RB, Jen JS, Molock FE (2000) Non-fouling surfaces produced by gas phase pulsed plasma polymerization of an ultra low molecular weight ethylene oxide containing monomer. Colloids Surf B 18:235–248

Xu Z, Marchant RE (2000) Adsorption of plasma proteins on polyethylene oxide-modified lipid bilayers studied by total internal reflection fluorescence. Biomaterials 21:1075–1083

Yan F, Dejardin P, Mulvihill JN, Cazenave JP, Crost T, Thomas M, Pusineri C (1992) Influence of a preadsorbed terpolymer on human platelet accumulation, fibrinogen adsorption, and ex vivo blood activation in hemodialysis hollow fibers. J Biomater Sci Polym Ed 3:389–402

Ye SH, Watanabe J, Iwasaki Y, Ishihara K (2005) In situ modification on cellulose acetate hollow fiber membrane modified with phospholipid polymer for biomedical application. J Membr Sci 249:133–141

Zembala M, Dejardin P (1994) Streaming potential measurements related to fibrinogen adsorption onto silica capillaries. Colloids Surf B 3:119

Zembala M, Adamczyk Z (2000) Measurements of streaming potential for mica covered by colloid particles. Langmuir 16:1593–1601

Zembala M, Adamczyk Z, Warszynski P (2001) Influence of adsorbed particles on streaming potential of mica. Colloids Surf A 195:3–15

Zembala M (2004) Electrokinetics of heterogeneous interfaces. Adv Colloid Interface Sci 112:59–92

Zoungrana T, Findenegg GH, Norde W (1997) Structure, stability, and activity of adsorbed enzymes. J Colloid Interface Sci 190:437–448

4 Dual Polarisation Interferometry: An Optical Technique to Measure the Orientation and Structure of Proteins at the Solid–Liquid Interface in Real Time

Neville Freeman

Abstract. The study of the orientation, structure, and function of proteins at interfaces in real time is demanding and complex in nature. For the last 40 years the primary means for the study of protein structure has been x-ray crystallography. This is, of course, a solid-state technique and not real time in nature. Over the last 20 years several techniques to address, at least in part, this important area have been adopted. These range from biosensors, which measure the rates of change of processes at interfaces, to analytical techniques such as neutron reflection, which are capable of providing detailed information on (protein) layer structures at interfaces. In this article a new analytical technique is described, dual polarisation interferometry (DPI), which combines the analytical nature of neutron reflection techniques with the real-time, bench-top accessibility associated with biosensors. Several examples of the measurement of protein orientation, structure and function are presented to demonstrate the value of the technique. A description of the fundamental physical principles of the measurement and verification of the technique are also provided.

4.1 Introduction

The growth, metabolism and replication of cells, the basic building blocks of life, depend very heavily on proteins. Proteins perform a vast range of functions of both an intracellular and intercellular nature, being expressed within the cells themselves. The profile of expressed proteins within a cell depends upon the metabolic status of the cell, its age and its local environment. Understanding the role that proteins play in the status of the cell is crucial to the understanding of the diseased state and is therefore of great importance within medical and pharmaceutical studies of disease. Their behaviour at interfaces (e. g. surfaces) is of particular relevance given that many biologically important processes are interfacial in nature.

Neville Freeman: Farfield Scientific Ltd, Farfield House, Southmere Court, Electra Way, Crewe Business Park, Crewe, Cheshire, CW1 6GU, UK, E-mail: nfreeman@farfield-scientific.com

Principles and Practice
Proteins at Solid–Liquid Interfaces
Philippe Déjardin (Ed.)
© Springer-Verlag Berlin Heidelberg 2006

To appreciate how proteins function and the diverse roles that they are capable of playing, an understanding of the structure of proteins and structural changes occurring in real time is required. Proteins are capable of undergoing substantial conformational and structural changes in the presence of a range of stimuli such as changes in environment, for example pH, the presence of small molecules, such as candidate drug molecules, or the presence of secondary binding partners (typically, but not limited to, other proteins).

The structure of a protein is determined by its primary structure, the sequence in which the amino acids that constitute its composition are covalently bound together. The nature of the amino acid sequences leads to regions of the molecule forming coils (alpha helices) or sheets (beta sheets), which define the secondary structure of the molecule. The molecule undergoes further organisation (folding and reordering) to define the tertiary structure of the protein. The secondary and tertiary structures are noncovalent in nature and a range of interactions contribute to the final structure, such as hydrogen bonding, electrostatic interactions and dispersion forces. These interactions occur between adjacent amino acid groups and may be mediated or altered by solvation, the ionic strength of the solution and a range of other environmental factors. Finally, these individual peptides often interact with other peptides to perform specific functions or to provide structural integrity, and this final structure of the protein is known as the quaternary structure.

The dynamic nature of the secondary and tertiary structures of proteins enables them to undergo structural changes in response to stimuli that are often related to their functional roles. Structurally distinct regions within a protein are often associated with specific functions, and these structures may be conserved to undertake similar functions across a range of different proteins. The shape of the protein, especially its external surface often provides pockets or clefts, which offer specific binding sites for small molecules or other proteins. Interactions with these sites is often described as specific binding and is associated with the activation or regulation of the activity of the protein.

The analysis of protein structure at the tertiary and quaternary levels, especially in real time, is a particularly challenging task, but is extremely important to the pharmaceutical industry and to protein researchers. Since the early successes in determining the x-ray crystal structure of myoglobin and haemoglobin (Kendrew et al. 1958; Muirhead and Perutz 1963; Perutz 1963), biochemists and pharmacologists have tended to rely on x-ray diffraction techniques for information on a protein's three-dimensional structure and its relationship to its function. Structure–function relationships are particularly important in order to gain a better understanding of how a particular protein operates or how drug molecules could be designed

to modulate the behaviour of a protein implicated in a disease mechanism. The importance of these studies is demonstrated by the current drive in pharmaceutical research towards structurally informed drug discovery.

X-ray diffraction techniques require a diffraction-quality protein crystal. Producing such crystals is extremely challenging and is often the rate-limiting, or even terminal step in the process of determining molecular structure. In the crystalline state the protein molecule is in a condition that is far from that found in vivo. The contributions of the crystal lattice, changes in solvation state and use of modifiers in order to obtain crystals, for example, all lead to a degree of uncertainty regarding the fidelity of the crystal structure when compared to the structure adopted by the protein in its natural environment. In addition, x-ray diffraction provides no information on the mechanisms by which structural change occurs. The best that can be achieved is the crystal structure of the native protein and the crystal structure of the protein in the presence of a small molecule (i. e. a candidate drug molecule). This provides the molecular structures of the starting condition (the native protein) and the molecular structure of the end point (when the protein has bound the small molecule). Whilst this is a highly information-rich technique, the crystallisation of proteins is an extremely difficult and time-consuming process and it is not uncommon for the drug discovery process to have to proceed in the absence of critical structural information.

The drug discovery process typically starts with the isolation and identification of proteins that, it is suspected, are implicated in the diseased state. Once this has been achieved the next key step is to obtain as much structural information as possible. This usually begins with attempts to obtain x-ray diffraction data to solve crystal structures, which can be a serious bottleneck in the discovery process. Membrane-bound proteins, which are currently of great interest to the pharmaceutical industry, have been found to be particularly difficult in this respect, representing a very small fraction of the protein structures available on the Brookhaven Protein Database (Berman et al. 2000). Even when structural information is available, the value is limited as the data provided is static, the protein being "frozen" in a crystal lattice, and few insights are offered into the mechanism by which the protein functions.

As a result of the limitations of structural information and its relationship to the function of a protein obtained through x-ray crystallography, several techniques have been developed in recent years to supplement the information provided by diffraction experiments. These include high-field nuclear magnetic resonance (NMR) and neutron reflection techniques. NMR techniques are useful but very data intensive (and the structures are somewhat ambiguous), whilst neutron reflection offers more limited structural information but can provide a limited degree of temporal information.

True real-time capabilities are offered by sensor techniques such as microcalorimetry, acoustic wave devices (predominantly quartz crystal microbalance) and optical techniques, including, for example, surface plasmon resonance (SPR). As a consequence, structural determination has tended to remain the preserve of x-ray crystallography, whilst function has tended to be determined using calorimetric, acoustic wave or optical techniques. The latter, often being at best semi-quantitative in nature, have tended to rely on temporal characteristics, measuring the kinetics of protein interaction events, which are then related to function. Any relationship between temporal sensor data and structure tends to be, at best, putative in nature. This has led to the separation of the structural and functional measurements, which requires the adoption of some significant assumptions. For readers wishing to obtain more general reviews on tagless biosensor platforms are directed towards reviews on this subject (Baird et al. 2001).

Recently, techniques have been developed that attempt to link structure and function. Certain modifications to acoustic-wave devices, utilising the characteristics of the dissipation of acoustic modes (sometimes referred to as 'QCM-D') can under some conditions provide information on the dimensionality of deposited thin films which, in conjunction with the mass loading (determined from the change in resonant frequency of the acoustic device), can offer some insights in to surface structure. In order to provide a full analytical treatment of such data, several significant assumptions must be made. QCM data is of relatively low resolution when compared with analogous optical techniques, which limits its utility in the pharmaceutically relevant area of protein–small molecule interactions. Optical approaches have been described; these include optical waveguide light spectroscopy (OWLS) (Tiefenthaler and Lukosz 1989), ellipsometry (Spaeth et al. 1997), coupled plasmon waveguide resonance (CPWR) (Salamon et al. 2000) and dual polarisation interferometry (DPI; Cross et al. 2003). OWLS provides relatively low-layer parameter and temporal resolution, whilst ellipsometry suffers from both resolution issues and ambiguity in terms of data interpretation. CPWR has found limited use in the life science arena but does not appear to have been widely adopted. The latter technique, DPI, involves exciting a waveguide structure with two polarisations of light, which provides two independent measures of the surface condition of the waveguide itself. From this data, the thickness and density (or refractive index) of thin-layer structures on the waveguide surface can be determined with relatively few assumptions to very high precision and with good temporal resolution. The technique has found broad application in life science and surface science research.

In the present article, the application of DPI will be explored. A general background, and introduction to the theoretical treatment of DPI has been provided at the end of this article (see Appendices 1–3).

4.2 Experimental Approaches Adopted

4.2.1 Typical Approach Adopted

In general it is best from an analytical perspective to undertake as much of the experimental procedure as possible on the DPI instrument itself. Thus, all chemistries that can be carried out across a typical temperature range of 10–40 °C in the liquid phase can in principle be undertaken on the instrument. The advantage of running entire experiments "on-instrument" is simple: it enables a very clear analysis of how much of each material is deposited on the sensor surface at each stage of the experimental procedure and under what conditions. This enables the use of very valuable diagnostic information when analysing the experimental data, and enables stoichiometric analysis of the interactions investigated to be undertaken with ease.

4.2.2 Experimental Protocols

Typical protocols start with a waveguide sensor chip that has been pre-functionalised with a covalently bound species such as free amine (coupled to the waveguide surface via silane chemistry) or free thiol (again covalently bound using silane chemistries). The chip is inserted into the instrument and the fluidic system is started (typically flowing running buffer at 100 µl min^{-1}) followed by a series of injections such as linker [e. g. homobifunctional linker such as bis(sulphosuccinimydyl) suberate, BS^3, an amine-amine linker], followed by protein followed by block [such as Tris(hydroxymethyl)aminomethane, Tris]. The surface is then ready to be challenged as required by the experimentalist.

4.2.3 Advantages

The advantages of this approach are that the condition of surface is very well understood throughout the experimental procedure. This enables stoichiometries of interactions to be investigated and rapid optimisation of the protocol to be undertaken where necessary. It also enables variations in the quality of the materials used to be analysed and taken into account when considering the experiment as a whole.

Table 1. Example of verification of dual polarisation interferometry (DPI) data with neutron reflection results (Freeman et al. 2004b). *[BSA]* Concentration of bovine serum albumin

Method	[BSA] (g dm^{-3})	Mass adsorbed pH 3 (ng mm^{-2})	Mass adsorbed pH 5 (ng mm^{-2})	Mass adsorbed pH 7 (ng mm^{-2})
Neutron reflectivity[a]	0.15	0.50	2.50	0.50
DPI	0.10	0.48	2.11	0.42

[a]Su et al. 1998b

Table 2. Example of verification of DPI data with x-ray crystal structure data (see Peters 1985) at pH 5

DPI (*Ana*Light® Bio200)	X-ray structure	
Thickness (Å)	Short Axis (Å)	Long Axis (Å)
44 (±4)	40 (±2)	140 (±2)

4.2.4 Verifying DPI as an Experimental Approach

DPI has been verified against a wide range of analytical techniques including x-ray crystallography, neutron reflection, fluorescence assays, dynamic light scattering, ellipsometry, electron microscopy, scanning probe microscopy and molecular modelling, and it has been found to be in good experimental agreement with all of these for a range of experimental systems. Some example data are provided in Tables 1 and 2.

An example of an experiment using nanoparticles is shown in Fig. 1. Here, 80-nm silica nanoparticles were flowed over a polyethyleneimine-treated sensor surface, allowing electrostatic interactions to adhere the particles to the polymer/sensor surface. The packing efficiency of the silica spheres is poor when compared to the polymer layer, hence the drop in the density on introduction of the silica nanospheres but the mass increases and the thickness of the layer increases to 78 nm, which is in excellent agreement with the expected result.

4.3 DPI: Applications

4.3.1 Introduction

DPI has been used to study a wide range of molecular systems. These range from studying the interfacial behaviour and orientation of pro-

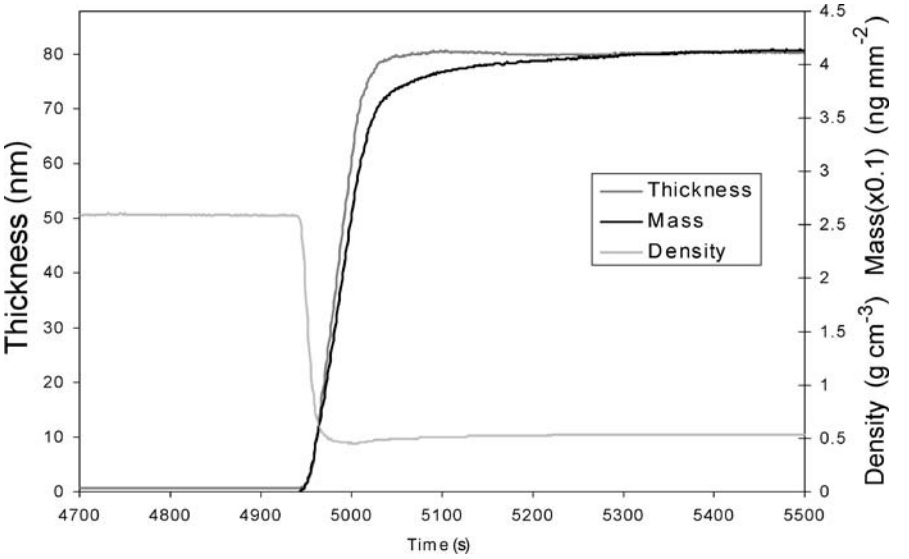

Fig. 1. Dual polarisation interferometry (DPI) experiment showing the thickness (*thin black line*), density (*thin grey line*) and mass (*thick black line*) profiles for a layer constructed of 80 nm silica nanospheres

tein molecules and the solid–liquid interface to the molecular interactions of model systems such as biotin–streptavidin, and subsequent structural changes through to the structural changes invoked when certain proteins bind metal ions. A selection of applications has been chosen for discussion here that illustrate the wide range of orientation and interaction studies that can be undertaken using DPI.

4.3.2 Protein Orientation

Lysozyme Orientation at the Silica–Water Interface

Lysozyme adsorption at the silica–water interface and subsequent layer structures were investigated. The build-up (and removal) of molecular layers adsorbing or reacting on a lightly doped silicon dioxide (silica) surface were measured in terms of thickness and refractive index changes over time. Lysozyme adsorption was monitored at a range of concentrations (from 0.03 g dm^{-3} to 4.0 g dm^{-3}) and at both pH 4 and pH 7 in a flow-through cell arrangement. Adsorbed layers ranging from 14 to 43 ± 1Å in thickness and 0.21 to 2.36 ± 0.05 mg m^{-2} in terms of mass coverage were observed at pH 4 with increasing lysozyme concentration, indicating a strong deformation of the monolayer over the low concentration range and formation of an al-

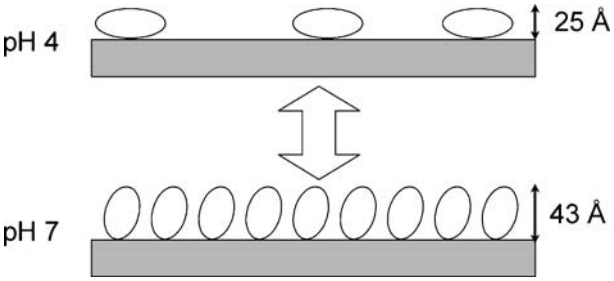

Fig. 2. Schematic representation showing the physisorbed lysozyme at pH 4 and pH 7 at 1 g dm^{-3} and 20 °C at the silica–water interface

most complete sideways-on bilayer in which the molecules were adsorbed with their short axis normal to the silica surface at the highest concentrations. At pH 7, the thickness of adsorbed layers varied from 16 to 54 ± 1Å, with significantly higher surface coverage (0.74–3.29 ± 0.05 mg m^{-2}) over the same lysozyme concentration range, again indicating structural deformation during the initial monolayer formation followed by a closely packed monolayer where the long axis of the lysozyme molecule was oblique to the silica surface at intermediate concentrations and a subsequent bilayer where the molecules of the second layer were oriented with the short axis normal to the silica surface at the highest concentrations. These experiments were repeated with a fixed lysozyme concentration of 1.0 g dm^{-3} whilst cycling the pH from 7 to 4 and back again or vice versa. Broadly reversible adsorption was observed, regardless of whether the pH was cycled or not. These observations agree with earlier studies undertaken using neutron reflection (Su et al. 1998a). A schematic representation of changes in orientation is shown in Fig. 2 (Freeman et al. 2004a).

4.3.3 Bovine Serum Albumin Structures at pH 3 and pH 7

DPI has been used as a high-resolution (< 0.01 nm), lab-based technique to determine the thickness and refractive index (density) of bovine serum albumin (BSA) molecules adsorbing or reacting at the solid–liquid interface in real time (up to ten measurements per second). Results from these studies of the adsorption of BSA on to a silicon oxynitride chip surface demonstrate how time-dependent molecular behaviour can be examined. Mechanistic and structural information relating to the adsorption process was obtained as a function of the solution pH. The results are shown in Fig. 3, and the schematic representation of the layer changes occurring with pH cycling are shown in Fig. 4.

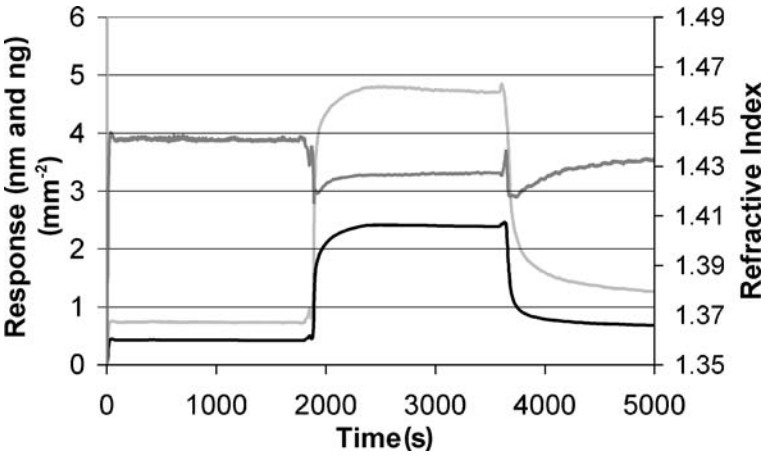

Fig. 3. Changes in layer structure as a function of cycling pH at a constant bovine serum albumin (BSA) concentration. *Light grey* thickness, *mid grey* refractive index (proportional to density), *dark grey* mass

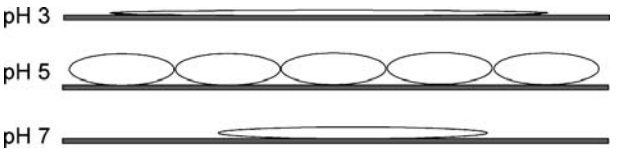

Fig. 4. Schematic diagram of the structure of the physisorbed BSA layer during the pH changes described for Fig. 3

4.3.4 Protein Orientation and Subsequent Activity

Optimised Antibody Immobilisation Protocol

The immobilisation of a mouse IgG3 antibody raised to cortisol (anti-cortisol) is summarised in Table 3. The experimental protocol was as follows. A thiol functionalised chip was first calibrated using standard calibrant solutions and then subjected to N-maleimidobutyryloxy-sulpho-succinimide ester (sulpho-GMBS), which is a thiol amine linker followed by protein G. Once the protein G had been immobilised (via the sulpho-GMBS linker) the surface was ready for the immobilisation of the IgG3 antibody itself. Protein G has the capability to orient the antibody by interacting specifically with the Fc region, ensuring that the antibody remains active once immobilised. As can be seen from Table 3, the layer thickness increases by over 15 nm on the addition of the antibody. This is entirely consistent with the long axis of the IgG3 antibody (typically 12–15 nm, the other two axes typically being of the order of 5–10 nm) being immobilised normal to the sensor surface. This is shown schematically in Fig. 5.

Table 3. Layer analysis for each layer of the oriented immobilisation protocol for the IgG3 anticortisol antibody. *GMBS N*-(γ-maleimidobutyryloxy)succinimide

Layer	Name	Thickness (nm)	Density (g cm^{-3})	Mass (ng mm^{-2})
1	GMBS	0.540	0.555	0.300
2	Protein G	0.826	0.810	0.669
3	IgG3 anti-cortisol	15.126	0.181	2.743

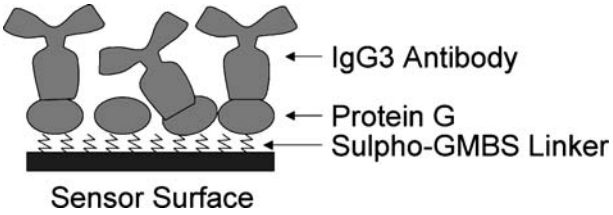

Fig. 5. Schematic diagram of the immobilisation of IgG3 anticortisol to the sensor chip surface. *GMBS N*-(γ-maleimidobutyryloxy)succinimide

Having prepared the immobilised antibody surface, it was repeatedly challenged with the antigen, cortisol. This is an extremely small molecule (molecular mass 372 Da) when compared to the antibody (molecular mass 160,000 Da). This situation is germane to many systems of interest to the life scientist and provides a considerable challenge for instrumentation scientists. As the size and mass of the protein, in this case an antibody, increases and the size and mass of the molecule that binds, in this case cortisol, decreases, so the signal to noise ratio diminishes. However, the sensitivity of DPI can be seen, from Fig. 6, to be entirely adequate to monitor the antigen-antibody binding event on injecting antigen across the immobilised antibody surface. During repeated injections of cortisol and subsequent washes, the thickness of the antibody layer increases and its density reduces on binding (which is reversed during the wash), which is indicative of a structural change occurring as a consequence of the binding process.

These structural changes occur despite the considerable difference in size between the antibody and antigen, the antibody surface undergoing a substantial structural change on binding the antigen. Each time the antibody surface is subjected to the antigen, an increase in the thickness of the layer (up to 0.5 nm at high antigen concentrations) and a commensurate decrease in density is observed. It should be noted that despite the density decrease, the overall layer mass increases on binding antigen. The relationship between the thickness and density of immobilised protein layers provides very strong evidence of specific binding events (Swann et al. 2004).

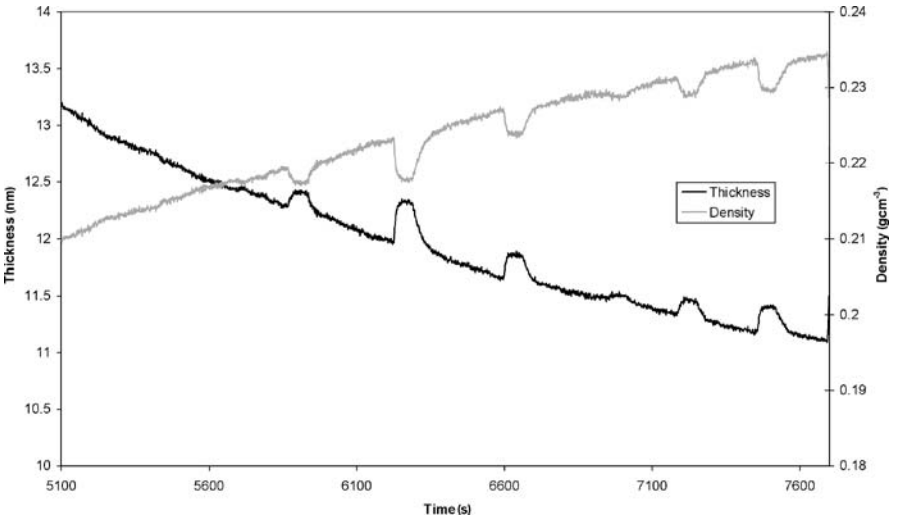

Fig. 6. Structural responses when anti-cortisol binds cortisol (at varying cortisol concentrations)

Both the mass increase and thickness increase can be used to determine the affinity constant for the binding interaction and in this case for the thickness change binding curve (see Fig. 7). These observations are consistent with the two flexible F_{AB} arms becoming more erect on binding antigen. From the mass values it was also possible to calculate the stoichiometry for the binding event, which at two antigen molecules per antibody is as would be expected for an IgG3 antibody. As the binding was repeated at a range of antigen concentrations it was also possible to calculate an affinity constant for the antigen binding. The value of 0.8 μM was obtained, which is within the range expected by the supplier of the antibody, strongly supporting the hypothesis that the observed structural changes were directly related to antibody–antigen binding events.

Poorly Optimised Antibody Immobilisation

This example is provided to demonstrate how the technique can be used to determine the orientation and structure of an immobilised antibody layer and subsequent blocking steps and to diagnose potential problems at an early stage. In this case, anti-ovalbumin has been immobilised to the sensor surface using the homobifunctional linker bis(sulphosuccinimydyl) suberate (BS^3). It can be seen that in this case the antibody goes down as a very thin layer and is therefore likely to be prone on the surface (Table 4). In such a condition, the antibody cannot function correctly and is likely to have a very low activity. This indeed was observed to be the case. The experiment was, however, continued and a blocking step was undertaken. It can be seen

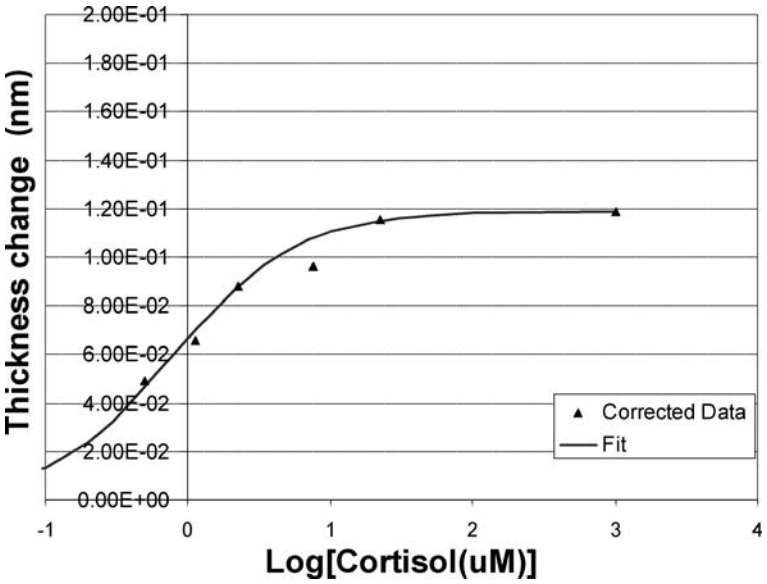

Fig. 7. Structural binding curve for the binding of cortisol to anti-cortisol

Table 4. Layer structure during the immobilised of anti-ovalbumin. *TM* Transverse magnetic, *TE* transverse electric, *Diff* phase difference, *Th* thickness, *RI* refractive index, BS^3 bis(sulphosuccinimydyl) suberate, *Ab* antibody

Name	Mass (ng mm^{-2})	TM Diff (rad)	TE Diff (rad)	Th (nm)	RI
BS^3	0.255	0.827	0.693	0.486	1.4303
Ab	0.720	1.526	1.151	3.334	1.3731

Table 5. Addition of blocking agent and antigen to the anti-ovalbumin surface

Name	Mass (ng mm^{-2})	TM Diff (rad)	TE Diff (rad)	Th (nm)	RI
Ab	0.720	1.526	1.151	3.334	1.3731
Block	1.406	2.179	1.715	6.117	1.3757
Antigen	1.446	0.121	0.094	6.403	1.3749

from Table 5 that the addition of a block, γ-globulin, simply increases the thickness of the layer present but does not increase its refractive index (and therefore its density). This suggests that the blocker in the experiment is not inserting between the layers as anticipated, but simply covering the surface of the prone antibody layer. Finally, when the antigen is added to the layer structure, this too appears to add additional layer thickness without increasing the layer density, suggesting that the antigen can only interact with the surface generated by the blocker.

Table 6. Example conditions and immobilisation strategies used with antibodies. *MW* Molecular weight, *HSA* human serum albumin, *+ve* positive, *-ve* negative, *ProBNP* precursor of brain natriuretic peptide

Antibody	Type	Immobilisation	Antibody Layer (nm)	Activity	Antigen (MW)	ΔThickness (nm)
Ovalbumin		$-NH_2$, BS^3	3.3	Inactive	5,000	None
HSA	IgG1	$-NH_2$, BS^3	6.4	Active <<1:1	67,000	+ve
Bi-ProBNP	Poly	$-NH_2$, SA, s-NHS-LC Biotin	6.7	Active 1:1	8,000	–ve
BSA	IgG1	$-NH_2$, BS^3, Protein G	6.0	Inactive	66.000	None
Cortisol (1)	IgG3	$-NH_2$, BS^3, Protein G	9.0	Active 2:1	362	+ve
Cortisol (2)	IgG3	–SH, s-GMBS, Protein G	15.1	Active 2:1	362	+ve

Using Structural Information to Optimise Antibody Activity

An example range of immobilisation strategies and antibody classes is shown in Table 6. It can be seen that active antibody surfaces can be obtained with a wide range of immobilisation strategies.

4.3.5 Protein Structure and Small Molecule Interactions

Introduction

Protein–small molecule interactions and the structural changes associated with binding are extremely important. Such interactions are of key importance to the pharmaceutical industry, whose main concern is the mediation of protein function by small (drug) molecules. Protein–small molecule interactions have been investigated using optical sensor technologies, sometimes referred to as biosensors (Ramsey 1998). However, the majority of this work has been undertaken by immobilising the small molecule to the surface of the sensor and then measuring the binding of the receptor to the surface. There are several advantages to undertaking experimentation in which the receptor is bound to the sensor surface, including reduced consumption of receptor, enabling quantitative assessment of the amount of small molecule that binds to the receptor and ultimately allowing the high throughput screening of pharmaceutical "lead" compounds. There

have been reports of the measurement of small-molecule binding using various SPR techniques for a limited number of systems (Davis and Wilson 2001; Frostell-Karlsson et al. 2000; Karlsson 1994; Karlsson et al. 2000). For the purposes of illustration, the model system, streptavidin – biotin, will be discussed here; this system has been reported in detail elsewhere (Swann et al. 2004).

Biotin Streptavidin

The surface immobilisation data shown in Fig. 8 shows that the layer thickness after immobilisation of the streptavidin is observed to increase by 6.63 nm. This is in good agreement with x-ray crystallographic structure data that suggests that the long axis of the apo-core-streptavidin molecule at pH 7.5 is around 6.8 nm (Weber et al. 1989) and the dimensions are consistent with the formation of a monolayer of immobilised protein on the sensor surface. The mass loading of the sensor surface enables calculation of the area per molecule surface coverage, which provides an additional indication of the likelihood of a monolayer having been formed. The calculated value of 4,350 $Å^2$ $molecule^{-1}$ is greater than the theoretical value of 3,000 $Å^2$ $molecule^{-1}$ for a fully saturated surface layer, which further suggests that a monolayer has been achieved. The detail of the experiment is shown in Fig. 9, the binding of D-biotin to streptavidin being clearly observed. Figure 9A shows the data, resolved into thickness and density for the binding event. On binding D-biotin, the streptavidin adlayer thickness decreases a small but measurable amount. This is to be expected as streptavidin is a relatively rigid globular protein. There is a commensurate increase in the density of the layer during the binding process. It is also

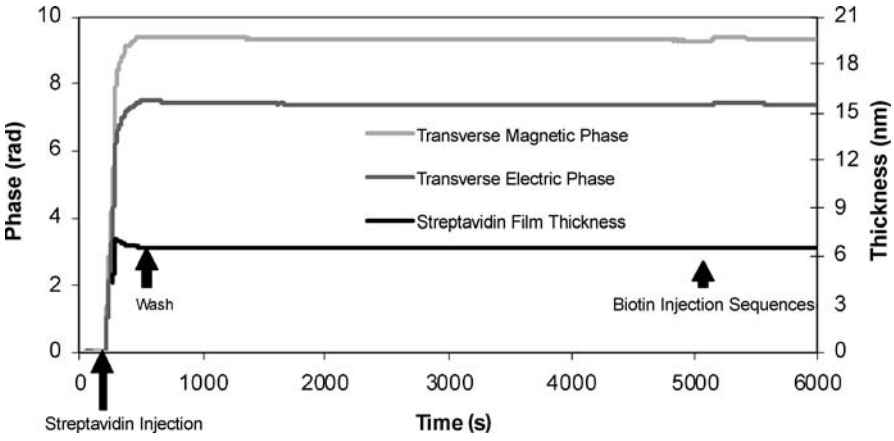

Fig. 8. Immobilisation of streptavidin to a biotinylated sensor surface

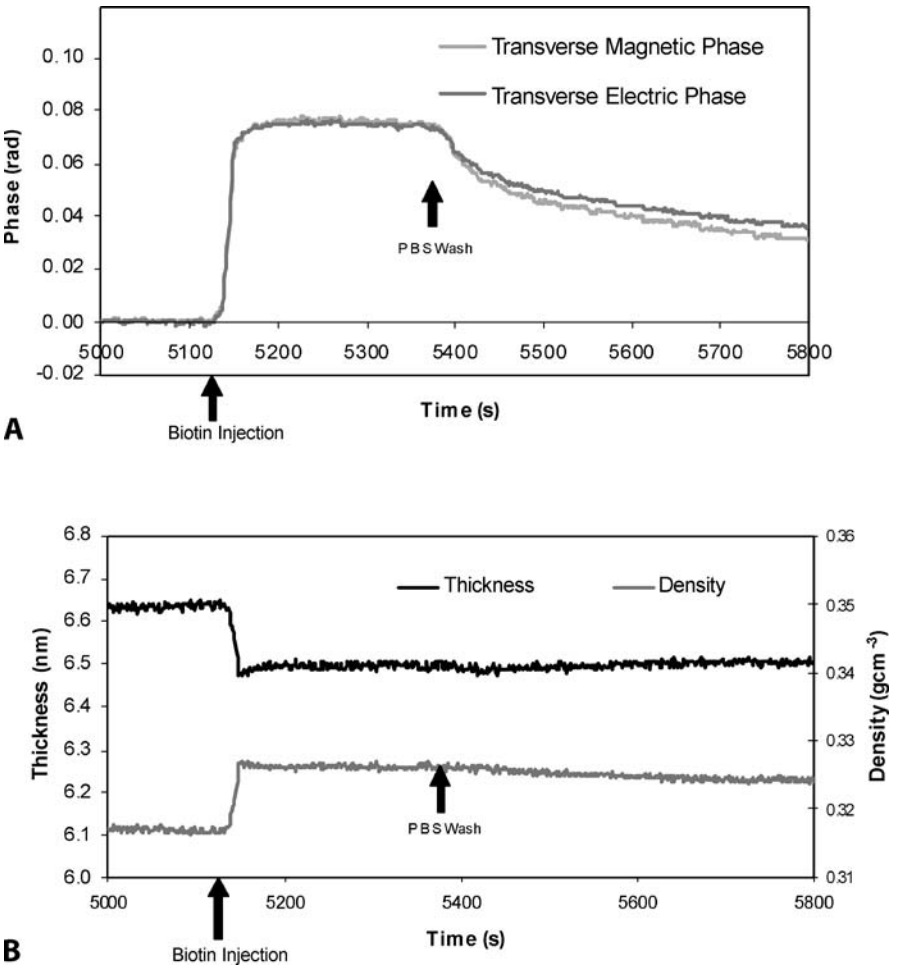

Fig. 9. Detail of the binding of free D-biotin to the streptavidin surface. **A** Raw phase data. **B** Resolved thickness and density over the same time period shown in **A** (Swann et al. 2004)

possible to calculate the mass of protein immobilised on the surface, the consequent mass of D-biotin bound and from the two, the stoichiometry of the interaction. Assuming 100% activity for the immobilised protein, the ratio of D-biotin binding to streptavidin was 2.1:1 which is extremely close to the 2:1 stoichiometry which would be expected if 2 of the available binding sites had been taken up in the surface immobilisation step.

It is generally accepted that when streptavidin binds to a biotin functionalised surface, two (of the four available) binding sites are occupied by surface immobilised species leaving two available for subsequent interactions (Jung et al. 2000). On binding D-biotin it is generally accepted that strepta-

vidin contracts. Studies by (Weber et al. 1989) suggest that a reduction in adlayer thickness of between 0.1 and 0.4 nm when comparing free streptavidin to the tetrameric adduct might be expected, depending upon the orientation of the protein. Data obtained using DPI to measure changes in a layer of bound streptavidin as it binds free D-biotin at pH 7.4 (Fig. 9), are in good agreement with the x-ray crystallographic evidence.

It is interesting to note from Figs. 8 and 9 that there is an apparent loss of material after the surface has been challenged with D-biotin (measured as phase shifts in radians for both the transverse electric, TE, and transverse magnetic, TM polarisations) on returning the solution phase to phosphate-buffered saline. This approximates to a loss, during the wash phase, of approximately 8 fg mm^{-2} s^{-1}. This process is not the reverse of the binding event. This might be attributed to the displacement of streptavidin from the surface as a consequence of the higher affinity of streptavidin for free D-biotin than for surface-bound D-biotin, as has been observed by Jung et al. (2000). The thickness and density profiles during the rinsing process support this hypothesis. The thickness during rinsing remains constant, whilst the density reduces very modestly implying that a small number of streptavidin molecules are removed during the rinse.

4.3.6 Protein Structure and Metal Ion Interactions

Transglutaminases

Transglutaminases are catalysts that are involved in the post-translational modification of proteins, forming isopeptide bonds at glutamine residues (Greenberg et al. 1991; Folk and Finnlayson 1997). The primary function of these enzymes appears to be in the stabilisation of tissues and, as such, their occurrence is widespread, being found in both extracellular and cellular fluids. There is evidence that transglutaminases may be bifunctional, also having capabilities to perform the role of G-proteins in cell signalling pathways (Monsonego et al. 1998; Nakoaka et al. 1994).

Factor XIII is one of the best characterised transglutaminases, being the last enzyme to be activated in the blood coagulation cascade, increasing the mechanical strength and chemical stability of blood clots. It is a tetramer consisting of two catalytic "a" subunits and two non-catalytic "b" subunits (which are thought to play a role in stabilising the "a" units). The protein-modifying activities of transglutaminases play a role in programmed cell death, cross-linking membrane and cytoskeletal proteins (Fesus et al. 1991; Siefring et al. 1978). This activity has been shown to be modulated by calcium and GTP (Achyuthan and Greenburg 1987; Bergamini et al. 1993). This modulation is thought to be related to putative conformational changes

induced by the modulators. Indirect analysis using shallow-angle neutron scattering and shallow-angle x-ray scattering (Cassadio et al. 1999) and circular dichroism spectroscopy (Di Venere et al. 2000) have suggested that there is a significant increase of 0.8 nm in the gyration radius of the protein on binding calcium, suggesting a significant broadening of the protein structure on binding. Efforts to elucidate conformational changes directly from crystallographic data have not been successful as it is thought that the active form (with calcium bound) is constrained by the crystal lattice (Fox et al. 1999). Reports on optical measurements of transglutaminase on the addition of calcium have also been reported in which anomalies in the expected responses have been attributed to likely conformational changes in the protein on binding calcium (Gestwicki et al. 2001).

Using DPI it has been possible to measure the conformational changes associated with calcium binding directly. The experiment was carried out as follows. The protein was immobilised to an amine functionalised sensor surface via free external amine groups on the protein using BS^3. A thickness increase of 5 nm was observed, which demonstrates that the disc-shaped molecule (approximately 15 nm in diameter and 5 nm thick) has been immobilised face-parallel to the chip surface, as would be expected using this immobilisation method. Once the protein surface was created, it was challenged with different concentrations of calcium chloride and chloride mole equivalents of sodium chloride. As can be seen from Fig. 10, the protein layer undergoes substantial conformational changes in the presence of calcium that do not occur in the presence of sodium. It was also possible, having conducted the experiment at a range of concentrations, to calculate the affinity constant for the interaction. The affinity constant has been calculated to be 1.16 mM, which compares well with the range of literature values for the interaction (0.2–3.0 mM; Mottahedeh and Marsh 1998). This clearly suggests that the structural changes observed are directly related to the binding of calcium.

4.4 Future Developments

The optical waveguide device can be considered to be an optical bench. As such, a wide variety of optical experiments can, in principle, be carried out either sequentially or, preferentially, simultaneously. Rather than listing the variety of such experiments, for the sake of brevity, just one extension to the DPI technique will be briefly discussed here.

Perhaps the most obvious additional experiment is to measure the extinction coefficient (the losses) of the sensing waveguide. These can be determined by measuring the contrast of the fringe image, which is a ratio-

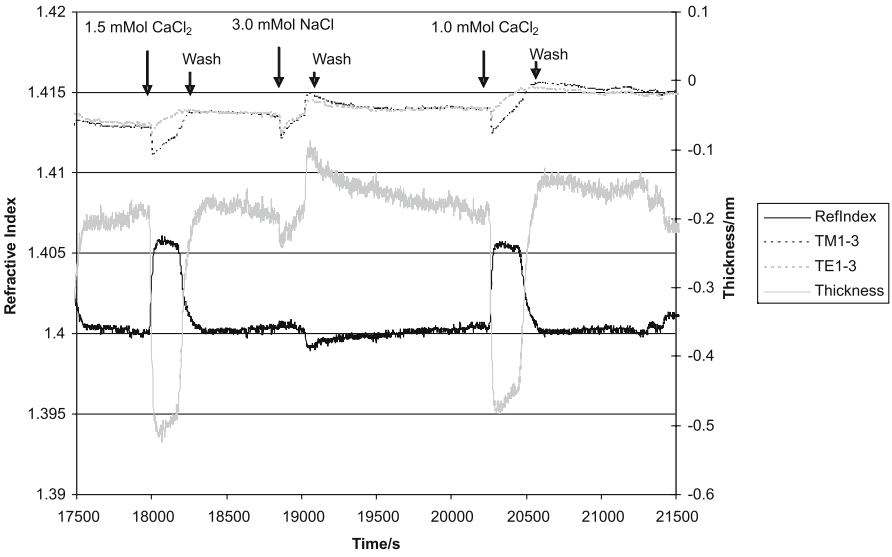

Fig. 10. The response of immobilised tissue transglutaminase to sodium and calcium chloride, demonstrating clear conformational changes with calcium but not with sodium. *Dashed lines* raw data, *Solid lines* resolved data, thickness and refractive (*Ref*) index

metric measure of the light passing down the upper (sensing) waveguide, and that passing down the lower (reference) waveguide. This data provides information on the structure of assemblies on the waveguide surface (e. g. nucleated or stochastic structures) and the degree of order (optical anisotropy) that they exhibit. Fringe image contrast has already been shown to provide a very valuable indicator of the early onset of crystallisation. Data relating to extinction coefficients is actively being developed at the present time. It has been demonstrated that the losses are not diffraction limited. Losses have been observed with particulates that are smaller than $\lambda/20$ (i. e. less than 32 nm). A full analytical solution for waveguide loss is now being sought to provide yet further information on the structure and orientation of proteins and the solid–liquid interface.

The other major area in which rapid developments are being made is the area of biological membrane mimics. There is considerable interest in proteins that reside in membranes and there is a strong requirement for the provision of biologically relevant membrane mimics on sensor surfaces. DPI is a particularly relevant measurement technique, as liposome and bilayer constructs can be monitored on the sensor surface, allowing the engineering of constructs that are similar to those found in nature. Technical progress and surface offerings relating to this area are expected to be dramatic.

4.5 Conclusions

It has been shown that DPI offers an analytical technique to provide information on the orientation and structure of proteins in real time. The technique relies on classical optics, which are well understood, and provides dimensional information to a very high resolution (typically better than 0.01 nm) and mass loadings to a resolution of around 100 fg mm^{-2}. It is possible not only to detect interactions between large proteins and small molecules, but also to quantify them and to determine stoichiometries. The technique described is not limited to the present measurement of thickness and refractive index of thin (protein) films, but has the potential to be extended to provide yet more detailed information relating to protein orientation and structure.

Acknowledgements. I would like to thank Professor David Fernig (Liverpool University), Dr. David Cullen, Dr. Kal Karim, Dr. Judith Taylor (Cranfield University), Professor Jian Lu (Manchester University) and Dr. Janos Voeroes (ETH Zurich) for their experimental expertise. I also gratefully acknowledge the experimental skills and diligence of Dr. Marcus Swann, Dr. Jonathan Popplewell and Dr. Louise Peel (Farfield Scientific) who undertook most of the experiments I have described. I would also like to Dr. Gerry Ronan (Farfield Scientific) and Dr. Marcus Swann for helpful discussions on the most appropriate ways to describe some of the physical concepts utilised by DPI. I would also thank Joanna Mosiezny (Farfield Scientific) for her patience and tenacity in preparing this document.

Appendix 1 DPI: Background

The need to obtain structural information and relate it to the function of proteins has never been greater. Below, one analytical technique, neutron reflection, and one sensor technique, SPR, are compared to demonstrate the strengths and weaknesses of the two approaches.

A.1.1 Neutron Reflection

As many biological processes occur at interfaces (Fragneto-Cusani 2001), an understanding of the structure of proteins as they function at the solid–liquid interface is very much sought after. One technique that has been used is neutron reflection. This has, over the last 25 years, been shown to be a very valuable technique for investigating inhomogeneities across such interfaces

(Fragneto-Cusani 2001). Data at the interface is obtained by measuring the reflected intensity of a well-collimated neutron beam in comparison to the excitation intensity. By comparing these measurements at a range of incident angles and excitation wavelengths, the concentration profile at the interface can be calculated. Given the short wavelengths of neutron radiation, the dimensions of the layer perpendicular to the interface can be obtained at sub-nanometre (i. e. molecular) resolution. In addition, the method can provide exquisite detail where it is possible to deuterate materials at the interface, as contrast variation can then be used to probe the cross-section of layers formed at the interface. The technique has not, however, been widely adopted by the life science community. This is due to the fact that the neutron reflection facilities, whilst having increased significantly worldwide, are remote centralised facilities, and the cost of access remains high. In addition, the temporal resolution is currently of the order of a minute or so (Bucknall et al. 1999), which is not sufficient to monitor the early stages of structural changes that proteins typically undergo. This is, however, a rapidly developing area and, as such, this limitation may be addressed.

A.1.2 Surface Plasmon Resonance

In the absence of the availability of structural information at an appropriate temporal resolution, several optical techniques have been utilised to provide information on the function of proteins. The most common optical method deployed has been SPR. The phenomenon of plasmon resonance was first observed in 1968 (Kretschmann and Raether 1968). The first commercial SPR based biosensors were released in 1990 and have proved useful in the study of equilibrium and kinetic aspects of the interactions of biological macromolecules (Shuck 1997). The basic optical configuration comprises a prism coated with a thin gold (or silver) layer (Fig. 11).

Light that is coupled into the prism is totally internally reflected at the metal-coated surface. When the angle of the incident light meets the resonant condition, surface plasmons, oscillating electromagnetic waves on the surface of the metal layer, are excited causing a reduction in the (energy) intensity of the reflected light. The surface plasmons have an associated electromagnetic field (evanescent field) that decays exponentially normal to the layer surface, which extends a few hundred nanometres from the metal surface. Changes in the refractive index (dielectric constant) within this region leads to changes in the observed resonance angle. Therefore, when macromolecules are adsorbed or desorbed in the immediate vicinity of the metallic sensor surface, the refractive index changes, leading to a commensurate change in the measured resonant angle. Commercially

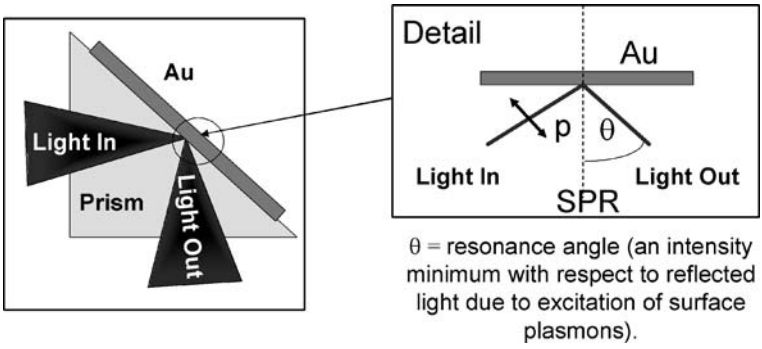

Fig. 11. Typical surface plasmon resonance (*SPR*) experiment

available instruments measure only the effective refractive index and therefore it is not possible to obtain analytical analyses of the structure of surface layers directly. Structural data cannot be obtained directly from SPR-based techniques, the information being confined to temporal information on the rate at which molecular associations and disassociations occur.

Appendix 2 DPI: Theory

There are two key aspects that need to be addressed to produce instrumentation of value to researchers in the field of drug discovery and protein science. The first is detailed information on complex three-dimensional molecular systems (proteins), the second is the exquisite sensitivity necessary to determine the binding of small molecules (drug molecules typically have a molecular mass of 200–500 Da) to large molecules (protein molecules span the range between 10,000 and 2,000,000 Da). Before we discuss the nature of DPI in detail, it is necessary to understand the basics of the propagation of light within a waveguide. A schematic is shown in Fig. 12.

It can be seen that whilst the majority of the light is confined to the core of the waveguide (depicted in grey), there is a residual, or evanescent, field that extends beyond the boundary of the core. The evanescent field can be seen to decay exponentially with distance from the waveguide surface and, as a result, only changes occurring within the first 100 nm or so of the waveguide surface will influence this field. Material changes in the refractive index in this region will affect the propagation speed within the waveguide as a consequence of changing the effective optical path. By allowing molecules of interest (e. g. proteins) to be attached to the sensing surface, it is possible to use this effect as a means to measure molecular interactions.

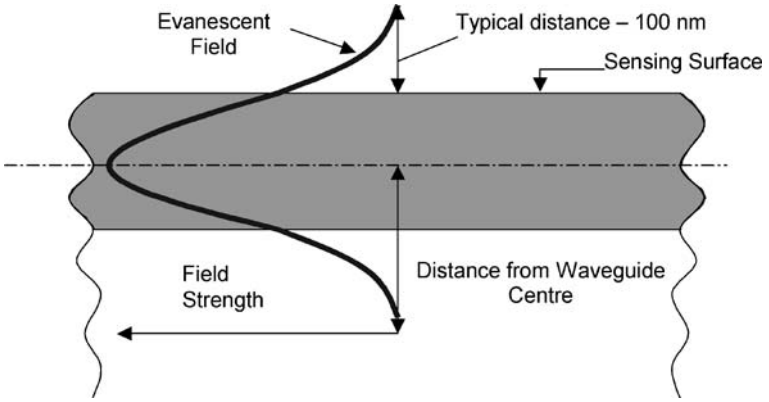

Fig. 12. Schematic of the optical intensity as light passes through a waveguide

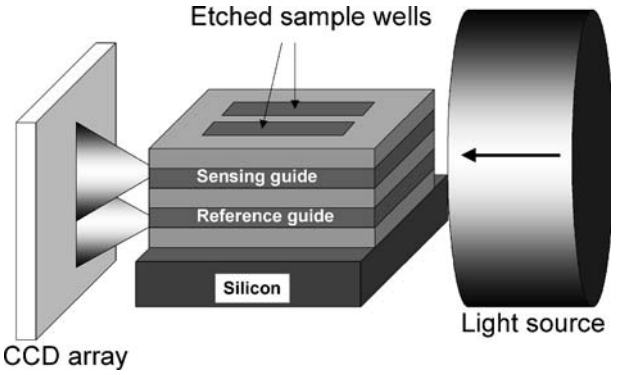

Fig. 13. Dual waveguide integrated inteferometer (Cross et al. 2004)

The precise measurement of optical path lengths can best be achieved using interferometric techniques. This involves comparing the path length of a measuring arm with that of a reference arm. DPI utilises a simple integrated interferometric configuration, as shown in Fig. 13. Here the optical path length of the upper sensing waveguide (variant) is compared with the optical path length of the lower reference waveguide (invariant). When the light is emitted from the structure and allowed to interfere in the far-field, the classic interference fringes of Young's famous double slits experiment are observed.

A comparison of the optical path lengths of the two waveguide arms is achieved as follows. First, the two waveguides are excited by a single coherent light source. The wavefront entering the interferometer is thus in phase on entering the structure. As molecules adhere to the surface of the sensing waveguide, changes in the refractive index at this boundary occur. This leads to changes in the effective optical path length of the top

waveguide only, which leads to changes in the phase between the light in the two waveguides. Thus, when the light now exits the two waveguides of the interferometer, they no longer hold the same phase relationship they did before the molecules were attached to the surface. This change manifests itself as a change in the position of the interference fringes.

Interferometers offer considerable advantages over angular measurements such as those made in SPR (see for comparison for Figs. 11 and 13), providing an exceedingly stable measurement platform with both high sensitivity and broad dynamic range. The stability of the measurement platform is achieved by the provision of a high-fidelity reference signal via the reference waveguide. Any minor deviations in the local environment or the output radiation will be compensated. The sensitivity is provided by measurement of the position of the interference fringes. Using standard algorithms it is possible to determine the fringe position to a very high accuracy, and therefore very subtle differences can be measured in the condition of the top sensing waveguide when compared to the lower reference waveguide.

So far we have described single-polarisation interferometry. This provides, albeit with extremely high sensitivity, very similar information to that provided using commercial SPR devices. Intrinsic to the physics of SPR is the restriction that monochromatic light of only a single polarization (TM) can excite the electromagnetic surface waves (Burrstein et al. 1974). The angular resonance position of excitation, whose measurement of change provides the basic assay data, is a single piece of information that reflects the changes to an optogeometric parameter of an interface layer that includes the average thickness and average density (through the refractive index) of the layer. It is not possible to unambiguously deconvolve these two aspects of the physical layer deposition (or removal) process (Flanagan and Pantell 1984).

At least two measurement parameters are needed to resolve the optogeometric parameters of a layer system. In areas of research demanding more detailed structural information, the output provided by such optical sensors may fall short of requirements. The folding and misfolding of proteins, for example, are increasingly topics of study in their connection with the onset of degenerative diseases such as Alzheimer's disease (Radford 2000). In the case of guided waves, no such restrictions to single measurements pertain.

In alternative evanescent wave techniques, an all-dielectric sensor surface is provided and excitation of bound or partially bound optical modes provides the measurement principle (Cush et al. 1993). In these structures, both TE and TM modes are allowed. Measurement of the excitation condition, by grating coupling for example, may be used to allow deconvolution of the thickness and refractive index of deposited layers (Nellen

et al. 1988). However, the individual modes are excited at well-separated coupling angles of incidence, which limits the rate and precision at which data collection can be performed and involves mechanical scanning over several degrees of arc.

Returning to DPI, the use of the second polarisation of light provides a second independent measurement of the layer condition. This relies on the fact that plane polarised light behaves differently in waveguide structures depending upon which polarisation is utilised. The differences in behaviour of the two polarisations result from the differences in the evanescent field profiles generated by the two polarisations. These are shown schematically in Fig. 14.

We can determine the expected optical path length for a given polarisation of light by invoking Maxwell's equations. Maxwell's equations describe how the electric and magnetic fields propagate through any medium. They describe how you must have an electric field if you have a magnetic one and vice versa, what the relationship between the two is, and the fact that they can only change in a gradual manner (no steps). They also relate the material properties to the field's propagation by describing two constants,

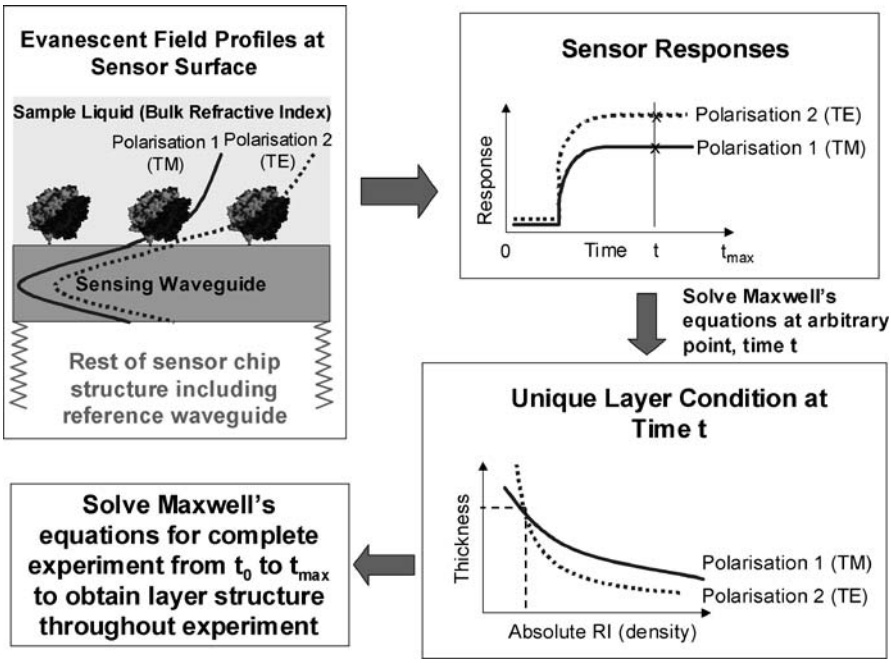

Fig. 14. Comparison of evanescent field decay in transverse magnetic (*TM*) and transverse electric (*TE*) polarisations and the subsequent responses when a layer structure is deposited. *RI* Refractive index

the dielectric constant for the material (the refractive index) and the magnetic permeability (which, assuming there is no magnetic material, is equal to 1). To solve Maxwell's equations, you start at the boundaries where you know the solution (in our case in the bulk liquid or in the middle of the waveguide stack where the values are zero and assume an arbitrary value in the waveguide itself) and at each interface you force the electric fields to be equal and the magnetic fields to be equal, but allow the field profiles to vary according to their relationships between these interfaces.

Having solved Maxwell's equations for one polarisation for light travelling along the waveguide and interacting with the thin film and whatever is above it (the bulk refractive index), you get a range of possible solutions where the phase could equate the thickness and refractive index of the layer. This is shown by the solid line in Fig. 14. Returning to Maxwell's equations, we can now look at the behaviour of the second polarisation. As can be seen in Fig. 14, the evanescent field profiles demonstrate different exponential decays with distance from the waveguide surface. In the first case the electric field was perpendicular to the waveguide and now, in the second, it will be parallel (and the magnetic field perpendicular). Now when we resolve Maxwell's equations, we get a different range of possible thicknesses and refractive indices for the deposited layer (see dotted line in Fig. 14). In effect, the waveguide appears to have a different refractive index for one polarisation when compared to the other.

The waveguide is obviously made of the same material so, assuming there is no optical or magnetic anisotropy (birefringence) that could cause this effect, the difference in optical properties must be entirely due to the physical geometries of the layer. When the two plots of allowable layer geometries are superimposed, one upon the other (see Fig. 14), a unique solution is obtained at the intersect, which corresponds to the actual optogeometric properties of the film. Thus, it can be seen that only modest assumptions (principally that the film is uniformly populated) need to be made in order to complete this analysis.

A more complete analysis of DPI can be found elsewhere (Cross et al. 2004).

Appendix 3 DPI: Implementation

A.3.1 Hardware

A schematic of the hardware employed to conduct DPI measurements is shown in Fig. 15. The output of a coherent light source, plane polarised (helium-neon laser, $\lambda = 632.8$ nm) is focussed (using a beam expander) on to the end face of a sensor chip (as described in Fig. 13). Between the light

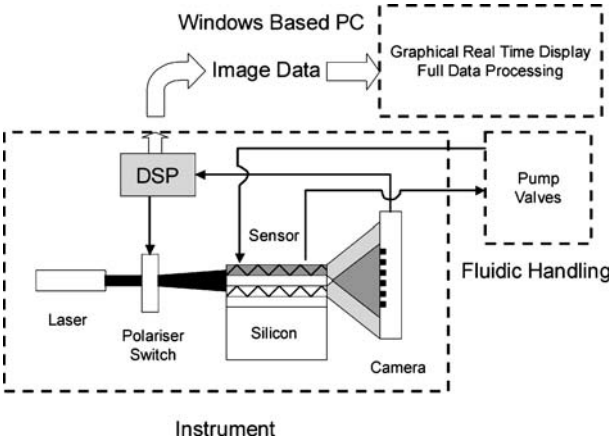

Fig. 15. Schematic diagram of a dual polarisation interferometer. *DSP* Digital signal processor

source and the waveguide structure there is a ferroelectric liquid crystal half-wave plate (polariser switch) to select the polarisation of light with which to excite the waveguide structure. This is controlled by the DSP, typically switching at 50 Hz. The high tolerance to input-coupling conditions of the waveguide structure is important here as refractive displacement of the beam occurs during the process of activating the polariser switch. However, displacement of the fringe image is observed during the switching process. The (diffracted) light output from the waveguide structure is allowed to fall on a camera (1024 × 1024 pixels). The image containing the interference fringe image is captured by the DSP. A fast Fourier transform algorithm is used to calculate any change in fringe position (phase) since the last measurement was made, and this is reported to an attendant PC. The polariser switch is set to admit the alternate polarisation and the process is repeated. These steps are repeated throughout the course of an experiment.

In addition to the optical train, there is also a fluidic train. The waveguide structure is brought into close proximity with a fluidic manifold that provides two flow-through cells, each of which is 2 µl in volume. One side of each flow cell comprises the active waveguide surface; it is this surface upon which proteins are immobilised and their behaviour and structure studied. The provision of the second flow cell enables biological control experiments to be conducted simultaneously. The fluidic set-up is such that standard high performance liquid chromatography equipment may be used (e. g. pumps, de-gassers and injection valves), which are familiar to most experimental practitioners.

As the instrument is measuring refractive indices to a very high accuracy, it is necessary to control the temperature very closely. An autonomous

Fig. 16. DPI. A bench-top instrument for the study of protein structure in real time (Cross et al. 2004)

temperature control unit using two-stage temperature control ensures that the temperature in the region of the waveguides is maintained at ±1 mK.

Once the data have been collected by the PC they are saved to disc and displayed in real time for the user to see. The data may also be resolved using Maxwell's equations to display the data in terms of thickness and refractive index. This information may be further manipulated to provide additional information such as mass per unit area and the volume fraction of the layer that is occupied. A dual-polarisation interferometer is shown in Fig. 16.

A.3.2 Data Analysis

Using the DPI techniques described above, it is possible to obtain thickness and refractive index data for layers deposited upon the surface of the sensing waveguide and calibrate the refractive index values for bulk solutions such as the phosphate-buffered saline running buffers. Given that the refractive index increments of proteins are quite consistent (Arwin 2000; Davis and Wilson 2000; Huglin 1972; Wen and Arakawa 2000), with typical values of 1.465, at a density of 0.71 g cm^{-3} it is possible to determine the mass of material deposited on the sensor surface using Eq. 1

$$\varrho_L = \varrho_p(n_L - n_s)/(n_p - n_s) \tag{1a}$$

$$m_L = \varrho_L \tau_L \tag{1b}$$

where ϱ_L is the adsorbed layer density, ϱ_p is the protein density, n_L is the adsorbed layer refractive index, n_p is the protein refractive index, n_s is the solution (bulk) refractive index, m_L is the mass loading per unit area and τ_L

is the adsorbed layer thickness. From the mass loading it is straightforward to calculate the area per molecule according to Eq. 2:

$$A = M_w/(N_a m_L) \tag{2}$$

where A is the area per molecule, M_w is the protein molecular weight and $N_a$is Avogadro's number.

By using the measured values for the refractive index of the bulk solution the volume fraction of the layer occupied by protein (ϕ_p) can also be calculated using Eq. 3:

$$\phi_p = (n_L^2 - n_s^2)/(n_p^2 - n_s^2) \tag{3}$$

After calculation of the parameters described above, it is possible to draw inferences not only regarding the gross structures of the deposited protein layers, but also the likely orientation of the protein molecules within the layers.

References

Achyuthan KE, GreenBurg CS (1987) Identification of a guanosine triphosphate–binding site on guinea pig liver transglutaminase. role of GTP and calcium ions in modulating activity. J Biol Chem 262:1901–1906

Arwin H (2000) Ellipsometry on thin organic layers of biological interest: characterization and applications. Thin Solid Films 377–378:48–56

Baird C L, Myszka DG (2001) Current and emerging commercial optical biosensors. J Mol Recognit 14:261–268

Bergamini CM, Signorini M, Caselli L, Melandri P (1993) Regulation of transglutaminase activity by GTP in digitonin-permeabilized Yoshida tumour cells. Biochem Mol Biol Int 30:727–732

Berman HM, Westbrook J, Feng Z, Gilliland G, Bhat TN, Weissig H, Shindyalov IN, Bourne PE (2000) The protein data bank. Nucleic Acids Res 28:235–242

Bucknall DG, Butler SA, Higgins JS (1999) ISIS Facility Annual Report 1998–99 RAL-TR-1998-050

Burstein E, Chen WP, Chen YJ, Hartstein A (1974) Surface polarisations – propagating electromagnetic modes at interfaces. J Vac Sci Technol 11:1004–1019

Cassadio R, Polverini E, Mariani P, Spinozzi F, Carsughi F, Fontana A, Polverino de Laureto P, Matteucci G, Bergamini CM (1999) The structural basis for the regulation of tissue transglutaminase by calcium ions. Eur J Biochem 262:672–679

Cross GH, Reeves AA, Brand S, Popplewell JF, Peel LL, Swann MJ, Freeman NJ (2003) A new quantitative optical biosensor for protein characterisation. Biosensors Bioelectron 19:383–390

Cross GH, Reeves A, Brand S, Swann MJ, Peel LL, Freeman NJ, Lu JR (2004) The metrics of surface adsorbed small molecules on the Young's fringe dual-slab waveguide interferometer. J Phys D Appl Phys 37:74–80

Cush R, Cronin JM, Stewart WJ, Maule CH, Molloy J, Goddard NJ (1993) The resonant mirror: a novel optical biosensor for direct sensing of biomolecular interactions.

Part I: principle of operation and associated instrumentation. Biosensors Bioelectron 8:347–354
Davis TM, Wilson WD (2000) Determination of the refractive index increments of small molecules for correction of surface plasmon resonance data. Anal Biochem 284:348–353
Davis TM, Wilson WD (2001) Surface plasmon resonance biosensor analysis of RNA–small molecule interactions. Methods Enzymol 340:22–51
Di Venere A, Rossi A, De Matteis F, Rosato N, Finazzi A, Mei G (2000) Opposite effects of Ca^{2+} and GTP binding on tissue transglutaminase tertiary structure. J Biol Chem 275:3915–3921
Fesus L, Piacentini M, Davies PJA (1991) Apoptosis: molecular mechanisms in programmed cell death. Eur J Cell Biol 56:170–177
Flanagan MT, Pantell RH (1984) Surface plasmon. Resonance and immunosensors. Electron Lett 20:968–970
Folk JE, Finnlayson JS (1977) The ε-(γ-glutamyl) lysine crosslink and the catalytic activity of transglutaminases. Adv Protein Chem 31:1–133
Fox BA, Yee VC, Pedersen LC, Le Trongi I, Bishop PD (1999) Identification of the calcium binding site and a novel ytterbium site in blood coagulation factor XIII by x-ray crystallography. J Biol Chem 274:4917–4923
Fragneto-Cusani G (2001) Neutron reflectivity at the solid/liquid interface: examples of applications in biophysics J Phys Condens Matter 13:4973–4989
Freeman NJ, Peel LL, Swann MJ, Lu JR (2004a) Lysozyme adsorption studies at the silica/water interface using dual polarization interferometry. Langmuir 20:1827–1832
Freeman NJ, Peel LL, Swann MJ, Cross GH, Reeves A, Brand S, Lu JR (2004b) Real time, high-resolution studies of protein adsorption and structure at the solid–liquid interface using dual polarisation interferometry. J Phys Condens Matter 16:S2493–S2496
Frostell-Karlsson A, Remaeus A, Roos H, Andersson K, Borg P, Hamalainen M, Karlsson R (2001) Biosensor analysis of the interaction between immobilized human serum albumin and drug compounds for prediction of human serum albumin binding levels. J Med Chem 43:1986–1992
Gestwicki JE, Hsieh HV, Pitner JB (2001) Using receptor conformational change to detect low molecular weight analytes by surface plasmon resonance. Anal Chem 73:5732–5737
Greenberg CS, Birckbichler PJ, Rice RH (1991) Transglutaminases: multifunctional crosslinking enzymes that stabilize tissues. FASEB J 5:3071–3077
Huglin MB (ed) (1972) Light Scattering from Polymer Solutions. Academic Press, NewYork
Jung LS, Nelson KE, Stayton PS, Campbell CT (2000) Streptavidins on mixed biotin-containing alkylthiolate monolayers. Langmuir 16:9421–9432
Karlsson R (1994) Real-time competitive kinetic analysis of interactions between low-molecular-weight ligands in solution and surface-immobilized receptor. Anal Biochem 221:142–151
Karlsson R, Kullman-Magnusson M, Hamalainen MD, Remaeus A, Andersson K, Borg P, Gyzander E, Deinum J (2000) Biosensor analysis of drug–target interactions: direct and competitive binding assays for investigation of interactions between thrombin and thrombin inhibitors. Anal Biochem 278:1–13
Kendrew JC, Bodo G, Dintzis HM, Parrish RG, Wyckoff H, Phillips DC (1958) A three-dimensional model of the myoglobin molecule obtained by x-ray analysis. Nature 181:662–666
Kretschmann F, Raether H (1968) Radiative decay of non-radiative surface plasmons excited by light. Z Naturforsch Teil A 23:2135–2136
Monsonego A, Friedmann I, Shasni Y, Eisenstein M, Schwartz M (1998) GTP dependent conformational changes associated with the functional switch between G document and crosslinking activities in brain-derived tissue transglutaminase. J Mol Biol 282:713–720

Mottahedeh J, Marsh R (1998) Characterization of 101-kDa transglutaminase from physarum polycephalum and identification of LAV1-2 as substrate. J Biol Chem 273:29888–29895

Muirhead H, Perutz MF (1963) Structure of haemoglobin. A three-dimensional Fourier synthesis of reduced human haemoglobin at 5.5 Å resolution. Nature 199:633–638

Nakoaka H, Perez DM, Back KJ, Das T, Husain A, Misono K, Im MJ, Graham RM (1994) Gh: a GTP-binding protein with transglutaminase activity and receptor signaling function. Science 264:1593–1596

Nellen Ph M, Tiefenthaler K, Lukosz W (1988) Integrated optical input grating couplers as biochemical sensors. Sens Actuators 15:285–295

Perutz MF (1963) X-ray analysis of hemoglobin. Science 140:863–869

Peters T (1985) Serum albumin. Adv Protein Chem 37:161–245

Radford SE (2000) Protein folding: progress made and promises ahead. Trends Biochem Sci 25:611–618

Ramsay G (ed) (1998) Commercial Biosensors: Applications to Clinical, Bioprocess and Environmental Samples. Wiley Interscience, New York

Salamon Z, Cowell S, Varga E, Yamamura HI, Hruby VJ, Tollin G (2000) Plasmon resonance studies of agonist/antagonist binding to the human δ-Opioid receptor: new structural insights into receptor–ligand interactions. Biophys J 79:2463–2474

Shuck P (1997) Surface plasmon resonance to probe the equilibrium and dynamic aspects of interactions between biological macromolecules. Annu Rev Biophys Biomol Struct 26:541–566

Siefring GE, Apostol AB, Velasco PT, Lorand L (1978) Enzymatic basis for the Ca++-induced cross-linking of membrane proteins in intact human erythrocytes. Biochemistry 17:2598–2604

Spaeth K, Brecht A, Gauglitz (1997) Studies on the biotin-avidin multilayer adsorption by spectroscopic ellipsometry. J Colloid Interface Sci 196:128–135

Su TJ, Lu JR, Thomas RK, Cui ZF, Penfold J (1998a) The conformational structure of bovine serum albumin layers adsorbed at the silica–water interface. J Phys Chem B 102:8100–8108

Su TJ, Lu JR, Thomas R K, Cui ZF, Penfold J (1998b) The effect of solution pH on the structure of lysozyme layers adsorbed at the silica–water interface studied by neutron reflection. Langmuir 14:438–445

Swann MJ, Peel LL, Carrington S, Freeman NJ (2004) Dual-polarization interferometry: an analytical technique to measure changes in protein structure in real time, to determine the stoichiometry of binding events, and to differentiate between specific and nonspecific interactions. Anal Biochem 329:190–198

Tiefenthaler K, Lukosz W (1989) Sensitivity of grating couplers as integrated-optical chemical sensors. J Opt Soc Am 6:209–220

Weber PC, Ohlendorf DH, Wendoloski JJ, Salemme FR (1989) Structural origins of high-affinity. biotin binding to streptavidin. Science 243:85–88

Wen J, Arakawa T (2000) Refractive index of proteins in aqueous sodium chloride. Anal Biochem 280:327–329

5 Total Internal Reflection Ellipsometry: Monitoring of Proteins on Thin Metal Films

Michal Poksinski, Hans Arwin

Abstract. A measurement technique based on ellipsometry performed under conditions of total internal reflection is presented here. This technique is called total internal reflection ellipsometry (TIRE). When extended with the surface plasmon resonance effect, TIRE becomes a powerful tool for monitoring protein adsorption on thin metal films. A brief description of TIRE is presented here together with some examples of measurement system setups. Two examples of applications are included, followed by a short presentation of possible future applications of TIRE.

5.1 Introduction

The main goal of this work is to review total internal reflection ellipsometry (TIRE) with special focus on its advantages for monitoring protein adsorption. The idea behind TIRE is not new; the background theory can be found in textbooks (Azzam and Bashara 1987; Pedrotti and Pedrotti 1996). However, the lack of powerful computing devices required for ellipsometric analysis has limited the development of TIRE (as well as its parent technique – ellipsometry) for quite a time. The situation has changed during recent decades, and TIRE has come to the attention of several scientists, who noticed its potential and advantages in many different areas of science (Bortchagovsky 1997; Okutani et al. 1998). Rekveld carried out some pioneering work using single-wavelength ellipsometry and a flow cell to study fibrinogen adsorption on titanium dioxide, but without sensitivity optimization (Rekveld 1997). Nowadays, depending on the application and experimental settings, TIRE can also be found under the names of internal reflection ellipsometry (IRE; Poksinski and Arwin 2004), (surface) plasmon enhanced ellipsometry ((S)PEE; Westphal and Bornmann 2002), or total reflection ellipsometry (TRE; Okutani et al. 1998). With enhancement of

Michal Poksinski, Hans Arwin: Laboratory of Applied Optics, Department of Physics, Chemistry and Biology, Linköping University, SE-581-83 Linköping, Sweden, E-mail: micpo@ifm.liu.se

Principles and Practice
Proteins at Solid–Liquid Interfaces
Philippe Déjardin (Ed.)
© Springer-Verlag Berlin Heidelberg 2006

the surface plasmon resonance (SPR) effect, this technique becomes powerful in the area of protein adsorption, where it is mostly used nowadays (Poksinski and Arwin 2004; Nabok et al. 2005). However, applications in other areas like liquid crystals (Okutani et al. 1998) and corrosion monitoring (Poksinski et al. 2003) are also of interest.

Development of measurement techniques in the area of protein adsorption is of special interest as it becomes more and more important to monitor proteins as close as possible to their natural environments. Interactions of different proteins with the surfaces of different materials are important to the scientific community (Caruso et al. 1997; Mårtensson et al. 1995; Tengvall et al. 1998). The TIRE technique is very attractive as it allows in situ studies of proteins adsorbed onto thin metal films, with a potential to provide the out-of-plane refractive index profile of the adsorbed material.

The objective of this work is to provide a general overview of the possible applications of TIRE for monitoring protein adsorption on thin metal films. The theoretical aspects of TIRE are presented in brief, followed by a description of experimental setups and examples of applications. Suggestions and comments about other possible applications are given at the end. More details regarding the theoretical aspects of TIRE, as well as sensitivity and accuracy considerations, can be found elsewhere (Arwin et al. 2004; Tompkins and Irene 2005; Poksinski and Arwin, unpublished data).

5.2
Total Internal Reflection Ellipsometry

Before discussing TIRE, it is useful to recall two important measurement techniques, one of which is based on the ellipsometric principle and the other on the SPR phenomenon. In brief, ellipsometry can be characterized as a measurement of the change of the state of polarization of light upon reflection on the sample surface (Fig. 1). As the light is not only re-

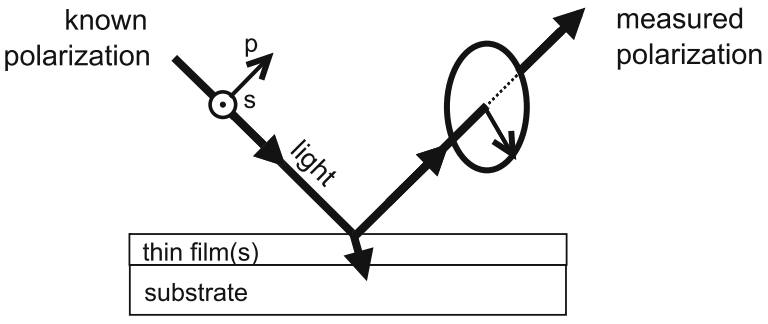

Fig. 1. The principle of ellipsometry (see text for details). *p* Parallel, *s* perpendicular

flected on the surface of a sample but also penetrates into the outermost material under the surface (and is then reflected and refracted further at each interface), the result of an ellipsometric measurement contains information about the optical parameters and morphology of the materials present (often as thin films) within the penetration depth of the light. The experimental data obtained from ellipsometry is usually expressed by the two parameters ψ and Δ (called ellipsometric angles). They are defined by the ratio ϱ of the complex-valued reflection coefficients R_p and R_s for light parallel (p) and perpendicular (s) to the plane of incidence, respectively, such that

$$\varrho = \frac{R_p}{R_s} = \tan\psi \exp(i\Delta) \tag{1}$$

The amplitude ratio of ϱ is thus given by $\tan\psi$, and Δ is the phase difference between the reflection coefficients in the p- and s-directions.

Ellipsometry is an indirect technique and ϱ contains all information about the structure and type of the investigated material in complex expressions. Thus, in most cases an ellipsometric measurement does not give direct information about one specific property of the sample. One exception is when measurements are performed on a flat ideal, film-free substrate; ϱ can then be directly inverted to provide the complex-valued refractive index of the substrate material. However, in general an appropriate optical model has to be developed and nonlinear regression has to be performed to obtain the values of the parameters of the material under investigation. Nowadays, modeling procedures are often built into the data acquisition software of ellipsometers. Also, databases of optical properties of various materials have been developed over the past decades (Palik 1985, 1991). All this makes ellipsometry a powerful measurement technique. More detailed information about ellipsometry can be found elsewhere (Azzam and Bashara 1987; Tompkins and McGahan 1999; Tompkins and Irene 2005).

Total internal reflection may occur when light is traveling from a medium with higher refractive index to a medium with lower refractive index, given that both media are transparent. Above a certain angle of incidence, called the critical angle, the light is totally reflected back into the higher refractive index medium, and no light passes into the low-index medium. However, due to the so-called evanescent field (Yeh 1988), part of the light penetrates the low-index medium. This forms the basis for the principles behind the SPR and TIRE.

The measurement technique of SPR takes its name from the phenomenon with the same name. SPR can be observed in many materials, but it is most significant in free electron materials, especially in metals like silver, gold, and copper. SPR can be excited under conditions of total internal reflection; a typical SPR setup is presented in Fig. 2 (Johansen et al. 2000b).

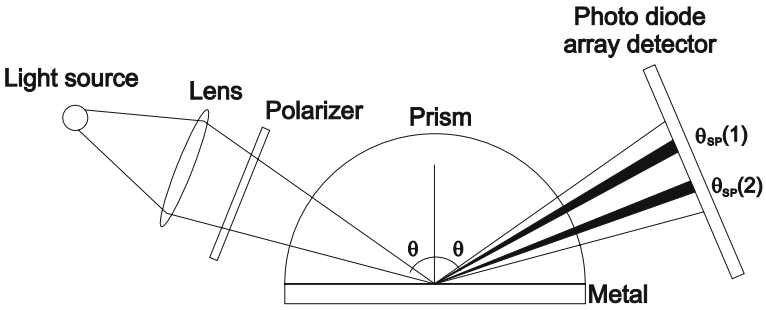

Fig. 2. Typical surface plasmon resonance setup with a fixed photodiode array detector and a focused light beam. Depending on the actual conditions (i. e., the refractive index of the adsorbed proteins) a surface plasmon can be excited at $\theta_{SP}(1)$ or $\theta_{SP}(2)$

The light, which has to be p-polarized is incident through the prism and is reflected at the interface between the glass and the thin metal layer. The requirements for excitation of SPR are fulfilled if the metal has suitable optical properties and thickness. The detector measures the intensity of reflected light. Under certain experimental conditions, which include angle of incidence, wavelength, and the presence and type of overlayer on the surface of the metal layer, all light can be coupled into a surface plasmon wave traveling along the metal surface. In this case no light is reflected and the detector reports zero intensity. When the angle of incidence is varied, a minimum (a "dip") in intensity is observed. The position of the dip turns out to be very sensitive to the presence of an overlayer on the metal surface and can be used for quantification (Johansen et al. 2000a). Nowadays, the SPR technique is widely used for studies of the behavior of proteins on various metal surfaces. Similarly to ellipsometry, this is an indirect technique, so modeling also needs to be applied to obtain information about the investigated material (adsorbed onto the metal surface). As SPR only has one measurement parameter (the changes in the dip position are monitored), it makes this technique powerful in the sensor area. Unfortunately, it is often very hard to obtain more complete information about the investigated material, so complementary techniques need to be applied.

The experimental setup used for TIRE (Fig. 3) is very similar to the SPR setup. However, in addition to the light source, polarizer, and detector, we introduce a second polarizer (called an analyzer), which is necessary to perform ellipsometric measurements. In the ellipsometric configuration described here, the analyzer is rotating. The detector signal is analyzed and provides ψ and Δ. In addition, notice that the polarizer azimuth is not in the p-direction as in SPR, but is typically fixed at 45° from the plane of incidence. Immediately one can observe the main difference between

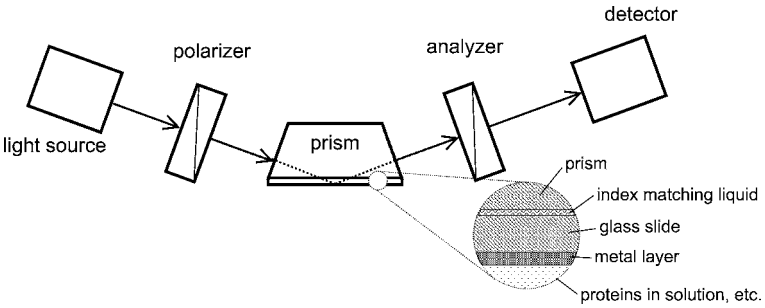

Fig. 3. Schematic view of the total internal reflection ellipsometry (TIRE) system (with a trapezoidal prism as an example). The magnified view (in the *circle*) shows the index-matching liquid inserted between the prism and glass slide, and the metal layer deposited on the glass slide (see text for details)

the TIRE and SPR techniques on one hand and traditional ellipsometry on the other: measurements are performed from the "back side" of the sample, in comparison to the "front side" measurements made in traditional ellipsometry. This is quite an advantage when in situ studies on protein adsorption are of interest – light does not need to travel through the liquid (which thus is allowed to be opaque), which minimizes disturbances in the measured signal. In comparison to SPR, TIRE provides two parameters, one containing information about intensity (ψ), quite similar to the intensity measured in SPR, and a second one, the phase difference (Δ), which is obtainable only in ellipsometry. If the measurement conditions are set so that the SPR effect is utilized, one can combine both techniques to obtain a powerful measurement technique with measurement detection limits normally unreachable for both traditional ellipsometry and SPR (Arwin and Poksinski, unpublished data). It should be noticed that in principle, the SPR effect is not necessary for the TIRE technique and it will still have some advantages (i. e., measurements is possible in opaque solutions), but the sensitivity will not be as good as when the SPR effect is employed. One should also notice that in most applications of the SPR technique, the angle of incidence is varied (with fixed wavelength), whereas in most cases of TIRE spectroscopy is performed (with a fixed angle of incidence). This should be noticed when comparing the results from both techniques.

The description presented herein is quite brief. However, it should be sufficient to get an overview of the phenomena and theoretical aspects of TIRE. Ellipsometry (Azzam and Bashara 1987; Tompkins and McGahan 1999; Tompkins and Irene 2005) and SPR (Liedberg et al. 1995; Raether 1988) are well-documented techniques, and complementary information about TIRE is also available (Arwin et al. 2004; Nabok et al. 2005; Poksinski et al. 2003; Poksinski and Arwin 2003, 2004; Rekveld 1997).

5.3 Experimental Setup

The most basic experimental setup for TIRE includes a glass slide with a thin metal film mounted on a prism and an ellipsometer. In addition, depending on the specific application and measurement conditions, components like a flow cell, a flow control system, application-specific data acquisition, and system control software are needed. These components can be universal, or application specific, depending on the user needs. The setup can be simplified to an absolute minimum if a sensor-type measurement tool is of interest, or extended with various additional components if complex analyses are in focus. It is impossible to give review of all possible experimental setups for TIRE, due to the continuous development and variety of possible setups. In the following paragraphs we try to give a general overview of the TIRE components of importance for protein studies, focusing on possible advantages and disadvantages of particular solutions. Examples of application-specific setups can be found later in this chapter. The suggestions and opinions presented here should be treated as comments and they certainly do not cover all possible aspects of the presented setups. One should notice that when a specific application is of interest, particular component types may depend on each other, and understanding of the right choice for the best possible results may not be straightforward.

The most specific part of the TIRE setup is a glass slide sample coupled to a glass prism. The samples may be the objectives for investigation by TIRE, or may serve as surfaces for additional treatments. In the case of protein adsorption studies, semitransparent metal layers are used. In principle, the metal layer can be deposited directly onto the prism surface, but in most cases it is deposited onto a glass slide, which then is mounted in optical contact with the prism. The glass slide should have the same optical properties as the prism. To avoid unnecessary interference from the prism–slide interface an index-matching liquid should be used. If TIRE should be extended with SPR, a thin layer of suitable metal (preferable gold, silver, or copper for the best effect) should be used on the glass slide. The thickness of the layer depends on the application, and again, in the case of SPR-enhanced TIRE it should be tuned to the specific application, prism type, and the wavelength range available on the ellipsometer. An example of a setup with an equilateral prism is presented in Fig. 4.

One of several possible prism geometries that can be used in TIRE is a triangular equilateral prism, which allows measurements at an angle of incidence of 60°. Other values for the angle of incidence are also possible with a 60° prism. However, one must then take into account the refraction of the incoming and outgoing light at the two prism–air interfaces, as the light is not incident normal to the prism surface. To obtain the best results,

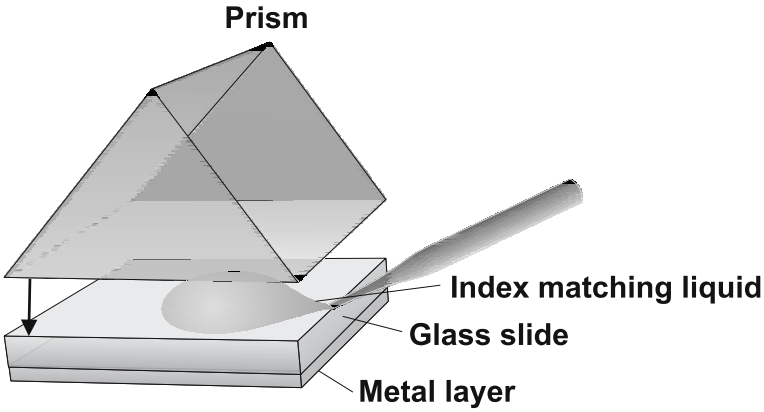

Fig. 4. Example of the prism and sample configuration for TIRE. Notice the index-matching liquid inserted between the prism and the glass slide and the metal layer deposited on the glass slide

a prism that is suitable for the specific application should be used. Again, in the case of protein adsorption studies, when the SPR effect is utilized, one should use a triangular (or for practical reasons trapezoidal, as the height of the prism increases with internal angle) prism with its internal angle close to the angle of incidence at which the SPR effect occurs for the selected wavelength, metal layer thickness, and material composition. To allow multiple angles of incidence one can use a prism with a polygonal shape, or a prism that together with the glass slide forms a half-cylindrical configuration; this is important to notice, as otherwise the light will be refracted on the air–glass interface, resulting in a different internal and external angle of incidence. With a half-cylindrical configuration, one also needs to remember that the incident parallel light beam from the ellipsometer has a certain, finite width and thus it will be focused at the side of the prism onto which the glass slide is mounted. This can minimize the sensing area, but also introduce unwanted effects due to the refraction of the peripheral parts of the beam on the prism surface. To avoid this, the light should be prefocused before entering the prism so that the whole beam is incident normal to the prism surface.

To be able to perform in situ studies, for example for monitoring the adsorption of proteins onto the surface, the prism and the glass slide with the metal layer have to be mounted in an appropriate flow cell. Virtually any type of flow cell can be used in a TIRE setup, although in most cases an application-specific design is preferred. In Fig. 5, an example of an injection-type flow cell is presented. In this type of cell the liquid is injected close to the sample surface and then pumped out from the top of the cell. The flow rate as well as solution mixing can be controlled by a computer-

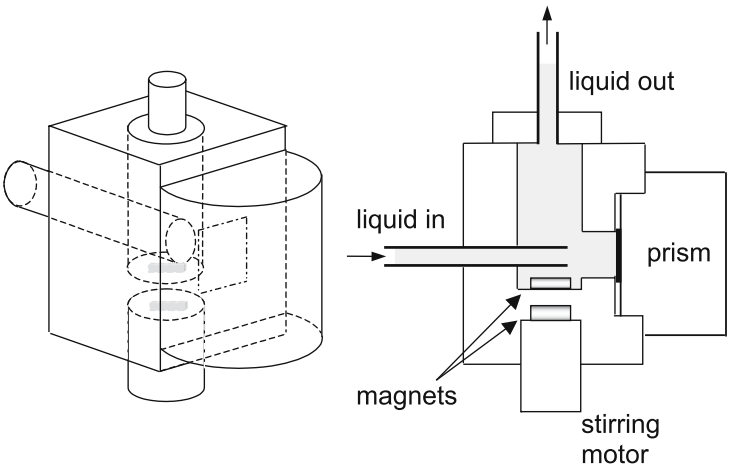

Fig. 5. Example of a flow cell used in a TIRE system for studies of protein adsorption. An half-cylindrical prism is shown here as an example

supported flow control system, either separate from or built into the data-acquisition software of the ellipsometer. Additional stirring in the cell can be achieved with the aid of a magnet rotated by an external motor, as shown in Fig. 5.

The measurement in a TIRE setup is performed with an ellipsometer. In most cases it is the most advanced (and expensive) part of the setup. TIRE can be performed with virtually any type of ellipsometer, either specially designed for the specific application or with a commercially available multipurpose ellipsometer. There are several types of ellipsometers available on the market today. They vary from very simple setups including laser-based single-wavelength ellipsometers with a fixed angle of incidence, to advanced multiwavelength, multiple-angle machines. Imaging ellipsometers with different scanning areas are also available. The wavelength range varies form ultraviolet to far-infrared. If a sensor-type setup for protein adsorption is of interest, one may pick up a green (502 nm) or red (632 nm) laser-based single-wavelength ellipsometer. For more detailed studies of, for example, multilayered protein structures, with full utilization of the SPR effect, a variable-angle spectroscopic ellipsometer is a better choice. An example on such an ellipsometer is shown in Fig. 6.

If measurements are to be performed in situ and a good monitoring over time is of importance one user a multiwavelength ellipsometer. This type of ellipsometer is capable of taking a full ellipsometric spectrum in a single shot, which speeds up measurements and provides much more data for analysis. A schematic illustration of a complete setup for TIRE is presented in Fig. 7.

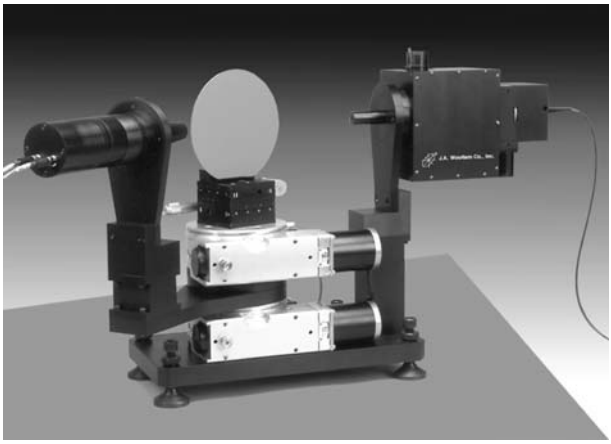

Fig. 6. Comercially available spectroscopic ellipsometer. Reprinted with permission from J.A. Woollam Co

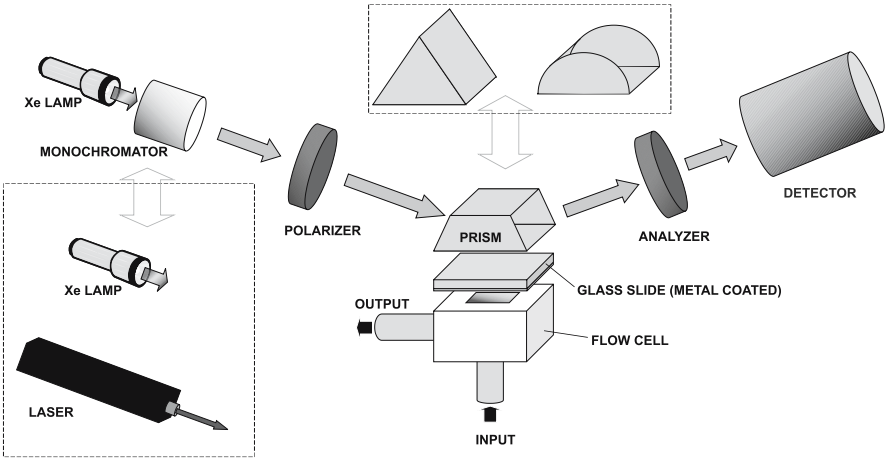

Fig. 7. A schematic overview of the TIRE system. Please observe the different prism configurations and ellipsometer systems available for measurements. With a white-light source (a Xe lamp without a monochromator), the detector must be wavelength selective (i. e., a grating with a diode array)

5.4 Application Examples

Three examples of possible applications of TIRE in the area of protein adsorption are presented here. The first example shows a potential for microstructural analysis of protein monolayers adsorbed onto metal films. The second example addresses problems with potential industrial rele-

vance. It also demonstrates one of the TIRE strengths – the possibility of measurement in opaque solutions. The final example illustrates a major TIRE advantage: extremely high sensitivity under SPR conditions. The experiments were performed with spectroscopic ellipsometers (M-88 and VASE) from J.A. Woollam; data analysis were performed with the WVASE32 software (J.A. Woollam Co).

In the first application example, TIRE is employed both in spectroscopic mode (in the wavelength range 400–1,200 nm) and in kinetic in situ mode for investigation of ferritin adsorption onto thin semitransparent gold films with a thickness of 43 nm. The measurements were performed at two angles of incidence: 60° and 65.5°. The second angle is optimized for the SPR effect for the gold layer thickness used. In this configuration the SPR phenomenon gives a large enhancement of the protein film thickness sensitivity. Adsorption of a monolayer of ferritin results in a change in Δ of more than 90° (Poksinski and Arwin 2004) compared to 3° in similar ordinary ellipsometric measurements on gold substrates (Mårtensson et al. 1995). This large sensitivity demonstrates a large potential for sensor applications. The 60° angle of incidence was included for comparison between SPR-enhanced TIRE and ordinary TIRE. Ellipsometric spectra before and after adsorption are presented in Fig. 8. Notice the difference in sensitivity between the two angles of incidence and the very large change in Δ close to the resonance (e. g., at a wavelength of 850 nm). The ferritin layer refractive index was then modeled with a Cauchy dispersion model, resulting in a layer thickness of 9.2 nm, which is in good agreement with the dimen-

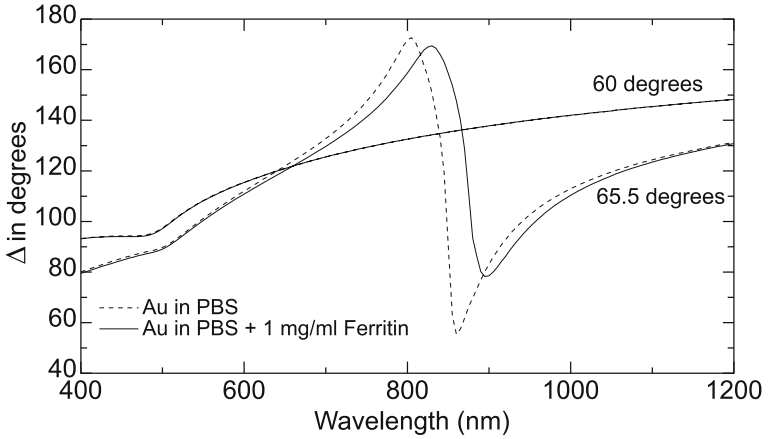

Fig. 8. Spectroscopic Δ data measured in TIRE mode on a thin gold film before and after the addition of ferritin to a final concentration of 1 mg/ml in a TIRE cell, recorded at the angles of incidence of 60° and 65.6°. The cell contains 2 ml of phosphate buffered saline (PBS). Reprinted with permission from Poksinski and Arwin (2004; copyright Elsevier)

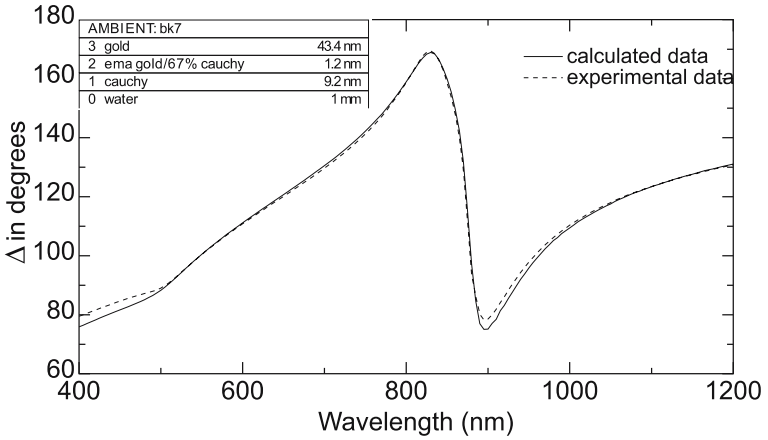

Fig. 9. Best fit to experimental TIRE data on a ferritin layer on a thin gold film. The insert shows the model used for the calculations. Reprinted with permission from Poksinski and Arwin (2004; copyright Elsevier)

sion of the ferritin molecules (Mårtensson et al. 1995). The fit is shown in Fig. 9 with the optical model as an insert. Further details, including the 1.2-nm interface layer, are described by Poksinski and Arwin (2004).

In the second example we demonstrate that TIRE can be used as sensor principle for measurements in a nontransparent ambient with the potential for industrial applications like in situ monitoring of growth of layers on the inside of pipelines. Adsorption from milk on gold, iron, and chromium surfaces, and subsequent cleaning with sodium hydroxide was chosen as a specific application example (Poksinski and Arwin 2003). The TIRE system used in this example was based on a rotating polarizer, multiwavelength ellipsometer (M88, J.A. Woollam Co.) equipped with a half-cylindrical prism configuration. The experiments were performed at an angle of incidence of 64° in the wavelength range 409–762 nm. The kinetic data reported here were recorded at 762 nm. Glass slides with 43-nm-thick layers of vacuum-deposited gold were exposed to water, milk, and NaOH in the order as presented at the bottom of Fig. 10. Adsorption and desorption onto the metal layer surface can be observed as changes in the ellipsometric angle ψ and Δ, as exemplified by Δ versus time in Fig. 10. To obtain a more detailed view of the adsorption process, spectroscopic data were taken at certain points (marked A–E in Fig. 10) during data acquisition. Spectroscopic data for an experiment using a gold layer are presented in Fig. 11. One should notice that the SPR effect was not fully utilized in this example due to the spectral range limitations of the ellipsometer used.

To further illustrate the large sensitivity obtainable, we show in Fig. 12 the kinetics of adsorption of human serum albumin (HSA) on a thin gold film.

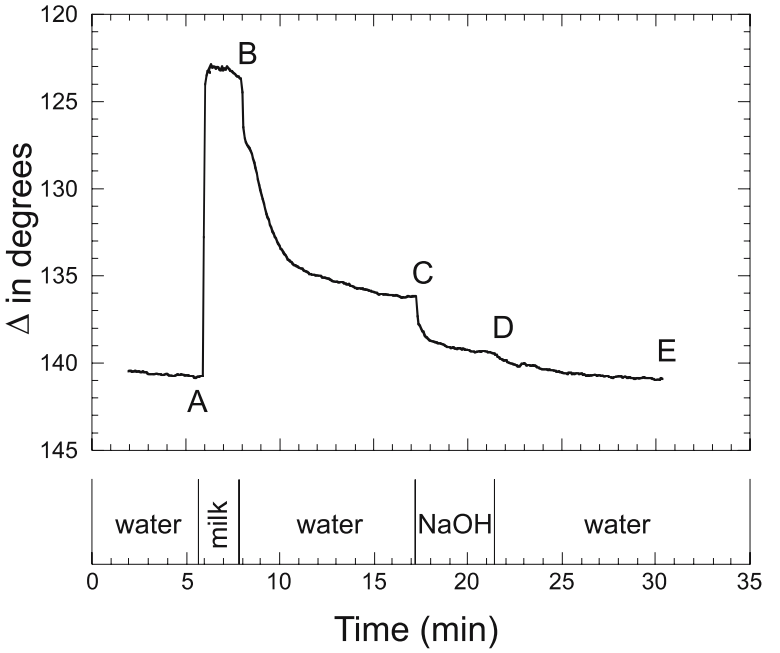

Fig. 10. Changes in the ellipsometric parameter Δ during adsorption from milk and subsequent cleaning on a gold surface measured at a wavelength of 762 nm and an angle of incidence of 64°. Changes in the liquid in the flow are marked with letters *A–E*. Reprinted with permission from Poksinski and Arwin (2003; copyright Elsevier)

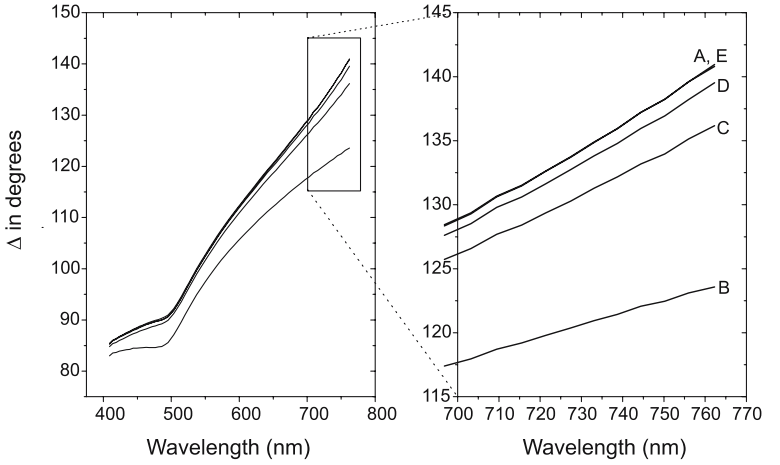

Fig. 11. Spectral ellipsometry changes due to adsorption from milk and subsequent cleaning. Spectroscopic data were measured in the wavelength range 409–762 nm at an angle of incidence of 64° (*left*). A magnification of part of the spectrum is also shown (*right*). The letters *A–E* refer to spectra recorded at times as shown in Fig. 10. For clarity, only Δ is presented. Reprinted with permission from Poksinski and Arwin (2003; copyright Elsevier)

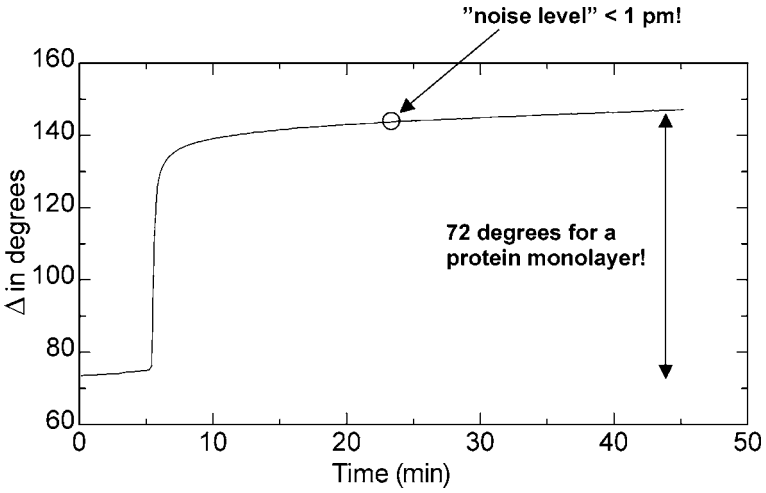

Fig. 12. Δ versus time in TIRE mode during adsorption of human serum albumin on a 45.8-nm gold layer in phosphate-buffered saline buffer (pH 7.4). The measurements were performed at an angle of incidence of 70° and a wavelength of 650 nm

HSA is a relatively small protein, and from the evaluation of ellipsometric data we find a layer thickness of 2.7 nm. Even for such a thin layer, we measure a change of 72° in Δ, with a noise level corresponding to an equivalent thickness of less than 1 pm.

5.5 Further Possibilities

The application examples mentioned earlier are just a few of the various experimental possibilities offered by TIRE. We would also like to point on two interesting applications for further studies. It can be observed that with appropriate tuning of the system (i. e., the combination of the components set up for the largest possible SPR effect) one can obtain sensitivities of several orders of magnitude larger in comparison to currently available similar techniques (e. g., ellipsometry, SPR). The large sensitivity of TIRE for thin layers opens up a pathway to analyze in detail the structure of thin protein layers. With further development of the models for the protein layers, mass distribution perpendicular to the surface may be resolved. Another application of TIRE can be a parallel study on, for example, protein adsorption performed simultaneously with TIRE and traditional ellipsometry with use of two ellipsometers on the same sample under the same measurement conditions. This will increase the information obtained in an experiment, and due to the specific response of each technique should allow more ac-

curate modeling of the layer (or layers) of adsorbed proteins. It could be especially useful when thicker multilayered protein complexes are used, as both techniques exhibit a reduced sensitivity with the increase of thickness of the adsorbed material. Both of these possible applications could allow better understanding of the behavior of proteins on metal surfaces.

Acknowledgements. We would like to thank Hasan Dzuho, Wojciech Grzegorczyk and Klaudia Sosnica for contributions to our TIRE development. We acknowledge the Swedish Research Council for financial support and the Knut and Alice Wallenberg foundation for generous support to instrumentation.

References

Arwin H, Poksinski M, Johansen K (2004) Appl Opt 43:3028–3036
Azzam RMA, Bashara NM (1987) Ellipsometry and Polarized Light. North Holland, Amsterdam
Bortchagovsky EG (1997) Proc SPIE 3094:239–249
Caruso F, Furlong DN, Kingshott P (1997) J Colloid Interface Sci 186:129–140
Johansen K, Arwin H, Lundström I, Liedberg B (2000a) Rev Sci Instrum 71:3530–3538
Johansen K, Lundström I, Liedberg B (2000b) Biosens Bioelectron 15:503–509
Liedberg B, Nylander C, Lundström I (1995) Biosens Bioelectron 10:I–IX
Mårtensson J, Arwin H, Nygren H, Lundström I (1995) J Colloid Interface Sci 174:79–85
Nabok AV, Tsargorodskaya A, Hassan AK, Starodub NF (2005) Total internal reflection ellipsometry and SPR detection of low molecular weight environmental toxins. Appl Surf Sci 246:381–386
Okutani S, Kimura M, Akahane T (1998) Jpn J Appl Phys 37:l600–l602
Palik ED (ed) (1985) Handbook of Optical Constants of Solids. Academic Press, Washington
Palik ED (ed) (1991) Handbook of Optical Constants of Solids II. Academic Press, San Diego
Pedrotti FL, Pedrotti LS (1996) Introduction to Optics. Prentice-Hall International, Upper Saddle River, NJ
Poksinski M, Arwin H (2003) Sens Actuators B 94:247–252
Poksinski M, Arwin H (2004) Thin Solid Films 455–456:716–712
Poksinski M, Dzuho H, Arwin H (2003) J Electrochem Soc 150:B536–B539
Raether H (1988) Surface Plasmons on Rough Surfaces and on Gratings. Springer Verlag, Berlin Heidelberg
Rekveld S (1997) Ellipsometric Studies of Protein Adsorption onto Hard Surfaces in a Flow Cell. Fedobruk, Enschede
Tengvall P, Lundström I, Liedberg B (1998) Biomaterials 19:407–422
Tompkins HG, Irene EA (eds) (2005) Handbook of Ellipsometry, William Andrew, Norwich, NY
Tompkins HG, McGahan WA (1999) Spectroscopic Ellipsometry and Reflectometry: a User's Guide. John Wiley & Sons, New York
Westphal P, Bornmann A (2002) Sens Actuators B 84:278–282
Yeh P (1988) Optical Waves in Layered Media, John Wiley & Sons, New York

6 Conformations of Proteins Adsorbed at Liquid–Solid Interfaces

Sylvie Noinville, Madeleine Revault

Abstract. Nonspecific adsorption of globular proteins induces conformational changes that depend upon both on the nature of the sorbent phase and on the structural stability of the protein. Because proteins can adopt various flexible three-dimensional structures under external perturbation, the surface contact with a sorbent phase can stabilise or not different conformers, which will influence the adsoprtion and desorption kinetics. Biophysical techniques such as Fourier transform infrared (FTIR) and circular dichroism spectroscopies enable the determination of the extent in secondary structures of the adsorbed protein at the aqueous–solid interface. Based on practical viewpoints of protein adsorption, we review the findings obtained in a wide range of sorbent phases such as mineral particles, colloidal systems, planar surfaces chemically modified by polymers, or self-assembled monolayers. We lay emphasis on the importance of obtaining insights into both structure and solvation during adsorption by the combined NH/ND isotope exchange and attenuated total reflectance (ATR)-FTIR techniques. We present illustrative cases of adsorption of proteins of low and high structural stabilities, bovine serum albumin and lysozyme, respectively, on either hydrophobic or hydrophilic supports.

6.1 Introduction

Over the past few years, numerous studies have aimed at understanding which driving forces govern protein adsorption at liquid–solid interfaces (Norde 1998, 2000). Spontaneous adsorption of protein molecules onto a solid sorbent will occur if the Gibbs energy of the system decreases. The enthalpic energy results from an electrostatic mechanism and H-bonding interactions, while the entropic contribution arises from the change of the initial ordered structure of the adsorbed protein as well

Sylvie Noinville, Madeleine Revault: Laboratoire de Dynamique, Interactions et Réactivité, CNRS-Université Pierre et Marie Curie, UMR 7075, 2 rue Henri Dunant, 94320 Thiais, France, E-mail: sylvie.noinville@glvt-cnrs.fr

Principles and Practice
Proteins at Solid–Liquid Interfaces
Philippe Déjardin (Ed.)
© Springer-Verlag Berlin Heidelberg 2006

as the rearrangement of water molecules and counterions at the interface. The protein folding is well known to be a highly cooperative process in solution. The denaturation of the globular proteins corresponds to a Gibbs energy in the 20–100 kJ mol^{-1} range, which is equivalent to the energy required for the disruption of 1–8 hydrogen bonds. Cooperative interactions do not involve the entire protein molecule, so that some partially folded conformations exist in solution as a result of local rather than global unfolding (Radford et al. 1992). When a denaturation process occurs in solution, the conformational entropy is offset by the enthalpy gain and the entropy loss due to the rearrangement of water molecules around the de novo external amino-acid distribution of the protein. When adsorbed onto a solid support, one external side of the protein molecules previously surrounded by water molecules is then in contact with the sorbent surface. Consequently, the mechanism of surface-induced conformational changes may be quite different from that causing protein unfolding in solution induced by denaturant addition or by heating. Recently, a high rate of partial unfolding of α-lactalbumin adsorbed on polystyrene (around 74 s^{-1}) was determined by nuclear magnetic resonance (NMR) experiments, compared to the lower rate of pH-induced global unfolding (Engel et al. 2004). Circular dichroism (CD) studies have shown the difference between the heat-induced unfolding of immunoglobulin and the surface-induced process when the protein is adsorbed on Teflon particles (Vermeer et al. 1998).

One common feature of the structure of the globular proteins is that the polar residues are located on the external surface and that most of the apolar amino acids are buried in the protein core. However, a significant fraction of the external surface of the protein molecule is composed of hydrophobic patches, which account for up to 40–50% (Branden and Tooze 1991; Dill et al. 1995; Richards 1977). If the external surface of the protein is polar as for the sorbent phase, some hydration water molecules are retained to solvate the protein charged residues and the surface charges. If the protein surface is rather apolar and the sorbent phase polar, or vice-versa, a dehydration of the protein–solid interface could occur. In the case of a hydrophobic character for both the protein surface and the solid support, structural changes of the proteins as well as variations in solvation states modify the entropy of the overall system (Boulkanz et al. 1997; Dorsey and Dill 1989; Gilpin 1993; Lu et al. 1998; Norde 1998). In some cases, the adsorption on hydrophobic supports induces a conformational change large enough to cause an average increase of the protein hydration (Boulkanz et al. 1995; McNay and Fernandez 1999). For both hydrophobic and hydrophilic supports, protein solvation and structural changes also depend on the pH and the ionic strength of the liquid phase, as these parameters indirectly influence the entropic forces (Baron et al. 1999; Giacomelli et al.

1999b; Haynes and Norde 1995; Kondo et al. 1991; Quiquampoix et al. 1993; Servagent-Noinville et al. 2000; Su et al. 1998b).

Of course, the adsorption process depends strongly on the chemical and electrical properties of the sorbent phase. Many studies concerning protein adsorption onto a polar charged support show that the major driving force is of coulombic nature (Gill et al. 1994; Lesins and Ruckenstein 1989; Quiquampoix et al. 1995; Servagent-Noinville et al. 2000; Su et al. 1998b). The design of electrostatically neutral surfaces is sought for their ability to reduce protein adsorption. In that case, the different hydration properties lead to repulsive hydration forces at close approach responsible for the inhibited adsorption (Herrwerth et al. 2003; Jeon et al. 1991). On hydrophobic supports, adsorption is driven by the reduction of interfacial energetics concomitant with the replacement of water molecules by the adsorbed proteins (Vogler 1998).

Besides these interactions between a single protein molecule and the solid phase, protein–protein interactions of either electrostatic or hydrophobic origin may also influence the accumulation of proteins at the liquid–solid interface. For both hydrophobic and hydrophilic supports, all of these parameters govern the specific orientation and the structure of the protein molecules inside the adsorbed layer (Malmsten 1998; Wahlgren et al. 1998). One approach with which to gain insight into the impact of hydrophobic or electrostatic interactions on the adsorption mechanism is to study protein adsorption on molecularly well-defined surfaces such as self-assembled monolayers (SAMs) on gold or silicon (Mrksich et al. 1995; Silin et al. 1997). Surface plasmon resonance (SPR) studies have shown that the propensity of SAMs of gradient wettabilities to adsorb proteins is related to the interfacial free energy of these surfaces, despite important exceptions (Sigal et al. 1998). Non-charged hydrophilic surfaces such as OH-terminated SAMs are generally correlated with low protein retention (Silin et al. 1997; Tengvall et al. 1998). Although ethylene-glycol-terminated SAMs are known to be highly resistant to protein adsorption, these supports are characterised by intermediate wettabilities (Herrwerth et al. 2003; Ostuni et al. 2001). The correlation between a macroscopic surface property such as wettability and protein adsorption seems to be restrictive to the choice of model proteins under investigation. However, a means with which to study the influence of one single isolated hydrophobic end-group on protein adsorption is provided by mixing two types of end-groups, one of which is a known repelling moiety, to build well-controlled hydrophobic patches inside the SAMs (Ostuni et al. 2003).

In general, the adsorption of proteins from aqueous solutions onto a solid support occurs via three major steps: (1) transport of protein molecules from the bulk to the interface, (2) contact of the protein molecules to the solid surface and (3) conformational changes of the protein molecules

during adsorption. Because the structural changes of the protein are kinetically controlled, accurate knowledge of the adsorption kinetics is of great importance. Most of the general patterns governing the kinetics of protein adsorption have been described in previous reviews (Brash 1996; Malmsten 1998; Ramsden 1998).

The structural rearrangement caused by the direct contact with the sorbent phase enables the existence of different conformers, which result from the way local unfolding could propagate along the entire molecule, depending on the intrinsic stability of the protein. In the case of strong protein–sorbent interactions, non-equilibrium states could be retained at the liquid–solid interface. Hence, protein adsorption could appear like an irreversible process, depending on different time scales. Moreover, structural changes of the protein involving more than 10% of the polypeptide backbone are generally associated with a spreading phenomenon, allowing a greater number of contacts with the sorbent phase (Jeon et al. 1994; Noinville et al. 2002; Su et al. 1998b). Hence, the desorption of even partially unfolded proteins becomes difficult. Besides, by spreading over the sorbent phase, the protein molecules delay or prevent the attachment of additional protein molecules. The adsorption rate and the conformational changes could depend on the surface coverage insofar as the adsorption takes place at a more and more modified interface. As a consequence, the layer of adsorbed proteins could be composed of a heterogeneous distribution of adsorbed conformers (Pitt and Cooper 1986; Zoungrana et al. 1997). A general trend in the adsorption of globular proteins is to distinguish between two classes associated with distinct adsorption behaviour in relation to their structural stabilities (Arai and Norde 1990; Kondo et al. 1991; Norde 1998). On one hand, the so-called "soft" proteins with low structural stability depict protein molecules with a high tendency to denature upon adsorption, even if the sorbent phase is weakly attractive (Table 1). On the other hand, "hard" proteins tend to adsorb less strongly on hydrophilic supports unless attractive electrostatic interactions prevail (Table 2). These hard proteins generally undergo minor conformational changes except when adsorbed onto hydrophobic supports. Recently, dynamic Monte Carlo simulations have corroborated the relationship between the native-state structural stability of the protein and its adsorption behaviour by computing the changes in the system entropy (Liu and Haynes 2005). One strategy to change the protein structural stability is to perform site-directed mutagenesis. The substitution of one single residue in the primary sequence of the protein provides mutants of different intrinsic stability and adsorption behaviour (Brash 1996; Malmsten et al. 2003). McGuire et al. (1995) studied protein adsorption of the wild type of bacteriophage T4 lysozyme and various mutants on flat silica surfaces. The variant with the lower structural stability displays the slowest adsorption kinetics, while it undergoes the largest

Table 1. Properties of "soft" proteins. *HAS* Human serum albumin, *BSA* bovine serum albumin, *β-Lg* β-lactoglobulin, *α-La* α-lactalbumin

Property	HSA	BSA	β-Lg	α-La
Molar mass (kD)	67	65	18.4	14
$\sum$Ni	586	582	162	123
Dimension[a] (Å^3)	30×80×80	30×80×80	36×36×36	37×32×25
Hydrophobicity[b] (J g^{-1})	–3.8			–5.8
10^{10}Compressibility[c] (m^2 N^{-1})	0.712	1.05	0.845	0.827
Isoelectric point	4.7	4.8	5.2	4.3
Secondary structure[a]				
%α-helix	67	67	10	29
%β-sheet	0	0	43	8
Reference	(Carter and Ho 1994)	(Carter and Ho 1994)	(Qin et al. 1998)	(Pike et al. 1996)
PDB entry[d]	1BMO		3BLG	1HFX

[a]X-ray data if available or sequence homology
[b]Privalov 1979
[c]Gekko and Hasegawa 1986
[d]Berman et al. 2000

Table 2. Properties of "hard" proteins. *Lys* Lysozyme, *Chym* chymotrypsin, *Cyt c* cytochrome c, *RNase* ribonuclease, *PDB* protein data bank

Property	Lys	Chym	Lipase	Cyt c	RNase
Molar mass (kD)	14	25	22	12	14
Dimension[a] (Å^3)	45×30×30	30×80×80	37×32×25	45×35×30	38×28×22
$\sum$Ni	129	245	269	104	124
Hydrophobicity[b] (J g^{-1})	–7.6				–8.7
10^{10} compressibility[c] (m^2 N^{-1})	0.467	0.415		0.339 [(e)]	0.112
Isoelectric point	11	8	4.4	10.7	9.4
Secondary structure[a]					
%α-helix	29	11	33	39	11.5
%β-sheet	6	51	26	0	33
Reference	(Wilson et al. 1992)	(Birktoft and Blow 1972)	(Lawson et al. 1994)	(Banci et al. 1997)	(Leonidas et al. 1997)
PDB entry[d]	1HEL	2CHA	1TIB	1AKK	1AFU

[a]X-ray data if available or sequence homology
[b]Privalov 1979
[c]Gekko and Hasegawa 1986
[d]Berman et al. 2000
[e]Chalikian et al. 1995

unfolding of α-helices, as shown by CD studies on silica nanoparticles (Billsten et al. 1998). The structural stability of the protein is a key factor in determining the rate of conformational changes for different mutants of human carbonic anhydrase I and II (Lundqvist et al. 2004; Malmsten et al. 2003). Recently, the rate of the surface-induced conformational change of the human carbonic anhydrase variants is indeed affected by the stability of the variant, but the average conformation of the final adsorbed state is not (Karlsson et al. 2005). Wild-type recombinant interferon γ and its Asp25-mutant have different adsorption behaviours, as studied on hydrophobic supports by Fourier transform infrared spectroscopy (FTIR) analysis (deCollongue-Poyet et al. 1996). The amount of the mutant adsorbed is lower than that of the wild-type protein. The contact with the hydrophobic support entails a different increase in the amount of polar helices and bend domains in mutant and wild types with respect to the conformation in solution. However, this mutation of one single residue does not change the protonation state of the interferon, but induces a local change in the packing of the α-helices. One drawback of site-directed genetic engineering or chemical modification used to modulate protein hydrophobicity or protein net charge is that it also alters the structure of the protein under study (van der Veen et al. 2004).

Due to the peculiar behaviour of protein molecules, the adsorption of protein to solid surfaces is the result of a large number of parallel and consecutive reaction steps, which render the study of the kinetics and thermodynamics of the protein–solid system difficult (Fang and Szleifer 2001). Models concerning the conformational changes of adsorbed proteins have been proposed for fitting experimental kinetics studies (Kridhasima et al. 1993; Pantazaki et al. 1998; Soderquist and Walton 1980). However, the main difficulty encountered in most theories of protein adsorption is to choose at which level to depict the protein–solid interface. As a starting point, the macroscopic description requires consideration of the globular protein as a rigid sphere with a net electrostatic charge on a plane surface (Roth and Lenhoff 1993). Some colloidal models account for conformational changes upon adsorption by considering the existence of different adsorbed conformers such as a folded state and a fully denatured state of the adsorbed protein (Van Tassel et al. 1998). A more sophisticated model is to depict the map of the protein surface, the distribution of positive and negative charges and the surface polarity. This methodology yields better predictions of interactions between like-charged proteins and surfaces (Asthagiri and Lenhoff 1997). The more sophisticated approach is to depict the protein using its three-dimensional structure. Early simulation studies of protein adsorption based on its full atomistic description have reported calculated energetics as a function of the orientation and the separation distance of the protein towards the surface in the case of uniformly charged support

(Yoon and Lenhoff 1992) or a polymer surface represented atomistically (Noinville et al. 1995; Roush et al. 1994). Most recent studies are focussed not only on the interaction energy and adsorbed amount, but also on the orientation of adsorbed proteins or peptides (Noinville et al. 2003; Zhou et al. 2003). Monte Carlo simulations of adsorption of immunoglobulins onto charged surfaces lay emphasis on the dependence of the protein orientation versus surface charge density, as previously shown experimentally (Zhou et al. 2003). A preferred orientation for the antibodies on the charged surface is determined when electrostatic interactions prevail over the hydrophobic ones. In all of these studies, the aqueous medium is described as a continuous dielectric medium. A simulation study of a small peptide of five residues is reported with explicit water molecules, demonstrating their orientational structure at a peptide–non-polar solid interface (Bujnowski and Pitt 1998).

6.2 Experimental Techniques

A short overview of the experimental methods currently used to follow adsorption kinetics is given in the literature (Kurrat et al. 1994). In this section, we will focus on biophysical methods that reveal the structural changes upon adsorption approaching the molecular scale. Then we will present methods that allow combined kinetics and structural data. Finally, we will detail methods that provide information about the distribution, orientation and solvation of the adsorbed proteins.

No experimental means of direct determination of protein structure are currently available at an atomistic scale when the protein is in contact with a solid surface. However, much progress has been made to gain structural insight at various aqueous–solid interfaces. In general, the biophysical methods allowing the determination of protein structure fall into two categories: one allowing high-resolution structural characterisation such as x-ray crystallography, neutron diffraction and NMR spectroscopy, and the second providing the extent of secondary structure or information on the tertiary structure using FTIR or CD techniques.

6.2.1 High-Resolution Structure of Proteins

Apart from x-ray crystallography and neutron diffraction dedicated to crystallised proteins, all other biophysical techniques that are well suited for proteins in solution could be adapted to interfacial analysis, although there

are limitations depending upon the heterogeneous character of the protein–sorbent phase under study. Recent progresses in NMR spectroscopy allows the determination of structures of small membrane proteins (up to 20 kDa) in detergent micelles (Booth et al. 2004; Tamm et al. 2003). This opens a new window into the study of the dynamics of proteins at the aqueous–fluid interface. A first high-resolution structural characterisation using solid-state NMR was carried out for statherin, a protein of around 5 kDa, adsorbed onto an inorganic support such as hydroxyapatite in the hydrated and lyophilised states (Long et al. 2001), enlightening the role of water in stabilising the helical structure of the adsorbed peptide. A combined study involving CD and NMR spectroscopies has shown the localised α-helix unfolding of small peptides adsorbed at an aqueous–colloidal interface (Read and Burkett 2003).

6.2.2 Secondary Structure of Proteins

The practical limitations encountered with high-resolution structural techniques such as isotope labelling, namely the size of the protein/colloid system and the size of the protein itself, mean that methods such as CD and vibrational spectroscopies remain attractive options. These low-resolution techniques provide a global estimation of the secondary structures (α-helix, β-sheet or random coil) without specifying the local region involved in the conformational transition. The latter techniques are suitable for studying proteins at liquid–solid interfaces in more or less restricted conditions. For CD spectroscopy, limitations arise from the significant scattering of the wavelength of interest due to the size of the sorbent particles. The use of silica nanoparticles of diameter not exceeding 20 nm has been developed specifically for CD experiments (Billsten et al. 1998). Adsorption of globular proteins of different structural stabilities has been studied by CD on charged silica nanoparticles (Giacomelli and Norde 2001; Kondo and Fukuda 1998; Kondo et al. 1991). These studies have shown that the largest conformational changes are observed for the adsorption of the less stable proteins such as BSA, myoglobin or haemoglobin. In contrast, the more rigid proteins such as cytochrome c, immunoglobulin G (IgG) and ribonuclease (RNase), which are characterised by their low adiabatic compressibility, are less unfolded by contact with the hydrophilic surface (Table 2).

Partially hydrophobic supports could be used for CD experiments by modification of silica particles by polymer silane coupling agents (Kondo et al. 1996) or by the use of Teflon latex nanoparticles (Giacomelli and Norde 2003; Zoungrana et al. 1997). Recent CD measurements of protein adsorption on silica nanoparticles of various diameters combined with

NMR have shown that the amount and the secondary structures of the adsorbed protein depend on the particle curvature (Lundqvist et al. 2004).

FTIR spectroscopy reveals not only changes in the global secondary structures of proteins (Byler and Susi 1986; Surewicz et al. 1993), but also allows determination of the average solvation states by hydrogen–deuterium (H/D) isotope exchange, as detailed later on (Mitchell et al. 1988; Muga et al. 1991) and can quantify the protonation states of the aspartate and glutamate side chains (Chirgadze et al. 1975). Transmission-FTIR spectroscopy is still used for direct comparisons between a protein in solution and the same protein adsorbed on various types of solid particles such as chromatographic supports (Boulkanz et al. 1997; Soderquist and Walton 1980) or clay minerals (Revault et al. 2005; Servagent-Noinville et al. 2000). The only limitation is a particle size not exceeding 10 μm. Conformational changes could be correlated with chromatographic retention times in the case of serum albumin and interferons (Boulkanz et al. 1995; Pantazaki et al. 1998).

A strategy for studying both adsorption kinetics and protein structural transition by FTIR is to use attenuated total reflection (ATR) mode at the liquid–planar solid interface (Ball and Jones 1995; Chittur 1998; van Straaten and Peppas 1991). In order to obtain a large variety of sorbent phases, many modification of the ATR crystal plate could be obtained either by deposition of lipids (Sharp et al. 2002) or polymers (Green et al. 1999; Lenk et al. 1989; Sukhishvili and Granick 1999) or by chemical grafting of SAMs (Cheng et al. 1994; Noinville et al. 2003). Adsorption kinetics may be monitored by measuring the time-dependent increase in the amide band in a flow system or in stationary conditions (Chittur et al. 1986; Jeon et al. 1992). The earliest ATR-FTIR experiments were devoted to the real-time adsorption kinetics of proteins of interest to biomaterials including immunoassays, protein chromatography, biosensors and biocatalysis (Cheng et al. 1994; Fu et al. 1993; Lenk et al. 1989; Müller et al. 1997; Ong et al. 1994). For instance, adsorption of IgG onto different supports was largely studied with respect to both the adsorbed amount and the structure to ensure antigen binding (Giacomelli et al. 1999a). The Y-shaped IgG molecules are composed of two F_{ab} segments and one F_c domain. The F_{ab} segments containing the binding sites show a different stability from the whole IgG molecules. The less structurally stable F_c fragment is more readily adsorbed than the F_{ab} fragments, thus affecting the orientation of the adsorbed IgG (Buijs et al. 1996).

6.2.3 Orientation, Localised Structural Information

The structural parameters of the adsorbed protein layers may be obtained by using intrinsic fluorescence spectroscopy on chromatographic supports

(Oroszlan et al. 1990), on silica and chemically modified silica slides (Buijs and Hlady 1997; Iwamoto et al. 1985). Furthermore, fluorescence polarisation measurements enable the study of the orientation and the rotational mobility of adsorbed proteins (Bos and Kleijn 1995; Tronin et al. 2002). Side-on or end-on orientations of lysozyme on hydrophobic and hydrophilic surfaces were deduced from kinetic measurements using FTIR (Wertz and Santore 2002). In some cases, polarised ATR measurements may allow the determination of the interfacial orientation of the protein in the adsorbed layer and have been mainly used to analyse the predominantly helical proteins inserted in lipid films (Frey and Tamm 1991; Houbiers et al. 2001; Martin et al. 2003). The molecular order of the whole protein is generally inferred from the measured dichroic ratios obtained for the stereoregular α-helical domains of the protein (Martin et al. 2003; Methot et al. 1996). On solid support, the molecular orientation of an α-helical peptide could be determined thanks to the specific hydrophobic interaction between the amphipathic peptide with the CH_3-terminated SAM (Noinville et al. 2003). The interpretation of polarised infrared data seems to be more difficult for the β-sheeted structure (Chittur 1998).

6.2.4 Spatial Distribution of Proteins in the Adsorbed Layer

Neutron reflectrometry in combination with water-contrast variation can probe the interfacial layer thickness with a resolution of a few angstroms and has provided information on mean structural conformations for globular protein layers at the aqueous–solid interface (Follows et al. 2004; Lu et al. 2005; Marsh et al. 1999; Tiberg et al. 2001).

Direct imaging methods like atomic force microscopy (AFM), surface force microscopy (SFM) and scanning tunnelling microscopy are well suited for probing the protein morphology on solid supports (Haggerty and Lenhoff 1993a). Most studies of the adsorption of proteins by AFM have been carried out using dry-sample imaging methods (Ortega-Vinuesa et al. 1998). The number of in situ experiments on adsorption at the liquid–solid interface is much more limited (Kim et al. 2002). These techniques provide complementary information about parameters such as the lateral distribution of protein molecules on surfaces and also allow direct measurements of forces between the adsorbent phase and a single protein (Claesson et al. 1995). With SFM, measurements of forces and distances between two proteins coated on mica surfaces have been evaluated for bovine serum albumin (BSA; Perez and Proust 1987) and for lysozyme (Haggerty and Lenhoff 1993b). By tracking the effect of the chemical properties using self-assembled monolayers as chemically patterned surfaces, many AFM

studies track the effect of the chemical properties as well as the surface topology of the sorbent support on the conformation of the individual protein molecules in the adsorbed layer (Li et al. 2003; Marchin and Berrie 2003; Patel et al. 1998; Wadu-Mesthrige et al. 2000).

6.2.5 Solvation Information

Upon exposure to D_2O, the amide proton of the protein backbone will exchange with the solvent deuterium. The H/D exchange rate depends upon pH, temperature and the structural environment of the amide proton (Gregory and Lumry 1985). Factors such as steric inaccessibility to the solvent, local charge distributions and internal hydrogen bonding will slow down the rate of amide proton exchange so that the kinetics of D_2O diffusion inside the protein core probes the accessibility of the solvent into random or structured internal domains and thus can give information on the protein tertiary structure. NMR or mass spectrometry and isotope-exchange techniques can be used to probe the tertiary structure or conformational stability of proteins (Huyghues-Despointes et al. 2001). For instance, these techniques were carried out for lysozyme before and after elution from reversed chromatographic phases (McNay and Fernandez 1999; Tibbs Jones and Fernandez 2003). The mass increase in the protein resulting from H/D exchange may be measured by mass spectrometry. For example, localised changes in the structural stability of myoglobin upon adsorption onto nanometer-sized silica particles have been studied with isotopic exchange mass spectrometry (Buijs et al. 2003).

Exchange-rate measurements can be performed directly on adsorbed proteins by infrared spectroscopy from the decrease of the so-called amide II absorption band as a function of pH (Servagent-Noinville et al. 2000). The amide II absorption band corresponds to the bending motions of the residual CONH groups resulting from the incubation of the protein in deuterated buffer. Two-dimensional (2D)-FTIR spectroscopy developed by Noda (1989) could be used to enhance the spectral resolution of both the amide I and II bands of proteins and to allow assignments of the conformation-sensitive component bands (Nabet and Pézolet 1997). Two-dimensional FTIR spectroscopy combined with isotopic exchange has revealed the assignment of the exchanging amide proton to changes in protein secondary structure induced by a ligand binding (Meskers et al. 1999). Surface-induced conformational changes of cytochrome c and of antimicrobial peptides have also been demonstrated by the use of 2D-FTIR spectroscopy (Lecomte et al. 2001; Noinville et al. 2003).

6.3 Surface Effects on Both Protein Structure and Solvation by the ATR-FTIR Technique

We investigate protein adsorption on three types of planar solid supports, classified as hydrophilic or hydrophobic model surfaces. The planar model supports are obtained by modifying the native silica surface of the ATR crystal with ω-functionalised alkylsilanes bearing a bromo or a methyl group at the end. The chemical transformation of the bromo-terminated SAMs enables the production of a polar aminated support (Noinville et al. 2003). Among the two hydrophilic supports, the native silica surface of the ATR crystal is used as a negatively charged surface, while the ND_2-terminated SAMs, still not protonated at pD 7.5, is considered as a neutral support. We will present infrared results performed with hydrosoluble proteins such as BSA and lysozyme chosen as illustrative cases of adsorption of respectively soft and hard proteins on the three different types of supports. Then we will present results that clarify the role of the protein nature and size specifically during adsorption onto hydrophobic supports.

Before reviewing the results concerning the surface-induced conformational changes, we introduce the specific processing of infrared spectra of proteins.

6.3.1 FTIR Spectral Analysis

Infrared spectra of proteins in aqueous media exhibit nine characteristic absorption bands, which represent different vibration modes of their peptide moiety. Among all the amide vibrational modes, the most frequently used in studies of protein secondary structure is the amide I band. This vibrational mode, which lies in the 1,600–1,700 cm^{-1} spectral range, corresponds to the stretching mode of the peptide carbonyls. This broad infrared absorption band, which is sensitive to protein conformation, is composed of multiple component bands whose wavenumber depends on whether the peptide carbonyls are hydrogen bonded to other peptide units, or to side-chains, or to the solvent. Each component band could be assigned to a different structural element such as the α-helix, β-sheet, or "free" peptide groups located in random hydrophobic or polar domains. Spectral correlation with the secondary structure in the amide I spectral region is well documented on model polypeptides (de Lozé and Fillaux 1972; Tsuboi 1964) and on a large number of globular proteins (Byler and Susi 1986; Goormaghtigh et al. 1994; Kalnin et al. 1990; Krimm and Bandekar 1986).

Because the broad amide I band is made of overlapping component bands, resolution enhancement techniques are necessary to extract useful structural information from the infrared spectra of proteins. The main mathematical methods used to analyse these infrared spectra are self-deconvolution or second-derivative processing and curve-fitting, and are well described in the literature (Dong et al. 1990; Dousseau and Pézolet 1990; Surewicz et al. 1993).

Prior to the infrared analysis, subtraction of the water contribution must be undertaken. Even if many algorithms are now available to subtract the water contribution from the infrared spectra of proteins, this protocol should be used with caution when dealing with adsorbed proteins. Indeed, the adsorption process could induce a change in solvation of both the proteins and the solid support. As a result, the water molecules present at the interface could be involved in hydrogen bonding, which shifts the broad water contribution band and render the subtraction of their infrared contribution difficult (Giacomelli et al. 1999a). The main advantage of performing infrared analysis of proteins in D_2O is to allow a direct comparison between the solvated state and the adsorbed state of the protein. With regard to determination of the secondary structure, a few minutes of incubation of the protein in a deuterated medium is enough to shift the amide I band from 2 to 10 cm^{-1}. Assignments of component bands of the so-called amide I' band are reported in different works on globular proteins (Chirgadze and Brazhnikov 1974; Goormaghtigh et al. 1994). The great advantage is the shift of the disordered component band of amide I centred at 1,650 cm^{-1} in H_2O to 1,640 cm^{-1} in D_2O, whereas the component bands relative to ordered structures (α-helices, β-sheets) are less affected upon deuteration (Wantyghem et al. 1990).

In our procedure, the curve fitting is performed on both the amide I' and amide II spectral regions and calculated as a linear combination of individual band components by iterative adjustments of only the heights of the components, the other parameters like profiles, widths and wavenumbers being fixed. Then the fractional areas of the band components are assumed to represent percentages of the different types of ordered or random domains of the protein. Since FTIR spectra and mathematical decompositions are all run in the same way, the resulting difference in the spectral analyses between the adsorbed state and the state in solution reveals semi-quantitatively the structural transition upon adsorption (Baron et al. 1999; Noinville et al. 2002; Revault et al. 2005; Servagent-Noinville et al. 2000; Wantyghem et al. 1990).

Moreover, the use of deuterated media enables the researcher to follow the NH/ND exchange of the all amide protons of the protein backbone by examining the reduction of the amide II band. Since the NH/ND exchange rate slows down with the strength of hydrogen bonding involved in stereo-

regular structures, it is also possible to extract information on the protein stability.

6.3.2 Proteins in Solution

A protein may adopt in solution various structures with more or less subtle differences, depending on temperature, protein concentration, pH, ionic strength or addition of co-solvent or lipids. The rapid FTIR analysis is well suited to probe the extent in secondary structures of the protein in the solution state used as reference for the adsorption experiments.

As an illustration, the lists of the amide I' component bands identified via second-derivative methods are reported in Table 3 for BSA and lysozyme in deuterated phosphate buffer (Noinville et al. 2002; Servagent-Noinville et al. 2000). For α-helical proteins such as BSA, our infrared spectroscopic analysis distinguishes a major group of regular helices giving a component band at 1,651 cm^{-1} from a minor group of irregular helices at 1,660 cm^{-1}. This latter component band at a higher wavenumber is attributed to helices packed in a more hydrophobic environment (Dousseau and Pézolet 1990; Rothshild and Clark 1979). Our results show that BSA is stabilised by a large amount of α-helical domains, representing 53% of the overall polypeptide backbone at pD 7.5 (Table 3). The x-ray structure of homologous serum albumins such as human serum albumin (HAS) gives approximately 67% of the α-helix (Carter and Ho 1994). The stability of the secondary structure of BSA is known to depend on pH. Previous infrared analysis based

Table 3. Assignments of the amide I' components and extent in secondary structure elements (expressed as a percentage of overall amide I' area) of BSA and lysozyme incubated for 4 h in deuterated phosphate buffer at pD 7.5

Assignments to ν(CO) peptide carbonyls	BSA		Lysozyme	
	Wave number (cm^{-1})	Area (%)	Wave number (cm^{-1})	Area (%)
Random domains	1681	12	1689	18
Random domains	1671		1670	
Hydrophobic α-helices	1660	14	–	–
α-helices	1651	39	1652	34
Hydrated random domains	1640	13	1641	27
Bent, β-strands or β-sheets	1630	23	1630	11
Self-association	1612	2	1610	10
Reference	(Servagent-Noinville et al. 2000)		(Noinville et al. 2002)	

on the same spectral decomposition predicted a 61% helix content for BSA at a pD equal to its isoelectric point (Servagent-Noinville et al. 2000). The intramolecular hydrogen bonds, visible at 1,630 cm^{-1} involving approximately 23% of the peptide groups correspond to bent domains in the BSA backbone. This is in agreement with secondary structure predictions estimating that around 23% of the structure in extended chain conformation would be predicted as β-strand (Carter and Ho 1994). In the random coil domains, BSA presents 13% of its carbonyl groups from peptide bonds involved in hydrogen bonding with water (1,640 cm^{-1}). Other random coil domains represent 12% of the BSA backbone, and self-associated domains only 2% (Table 3). The component band located in the 1,610–1,620 cm^{-1} spectral region appears mainly after denaturation of a protein, as reported for cytochrome c (Muga et al. 1991) and for lectins (Wantyghem et al. 1990). This low wavenumber component is attributed to peptide CO, which is involved in intermolecular β-sheets or in self-association or aggregation, and is often found in amyloid peptides or in oligomeric prions (Revault et al. 2005; Sokolowski et al. 2003).

While the crystal structure of lysozyme reveals that 28% of the residues are in α-helical conformation (Wilson et al. 1992), the FTIR analysis gives an α-helix content of 34%. The crystallised lysozyme also contains a relatively high amount of 3_{10}-helix (11%). If we assume that the absorption frequencies of 3_{10}-helix and α-helix are closed enough to form only one component band at around 1,650 cm^{-1}, the helical content in lysozyme reaches 39%. Different infrared absorption frequencies for this infrequent 3_{10}-helical conformation in globular proteins have been found in the literature. It has been proposed that 3_{10}-helices absorb at a lower frequency than α-helices in D_2O solutions due to their tighter geometry (Prestrelski et al. 1991), rather than at 1,665 cm^{-1} as previously reported (Krimm and Bandekar 1986). The amount of hydrogen-bonded peptide CO with water molecules found for lysozyme is rather large (around 27%). Following the attribution given by Prestrelski et al., some of this H-bonded peptide CO absorbing at 1,640 cm^{-1} would in fact be involved in a 3_{10}-helix. Concerning β-structure, only 6% of the residues in the crystalline state of lysozyme are in β-strands (Wilson et al. 1992), whereas 11% of H-bonded peptide groups involved in β-structure are found by FTIR. Some of the peptide carbonyls considered as turns (35%) or as bends (4.6%) in the secondary structure from the x-ray data are interleaved between peptide CO involved in β-strands so that they could either contribute to the infrared band at 1,630 cm^{-1} if hydrogen-bonded, or to the infrared band attributed to peptide CO involved in loops in polar environments at 1,670 cm^{-1} if non-hydrogen bonded (Wantyghem et al. 1990).

6.3.3
Surface-Induced Conformational Changes of a Soft Protein: BSA

In general, proteins with low structural stability tend to adsorb on both hydrophobic and hydrophilic supports via a gain in conformational entropy. In the case of hydrophilic support, the soft proteins undergo more severe unfolding of the ordered structure because of a stronger increase in conformational entropy to compensate for the repulsive coulombic interaction on an electrostatically repelling surface.

Changes in Solvation due to Adsorption

The NH/ND exchange that BSA undergoes in response to exposure to the deuterated buffer is monitored by the amide II:amide I' ratio measurements and is shown in Fig. 1. At time zero, the exchange always involves the fully CONH protein. Within 10 min of incubation in deuterated buffer, 70% of the peptide CONH in BSA becomes COND, corresponding to the fast-exchangeable peptide protons of the readily water-accessible external residues of the protein. It takes more than 2 h to further exchange 12% of peptide NH of the BSA backbone. These slower-exchanging protons are located in the more internal domains or in the more hydrophobic secondary structures of the protein (Gregory and Lumry 1985). The right part of Fig. 1 shows the residual NH content and the protein adsorption density (Γ) recorded over time concomitantly during BSA adsorption on negatively charged hydrophilic (Fig. 1A), neutral hydrophilic (Fig. 1B) and hydrophobic support (Fig. 1C).

On hydrophobic support (Fig. 1C), BSA is adsorbed quite fast, within 10 min, while the peptide NH content decreases drastically to 5%. The larger solvation of the peptide carbonyls induced by adsorption is due to the diffusion of D_2O molecules into the protein core and is directly correlated with the changes in secondary structure of BSA (Fig. 2C). The BSA molecules lose 12% of their helical domains when they become adsorbed onto the CH_3-terminated SAMs, while the bent domains remain unchanged. The large unfolding of both the hydrophobic and polar helices involves the increase in the extent of self-associated and hydrated random domains, respectively (Servagent-Noinville et al. 2000). The internal hydrophobic domains of the protein are drafted towards the hydrophobic surface, increasing the solvation of 15% of the overall polypeptide backbone (Fig. 1C). The penetration of D_2O molecules into the adsorbed proteins is correlated specifically with the increase in the content of the hydrated random domains (Fig. 2C). A similar structural transition has been observed for HSA adsorbed onto a reversed-phase chromatographic support (Boulkanz et al. 1997).

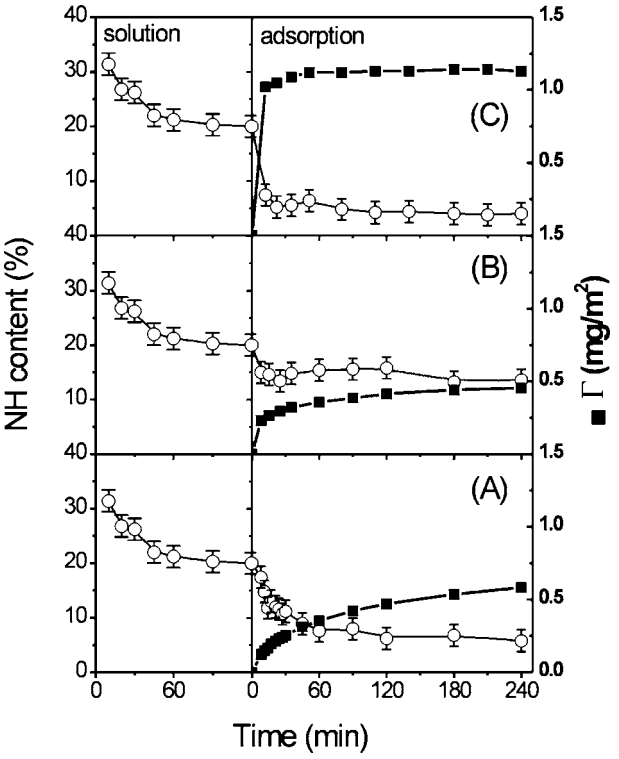

Fig. 1. Solvation changes (-○-) and adsorbed amount (-■-) of bovine serum albumin (BSA) adsorbed at a bulk concentration of 500 μg ml^{-1} in deuterated phosphate buffer and pD 7.5 onto different solid supports: a pure silica surface (**A**), ND_2-terminated SAMs (**B**)and CH_3-terminated SAMs (**C**). The left part of the graphs (i.e. left of time 0) shows the isotope exchange of the BSA in solution prior to adsorption (right part). The residual NH content (expressed as a percentage of the overall peptide carbonyls) is monitored by the amide II:amide I' ratio measurements. The adsorbed amount (Γ) of BSA is calculated from the adsorption density equation (Sperline et al. 1987)

In contrast with the adsorption onto a hydrophobic support, the adsorption onto hydrophilic supports leads to weaker adsorbed amounts of BSA. At a pH above the isoelectric point, the negatively charged BSA molecules do adsorb onto the negatively charged silica surface, but change their solvation states. Indeed the residual NH content of BSA decreases from 20% to around 5% as the surface coverage increases on the negatively charged silica. This change in tertiary structure due to the contact of the protein with the repelling silica surface is also linked to the large unfolding of α-helices involving 13% of the overall peptide carbonyls (Fig. 2A).

The adsorption of BSA on the ND_2-terminated SAMs is as slow as those on the repelling hydrophilic surface, but entails a weaker NH/ND exchange

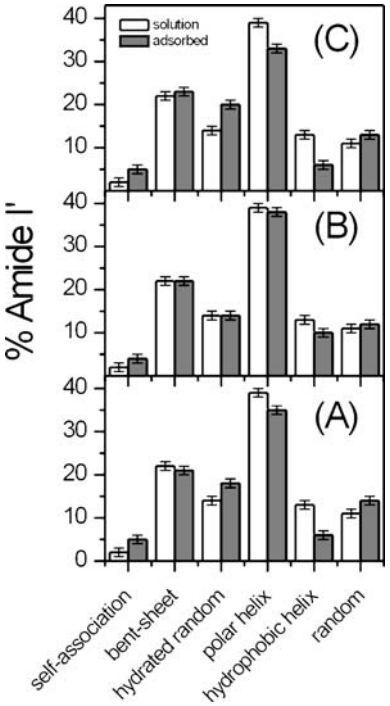

Fig. 2. Comparison of secondary structures of BSA resulting from our spectral analysis in a deuterated solution and adsorbed at a bulk concentration of 500 μg ml^{-1} and pD 7.5 on different solid supports: a pure silica surface (**A**), ND_2-terminated SAMs (**B**) and CH_3-terminated SAMs (**C**). The given percentage of amide I' values were recorded at 4 h in solution (*clear bars*) and for adsorption (*filled bars*)

(Fig. 1B), which is corroborated by a weaker conformational change of the protein. The adsorption of BSA onto the electrostatically neutral support unfolds the most hydrophobic helical domains at 1,660 cm^{-1}, involving around 4% of the overall backbone. The loss of these hydrophobic helical domains implies an increase in self-association. The structural change of the homologous HSA adsorbed to a positively charged hydrophilic surface such as an ion-exchanger chromatographic support also entails a small fraction of the overall peptide carbonyls (Pantazaki et al. 1998).

Adsorption Kinetics and Conformational Changes

The rates at which BSA was adsorbed onto the three different types of support were measured at a bulk concentration of 500 μg ml^{-1} (Fig. 1). The adsorbed amounts of BSA (Γ) increase with time and reach a plateau after 10 h for the negatively charged silica (not shown on Fig. 1A), after 4 h for the electrostatically neutral support (Fig. 1B) and after 60 min for the hydrophobic support (Fig. 1C).

The adsorbed amount of BSA on the repelling silica surface reaches a value of 0.45 mg m^{-2} and 0.7 mg m^{-2} after 2 and 10 h, respectively. Under identical conditions of bulk concentration at a D_2O–silica surface, the adsorbed amount of BSA determined by specular neutron reflection reached

a limiting value of 2.5 mg m^{-2} at a pH close to the isoelectric point of the protein, but was found to be only 0.5 mg m^{-2} at pH 7 (Su et al. 1998a). The maximum amount of adsorbed protein molecules is generally observed at the adsorption pH close to the isoelectric point thanks to the minimisation of electrostatic repulsions between the protein and the support (Giacomelli et al. 1999b; Norde 1998). The structural stability of BSA is known to be strongly pH-dependent. The higher α-helical content for BSA molecules at the isoelectric point suggests that the molecular shape of BSA is more compact than at higher levels of pH (Servagent-Noinville et al. 2000). However, the negatively charged silica induces a large unfolding of the α-helices by attracting the external positively charged Lys (aminium) and Arg (iminium) residues of the BSA molecules, causing the disruption of internal salt bridges between carboxylate side chains and the positively charged residues. The adsorption kinetics of BSA at a bulk concentration of 186 μg ml^{-1} on hydrophilic silica-titania surfaces reported by Kurrat et al. (1997) gave a Γ value of 1.3 mg m^{-2} in HEPES buffer and a value lower than 0.1 mg m^{-2} in phosphate buffer. Another research team found adsorption densities for BSA adsorbed on pure silica reaching 1.4 mg m^{-2} at a higher bulk concentration of 1,800 μg ml^{-1} (Kridhasima et al. 1993). It should be noted that the limit value for adsorption density depends strongly upon the protein concentration (Malmsten 1998). Furthermore, the above discrepancy between the reported Γ values for BSA could be due not only to the variable charge densities between the various oxide surfaces used in the different works, but also to the influence of counterions on the external charge distribution of the protein and on the protein structure itself.

By assuming that the adsorption plateau corresponds to the formation of a close-packed monolayer, the average cross-sectional area of the protein adsorbed is calculated and compared to the theoretical values calculated from the molecular dimension of the protein. The calculated cross-sectional areas of a BSA molecule adsorbed onto bare silica and CH3-terminated SAMs are 155 and 97 nm^2 $molecule^{-1}$, respectively. One work also found cross-sectional areas of 99 and 100 nm^2 $molecule^{-1}$ for BSA adsorbed onto hydrophobic polyurethane films at pH 7.0 by the ATR technique (Jeon et al. 1994). According to the three-dimensional heart-shape of the BSA molecule (Table 1), the cross-sectional area of the native BSA is either 24 or 28 nm^2 $molecule^{-1}$, depending on an end-on or side-on orientation, respectively. The five-fold or four-fold increase in the average cross-sectional area of an adsorbed BSA molecule corresponds to a spreading of the protein either on the repelling hydrophilic or on the hydrophobic support, and is correlated in both cases to the large unfolding of the protein stereoregular structure upon adsorption.

In contrast, the average conformation of the adsorbed BSA molecules on the neutral hydrophilic support is unchanged compared to the solvated

state (Fig. 2B). If the molecular shape of the protein corresponds to that of the native state, the adsorption density of 0.45 mg m^{-2} obtained on the ND_2-terminated SAMs corresponds to the formation of an incomplete or loosely-packed monolayer. This is in agreement with the general findings of the poor affinity of proteins towards neutral surfaces (Herrwerth et al. 2003; Ostuni et al. 2001; Silin et al. 1997; Tengvall et al. 1998).

6.3.4 Surface-Induced Conformational Changes of a Hard Protein: Lysozyme

Changes in Solvation due to Adsorption

As illustrated in Fig. 3, a first extremely rapid isotopic exchange occurs within the first 10 min of incubation of lysozyme in the deuterated buffer, corresponding to the exchange in COND of 70% of the amino acid residues. The residual NH content of lysozyme after 2 h of incubation reaches 21% in pure phosphate buffer (Figs. 3A,C) and 16% in phosphate-buffered saline (Fig. 3B). The ionic strength is known to influence the NH/ND isotope exchange kinetics of proteins (Gregory and Lumry 1985).

The adsorption of lysozyme with a positive net charge on the pure silica surface is driven mainly by electrostatic interactions (Robeson and Tilton 1996; Wahlgren et al. 1993). The adsorbed amounts of lysozyme are increased at low ionic strength, as illustrated in Fig. 3A compared to Fig. 3B. The first molecules of lysozyme adsorbed on the negatively charged silica do not change their solvation state since their residual NH content is rather unchanged compared to the equilibrium NH content of the protein in solution. The effect of ionic strength is to limit both the adsorbed amount of lysozyme and the NH/ND exchange of the adsorbed molecules (Fig. 2B). Since the diffusion of D_2O inside the adsorbed molecules of lysozyme is limited, no increase in hydrated random domains is observed (Figs. 4A,B). The adsorption of the positively charged lysozyme on the silica surface does not induce a significant change in either solvation or in secondary structure (Figs. 4A,B). The more exchanged states of adsorbed lysozyme in phosphate buffer appear when the adsorption density Γ exceeds the limit value of 1.25 mg m^{-2}. This limit value of adsorption density could correspond to the adsorption of lysozyme in a side-on orientation, as reported by other groups (Claesson et al. 1995; Wahlgren et al. 1995). The fast adsorption process is considered to form a basal monolayer of lysozyme in native structure, and the slower process could correspond to the multilayer growth. In the second step, the subsequent adsorbed molecules of lysozyme would be more solvated than in the former monolayer (see Fig. 3A), although they did not undergo a conformational change on the negatively charged silica. Ball and

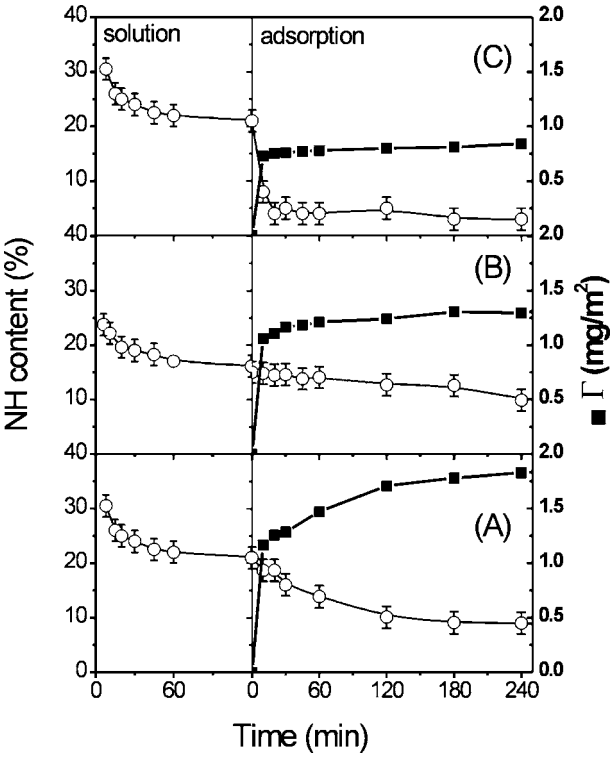

Fig. 3. Solvation changes (-○-) and adsorbed amount (-■-) of lysozyme adsorbed at a concentration of 250 μg ml^{-1} and pD 7.5 at different liquid–solid interfaces: a deuterated phosphate buffer–pure silica surface (**A**), deuterated phosphate buffer with 10 mM NaCl–pure silica surface (**B**) and deuterated phosphate buffer–CH_3-terminated SAMs (**C**). The residual NH content (expressed as a percentage of the overall peptide carbonyls) is monitored by the amide II:amide I' ratio measurements. The adsorbed amount (Γ) of lysozyme is calculated from the adsorption density equation (Sperline et al. 1987)

Ramsden (2000) showed that lysozyme exhibits also a two-step adsorption kinetics on a hydrophilic silica-titania surface. Surface apparatus studies of lysozyme adsorbed onto mica suggest that lysozyme could exist as a dimer forming a partial bilayer (Blomberg et al. 1998). Su et al. (1998b) showed that the adsorbed lysozyme on silica retains its tertiary structure and that no significant denaturation occurs. The results of their neutron reflection studies suggest that the structural arrangement of the adsorbed lysozyme at the aqueous–silica interface is determined by the lateral electrostatic repulsion, which in turn is dependent on the jamming within the bilayers and the net charge of the protein at a given pH. From x-ray data, the basic and acidic residues of lysozyme are known to have an uneven distribution at its periphery (Wilson et al. 1992). A preferred orientation at low surface

coverage would place the external basic residues of lysozyme facing the negatively charged silica surface. Consequently, this preferred orientation decreases the electrostatic repulsion between adjacent protein molecules and maximises the surface attraction, as already suggested by Haggerty and Lenhoff (1993b).

Many studies have underlined the orientation effect, which could occur during adsorption. When the bulk concentration of protein is low, a side-on orientation of the adsorbed molecules could be favoured. Rather, adsorption at a higher bulk concentration could lead to an end-on configuration due to a stronger protein–protein interaction, yielding to a more compact adsorbed layer. Obviously, the presented simplistic calculation from the adsorbed amount does not take into account that in some cases, the jamming coverage could be less than unity (Arai and Norde 1990) and the possibility of coexistence of different orientations of the adsorbed proteins at the interface (Su et al. 1998b). For instance, the experimental determinations of the thickness or the lateral distribution by other techniques is necessary to determine whether the formation of an incomplete monolayer or a loosely packed monolayer has occurred within side-on or end-on orientations.

Adsorption Kinetics and Conformational Changes

For adsorption on the CH_3-terminated SAMs, the adsorption plateau is rapidly reached within 30 min, meanwhile the residual NH content decreases drastically to a plateau value of 5%. As for BSA adsorbed onto a hydrophobic support, some D_2O molecules penetrate inside the lysozyme core and solvate more amide CONH bonds because of the changes in secondary structure induced by adsorption (Noinville et al. 2002). However, the major conformational change concerning lysozyme adsorbed onto a hydrophobic surface consists in an α-helix to β-sheet structural conversion (Noinville et al. 2002; Yokoyama et al. 2003). The maximum adsorbed amount of lysozyme of 0.8 mg m^{-2} corresponds to the close packing molecules with a cross-sectional area of 29 nm^2 (Fig. 3C). The increase in the cross-sectional area of adsorbed lysozyme could be a consequence of the conformational changes of the molecules requiring a larger area of contact with the hydrophobic surface. The losses of 12% of peptide carbonyls in helical structure and of 5% in random hydrated domains give rise to 8% of CO in β-structured domains and 7% of CO in self-associated domains (Noinville et al. 2002). Since one part of the newly formed domains is β-sheeted, the molecular shape of adsorbed molecules of lysozyme is expected to be less spread than the soft BSA. The lower content in random hydrated domains of the adsorbed lysozyme is linked to the dehydration of the protein–hydrophobic support (Fig. 4C). The released peptide carbonyls natively involved in the helical structure of lysozyme could not form hydrogen bonds

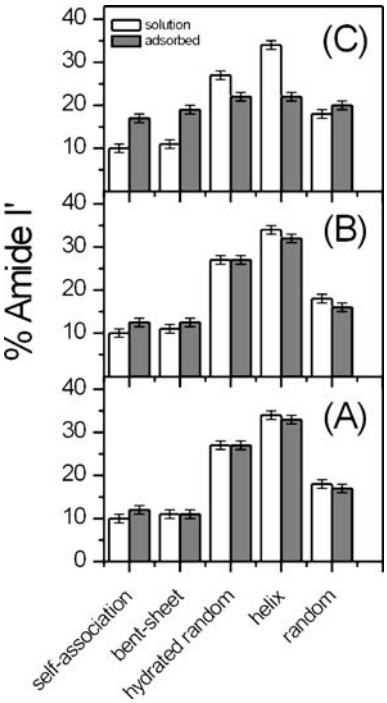

Fig. 4. Comparison of secondary structures of lysozyme resulting from our spectral analysis in a deuterated solution and adsorbed at a bulk concentration of 250 μg ml^{-1} and pD 7.5 at different liquid–solid interfaces: a deuterated phosphate buffer–pure silica surface (**A**), deuterated phosphate buffered saline–pure silica surface (**B**) and deuterated phosphate buffer–CH_3-terminated SAMs (**C**). The given percentage of amide I' values were recorded at 4 h in solution (*clear bars*) and for adsorption (*filled bars*), so that corresponds to the maximum adsorbed amount of lysozyme reported in Fig. 3

with water molecules since there are no more present at the dehydrated hydrophobic interface. The unfolded peptide carbonyls do form hydrogen bonds that are involved either in intramolecular domains (β-sheets) or in intermolecular self-associated domains. The global structural change in lysozyme caused by adsorption onto a hydrophobic support involves a small loss of stereoregular structures concerning 4% of the polypeptide backbone against 13% for the soft BSA (Noinville et al. 2002).

6.3.5 Folding or unfolding of proteins on hydrophobic supports

The mainly β-sheeted serine proteinase such as α-chymotrypsin has a high structural stability like lysozyme, but undergoes a large unfolding of its β-sheets upon adsorption on hydrophobic support (Baron et al. 1999; Zoungrana et al. 1997). The released peptide carbonyls form mainly intermolecular hydrogen bonds with neighbouring peptide segments, increasing the self-associated domains in the adsorbed layer of α-chymotrypsin (Noinville et al. 2002). Adsorption on hydrophobic surfaces may result in an increased or decreased order in protein structure, whether the balance between the energetically favourable interaction and the conformational

entropy is positive or not. For instance another serine enzyme such as *Humicola lanuginosa* lipase, with a higher overall hydrophobicity than the above proteinase, adsorbs onto the hydrophobic support with a gain in its stereoregular α/β fold (Noinville et al. 2002). Some antimicrobial peptides known to be randomly coiled in solution adsorb onto hydrophobic supports by forming amphipathic helices with the hydrophobic external side of the helix oriented towards the support and the polar side to the interfacial solution (Noinville et al. 2003). Surface-induced conformational changes of the amyloid β-peptide have been studied using CD spectroscopy on Teflon particles (Giacomelli and Norde 2003). The authors show that the hydrophobic support promotes α-helix formation at low surface coverage, but leads to a more enriched β-sheeted structure at high surface coverage, probably initiating self-aggregation. Even if the extent and the pathways of structural conversion in the case of very flexible polypeptides such as amyloid peptides or prions are still complex to tackle, the effect of the contact with a solid phase is to stabilise adsorbed conformers, which could inhibit protein aggregation by the complex interplay of electrostatic and hydrophobic interactions (Revault et al. 2005).

6.4 Conclusion

The initial events involved in protein adsorption causing solvation or conformational changes can occur at the microsecond to millisecond timescales, whereas conformational rearrangement as well as orientation and lateral distribution can occur over much longer time within the layer of adsorbed proteins. As a consequence, the biological function of the immobilised proteins is more or less altered depending on the adsorption history. Combined progress in structural biology and nanoscale-patterned surfaces should lead to a better knowledge of the surface-induced conformational changes of proteins, determining their enzymatic and cell-binding activities or their recognition or pathogenic functions.

References

Arai I, Norde W (1990) The behavior of some model proteins at solid–liquid interfaces. I, adsorption from single protein solutions. Colloids Surf A 51:1–15

Asthagiri D, Lenhoff AM (1997) Influence of structural details in modeling electrostatically driven protein adsorption. Langmuir 13:6761–6768

Ball A, Jones RAL (1995) Conformational changes in adsorbed proteins. Langmuir 11:3542–3548

Ball V, Ramsden JJ (2000) Analysis of hen egg white lysozyme adsorption on Si(Ti)O2 | aqueous solution interfaces at low ionic strength: a biphasic reaction related to solution self-association. Colloids Surf B 17:81–94

Banci L, Bertini I, Gray HB, Luchinat C, Reddig T, Rosato A, Turano P (1997) Solution structure of oxidized horse heart cytochrome c. Biochemistry 36:9867–9877

Baron M-H, Revault M, Servagent-Noinville S, Abadie J, Quiquampoix H (1999) Chymotrypsin adsorption on montmorillonite, enzymatic activity and kinetic FTIR structural analysis. J Colloid Interface Sci 214:319–332

Berman HM, Westbrook J, Feng Z, Gilliland G, Bhat TN, Weissig H, Shindyalov IN, Bourne PE (2000) The protein data bank. Nucleic Acids Res 28:235–242

Billsten P, Carlsson U, Elwing H (1998) Studies on the conformation of adsorbed proteins with the use of nanoparticle technology. In: Malmsten M (ed) Biopolymers at Interfaces. Marcel Dekker, New York, pp 627–650

Birktoft JJ, Blow DM (1972) Structure of crystalline-chymotrypsin. V. The atomic structure of tosyl-chymotrypsin at 2 A resolution. J Mol Biol 68:187–240

Blomberg E, Claesson PM, Froberg JC (1998) Surfaces coated with protein layers: a surface force and ESCA study. Biomaterials 19:371–386

Booth V, Waring A, Walther F, Keough K (2004) NMR structures of the C-terminal segment of surfactant protein B in detergent micelles and hexafluoro-2-propanol. Biochemistry 43:15187–15194

Bos MA, Kleijn JM (1995) Determination of the orientation distribution of adsorbed fluorophores using TIRF. I. Theory Biophys J 68:2566–2572

Boulkanz L, Balcar N, Baron M-H (1995) FTIR analysis for structural characterization of albumin adsorbed on the reversed-phase support RP-C6. Appl Spectrosc 49:1737–1746

Boulkanz L, Vidal-Madjar C, Balcar N, Baron M-H (1997) Adsorption mechanism of human serum albumin on a reversed-phase support by kinetic, chromatographic, and FTIR methods. J Colloid Interface Sci 188:58–67

Branden C, Tooze J (1991) Introduction to Protein Structure. Garland, New York

Brash JL (1996) Behavior of proteins at interfaces. Curr Opin Colloid Interface Sci 1:682–688

Buijs J, Hlady V (1997) Adsorption kinetics, conformation, and mobility of the growth hormone and lysozyme on solid surfaces, studied with TIRF. J Colloid Interface Sci 190:171–181

Buijs J, Norde W, Lichtenbelt JWT (1996) Changes in the secondary structure of adsorbed IgG and $F(ab')_2$ studied by FTIR spectroscopy. Langmuir 12:1605–1613

Buijs J, Ramstrom M, Danfelter M, Larsericsdotter H, Hakansson P, Oscarsson S (2003) Localized changes in the structural stability of myoglobin upon adsorption onto silica particles, as studied with hydrogen/deuterium exchange mass spectrometry. J Colloid Interface Sci 263:441–448

Bujnowski AM, Pitt WG (1998) Water structure around enkephalin near a PE surface: a molecular dynamics study. J Colloid Interface Sci 203:47–58

Byler DM, Susi H (1986) Examination of the secondary structure of proteins by deconvolved FTIR spectra. Biopolymers 25:469–487

Carter DC, Ho JX (1994) Structure of serum albumin. Adv Protein Chem 45:155–203

Chalikian TV, Gindikin VS, Breslauer KJ (1995) Volumetric characterizations of the native, molten globule and unfolded states of cytochrome c at acidic pH. J Mol Biol 250:291–306

Cheng S-S, Chittur KK, Sukenik CN, Culp LA, Lewandowska K (1994) The conformation of fibronectin on SAM with different surface composition: an FTIR/ATR study. J Colloid Interface Sci 162:135–143

Chirgadze YN, Brazhnikov EV (1974) Intensities and other spectral parameters of infrared amide bands of polypeptides in the a-helical forms. Biopolymers 13:1701–1712

Chirgadze YN, Fedorov OV, Trushina NP (1975) Estimation of amino acid residue side-chain absorption in the infrared spectra of protein solutions in heavy water. Biopolymers 14:679–694

Chittur KK (1998) FTIR/ATR for protein adsorption to biomaterial surfaces. Biomaterials 19:357–369

Chittur KK, Fink DJ, Leininger RI, Hutson TB (1986) Fourier transform infrared spectroscopy/attenuated total reflection studies of protein adsorption in flowing systems: approaches for bulk correction and compositional analysis of adsorbed and bulk proteins in mixtures. J Colloid Interface Sci 111:419–433

Claesson PM, Blomberg E, Froberg JC, Nylander T, Arnebrant T (1995) Protein interactions at solid surfaces. Adv Colloid Interface Sci 57:161–227

de Collongue-Poyet B, Sebille B, Baron M-H (1996) Chromatography of the Interferon γ and the analogue II: FTIR analysis. Biospectroscopy 2:101–111

de Lozé C, Fillaux F (1972) Spectroscopic study of monosubstituted amides II. rotation isomers in amides substituted by aliphatic side-chain models. Biopolymers 11:2063–2077

Dill KA, Bromberg S, Yue K, Fiebig KM, Yee DP, Thomas PD, Chan HS (1995) Principles of protein folding – a perspective from simple exact models. Protein Sci 4:561–602

Dong A, Huang P, Caughey WS (1990) Protein secondary structures in water from second-derivative amide I infrared spectra. Biochemistry 29:3303–3308

Dorsey JD, Dill KA (1989) The molecular mechanism of retention in reversed-phase liquid chromatography. Chem Rev 89:331–346

Dousseau F, Pézolet M (1990) Determination of the secondary structure content of proteins in aqueous solutions from their amide I and amide II infrared bands. Comparison between classical and partial least-squares methods. Biochemistry 29:8771–8779

Engel MFM, Visser AJWG, van Mierlo CPM (2004) Conformation and orientation of a protein folding intermediate trapped by adsorption. Proc Natl Acad Sci U S A 101:11316–11321

Fang F, Szleifer I (2001) Kinetics and thermodynamics of protein adsorption: a generalized molecular theoretical approach. Biophys J 80:2568–2589

Follows D, Holt C, Nylander T, Thomas RK, Tiberg F (2004) Beta-casein adsorption at the silicon oxide–aqueous solution interface: calcium ion effects. Biomacromolecules 5:319–325

Frey S, Tamm LK (1991) Orientation of melittin in phospholipid bilayers: a polarized attenuated total reflection infrared study. Biophys J 60:922–930

Fu F-N, Fuller MP, Singh BR (1993) Use of Fourier transform infrared/attenuated total reflectance spectroscopy for the study of surface adsorption of proteins. Appl Spectrosc 47:98–102

Gekko K, Hasegawa Y (1986) Compressibility–structure relationship of globular proteins. Biochemistry 25:6563–6571

Giacomelli CE, Bremer MGEG, Norde W (1999a) ATR–FTIR study of IgG adsorbed on different silica surfaces. J Colloid Interface Sci 220:13–23

Giacomelli CE, Esplandiu MJ, Ortiz PI, Avena MJ, Pauli CPD (1999b) Ellipsometric study of bovine serum albumin adsorbed onto Ti/TiO_2 electrodes. J Colloid Interface Sci 218:404–411

Giacomelli CE, Norde W (2001) The Adsorption–desorption cycle. Reversibility of the BSA–silica system. J Colloid Interface Sci 233:234–240

Giacomelli CE, Norde W (2003) Influence of hydrophobic Teflon particles on the structure of amyloid beta-peptide. Biomacromolecules 4:1719–26

Gill DS, Roush DJ, Willson RC (1994) Adsorption heterogeneity and thermodynamic driving forces in anion-exchange equilibria of cytochrome b5. J Colloid Interface Sci 167:1–7

Gilpin RK (1993) Conformational changes and molecular dynamics of simple silica immobilized systems. J Chromatogr A 656:217–229
Goormaghtigh E, Cabiaux V, Ruysschaert JM (1994). Determination of soluble and membrane protein structure by Fourier transform infrared spectrosocpy I. Assignments and model compounds. In: Hiderson HJ, Ralston GB (eds) Subcellular Biochemistry. Plenum Press, New York, pp 329–362
Green RJ, Hopkinson I, Jones RAL (1999) Unfolding and intermolecular association in globular proteins adsorbed at interfaces. Langmuir 15:5102–5110
Gregory RB, Lumry R (1985) Hydrogen-exchange evidence for distinct structural classes in globular proteins. Biopolymers 24:301–326
Haggerty L, Lenhoff AM (1993a) STM and AFM in biotechnology. Biotechnol Prog 9:1–11
Haggerty L, Lenhoff AM (1993b) Analysis of ordered arrays of adsorbed lysozyme by scanning tunneling microscopy. Biophys J 64:886–895
Haynes CA, Norde W (1995) Structures and stabilities of adsorbed proteins. J Colloid Interface Sci 169:313–328
Herrwerth S, Eck W, Reinhardt S, Grunze M (2003) factors that determine the protein resistance of oligoether self-assembled monolayers – internal hydrophobicity, terminal hydrophilicity, and lateral packing density. J Am Chem Soc 125:9359–9366
Houbiers MC, Wolfs CJAM, Spruijt RB, Bollen YJM, Hemminga MA, Goormaghtigh EU (2001) Conformation and orientation of the gene 9 minor coat protein of bacteriophage M13 in phospholipid bilayers. Biochim Biophys Acta 1511:224–235
Huyghues-Despointes BM, Pace CN, Englander SW, Scholtz JM (2001) Measuring the conformational stability of a protein by hydrogen exchange. Methods Mol Biol 168:69–92
Iwamoto GK, Winterton LC, Stoker RS, van Wagenen RA, Andrade JD, Mosher DF (1985) Fibronectin adsorption detected by interfacial fluorescence. J Colloid Interface Sci 106:459–464
Jeon JS, Sperline RP, Raghavan S (1992) Quantitative analysis of adsorbed serum albumin on segmented polyurethane using FT-IR/ATR spectroscopy. Appl Spectrosc 46:1644–1648
Jeon JS, Raghavan S, Sperline RP (1994) Quantitative analysis of albumin adsorption onto uncoated and poly(ether)urethane-coated ZnSe surfaces using the attenuated total reflection FTIR technique. Colloids Surf A 92:255–265
Jeon SI, Lee JH, Andrade JD, De Gennes PG (1991) Protein–surface interactions in the presence of polyethylene oxide: I. Simplified theory. J Colloid Interface Sci 142:149–158
Kalnin NN, Baikalov IA, Venyaminov S (1990) Quantitative IR spectrophotometry of peptide compounds in water (H_2O) solutions. III. Estimation of the protein secondary structure. Biopolymers 30:1273–1280
Karlsson M, Ekeroth J, Elwing H, Carlsson U (2005) Reduction of irreversible protein adsorption on solid surfaces by protein engineering for increased stability. J Biol Chem 280:25558–25564
Kim DT, Blanch HW, Radke CJ (2002) Direct imaging of lysozyme adsorption onto mica by atomic force microscopy. Langmuir 18:5841–5850
Kondo A, Fukuda H (1998) Effects of adsorption conditions on kinetics of protein adsorption and conformational changes at ultrafine silica particles. J Colloid Interface Sci 198:34–41
Kondo A, Oku S, Higashitani K (1991) Structural changes in protein molecules adsorbed on ultrafine silica particles. J Colloid Interface Sci 143:214–221
Kondo A, Urabe T, Yoshinaga K (1996) Adsorption activity and conformation of [alpha]-amylase on various ultrafine silica particles modified with polymer silane coupling agents. Colloids Surf A 109:129–136
Kridhasima V, Vinaraphong P, McGuire J (1993) Adsorption kinetics and elutability of α-Lactalbumin, β-Casein, β-Lactoglobulin, and BSA at hydrophobic and hydrophilic interfaces. J Colloid Interface Sci 161:325–334

Krimm S, Bandekar J (1986) Vibrational spectroscopy and conformation of peptides, polypeptides, and proteins. Adv Protein Chem 38:181–364

Kurrat R, Prenosil JE, Ramsden JJ (1997) Kinetics of human and bovine serum albumin adsorption at silica–titania surfaces. J Colloid Interface Sci 185:1–8

Kurrat R, Ramsden JJ, Prenosil JE (1994) Kinetic model for serum albumin adsorption: experimental adsorption. J Chem Soc Faraday Trans 90:587–590

Lawson DM, Brzozowski AM, Rety S, Verma C, Dodson GG (1994) Probing the nature of substrate binding in Humicola lanuginosa lipase through x-ray crystallography and intuitive modelling. Protein Eng 7:543–550

Lecomte S, Hilleriteau C, Forgerit JP, Revault M, Baron MH, Hildebrandt P, Soulimane T (2001) Structural changes of cytochrome c(552) from Thermus thermophilus adsorbed on anionic and hydrophobic surfaces probed by FTIR and 2D-FTIR spectroscopy. Chembiochem 2:180–189

Lenk TJ, Ratner BD, Gendreau RM, Chittur KK (1989) IR spectral Changes of bovine serum albumin upon surface adsorption. J Biomed Mater Res 23:549–569

Leonidas DD, Shapiro R, Irons LI, Russo N, Acharya KR (1997) Crystal structures of ribonuclease A complexes with 5'-diphosphoadenosine 3'-phosphate and 5'-diphosphoadenosine 2'-phosphate at 1.7 Å resolution. Biochemistry 36:5578–5588

Lesins V, Ruckenstein E (1989) Chromatographic probing of protein-sorbent interactions. J Colloid Interface Sci 132:566

Li L, Chen S, Jiang S (2003) protein adsorption on alkanethiolate self-assembled monolayers: nanoscale surface structural and chemical effects. Langmuir 19:2974–2982

Liu S, Haynes C (2005) Energy landscapes for adsorption of a protein like HP chain as a function of native state stability. J Colloid Interface Sci 284:7–13

Long JR, Shaw WJ, Stayton PS, Drobny GP (2001) Structure and dynamics of hydrated statherin on hydroxyapatite as determined by solid-state NMR. Biochemistry 40:15451–15455

Lu JR, Perumal S, Zhao X, Miano F, Enea V, Heenan RR, Penfold J (2005) Surface-induced unfolding of human lactoferrin. Langmuir 21:3354–3361

Lu JR, Su TJ, Thirtle PN, Thomas RK, Rennie AR, Cubitt R (1998) The denaturation of lysozyme layers adsorbed at the hydrophobic solid/liquid surface studied by neutron reflection. J Colloid Interface Sci 206:212–223

Lundqvist M, Sethson I, Jonsson B-H (2004) Protein adsorption onto silica nanoparticles: conformational changes depend on the particles' curvature and the protein stability. Langmuir 20:10639–10647

Malmsten M (1998) Formation of adsorbed protein layers. J Colloid Interface Sci 207:186–199

Malmsten M, Arnebrant T, Billsten P (2003). Interfacial behavior of protein mutants and variants. In: Malmsten M (ed) Biopolymers at Interfaces. Marcel Dekker, New York, pp 95–113

Marchin K, Berrie C (2003) Conformational changes in the plasma protein fibrinogen upon adsorption to graphite and mica investigated by AFM. Langmuir 19:9883–9888

Marsh RJ, Jones RAL, Sferrazza M (1999) Neutron reflectivity study of the adsorption of β-lactoglobulin at a hydrophilic solid/liquid interface. J Colloid Interface Sci 218:347–349

Martin I, Goormaghtigh E, Ruysschaert J-M (2003) Attenuated total reflection IR spectroscopy as a tool to investigate the orientation and tertiary structure changes in fusion proteins. Biochim Biophys Acta 1614:97–103

McGuire J, Wahlgren MC, Arnebrant T (1995) Structural stability effects on the adsorption and dodecyltrimethylammonium bromide-mediated elutability of bacteriophage t4 lysozyme at silica surfaces. J Colloid Interface Sci 170:182–192

McNay JL, Fernandez EJ (1999) How does a protein unfold on a reversed-phase liquid chromatography surface? J Chromatogr A 849:135–148
Meskers S, Ruysschaert J-M, Goormaghtigh E (1999) H–D exchange of streptavidin and its complex with biotin studied by 2D ATR FTIR spectroscopy. J Am Chem Soc 121:5115–5122
Methot M, Boucher F, Salesse C, Subirade M, Pezolet M (1996) Determination of bacteriorhodopsin orientation in monolayers by infrared spectroscopy. Thin Solid Films 284–285:627–630
Mitchell RC, Haris PI, Fallowfield C, Keeling DJ, Chapman D (1988) Fourier transform infrared spectroscopic studies on gastric H^+/K^+–ATPase. Biochim Biophys Acta 941:31–38
Mrksich M, Sigal GB, Whitesides GM (1995) Surface plasmon resonance permits in situ measurement of protein adsorption on self-assembled monolayers of alkanethiolates on gold. Langmuir 11:4383–4385
Muga A, Mantsch HH, Surewicz WK (1991) Membrane binding induces destabilization of cytochrome c structure. Biochemistry 30:7219–7224
Müller M, Werner C, Grundke K, Eichhorn KJ, Jacobash HJ (1997) ATR-FTIR spectroscopy of proteins adsorbed on biocompatible cellulose films. Mikrochim Acta 14:671–674
Nabet A, Pézolet M (1997) Two dimensional FT-IR spectroscopy:a poxerful method to study the secondary stucture of proteins using H–D exchange. Appl Spectrosc 51:466–469
Noda I (1989) Two-dimensional infrared spectroscopy. J Am Chem Soc 111:8116–8118
Noinville S, Bruston F, Revault M, Baron M-H, Nicolas P (2003) Conformation, orientation and adsorption kinetics of Dermaseptin B2 onto synthetic supports at aqueous/solid interface. Biophys J 85:1196–1206
Noinville S, Revault M, Baron M-H, Tiss A, Yapoudjian S, Ivanova M, Verger R (2002) Conformational changes and orientation of Humicola lanuginosa lipase on a solid hydrophobic surface:an in situ interface FTIR-ATR study. Biophys J 82:2709–2719
Noinville V, Vidal-Madjar C, Sébille B (1995) Modeling of protein adsorption on polymer surfaces. Computation of adsorption potential. J Phys Chem 99:1516–1522
Norde W (1998) Driving forces for protein adsorption at solid surfaces. In: Malmsten M (ed) Biopolymers at Interfaces. Marcel Dekker, New York, pp 27–54
Norde W (2000) Proteins at solid surfaces. In: Baszkin A, Norde W (ed) Physical Chemistry of Biological Interfaces. Marcel Dekker, New York, pp 115–136
Ong JL, Chittur KK, Lucas LC (1994) Dissolution/reprecipitation and protein adsoprtion studies of calcium phosphate coatings by FTIR/ATR techniques. J Biomed Mater Res 28:1337–1346
Oroszlan P, Blanco R, Lu XM, Yarmush D, Karger BL (1990) Intrinsic fluorescence studies of the kineticsmechanism of unfolding of a-lactalbumin on weakly hydrophobic chromatographic surfaces. J Chromatogr 500:481–502
Ortega-Vinuesa JL, Tengvall P, Lundstrom I (1998) Aggregation of HAS, IgG, and fibrinogen on methylated silicon surfaces. J Colloid Interface Sci 207:228–239
Ostuni E, Chapman RG, Holmlin RE, Takayama S, Whitesides GM (2001) A survey of structure–property relationships of surfaces that resist the adsorption of protein. Langmuir 17:5605–5620
Ostuni E, Grzybowski B, Mrksich M, Roberts C, Whitesides G (2003) Adsorption of proteins to hydrophobic sites on mixed self-assembled monolayers. Langmuir 19:1861–1872
Pantazaki A, Baron M-H, Revault M, Vidal-Madjar C (1998) Characterization of human serum albumin adsorbed on a porous anion-exchange support. J Colloid Interface Sci 207:324–331
Patel N, Davies MC, Heaton RJ, Roberts CJ, Tendler SJB, Williams PM (1998) A scanning probe microscopy study of the physisorption and chemisorption of protein molecules onto carboxylate terminated self-assembled monolayers. Appl Phys A 66:S569–S574

Perez E, Proust JE (1987) Forces between mica surfaces covered with adsorbed mucin across aqueous solution. J Colloid Interface Sci 118:182–191

Pike AC, Brew K, Acharya KR (1996) Crystal structures of guinea-pig, goat and bovine alpha-lactalbumin highlight the enhanced conformational flexibility of regions that are significant for its action in lactose synthase. Structure 4:691–703

Pitt WG, Cooper SL (1986) FTIR-ATR studies of the effect of shear rate upon albumin adsorption onto polyurethaneurea. Biomaterials 7:340–347

Prestrelski SJ, Byler DM, Thompson MP (1991) Infrared spectroscopic discrimination between a- and 3_{10}-helices in globular proteins. Int J Pept Protein Res 37:508–512

Privalov PL (1979) Stability of proteins:small globular proteins. Adv Protein Chem 33:167–241

Qin BY, Bewley MC, Creamer LK, Baker HM, Baker EN, Jameson GB (1998) Structural basis of the Tanford transition of bovine beta-lactoglobulin. Biochemistry 37:14014–14023

Quiquampoix H, Abadie J, Baron M-H, Leprince F, Matumoto-Pintro PT, Ratcliffe RG, Staunton S (1995). Mechanisms and consequences of protein adsorption on soil mineral surfaces. In: Horbett TA, Brash JL (eds) Proteins at Interfaces. II. Fundamentals and Applications. American Chemical Society, Washington, DC, pp 321–333

Quiquampoix H, Staunton S, Baron M-H, Ratcliffe RG (1993) Interpretation of the pH dependence of protein adsorption on clay mineral surfaces and its relevance to the understanding of extracellular enzyme activity. Colloids Surf A 75:85–93

Radford SE, Buck M, Topping KD, Dobson CM, Evans PA (1992) Hydrogen exchange in native and denatured states of hen egg-white lysozyme. Proteins 14:237–248

Ramsden JJ (1998) Kinetics of protein adsorption. In: Malmsted M (ed) Biopolymers at Interfaces. Marcel Dekker, New York, pp 321–361

Read MJ, Burkett SL (2003) Asymmetric [alpha]-helicity loss within a peptide adsorbed onto charged colloidal substrates. J Colloid Interface Sci 261:255–263

Revault M, Quiquampoix H, Baron MH, Noinville S (2005) Fate of prions in soil:trapped conformation of full-length ovine prion protein induced by adsorption on clays. Biochim Biophys Acta 1724:367–374

Richards FM (1977) Areas, volumes, packing and protein structure. Annu Rev Biophys Bioeng 6:151–176

Robeson JL, Tilton RD (1996) Spontaneous reconfiguration of adsorbed lysozyme layers observed by total internal reflection fluorescence with a pH-sensitive fluorophore. Langmuir 12:6104–6113

Roth CM, Lenhoff AM (1993) Electrostatic and vander Waals contribution to protein adsorption: computation of equilibrium constants. Langmuir 9:962–972

Rothshild KJ, Clark NA (1979) Polarized infrared spectroscopy of oriented purple membrane. Biophys J 25:473–488

Roush DJ, Gill DS, Willson RC (1994) Electrostatic potentials and electrostatic interaction energies of rat cytochrome b5 and a simulated anion-exchange adsorbent surface. Biophys J 66:1290–300

Servagent-Noinville S, Revault M, Quiquampoix H, Baron M-H (2000) Conformational changes of BSA induced by adsorption on different clay surfaces: FTIR analysis. J Colloid Interface Sci 221:273–283

Sharp JS, Forrest JA, Jones RA (2002) Surface denaturation and amyloid fibril formation of insulin at model lipid–water interfaces. Biochemistry 41:15810–15819

Sigal GB, Mrksich M, Whitesides GM (1998) Effect of surface wettability on the adsorption of proteins and detergents. J Am Chem Soc 120:3464–3473

Silin V, Weetall H, Vanderah DJ (1997) SPR studies of the nonspecific adsorption kinetics of human IgG and BSA on gold surfaces modified by self-assembled monolayers (SAMs). J Colloid Interface Sci 185:94–103

Soderquist ME, Walton AG (1980) Structural changes in proteins adsorbed on polymer surfaces. J Colloid Interface Sci 75:386–392

Sokolowski F, Modler AJ, Masuch R, Zirwer D, Baier M, Lutsch G, Moss DA, Gast K, Naumann D (2003) Formation of critical oligomers is a key event during conformational transition of recombinant syrian hamster prion protein. J Biol Chem 278:40481–40492

Sperline RP, Muralidharan S, Freiser H (1987) In situ determination of species adsorbed at a solid–liquid interface by quantitative infrared attenuated total reflectance spectrophotometry. Langmuir 3:198–202

Su TJ, Lu JR, Thomas RK, Cui ZF, Penfold J (1998a) The conformational structure of bovine serum albumin layers adsorbed at the silica–water interface. J Phys Chem B 102:8100–8108

Su TJ, Lu JR, Thomas RK, Cui ZF, Penfold J (1998b) The adsorption of Lysozyme at the silica–water interface: a neutron reflection study. J Colloid Interface Sci 203:419–429

Sukhishvili SA, Granick S (1999) Adsorption of human serum albumin:dependence on molecular architecture of the oppositively charged surface. J Chem Phys 110:10153–10161

Surewicz WK, Mantsch HH, Chapman D (1993) Determination of protein secondary structure by Fourier transform infrared spectroscopy:a critical assessment. Biochemistry 32:389–394

Tamm LK, Abildgaard F, Arora A, Blad H, Bushweller JH (2003) Structure, dynamics and function of the outer membrane protein A (OmpA) and influenza hemagglutinin fusion domain in detergent micelles by solution NMR. FEBS Lett 555:139–143

Tengvall P, Lundstrom I, Liedberg B (1998) Protein adsorption studies on model organic surfaces:an ellipsometric and infrared spectroscopic approach. Biomaterials 19:407–422

Tibbs Jones T, Fernandez EJ (2003) [alpha]-Lactalbumin tertiary structure changes on hydrophobic interaction chromatography surfaces. J Colloid Interface Sci 259:27–35

Tiberg F, Nylander T, Su TJ, Lu JR, Thomas RK (2001) Beta-casein adsorption at the silicon oxide–aqueous solution interface. Biomacromolecules 2:844–850

Tronin A, Edwards AM, Wright WW, Vanderkooi JM, Blasie JK (2002) Orientation distributions for cytochrome c on polar and nonpolar interfaces by total internal reflection fluorescence. Biophys J 82:996–1003

Tsuboi M (1964) Some problems in the infrared spectra of polypeptides and polynucleotides. Biopolymers 1:527–547

van der Veen M, Norde W, Stuart MC (2004) Electrostatic interactions in protein adsorption probed by comparing lysozyme and succinylated lysozyme. Colloids Surfaces B:Biointerfaces 35:33–40

van Straaten J, Peppas NA (1991) ATR-FTIR analysis of protein adsorption on polymeric surfaces. J Biomater Sci Polym Ed 2:113–121

Van Tassel PR, Guemouri L, Ramsden JJ, Tarjus G, Viot P, Talbot J (1998) A Particle-level model of irreversible protein adsorption with a postadsorption transition. J Colloid Interface Sci 207:317–323

Vermeer AWP, Bremer MGEG, Norde W (1998) Structural changes of IgG induced by heat treatment and by adsorption onto a hydrophobic Teflon surface studied by circular dichroism spectroscopy. Biochim Biophys Acta 1425:1–12

Vogler EA (1998) Structure and reactivity of water at biomaterial surfaces. Adv Colloid Interface Sci 74:69–117

Wadu-Mesthrige K, Amro NA, Liu GY (2000) Immobilization of proteins on self-assembled monolayers. Scanning 22:380–388

Wahlgren M, Arnebrant T, Lundstrom I (1995) The Adsorption of lysozyme to hydrophilic silicon oxide surfaces: comparison between experimental data and models for adsorption kinetics. J Colloid Interface Sci 175:506–514

Wahlgren M, Welin-Klintström S, Karlsson CA-C (1998). Interactions between proteins and surfactants at solid interfaces. In: Malmsten M (ed) Biopolymers at Interfaces. Marcel Dekker, New York, pp 485–512

Wahlgren MC, Arnebrant T, Paulsson MA (1993) The adsorption from solutions of β-lactoglobulin mixed with lactoferrin or lysozyme onto silica and methylated silica surfaces. J Colloid Interface Sci 158:46–53

Wantyghem J, Baron M-H, Picquart M, Lavialle F (1990) Conformational changes of Robinia pseudoacacia lectin related to modifications of the environment: FTIR investigation. Biochemistry 29:6600–6609

Wertz CF, Santore MM (2002) Adsorption and reorientation kinetics of lysozyme on hydrophobic surfaces. Langmuir 18:1190–1199

Wilson KP, Malcolm BA, Matthews BW (1992) Structural and thermodynamic analysis of compensating mutations within the core of chicken egg white lysozyme. J Biol Chem 267:10842–10849

Yokoyama Y, Ishiguro R, Maeda H, Mukaiyama M, Kameyama K, Hiramatsu K (2003) Quantitative analysis of protein adsorption on a planar surface by Fourier transform infrared spectroscopy: lysozyme adsorbed on hydrophobic silicon-containing polymer. J Colloid Interface Sci 268:23–32

Yoon BJ, Lenhoff AM (1992) Computation of the electrostatic interaction energy between a protein and a charged surface. J Phys Chem 96:3130–3134

Zhou J, Chen S, Jiang S (2003) Orientation of adsorbed antibodies on charged surfaces by computer simulation based on a united-residue model. Langmuir 19:3472–3478

Zoungrana T, Findenegg GH, Norde W (1997) Structure, stability and activity of adsorbed enzymes. J Colloid Interface Sci 190:437–448

7 Evaluation of Proteins on Bio-Devices

Satoka Aoyagi, Masahiro Kudo

Abstract. The evaluation of proteins on bio-devices is one of the most important issues in biotechnology fields. In particular, evaluation of the changes in orientation and partial changes in structure of immobilized proteins are required for the development of sophisticated bio-devices. There are various methods being developed for protein evaluation. In this chapter, time-of-flight secondary ion mass spectrometry (TOF-SIMS), one of the most sensitive surface analysis methods, is described in terms of protein measurement. TOF-SIMS is useful for the evaluation of bio-device surfaces because it provides a submicron-scale mapping, orientation, and conformation of immobilized proteins on devices. In addition, TOF-SIMS requires no pretreatment of samples, such as labeling with a fluorescent probe or coating with metallic thin films, to prepare the samples. In the near future, conformation change of proteins after reactions or environmental change, such as changes in pH and orientation of binding sites of immobilized protein, will be measured with TOF-SIMS based on the analysis of partial chemical structures.

7.1 Introduction

This article describes the evaluation and observation of proteins immobilized on substrates by means of time-of-flight mass spectrometry (TOF-SIMS), and discusses briefly the evaluation of reactions between immobilized protein and free protein using TOF-SIMS imaging at the submicron level.

The monitoring of proteins on material surfaces is useful for the development of high-performance bio-devices such as artificial organs and biosensors. TOF-SIMS is one of the most useful techniques for the eval-

Satoka Aoyagi: Faculty of Life and Environmental Science, Department of Regional Development, Shimane University 1060 Nishikawatsu-cho, Matsue-shi, Shimane, 690-8504, Japan, Shimane University, Japan, E-mail: aoyagi@life.shimane-u.ac.jp

Masahiro Kudo: Department of Materials and Life Science, Seikei University, Japan

Principles and Practice
Proteins at Solid–Liquid Interfaces
Philippe Déjardin (Ed.)
© Springer-Verlag Berlin Heidelberg 2006

uation of bio-device surfaces, because it provides a submicron-scale look at the distribution of proteins on materials. In addition, TOF-SIMS requires no pretreatment of samples, such as labeling with a fluorescent probe or coating with metallic thin films, to prepare the samples, although radioisotope labeling is sometimes employed to enhance detection sensitivity. Furthermore, both the identification of proteins and investigation of the orientation of immobilized proteins may be carried out using this technique. However, at present TOF-SIMS is not suitable for the ionization of large molecules such as proteins. Therefore, special data analysis techniques have often been employed for the characterization of TOF-SIMS spectra, utilizing fragment ions from large molecules.

Secondary ion mass spectrometry (SIMS) is a method for detecting ions, including those molecular ions produced by collisions between primary ions and atoms and molecules on a sample surface. SIMS provides qualitative and quantitative information on the sample surfaces via mass spectra, depth profile, chemical structure, and chemical mapping, in the form of secondary ion images. TOF-SIMS is one of the SIMS techniques carried out with a TOF mass spectrometer, which is the most sensitive analyzer, and which has the widest mass spectrum range.

Certain analytic techniques have often been employed for the characterization of TOF-SIMS spectra with fragment ions from large molecules such as proteins and polymers, because TOF-SIMS is not suitable for the ionization of intact macromolecules. In particular, there is a problem in the case of the measurement of proteins with TOF-SIMS: since every protein consists of the same 20 amino acids, it is difficult to discriminate between proteins based on a simple comparison of the fragment ions. Certain types of polymers also have this same problem. In order to overcome this problem, appropriate spectrum analysis techniques are needed.

Multivariate analysis techniques, such as principal component analysis (PCA) and linear discriminant analysis (LDA), have been employed to interpret TOF-SIMS spectra using fragment ions related to proteins (Belu et al. 2003; Lhoest et al. 1998, 2001; Mantus et al. 1993; Wagner and Castner 2001; Wagner et al. 2002, 2004). PCA is especially useful for characterizing the TOF-SIMS spectra of protein samples. However, it is sometimes difficult to select specific peaks for the chemical imaging of proteins with PCA. Accordingly, information theory (Shannon and Weaver 1947) has been employed to analyze TOF-SIMS data on protein-containing biomaterials (Aoyagi et al. 2003). This innovation is now sufficiently developed so as to be able to obtain chemical images of protein samples. Mutual information (Shannon and Weaver 1947; Eckschlager et al. 1990), a technical term defined by information theory, characterizes the specificity of every peak in the TOF-SIMS spectra of a sample compared with another sample, such as a reference sample. With mutual information specific, the desired peaks

can be selected out of a great number of peaks that appear in TOF-SIMS spectra. In this article, the application of TOF-SIMS to protein measurement is described, and the latest research in this field is reviewed.

7.2 Time-of-Flight Secondary Ion Mass Spectrometry (TOF-SIMS)

7.2.1 Principles of TOF-SIMS

TOF-SIMS is a SIMS technique that utilizes a time-of-flight mass analyzer to enhance its sensitivity and expand its range of application (Vickerman and Briggs 2001). TOF-SIMS provides a characterization of complex sample surfaces such as protein-adsorbed materials, and chemical mapping information, for example, the imaging of the distribution pattern of a particular protein.

SIMS refers to the mass spectrometry of ionized particles (secondary ions) emitted by a beam of primary ions bombarding a surface. SIMS provides a characterization of a target surface by means of mass spectra, depth profiles, and secondary ion images. Surface mass spectra allow the identification and quantification of all constituent elements, isotopes, and molecular species via: (1) the controlled desorption of atoms and molecular species, (2) the efficient ionization of these desorbed particles, and (3) the unambiguous identification of the generated ions by their charge:mass ratios.

A detailed understanding of the interactions between ions and material surfaces, such as the phenomenon of sputtering, for example, is crucial for an appropriate application of SIMS. A beam of primary ions bombards a surface, leading to interactions that cause the emission of a variety of types of secondary particles, including secondary electrons, photons, neutrons, and positive and negative secondary ions from the sample, some of which recoil, so that the primary ions are scattered or implanted. The sputtering yield depends on the energy of the primary ions, the particular elements, the measurement conditions, and the encasing atmosphere (Benninghoven et al. 1987; Bubert and Jenett 2002; Vickerman and Briggs 2001). The processes of secondary-ion generation include sputtering and ionization processes that have not yet been fully clarified, although several simulations have been carried out and hypotheses put forward (Benninghoven et al. 1987; Krantzman et al. 2001). The ions emitted from organic samples are analyzed in a mass spectrometer, resulting in positive or negative mass

spectra consisting of the parent and fragment ion peaks characteristic of the surface. The major portion of the secondary particles are neutrons, while only a fraction of the $\sim 10^{-6}$–10^{-1} of the total are positively or negatively charged, and are called secondary ions (Benninghoven et al. 1993). Typical secondary ions from organic samples on metallic substrates are $Me^{+/-}$, $[M + H]^+$, $[M - H]^-$, $[M + Sa]^+$ and $[M + Me]^+$, where Me is a metal such as Ag, M is a molecule, H is hydrogen, and Sa is either Na or K.

SIMS currently employs two modes of measurement, dynamic and static. In the dynamic mode, primary ions with high current densities are used to bombard a sample surface, damaging the surface. Although the dynamic mode has an extremely high sensitivity, it is not applied to organic samples because the damage is too extensive to obtain useful chemical information. In the static mode samples are sputtered softly with low current densities to conserve chemical structures. In TOF-SIMS, pulsed primary ions with high current densities are used to obtain a high sensitivity and to prevent damage destroying the chemical structures.

TOF-SIMS is suitable for highly sensitive detection because TOF MS offers extremely high transmission in combination with parallel detection of all masses. Moreover, TOF-SIMS is able to prevent insult of a sample from charge-up using a low-energy ($\leq$ 20 eV) electron flood gun, which is pulse-controlled with a primary ion beam. In addition, with TOF-SIMS, biomaterials, including proteins, are qualitatively and quantitatively measurable, and the distribution of particular molecules may also be ascertained.

All emitted secondary ions are accelerated to a given potential, V (2–22 keV) and all ions with the same electric charge have the same kinetic energy in the TOF mass analyzer, as shown in Fig. 1. The velocity of each secondary ion depends on its weight, as shown in Eq. 1:

$$qE = (1/2)mv^2 \tag{1}$$

where q is the charge of the secondary ion (C), E is a given voltage (V), m is the weight of the secondary ion (kg), and v is the velocity of the secondary ion (m/s).

The ions are allowed to drift through a path of a given length, L (m) for time t (s), before reaching the detector:

$$L = vt \tag{2}$$

Therefore, ions having a mass-to-charge ratio, m:q, can be calculated using Eqs. 1 and 2:

$$m/q = t^2(2E/L^2) \tag{3}$$

Figure 2 shows the relationship between the time-of-flight and the mass of each secondary ion. The lighter ions reach the detector faster.

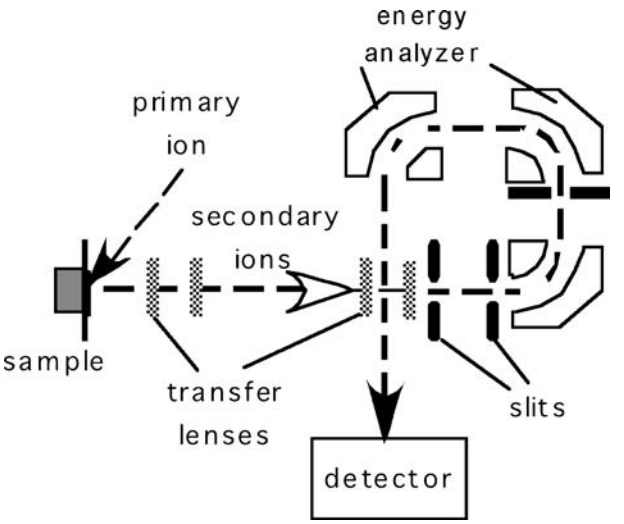

Fig. 1. Schematic of time-of-flight secondary ion mass spectrometry (TOF-SIMS; Cyclone type)

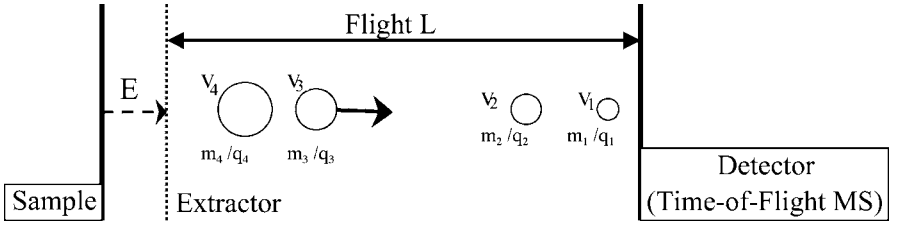

Fig. 2. Principles of the time-of-fight mass spectrometer (TOF-MS)

To date, liquid metal ion sources (LMIS) with low melting-point temperatures have been used mainly as the primary ion source for TOF-SIMS, because, $^{69}Ga^+$ ions (melting point 30°) in particular can be focused to a 50-nm minimum-diameter probe, while being pulsed at frequencies of up to 50 kHz and rastered at the same time.

Polyatomic ion sources such as Au_x^+ (the gold cluster ion), Bi_x^+ (the bismuth cluster ion), and C_{60}^+ (Postawa et al. 2003, 2004; Vickerman and Briggs 2001) have recently been developed and recognized to be useful for the measurement of biomaterials, especially proteins, because they produce a greater amount of the larger-fragment ions from proteins and polymers than the conventional primary ion sources. The production of larger-fragment ions from proteins is required for complicated samples that include several proteins. A further innovation of the ionization enhancement technique for SIMS will be required in order to obtain clear images of each individual protein.

7.2.2
TOF-SIMS Spectra and Secondary-Ion Images

Chemical Identification

TOF-SIMS produces mass spectra of positive and negative secondary ions from the outer few nanometers of material surfaces under static conditions. Secondary ions, including molecular ions, suggest the chemical structures and components of sample surfaces with a high mass resolution of over several 1000 atomic mass units (amu). In the case of an analysis of organic materials such as proteins, however, the organic analyte molecule cation yield is low. In order to achieve high yields of large molecular ions in SIMS with proteins, cationization of sputtered particles by means of complexation with substrate atoms is often used (Benninghoven et al. 1993; Wojciechowski et al. 2001). In these analyses, an organic analyte is deposited onto a clean metal surface, such as silver.

Chemical Imaging

The chemical components, elements, and molecules of a sample can be mapped by focusing the primary gallium ion beam to a diameter of 50 nm (the gold cluster ions and bismuth cluster ions may have the same spatial resolution; Winograd 1993) and rastering the sample surface as shown in Fig. 3. In order to obtain meaningful chemical images it is important to

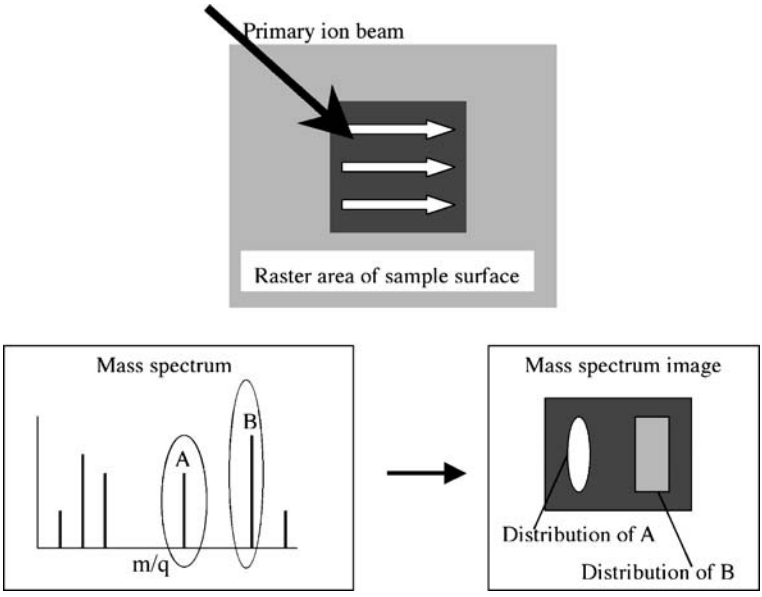

Fig. 3. Schematic of TOF-SIMS imaging

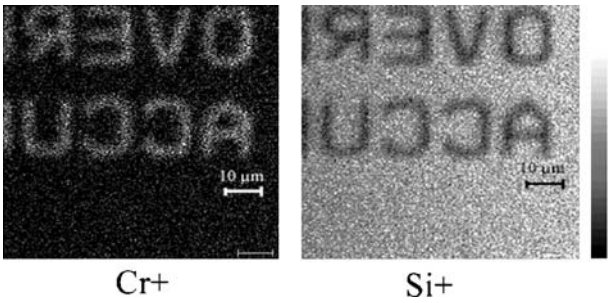

Fig. 4. TOF-SIMS images of chromium positive ion (*left*) and silicon positive ion (*right*) on a patterned glass plate

ensure a static condition by estimating the primary ion dose (Marletta et al. 1990); this will allow observation of the outer sample surfaces. Figure 4 shows some examples of secondary ion images obtained using chromium and silicon ions on a microscale patterned glass plate, on which the letters are patterned with chrome. These TOF-SIMS images were obtained with a gallium ion source.

Quantification

Quantitative analysis with TOF-SIMS requires very careful handling, as is the case with other SIMS applications, because the secondary ion yield depends on several sensitive factors, such as the sample matrix and elements involved, which are not directly proportional to the concentration of the components in the samples (Belu et al. 2003; Benninghoven et al. 1987).

The matrix effect is one of the most important factors in quantitative analysis with TOF-SIMS. The variability of the ion yield is constrained by changes in the surface composition. An identical substance does not have the same secondary ion yield in a different chemical environment, so simple comparisons among TOF-SIMS spectra are very difficult to carry out.

7.2.3 Data Analysis

Data analysis techniques are required when protein samples are measured with TOF-SIMS because it is difficult to obtain large intact molecular ions with enough intensity using current TOF-SIMS techniques. Since all proteins consist of the same 20 amino acids, TOF-SIMS spectra of protein-adsorbed films cannot be readily differentiated by the straightforward presence or absence of unique peaks. Proteins are large molecules, approximately 1–20 nm, and secondary ions from proteins are necessarily

from only partial areas or regions of the molecule. TOF-SIMS enables direct qualification and quantification of a protein sample from only partial information from a protein surface by utilizing analysis techniques appropriate to TOF-SIMS spectra, techniques such as multivariate analysis and information theory.

Although the latest SIMS techniques using the cluster ions as primary ion sources enable to obtain larger molecular ions from proteins, these SIMS spectra require data analysis methods because of the similarity of fragment ions. In addition, the orientation of immobilized proteins can be evaluated by means of TOF-SIMS spectra, because fragment ions provide useful information about the partial chemical structures of immobilized proteins.

Multivariate Analysis Techniques

Multivariate analysis techniques such as PCA (Huberty 1994; Jackson 1980; Wagner et al. 2004; Wold 1976, 1987) and LDA provide useful tools for gaining important information from large data sets (Mantus et al. 1993; Lhoest et al. 1998; Wagner et al. 2003b). PCA involves a mathematical procedure that transforms a number of correlated variables into a smaller number of uncorrelated variables called principal components (PCs). PCA can reduce the dimensionality of multidimensional space while retaining a large amount of the original information in the data. For example, two-dimensional data may be transformed into one-dimensional data, as shown in Fig. 5. The first PC accounts for as much of the variability in the data as possible, and each succeeding component accounts for as much of the remaining variability as possible. Moreover, PCA is one of the unsupervised pattern-recognition techniques, and therefore provides results that are unbiased by human input.

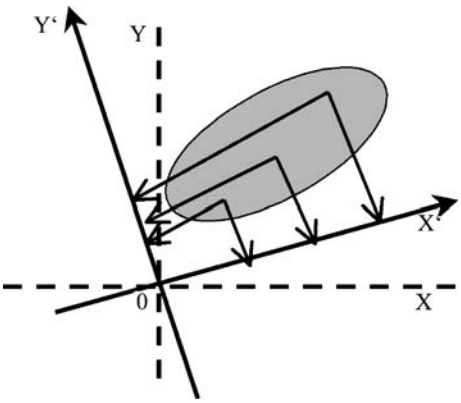

Fig. 5. Schematic of the principal component analysis (PCA) concept; concentration of the original information

PCA had been employed to characterize the SIMS mass spectra of polymers (Vanden Eynde and Bertrand 1999). PCA has also been applied to interpretations of the TOF-SIMS spectra of protein samples and extended the application of TOF-SIMS measurement to biomaterials. The following are the TOF-SIMS data analysis steps carried out in PCA. Prior to analysis, several peaks are selected from each spectrum. One of the selection criteria can be based on SIMS studies of amino acid homopolymers, as reported by Mantus et al. (1993). The intensities of the secondary ion peaks are normalized to the total ion count before PCA in order to correct for the differences in total secondary ion yield from spectrum to spectrum. Moreover, before applying PCA to a data set, it is necessary to properly pretreat the data to assure that the variance patterns highlighted are truly related to the chemical differences between the samples and not mathematical differences in peak intensities (Wagner et al. 2004).

A typical data set X with m samples and n peaks then can be written as a matrix, with m rows and n columns. These are transformed into PCs by multiplication of the appropriate matrix. The scores of each PC suggest the character of each sample, and it is one of the advantages of PCA that the analyst can easily determine how unspecified data fit within a particular data category by considering the scores and loadings. The score plot of the first two or three scores reveals the groupings, outlines, and other strong patterns in the data. Since PCA can be applied to any data matrix and is an unsupervised and hence unbiased analysis, it is recommended as an initial step in any multivariate analysis so as to obtain a first look at the structure of the data, to help identify outliers, to delineate classes, and so on. However, when the objective is classification or relating one set of variables to another, there are extensions of PCA that are more efficient for these purposes.

Discriminant analysis techniques such as LDA are methods for discriminating between several groups of discriminant function, and it is also one of the supervised analysis techniques. Origins of data are considered during the calculation of LDA to relate data from the same group samples. LDA is especially applied to find specific secondary ion peaks that will be used to characterize the samples.

Information Entropy

Mutual information, which is defined by information theory (Shannon and Weaver 1947), was employed to select peaks from numerous candidates in the TOF-SIMS spectra of proteins (Aoyagi et al. 2003, 2004a, b). Mutual information (Eckschlager 1990; Shannon and Weaver 1947) is obtained by subtracting *a posteriori* entropy (uncertainty) from *a priori* entropy (uncertainty). In this formulation, a posteriori entropy is defined as information entropy that occurs after an event.

The calculation steps are as follows. Suppose the number of TOF-SIMS spectra is N and they are classified in two categories, the sample and the reference sample. The number of spectra belonging to the sample is n(a1) and that belonging to the reference sample is n(a2). In terms of sample categories, information entropy S(A) is defined by the following equation:

$$S(\mathrm{A}) = -\sum p(\mathrm{ai}) \log_2 p(\mathrm{ai}) \tag{4}$$

where the probability $p(\mathrm{ai}) = n(\mathrm{ai})/N (I = 1, 2)$ and S(A) is the amount of information needed to determine the a priori category of a spectrum. With a certain peak threshold V, the set of spectra are split into two subsets B1 and B2. The peak intensity greater than V is classified as B1 and the number of the spectra containing these peaks as n(b1), and that less than V is classified as B2 and the number of the spectra containing these peaks as n(b2). Therefore, the information entropy of splitting induced by V, S(B) is defined by the equation:

$$S(\mathrm{B}) = -\sum p(\mathrm{bj}) \log_2 p(\mathrm{bj}) \tag{5}$$

where the probability $p(\mathrm{bj}) = n(\mathrm{bj})/N (j = 1, 2)$

Mutual information I(A;B) is defined by equation:

$$I(\mathrm{A};\mathrm{B}) = S(\mathrm{A}) - S(\mathrm{A}|\mathrm{B}) \tag{6}$$

$$S(\mathrm{A}|\mathrm{B}) = -\sum \sum p(\mathrm{bj}) p(\mathrm{ai}|\mathrm{bj}) \log_2 p(\mathrm{ai}|\mathrm{bj}) \tag{7}$$

where the probability $p(\mathrm{ai}|\mathrm{bj}) = n(\mathrm{ai}|\mathrm{bj})/n(\mathrm{bj})$, S(A) is the a priori uncertainty and S(A|B) is the a posteriori uncertainty. The term n(ai|bj) is the number of spectra belonging to sample category i out of the spectra containing peaks greater than V. The best value of V is chosen to provide the largest I(A;B). When I(A;B) = S(A), the peak intensity of each spectrum is classifiable into the correct category.

For example, there are TOF-SIMS spectra of two samples, A and B. We can compare the intensities of a certain peak. In case 1, the intensities of the peak cannot be classified with an appropriate threshold V. Therefore, *a priori* entropy equals the *a posteriori* entropy. This *a posteriori* entropy is information entropy after the estimation of the peak intensity with threshold V. In this case, the mutual information is zero. In other words, nothing is clarified by evaluation of the peak intensity with V. In case 2, peaks are completely classified by the threshold V. Therefore, the *a posteriori* entropy is zero, and the mutual information is 1. In other words, when mutual information equals the *a priori* entropy, this peak is the most important peak for classifying the samples.

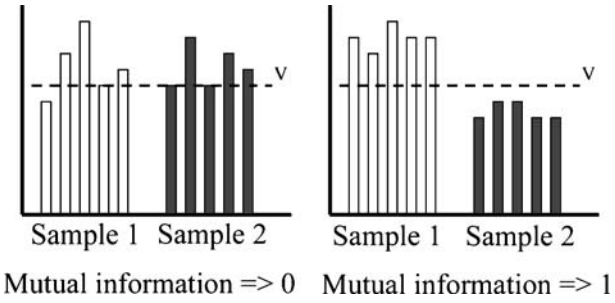

Fig. 6. Classification concept based on mutual information

Others

Partial least square regression was also applied to an interpretation of TOF-SIMS spectra (Wagner et al. 2004b), and an artificial neural network (ANN) was employed to chemically classify the SIMS spectra of adsorbed protein films. Sanni et al. (2002) reported a comparison of PCA and ANN in the characterization of protein spectra, and indicated the superiority of the ANN technique to distinguish the spectra of all of the adsorbed protein films using the entire mass spectrum. Other chemometric (Eckschlager et al. 1990; Gallagher et al. 2004; Vogt and Mizaikoff 2003) analysis techniques should also prove helpful for the correct interpretion of the TOF-SIMS spectra of complicated samples.

7.3 Analysis of Proteins on Bio-Devices

TOF-SIMS is used to analyze the characterization, distribution, conformation, and orientation of proteins on substrates. TOF-SIMS analysis techniques have been applied to a certain extent to the surface and interface investigation of bio-devices such as biosensors and implant materials. Since these protein analysis TOF-SIMS techniques are only just being developed, the use of some of them is currently limited. In the near future, TOF-SIMS techniques will provide the most important information on proteins at solid–liquid interfaces. In this article we describe the latest examples of application of TOF-SIMS to the evaluation of proteins on bio-devices.

7.3.1 Characterization of Proteins on Substrates

The characterization of the proteins adsorbed, or immobilized, on substrates by TOF-SIMS has contributed to the development of other analyti-

cal techniques. In 1986, the isolation of an apolipoprotein was studied with TOF-SIMS (Jabs et al. 1986), and an accurate evaluation of the molecular weight of peptides was obtained. Moreover, it became evident at that time that it was feasible using this method to monitor on a microscale basis the genetic polymorphisms of proteins and posttranslational modifications.

Kröger et al. (1998) reported the surface analysis of an optical immunosensor using TOF-SIMS; however, in this research, the role of TOF-SIMS was in fact subsidiary and quite limited, targeted to the mere finding of a product of a reaction. There have really been very few repots on the surface analysis of biomaterials carried out mainly by TOF-SIMS until the twenty-first century. Although TOF-SIMS is very useful for simple chemical analysis with x-ray photoelectron spectroscopy (XPS; Léonard et al. 2001; Lhoest et al. 1998; Wagner et al. 2003a), it has recently been shown that TOF-SIMS is in fact the most useful tool for characterizing complicated samples, including samples comprising of biological molecules.

In order to analyze the interactions between artificial surfaces and proteins, a spectral interpretation protocol is required. There are numerous possible fragment ions from proteins out of the various combinations of the constituent 20 amino acids. Since it is difficult to estimate every combination, homopolymers of 16 amino acids were examined with static SIMS by Mantus et al. (1993). The results were used to establish the first step of a spectral interpretation protocol for protein surfaces. Both positive and negative ion mass spectra were estimated by Mantus et al., and negative ion mass spectra were found to afford much less information than the mass spectra of the positive ions. Wagner and Castner (2001) reported the same result, confirming that positive ion mass spectra are the most suitable for protein analysis with SIMS. Subsequently, plasma proteins adsorbed to titanium substrate were analyzed with static SIMS based on this protocol. Moreover, the adsorption of fibronectin was investigated using TOF-SIMS based on this protocol (for proteins) in comparison with two other techniques, radiolabeling and XPS (Lhoest et al. 1998). As a result, it was found that the TOF-SIMS peaks characteristic of proteins exhibit differences in reduced intensity between the two substrates. It was suggested that these differences, which are not detectable by XPS, are attributable to different orientations and/or conformations of the proteins.

Investigation of the SIMS spectra for amino acid homopolymers can provide helpful information, but detailed studies of protein spectra have not been forthcoming because of the complexity of the mass spectra involved. Therefore, multivariate analysis techniques such as PCA have been applied to analyze the SIMS spectra. PCA reduces a large set of correlated variables, such as peak intensities in a mass spectrum, to a smaller number of uncorrelated variables referred to as PCs, as described above. Lhoest et al. (2001) reported characterization of adsorbed proteins such as bovine serum albu-

min (BSA), bovine plasma fibrinogen, bovine plasma fibronectin (Fn), and chicken egg white lysozyme, on mica and polytetrafluoroethylene (PTFE) substrates using TOF-SIMS with PCA. According to this research, PCA was implemented to enable the classification of several reference, positive-ion protein spectra according to protein and substrate type, and the combination of TOF-SIMS with PCA indeed did enable such a classification. The combination proved capable of classifying proteins by type in cases of pure protein spectra based on the score plots for each sample, and the relative surface concentration in the case of the binary protein spectra for BSA and Fn was based on a ratio of the peak intensities. Since BSA and Fn have large differences in their respective amino acid compositions, it is relatively easy for PCA to differentiate between the two proteins on the surface. The relative concentrations of BSA and Fn can be tracked using the ratio of the intensities of certain peaks, some ratios are more prevalent in one protein than in the other; for example, the ratios of threonine to glutamic acid or phenylalanine to tryptophan (BSA: Glu 10.12%, Phe 4.63%, Thr 5.66%, and Trp 0.34%, Fn: Glu 5.96%, Phe 2.03%, Thr 10.68%, and Trp 1.68%). The position of each peak in the loading plot represents its influence on the score plot, and supported the amino acid composition of BSA and Fn.

A variety of proteins on mica and PTFE substrates have been evaluated by means of TOF-SIMS and multivariate analysis, for example the PCA and LDA carried out by Wagner and Castner (2001, 2003) and Wagner et al. (2002, 2003a,b). LDA enhanced both the discrimination between groups and classification of unknowns because of its supervised nature. The TOF-SIMS spectra for albumin, collagen, cytochrome C, fibrinogen, fibronectin, hemoglobin, lactoferin, lysozyme, myoglobin, and transferrin films adsorbed onto PTFE were classified by PCA and LDA (Wagner and Castner 2001). Furthermore, it has been shown that qualitative information is obtainable for complex plasma and serum protein films using the multivariate analysis results from single-protein TOF-SIMS spectra. Quantitative results are also obtainable for binary adsorbed protein films, although such results depend on the substrate chemistry and morphology (Wagner et al. 2003b).

The TOF-SIMS measurement of proteins on metallic substrates and PTFE is an easier application of TOF-SIMS to biomaterials (Aoyagi et al. 2004b; Davies et al. 1996; Heard et al. 2001; Poleunis et al. 2002; Pradier et al. 2002; Wagner and Castner 2004), because ions from metal substrates and polymer substrates free of nitrogen, such as PTFE, can be distinguished from protein fragment ions quite easily. In addition, the latest research has demonstrated that cluster primary ions, such as the gold cluster, the bismuth cluster ions, and C_{60}^+ ions enhance peptide molecular ion yields. Tempez et al. (2004) reported that there are advantages of using large polyatomic gold clusters, Au_{400}^+, as the primary ion: (1) enhanced secondary ion yield of the intact molecule, (2) significantly improved S/N ratio, and (3) reduced

fragmentation. Similar advantages are also indicated in the case of using smaller cluster ions such as Au_3^+. Examples with the cluster primary ions will be described here later.

7.3.2 Investigation of Conformation and Orientation of Proteins on Substrates

Based on the investigation of fragment ions from proteins, information on the conformation and orientation of the proteins can be evaluated using TOF-SIMS spectra. TOF-SIMS produces important fragment ions with information regarding chemical structures at the uppermost surfaces of the samples. The surface is bombarded with a pulsed primary ion beam, inducing the desorption of particles. Because of the matrix effect, the desorption probability of particles and the formation probability of particular secondary ions strongly depend on the surface chemical structure, orientation, and molecular ambience (i.e., TOF-SIMS can be used to analyze not only the surface composition per se, but also the orientation and steric arrangement of molecules).

Since the sampling depth of TOF-SIMS in the static mode is approximately 1 nm, a thickness much less than for most proteins, TOF-SIMS is able to detect information about the conformation and orientation of proteins on substrates. There are two interesting approaches to the conformation and orientation of proteins on substrates that have been proposed in recent publications: one (Leufgen et al. 2003) is based on SF_5 primary ions and the gentle ionization effect of gold substrate, and others (Coullerez et al. 2003; Xia and Castner 2003) are based on spectrum analysis by PCA.

Leufgan et al. (2003) have reported the investigation of a template-assembled synthetic (TASP) protein conformation and its orientation in self-assembled monolayers (SAM) by means of TOF-SIMS. In this study, both the presence and molecular orientation of the TASP molecule can be monitored by TOF-SIMS, and furthermore, the influence of self-assembly protocols on the TASP molecular surface orientation, which can be studied though Fourier transform infrared spectroscopy and surface plasmon resonance are not able to offer data applicable to these targets.

Xia et al. (Xia and Castner 2003; Xia et al. 2002) have investigated the preservation of the structure of adsorbed protein film during drying procedures in ultrahigh vacuum surface analysis techniques such as SIMS. Two methods, trehalose protection and glutaraldehyde fixation, were studied to preserve adsorbed protein structures under an ultrahigh vacuum conditions. Using the combination of PCA and static TOF-SIMS, it was found that trehalose protection could reduce the conformational change of fibrinogen

upon drying, and in particular prevent it from unfolding and thus exposing its hydrophobic domains. In addition, it has been indicated that the other method, glutaraldehyde fixation, is a valuable alternative stabilizing method, since the structural differences observed between glutaraldehyde-fixed protein films before and after drying are very similar to those observed between trehalose-protected and -unprotected dried protein films.

7.3.3 Imaging of Protein Distribution

TOF-SIMS is the most useful technique for evaluating proteins on surfaces because it provides chemical mapping at a high spatial resolution. The chemical mapping of oligopeptides immobilized on an array of gold microelectrodes was obtained as secondary ion images with the peptide-dried ion $C_4H_8N^+$ (Mathieu 2001). In this case, the peptide image was obtained by conventional spectrum analysis, because components of the substrate were different from the peptide, and the fragment ions from the substrate and the peptide were therefore readily distinguishable.

One specific kind of protein found on substrates, which are composed of substances different from proteins, such as metallic substrates and polymers free of nitrogen, can be easily imaged by conventional TOF-SIMS techniques (Aubagnac et al. 1999; Belu et al. 2001). However, it is difficult to obtain one specific protein mapping from out of a collection of other proteins, especially on complicated materials containing nitrogen, because TOF-SIMS is not suitable for the ionization of large, intact molecules. In order to obtain chemical images of proteins, the specific peaks related to each protein must be selected from out of the TOF-SIMS spectra. Therefore, appropriate data analysis techniques are required for the characterization of TOF-SIMS spectra with fragment ions from large molecules. Moreover, since every protein consists of the same 20 amino acids, it is extremely difficult to discriminate between proteins based on a simple comparison of the fragment ions. Multivariate analysis techniques such as PCA and LDA have been employed to interpret TOF-SIMS spectra using fragment ions related to proteins.

Although LDA is considered suitable for the selection of specific peaks, the selection process requires either a great deal of data, or pretreatment of the data so as to prevent spurious discrimination. Fragment ions from bio-devices are often unpredicted because they contain complicated chemical additives in order to make them highly biocompatible and have high performance. In addition, since some of fragment ions from substrate materials generate complicated protein-like fragment ions, it is difficult to select appropriate peaks of fragment ions for data analysis of TOF-SIMS

spectra. Therefore an analysis technique which can be applied all peaks in spectra is required. Information theory has been employed to help analyze TOF-SIMS data on biomaterials containing proteins to enable a selection of several important peaks from all peaks (Aoyagi et al. 2003, 2004a,b).

Mutual information, as defined by information theory, describes the specificity of every peak in the TOF-SIMS spectra of a sample in comparison with another sample, such as a reference sample. With mutual information, important and specific peaks can be selected out of numerous candidate peaks, even in numbers ranging from several hundreds to 1,000 or more. Then selected peaks, however, should be checked based on their peak properties, such as chemical structures, noises, and distributions, because sometimes inappropriate peaks are selected by means of automatic analysis. Finally, the selected specific peaks provide the distribution of a particular protein on bio-devices. For example, Fig. 7 shows the distribution of immobilized protein on a glass surface with a chromium pattern. Protein molecules are immobilized on the glass surface through a covalent bond using the hydroxyl group. The images of amino acid fragment ions related to the protein mach the image of the glass surface shown by the Si^+ image.

The protein adsorption that takes place on hollow-fiber dialysis membranes with nanosized pores, which are used for the treatment of patients

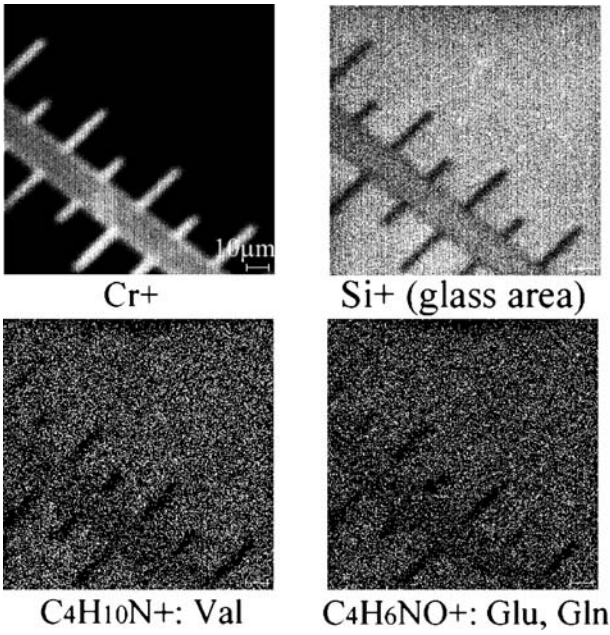

Fig. 7. TOF-SIMS images of amino acid fragment ions related to proteins on a chromium-patterned glass surface

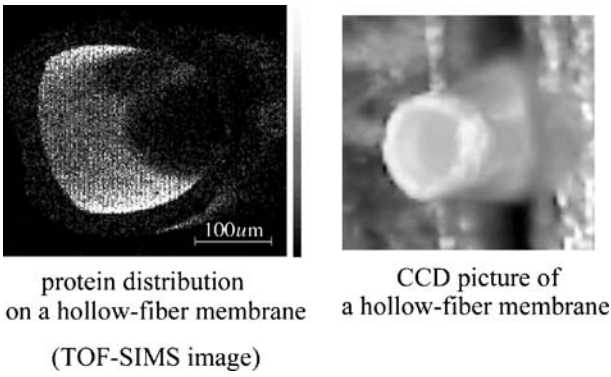

Fig. 8. TOF-SIMS image of protein adsorbed onto hollow-fiber membranes

with renal failure, has been evaluated by TOF-SIMS imaging in an effort to develop higher-performance dialysis techniques. The adsorption of a model protein, BSA, onto three commercially available, hollow-fiber dialysis membranes of different components and different structures, was measured with TOF-SIMS, and then the SIMS spectra were analyzed in the light of mutual information to select specific peaks for chemical imaging (Aoyagi et al. 2003, 2004a).

Figure 8 shows the secondary ion images of BSA adsorbed onto hollow-fiber membranes composed of polyacrylonitrile, according to the secondary positive ions related to the adsorbed BSA obtained from TOF-SIMS data analyzed with mutual information. Since TOF-SIMS secondary ion images are influenced by sample topography and the useful ion yield is dependent on certain chemical features, chemical images are needed for comparison with the total ion images.

The distribution and immobilization processes (Aoyagi et al. 2005; Chatterjee 2004; Hagenhoff 1995; Loyd and O'Keefe 2004) of proteins on biosensor surfaces have been measured using TOF-SIMS with mutual information or multivariate analysis. In order to allow a detailed control and specific tailoring of interfaces, a surface analytical tool is required that is able to localize, identify, and quantify the molecular structures of interest (Souda 2004). The distribution patterns of two proteins on a glass plate have been observed by TOF-SIMS imaging (Aoyagi et al. 2005). Both protein A, immobilized on the glass plate, and immunoglobulin G (IgG), bound to the immobilized protein A, were measured with TOF-SIMS and then their spectra were analyzed using PCA and mutual information. The PC score plots indicate that the fragment ions from protein A and those from the IgG could be distinguished with the TOF-SIMS spectra, and chemical images were obtainable based on mutual information. The TOF-SIMS images of

each protein reveal the distributions of protein A and IgG on the glass plate, and indicate that protein A is immobilized on the plate homogeneously, and that the reaction between the immobilized protein A and the IgG is not specifically localized.

This technique will be of special value for the evaluation of bio-devices containing biomolecules on their surfaces in order to confirm both the immobilization processes and the orientation of the immobilized molecules.

7.3.4 Other Points and Future Directions

In terms of the study of protein at interfaces, the interaction between water molecules is one of the most important points. However, it is difficult to consider the influence of water accurately because water is a complex and poorly understood liquid. Souda (2004a,b,c), Kawanowa et al. (2004), and Gunster and Souda (2005) have reported the study of hydration of organic substances on the water–ice surface using temperature-programmed TOF-SIMS. This technique will contribute to aid protein study in future.

In order to analyze complicated biomaterials, for example living materials such as internal organs and tissues as well as multifunctional biosensors, new TOF-SIMS techniques will be needed for the measurement of biopolymers. Among the innovations needed will be: (1) enhancement of the level of ionization of important secondary ions for the characterization and imaging of samples, and (2) production of intact or larger-fragment ions from biopolymers to allow the characterization and distinction of each protein and polymer. The enhancement of cationization by alkaline metals such as silver and gold (Bourdos et al. 2000; Wojciechowski et al. 2001) has been used for SIMS techniques and should also prove effective for protein measurement. Postionization by laser-secondary neutral mass spectrometry (SNMS; Dambach et al. 2004; Schnieders and Benninghoven 2000) and matrix-enhancement SIMS (Delcorte et al. 2004; Malyarenko et al. 2004; Wu and Odom 1996), based on matrix-assisted-laser-desorption/ionization-like sample preparation, are both expected to help provide more useful information.

Currently, cluster primary ions (Kollmer 2004; Thompson et al. 2004) such as C_{60}^+, Au_3^+ and Bi_3^+, which produce larger-fragment ions from proteins, are employed in the analysis of biomaterials (Xu et al. 2004). In particular, the C_{60}^+ ion source produces much larger fragment ions from macromolecules, such as proteins with measured intensities of up to 10,000 times greater than those obtained using a Ga^+ ion source (Postawa et al. 2003). In terms of spatial resolution, however, the C_{60}^+ ion source does not have the submicron-scale but rather one of approximately several microns

in size, and the Au_3^+ ion source has the same scale as that of the Ga^+ ion source (Kingshott et al. 2002; i. e., a submicron-scale spatial resolution), although its sensitivity for large fragment ions is not as high as the C_{60}^+ ion source.

Moreover, with integrating SIMS techniques including conventional techniques and novel ones, the protein depth profile, which provides information about the total chemical structure of a protein molecule immobilized on a device, will be developed in the near future

7.4 Summary

TOF-SIMS is a promising technique for evaluating proteins on bio-devices and for providing useful information about protein distribution at submicron spatial resolution, orientation, and conformation of immobilized proteins on devices. For example, TOF-SIMS spectra are able to contribute to an evaluation of the protein resistance of a polymer surface and protein formation dependent on treatment processes, and TOF-SIMS imaging provides information on the distribution of protein adsorption on artificial organs such as artificial kidneys. In addition, the reaction between protein immobilized on a solid surface and free protein in a solution is evaluated by means of TOF-SIMS techniques. In the near future, protein conformation changes after reactions or environmental changes, such as pH change and orientation of binding sites of immobilized protein, will be measured with TOF-SIMS based on the analysis of partial chemical structures.

SIMS spectra analysis techniques are necessary to interpret complicated and unpredictable SIMS data, even though SIMS with the cluster primary ion sources enhances the intensity of high-mass secondary ions. In addition, further improvements are required with respect to the production of larger and greater numbers of fragment ions and the methods of preparation of the bio-samples to enhance sensitivity. Both analysis and ion-production techniques will be considerably improved in the near future, and hence will enable a more precise measurement of various proteins on bio-devices.

References

Aoyagi S, Hayama M, Hasegawa U, Sakai K, Tozu M, Hoshi T, Kudo M (2003) TOF-SIMS imaging of protein adsorption on dialysis membrane by means of information entropy. eJ Surf Sci Nanotechnol 1:67–71

Aoyagi S, Hayama M, Hasegawa U, Sakai K, Tozu M, Hoshi T, Kudo M (2004a) Estimation of protein adsorption on dialysis membrane by means of TOF-SIMS imaging. J Membr Sci 236:91–99

Aoyagi S, Hiromoto S, Hanawa T, Kudo M (2004b) TOF-SIMS investigation of metallic material surface after culturing cells. Appl Surf Sci 231–232:470–474
Aoyagi S, Kawashima Y, Kudo M, (2005) TOF-SIMS imaging technique with information entropy. Nucl Instrum Methods Phys B 232:146–152
Aubagnac JL, Enjalbal C, Drout C, Combarieu R Martinez J (1999) Imaging time-of-flight secondary ion mass spectrometry of solid-phase peptide syntheses. J Mass Spectrom 34:749–754
Belu AM, Graham DJ, Castner DG (2003) Time-of-flight secondary ion mass spectrometry: techniques and applications for the characterization of biomaterial surfaces. Biomaterials 24:3635–3653
Belu AM, Yang Z, Aslami R Chilkoti A (2001) Enhanced TOF-SIMS imaging of a micropatterned protein by stable isotope protein labeling. Anal Chem 73:143–150
Benninghoven A, Hagenhoff B, Niehuis E (1993) Surface MS: probing real-world samples. Anal Chem 65:630–640
Benninghoven A, Rüdenauer FG, Werner HW (1987) Secondary Ion Mass Spectrometry (Chemical Analysis vol 86). Wiley & Sons, New York
Bourdos N, Kollmer F, Benninghoven A, Ross M, Sieber M, Galla HJ, (2000) Analysis of lung surfactant model systems with time-of-flight secondary ion mass spectrometry. Biophys J 79:357–369
Bubert H, Jenett H (2002) Surface and Thin Film Analysis. Wiley-VCH Verlag, Germany
Chatterjee R (2004) Application of TOF-SIMS to monitor coating processes on biological and organic surfaces. Appl Surf Sci 231–232:437–441
Coullerez G, Baborowski J, Viornery C, Chevolot Y, Xanthopoulos N, Ledermann N, Muralt P, Setter N, Mathieu HJ (2003) Imaging by time-of-flight secondary ion mass spectrometry of plasma patterned metal and oxide thin films. Appl Surf Sci 203:527–531
Dambach S, Fartmann M, Kriegeskotte C, Brüning C, Wiesmann HP, Lipinsky D, Arlinghaus HF (2004) Laser-SNMS analysis of apatite formation in vitro. Appl Surf Sci 231–232:506–509
Davies J, Nunnerley CS, Paul AJ (1996) A correlative study of the measurement of protein adsorption to steel, glass, polypropylene, and silicone surfaces using TOF-SIMS and dynamic contact angle analyses. Colloids Surf B 6:181–190
Delcorte A, Hermans S, Devillers M, Lourette N, Aubriet F, Muller JF Bertrand P (2004) Desorption/ionization of molecular nanoclusters: SIMS versus MALDI. Appl Surf Sci 231–232:131–135
Eckschlager K, Stepanek V, Danzer K (1990) A review of information theory in analytical chemometrics. J Chemom 4:195–216
Gallagher NB, Shaver JM, Martin EB, Morris J, Wise BM, Windig W (2004) Curve resolution for multivariate images with applications to TOF-SIMS and Raman. Chemom Intell Lab Syst 73:105–117
Gunster J, Souda R (2005) Water condensation on a hydrophobic surface: a structural self-trapping system. Phys Rev B 71:041407
Hagenhoff B (1995) Surface mass spectrometry – application to biosensor characterization. Biosensors and Bioelectronics 10:885–894
Heard PJ, Feeney KA, Allen GC, Shewry PR (2001) Determination of the elemental composition of mature wheat grain using a modified secondary ion mass spectrometer (SIMS). Plant J 30:237–245
Huberty CJ (1994) Applied Discriminant Analysis. Wiley & Sons, New York
Jabs HU, Assmann G, Greifendorf D, Benninghoven A (1986) High performance liquid chromatography and time-of-flight secondary ion mass spectrometry: a new dimension in structural analysis of apolipoproteins. J Lipid Res 27:613–621

Jackson JE (1980) Principal Components and factor analysis: part I – principal components. J Qual Technol 12:201–213

Kawanowa H, Kondo M, Gotoh Y, Souda R (2004) Hydration and H/D exchange of CH3OH adsorbed on the D_2O-ice surface studied by time-of-flight secondary-ion mass spectrometry (TOF-SIMS). Surf Sci 566:1190–1195

Kingshott P, Mcarthur S, Thissenm H, Castner DG, Griesser HJ (2002) Ultrasensitive probing of the protein resistance of PEG surfaces by secondary ion mass spectrometry. Biomaterials 23:4775–4785

Kollmer F (2004) Cluster primary ion bombardment of organic materials. Appl Surf Sci 231–232:153–158

Krantzman KD, Postawa Z, Garrison BG, Winograd N, Stuart SJ, Harrison JA (2001) Understanding collision cascades in molecular solids. Nuclear Instrum Methods Phys Res B 180:159–163

Kröger D, Katerkamp A, Renneberg R, Cammann K (1998) Surface investigations on the development of a direct optical immunosensor. Biosensors Bioelectron 13:1141–1147

Leufgen K, Mutter M, Vogel H, Szymczak W (2003) Orientation modulation of a synthetic polypeptide in self-assembled monolayers: a TOF-SIMS study. J Am Chem Soc 125:8911–8915

Lloyd KG, O'Keefe DP (2004) Re-discovering surface mass spectrometry: chemical mapping from micro to macro. Appl Surf Sci 231–232:207–216

Léonard D, Chevolot Y, Heger F, Martins J, Crout DHG, Sigrist H, Mathieu HJ (2001) TOF-SIMS and XPS study of photoactivatable reagents designed for surface glycoengineering: part III. 5-Carboxamidopentyl-n-[m-[3-(trifluoromethyl)diazirin-3-yl]phenyl-β-D-galactopyranosyl]-(1->4)-1-thio-β-D-glucopyranoside (lactose aryl diazirine) on diamond. Surf Interface Anal 31:457–464

Lhoest JB, Detrait E, van den Bosch de Aguilar P, Bertrand P (1998) Fibronectin adsorption, conformation, and orientation on polystyrene substrates studied by radiolabeling, XPS, and ToF SIMS. J Biomed Mater Res 41:95–103

Lhoest JB, Wagner MS, Tidwell CD, Castner DG (2001) Characterization of adsorbed protein films by time of flight secondary ion mass spectrometry. J Biomed Mater Res 57:432–440

Malyarenko DI, Chen H, Wilkerson AL, Tracy ER, Cooke WE, Manos DM, Sasinowski M, Semmes OJ (2004) Ga^+ TOF-SIMS lineshape analysis for resolution enhancement of MALDI MS spectra of a peptide mixture. Appl Surf Sci 231–232:357–361

Mantus DS, Ratner BD, Carlson BA, Moulder JF (1993) Static secondary ion mass spectrometry of adsorbed proteins. Analy Chem 65:1431–1438

Marletta G, Catalano SM, Pignataro S (1990) Chemical reactions induced in polymers by keV ions, electrons and photons. Surf Interface Anal 16:407–411

Mathieu HJ (2001) Bioengineered material surfaces for medical applications. Surf Interface Anal 32:3–9

Poleunis C, Rubio C, Compère C, Bertrand P (2002) Role of salts on the BSA adsorption on stainless steel in aqueous solutions. II. TOF-SIMS spectral and chemical mapping study. Surf Interface Anal 34:55–58

Postawa Z, Czerwinski B, Szewczyk M, Smiley EJ, Winograd N, Garrison BJ (2003) Enhancement of sputtering yields due to C60 versus Ga bombardment of Ag{111} as explored by molecular dynamics simulations. Anal Chem 75:4402–4407

Postawa Z, Czerwinski B, Szewczyk M, Smiley EJ, Winograd N, Garrison BJ (2004) Microscopic insights into the sputtering of Ag{111} induced by C 60 and Ga bombardment. J Phys Chem B 108:7831–7838

Pradier CM, Costa D, Rubio C, Compère C, Marcus P (2002) Role of salts on BSA adsorption on stainless steel in aqueous solutions. I. FT–IRRAS and XPS characterization. Surf Interface Anal 34:50–54

Sanni OD, Wagner MS, Briggs D, Castner DG, Vickerman JC (2002) Classification of adsorbed protein static TOF-SIMS spectra by principal component analysis and neural networks. Surf Interface Anal 33:715–728

Schnieders A, Benninghoven A (2000) Detection and quantification of metals in organic materials by laser – SNMS with nonresonant multiphoton ionization. Analytical Chemistry 72:4289–4295

Shannon CE, Weaver W (1947) The Mathematical Theory of Information. University of Illinois Press, Urbana, IL

Souda R (2004) Interactions of water with pyridine and benzene studied by TOF-SIMS. J Phys Chem B 108:283–288

Souda R (2004) Solvation of octane at water- and methanol-ice surfaces and surfactant effect of methanol at octane–water interface studied by temperature-programmed TOF-SIMS. J Phys Chem B 108:12159–12163

Souda R (2004) Hydration of polar and noepolar molecules at the surface of amorphous solid water. Phys Rev B 70:1–8

Tempez A, Schultz JA, Della-Negra S et al (2004) Orthogonal time-of-flight secondary ion mass spectrometric analysis of peptides using large gold clusters as primary ions. Rapid Commun Mass Spectrom 18:371–376

Thompson CE, Jungnickel H, Lockyer NP, Stephens GM, Vickerman JC (2004) TOF-SIMS studies as a tool to discriminate between spores and vegetative cells of bacteria. Appl Surf Sci 231–232:420–423

Vanden Eynde X, Bertrand P (1999) Quantification of polystyrene blend surfaces based on end group TOF-SIMS analysis. Appl Surf Sci 141:1–20

Vickerman JC, Briggs D (2001) TOF-SIMS: Surface Analysis by Mass Spectrometry. IM Publications and Surface Spectra, UK

Vogt F, Mizaikoff B (2003) Introduction and application of secured principal component regression for analysis of uncalibrated spectral features in optical spectroscopy and chemical sensing. Anal Chem 75:3050–3058

Wagner MS, Castner DG (2001) Characterization of adsorbed protein films by time-of-flight secondary ion mass spectrometry with principal component analysis. Langmuir 17:4649–4660

Wagner MS, Castner DG (2003) Characterization of adsorbed protein films using time-of-flight-secondary ion mass spectrometry and multivariate analysis. Appl Surf Sci 203–204:698–703

Wagner MS, Castner DG (2004) Analysis of adsorbed proteins by static time-of-flight secondary ion mass spectrometry. Appl Surf Sci 231–232:366–376

Wagner MS, Graham DJ, Ratner BD, Castner DG (2004) Maximizing information obtained from secondary ion mass spectra of organic thin films using multivariate analysis. Surface Sci 570:78–97

Wagner MS, Horbett TA, Castner DG (2003a) Characterizing multicomponent adsorbed protein films using electron spectroscopy for chemical analysis, time-of-flight secondary ion mass spectrometry, and radiolabeling: capabilities and limitations. Biomaterials 24:1897–1908

Wagner MS, Shen M, Horbett TA, Castner DG (2003b) Quantitative analysis of binary adsorbed protein films by time of flight secondary ion mass spectrometry. J Biom Mater Res 64A:1–11

Wagner MS, Tyler BJ, Castner DG (2002) Interpretation of static time-of-flight secondary ion mass spectra of adsorbed protein films by multivariate pattern recognition. Anal Chem 74:1824–1835

Winograd N (1993) Ion beams and laser postionization for molecule-specific imaging. Anal Chem 65:622–629

Wojciechowski I, Delcorte A, Gonze X, Bertrand P (2001) Mechanism of metal cationization in organic SIMS. Chem Phys Lett 346:1–8
Wold S (1976) Pattern Recognition 8. Pergamon, UK
Wold S (1987) Principal Component Analysis. Chemom Intell Lab Syst 2:37–52
Wu KJ, Odom RW (1996) Matrix-enhanced secondary ion mass spectrometry: a method for molecular analysis of solid surfaces. Anal Chem 68:873–882
Xia N, Castner DG (2003) Preserving the structure of adsorbed protein films for time-of-flight secondary ion mass spectrometry analysis. J Biomed Mater Res 67A:179–190
Xia N, May CJ, McArthur SL, Castner DG (2002) Time-of-flight secondary ion mass spectrometry analysis of conformational changes in adsorbed protein films. Langmuire 18:4090–4097
Xu J, Ostrowski O, Szakal C, Ewing AG, Winograd N (2004) TOF-SIMS imaging with cluster ion beams. Appl Surf Sci 231–232:159–163

8 Fibronectin at Polymer Surfaces with Graduated Characteristics

Tilo Pompe, Lars Renner, Carsten Werner

Abstract. Globular proteins adsorbed onto artificial materials often exhibit different functional characteristics due to an altered availability for molecular interactions. This effect is caused by the patterns of substrate–protein interactions and is attributable to conformational changes as well as to the orientation and/or the anchorage of the surface-confined proteins. To highlight this interrelation we report a detailed experimental investigation of the adsorption and displacement of fibronectin, a key protein of the extracellular matrix that enables cell adhesion, at a set of polymer thin films with various hydrophilicity, charge density and swelling characteristics. The patterns of protein displacement were analysed quantitatively for several substrates and adsorbed protein amounts, referring to a model recently suggested by Huetz et al. (Langmuir 11:3145–3152, 1995). The patterns of protein displacement were related to the substrate characteristics and the conditions applied during the formation of the protein layer (i. e. the solution concentration). These findings were compared with the reorganisation of adsorbed fibronectin on the compared polymer substrates by endothelial cells in culture. The results demonstrate that a certain binding strength of fibronectin is required to support the cell-driven formation of fibronectin fibrils, which, in turn, is an important prerequisite for the differentiation of the cells.

8.1 Introduction

Materials surfaces exposed to biofluids acquire biopolymer layers that undergo dynamic changes during time. The biomolecules adsorb, desorb and displace each other and may become subject to structural (conformational) changes caused by the altered local environment. Cells respond to the molecular characteristics of the biointerfacial layers by adhesion, motility

Tilo Pompe, Lars Renner, Carsten Werner: Leibniz Institute of Polymer Research Dresden, Max Bergmann Center of Biomaterials Dresden, Hohe Str. 6, 01069 Dresden, Germany, E-mail: carsten.werner@mbc-dresden.de

Principles and Practice
Proteins at Solid–Liquid Interfaces
Philippe Déjardin (Ed.)
© Springer-Verlag Berlin Heidelberg 2006

and the attainment of certain activities or functions. Among the secondary cellular processes, the secretion and degradation of matrix biopolymers and the reorganisation of these molecules into complex structures play a prominent role and determine the patterns of interaction between living and non-living matter at a vast majority of interfaces.

The very complex and dynamic nature of the biomolecular adlayers of materials arises from the complex composition of the biofluids and the biomolecules contained therein, their conformational changes during adsorption and the different interactions involved in the adsorption process. Therefore, and despite of a wealth of detailed investigations of various systems, a comprehensive model of protein adsorption at solid–liquid interfaces is still missing. Haynes and Norde (1994) pointed out that the interplay of hydrophobic and polar interactions, hydrogen bonds, van der Waals interaction, and entropic and structural forces determines protein adsorption in almost any setting.

The dynamics of the protein adsorption process onto solid surfaces and the involved conformational changes have been unravelled and modelled for various single-protein systems (Calonder and Van Tassel 2001; Haynes and Norde 1994; Huetz et al. 1995; Wertz and Santore 2002). Despite the complexity of interlinked processes involved even in the adsorption of a single protein, several investigations could establish general ideas on adsorption, desorption, and exchange from complex protein solutions. An early and widely known finding is referred to as the "Vroman effect" (Bamford et al. 1992), stating a sequential displacement of proteins from surfaces in a size-dependent manner with large proteins exhibiting the highest surface affinity due to the higher number of interacting segments. While convincingly explaining some systems, this simple picture cannot hold true for protein displacement processes in general. However, protein exchange experiments provide a valuable and realistic measure of the interaction strength of proteins with solid substrates, as was demonstrated by Grinell and Feld (1981).

Starting from these findings we analysed the impact of protein–substrate anchorage in the context of cell culture experiments to determine the environmental signals that trigger the fate decisions of adherent endothelial cells. We focussed on fibronectin (FN) as a key protein of the extracellular matrix that enables cell adhesion. A set of polymer surfaces was used as substrates; these were established from different alternating maleic anhydride copolymers. Covalently attached thin films of these copolymers allowed us to create a platform of substrates with graduated surface physicochemistry that was thoroughly characterised (Pompe et al. 2003b). In detailed protein adsorption and exchange studies, the adsorption kinetics and binding strength were studied and correlated to the protein surface concentration, protein conformation and surface interaction parameters

(Renner et al. 2004, 2005). Finally, the corresponding cellular interaction was investigated in cell adhesion and protein reorganisation experiments using endothelial cells (Pompe et al. 2003a, 2005a).

8.2 Gradated Substrate Physicochemistry

Addressing the very obvious need to establish structure–property relationships in biointerfacial processes, several approaches for the preparation of materials with controlled variation of the surface characteristics have been suggested over the last few years. In our approach, alternating maleic acid anhydride copolymers have been used as covalently attached coatings in order to switch the chemical reactivity of solid substrates towards biopolymers and to precisely adjust their physicochemical characteristics. Towards that aim, alternating maleic acid anhydride copolymers (Trivedi and Culbertsen 1982) were deposited as thin films on carrier materials. Through the choice of the comonomer and via conversions of the reactive anhydride moieties, a wide variety of surface parameters can be adjusted. While earlier works already made use of the high reactivity of maleic anhydrides for several surface modification concepts (Chapman et al. 2000; Jenkins et al. 2000), we have been able to demonstrate additional options of maleic anhydride copolymer coatings for the gradual variation of physicochemical surface characteristics with specific biomolecular functionalities and lateral constraints independent of the underlying substrate (Pompe et al. 2003b; Schmidt et al. 2002).

In the experiments reported herein, the latter features of alternating maleic anhydride acid copolymers were used to vary the polar–non-polar balance of the molecules as well as the structural characteristics of the macromolecules in polar and non-polar environments and, through this, the surface free energy and charge density of the copolymer films. It is hypothesised that the choice of comonomer influences the non-specific biopolymer binding (Malmsten 1998). To restrict the interactions with biopolymers to non-covalent ones the high reactivity of the anhydride moieties can be "switched off" by hydrolysis, creating surfaces that are characterised by the interplay between carboxylic acid groups and the features of the comonomer subunits.

To cover a broad range of interaction strengths, the following copolymers were utilised: -poly(octadecene-*alt*-maleic anhydride) (POMA), -poly-(propene-*alt*-maleic anhydride) (PPMA) and -poly(ethylene-*alt*-maleic anhydride) (PEMA).

Molecular images of the characteristic repeating units allow the visualisation of the decreasing ratio of the size of the non-polar comonomer

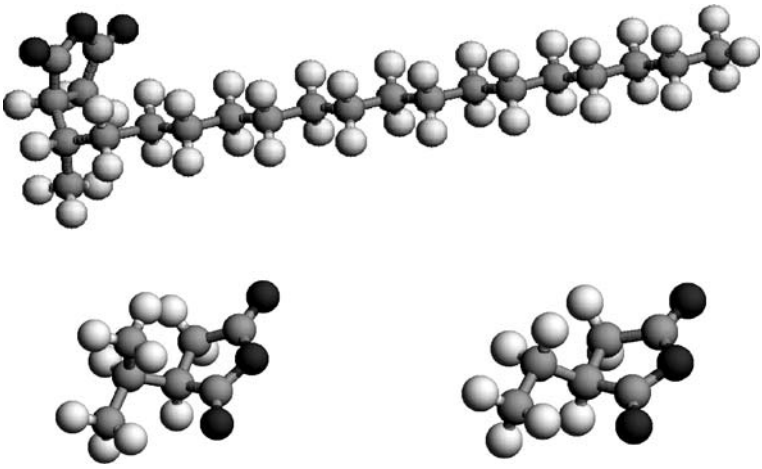

Fig. 1. A,B Molecule models of the repeating units of different copolymers: POMA (*top*), PPMA (*bottom left*) and PEMA (*bottom right*)

side chain and the polar anhydride group in the different copolymers in the order PEMA < PPMA < POMA (Fig. 1). Already from these images a tendency of the extended alkyl chains of POMA to self-assemble can be anticipated.

Thin films of the maleic acid anhydride copolymers were prepared by spin-coating, solution casting or adsorption on top of amine-bearing surfaces. Covalent attachment of the copolymers – realised through spontaneous reaction of the anhydride functions with the amines of the substrate – efficiently prevented delamination, reordering and dewetting of the films during further modification and application. Amino functionalisation of the substrates was achieved on SiO_2 surfaces (glass coverslips or silicon wafers) by silanisation with 3-aminopropyl-dimethylethoxy-silane. Polymer substrates were amino-functionalised by surface-selective, low-pressure plasma treatments in ammonia atmospheres (Nitschke et al. 2002; Tusek et al. 2001) or by oxygen plasma modification with subsequent amino-silane functionalisation.

The film thickness of the dry copolymer coatings was determined to be between 3 and 6 nm by ellipsometry for covalently attached layers (Table 1). The concentrations of accessible anhydride moieties of about 10^{14} /cm^2 were estimated from x-ray photoelectron spectroscopy (XPS) data via determination of the sulphur and nitrogen content of the surface after a reaction with 50 mM methionine amide hydrochloride in buffer solution for 1 h (Table 1). The determination assumes a density of 2.85 g/cm^3 of the detected SiO_2 from the silicon substrate and a mean attenuation length of the XPS signal in the substrate and the surface layer of about 3 nm (Mark et al.

Table 1. Physicochemical parameters of the maleic anhydride copolymer thin films used

Parameter	POMA	PPMA	PEMA
Thickness[1] (±0.5 nm)	3.5 nm	3.0 nm	4.5 nm
Anhydride surface density[2]	9×10^{13}/cm^2	3×10^{14}/cm^2	7×10^{14}/cm^2
Water contact angle[3] (±3 °C)	100°	38°	26°

[1]Determined by ellipsometry
[2]Determined by XPS after methionine amid conversion
[3]Measurement of hydrolysed copolymer surfaces

1987; Pompe et al. 2005b). Within this routine the elemental compositions (C, N, S, Si) of the layer components (SiO_2, maleic anhydride copolymer, methionine amide) were fitted to the XPS data in a least-square sense. The aminosilane surface concentration was set to a fixed value of 5×10^{14} /cm^2, which was determined independently on surfaces without copolymer films using the same method. Data collected using this approach reflect the anhydride density accessible for the reaction with amines from aqueous solutions, which is of interest in our set-up. The estimated anhydride surface concentrations for POMA, PPMA and PEMA agree well with the expectation of higher values for smaller comonomers (Table 1). Furthermore, the ratio of calculated anhydride to comonomer units shows the better accessibility of anhydride moieties for the more hydrophilic copolymers. The same tendency manifests itself in differences in the hydrophobicity of the copolymer films (Mark et al. 1987). A decreasing mass content of the polar anhydride component leads to a decrease in the surface energy. This was confirmed by measurements of the advancing water contact angles, which revealed differences in the hydrophobicity of the films related to the size of the hydrocarbon structure in the comonomer units (Table 1).

The physicochemical surface characteristics of the covalently attached thin films of the maleic anhydride copolymers were found to be graduated over a wide range in a well-defined manner. The variation in the degree of hydrophobicity and the density of functional anhydride moieties suggests not only an influence on the interaction strength with biopolymers, but furthermore, a variation in the structural characteristics of the copolymer films ranging from a hydrophobic, water-insoluble film (POMA) to point-attached, water-soluble copolymer chains (PEMA). The copolymer film characteristics under physiological buffer conditions were studied in a different set of experiments, as reported elsewhere (Pompe et al. 2005b). The swollen film thickness was determined from deflection–separation curves of scanning force microscope measurements and cross-checked by investigations with a quartz crystal microbalance with dissipation measurements (QCM-D). As expected, POMA exhibits no swelling, in contrast to PPMA and PEMA, which swell by a $N^{3/5}$ scaling known from free polymer chains

in a good solvent, or also termed a "mushroom" regime in the context of polymer brushes (Binder 2002). It was concluded that the copolymer chains are coupled to the amino groups on the substrate surface with a rather low frequency. The individual chains seem to have only one or very few grafting points to the surface, so they still behave like free copolymer chains with respect to the scaling to their molar mass. Changing the pH value to pH 3.0 led to a shrinkage in film thickness, which can be attributed to the change in ionisation of the primary and secondary carboxylic acid groups ($pK_{a1} = 3.0$ and $pK_{a2} = 7$; Dubin and Strauss 1967, 1970; Osaki and Werner 2003; Sugai and Ebert 1986). There exists a sensitive balance of repulsive electrostatic forces of the polar acid groups and attractive hydrophobic interactions of the non-polar alkyl moieties.

It follows, that not only the pH value but also the ionic strength can affect the degree of swelling of the copolymer films. As shown exemplarily in Fig. 2 for a PPMA film in different concentrations of phosphate-buffered saline (PBS) solution, this dependency is very pronounced in the range between 10^{-1} M and 10^{-3} M, but can be neglected above 10^{-1} M or below 10^{-3} M. While below 10^{-3} M the chains are probably almost fully stretched, the negligible shrinkage above 10^{-1} M can be attributed to the fully screened charges of the carboxylic acid groups. Because of this low degree of swelling under physiological conditions (10^{-1} M PBS) only minor or negligible influences of the compression of expanded polymer chains or protein penetration within the copolymer layers are expected for the protein exchange experiments reported below.

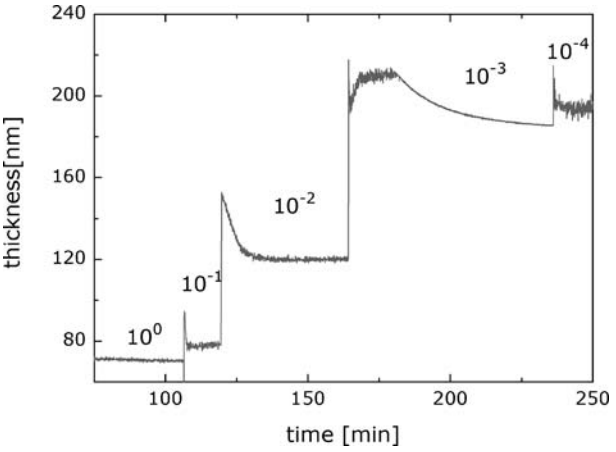

Fig. 2. Thickness of swollen films of hydrolysed PPMA at different ionic strengths of phosphate-buffered saline solutions, measured using a quartz crystal microbalance with dissipation measurements. The ionic strength at the different time points is indicated by the molar concentration of the buffer solution

Based on this knowledge of the physicochemical characteristics of the above-described set of copolymer thin films, the interactions directing protein anchorage and displacement could be analysed for the prominent example of surface-bound FN. The results obtained are reported in the subsequent sections.

8.3 Fibronectin Exchange at a Constant Surface Concentration

In a first set of experiments, interfacial FN exchange was studied at various compositions of the protein solution applied for the displacement. Homoexchange by FN as well as heteroexchange by human serum albumin (HSA) was measured by fluorescence confocal laser scanning microscopy (LSM), which was supported by high-performance liquid chromatography (HPLC)-based amino acid quantification. Based upon preceding studies (Salchert et al. 2003), the adsorbed amount of FN onto the polymeric surfaces was quantified by HPLC-based amino acid analysis. Time- and concentration-dependent adsorption experiments revealed that the surface coverage has almost reached a steady state at the chosen solution concentration of 50 μg/ml after 1 h of adsorption. Figure 3 indicates the quantity of adsorbed protein on the three copolymer surfaces.

The adsorbed amount of FN implies no simple side-on adsorption of the protein. An assumptive monolayer, supposing a side-on adsorption of a molecule with two arms of 60 nm length and 2.5 nm in diameter (Haeberli 1998), is calculated to be 0.25 μg cm^2. However, in a realistic scenario,

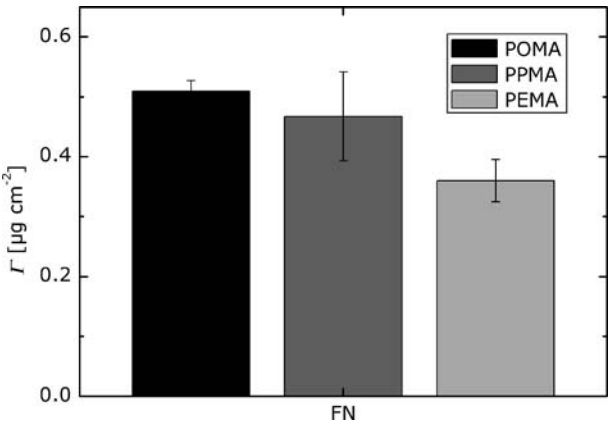

Fig. 3. Initially adsorbed surface concentration (Γ) of fibronectin (FN) on POMA, PPMA, and PEMA from a solution concentration of 50 μg/ml after 1 h of adsorption

adsorbed protein layers cannot be considered to create a homogeneous structure. The amount of FN gained may be attributed to the heterogeneity in the orientation of the adsorbed protein molecules, because a heterogeneous protein layer could combine both, side-on and end-on orientation in a random distribution.

FN exchange was studied immediately following the adsorption process only interrupted by rinsing with PBS. The kinetics of the surface coverage of rhodamine-conjugated FN, as determined by LSM measurements, showed distinct differences for the compared polymer films and exchange solutions. Both homo- and heteroexchange solutions were applied at a concentration of 50 µg/ml. The FN surface concentration during exchange is exemplarily shown on POMA for hetero- and homoexchange in Fig. 4A, and for heteroexchange by HSA at the three copolymer surfaces in Fig. 4B.

FN exerted a bigger impact on the displacement of the preadsorbed FN than HSA on POMA. In addition, the heteroexchange demonstrates the impact of the physicochemical characteristics of the polymer substrates, with an increasing exchange occurring on the more polar surfaces. The higher amount of FN exchanged on the hydrophilic surfaces (PEMA, PPMA) correlates with a stronger anchorage of FN at hydrophobic surfaces. Noticeable in Fig. 4 is that there is a fast decline during the first few hours of observation and an attenuation of the curves towards the later stages. We detected this as a general trend in all exchange experiments, which is in agreement with earlier published findings (Huetz et al 1995; Wertz and Santore 2002). Huetz et al. (1995) reported data indicating a similar behaviour for a model system of immunoglobulin molecules displaced by fibrinogen on a silica surface. The exchange mechanism was classified into a fast exchange step, followed by a slower step independent of the solution containing the molecules. The latter is apparently in contrast to our observation. Nevertheless, we have been able to describe the exchange process with two exponential functions on the basis of this theoretical approach with a coverage-dependent exchange kinetics giving,

$$\frac{\partial \Gamma}{\partial t} = -\frac{1}{\tau}\Gamma \tag{1}$$

where Γ and τ are surface coverage and desorption time constant, respectively. Assuming two protein species, fast (A) and slowly (B) desorbing, leads to:

$$\Gamma(t) = \Gamma_A \exp(-\frac{t}{\tau_A}) + \Gamma_B \exp(-\frac{t}{\tau_B}) \tag{2}$$

The results of the exponential fits to the measured exchange kinetics are summarised in Table 2. It is interesting to note that protein exchange

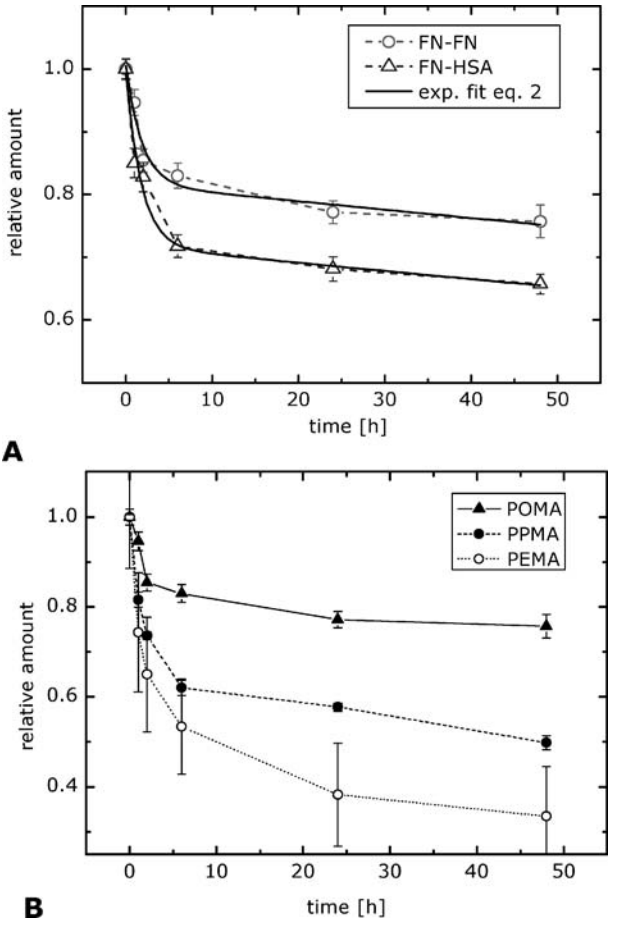

Fig. 4. A Displacement of adsorbed FN by FN and human serum albumin (*HSA*) on POMA (*circles*) and PPMA (*triangles*), and **B** by HSA on POMA, PPMA and PEMA. Relative amounts of preadsorbed protein remaining after incubation with different protein solutions were measured by laser scanning microscopy (LSM). The exponential fit (Eq. 2) is shown exemplarily in **A** (*solid lines*)

Table 2. Summary of the fit parameters of the exponential approach describing hetero- and homoexchange of fibronectin (*FN*) on maleic anhydride copolymer surfaces

Copolymer	Heteroexchange by HSA				Homoexchange by FN			
	$\tau_A(h)$	$\tau_B(h)$	Γ_A (μg/cm^2)	Γ_B (μg/cm^2)	$\tau_A(h)$	$\tau_B(h)$	Γ_A (μg/cm^2)	Γ_B (μg/cm^2)
POMA	1.8	530	0.19	0.81	1.8	530	0.27	0.73
PPMA	1.5	190	0.35	0.65	1.4	67	0.54	0.46
PEMA	1.3	83	0.44	0.56	2.1	266	0.2	0.8

was observed for FN on the hydrophobic POMA, which is in contrast to the findings of several earlier findings (Capadona et al. 2003; Pettit et al. 1992) on various different hydrophobic surfaces. However, desorption of small fractions of adsorbed protein layers was also reported in the literature (Wertz and Santore 2002). This confirms that protein adsorption phenomena do not simply depend on any single surface property, like hydrophobicity, but depend on a balance of several interactions.

In addition we were able to reliably convert the relative amount of adsorbed protein into absolute amounts with the aid of fluorescent calibration beads (for details see Renner et al. 2004). The conversion allows a more valuable comparison between the exchange kinetics of the protein amounts on both polymer surfaces and a rescaling to the quantitative surface coverage by the HPLC data. The calibrated absolute fluorescence intensities were shown to correlate well with the HPLC data by introducing the ratio between the amounts adsorbed onto PPMA and POMA (A_{PP}:A_{PO}). We gained values, which differ in the range of the mean error (Table 3), and concluded that the HPLC data corresponds to the converted absolute amount. Based on this correlation, the exchange kinetics measured by LSM could be rescaled to reflect the dynamic change of the surface coverage quantitatively.

Starting from there, the homo- and heteromolecular exchange of FN on the different copolymers could be analysed in more detail. The results shown in Fig. 5 for the homomolecular exchange indicate an exchange accompanied by additional adsorption on both polymer surfaces. The HPLC data indicate that although after the initial adsorption time of 1 h the amount of adsorbed FN increases further, it does so very slowly. This process can be attributed to conformational changes, reorganisation of the adsorbed protein layer or exchange of protein with adsorption in different orientations. Such processes are already known from the literature to occur over long time scales (Calonder et al. 2001; Haynes and Norde 1994; Nygren 1993; Wertz and Santore 1999). The exchange process is illustrated by the LSM data indicating the amount of remaining FN from the initial adsorption step with a more intense exchange on the hydrophilic PPMA surface.

A similar behaviour was measured for the heteromolecular exchange of FN on the two copolymer surfaces (Fig. 6). On the hydrophilic PPMA sub-

Table 3. Comparison of high-performance liquid chromatography (*HPLC*) data and converted absolute laser scanning microscopy (*LSM*) data using the mass or intensity ratios A_{PPMA}:A_{POMA}

	FN	HSA
LSM	0.89 ± 0.2	0.46 ± 0.17
HPLC	0.92 ± 0.15	0.62 ± 0.1

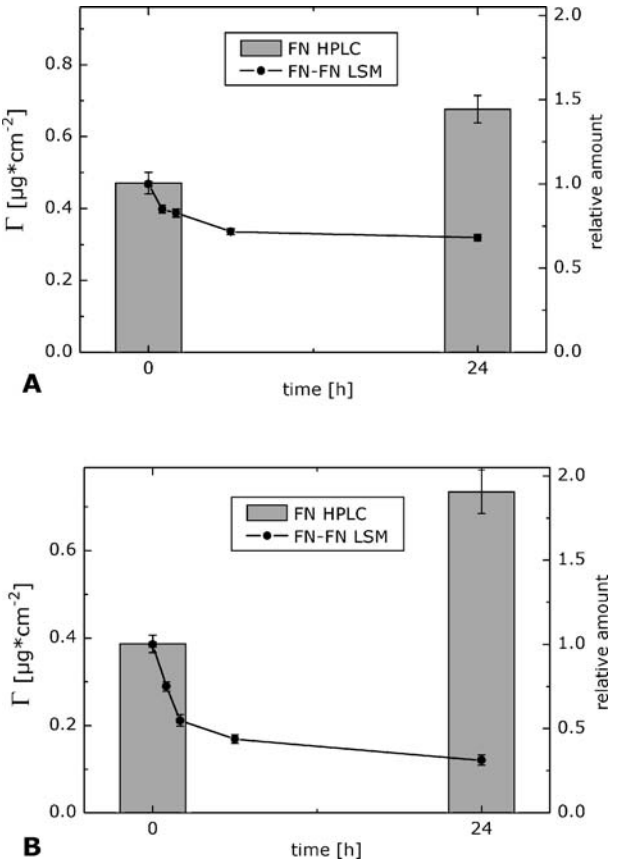

Fig. 5. **A** Homomolecular exchange of FN on POMA and **B** on PPMA, as measured by high-performance liquid chromatography (HPLC; *grey bars*) and LSM (*circles* and *solid lines*)

strate, more FN is displaced by HSA. Again, an increase in the total amount of adsorbed protein could be observed, which was attributed to conformational changes and exchange processes, as observed for the homomolecular system. The exchange kinetics clearly indicate a higher affinity of FN towards hydrophobic surfaces. Furthermore, the data given in Fig. 6 provide further evidence for the good agreement between HPLC and LSM analyses and proof of the reliability of the LSM measurements. While the influence of the fluorochrome on the adsorption and the exchange properties of the proteins might be critical in the LSM experiments, the agreement with the HPLC data of the unlabelled proteins indicate that the label has no influence on the adsorption and the exchange processes at the analysed settings. While HPLC provides more quantitative data, this ex situ method is limited to lower numbers of time points.

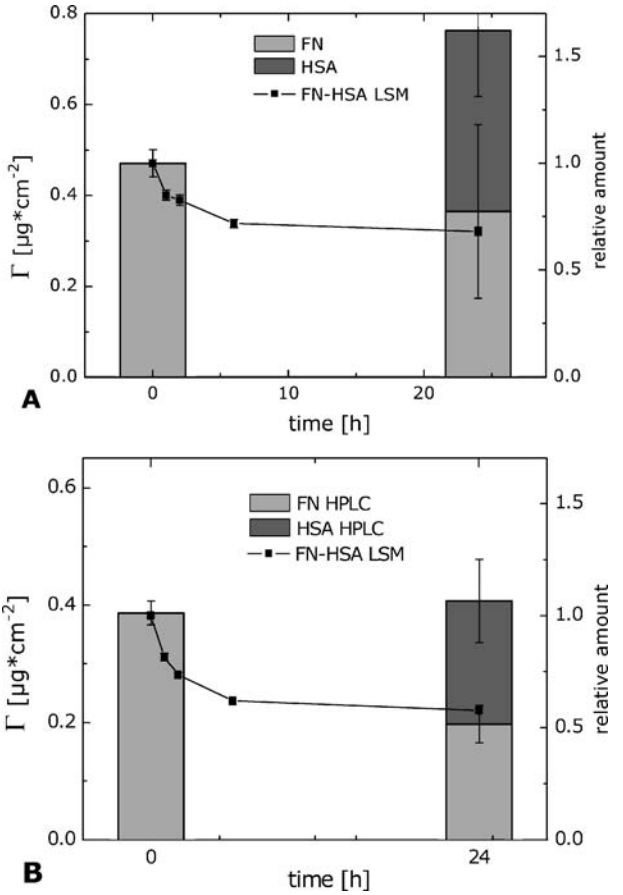

Fig. 6. **A** Heteromolecular exchange of FN by HSA solutions on POMA and **B** PPMA, as measured by HPLC (*bars*) and LSM (*circles* and *solid lines*)

The results can be qualitatively summarised as follows: (1) homo- and heteroexchange of FN occur on surfaces that exhibit different degrees of polarity, and (2) FN exhibits a higher affinity to the hydrophobic substrates as compared to the more hydrophilic and more negatively charged substrates. Extending this qualitative picture, a multivariate regression analysis was applied in order to reveal the relevance of interaction parameters in the complex setting of different exchange processes on different copolymer surfaces (Renner et al. 2004). The linear model used therein could already elucidate several important features of the analysed processes, like the significant influence of the protein solution applied in the displacement experiments on τ_A and τ_B and of the substrate hydrophobicity on the exchange and non-exchanged amounts Γ_A and Γ_B. However, the simplicity of

the linear approach and the assumed interaction schemes did not allow for a satisfactory description of the complex protein interaction processes during protein exchange on solid substrates. In a more restricted approach with a smaller number of variables, a convincing trend of the time constants τ_A and τ_B of the FN heteroexchange following the anhydride concentration of surfaces (used as a measure of surface polarity) can be shown (Fig. 7). As the balance of the polar maleic acid groups and the hydrophobic components of the comonomers dominates the copolymer surface characteristics, a major impact of this parameter on protein–substrate interactions can be expected. Matching this expectation, a correlation of the FN anchorage –

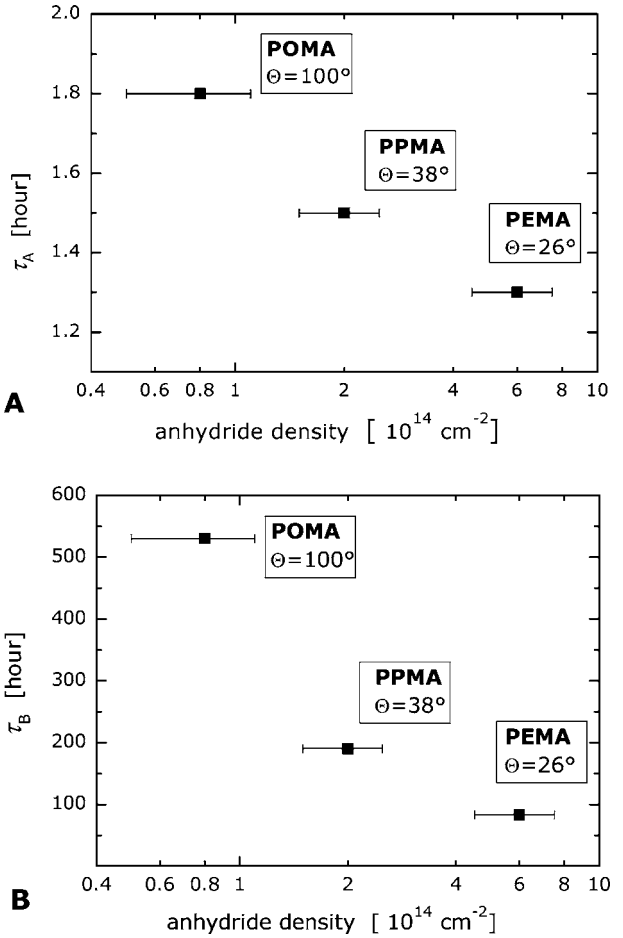

Fig. 7. FN anchorage strength measured in terms of the time constants τ_A (**A**) and τ_B (**B**) of FN heteroexchange by HSA versus the anhydride concentration of the maleic anhydride copolymer surfaces.

expressed by the exchange time constants τ_A and τ_B – to the surface polarity – characterised by the anhydride density – is observed.

In view of this result we may conclude that protein displacement experiments allow for the characterisation of protein–substrate interactions and permit the establishment of a quantitative link between the derived features of the exchange processes and the substrate characteristics.

8.4 Fibronectin Exchange at Variable Surface Concentrations

Another set of experiments that enables determination of the characteristics of FN layers containing various amounts of protein will now be described. As it will be seen later on, this kind of analysis can be used to derive additional features about the interaction strength of adsorbed FN molecules and to conclusions about conformational changes of the adsorbed proteins.

FN layers were adsorbed from solutions of 2.5, 5, 10 and 50 µg/ml FN in PBS onto hydrolysed POMA and PPMA surfaces; the adsorption process was monitored by QCM-D. The changes in mass and viscoelastic properties caused by the formation of adlayers were determined from the measured changes in resonance frequency and damping characteristics (energy dissipation) of the quartz crystal. As discussed in detail elsewhere (Renner et al. 2005), the difference in the relationship between mass increase and change in damping allowed us to consider FN layers as being "stiffer" on POMA, with a more compact protein conformation and stronger binding to the surface. Strong hydrophobic interactions apparently cause the tight binding of FN to be most pronounced at low coverage. At very high coverage the FN molecules may bind more loosely even on POMA due to protein–protein in plane interactions and competition of proteins for surface sites, leading to a more weakly bound layer structure with higher dissipation. This interpretation is supported by comparing the FN surface coverage determined by QCM-D and HPLC. As in the QCM-D measurement the water mass content incorporated or coupled to the protein layer or bound as hydration shells to FN molecules is included in the mass determination, an effective density, ϱ_{eff}, of the adsorbed layer can be calculated as introduced by Höök et al. (2001):

$$\varrho_{eff} = \frac{m_{layer}}{V_{layer}} = \frac{m_{QCM}}{\frac{m_{Prot}}{\varrho_{Prot}} + \frac{m_{Solv}}{\varrho_{Solv}}} \tag{3}$$

$$m_{Solv} = m_{QCM} - m_{HPLC} \tag{4}$$

where the values of m_{layer} and $m_{Prot}(= m_{HPLC})$ are taken from measurement data. The solvent and protein densities are set to $\varrho_{Solv} = 1{,}000\,kg/m^3$ and

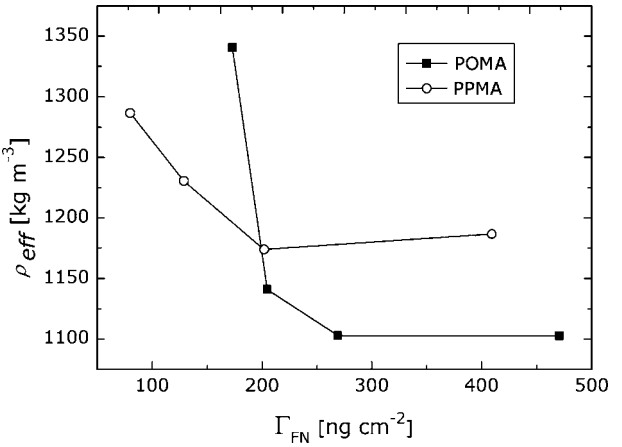

Fig. 8. Effective density ϱ_{eff} of the FN layer versus the surface coverage determined by HPLC (according to Eq. 4)

ϱ_{Prot} = 1,370 kg/m^3 according to Quillin and Matthews (2000). By using this equation, the density can be calculated for the dependence on the FN solution concentration during adsorption, as presented in Fig. 8. A strong change in the layer composition is observed for POMA surfaces, in contrast to a smaller change in the density for PPMA surfaces. The decrease in surface density corresponds to the change of coupling of water into the FN layer.

One can conclude that FN adsorbs on POMA at lower coverage in a very compact form with strong conformational changes due to the strong hydrophobic interaction. At higher coverage it still adsorbs in a more globular form with a strong affinity to the surface. The globular shape, similar to the shape in solution, probably leads to the high water content in the FN layer and the higher surface coverage in comparison to the PPMA surface.

On the hydrophilic PPMA, the adsorption of FN was assumed to occur in a more expanded state due to the influence of electrostatic interactions. The lower affinity to the surface does apparently not strongly change the conformation. However, the electrostatic interactions may open the globular structure of the dissolved FN. Thus, less water can be coupled into FN molecules. Furthermore, the electrostatic proteinsubstrate interaction probably decreases the number of free charges, which may cause a thinner hydration shell and smaller changes in the effective layer density.

The hypothesis of varying conformational changes with varying surface coverage is further supported by the estimation of the coverage of a densely packed monolayer of FN dimers with a monomer of 60 nm length and 2.5 nm in diameter. A surface coverage of approximately 250 ng/cm^2 is determined. As seen in Fig. 8, the decrease in the effective layer density

levels off at about this surface coverage, because above this coverage the adsorbing proteins cannot spread as much and the overlapping of FN molecules during adsorption should increase. By that, the adsorbing FN molecules exhibit only a less intense interaction, with the polymer substrate inducing only minor changes of the conformational state of the whole FN molecule.

The conformational changes were verified by immunofluorescence analysis with monoclonal antibodies to the heparin-binding domain near the C-terminus (Clone FNH3-8) and a domain near the primary cell binding domain (Clone FN12-8). Figure 9 shows the differences in antibody binding on the FN-coated polymer surfaces. It clearly demonstrates stronger conformational changes near the cell binding domain (FN12-8) for POMA by the lower antibody binding, especially at low FN coverage. For the heparin-binding domain (FH3-8), only a slightly lower antibody binding is observed for POMA. These findings support the QCM-D data, pointing to stronger conformational changes of FN on the hydrophobic POMA at low coverage.

Based upon this characterisation of the state of adsorbed FN at variable surface coverage, FN heteroexchange experiments were conducted to reveal the correlation of the above findings to the FN displacement characteristics. As shown in Fig. 10, at low initial surface coverage FN was barely displaced by HSA on the hydrophilic PPMA surface. Increasing the initial surface coverage led to an increase in the relative amount of displaced FN by as high as 50% for the highest absolute surface coverage of 409 ng/cm^2 (for details on HPLC results see Renner et al. 2005). In contrast (Fig. 10B), FN adsorbed onto POMA was displaced by to up to 30%, with no significant

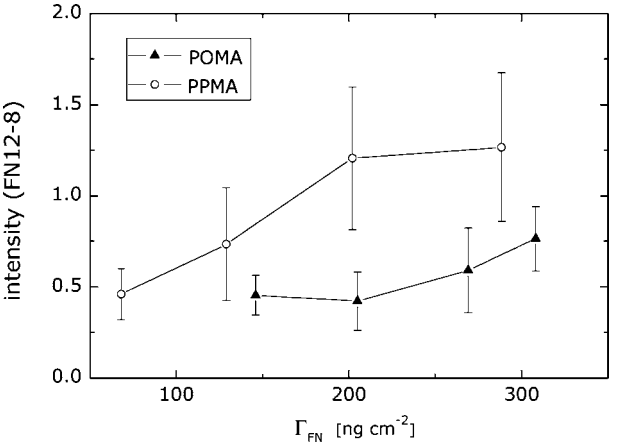

Fig. 9. Relative fluorescence intensities of antibody binding (Clone FN12-8) to FN layers on POMA (*filled triangles*) and PPMA (*open circles*)

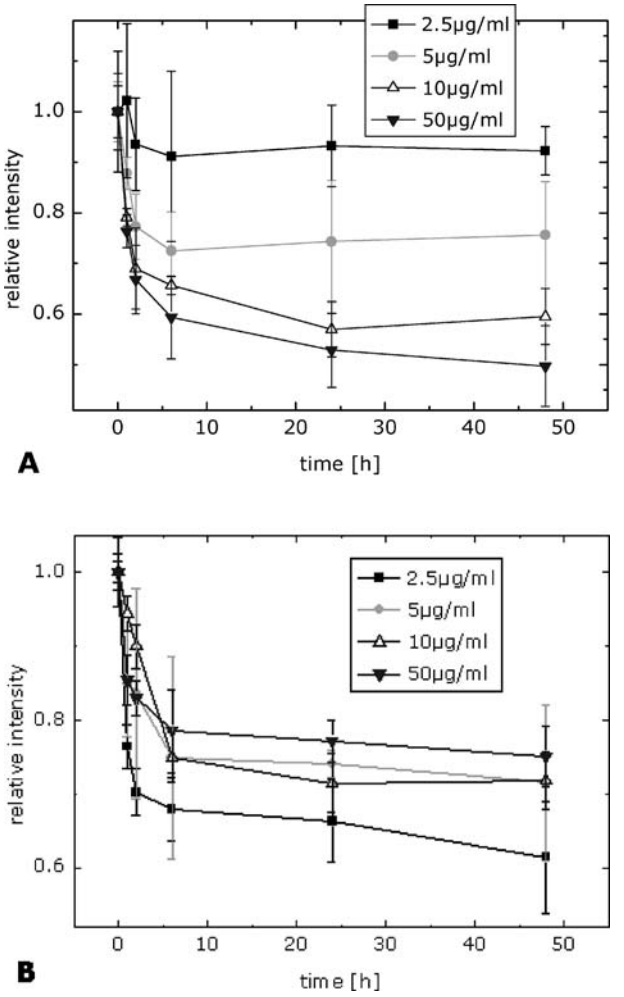

Fig. 10. FN surface coverage versus time during protein exchange by HSA (50 µg/ml) on PPMA (**A**) and on POMA (**B**)

difference caused by the initial surface coverage. A slightly higher relative displacement of the pre-adsorbed FN species was determined only for the lowest surface coverage. Plotting the absolute FN surface coverage versus time (Fig. 11) for different initial coverages on each substrate indicates that different absolute amounts were displaced on PPMA, while approximately similar amounts were exchanged on POMA surfaces. The comparison of the absolute surface coverage at late stages of displacement on PPMA reveals a limiting non-displaceable fraction of surface-bound FN, which was concluded to be independent of the initial surface coverage.

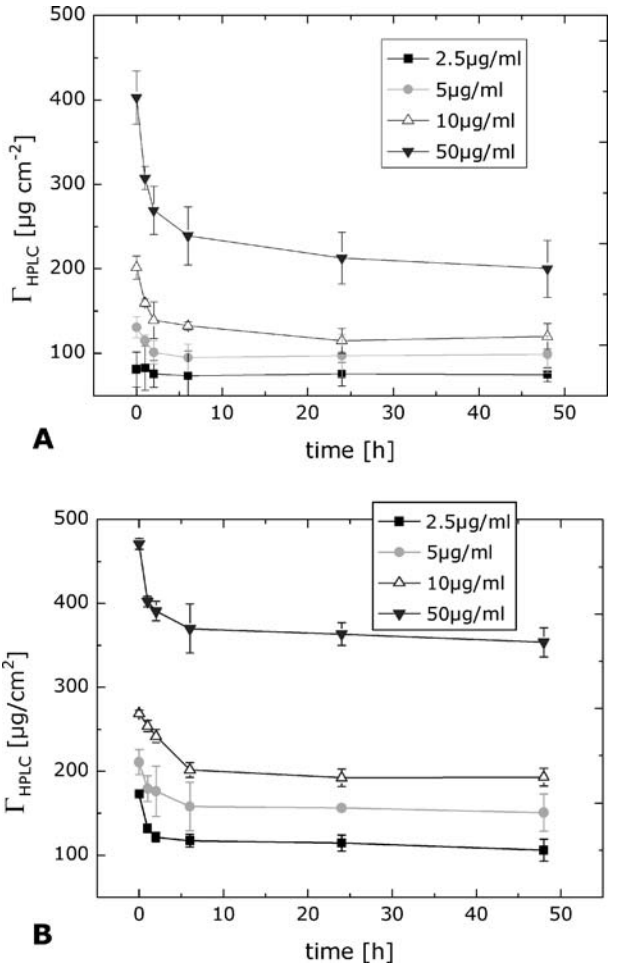

Fig. 11. FN surface coverage versus time during protein exchange by HSA rescaled from Fig. 10 with respect to HPLC data at initial coverage on PPMA (**A**) and POMA (**B**)

The displacement rate was then further evaluated by fitting the exponential decay of the observed kinetics as described earlier. As postulated earlier, in this study a non-displaceable FN fraction might occur for a low FN coverage on PPMA. By using the model equation described above (Eq. 2), this should manifest itself as a drastic increase of the second time constant. Figure 12 shows the parameters of the kinetic fits as they depend on the surface coverage. The regression coefficient of the fits was always $R^2 > 0.97$. For the POMA surface the time constants of the fast and slowly desorbed FN species show no clear trend. However, on the PPMA surface the slow time constant was found to be one order of magnitude higher for low coverage

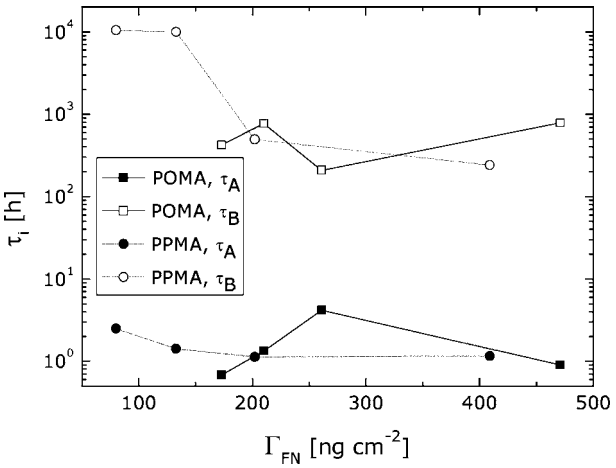

Fig. 12. Time constants of the exponential fit of the FN displacement in dependence on FN surface coverage. Values were determined by fits to the averaged values shown in Fig. 10 with $R^2 > 0.97$

than for higher ones, indicating almost no displacement, comparable to the results on POMA.

In summary, the following conclusions can be drawn from the FN adsorption and heteroexchange experiments with FN layers at different degrees of surface coverage:

1. During adsorption FN builds a more rigid layer on POMA in a more compact form with stronger conformational changes as a result of the strong hydrophobic interactions with the long alkyl chains of the comonomer. The more globular structure of the protein molecules allows a high amount of water to be coupled into the FN layer.
2. Similar amounts are thus displaced independent of the surface coverage, because every molecule adsorbs in a compact form and there is no potential for further spreading due to "fixation" of the protein in the initially adsorbed shape by strong hydrophobic interactions with the substrate.
3. On PPMA the characteristics of the FN layer is apparently more determined by electrostatic interactions involving the carboxylic acid groups, leading to looser binding of molecules in a more open form, however with less overall conformational changes. We suppose that FN molecules adsorb in totally lower amounts. Less water is coupled into this FN layer, where the open form of the molecules and the electrostatic origin of their binding are thought to be the main reasons for the smaller coupled hydration shell in comparison to POMA.

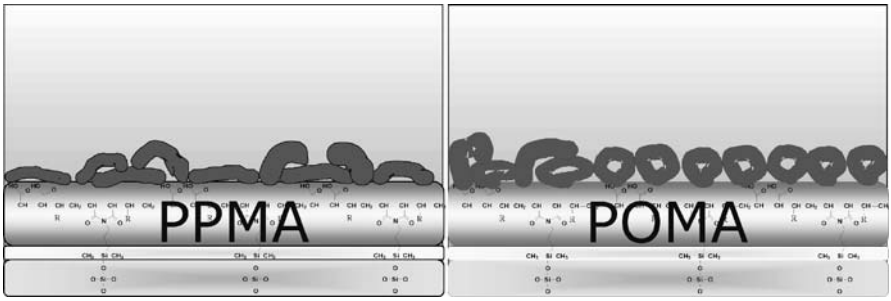

Fig. 13. Schematic representation of the suggested interfacial structure of FN on hydrophilic PPMA (*left*) and hydrophobic POMA (*right*) surfaces

4. The stronger influence of electrostatic interactions on PPMA substrates leads to a weaker binding and a higher spreading potential of FN. By varying the surface coverage, FN molecules adsorb with a different degree of spreading due to the different space available. This behaviour results in a dependence of the exchange characteristics on the surface coverage with less exchange at low surface coverage.

This interpretation is based on the earlier suggested random sequential adsorption model (Evans 1993; Schaaf and Talbot 1989; Van Tassel et al. 1996) with relaxation and spreading of adsorbed proteins being dependant on the available space, and hypothetically sketched in Fig. 13. For POMA the strong interaction prevents further spreading and the HSA displacement follows a similar pattern at each surface coverage. However, on PPMA the FN molecules spread very well at low surface coverage and remain in a non-displaceable state. Above a surface coverage of approximately 100 ng/cm^2 the FN molecules cannot fully spread and may partially overlap, resulting in an increase of the exchange probability by the HSA molecules.

The reported findings on the different states of FN on both substrates agree well with established models and reported data for protein adsorption. Norde et al. (Arai and Norde 1990a b; Norde and Favier 1992) discussed the influence of electrostatic charge and hydrophobic properties on the adsorption of various model proteins. Regarding the surface properties, FN attaches with a higher affinity to POMA by exposing the hydrophobic core of the protein towards the hydrophobic surface, which results in an increased binding strength and stronger conformational changes at the level of the secondary structure. On PPMA the electrostatic interactions may lead to a change in the tertiary structure by opening the globular form; however, less changes occur in the secondary structure due to the weaker interaction with the substrate (as compared to POMA). Importantly, the hypothesised change in the tertiary structure is supported by the obser-

vations of Bergkvist et al. (2003) revealing elongated FN molecules on hydrophilic surfaces and globular compact molecules on hydrophobic substrates. Studies on FN and FN-fragment adsorption onto CH_3- and COOH-terminating self-assembled monolayers (Keselowsky et al. 2003; Wilson et al. 2004) found similar conformational changes in dependence on the substrate surface chemistry by binding different monoclonal antibodies and using molecular dynamic simulations.

Taken together, it is obvious that a wealth of details on the anchorage, the kind of interaction and the conformational changes of proteins at interfaces can be derived from protein heteroexchange experiments enabled by the combination of complementary analytical techniques.

8.5 Relevance of the Interfacial Constraints of Fibronectin for Cell-Matrix Adhesion

Protein exchange experiments, as summarised in the preceding sections, reveal the strength of protein–substrate interactions and the resulting influences on protein conformation. The obtained insights gain special importance where they provide new options for the modulation of the functionality of the immobilised proteins towards living systems. Along that line, the presented results were successfully employed to elucidate recent findings of in vitro cell adhesion experiments, which are described in detail elsewhere (Pompe et al. 2003a, 2005a). Briefly, endothelial cells were grown on the described set of hydrolysed maleic anhydride copolymer surfaces with a pre-adsorbed FN layer on top. The cell-driven reorganisation of FN into fibrillar structures was analysed at 50 min after cell seeding. The obtained fibrils, as exemplarily shown in Fig. 14, exhibit distinct differences in density and length depending on the above-described characteristics of the substrate surface. A two-dimensional autocorrelation analysis was applied to reveal periodic features in the fibrillar pattern (Pompe et al. 2004b). As shown in Fig. 15, the dependency of the FN patterns on the substrate characteristic was found, which could be correlated to the FN–substrate anchorage reflected by the time constant of FN heteroexchange experiments (taken from Table 2). The mean distance of the FN fibrils was determined to be in the range of $2.6 \pm 0.7\,\mu m$ for the POMA substrate with the high adsorption strength of FN, down to $1.8 \pm 0.4\,\mu m$ for the PEMA substrate with the lowest FN anchorage.

Beyond the obvious mechanistic interrelation of distinct interfacial modes of a given adhesive protein and the resulting characteristics of the cell-matrix adhesion at the artificial substrate, a most important consequence of this functional modulation of FN was observed: only the weakly

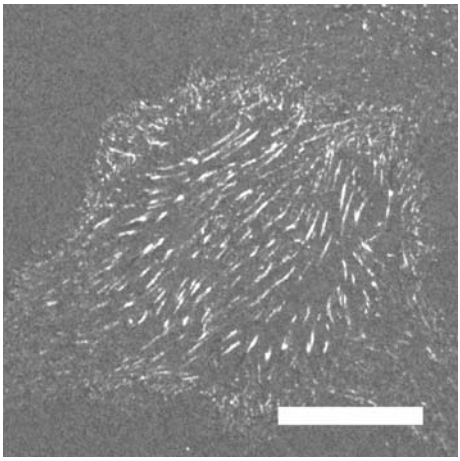

Fig. 14. LSM image of rhodamine-conjugated FN reorganised by endothelial cells on a PPMA substrate. Scale bar: 20 μm

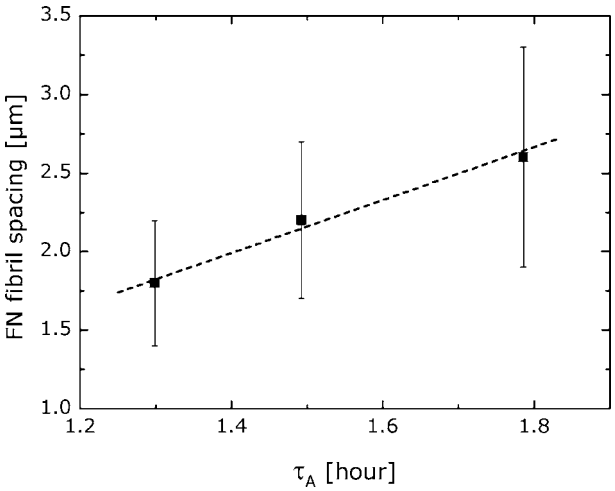

Fig. 15. FN fibrillar spacing is dependent on the time constant τ_A of FN heteroexchange

bound FN layers on the less hydrophilic copolymer substrates were found to enable the differentiation of adherent endothelial cells into capillary networks – a process required for almost any engineered tissue (Pompe et al. 2004a).

These observations allow us to conclude that protein heteroexchange experiments are a most adequate tool for quantitatively unravelling and predicting cellular processes in contact with biomaterials.

References

Arai T, Norde W (1990a) The behavior of some model proteins at solid–liquid interfaces. 1. Adsorption from single protein solutions. Colloids Surf 51:1–15

Arai T, Norde W (1990b) The behavior of some model proteins at solid–liquid interfaces. 2. Sequential and competitive adsorption. Colloids Surf 51:17–28

Bamford CH, Cooper SL, Tsurutta T (eds) (1992) The Vroman Effect. VSP, Utrecht

Bergkvist M, Carlsson J, Oscarsson S (2003) Surface-dependent conformations of human plasma fibronectin adsorbed to silica, mica, and hydrophobic surfaces, studied with use of atomic force microscopy. J Biomed Mater Res 64A:349–356

Binder K (2002) Scaling concepts for polymer brushes and their test with computer simulation. Eur Phys J E Soft Matter 9:293–298

Calonder C, Tie Y, Van Tassel PR (2001) History dependence of protein adsorption kinetics. Proc Natl Acad Sci U S A 98:10664–10669

Calonder C, Van Tassel PR (2001) Kinetic regimes of protein adsorption. Langmuir 17:4392–4395

Capadona JR, Collard DM, García AS (2003) Fibronectin adsorption and cell adhesion to mixed monolayers of tri(ethylene glycol)- and methyl-terminated alkanethiols. Langmuir 19:1847–1852

Chapman RG, Ostuni E, Yan L, Whitesides GM (2000) Preparation of mixed self-assembled monolayers (SAMs) that resist adsorption of proteins using the reaction of amines with a SAM that presents interchain carboxylic anhydride groups. Langmuir 16:6927–6936

Dubin PL, Strauss UP (1967) Hydrophobic hypercoiling in copolymers of maleic acid and alkyl vinyl ethers. J Phys Chem 71:2757–2759

Dubin PL, Strauss UP (1970) Hydrophobic bonding in alternating copolymers of maleic acid and alkyl vinyl ethers. J Phys Chem 74:2842–2847

Evans JW (1993) Random and cooperative sequential adsorption. Rev Mod Phys 65:1281–1329

Grinnell F, Feld MK (1981) Adsorption characteristics of plasma fibronectin in relationship to biological activity. J Biomed Mater Res 15:363–381

Haeberli A (ed) (1998) Human protein data. Wiley-VCH, Weinheim

Haynes CA, Norde W (1994) Globular proteins at solid/liquid interfaces. Colloids Surf B2:517–566

Höök F, Kasemo B, Nylander T, Fant C, Scott K, Elwing H (2001) Variations in coupled water, viscoelastic properties, and film thickness of a Mefp-1 protein film during adsorption and cross-linking: a quartz crystal microbalance with dissipation monitoring, ellipsometry, and surface plasmon resonance study. Anal Chem 73:5796–5804

Huetz Ph, Ball V, Voegel J-C, Schaaf P (1995) Exchange kinetics for a heterogeneous protein system on a solid surface. Langmuir 11:3145–3152

Jenkins ATA, Hu J, Wang YZ, Schiller S, Foerch R, Knoll W (2000) Pulsed plasma deposited maleic anhydride thin films as supports for lipid bilayers. Langmuir 16:6381–6384

Keselowsky BG, Collard DM, Garcia AJ (2003) Surface chemistry modulates fibronectin conformation and directs integrin binding and specificity to control cell adhesion. J Biomed Mater Res 66A:247–259

Malmsten M (ed) (1998) Biopolymers at Interfaces. Dekker, New York

Mark HF, Bikales NM, Overberger LG, Menges G (1987) Maleic and Fumaric Polymers Encyclopedia of Polymer Science and Engineering, vol 9. Wiley-VCH, New York

Nitschke M, Schmack G, Janke A, Pleul D, Werner C (2002) Low pressure plasma treatment of poly(3-hydroxybutyrate): toward tailored polymer surfaces for tissue engineering scaffolds. J Biomed Mater Res 59:632–638

Norde W, Favier JP (1992) Structure of adsorbed and desorbed proteins. Colloids Surf 64:87–93
Nygren H (1993) Nonlinear kinetics of ferritin adsorption. Biophys J 65:1508–1512
Osaki T, Werner C (2003) Ionization characteristics and structural transitions of alternating maleic acid copolymer films. Langmuir 19:5787–5793
Pettit DK, Horbett TA, Hoffman AS (1992) Influence of the substrate binding characteristics of fibronectin on corneal epithelial cell outgrowth. J Biomed Mater Res 26:1259–1275
Pompe T, Kobe F, Salchert K, Jørgensen B, Oswald J, Werner C (2003a) Fibronectin anchorage to polymer substrates controls the initial phase of endothelial cell adhesion. J Biomed Mater Res 67A:647–657
Pompe T, Zschoche S, Salchert K, Herold N, Gouzy M-F, Sperling C, Werner C (2003b) Maleic anhydride copolymers – a versatile platform for molecular biosurface engineering. Biomacromolecules 4:1072–1079
Pompe T, Markowski M, Werner C (2004a) Modulated fibronectin anchorage at polymer substrates controls angiogenesis. Tiss Eng 10:841–848
Pompe T, Mitdank C, Werner C (2004b) Quantitative analysis of fibronectin fibrillogenesis by endothelial cells on biomaterials. J Phys Condens Matter 16:2421–2426
Pompe T, Keller K, Mitdank C, Werner C (2005a) Fibronectin fibril pattern displays the force balance of cell-matrix adhesion. Eur Biophys J 34:1049–1056
Pompe T, Renner L, Grimmer M, Herold N, Werner C (2005b) Functional films of maleic anhydride copolymers under physiological conditions. Macromol Biosci 5:890–895
Quillin ML, Matthews BW (2000) Accurate calculation of the density of proteins. Acta Cryst D56:791–794
Renner L, Pompe T, Salchert K, Werner C (2004) Dynamic alterations of fibronectin layers on copolymer substrates with graded physicochemical characteristics. Langmuir 20:2928–2933
Renner L, Pompe T, Salchert K, Werner C (2005) Fibronectin displacement at polymer surfaces. Langmuir 21:4571–4577
Salchert K, Pompe T, Sperling C, Werner C (2003) Quantitative analysis of immobilized proteins and protein mixtures by amino acid analysis. J Chromatogr A 1005:113–122
Schaaf P, Talbot J (1989) Kinetics of random sequential adsorption. Phys Rev Lett 62:175–178
Schmidt U, Zschoche S, Werner C (2002) Modification of poly(octadecene-alt-maleic anhydride) films by reaction with functional amines. J Appl Polymer Sci 87:1255–1266
Sugai S, Ebert G (1986) Conformations of hydrophobic polyelectrolytes. Adv Colloid Interface Sci 24:247–282
Trivedi BC, Culbertsen BM (1982) Maleic Anhydride. Plenum, New York
Tusek L, Nitschke M, Werner C, Stana-Kleinschek K, Ribitsch V (2001) Electrokinetic characterization of NH_3 plasma treated PA 6 foils. Colloids Surf A 195:81–95
Van Tassel PR, Talbot J, Tarjus G, Viot P (1996) Kinetics of irreversible adsorption with a particle conformational change: a density expansion approach. Phys Rev E Soft Matter 53:785–798
Wertz CF, Santore MM (1999) Adsorption and relaxation kinetics of albumin and fibrinogen on hydrophobic surfaces: single-species and competitive behavior. Langmuir 15:8884–8894
Wertz CF, Santore MM (2002) Fibrinogen adsorption on hydrophilic and hydrophobic surfaces: geometrical and energetic aspects of interfacial relaxations. Langmuir 18:706–715
Wilson K, Stuart SJ, Garcia A, Latour RA Jr (2004) A molecular modeling study of the effect of surface chemistry on the adsorption of a fibronectin fragment spanning the 7-10th type III repeats. J Biomed Mater Res 69A:686–698

9 Development of Chemical Microreactors by Enzyme Immobilization onto Textiles

Christophe Innocent, Patrick Seta

Abstract. Advanced biotechnological techniques are now being used in the chemical engineering of membrane processes, notably enzyme immobilization procedures, biosensors, and, more recently, proteomics. The knowledge and increasingly fine control of the production and reactivity of enzymes also profits research whose aim is to use on a large scale the catalytic material properties of biocatalysts (enzymes). These materials with reactive properties could be introduced into membrane technology, opening as a new field the treatment of liquid media according to the concept of membrane bioreactors, where the membrane itself acts as the chemical reactor. As will be discussed herein, the ionic-exchanging textiles will be involved in this futurology.

9.1 Introduction

The concept of the chemical microreactor is becoming increasingly important not only because the industrial community must now protect the environment, but also in the developments in biotechnology and in the field of health. With regard to the increasing need to protect the environment, for example, there is a need for the development of waste treatment processes that are more effective and are easily combined or coupled with other processes, or still better able to fulfill several functions in only one operation (unitary process). Membrane technology, and in particular the processes involved in separation already utilize this concept of unitary operation, and the concept of catalytic membranes has experienced significant developments as regards, for example, gas treatment (Dalmon 1997). The chemical reactivity of liquid media has also been tested with membrane bioreactors, where the membrane is not the site of chemical or biochemical reactions of transformation. In such bioreactors the membrane is just a separator

Christophe Innocent, Patrick Seta: European Membrane Institute, UMR 5635 (ENSCM-UMII-CNRS), Université Montpellier 2, CC 047, 34095 Montpellier Cedex 5, France, E-mail: christophe.innocent@iemm.univ-montp2.fr, pseta@iemm.univ-montp2.fr

Principles and Practice
Proteins at Solid–Liquid Interfaces
Philippe Déjardin (Ed.)
© Springer-Verlag Berlin Heidelberg 2006

that confines the biological medium and isolates it from the rest of the system, and allows the separation of chemical entities either downstream from the membrane for the recovery of products, which may be considered as valuable chemicals (recovery), or upstream in order to avoid parasitic inhibiting effects on the maintenance of the active biomass.

Work in this field is moving increasingly toward the evaluation of membranes that are able to fulfill two functions, namely efficient selective separation and catalytic reactivity, whereby the membrane catalyzes chemical reactions, the objective being to convert input products into output products that are either less toxic or have a greater value.

The biocatalysts, in this case the enzymes, have a place of choice in this prospective work, which profits from the contributions of other fields of biotechnology such as biocompatibility studies for the development of membranes for hemodialysis (Eltsefon et al. 1988; Ishihara et al. 1999), artificial organs (Schmidt 1996), or biosensors (Cosnier et al. 1999).

Various routes for enzyme immobilization will be discussed herein, as well as an evaluation of their respective performances when grafted by more or less soft chemical reactions (Green and Hill 1984) or attached by molecular recognition (Rao et al. 1999).

It has been suggested that the two essential criteria for discrimination are the specific activity of the enzymes and the lifetime of their activity compared to that of the same active enzymes in homogeneous medium (batch processing). Some work has shown that fibrous systems are good candidates for the development of systems that have properties that are comparable to those of catalytic membranes embedded with enzymes, and properties similar to those of filtration membranes (Freitas dos Santos et al. 1997). With this intention, it is necessary to have materials bearing chemical sites that are favorable for the attachment of enzymes. The sites involved in this chemistry are generally carboxylic acid, hydroxyls, and amino or quaternary ammonium groups, which are created on the surface of these porous materials by various means such as direct chemical surface treatment, plasma, or ultraviolet (UV) activation. The reactive sites thus created allow the attachment of the enzymes by using coupling reagents such as tosyl chloride, dicyclohexylcarbodiimide, and glutaraldehyde. Approaches aiming at creating biocompatible environments consist of modifying the surface of polymeric filtration membranes by grafting of functional groups like sugars and polypeptides (Deng et al. 2004) and then to adsorb enzymes like lipase, the activity of which is preserved in such environment.

Another method of creating a biocompatible environment is biomimetic inspiration, which was shown to be effective for enzyme attachment and was derived from protein analysis techniques (enzyme-linked immunosorbent assay) and then used for the development of biosensors (Iqbal et al.

2000; Vo-Dinh and Cullum 2000). It utilizes the very strong and specific interaction between the small protein avidin for biotin. Because of its tetrameric structure, avidin has four sites of recognition that are accessible to biotin. Various proteins and enzymes are easily biotinylated, and this mode of enzyme grafting has already been used for electrode production as well as for membranes that are made up of conducting fibers. Fibers that are covered with a polypyrrole electron-conducting polymer layer (deposited by electropolymerization), similarly to bioenzymatic electrodes such as glucose oxidase biosensors (Coche-Guerente et al. 1994), are stabilized, thus increasing the lifetime of the molecular-recognition-type enzymes fixed by this immobilization procedure.

Another approach that was inspired by the biomimetic method consists of utilizing neutral and ion-exchanging textiles as a support for immobilization. The main advantage of these textiles is primarily their availability and the diversity of the reactor structures that are accessible. This approach will be discussed in the following review, where two cases will be presented: enzyme immobilization on insulating textiles and enzyme attachment on electron-conducting textiles. In the latter case, an electric conductor is used as the supporting material for the enzymes. The ability to introduce these new catalytic materials in a chain of coupled processes, especially electrocatalysis, will be emphasized.

9.2
Nonconducting Cellulosic Textiles

9.2.1
Pepsin and Trypsin Immobilization on Cotton

Cotton, which is used for the manufacture of clothes is not expensive and is highly accessible, has been used with success in the immobilization of enzymes and microorganisms, and in the fermentation process (Albayrak and Yang 2002). Cotton covered with polyethyleneimine has recently been used as a support for the immobilization of glucose oxidase (Kumar et al. 1997), urease (Kamath et al. 1988), and invertase (Yamazaki et al. 1984) by ionic adsorption followed by reticulation with glutaraldehyde. Cotton fibers that have a skeleton of cellulose (Fig. 1) can be activated with a variety of reagents such as cyanogen bromide (CNBr), sulfonyl chlorides, and periodates to form covalent bonds with the enzyme (Confort et al. 1989). The activation of cellulose by CNBr produces a slightly reactive cyclic imidocarbonate with a labile bond that provokes the release of the coupled catalyst (Confort et al. 1988). However, CNBr is poisonous, and its use implies some serious health risks during the activation because of the

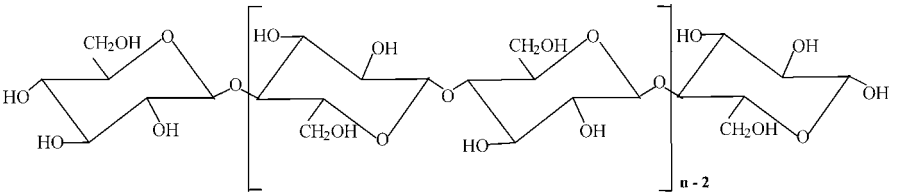

Cellulose

Fig. 1. Basic structure of cellulose molecules

possible presence of cyanate residues during food ingredient production (Giacomini et al. 1998).

Chloride p-toluenesulfonyl (tosyl chloride) is one of the least expensive reagents that can be used to activate hydroxyl groups under moderate conditions (Albayrak and Yang 2002). While 2,2,2-trifluoroethanesulfonyl chloride (tresyl chloride) is more reactive than tosyl chloride, it is extremely expensive and too volatile to be used conveniently, unlike tosyl (Albayrak and Yang 2002). Tosylated materials are stable in a dilute acidic environment (e.g., pepsin in an acidic environment) and the covalent bond formed after the displacement of the tosyl should be very strong and stable.

Among the proteolytic enzymes, immobilized proteases have shown better properties regarding activity and stability. They catalyze the hydrolysis of certain peptide bonds in protein molecules. The general reaction is illustrated in Fig. 2.

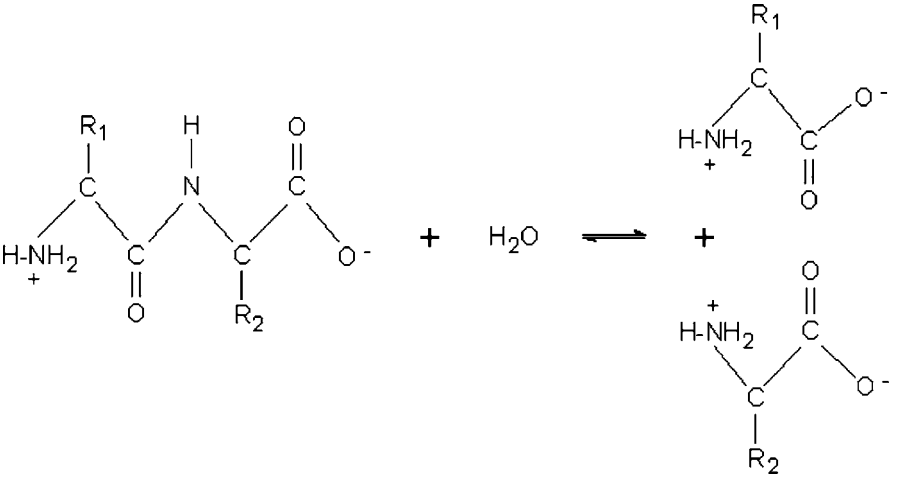

Fig. 2. Hydrolysis of peptide bonds in protein molecules (a reaction that is catalyzed by immobilized proteases)

Proteases attack proteins in two ways, yielding different products. Endoproteases attack peptide bonds in the interior of the peptide chain, yielding smaller polypeptides and peptides. Exoproteases act as cleaving agents of single amino acids from either end of the peptide chain. The pancreatic enzyme trypsin, which facilitates the digestion of proteins, breaks a peptide bond adjacent to the basic amino acid residues of lysine and arginine, whilst the enzyme chymotrypsin, another digestive enzyme, hydrolyzes the peptide bond adjacent to aromatic amino acid residues (phenylalanine, tryptophan, and tyrosine). These two enzymes have serine at the active site and are referred to as serine proteases. Pepsin effects a direct interaction between the peptide bonds and two aspartate radicals, which play alternatively the role of acid and basic catalysts. It is supposed that one of the carboxylic radicals of aspartate is dissociated whilst the other is protonated.

Cotton was chosen for its highly porous fibrous structure and its high mechanical strength. Hence, it allows high flow rates and efficient mass transfer through the matrix, properties that are advantageous not only during treatments for chemical activation and enzyme immobilization, but also for the applications of immobilized enzymes. For this reason, in the present work we are interested in the establishment of cotton catalytic materials upon which the proteases pepsin and trypsin will be immobilized in an irreversible manner using covalent bonding via tosyl chloride activation.

Tosylation of Cotton and Enzyme Immobilization

The cotton used was obtained locally and had a density of 1.27 g/cm^3. The value of specific surface for the cotton fibers was about 55×10^3 m^2/kg (Kaewprasit et al. 1998). The immobilization procedure comprised four main steps: mercerization of the cotton with NaOH, pretreatment with pyridine, tosyl activation of the cotton, and enzyme coupling to the cotton fibers. For mercerization, 0.1 g of cotton was soaked in 10 ml of 3 N NaOH solution for several hours (24 h, but about 4 h can be sufficient; Albayrak and Yang 2002). The cotton was then rinsed thoroughly with distilled water to remove the excess NaOH. The wet cotton was blotted between paper towels to remove as much water as possible. Then blotted cotton was then further rinsed with dry acetone to remove water. A sample of 10 ml dry pyridine was then added to the cotton and incubated for (pyridine pretreatment) 18 h.

For tosylation of the cotton, 10 ml of a 5-M tosyl solution (in excess) in dry acetone was added to 0.1 g of the pyridine-pretreated cotton, without removing the pyridine, for 48 h. When tosylation was completed, the cotton was removed from the reaction mixture and washed first with acetone and then with excess amounts of a 10 mM HCl solution to remove tosyl and

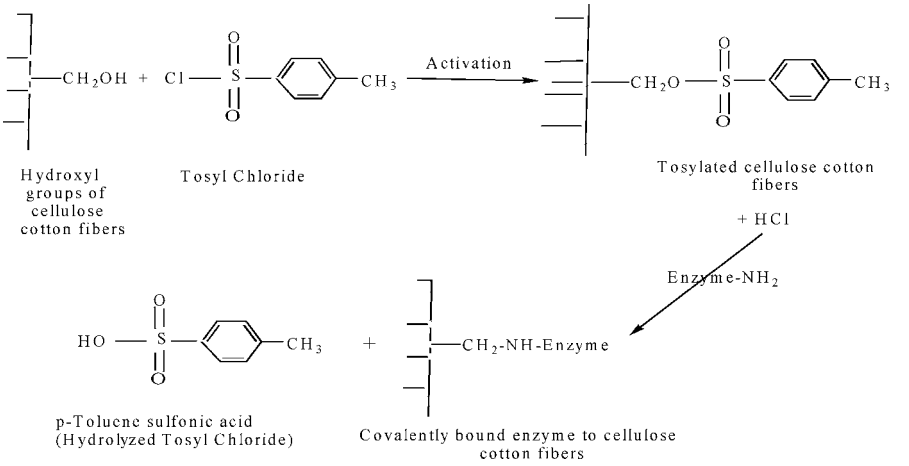

Fig. 3. Mechanism of the enzyme immobilization on the cotton fibers by tosyl chloride activation

pyridine residues from the cotton. Tosyl-activated cotton was kept in 10 mM HCl solution and stored at 4 °C until used for enzyme immobilization.

Enzyme immobilization was carried out by immersing 0.1 g of cotton for 2 h in 4 ml of a 10-mM HCl solution in the case of pepsin, and Tris-HCl, $CaCl_2$ (pH 7.5) in the case of trypsin, containing 2 mg of enzyme. After immobilization, the cotton was rinsed with copious amounts of the same acid or buffer solution and then kept in it. Enzyme activity was determined immediately and with time. All reactions during tosyl activation and enzyme immobilization were carried out in 20-ml flasks at room temperature and shaken at 200 rpm. The flasks were tightly sealed with rubber stoppers to prevent evaporation of the reactants and solvents.

The proposed mechanism for cotton tosylation followed by enzyme immobilization is described in Fig. 3.

Enzyme Activity Assay

The activity of the immobilized enzyme on cotton is measured with porcine hemoglobin and *N*-benzoyl-L-arginine-p-nitroanilide (BAPNA) as substrates. The specific reactions are given schematically in Fig. 4. In the case of pepsin in solution, the activity was assayed using a solution of 2% hemoglobin in 10 mM HCl as a substrate. A volume of 1 ml enzyme extract in HCl was incubated at 37 °C with 5 ml of substrate for 10 min. The reaction was terminated using 10 ml of 5% trichloroacetic acid (TCA) and left to incubate for 5 min. The mixture was then filtered. Absorbance was recorded at 280 nm. For blank reading, TCA was added to substrate prior

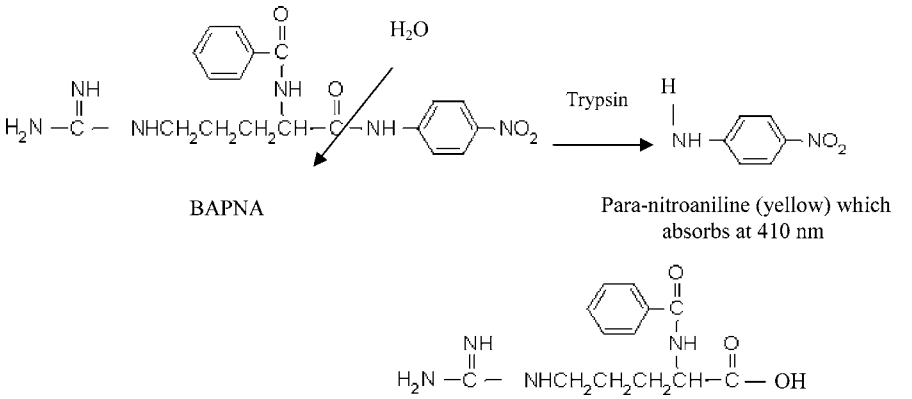

Fig. 4. Measurement of the activity of immobilized enzyme of cotton using *N*-benzoyl-L-arginine-p-nitroanilide (BAPNA) as a substrate

to the addition of enzyme extract. Specific activity (U) is expressed as:

$$\frac{\left(\begin{array}{c}\text{absorbance value (supernatant)}\\ -\text{absorbance value (blank)}\end{array}\right) \times 1000 \times \text{dilution factor}}{10\,\text{mn} \times \text{mg protein in the assay}} \quad (1)$$

Trypsin activity in solution was assayed using BAPNA as substrate. A 43.5-mg sample of BAPNA was dissolved in 2 ml of dimethylsulfoxide, and the mixture increased to 100 ml with 0.05 M Tris-HCl buffer. A volume of 0.25 ml enzyme extract was mixed with 4 ml of freshly prepared BAPNA substrate solution and left for 10 min at 25 °C before adding 5 ml of 30% acetic acid to stop the reaction. The absorbance of the resulting solution was determined at 410 nm, where p-nitroaniline absorbs, followed by the calculation of Trypsin activity using the following formula:

$$\frac{\text{absorbance value of product} \times 1000 \times \text{volume of reaction mixture}}{10\,\text{mn} \times 8{,}800 \times \text{mg protein in the assay}} \quad (2)$$

where 8,800 is the extinction coefficient of p-nitroaniline at 410 nm (M^{-1}/cm).

In the case of pepsin and trypsin immobilized on the cotton, the substrates were circulated continuously into an experimental setup containing the enzyme fixed on the cotton, as described in Fig. 5. After a reaction time of 10 min, the solution was collected and analyzed as before. TCA and acetic acid were not added to the cotton to avoid denaturation of the enzyme attached to the cotton fibers.

Absorbances at 280 nm and 410 nm of the products solutions were measured with a UV-visible spectrophotometer. The amount of the enzyme

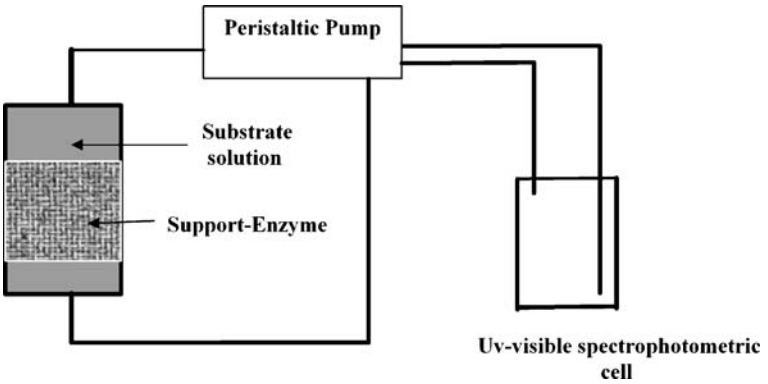

Fig. 5. Experimental setup for measurement of the activity of immobilized enzymes

coupled onto the tosylated cotton was determined from the initial amount of protein present in the enzyme-coupling solution, subtracting the final total protein amounts present in the remaining coupling and washing solutions. The coupling yield (%) of the enzyme was then calculated from the amount of enzyme coupled to the cotton cloth divided by the initial total amount of the enzyme present in the coupling solution.

After calculating the enzyme activity, we can convert it to a concentration of transformed products, given that one unit catalyzes the hydrolysis of 1 μmol of substrate per minute at a definite temperature and pH.

Fourier transform infrared spectra for the cotton before and after contact with tosyl chloride are shown in Fig. 6. These spectra showed that specific peaks related to –C–O–SO_2–C– were observed at 1,180 and 1350/cm on the spectrum of the tosylated cotton. This indicates that tosyl chloride reacts with the primary hydroxyl groups of the cotton according to the mechanism described in Fig. 3.

On the other hand, the enzyme solution during the course of enzyme coupling to tosylated cotton was scanned in the UV-visible range from 200 to 700 nm. The spectra taken before contact with the tosylated cotton, and after 2 and 6 h of contact are shown in Fig. 7. As can be seen in this figure, the enzyme peak (at 280 nm) was higher for the solution that initially contained more enzymes. However, at 2 and 6 h, a big part of enzyme disappeared and an increase in tosyl content in the solution was observed, as expressed by an increase of the absorbance of the specific peak at 261 nm. The simultaneous increase in tosyl and decrease in enzyme concentrations clearly suggests that the degree of enzyme coupling is accompanied by a displacement of tosyl, following the nucleophilic substitution mechanism for enzyme immobilization. Therefore, it could be concluded that tosyl was covalently bound to the hydroxyl groups and behaved as a leaving agent

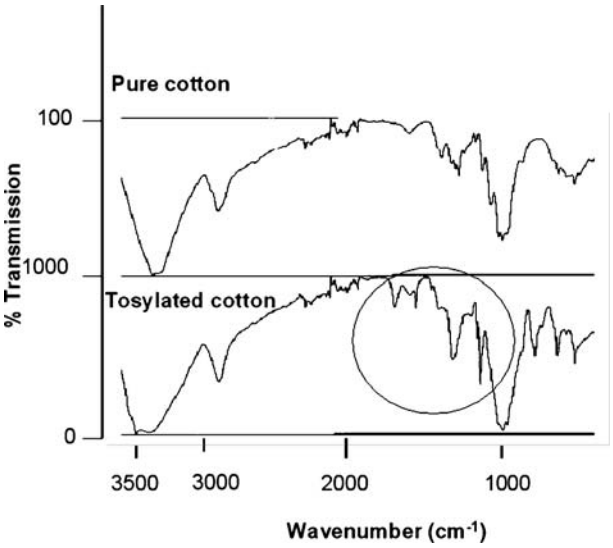

Fig. 6. Fourier transform infrared spectra of pure cotton and tosylated cotton

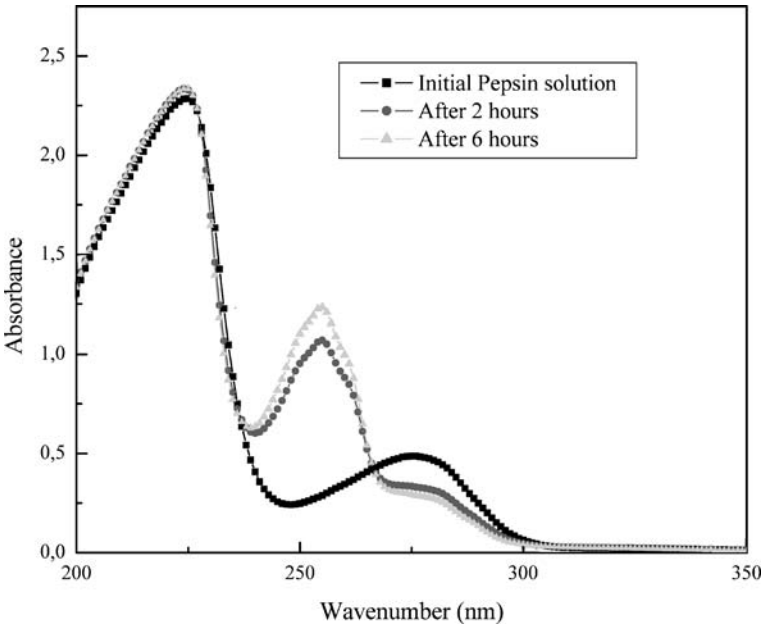

Fig. 7. Scanning ultraviolet spectra of the enzyme-coupling solutions taken before contact with the cotton (*black squares*) and at 2 (*red circles*) and 6 h (*green triangles*) after the coupling reaction

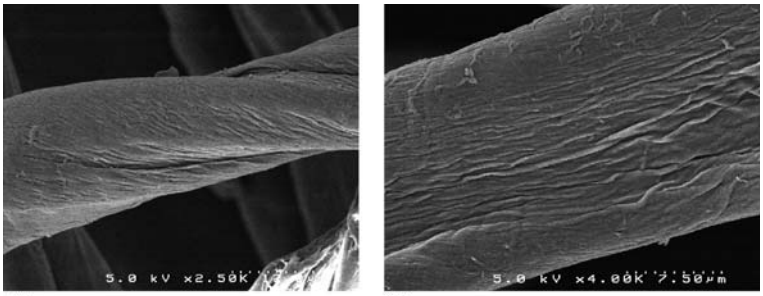

Fig. 8. Scanning electron micrographs of the cotton fibers before (**A**) and after (**B**) contact with the tosyl chloride solution

and was subsequently replaced by the enzyme, leading to a covalent linkage according to the mechanism shown in Fig. 3.

Scanning electron micrographs were recorded to compare the morphology of the modified cotton with that of the unmodified cotton. All samples were dried in vacuum and gold-coated. Figure 8A,B show the top surfaces of both cotton samples. We could not see any difference in the morphology of both materials, which demonstrates that no change occurred in the physical structure of the cotton fibers following activation of the hydroxyl radicals via tosylation.

Pepsin had the highest activity at pH 1.5, which decreased with increasing pH. Over pH 3 almost 90% of the relative activity was lost, and no activity was detected beyond pH 5. The optimum pH for trypsin was observed at around pH 8. No trypsin activity was measured at a pH below 4 or over 12. These values are in accordance with the data reported in literature (Devi et al. 1990). For both enzymes this process (loss of activity by changing the pH) was irreversible. The instability of acidic proteases towards the alkaline pH region contrasted with the behavior of gastric protease of many of the lower vertebrate species.

Exchange Capacity of the Cotton Fibers

The number of exchangeable hydroxyl groups (exchange capacity) of the cotton fibers was determined by shaking 0.18 g of cotton in 10 ml of a solution of 1 M NaOH for 24 h to ensure that a maximum of the cotton OH sites were exchanged (substitution of H^+ by Na^+). The cotton was then rinsed thoroughly to remove the excess NaOH. It was then shaken for 24 h in 10 ml of a solution of 1 N HCl to exchange Na^+ ions with H^+. The difference in pH (or difference in Na^+ concentration) before and after exchange allowed us to calculate the number of active sites (or the exchange capacity) of the

Table 1. Quantities of enzyme in the different phases. Initial quantity of enzyme: 2 mg in 4 ml; *m*(cotton) = 0.1 g

Enzyme	Solution after contact (mg)	Washing solutions (mg)	Immobilized quantity (mg)	Yield (%)
Pepsin	0.0677	1.857	0.075	3.8
Trypsin	0.0235	1.889	0.087	4.4

Table 2. Enzyme exchange capacity of the cotton. *m*(cotton) = 0.1 g which corresponds to a surface of 5.5×10^{20} Å^2; molecular mass (MM) pepsin = 36,000 g/mol, MM trypsin = 23,000 g/mol

Enzyme	Number of enzyme molecules fixed/g of cotton	Number of enzyme molecules fixed/Å^2 of cotton	Yield (%)
Pepsin	125.3×10^{14}	2.28×10^{-6}	0.63
Trypsin	228.8×10^{14}	4.16×10^{-6}	2.28

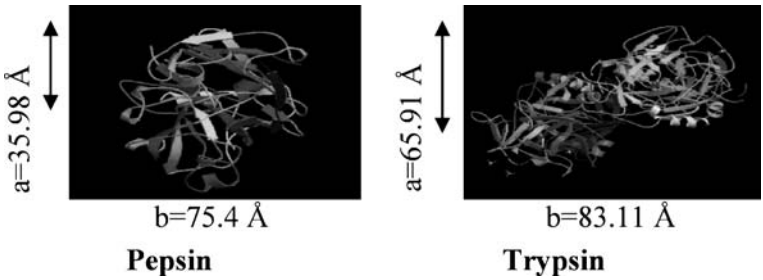

Fig. 9. Areas taken up by a molecule of pepsin (*left*) and trypsin (*right*)

cotton fibers. The value found was 6.56×10^{18} protons exchanged on 0.18 g of cotton, which corresponds to 6×10^{-3} active sites/Å^2 (i.e., about 5 meq of protons/g of cotton), in turn, to an exchange capacity of 3.6×10^{19} protons/g of cotton (0.18 g of cotton used corresponds to a surface of 9.9×10^{20} Å^2). This value was used for calculating the yield of enzyme fixation.

For enzyme immobilization we used 0.1 g cotton, which corresponds to 5.5×10^{20} Å^2, taking into account the specific area of the cotton given above. Table 1 gives the different quantities of enzymes fixed on the cotton fibers, assuming that the specific activity of the immobilized enzyme was the same as that in solution. Table 2 gives the exchange capacity values obtained for both proteases calculated using the value of the specific area of cotton fibers given above. Pepsin and trypsin molecules occupy a mean area of 438,000 Å^2 and 240,000 Å^2, respectively (Fig. 9).

Kinetic Analysis of the Enzyme Activity

The evolution of product formation was linearly dependent on time during the first minutes of the reaction. From the Michaelis-Menten kinetic model, constants, K_m, of pepsin and trypsin were obtained and maximal rates, V_{max}, were calculated by expressing $1/V_i$ versus 1/[S]. The different results obtained for both enzymes are summarized in Table 3.

V_{max} and K_m values of immobilized enzyme were slightly higher than those of the free enzyme in solution. These results were most likely due to the following factors. The immobilized enzymes did not have the same accessibility to the substrates than the soluble enzymes. This could be explained by the fact that a higher concentration of substrate was needed to enhance the collisions with the immobilized enzyme as compared to the same amount of soluble enzyme, and resulting in an increased K_m. In the case of pepsin, adsorption of a substrate such as hemoglobin could also be responsible for the increase in V_{max} as compared to the free enzyme.

Table 3. Values of Michaelis-Menton constant, K_m, and maximum reaction rate, V_{max}

Enzyme	V_{max} (mol/l/min)		K_m (mol/l)	
	In solution	On cotton fibers	In solution	On cotton fibers
Trypsin	2.79×10^{-4}	3.11×10^{-4}	1.64	7.31
Pepsin	0.032	0.22	1.4×10^{-4}	3.42×10^{-4}

Long-Term Stability

The stabilities of enzymes in solution and immobilized on the cotton fibers were estimated by following their respective activities with time. Figure 10A,B shows a decrease in activity over time in both cases. However, the activities of immobilized enzymes on cotton fibers remained higher

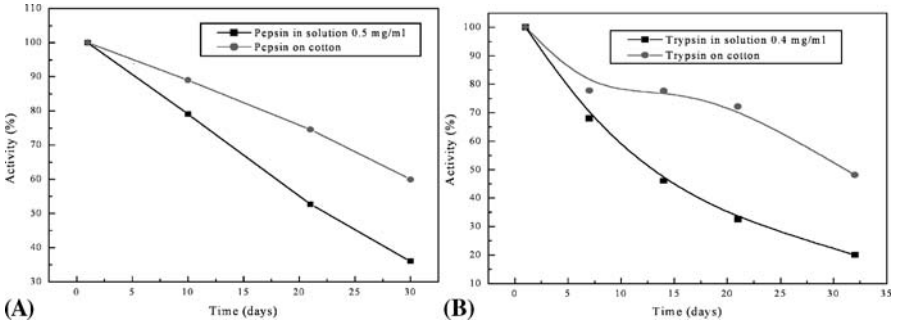

Fig. 10. Stability of pepsin (**A**) and trypsin (**B**) in solution and immobilized on cotton fibers

than that in solution (about 1.66 times higher in the case of pepsin and 2.4 in the case of trypsin). A life-time of over 1 month for the enzyme-modified cotton biocatalytic material, corresponding to a loss of only the half of the initial activity, was observed, which represents to some extent an appreciable stabilization of the enzyme reactivity by the immobilization process.

In conclusion, the feasibility and the efficiency of the elaboration of an enzymatic membrane made of proteases immobilized onto cotton fibers by tosyl activation is demonstrated. Cotton was activated with tosyl chloride and used as a novel fibrous matrix for biocatalyst immobilization. The described procedure is simple, inexpensive, and industrially applicable; moreover, it provides highly active and stable immobilized biocatalyst support. The very simple method for immobilization using tosyl-activated cotton and the appreciable working lifetime (over 1 month) of the cotton-immobilized enzyme reactor should have many applications in industrial biocatalysis (e.g., peptide production with pepsin and synthesis of insulin with trypsin).

9.2.2 Immobilization of Uricase and Xanthine Oxidase on Ion-Exchanging Textiles

Ion-exchanging textiles have been used as organic supports for enzyme immobilization with the aim of developing reactive woven materials that can be substituted into membrane systems in bioreactors or that can act, for instance, as reactive bags for waste treatment devices, thus extending the range of their potential applications. The cationic or anionic sites of ion-exchanging textiles are used for enzyme immobilization by classical chemical routes (chemical bonding) and by a biomimetic molecular recognition attachment process (complexation between biotin and avidin). As a result of the comparison between both processes used for enzyme immobilization, it has been shown that the biomimetic latter route is much more efficient than the classical routes, improving both the enzyme specific activity and their lifetime.

The chemical structure of the matrix of the ion-selective membranes used in electromembrane processes (for instance electrodialysis) is not very different from that of ion-exchanging textiles. These membranes can be associated with textiles in coupled processes like electrodeionization (Dejean et al. 1997) or, better still, can be substituted into membranes for applications such as chemical conversion.

The association of textile and enzyme is already used in the textile industry. Enzymes can be used in diverse textile areas ranging from fabric prepa-

ration to fabric destruction. Enzymes may be used at each wet-processing step, for example lipase or amylase for resizing, pectinase or cellulase for scouring (Buschle-Diller et al. 1998), and oxidoreductase for bleaching, dying, and finishing (Nolan Etters 1998). Immobilization of an enzyme on the textile can be utilized in the development new functionalized textiles for use not only in the clothing industry, but also as a catalytic material. Moreover, the porosity of a textile with associated enzyme catalytic activity can allow to the production of a kind of chemically reactive enzyme filtration membrane.

We present here few examples of a system comprising an ion-exchanging tissue, in the core of which enzymes acting as catalysts have been grafted either by a chemical route or by a biomimetic molecular recognition process (complex formation).

Comparison between the activity of tissues immobilizing enzymes by covalent bonding and that immobilizing enzymes by molecular recognition reveals that the latter biomimetic immobilization process is more effective, presumably because of the mildness of this process, which preserves the specific activity of the immobilized enzyme.

Textile supports are made of nonwoven cellulose fibers that are modified by ion-exchange groups (carboxylic, tertiary amine, or ammonium). The grafting ratio is 20%, with an average polymerization degree of 50–200, the specific mass and the cut-off being 450 g/m^2 and 0.1 mm, respectively (Institut Textile de France 1987).

Enzyme immobilization by Chemical Grafting

Two different ways have been used to anchor enzymes covalently onto the surface of textile fibers: (1) reaction with periodate on the cellulose chain, and (2) using a coupling agent to graft the enzyme onto the functional group of the textile. The first activation procedure involves the production of aldehyde groups on the cellulose chain via a reaction with periodate. A piece of textile (4 cm^2) was treated with 10 ml of 0.5 M sodium periodate for 90 min in the dark. The tissue was then thoroughly washed with distilled water and dried at 50 °C for 2 h. Then the modified textile was then immersed in 4 ml of enzyme solution, for instance urease (1 mg/ml), for 24 h.

The second procedure involves a coupling agent, such as 1,4-phenylene-diisothiocyanate. It has been shown previously that this coupling agent allows the grafting of an enzyme onto a polymer support (Marchand Brynaert 1999) via a reaction with the amino groups. The textile was immersed in 4 ml of the 1,4-phenylene-diisothiocyanate solution (4.3 mM) in dry toluene for 12 h. The textile was then rinsed with toluene and immersed in 4 ml of enzyme aqueous solution (1 mg/ml) for 24 h.

Enzyme Immobilization by Molecular Recognition

Cation-exchange textiles are modified according to the following procedure: a sample of textile (4 cm^2) is immersed in NaOH and urea solution (1 M) for 12 h to graft amino groups on carboxylic acid functions. Biotin is attached to this amino group using *N*-hydroxysuccinimide biotin as a coupling reagent (0.4 mg/ml for 12 h at room temperature). Anion-exchange textiles are modified directly by immersion in a sulfo-*N*-hydroxysuccinimide biotin (0.4 mg/ml) aqueous solution for 12 h. All textiles are then thoroughly rinsed with distilled water and stored at room temperature before being used.

Textile Characterization

Cellulose copolymer textiles are modified by plasma irradiation treatment to graft ionic groups onto the fiber. The number of ionic groups are deduced from the ion-exchange capacity of the textile, as measured by determining of the amount of fixed ions on the textile (Yakup Arica 2000). The experimental procedure will now be described.

For anion-exchange textiles, the tissues are equilibrated in sodium chloride solution (1 M) for 24 h. Solutions are changed three times (the corresponding total volume is 500 ml/cm^2 of textile). The textiles are then rinsed with demineralized water and dried at 50 °C overnight. Then they are immersed in nitric acid solution (0.1 M) for 24 h to exchange chloride ions with nitrate ions. The concentration of chloride ions is determined by titration with silver nitrate. The final titration point is determined by potentiometric measurement.

Cation-exchange textiles are equilibrated in sodium hydroxide solution (1 M) for 24 h. After rinsing with demineralized water and drying at 50 °C overnight, the textiles are immersed for 24 h in HCl solution (0.1 M) to exchange sodium ions with protons. Sodium ion concentration is then analyzed by photometric measurement.

The exchange capacity (EC) is calculated as the ratio of co-ion in solution per unit of weight of dry textile.

$$\mathrm{EC} = C \cdot V/M \tag{3}$$

C being the co-ion concentration, V the volume of the solution, and M the mass of dry textile.

Enzyme Biotinylation

A biotinylated enzyme is prepared by adding a fixed amount (2 mg/ml) of enzyme solution, either urease, uricase, or xanthine oxidase), in 100 mM phosphate buffer, pH 7.5, to 100 times mole excess of biotin-amidocaproate *N*-hydroxysuccinimide ester. The biotinylated reaction is carried out at

room temperature in a vial with constant stirring for 3 h. After this, 10 mg of glycine is added to react with the unused biotin. Removal of all small-molecular-weight reactants and products is achieved by chromatography through a Sephadex G 25 column from SIGMA (USA) (with a cut-off at molecular weight 25,000).

Fixation of Enzyme on the Textile

The biotin-modified textile support is rinsed with distilled water and immersed in 2 ml of an aqueous solution of avidin (1 mg/ml) for 1 h. The resulting porous material is washed with distilled water and immersed in a solution of 2 ml biotinylated enzyme (2 mg/ml) for 1 h and then washed again with distilled water.

Membrane Textile Device

The modified textile is tightly packed (0.5 cm in thickness) into a glass column of 1 cm in diameter, 10 cm high for chromatography. The column is filled with the studied solution at the top of the column, and this solution flows through by gravity or is circulated by pumping with a peristaltic pump (flow rate: 2 ml/min) and is analyzed at its exit

Enzymatic Activity Measurements

Urease catalyzes the hydrolysis of urea, producing ammonium and carbonate ions according to the following reaction:

$$NH_2CONH_2 + 2H_2O \rightarrow 2NH_4^+ + CO_3^{2-} \quad (4)$$

Determination of the activities of the free and immobilized urease is carried out by measuring the production of ammonium according to a procedure given by Sigma (Sigma catalog no. 535) with a blood urea nitrogen (BUN) acid reagent and BUN color reagent (Sigma). A calibration curve is established by mixing 3 ml of BUN acid reagent with 2 ml of BUN color reagent and 1 ml of sample solution (urea concentration between 2 and 60 mM) and maintaining the mixture at precisely 80 °C for 10 min. After cooling, the respective absorbances at 524 nm are recorded (Coche-Guérente et al. 1995).

Uricase activity is measured by spectrophotometric detection of the uric acid according to a Sigma procedure (Sigma catalog no. 292). The reaction is monitored by the absorbance change at 292 nm. Since uric acid absorbs at 292 nm and the end product of the reaction does not, the decrease in absorbance is proportional to the decrease in the uric acid concentration and thus to the uricase activity (the extinction coefficient of the uric acid solution at 292 nm, ε_{292} = 12,200/mol/cm).

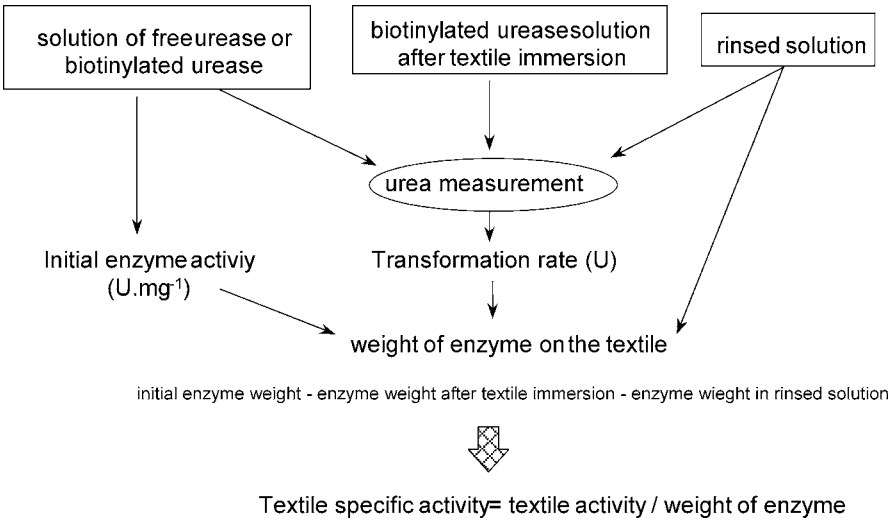

Fig. 11. Description of the procedure used for the determination of the specific enzyme activity of the textile

Xanthine oxidase activity is measured by spectrophotometric detection at 292 nm of the produced uric acid or from the amount of hydrogen peroxide produced with xanthine as substrate (Coche-Guérente et al. 1995). The hydrogen peroxide concentration is determined according to analytical methods that have been described previously (Green and Hill 1984; peroxidase activity determination from SIGMA) based on enzymatic reactions with peroxidases.

The enzyme-specific activity of the modified textiles is calculated in the case of urease immobilization after determining the weight of the enzyme on the textile and the enzyme activity of the material. Figure 11 depicts the measuring procedure used to estimate the weight of enzyme immobilized on the textile. The recording of the activity of the enzyme solution allows us to know the corresponding weight of enzyme (knowing the initial specific activity of the enzyme).

Ion-exchange textiles have been used to achieve enzyme immobilization, as their ion-exchanging groups can react with the biotin groups of biotinylated enzymes. Three types of textile have been used: carboxylic acid, tertiary amine and quaternary ammonium groups, as cation and anion exchangers, respectively (Fig. 12).

Table 4 shows the evolution of the ion exchange capacity (EC) of a textile before and after chemical modification (biotin attachment). In the case of the carboxylic acid tissue, the EC value is in good agreement with the proposed reaction scheme for the attachment of biotin to the COO^- groups.

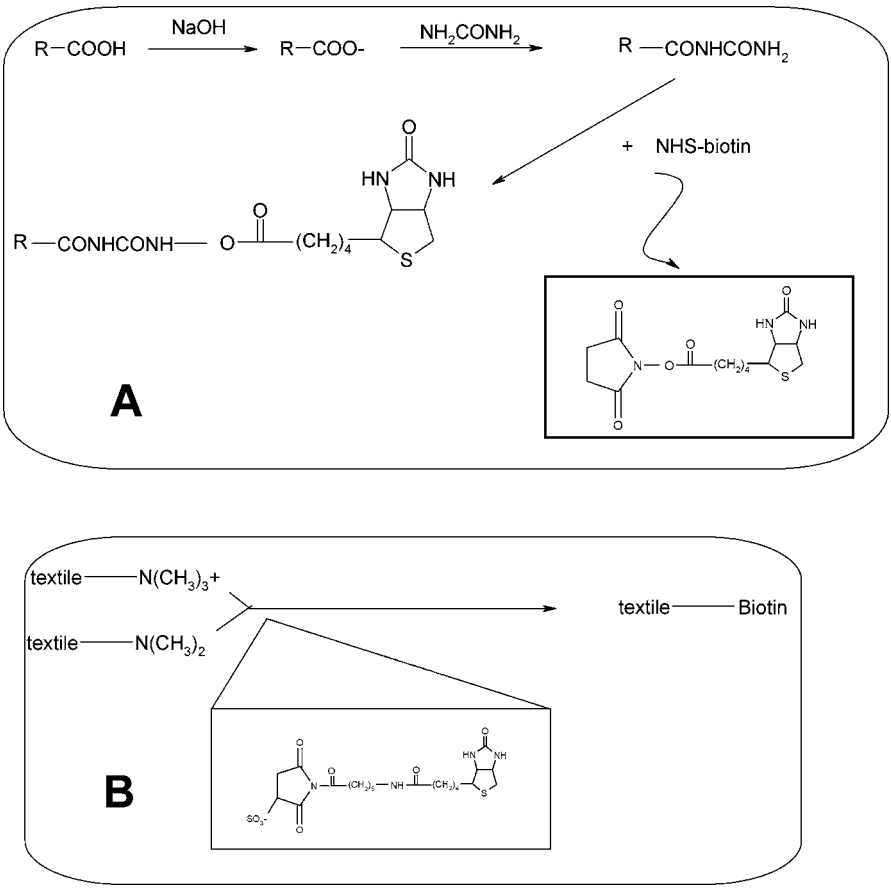

Fig. 12. Chemical reactions used to modify a textile support by biotin attachment: (**A**) cation exchanger textile (carboxylic acid groups) and (**B**) anion exchanger textile bearing amino groups

Table 4. Exchange capacity of different textiles before and after chemical modification (biotin anchorage). *Carbox* Carboxylic acid, *N Tert* tertiary amine, *N Quat* quaternary ammonium, *EC* exchange capacity, *Max* maximum

	Carbox	Carbox Biotin	N Tert	N Tert Biotin	N Quat	N Quat Biotin
EC (meq/g)[a]	3.0	2.3	1.8	2.6	0.3	2.2
Exchange capacity (meq/g)[b]	2–5	–	Max 1.6	–	0.4–1	–

[a]Measured in this work
[b]From IFTH data

After the reaction, the textile lost its ion EC. Conversely, in the case of tertiary amine groups, these groups are quaternized during the reaction and the anion EC is increased after modification.

Urease Immobilization by Molecular Recognition

The first step for enzyme entrapment is the synthesis of a biotinylated urease. The amount of enzyme immobilized is calculated by kinetic measurements. Assuming that the enzyme keeps its activity after immobilization, the weight of immobilized enzyme is given by:
$W_t = W_i - W_{im} - W_r$, where W_t, W_i, W_{im}, and W_r are the weight of enzyme attached to the textile, the weight of enzyme in the initial solution, the weight of enzyme in the solution after textile immersion, and the weight of enzyme in the rinsed solution, respectively.

Textile activity is obtained by spectrophotometric measurement of the urea consumed by the enzyme reaction. The kinetic parameters corresponding to the activity of the immobilized enzyme are calculated from the absorbance curve versus time (Fig. 13).

As far as the specific activity is concerned, this parameter is determined by the ratio of enzyme textile activity to the weight of enzyme. With an initial weight of enzyme in solution of 0.41 mg, absorbance measurements gave a final weight of enzyme on the textile of 0.081, 0.151, and 0.26 mg for carboxylic acid, quaternary ammonium, and tertiary amine textile, respectively. The corresponding specific activities are 1617, 927, and 504 U/mg for carboxylic acid, ammonium, and tertiary amine textiles, respectively.

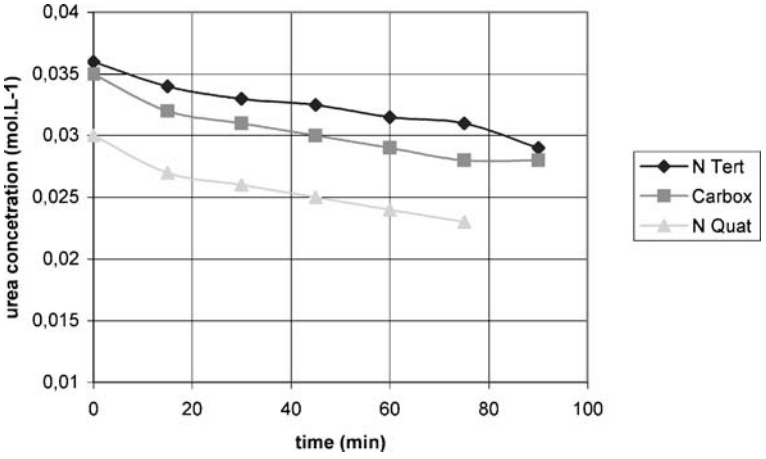

Fig. 13. Urea concentration versus time at the exit of the column; flow rate = 1 ml/min. *N Tert* Tertiary amine, *Carbox* carboxylic acid, *N Quat* quaternary ammonium

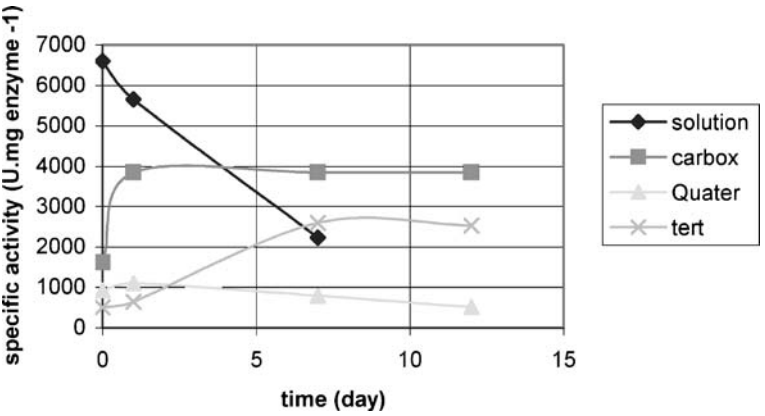

Fig. 14. Stability curve obtained from the free urease and immobilized urease on three different textile supports: carboxylic acid (*carbox*, *pink squares*), quaternary ammonium (*Quater*, *yellow triangles*), and tertiary amine (*tert*, *green crosses*)

Figure 14 represents the variations with time of the specific urease activity of textiles bearing different reactive groups in comparison with that of the corresponding enzyme in solution. The activity of free enzyme in solution decreases almost linearly in the first days of storage. Conversely, the textile activity remains more stable after 24 h (or a few days) and was even shown to be almost constant over a period of 45 days in the case of carboxylic acid textile. The biomimetic immobilization process allows the maintenance of good stability for the enzyme by protecting the it from deactivation. The enzyme immobilized on the textile kept 57% of its initial activity in solution. This result demonstrates the efficiency of this immobilization method as compared to the covalent grafting method (Yakup Arica 2000). An increase in enzyme activity after a few days of storage has already been observed in the case of glucose oxidase immobilized in a polymer matrix (Coche-Guérente et al. 1995).

Chemical Immobilization of Urease

In order to establish the influence of protein group in avidin-biotin technology on the efficiency of enzyme immobilization, covalent enzyme fixation was carried out with two different routes according to some examples given in literature: using periodate oxidation of cellulose, and using 1,4 phenylenediisothiocyanate as a coupling agent. The first method is based on a direct chemical reaction with cellulose, which brings onto the textile matrix a great number of reactive aldehyde functions. In the second procedure, a coupling reagent intervenes, allowing the grafting of enzymes on the functionalized groups of the textile. The amount of enzyme im-

Table 5. Reaction rate and specific activity for different modified textile measured by spectrophotometric determination of urea concentration (see experimental section)

		Rate (U)	Activity (U/mg)
Tertiary amine	Periodate	194	52
	Thiocyanante	40	–
	Biotin	131	504
Ammonium	Periodate	156	43
	Thiocyanante	38	–
	Biotin	140	927
Carboxylic	Periodate	189	50
	Thiocyanante	33	
	Biotin	131	1617

mobilized according these procedures was estimated to lie in the range of 90–95% of the amount of initial enzyme in contact with the textile. The weight of enzyme on a piece of tissue (4 cm^2) was about 3.8 mg. The covalent bonding is a highly effective method for irreversible enzyme immobilization; however, experiments devoted to enzyme activity have confirmed that the enzyme is severely deactivated by the chemical treatments involved in the protocols for enzyme covalent bonding onto the textile surface. The large amount of enzyme fixed onto the textile support cannot overcome the effect of deactivation due to these treatments, and as a result, the samples exhibited a poor specific activity as compared to those realized according to the biomimetic route, as depicted in Table 5.

In Table 2, the reaction rate and specific activity values obtained with different immobilization methods are compared. This table shows clearly that avidin-biotin technology provides a good specific activity, in all cases much higher than that obtained with chemical grafting, whichever the chosen functional reactive group brought by the textile. The presence of a protein group such as avidin, close to the enzyme prevents deactivation and as a result preserves the catalytic activity. Moreover, this technology largely extends the stability of the bioactive species over a long period, thanks to the microenvironment created around the immobilized enzyme.

Since urease has been immobilized while maintaining reasonable stability and good efficiency, our immobilization method on the textile support has been generalized to other types of enzymes such as oxidase or decarboxylase.

Xanthine Oxidase and Uricase Immobilization

The efficiency of the immobilization method being demonstrated with urease and in order to prove the potentiality of the molecular recognition

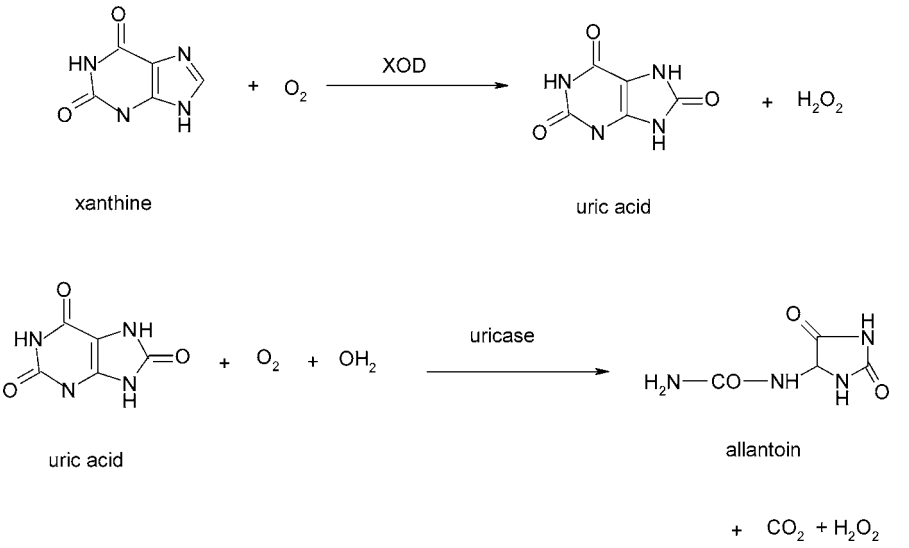

Fig. 15. Catalytic chemical reactions achieved by xanthine oxidase and uricase

process, different types of enzyme have been fixed onto textiles: xanthine oxidase, which allows the chemical transformation of xanthine into uric acid, and uricase, which transforms uric acid into allantoin (see the reaction scheme shown in Fig. 15). The enzymatic transformation of xanthine into uric acid determined from the increase in the absorbance at 290 nm (production of uric acid) is shown in Fig. 16, for the different studied ion exchanging textiles.

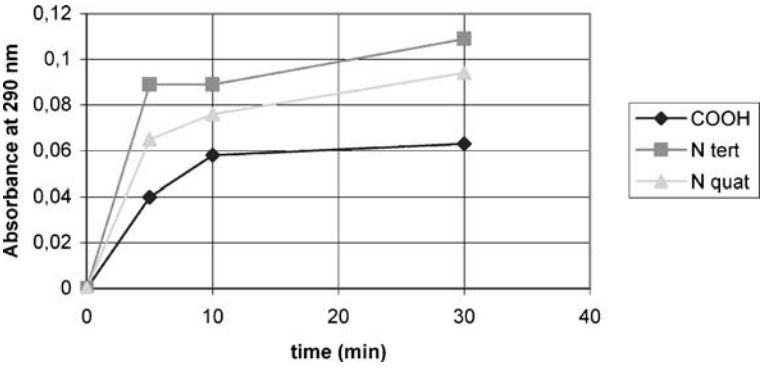

Fig. 16. Absorbance values recorded at 290 nm at the exit of the column after injection of 40 ml of a xanthine (1.2×10^{-4} M) in 5×10^{-2} M phosphate buffer solution (pH 7.5)

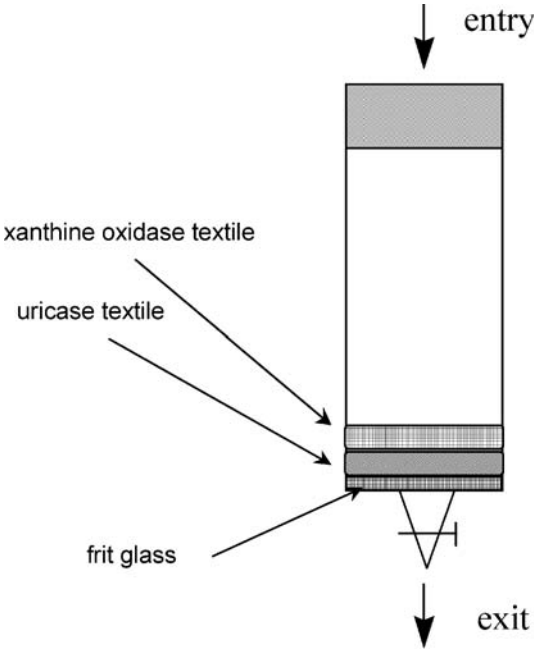

Fig. 17. Experimental device for a sequential bienzymatic process

After having demonstrated the feasibility of this method for xanthine substrate removal, we have sophisticated the process by simply adding in the column another textile modified by uricase. Figure 17 represents the set-up used in a sequential bienzymatic process, which allows both the degradation of xanthine and of uric acid, which is the reaction product of the first enzyme reaction in the flow cell.

Spectrophotometric measurements have been achieved at the exit column. Two different wavelengths have been used to demonstrate the decrease in xanthine concentration (273 and 290 nm). The production of uric acid would result in an increase in the absorbance at 290 nm; however, a reduction in the optical density recorded at 290 nm was observed, and this was attributed to the reduction in xanthine concentration, which would lead to an increase, if the second reaction involving uricase was not effective . In fact this means that no production of uric acid can be recorded, as the reaction across the second enzyme layer immobilizing uricase is highly efficient. The observed decrease in fact corresponds to the reduction in xanthine concentration. Even if the main optical absorption region of xanthine is 273 nm, it also absorbs at 290 nm (main absorption band of uric acid), but with a lower absorption coefficient. At these two wavelengths,

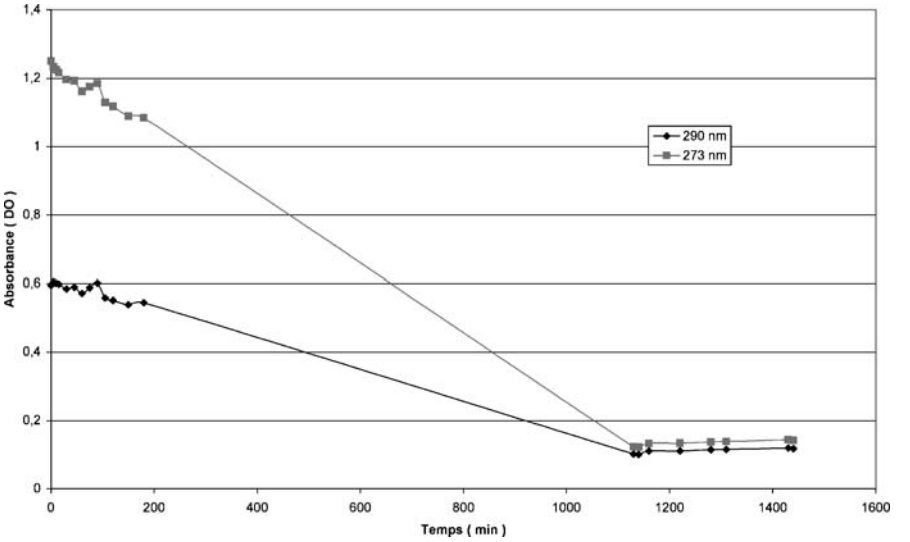

Fig. 18. Absorbance change versus time measured at 273 (*pink squares*) and 290 nm (*navy blue diamonds*) in the flow at the exit of the column

the slopes of the two linear variations of absorbance with time are shown in Fig. 18, allow us to calculate the reaction rate decrease knowing the molar extinction coefficients at 273 and 290 nm, respectively. The same obtained value of the reaction rate (12 µmol/min) demonstrates that no production of uric acid occurred during the time of the experiment, during which all of the xanthine was converted to allantoin. The uric acid enzymatically produced in the course of the flow across the first textile is totally consumed by the enzymatic reaction on the second textile. These data show the high efficiency of the bienzymatic process, which results in the sequential action of the two enzyme modified textiles.

Catalase Immobilization

In order to extend the domain for applications of such enzyme textile membrane to hydrogen peroxide dismutation, immobilization of catalase has been achieved. Catalase is a hydrogen peroxidase oxidoreductase enzyme that catalyzes the dismutation of hydrogen peroxide according to the following reaction scheme:

$$H_2O_2 + H_2O_2 \rightarrow O_2 + 2H_2O \quad (5)$$

The catalytic mechanism has been followed during a long working period by hydrogen peroxide measurements (see experimental section). Figure 19 shows the long-term stability of the catalase-modified textile.

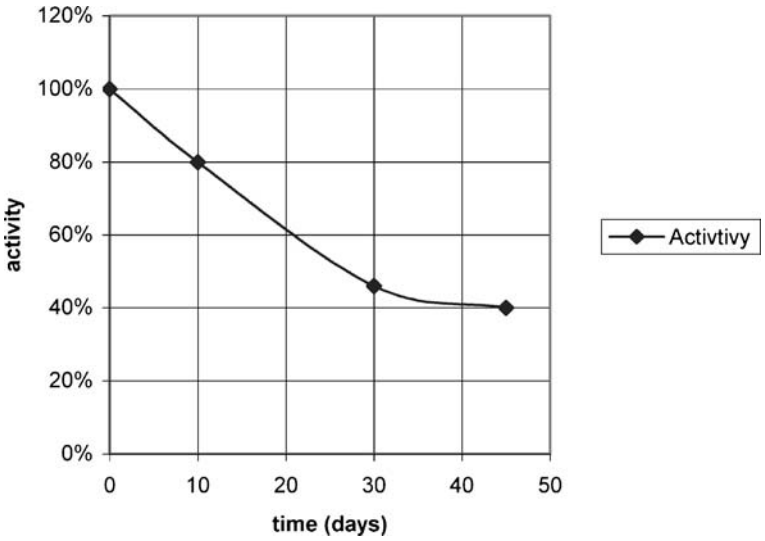

Fig. 19. Variation of the enzyme activity of a textile immobilizing catalase versus working time

Conclusion

The main feature of textiles modified by enzymes immobilized according to the biotin-avidin molecular recognition process as compared to the covalent linkage, is the much higher efficiency of the former. This efficiency is the result of the lower deactivation of the enzymes immobilized in this way, and can be attributed to the creation of microenvironments that are presumably favorable to the preservation of the protein structure of the enzyme and of the accessibility of the catalytic site.

Conversely, the covalent linkage ensure a very high content of immobilized enzymes onto the textile fibers; however, most of the covalently enzymes bound were shown to be inactive.

9.2.3 Urease Electrodialysis Coupling

We present in the last part of this chapter an application of the concept of enzyme-modified textiles based on urease immobilization in a coupling process (reaction–separation), the separation being achieved by coupling to an electromembrane process. Various technologies have been proposed for the recycling of wastewater (Dean 1991). In many cases removal of urea is difficult (for example, rejection by reverse osmosis membranes is weak; Lee and Lueptow 2001). However, one approach to handling urea is to hydrolyze it with urease immobilized on a support material (Schussel

and Atwater 1995). Urea was shown to be efficiently removed from aqueous solutions by combining a catalytic reaction and ionic migration through an ion-exchange membrane in an electrodialysis cell. (Huang and Chen 1992, 1993). As urease allows the hydrolysis of urea with the production of ammonium and carbonate ions, these produced cations and anions can be separated by electrodialysis across cation- and anion-exchange membranes.

As an indication of the efficiency of this coupling process, urea and its by-products were totally removed from the treated aqueous solutions. Moreover, the migration through the membrane of ionic reaction products has an additional advantage, since it avoided the kinetic inhibition of the enzymatic reaction due to the back reaction.

Carboxylic textiles were modified by immersion in NaOH and urea solution (1 M) for 12 h to graft amino groups onto carboxylic acid molecules. Biotin was attached to this amino group using *N*-hydroxy-succinimide biotin as a coupling reagent (0.4 mg/ml for 12 h at room temperature). Anion exchange textiles were modified directly by immersion in a sulfo-*N*-hydroxy-succinimide biotin (0.4 mg/ml) aqueous solution for 12 h.

A biotinylated urease was prepared by adding a fixed amount (2 mg/ml) of urease solution (EC 3.5.1.5, type III) from Jack Bean, in phosphate buffer 100 mM, pH 7.5, to 100 times mole excess of biotin-amidocaproate *N*-hydroxysuccinimide ester.

The biotin-modified textile support immersed in a 2 ml avidin aqueous solution (1 mg/ml) for 1 h was then immersed in 2 ml of biotinylated enzyme solution (2 mg/ml) for 1 h and then washed again with distilled water before the attachment of biotinylated urease.

A laboratory cell for assays of catalytic substrate transformation composed of three compartments separated by two ion-exchange membranes was used for the coupling with electrodialysis (Dejean et al. 1997). The modified textile was squeezed between the anion- and the cation-exchange membranes in the central compartment. The solution flowed continuously between both membranes across the textile enzyme membrane as in a frontal filtration.

A urea (10^{-2} M) solution circulated in the central compartment while molar sodium hydroxide solution and molar sulfuric acid solution circulated in anodic and cathodic compartments, respectively. Urease catalyzes the hydrolysis of urea producing ammonium and carbonate ions according to reaction (1). The determination of the activities of the free and immobilized urease was carried out by measuring of the ammonium production with blood urea nitrogen (BUN) acid reagent and BUN color reagent (Sigma product).

Figure 20 shows the specific activity of immobilized urease as compared to free enzyme. It is clear that immobilization via avidin-biotin technology

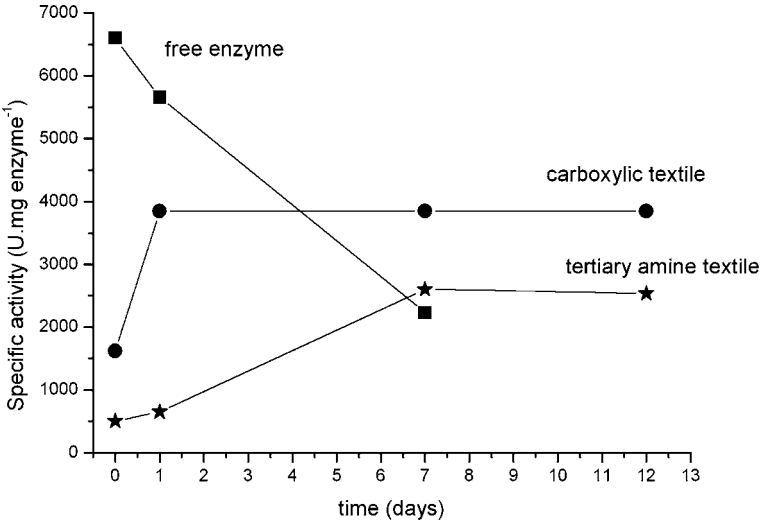

Fig. 20. Specific activity of free urease and immobilized urease on the textile support (1 enzymatic unit corresponds to the degradation of 1 μM of urea at 20 °C in phosphate buffer pH = 8.5)

on the textile support allows the maintenance of the catalytic activity of the enzyme. The electrical field was applied to the electrodialysis cell with the textile inserted in the central compartment and clipped between the two ion-exchange membranes (Fig. 21).

Figures 22 and 23 depict the ammonium concentration evolution in the cathodic and central compartments, respectively. Three current densities were used (1, 5, and 10 mA/cm^2). In the central compartment, the ammonium concentration produced by the enzymatic reaction decreases as the current density increases. The cations are transported through the cation-exchange membrane to the cathodic compartment owing to the driving force of electric field. In the central compartment, ammonium and carbonate ions are produced by the enzymatic reaction. When the current is increased in the electrodialysis cell the ammonium ion concentration decreases as the concentration in the cathodic compartment increases, because of the efficiency of the transport process across the cation-exchange membrane due to the driving force of the electrical field. Moreover, the efficiency of the transport of the ions produced by the enzymatic reaction is also demonstrated since no ammonium ions are detected in the anodic compartment. A weak leakage of ammonium through the anion-exchange membrane is detected at high current density after 90 min of working (only 1% of total ammonium concentration). The values of pH are kept constant during the process in anodic and cathodic compartments due to the high

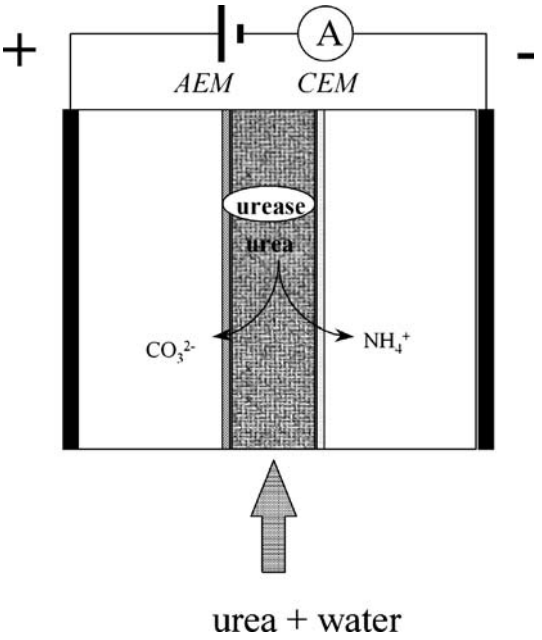

Fig. 21. Scheme of electrodialysis cell incorporating an enzyme modified textile. *AEM*: anion exchange membrane , *CEM*: cation exchange membrane

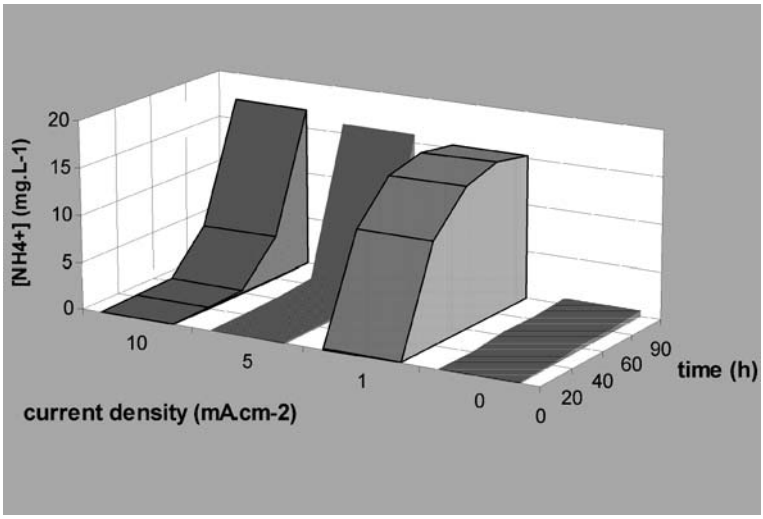

Fig. 22. Ammonium concentration in cathodic compartment versus time of electrodialysis and applied current density

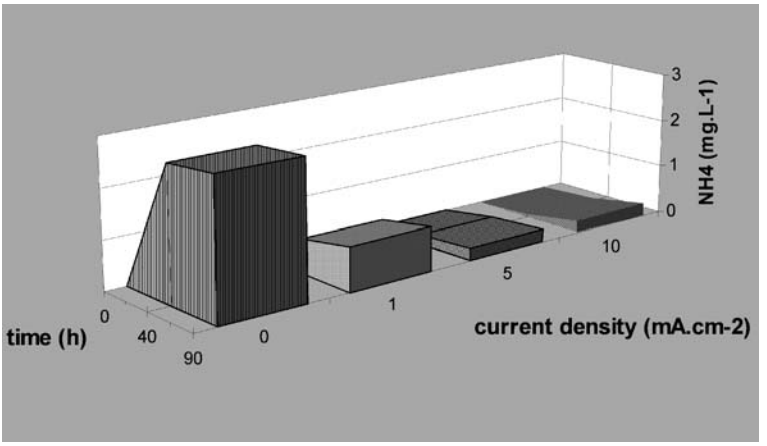

Fig. 23. Ammonium concentration in central compartment versus time of elctrodialysis and applied current density

volume used and the weak current density. Conversely, the pH in the central compartment is changed (initially pH 8.5, dropping to pH 7 after 90 min of the process).

In conclusion, in the prospect of achieving a complete removal of specific compounds such as organic pollutants by an enzymatic process represents an interesting example whereby the coupling between a chemical reaction process and membrane separation technology allows the complete treatment of a liquid phase.

9.3 Electron-Conducting Textile

9.3.1 Enzyme Immobilization on Carbon Felt

The concept of the membrane reactor has been increasingly researched in recent years because it has been postulated that the membrane core of a filtration membrane could itself be a reactive phase. Thus, the membrane would bring in addition the ability to chemically transform compounds that are solubilized in the permeate. This type of chemical transformation is very efficient because the process is a catalytic one.

We have already described the immobilization of biotinylated enzymes by a specific and irreversible biotin–avidin molecular recognition process. We generalized this process of enzyme immobilization to another enzyme

(i.e., catalase), which has been biotinylated prior to membrane immobilization because catalase is not a commercially available biotinylated enzyme. We have measured the kinetic parameters of the enzymatic reaction (hydrogen peroxide dismutation) in the membrane system. A comparison of the deduced rate parameters with those of the free respective enzymes reveals a slight decrease in the reactivity of the enzymes immobilized on the polypyrrole membrane compared to that of the free enzymes, but far from the loss of reactivity generally observed until now with enzymes immobilized by using more classical routes such as chemical bonding. Moreover, the long-term stability of the membrane in terms of reactivity also appeared to increase.

Electrochemical polymerization of the pyrrole–biotin monomers was carried out in a classical three-electrode cell, the same as those commonly used in cyclic voltammetry experiments. The working electrode was carbon felt (1.5 × 05 × 0.5 cm). Hydrogen peroxide dismutation was achieved with a flow of 30 cm^3 hydrogen peroxide 10^{-2}M solution across a membrane held in a column, as shown in Fig. 24.

Biotinylation of Catalase

A biotinylated catalase was prepared by adding a fixed amount (2 mg/ml) of catalase solution (phosphate buffer 100 mM pH 6.0) to a 100 times molar excess of biotinamidocaproate *N*-hydroxysuccinimide ester. The biotinylated reaction was carried out in a vial under constant stirring at room temperature for 3 h. At this time, 10 mg of glycine was added to react with the unused biotin. Removal of all small-molecular-weight reactants and products was achieved by chromatography through a Sephadex G 25 column from SIGMA (USA) (molecular weight cut off of 10,000).

Enzymatic Membrane Preparation

The enzymatic membrane was prepared in a three-electrodes cell as follows: monomer 1 (2 mM) in 0.1 M $NaClO_4$ acetonitrile, was electropolymerized on a 1.5 × 0.5 × 0.5 cm carbon felt from Carbone Industrie, France). The specific surface per volume unit of about 42 cm^2/cm^3 has been estimated, as in Coche and Moutet (1987), by recording the electrochemical signal of reduction of an electroactive compound such as ferricyanide ion. The porosity of the felt used is about 95% (Gonzalez-Garcia et al. 1999).

The polypyrrole-biotin modified support was rinsed with distilled water and immersed in 2 ml of avidin aqueous solution (1 mg/ml) for 1 h. The resulting porous carbon membrane was washed with distilled water and immersed in 2 ml of biotinylated enzyme solution (2 mg/ml) for 1 h and then washed again with distilled water.

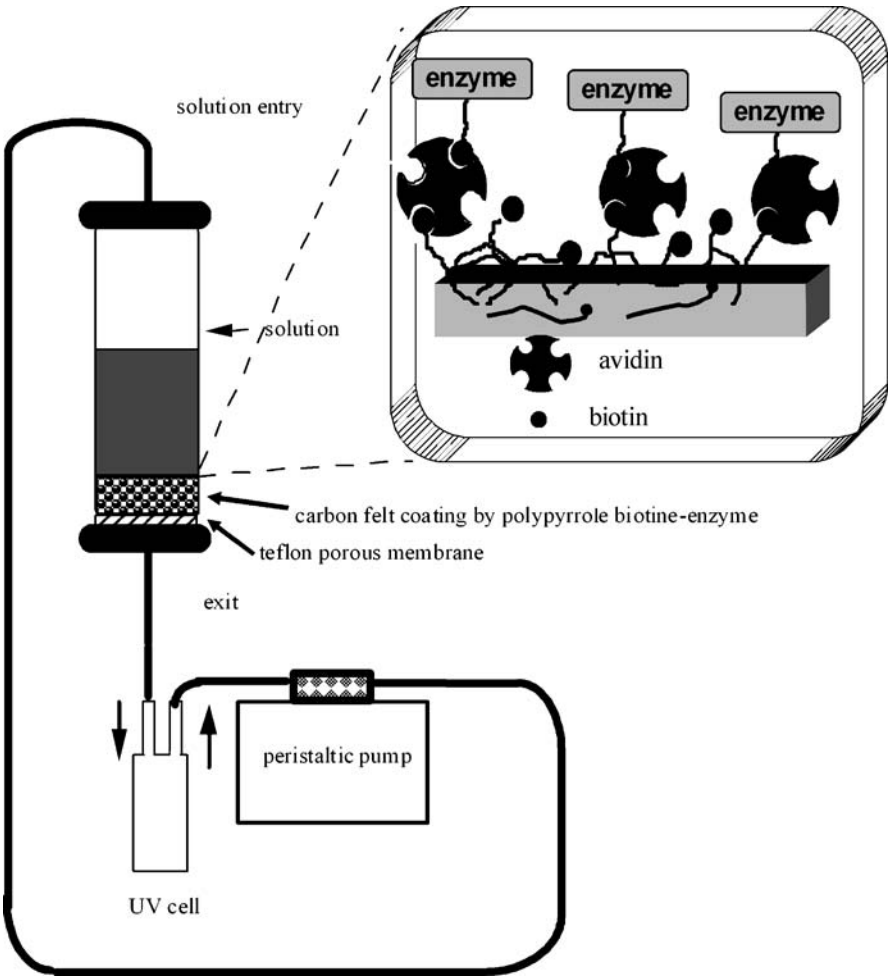

Fig. 24. Schematic diagram of the enzymatic membrane device. Glass column dimensions diameter 1 cm, height 10 cm. The inset represents the enzyme linkage of the biotinylated enzyme to the electropolymerized polypyrrole-biotin by the avidin-biotin molecular recognition process

Membrane Device

The modified carbon felt was tightly packed (0.5 cm in thickness) into a 1-cm-diameter, 10-cm-high glass column for chromatography. The column was filled with the studied solution at the top of the column and the solution flowing through the membrane was analyzed at the exit (Fig. 24). The solution was circulated by pumping with a peristaltic pump and maintained at 20 °C. Thanks to the high porosity of the felt, no strong limitation of the liquid flow occurred in the column during the filtration process.

Hydrogen Peroxide Measurements

The following analytical methods (Green and Hill 1984; peroxidase activity determination from SIGMA) were used to detect changes in hydrogen peroxide concentration changes.

Reduction of H_2O_2 catalyzed by peroxidase in the presence of pyrogallol: a mixture of pyrogallol (at a concentration not lower than the H_2O_2 one) and peroxidase (POD) was added to the H_2O_2 aqueous solution. The measured change in absorbance at 420 nm corresponding to purpurogallin formation ($\varepsilon = 248/M/cm$) is directly related to the H_2O_2 concentration decrease according to Eqs. 4 and 5:

$$H_2O_2 + POD_{red} \rightarrow POD_{ox} + H_2O \quad (6)$$

$$POD_{ox} + \text{pyrogallol} \rightarrow \text{purpurogallin} + POD_{red} \quad (7)$$

The co-oxidation of phenol and antipyrin was catalyzed by peroxidase. A mixture of phenol, 4-amino-antipyrin (at concentrations not lower than half the concentration of H_2O_2) and peroxidase was added to the H_2O_2 aqueous solution. The change in absorbance was recorded at 505 nm ($\varepsilon = 6.4 \times 10^3$/M/cm), which corresponds to the wavelength maximum of the absorption band of the quinone-imine produced by the co-oxidation of phenol and antipyrin catalyzed by the peroxidase.

For high concentrations of H_2O_2 ($\gg 10^{-2}$ M), a direct spectroscopic measurement was used. The optical density of the solution was recorded at 240 nm and the resulting concentration was calculated using a value of 39.4/mol/cm (Aebi 1984) for the molar extinction coefficient of H_2O_2.

Poly(pyrrole-biotin) Film Characterization

The structure of the film was assessed by scanning electron microscopy. The polymerization of the pyrrole–biotin monomer was carried out on a carbon felt. Figure 25 shows photographs of polymer deposition on the carbon surface. The latter illustrates that the electrochemical addressing of polymer films allows the spatially controlled functionalization of surfaces whatever their shape and size are. We recently demonstrated by gravimetric measurements that the immobilization of avidin on biotinylated polypyrrole films via bioaffinity interactions provides a compact avidin monolayer (Cosnier et al. 2001). Figure 25C shows this specific binding event of avidin onto polymerized biotin leading to a smoothed polypyrrole–air interface.

Peroxidase Immobilization

Amount of Immobilized Enzyme

The amount of POD immobilized on the carbon felt after electropolymerization were determined by enzymatic activity measurements. The

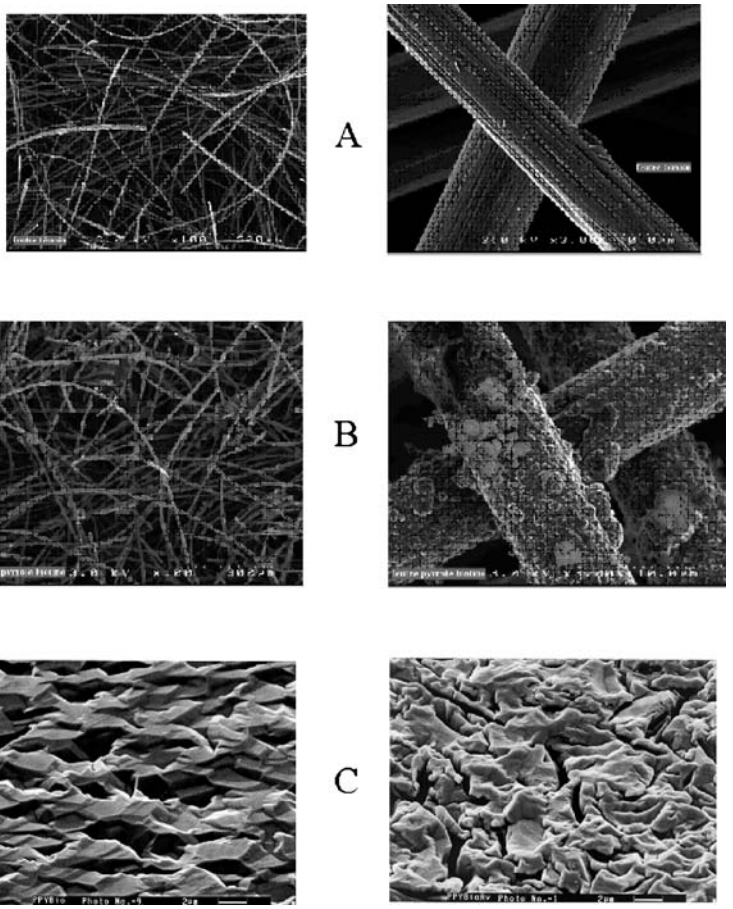

Fig. 25. Micrographs of carbon felt before (**A**) and after modification by electropolymerization of pyrrole-biotin monomer (**B**) and deposited on platinum surface (**C**) before (*left*) and after (*right*) complexation with avidin

enzyme solutions were analyzed before and after contact with the carbon tissue and the amount of enzyme actually grafted in the polymer matrix was calculated in the same way as described previously in the experimental section. The results demonstrate that 1.6 mg of enzyme was anchored in the polymeric matrix, corresponding to 83% of the initial amount of enzyme (2 mg) put in contact with the carbon felt modified by the polymer. The amount of fixed active enzyme in the membrane is around 4.1 mg/cm^3, which corresponds to approximately 0.1 mg/cm^2 of the effective surface. Taking into account the fact that the theoretical maximum surface coverage for a close-packed avidin monolayer corresponds to 3.3–5×10^{12} molecules/cm^2 (Cosnier 1999), the maximum amount of an-

chored POD should be 0.22–0.33 mg/cm^2. The specific anchoring of POD by avidin–biotin bridges thus constitutes an efficient approach for the functionalization of the whole structure of a carbon felt. The specific recognition between avidin and biotinylated enzyme allows a strong increase in enzyme grafting as compared to other matrices (Cosnier and Innocent 1993). Thus, the complexation between biotin and avidin appears to be limited by a steric interaction, whereby the smaller the enzyme size, the more efficient the immobilization. The same result has been reported for enzyme immobilization in the case of polypyrrole derivatives for biosensor elaboration (Cosnier and Innocent 1993).

Membrane Working

An equimolecular aqueous solution of H_2O_2 and pyrogallol (5×10^{-3} M) passed through the POD membrane and was analyzed by absorption spectroscopy. In the course of the transfer across the membrane, H_2O_2 is reduced by the immobilized POD, which in turn oxidizes pyrogallol into purpurogallin (see Eqs. 1 and 2). The amount of purpurogallin detected corresponds to the quantity of H_2O_2 consumed by the enzymatic reaction. The chemical yield of the membrane process corresponds to the ratio between the number of purpurogallin molecules produced and the number of H_2O_2 molecules introduced into the column. A value of 0.8 was obtained for this ratio. This value, although satisfying by itself, can be improved by a recirculation of the feed solution through the enzymatic membrane.

After a recirculation time of 30 min (which corresponds to six passages of the feed solution volume through the membrane), all of the initial H_2O_2 was oxidized by the enzymatic catalytic membrane. Figure 26 shows the rate of consumption of H_2O_2 (initial concentration 5×10^{-3} M) versus time, whereby the exit solution is continuously injected into the column, thus allowing a constant flow through the enzymatic membrane. The remarkable efficiency of this H_2O_2 degradation process is explained by the peculiar molecular interaction process used for the enzyme attachment in the immobilization procedure. In this way the enzyme was neither altered nor denatured as a result of avidin–biotin complexation and the catalytic activity was maintained in the membrane. The measurement of the specific activity of the free POD in solution related to pyrogallol transformation into purpurogallin indicates 200 U/mg of enzyme (a value not very far from that notified by the supplier, 240 U/mg). The membrane enzyme activity determined in the same experimental conditions was 117 U/mg. This value corresponds to 58% of free enzyme activity. Thus, the remaining activity of the immobilized enzyme is markedly higher than those reported previously with other immobilization methods based on electrogenerated polymer films (only 4% of free peroxidase activity; Coche-Guérente et al.

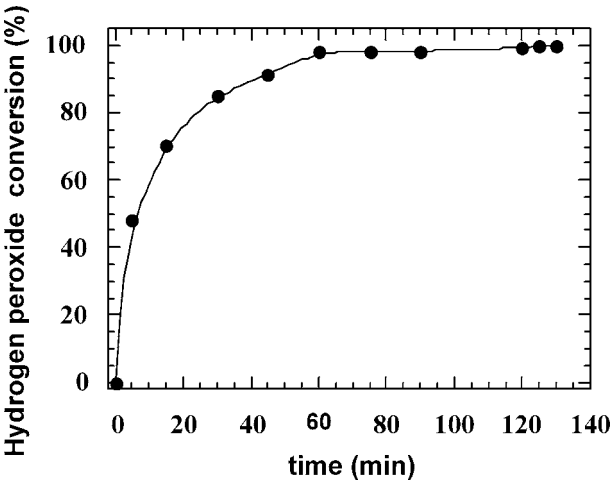

Fig. 26. Conversion ratio versus time of H_2O_2 solution (10^{-3} M) with peroxidase membrane (membrane thickness 1 cm, flow rate 1 ml/min)

1995) and 9% of free polyphenol oxidase activity (Cosnier and Innocent 1993) is maintained in the polymer matrix. This clearly illustrates the advantages offered by a soft attachment of the enzyme molecules, which preserves their conformational flexibility and hence their activity.

Dependence on pH

The optimum pH range for reactivity of the catalytic membrane was investigated with H_2O_2 (5×10^{-3} M) as a substrate and a circulation time of 15 min (flow rate: 2 ml/min). In the pH range of 4.7–8.3 the enzyme membrane shows a typical bell-shaped response; t. The maximum efficiency is obtained for pH 6.8 (Fig. 27). This value is in good agreement with that determined with free POD in solution (Worthington 1988). The kinetic experiments presented below were performed at pH 6.8, which corresponds to the pH of maximum efficiency for the immobilized enzymes.

Kinetic Parameters

Kinetic analysis was carried out by recording the solution substrate concentration of the at the column exit. According to the investigation reported previously (Wang et al. 1996), the immobilized enzyme reactivity in the carbon felt was estimated by considering the residence time of the substrate solution in the membrane. The mean residence time, t_r, of solute in the porous material can be calculated using the following equation:

$$t_r = L/J \tag{8}$$

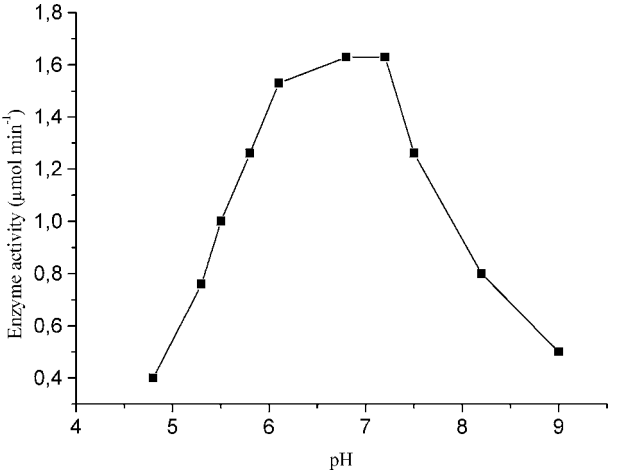

Fig. 27. Effect of pH on the enzyme activity of the membrane

where L is membrane thickness and J is volume flux of the solution; J is equal to the ratio of flow to membrane surface. The reaction rate is calculated as $V = \Delta C/t_r$, where ΔC is the concentration decrease of H_2O_2 in the flowing solution.

Peroxidase Membrane Case

Figure 28A depicts the relationship between the reaction rate and substrate concentration in the case of a POD membrane. The rate follows a classical enzymatic kinetic curve. The first step corresponds to a linear part (weak substrate concentration). For high substrate concentrations, saturation of the reaction rate is observed and the maximal value obtained is due to saturation of active enzyme sites.

Figure 28B shows the corresponding Lineweaver-Burk plot for the immobilized POD membrane. From the obtained slope (K_M/V_M) and intercept ($1/V_M$) for the linear relationship, both K_M and V_M are estimated to be 1.45×10^{-4} M and 1.8×10^{-3} M/s, respectively.

Catalase Membrane Case

In order to use the enzyme membrane for H_2O_2 dismutation, immobilization of catalase has been achieved. A simplified scheme for the mechanism underlying the catalase reaction may be described by the following two equations (Chance 1948; Nicoholls and Schonbaum 1963):

$$\text{cat(OH)}_4 + \text{H}_2\text{O}_2 \leftrightarrow \text{cat(OH)}_3\text{OOH} + \text{H}_2\text{O} \quad (9)$$

$$\text{cat(OH)}_3\text{OOH} + \text{H}_2\text{O}_2 \rightarrow \text{cat(OH)}_4 + \text{O}_2 + \text{H}_2\text{O} \quad (10)$$

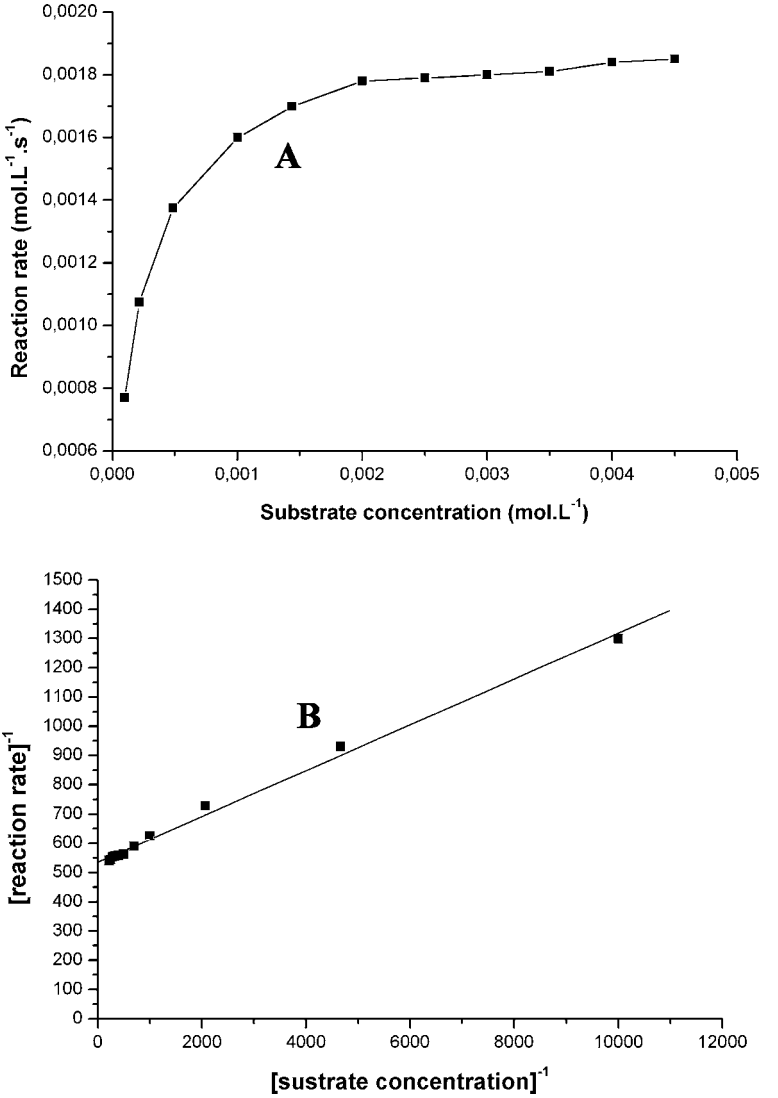

Fig. 28. Reaction rate of H_2O_2 dismutation with POD-polypyrrole membrane (**A**) and Lineweaver-Burk plot of the POD-polypyrrole membrane (**B**); residence time, t_r = 42 s, membrane thickness 1 cm, flow rate 1 ml/min

where $cat(OH)_4$ is native catalase and $cat(OH)_3OOH$ the oxidized enzyme complex.

A kinetic study was carried out both with the peroxidase and the catalase membrane in order to understand the effect of immobilization by avidin-biotin technology. In some cases, the treatment of the kinetics re-

Table 6. Kinetic parameters: Michaelis constants (V_M and K_M) for catalase and peroxidase

	k^*[E]	k (/s/mg)	K_M (mol/l)	V_M (mol/l/s)
Free catalase	1×10^{-2}	0.125	3.26×10^{-2}	
Biotinylated catalase	9×10^{-4}	0.011	9.5×10^{-3}	0.11
Immobilized catalase	5×10^{-2}	0.031	7	3×10^{-2}
Immobilized peroxidase			1.45×10^{-4}	1.8×10^{-3}

sults with a classical Lineweaver-Burk plot gives a negative value for the extrapolated reaction rate. This suggests that the maximum reaction rate of enzymatic reaction is negative, which does not make any sense. For instance, for cases in which zero or negative y-intercepts are obtained, the K_M is much larger than the total experimentally accessible substrate concentration and the simplified Michaelis-Menten model does not apply. The same phenomenon has been observed previously with another enzymes such as lipase (Freeman et al. 2000). This is the reason why in Table 6 we preferred to use the catalytic constant (k) to compare the activity of the different enzymes.

The catalytic constant (expressed as per seconds per milligram normalized to a constant amount of enzyme) for the immobilized catalase is defined as the ratio of the slope of the curve reaction rate versus substrate concentration. This value is four times lower than that of the free catalase. This result is in good agreement with those values obtained for catalase immobilized on cellulose (Eremin et al. 1995). However, it is interesting to note that for catalase, biotinylation of the enzyme decreases the rate by a factor of about 10, whilst immobilization enhances the rate as compared to that of the biotinylated enzyme in solution. The K_M value drastically increases when catalase is immobilized by avidin-biotin recognition. This value is not a significant physical parameter as it corresponds to an unrealistic concentration of H_2O_2. At these high concentrations the catalase should be totally deactivated by the substrate (Vasudevan and Weiland 1990). Enzyme immobilization, for instance in polymeric hydrogels (Arica et al. 1999), has been shown to exhibit a large K_M value. A strong increase in the value of K_M means that the kinetic parameters are affected by enzyme immobilization, presumably due to the steric effects, which significantly decrease the catalytic reaction rate.

Membrane Stability

The enzymatic membrane was stored at 4 °C in buffer solution. Assays were performed at different storage times. Figure 29 illustrates membrane stability measured in the case of POD immobilization as the H_2O_2 concentration converted to purpurogallin, starting from a 5×10^{-5} M equimolar H_2O_2-

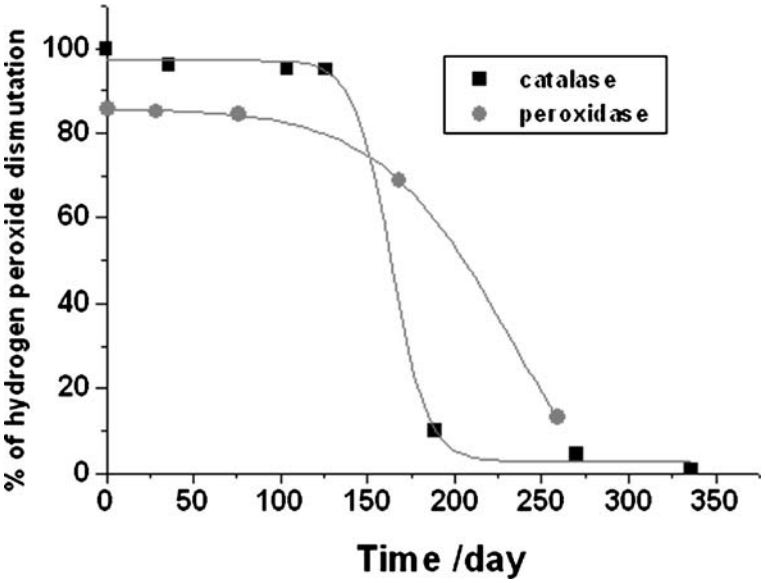

Fig. 29. Enzyme activity (in %) of the POD-membrane (●) and catalase membrane (■) after storage at 4 °C in buffer solution. Activities were measured with hydrogen peroxide concentration of 10^{-3} M after circulation time of 20 min (flow rate: 1 ml min^{-1})

pyrrogallol aqueous solution flowing across the membrane. In the case of catalase immobilization, the same operational stability with an initial H_2O_2 concentration of 2×10^{-2} M, was recorded. No significant decrease in enzyme activity was observed after 140 days and 8 h of cumulative dismutation reaction with a flow rate of 2 ml/min. The enzymatic membrane was remarkably stable compared to membranes made by other immobilization methods (Coche-Guérente et al. 1995; Cosnier 1999; Cosnier and Innocent 1993) and thus it should be noted that the enzyme was actually irreversibly immobilized. In the case of catalase immobilization, the stability is also satisfying; a loss of enzyme activity was only observed after 140 days of storage in buffer solution at 4 °C.

Conclusion

In this work the efficiency of the immobilization method based on avidin-biotin technology linked to an intermediate electropolymerized polymer layer onto carbon fibers for the building of a catalytic filtration membrane has been demonstrated. The enzyme activity of this new type of membrane along with the kinetic parameters have been determined in the case of the dismutation of H_2O_2. These rate parameters are not too much affected by the immobilization process, as the loss of reactivity as compared to free

enzymes was shown to be moderate. Moreover, the long-term stability of the catalytic activity of this type of reactive membrane makes it a promising candidate for practical application in membrane technology for liquid transformations.

9.3.2 Electrocatalysis Coupling with Enzyme-Conducting Textile Catalytic Reactivity

The electrical conducting properties of the carbon felt grafted with redox enzymes with the aid of a polypyrrole polymer layer, allow the electrochemical coupling or electrochemical transformation of the reactants involved in the activity of redox enzymes linked to such immobilization supports. As the enzyme support acts as an electrically conducting membrane, coupling via an electrochemical process is a simple means to intervene in the catalytic enzyme reaction. The electrochemical reaction has been used successfully for the regeneration of a substrate of the enzyme (converting a product of the enzyme activity into substrate) or even for the production of substrate in the vicinity of the enzyme

These two processes have been demonstrated with peroxidase. In a first example the cosubstrate of the peroxidase reaction, for instance $Fe(CN)_6^{4-}$, which is oxidized by peroxidase, is reduced electrochemically on the conducting textile biased to a negative electric potential. In the second example, H_2O_2, a substrate of peroxidase, is electrochemically produced by the reduction of oxygen, applying a reducing electrical potential to the conducting textile (in the latter case the textile acts as a working electrode for oxygen reduction).

Electrochemical Regeneration of an Enzyme Cosubstrate: Peroxidase Activity

A carbon felt modified by electro-deposition of a polypyrrole biotin layer to which biotinylated horseradish peroxidase (HRP) is attached by the molecular recognition process involving the biotin-avidin interaction (described in Chap. 1) has been introduced in a simple reactor where a solution of the enzyme reactants (H_2O_2 and $Fe(CN)_6K_4$) flow across the enzyme-modified carbon felt (Fig. 30). The conducting enzyme support is connected to a potentiometer as a working electrode biased to a potential at which the reduction of $Fe(CN)_6K_3$ occurs. The reaction is initiated by the addition of a low concentration of $Fe(CN)_6K_4$ to start the enzyme catalytic reaction, and the enzyme turnover is maintained by the electrochemical coupling, as the cosubstrate of the HRP: $Fe(CN)_6K_4$ is electrochemically regenerated from the oxidized form $Fe(CN)_6K_3$ formed in the reactor. The electrochemical coupling process is shown in Fig. 30.

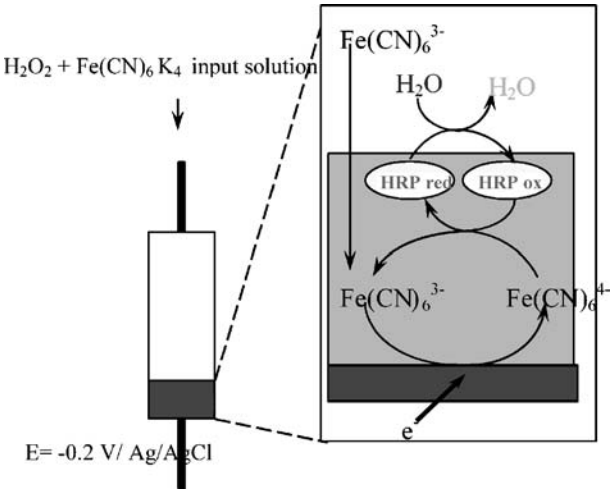

Fig. 30. Scheme of the working principle of peroxidase (HRP) immobilized on carbon felt covered with a polypyrrole biotin polymer. The HRP is attached to the polymer surface by biotin-avidin molecular recognition linkage. The regeneration of the redox mediator $Fe(CN)_6^{4-}$ is achieved biasing the carbon felt at –0.2 V versus an Ag/AgCl electrode

The variation of the $Fe(CN)_6K_3$ concentration is followed by absorption spectroscopy at 305 nm. Depending on the initial concentration of the $Fe(CN)_6K_4$ cosubstrate, for a given initial H_2O_2 concentration, the production of oxidized $Fe(CN)_6^{3-}$ species increases (see Fig. 31), which is an indication of the activity of the immobilized peroxidase. After a given time, the concentration of $Fe(CN)_6K_3$ decreases in the reactor as a result of the electrocatalytic coupling effect regenerating the cosubstrate. This effect is also evidenced by the reduction in the concentration of H_2O_2 as the enzyme activity is started.

The concentration of $Fe(CN)_6K_3$ affects the initial slope of the ferricyanide production as well as that of the related H_2O_2 dismutation, but the slope ratios do not vary exactly in the same proportion. The more probable explanation for this is the diffusion-limited process of access of reactants to the immobilized enzymes sites in the core of the grafted textile.

However, the data shown in Fig. 32 indeed confirm the electrocatalysis coupling, as the amount of H_2O_2 converted is much higher than that of ferricyanide initially introduced in the reactor. After about 50–60 min, as 1 mole of H_2O_2 necessitates 1 mole of $Fe(CN)_6K_3$ to be converted into products, the initial ferricyanide concentration introduced in the reactor has been approximately regenerated 100 times by the electrical reduction coupling at the carbon felt surface.

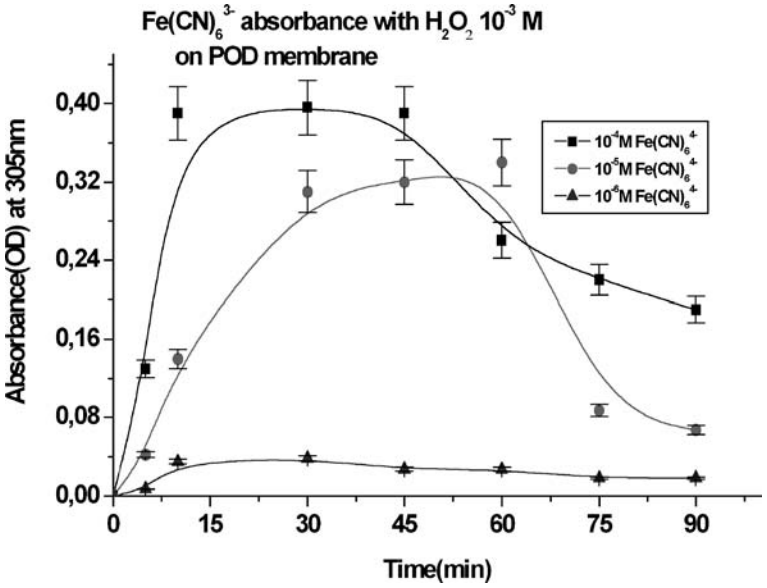

Fig. 31. Variation with time of the potassium ferricyanate absorbance for different initial concentrations of $Fe(CN)_6K_4$ in 10^{-3} M H_2O_2 solution (the carbon felt is electrically biased at –0.2 V versus Ag/AgCl electrode)

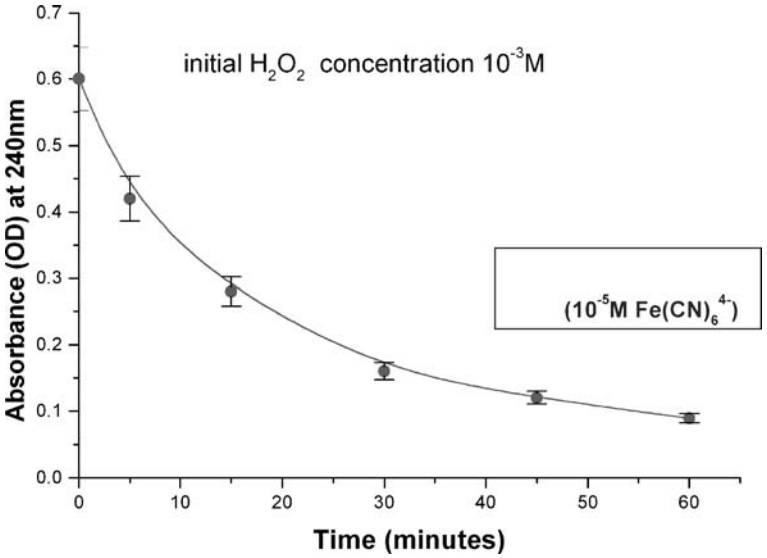

Fig. 32. Change in the H_2O_2 substrate concentration during the HRP reactivity under coupling with electrocatalysis

Electrochemical Production of an Enzyme Substrate

Another illustration of the interest of the electrical connection of the enzyme textile support is the possible production, for instance, of the substrate of a peroxidase activity. The electrochemical production of H_2O_2 is used in water treatment processes (Drogui et al. 2001), and it can be used similarly here for the working function of HRP immobilized onto a carbon felt.

The direct reduction of oxygen onto the carbon felt surface was achieved by biasing the substrate at –0.5 V/ECS, where the oxygen reduction occurs according to the classical electrochemical reaction:

$$O_2 + 2H^+ + 2e^- \rightarrow \frac{1}{2}H_2O_2 \tag{11}$$

The scheme shown in Fig. 33 depicts the working conditions of the enzyme reactor used in association with the electrochemical production of the HRP substrate, the chosen cosubstrate being pyrogallol, and oxygen fed in the reactor by gas bubbling. As in the case of the regeneration of the HRP cosubstrate described in the previous paragraph, the coupling efficiency is evidenced by the data shown in Fig. 32.

One of the products of the enzyme catalytic process, purpurogallin, is clearly formed from the pyrogallol fed into the reactor. The purpurogallin concentration depends on that of the initially introduced pyrogallol, showing that the H_2O_2 substrate is electrochemically produced in sufficient

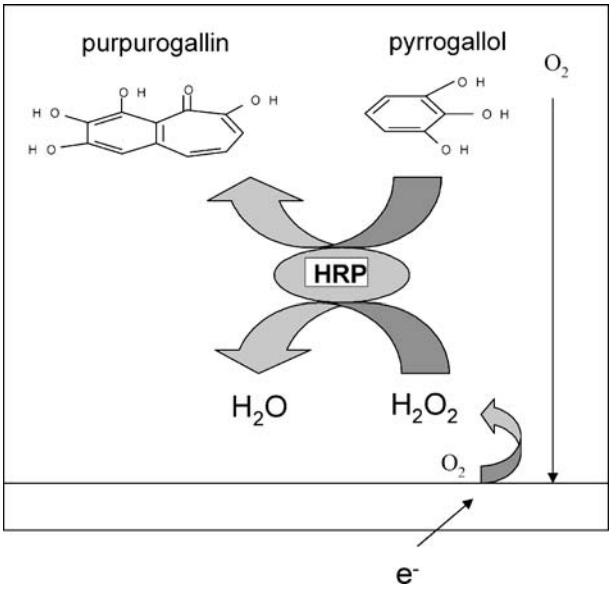

Fig. 33. Scheme of the catalytic reactions on the surface of a modified textile

amount from oxygen fed into the reactor, and does not limit the kinetics of the enzyme reaction.

Conclusion

In conclusion, the two examples mentioned in this section demonstrate that the immobilization of enzymes by a molecular recognition process onto textiles composed of electron-conducting fibers can be coupled to electrocatalysis. This coupling is efficient, even if in the described data some kinetic limitations are noticeable, due presumably to limited diffusion processes of species in the vicinity of the enzyme reactive sites in the textile core. However, as these experiments have been achieved in a very simple laboratory enzyme reactor, better optimization of the reactor design should emphasized this point.

Acknowledgements. We are very indebted to N. Bouhaine at the Department of Chemistry, Badji Mokhtar University, BP 12, 23000 Annaba, Algérie, and to A. Gherrou at the Faculty of Chemistry, USTHB, 16111 Bab Ezzouar, Algérie for their contributions to the experiments involving trypsin and pepsin grafted onto cotton. The authors also thank Professor Zhi-Kang XU and Dr. Zhen-Mei LIU at the Institute of Polymer Science, Zhejiang University, Hangzhou, 310027 People's Republic of China, for their collaboration in the domain of enzyme modifications of membranes in the frame of the Advanced Research Program (PRA 03-05) between France and China.

References

Aebi HE (1984) Methods of Enzymatic Analysis, vol. 3, (3rd edn). Verlag Chemie, Berlin, p 273

Albayrak N, Yang ST (2002) Immobilisation of *Aspergillus oryzae* galactosidase on tosylated cotton cloth. Enzyme Microb Technol 31:371–383

Arica MY, Oktem H A, Oktem Z, Tuncel SA (1999) Immobilization of catalase in polyisopropylacrylamide-co-hydroxyethylmethacrylate thermally reversible hydrogels. Polym Intern 48:879–887

Buschle-Diller G, El Mogahzy Y, Inglesby MK, Zeronian SH (1998) Effects of scouring with enzyme, organic solvents, and caustic soda on the properties of hydrogen peroxide bleached cotton yarn. Text Res J 68:920–929

Chance B (1948) The enzyme-substrate compounds of catalase and peroxides Nature 161:914–917

Coche-Guérente L, Cosnier S, Innocent C, Mailley P (1995) Development of amperometric biosensors based on the immobilization of enzymes in polymer films electrogenerated from a series of amphiphilic pyrrole derivatives. Anal Chim Acta 311:23–30

Coche-Guerente L, Deronzier A, Mailley P, Moutet JC (1994) Electrochemical immobilization of glucose oxidase in poly(amphiphilic pyrrole) films and its application to the preparation of an amperometric glucose sensor. Anal Chim Acta 289:143–153

Coche L, Moutet JC (1987) Catalysis of 1,2-dibromo-1,2-diphenylethane reduction on platinum and carbon felt electrodes coated by polypyrrole films containing 4,4′-bipyridinium groups. J Electroanal Chem 224:111–124

Confort AR, Albert EC, Langer R (1989) Immobilized enzymes cellulose hollow fibers: part I: immobilization of heparinase. Biotechnol Bioeng 34:1366–1373

Confort AR, Mullon CJP, Langer R (1988) The influence of bond chemistry on immobilized enzyme systems for ex vivo use. Biotechnol Bioeng 32:554–563

Cosnier S (1999) Biomolecule immobilization on electrode surfaces by entrapment or attachment to electrochemically polymerized films. A review. Biosens Bioelectron 14:443–460

Cosnier S, Innocent C (1993) A new strategy for the construction of a tyrosinase-based amperometric phenol and *o*-diphenol sensor. Bioelectrochem Bioenerg 31:147–160

Cosnier S, Perrot H, Wessel R (2001) Biotinylated polypyrrole modified quartz crystal microbalance for the fast and reagentless determination of avidin concentration. Electroanalysis 13:971–982

Cosnier S, Stoytcheva M, Senillou A, Perrot H, Furriel RPM, Leone FA (1999) A biotinylated conducting polypyrrole for the spatially controlled construction of amperometric biosensor. Anal Chem 71:3692–3697

Dalmon J-A (1997) Catalytic membrane reactors. In: Ertl G, Knözinger H, Weitkamp J (eds) Handbook of Heterogeneous Catalysis. Wiley-VCH, Weinheim, pp 1387–1398

Dean RB (1991) Processes for water reclamation. Waste Manage Res 9:425–430

Dejean E, Laktionov E, Sandeaux J, Sandeaux R, Pourcelly G, Gavach C (1997) Electrodeionization with ion-exchange textile for the production of high resistivity water: influence of the nature of the textile. Desalination 114:165–173

Deng HT, Xu ZK, Wu J, Ye P, Liu ZM, Seta P (2004) A comparative study on lipase immobilized polypropylene microfiltration membranes modified by sugar-containing polymer and polypeptide. J Mol Catal B Enzym 28:95–100

Devi S, Guthrie JT, Beddows CG (1990) The immobilization of trypsin onto irradiated oxidized natural rubbers converted to the natural rubber-g-Co-HEMA system. Radiat Phys Chem 36:703–707

Drogui P, Elmaleh S, Rumeau M, Bernard C, Rambaud A (2001) Hydrogen peroxide production by water electrolysis: application to disinfection. J Appl Electrochem 31:877–882

Eltsefon BS, Vengerova NA, Vysotina TA, Rudman AR, Yermakova LN, Irkley VM, Ryabchenko AS, Kuznetsova NA, Lykovykh LM (1988–89) Structure and transport properties of the Ultracell membrane for hemodialysis. Biomater Artif Cells Artif Organs 16:967–975

Eremin AN, Otyutskii SV, Metelissa DI (1995) Properties of catalase immobilized on cellulose in aqueous and micellar media. Kinet Catal 36:776–784

Freitas dos Santos LM, Pavasant P, Strachan LF, Pistikopoulos EN, Livingston AG (1997) Membrane attached biofilms for waste treatment – fundamentals and applications. Pure Appl Chem 69:2459–2469

Freeman KS, Tang TT, Shah RDE, Kiserov DJ, Gown LB (2000) Activity and stability of lipase in AOT reversed micelles with bile salt cosurfactant. J Phys Chem B 104:9312–9316

Giacomini C, Villarino A, Franco-Fraguas L, Batista-Viera F (1998) Immobilization of galactosidase from *Kluveromyces lactis* on silica and agarose: comparison of different methods. J Mol Catal B Enzym 4:313–327

Gonzalez-Garcia J, Bonete P, Exposito E, Montiel V, Aldaz A, Torregrosa-Marcia R (1999) Characterization of a carbon felt electrode: structural and physical properties. J Mater Chem 9:419–426

Green MJ, Hill HAAO (1984) Chemistry of dioxygen. Methods Enzymol 105:3–22

Huang TC, Chen DH (1992) A study of removal of urea from aqueous solution with immobilized urease and electrodialysis. J Chem Tech Biotechnol 55:191–199

Huang TC, Chen DH (1993) Coupling of urea hydrolysis ammonium removal in an electrodialyzer with immobilized urease. Chem Eng Commun 1205:191–201
Institut Textile de France (1987) Celluloses greffees Capt'ion: un echangeur d'ions à cinetique rapide, document technique
Iqbal SS, Bruno MW, Bronk JG, Batt BV Chambers CA (2000) A review of molecular recognition technologies for detection of biological threat agents. Biosens Bioelectron 15:549–578
Ishihara K, Shinozuka T, Hanazaki Y, Iwasaki Y, Nakabayashi N (1999) Improvement of blood compatibility on cellulose hemodialysis membrane: IV. Phospholipid polymer bonded to the membrane surface. J Biomater Sci Polym Ed 10:271–282
Kaewprasit C, Hequet E, Abidi N, Gourlot JP (1998) Application of methylene blue adsorption to cotton fiber specific surface area measurement: Part I. Methodology. J Cotton Sci 2:164–173
Kamath N, Melo JS, D'Souza SF (1988) Urease immobilized on polyethyleneimine cotton cloth. Appl Biochem Biotechnol 19:251–258
Kumar SD, Kulkarni AV, Kalyanraman R, Krishnamoorthy TS (1997) Whole blood glucose determination using glucose oxidase immobilized on cotton cheese cloth. Anal Chim Acta 338:135–140
Lee S, Lueptow R M (2001) Membrane rejection of nitrogen compound. Environ Sci Technol 35:3008–3018
Marchand Brynaert J (1999) Surface functionalization of polymer membranes. In: Smith Sorensen T (ed) Surface Chemistry and Electrochemistry of Membranes, Surfactant Science Series, vol 79. Marcel Dekker, New York, pp 91–124
Nicoholls P, Schonbaum GR (1963) Catalases. In: Boyer P, Lardy H, Myrback K (eds) The Enzymes, vol. VIII (2nd edn). Academic Press, New York, pp. 147–225
Nolan Etters J (1998) Emerging opportunities for enzyme use in textiles. Colourage Annu 87–92
Rao S, Anderson KW, Bachas LG (1999) Controlled layer-by-layer immobilization of horseradish peroxidase. Biotechnol Bioeng 65:389–396
Schussel LJ, Atwater JE (1995) A urease bioreactor for water reclamation aboard manned spacecraft. Chemosphere 30:985–994
Schmidt B (1996) Membranes in artificial organs. Artif Organs 20:375–380
Vasudevan PT, Weiland RH (1990) Deactivation of catalase by hydrogen peroxide. Biotechnol Bioeng 36:783–789
Vo-Dinh, Cullum BM (2000) Biosensors and bioships: advances in biological and medical diagnostics. Fresenius J Anal Chem 336:540–551
Wang H Y, Kobayashi T, Saitoh H, Fujii N (1996) Porous polydimethyl-siloxane membranes for enzyme immobilization. J Appl Polym Sci 60:2339–2346
Worthington BC (1988) Peroxidase. In: Worthington Enzyme Manual. Worthington Biochemical Co. Freehold, 254
Yakup Arica M (2000) Epoxy-derived pHEMA membranes for use bioactive macromolecules immobilization: covalently bound urease in a continuous model system. J Appl Polym Sci 77:2000–2008
Yamazaki H, Cheok RKH, Fraser ADE (1984) Immobilization of invertase on polyethyleneimine-coated cotton cloth. Biotechnol Lett 6:165–170

10 Approaches to Protein Resistance on the Polyacrylonitrile-based Membrane Surface: an Overview

Ling-Shu Wan, Zhi-Kang Xu, Xiao-Jun Huang

Abstract. Protein adsorption and/or deposition at the surface of polymeric membranes play important roles in membrane separation processes. Although polyacrylonitrile-based membranes have been used successfully in many fields, surface modifications to improve the protein resistance and hemocompatibility have received considerable interest. Various methods such as copolymerization, grafting, physical adsorption, biomacromolecule immobilization, and biomimetic modification, have been explored to build a friendly microenvironment for proteins, especially enzymes, at the membrane surface. Herein, the behaviors of proteins at the surfaces of polyacrylonitrile-based membranes are reviewed.

10.1 Introduction

Polyacrylonitrile (PAN) exhibits good thermal stability, mechanical strength, and membrane formation properties, and microporous PAN membranes are commercially available. However, its relatively poor hydrophilicity and biocompatibility hinder this type of membrane in further applications. Just like other ultrafiltration membranes, PAN-based membranes face an unavoidable problem with regard to their applications: a progressive decline in flux and a change of membrane selectivity. This phenomenon, more commonly known as membrane fouling, is attributed mainly to concentration polarization and protein fouling. Protein fouling, including adsorption/deposition on the membrane surface and pore blockage, generally results in a largely irreversible decline of flux. Many researchers have therefore provided important insights into the effects of interactions between proteins and membranes or between proteins. On the other hand, PAN-based membranes have also been used as blood-contacting materials in hemodialysis, plasmapheresis, plasma fractionation, leukofiltration, and artificial livers (Krasteva et al. 2002; Sun et al.

Ling-Shu Wan, Zhi-Kang Xu, Xiao-Jun Huang: Institute of Polymer Science, Zhejiang University, Hangzhou 310027, People's Republic of China, E-mail: xuzk@ipsm.zju.edu.cn

Principles and Practice
Proteins at Solid–Liquid Interfaces
Philippe Déjardin (Ed.)
© Springer-Verlag Berlin Heidelberg 2006

2003). During these processes protein adsorption occurs rapidly, within seconds to minutes after the first blood contact. In addition to the aforementioned disadvantages of flux decline and change in selectivity, protein adsorption can trigger the cascading chemical reactions of clotting factors, which is followed by platelet adhesion and activation of the coagulation pathways, leading to thrombus formation (Dee et al. 2002).

It seems that proteins at the membrane surface stand at the center of membrane filtration processes, especially for the blood-contacting membranes. Proteins, not only model proteins of membrane fouling such as bovine serum albumin (BSA), but also a special protein type, enzymes, must be taken into account. Protein molecules should not be thought of as rigid structures. As we know, proteins are flexible chains that have been coiled, folded, and bent to assume a particular three-dimensional conformation. Changes in the microenvironment of proteins can alter the conformation of the molecules. Likewise, proteins experience structural alterations during interactions with solid surfaces, such as charged or noncharged membrane surfaces. As for protein fouling, protein denaturation and aggregation may result in radically different deposition compared to native proteins. Thus, keeping protein adsorption at a low level, thus allowing only little changes in its conformation, should be beneficial to membrane fouling.

Many approaches have been explored to build a friendly and biocompatible interface between protein and membrane. Among them, surface modifications to increase the hydrophilicity and to introduce steric hindrance and/or a biomimetic layer on the membranes have received considerable attention. Herein, we will review some recent progress in the field of protein resistance at PAN-based membrane surfaces, as effected by various surface modification methods.

10.2 Copolymerization Procedures

Acrylonitrile can be easily copolymerized with a variety of comonomers (Krasteva et al. 2002). Copolymerizations of hydrophilic/functional monomers such as maleic acid (Nie et al. 2004a,b), *N*-vinyl-2-pyrrolidone (Groth et al. 2002; Krasteva et al. 2002; Wan et al. 2005), α-allyl glucoside (Xu et al. 2003, 2004), 2-hydroxyethyl methacrylate (HEMA; Huang et al. 2005a,b), acrylamides (Musale and Kulkarni 1996, 1997), and *N*-vinylimidazol (Godjevargova et al. 2000) with acrylonitrile have been performed to improve the properties of PAN-based membranes. Modifications through copolymerization are capable of improving the bulk property of polyacrylonitrile to some extent. Furthermore, the surface properties of the membrane can also be greatly improved, because the amount of incorporated comonomers

can be accurately tuned, and the hydrophilic moieties of the comonomer may migrate to the membrane surface to minimize the surface energy when used in an aqueous environment.

Carbohydrates exist in many forms and play important roles in natural living systems. Their highly hydrophilic characteristics together with their innate compatibility with biomolecules may meet the demands of protein resistance and have led to considerable interest in the synthesis of their polymers. We have synthesized the copolymer of acrylonitrile with α-allyl glucoside using the process of water-phase precipitation copolymerization (Xu et al. 2003). Copolymer membranes with different contents of α-allyl glucoside were prepared using a phase inversion process (Xu et al. 2004). The formula of α-allyl glucoside and the water contact angle of the membranes are shown in Figs. 1 and 2, respectively. BSA was chosen as a model protein to investigate the protein resistance of these copolymer membranes and typical results are shown in Fig. 3. It is well known that the hydrophobic interaction between the membrane surfaces and proteins plays a very important role in the nonselective adsorption of protein onto those membrane surfaces. Materials that possess a hydrophilic surface usually show relatively low nonselective adsorption for proteins or cells. Carbohydrate-containing polymers are highly hydrophilic materials, a property that can be confirmed by water-contact angle measurements; however, some recognize the biomolecules or cells because of the "cluster effect". Therefore, the hydrophilicity and recognition function of the carbohydrate moieties have different effects on the adsorption of proteins or cells.

It can be seen from Fig. 1 that the adsorbed amount of BSA decreases almost linearly with increases in α-allyl glucoside content in the copolymer: the higher BSA concentration may lead to the larger amount of BSA adsorbed. The decrease in BSA adsorption can be ascribed mainly to the improvement in hydrophilicity by the carbohydrate moieties for the membrane surface. Macrophage adhesion was also performed on these membranes to evaluate their biocompatibility; the results are shown in

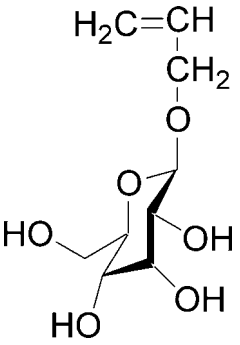

Fig. 1. Chemical structure of α-allyl glucoside

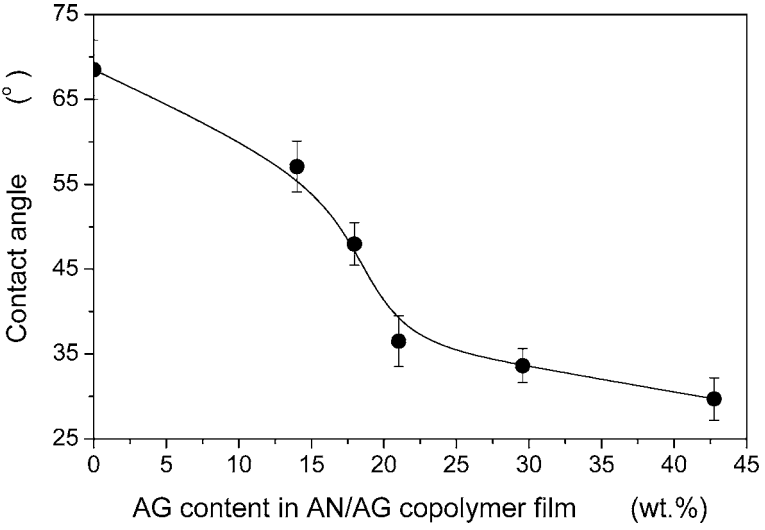

Fig. 2. Relationship between the contact angle and the content of α-allyl glucoside (*AG*) in the acrylonitrile/α-allyl glucoside (*AN/AG*) copolymer membranes

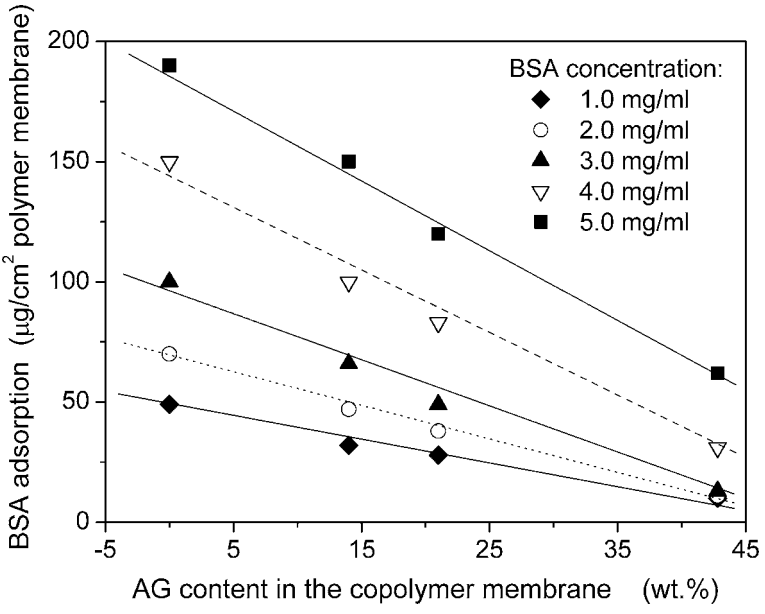

Fig. 3. Adsorption of bovine serum albumin (BSA) onto AN/AG copolymer membranes

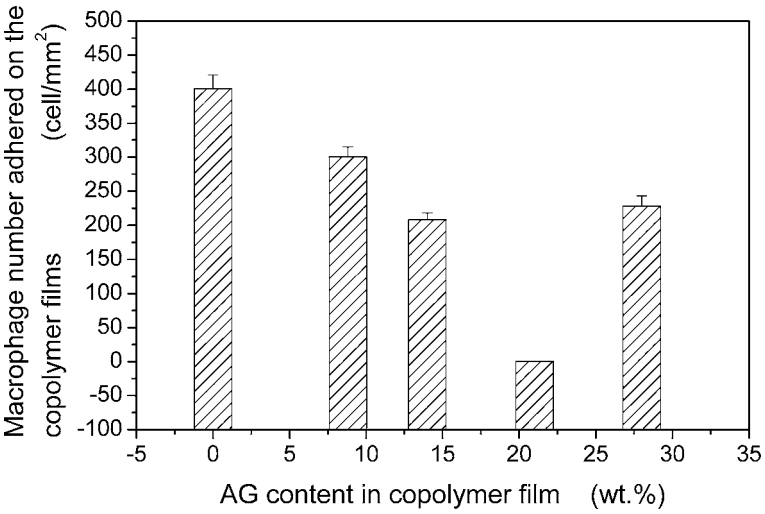

Fig. 4. Relative macrophage number versus AG content in AN/AG copolymer membranes

Fig. 4. It was clearly demonstrated that the number of macrophages that adhered onto the copolymer membranes decreased sharply when compared with that on the polyacrylonitrile membranes. However, it seems that the macrophage adhesion number increased again when the content of α-allyl glucoside exceeded around 20 wt %. This might be due to the "cluster effect" of the carbohydrate moieties in the copolymer chains. It was reported that the carbohydrate density strongly affects the specific interactions between carbohydrate moieties and cells, and that the binding affinity is drastically enhanced by multivalent carbohydrate ligands (the "cluster effect").

Poly(*N*-vinyl-2-pyrrolidone) has excellent biocompatibility with living tissues. *N*-vinyl-2-pyrrolidone is also a potential comonomer for the chemical modification of polyacrylonitrile membranes by copolymerization. Groth and coworkers (Groth et al. 2002; Krasteva et al. 2002) synthesized copolymers of acrylonitrile with *N*-vinyl-2-pyrrolidone using a solution copolymerization process. They used this type of copolymer membrane as culture substrate for human skin fibroblasts for the development of an artificial skin. The attachment, morphology, and growth of hepatocytes on this copolymer membrane were also investigated. They proposed that there was no simple relationship between the wettability of the membrane and its ability to support cell adhesion and function. It was also suggested that this copolymer containing *N*-vinyl-2-pyrrolidone can be considered as an interesting substrate if sufficient numbers of hepatocytes are seeded to promote sufficient functionality for a biohybrid liver support system.

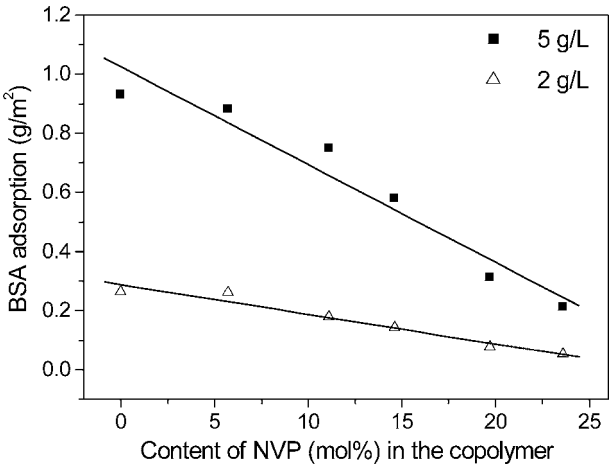

Fig. 5. Adsorption of BSA at different concentrations (2 g/l *open triangles*; 5 g/l *filled squares*) on acrylonitrile/*N*-vinyl-2-pyrrolidone copolymer films with various NVP content

Acrylonitrile/*N*-vinyl-2-pyrrolidone copolymers with different contents of *N*-vinyl-2-pyrrolidone were also synthesized by us using a water-phase precipitation copolymerization process. It was found that the introduction of *N*-vinyl-2-pyrrolidone into PAN did not change the water contact angles much, and this is in accord with the findings of Groth et al. (2002). However, as shown in Fig. 5, BSA adsorption was remarkably depressed with increasing content of *N*-vinyl-2-pyrrolidone in the copolymer. The results of platelet adhesion also confirmed the improvement in the biocompatibility of PAN afforded by the incorporation of *N*-vinyl-2-pyrrolidone. One can envisage that the protein fouling on this copolymer membrane surface might be reduced or even partly eliminated.

How do polymers containing *N*-vinyl-2-pyrrolidone achieve excellent biocompatibility? Hayama et al. (2004) insisted that the biocompatibility of membranes containing *N*-vinyl-2-pyrrolidone was dependent on both the number of *N*-vinyl-2-pyrrolidone units and their surface structures. They proposed that the higher the regularity of the polymer particle structure in the wet condition, the lower the wet:dry ratio surface roughness and the larger the wet:dry ratio of the polymer particle diameter. That is, the more the polymer particles swell as a result of wetting, the greater the biocompatibility.

We have synthesized the copolymers of acrylonitrile with maleic acid using the water phase precipitation copolymerization process (Nie et al. 2004c), which were denoted as PANCMA. Ultrafiltration hollow-fiber membranes of these copolymers with different molecular weights and contents of maleic acid were also prepared by a dry–wet phase inversion process. The

carboxyl groups on the membrane surfaces were then converted into anhydride groups by refluxing the membranes in acetic anhydride; the resultant membrane was denoted as PANCMAn. Although the amount of protein adsorbed onto both PANCMA and PANCMAn membranes were large, it was obvious that the former, with a BSA adsorption of 2.31 g/m^2, was more protein resistant than the latter, with a BSA adsorption of 4.02 g/m^2. Based on the fact that the water contact angle on the PANCMA membrane was 55 °C, which was smaller than that on the PANCMAn membrane (65 ∘ C, this different adsorption behavior of BSA might be ascribed to differences in the surface hydrophilicity.

Musale and Kulkarni (1996) investigated the fouling reduction in membranes fabricated from PAN and acrylonitrile-based copolymers with increasing acrylamide content. They suggested that membranes containing acrylamide were more hydrophilic, had a smaller dispersion force component of the surface energy and a smaller negative zeta potential than those prepared from PAN. The effect of the surface chemistry of these membranes with similar pore sizes was studied through the ultrafiltration of BSA as a function of feed pH. It was found that the PAN membrane exhibited relatively low BSA transmission rates throughout the pH range 4.0–7.5. However, the acrylamide-containing membranes exhibited marked increases in BSA transmission at pH values above the protein isoelectric point (pH 4.8). This might be ascribed to the combined effects of improved hydrophilicity/reduced dispersive surface energy and less electrostatic repulsion between the copolymer membranes and BSA. On the contrary, at pH values below the isoelectric point (pH 4.8), all of the membranes had a low BSA transmission due to strong adsorption resulting from attractive electrostatic interactions. They also found that the permeate flux and flux recovery increased for all membranes with increasing feed pH. This might be partly attributed the decreasing electrostatic attraction and increasing electrostatic repulsion between BSA and the membrane surface. At any given pH, the data comparison of permeate fluxes and flux recoveries indicated less fouling of the surface in the case of the acrylamide-containing membrane. In other words, the acrylamide-containing PAN membrane had a greater protein resistance.

Hemoglobin, a protein with a similar molecular weight to BSA but that is more hydrophobic, was also used by Musale and Kulkarni (1997) as a model protein in the ultrafiltration of PAN membranes containing acrylamide. In this case, because the hydrophobic interactions were strong, the rejection was relatively constant and the flux exhibited a minimum at the isoelectric point, while it increased monotonically through the copolymer membranes. It was also proposed that hemoglobin would be adsorbed preferentially on the membrane surface during the ultrafiltration of mixed proteins of hemoglobin and BSA.

A copolymer of acrylonitrile and *N*-vinylimidazol was synthesized by Godjevargova et al. (2000) and its ultrafiltration membrane was used for glucose oxidase immobilization. They found that the enzyme bound on the copolymer membrane had high relative activity (91%). One can envisage that the membrane containing *N*-vinylimidazol provided the immobilized enzyme with a good microenvironment and could optimize the conformation of enzyme for catalysis.

10.3 Poly(ethylene glycol) Tethering

Surface graft polymerization is one of the most commonly used methods of grafting, including radical, radiation, plasma, and ultraviolet initiated graft polymerization. In general, grafting modification changes the surface properties of a polymer membrane in a defined selective way while preserving its bulk/macroporous structure. The physicochemical properties of the membrane surfaces change to a great extent after modifications. Therefore, interactions with solutes such as proteins with a membrane can be changed accordingly, which may cause protein resistance.

Many researchers have developed various technologies to realize surface grafting. Meanwhile, a great variety of monomers were chosen to improve the protein resistance of PAN membranes. Ulbricht and Belfort (1996) studied the surface and permeation properties of PAN and polysulfone membranes after treatment with low-temperature plasma and subsequent grafting with HEMA. They indicated that PAN ultrafiltration membranes hydrophilized by simple water/He plasma treatment exhibited a strongly reduced impact of protein adsorption on membrane fouling, and hence enabled higher filtrate fluxes with the same protein retention. Based on the results of BSA ultrafiltration, they also proposed that the reduction of protein surface adsorption by increased membrane surface hydrophilicity could diminish the tendency of protein fouling, thus compensating for a loss in hydraulic permeability due to the grafting modification.

Being different from some monomers such as acrylamide and acrylic acid, poly(ethylene glycol) (PEG) is well-known for its extraordinary ability to resist protein adsorption because of its hydrophilicity, large excluded volume, and unique coordination with surrounding water molecules in an aqueous medium (Nie et al. 2003, 2004b, d; Xu et al. 2005). Surface-grafted PEG has also rendered ultrafiltration membranes resistance to protein fouling. In order to improve the protein resistance and blood compatibility of the PANCMA membrane, the carboxyl groups on the membrane surfaces were converted into anhydride groups by refluxing the membranes in acetic anhydride, and then these anhydride groups are subjected to an esterifica-

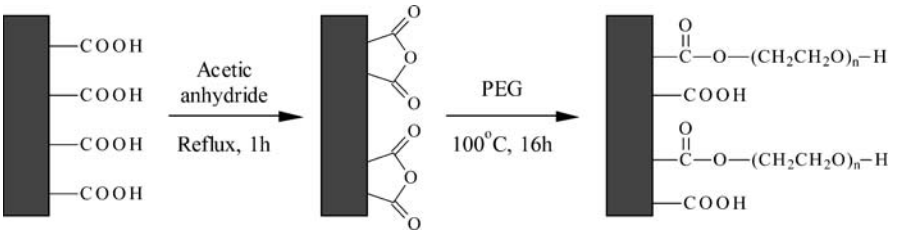

Fig. 6. Illustration of the preparation of acrylonitrile/maleic acid copolymer membrane and its grafting with poly(ethylene glycol) (*PEG*)

tion reaction with PEG containing hydroxyl end groups, as illustrated in Fig. 6.

For surface grafting modification, the grafting degree or the amount of grafted polymer is important to the surface properties of membrane. The grafting degree can be tuned by changing the conditions of modification during radiation-, plasma-, or ultraviolet-initiated graft polymerization. In order to investigate the effect of the grafting degree of PEG on the protein resistance of the membrane, PANCMA membranes with different contents of maleic acid were fabricated and then PEG was immobilized onto these membrane surfaces according to the procedure described above. The typical characteristics of the PANCMA and PEG-grafted membranes are summarized in Table 1. It can be seen from Table 1 that the grafting degree of PEG increased with the content of maleic acid, and the hydrophilicity (depicted as water contact angle) increased in the same order.

To investigate the filtration performances of this series of membranes, dynamic protein adsorption experiments were carried out. Typical results for the permeation fluxes of water and BSA solution through all membranes are shown in Figs. 7 and 8. The symbols, J_{w0} and J_p are defined as the flux

Table 1. Typical characteristics of the acrylonitrile/maleic acid copolymer (PANCMA) and poly(ethylene glycol) (PEG)-grafted membranes. *CA* Water contact angle, *GD* grafting degree

Polymer[a]	Content[b]	CA (°C[c])	Polymer[d]	GD[e]	CA (°C)
PANCMA04	3.69	48.2	PANCMA04-g-PEG400	7.19	31.4
PANCMA07	7.48	42.4	PANCMA07-g-PEG400	13.17	24.2
PANCMA11	11.45	37.1	PANCMA11-g-PEG400	16.84	21.1

[a,b]The number following "PANCMA" refers to the mol content of maleic acid in the copolymer

[c]Measured by the sessile drop method

[d]PEG400-grafted PANCMA membrane with different maleic acid contents

[e]Calculated from the weights of a membrane before and after grafting reaction (wt%)

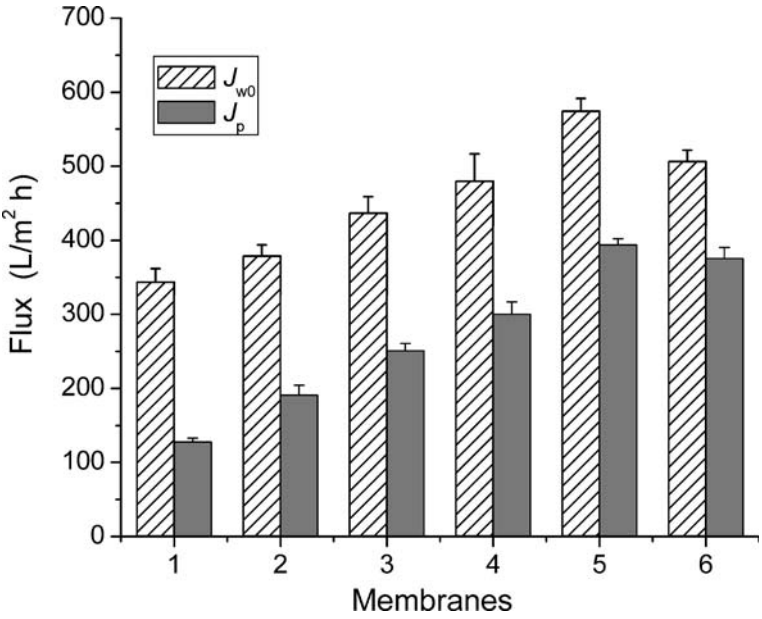

Fig. 7. Permeation fluxes of deionized water (J_{w0}, *hatched column*) and BSA solution (J_p, *shaded column*) through: PANCMA04 (1), PANCMA07 (2), PANCMA11 (3), PANCMA04-g-PEG400 (4), PANCMA07-g-PEG400 (5), and PANCMA11-g-PEG400 membranes (6). The number following "PANCMA" and "PEG" refers to the mole content of maleic acid and PEG, respectively, in or grafted onto the copolymer, respectively. *PANCMA* acrylonitrile/maleic acid copolymer

of deionized water and BSA solution, respectively. As can be seen from Fig. 7, for all PANCMA membranes, both J_{w0} and J_p membranes increased with the content of carboxyl groups, and the PEG-grafted membranes had higher fluxes than all nongrafted membranes. However, it was interesting that the J_{w0} and J_p of the PANCMA11-g-PEG400 (i. e., the membrane with the largest grafting degree) of PEG, were smaller than that of PANCMA07-g-PEG400 (i. e., a membrane with a moderate grafting degree). This may be due to the pore plugging of the membrane with the high graft degree of PEG. Figure 8 shows the percent of total fouling $[(1 - J_p/J_{w0}) \times 100]$, the flux recovery following water cleaning $[(J_{w1} - J_p)/(J_{w0} - J_p) \times 100$, where J_{w1} denotes water permeation flux after water cleaning], and the flux recovery as a result of chemical cleaning $[(J_{w2} - J_{w1})/(J_{w0} - J_p) \times 100$, where J_{w2} denotes the water permeation flux after chemical cleaning]. It can be clearly seen that the PEG-grafted membranes possessed lower total fouling and higher flux recovery.

Figure 9 shows the results of static protein adsorption for membranes with different contents of carboxyl groups or grafting degree of PEG. It

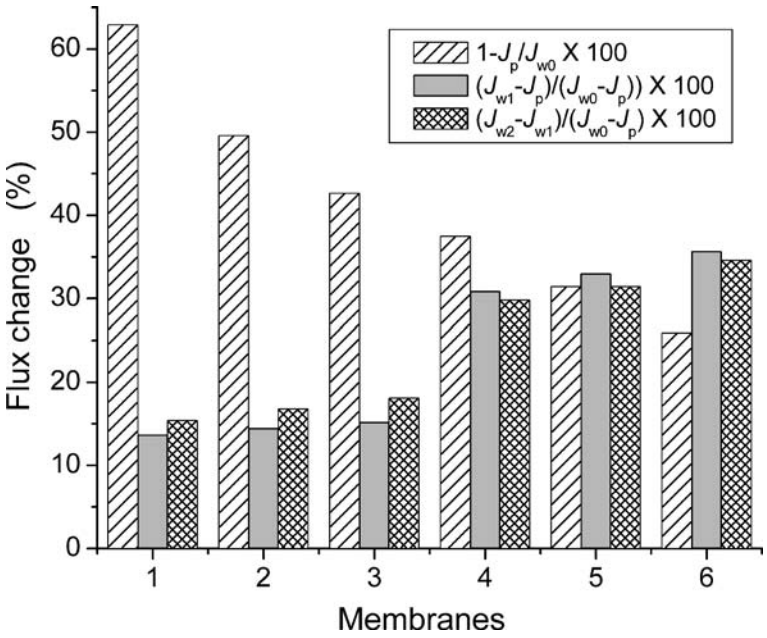

Fig. 8. Flux changes of: PANCMA04 (1), PANCMA07 (2), PANCMA11 (3), PANCMA04-g-PEG400 (4), PANCMA07-g-PEG400 (5), and PANCMA11-g-PEG400 (6) membranes during filtration (*hatched columns*) and after water cleaning (*black columns*) and chemical cleaning (*crosshatched columns*)

can be seen that, the higher the content of carboxyl groups or PEG, the smaller the amount of static BSA adsorption. In addition, the PEG-grafted membranes had a greater degree of protein resistance than the PANCMA membranes. This result implied that the grafting modification with PEG rendered the membrane somewhat protein resistant.

To investigate the protein resistance of the PEG-grafted membrane, PEGs with various molecular weights were grafted onto the PANCMA membrane. Water contact angle and water absorption measurements were used to characterize the relative hydrophilicity of the membrane surface. It can be seen from Fig. 10 that the PEG400-grafted membrane showed the greatest degree of water absorption and the smallest water contact angle. This is interesting and can be simply explained as follows. Although the PANCMA04-g-PEG200 membrane has the largest number of PEG chains per unit area, namely grafting density, the chain is short and of relatively low hydrophilicity. On the other hand, it is more difficult to graft PEG600 and PEG1000 onto the membrane surface; therefore, the hydrophilicity of the corresponding membranes also decreases. It seems that to obtain an optimal protein-resistant membrane, PEG of a moderate molecular weight should

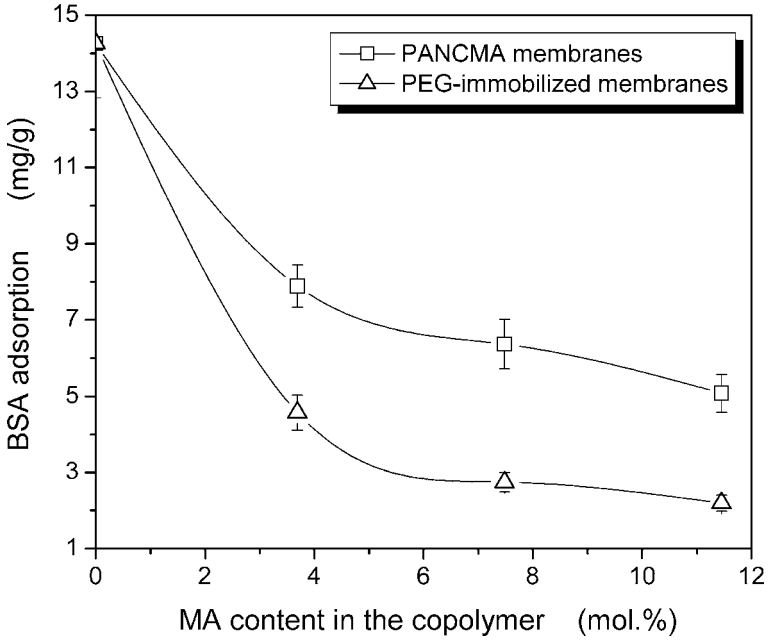

Fig. 9. Relationship between static BSA adsorption and maleic acid (*MA*) content in PANCMA for the original (*squares*) and PEG-grafted (*triangles*) membranes

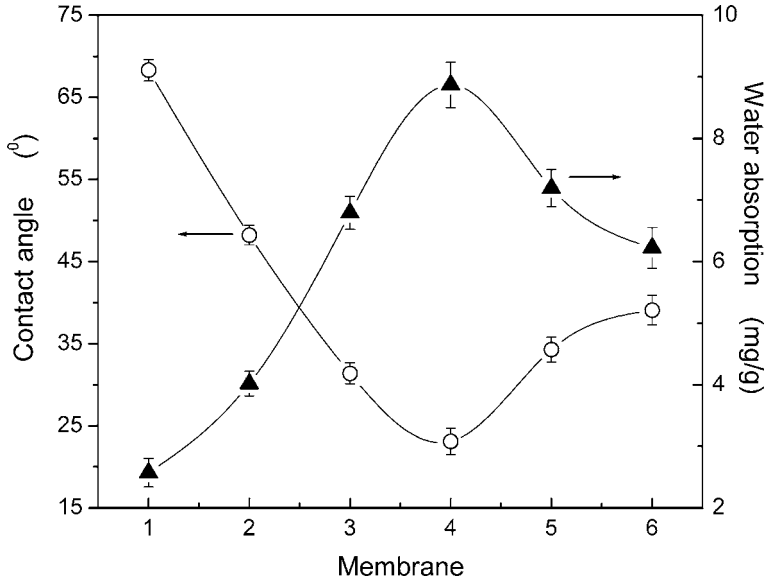

Fig. 10. Effects of the molecular weight of PEG on the water contact angle (*open circles*, left y axis) and water absorption (*filled triangles*, right y axis) of: polyacrylonitrile (PAN; 1), PANCMA3 (2), PANCMA04-g-PEG200 (3), PANCMA04-g-PEG400 (4), PANCMA04-g-PEG600 (5), and PANCMA04-g-PEG1000 (6) membranes

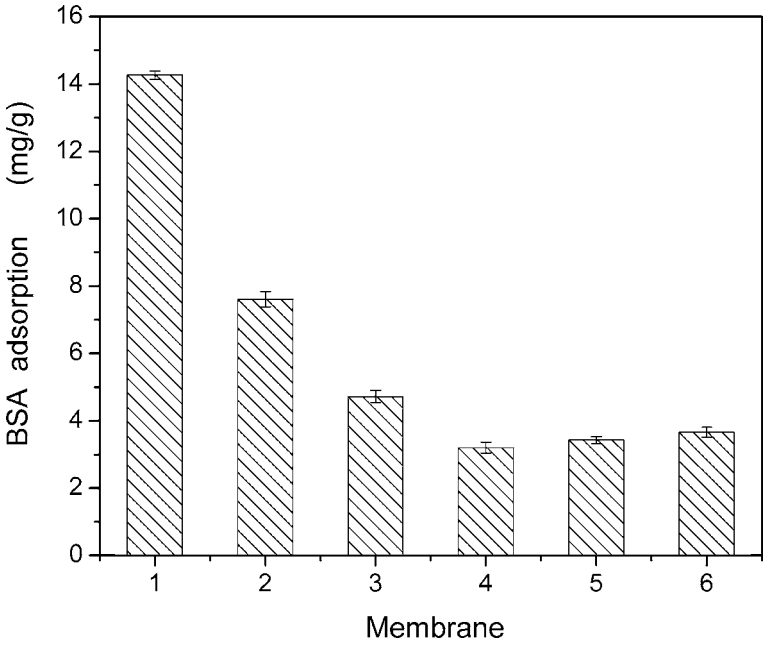

Fig. 11. Relationship between the molecular weight of PEG and static BSA adsorption on: PAN (1), PANCMA04 (2), PANCMA04-g-PEG200 (3), PANCMA04-g-PEG400 (4), PANCMA04-g-PEG600 (5), and PANCMA04-g-PEG1000 (6) membranes

be suitable because of the balance between the grafting density and the length of the hydrophilic chain segments. Figure 11 shows the results of static protein adsorption experiments on membranes grafted with different molecular weights of PEG. It can be seen that little protein is adsorbed on PEG-grafted membranes.

10.4 Physical Adsorption

One of the commonest methods of modifying the surface properties of a membrane is to coat that membrane, which has the desired bulk properties, with an agent that has the desired surface properties. Mostly, coating is based on the physical adsorption of an agent on the membrane surface. Hence, the stability and durability of the coating agent is one of the key factors.

Déjardin et al. (Etheve et al. 2003; Thomas et al. 2000;Valette et al. 1999; Yan et al. 1992) reported a series of studies on modification of the physical adsorption properties of PAN-based membranes. Two types of poly-

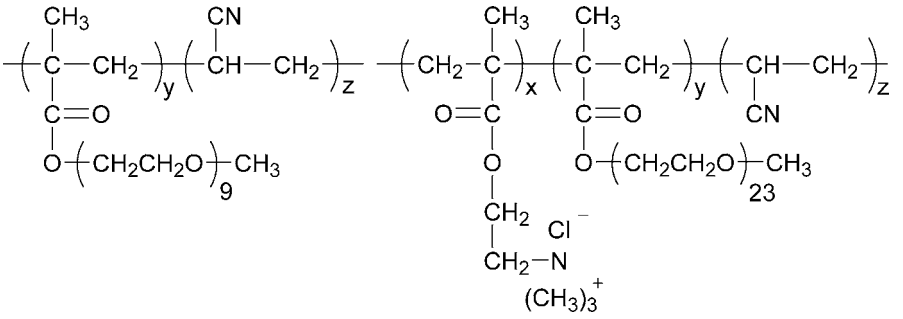

Fig. 12. Schematic representation of the structure of the copolymer and terpolymer derived from acrylonitrile, poly(ethyleneoxide) methacrylate and trimethylaminoethyl chloride methacrylate

mers, namely copolymers and terpolymers, were synthesized as depicted in Fig. 12. In the case of preadsorption with the terpolymer, platelet accumulation was considerably reduced. The effect on albumin and fibrinogen adsorption following preadsorption with the copolymer was also investigated. They found that whatever the pH of preadsorption, passivation efficiency was zero for copolymers with a high content of poly(ethyleneoxide) side chains, while a maximum reduction in adsorbance of 60% was attained with a copolymer containing 79 mol% acrylonitrile. They proposed that a higher content of acrylonitrile in the copolymer might improve the anchoring of the copolymer onto the membrane surface and therefore prevent protein adsorption more effectively than in the case of copolymers with a lower content of acrylonitrile, which is more readily displaced from the surface by proteins. Based on this consideration, the terpolymer was also synthesized and physically adsorbed onto the membrane. A reduction of at least 87% in fibrinogen adsorbance was obtained. They have also reported that although this water-soluble terpolymer might be leached out during these experiments, such a leaching should be low enough that it would not affect the prevention of protein adsorption. They also found that the levels of activation of blood components by the preadsorbed PAN-based membrane were lower than those of controls. Based on these results, it can be concluded that this physical adsorption modification did afford protein resistance.

In the study of Thomas et al. (2000), positively-charged poly(ethyleneimine) was physically adsorbed onto various PAN-based hemodialysis membranes, probably creating a repelling and water-swollen layer for proteins. Participating in the contact-phase activation of the endogenous blood-coagulation cascade, high-molecular-weight kininogen was chosen as a model protein to study the protein resistance of these membranes. It was found that both kininogen adsorption and contact-phase activa-

tion was greatly reduced, irrespective of the pH value (between 7.0 and 7.8). They (Etheve et al. 2003) also performed lysozyme adsorption on a hemodialysis sulfonated PAN membrane with and without preadsorbed poly(ethyleneimine) on the external faces. They found that over a long time period, the total adsorbed amount of lysozyme adsorbed was unaffected by preadsorption of the membrane with poly(ethyleneimine). However, it was found that the poly(ethyleneimine) layer led to significantly slower kinetics of adsorption at pH 7.2 in Tris buffer. Thus, it can be inferred that surface preadsorption by a high-molecular-weight poly(ethyleneimine), while preventing the activation of contact-phase activation, did not inhibit the high capacity of the membrane to adsorb small proteins.

Both cytochrome C and α-lactalbumin are low-molecular-weight proteins. The former is positively charged in an aqueous solution at pH 7.4 and the latter is negatively charged. Based on the results of the adsorption of these two low-molecular-weight proteins on different hemodialysis membranes, Valette et al. (1999) suggested that the observed differences in the adsorbance of proteins were mostly due to the different microstructure, chemical nature, and surface charge of the membrane.

10.5 Biomacromolecule Immobilization

Since PAN is one of the most important polymeric materials used in blood-contacting devices, efforts have been taken to build a blood-compatible surface. A well-known anticoagulant, heparin, which can catalytically increase the formation rate of antithrombin III and inhibit thrombin and some other coagulating proteases, is commonly used to treat patients who submit to hemodialysis. Heparin is a mixture of variably sulfated polysaccharide chains composed of repeating units of D-gluosamine and either L-iduronic or D-glucuronic acids, as well as some other biomacromolecules such as chitosan, insulin. Together with some proteins, heparin has been proved to be an effective agent in curtailing thrombosis and is effective when immobilized onto polymer surfaces.

In order to modify a PAN membrane to endow antibacterial activity and anticoagulation activity, Lin et al. (2004) immobilized the surface of PAN membrane with a chitosan/heparin complex, denominated as PAN-C/H. The anticoagulation activity was evaluated using protein adsorption, platelet adhesion, and coagulation time including activated partial thromboplastin time, prothrombin time, fibrinogen time, and thrombin time. Their immobilization procedure is shown in Fig. 13.

They reported that the hydrophilicity of the membrane after biomacromolecule-induced immobilization increased slightly. However, the be-

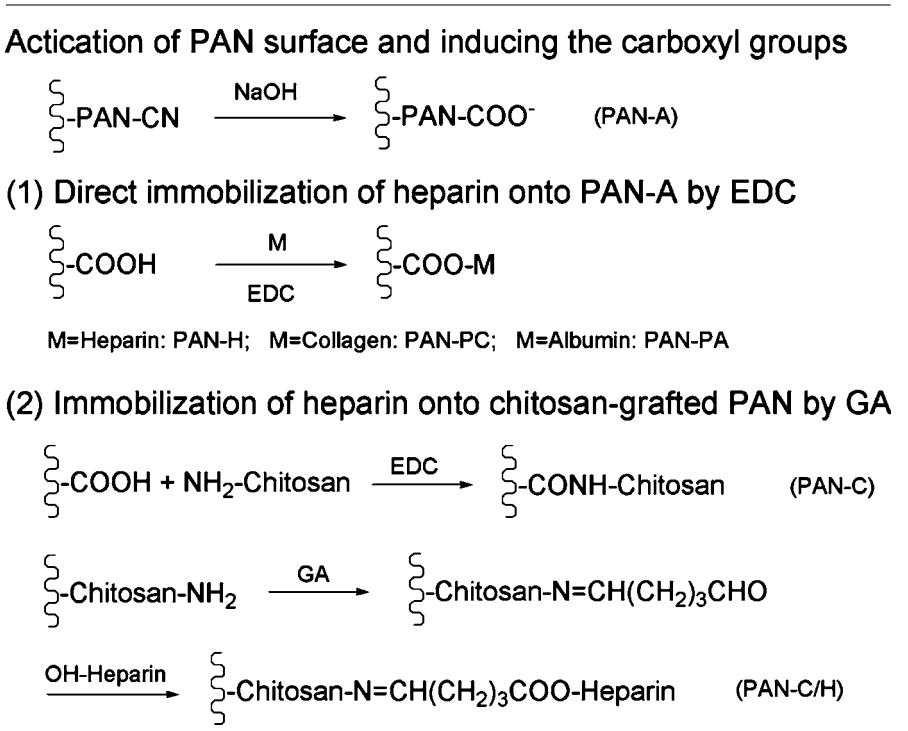

Fig. 13. Chemical scheme of biomacromolecule-immobilized PAN membranes. **A** Direct reaction of heparin, collagen, or albumin. **B** Chitosan (*C*)/heparin (*H*) conjugate reaction. *EDC N*,*N*-(3-dimethylaminopropyl)-*N*'-ethyl carbodiimide, *GA* glutaraldehyde, *PAN-A* activated PAN membrane, *PAN-H* heparin-grafted PAN membrane, *PAN-PC* collagen-grafted PAN membrane, *PAN-PA* albumin-grafted PAN membrane, *PAN-C* chitosan-grafted PAN membrane, *PAN-C/H* chitosan/heparin-complex-grafted PAN membrane

havior of protein adsorption onto membranes depended significantly on the surface characteristics, hydrophilicity, roughness, surface charge and chemistry. As shown in Table 2, the adsorbed amount of human serum albumin (HSA) and human plasma fibrinogen (HPF) on PAN-C/H was reduced to 38% and 26%, respectively, of those of PAN. The isoelectric point of HSA and HPF in the blood are 4.8 and 5.5, respectively; thus these proteins carry a negative charge in the normal blood circumstance (pH 7.4). Lin et al. (2004) proposed that, after hydrolysis, PAN-A carries a negative charge ($-COO^-$), thus the protein adsorption was reduced. On the other hand, chitosan is a weak base with a pK_a of 6.5, thus PAN-C carries positive charge ($-NH_3^+$) at pH 7.4. The adsorption of these two proteins was promoted because of the electrical attraction; however, when PAN-C was heparinized, the repulsive SO_3^- and COO^- on heparin reduced the adsorp-

Table 2. Platelet adhesion and plasma protein adsorption on the PAN-based membranes surfaces

Membrane type	Platelet adhesion numbers (cells/mm^2)	HAS adsorption (μg/cm^2)	HPF adsorption (μg/cm^2)
PAN	4810±38	279.7±14.9	564.3±16.1
PAN-A	3811±28	261.7±12.5	501.3±15.2
PAN-C	6689±57	288.3±13.9	615.3±14.3
PAN-H	1770±15	154.4±11.9	211.3±12.7
PAN-C/H	1623±16	145.4±12.5	147.9±15.6
PAN-PA	2584±26	–	237±14
PAN-PC	6050±40	–	588±29

tion of proteins. To sum up, they considered that electrical attraction or repulsion might play a key role in the adsorption of protein.

Lin et al. (2004) found that both the protein adsorption and platelet adhesion on the heparin-immobilized PAN membrane surface had the same trend; that is, a higher heparin immobilizing density yielded a lower plasma protein adsorption and lower platelet adhesion on the surface. They also pointed out, however, that the hydrophilic PAN-C surface caused more protein adsorption and a reduction of platelet adhesion was not observed. They proposed that a hydrophilic surface did not always correspond to protein resistance and suppression of platelet adhesion.

In some cases the proteins themselves were immobilized onto the membrane surface to improve the hemocompatibility. As we known, fibrinogen activates and albumin inhibits the adhesion of platelets (Klee and Hocker 2000). Therefore, albumin was often physically adsorbed or covalently immobilized onto the membrane surface. Liu et al. (2005) studied the hemocompatibility of PAN membranes covalently immobilized with either collagen (denoted as PAN-PC), which promoted platelet adhesion, or HSA (denoted as PAN-PA), which inhibited platelet adhesion. It can be seen from Table 2 that both platelet adhesion and HPF adsorption were promoted on PAN-PC membrane even compared with original PAN membrane. Both the platelet adhesion and the HPF adsorption of PAN-PA membranes stood almost at the same level with those of the PAN-H membrane. They found that immobilization with HSA resulted in a rougher surface morphology of the PAN membrane, reduced platelet adhesion, fibrinogen adsorption, prolonged the blood coagulation times, and reduced leukopenia and anaphylatoxin. Collagen-immobilized PAN membranes, however, exhibited the opposite effect when contacting blood, although they induced the least complement activation. They indicated that not all plasma proteins are capable of improving hemocompatibility.

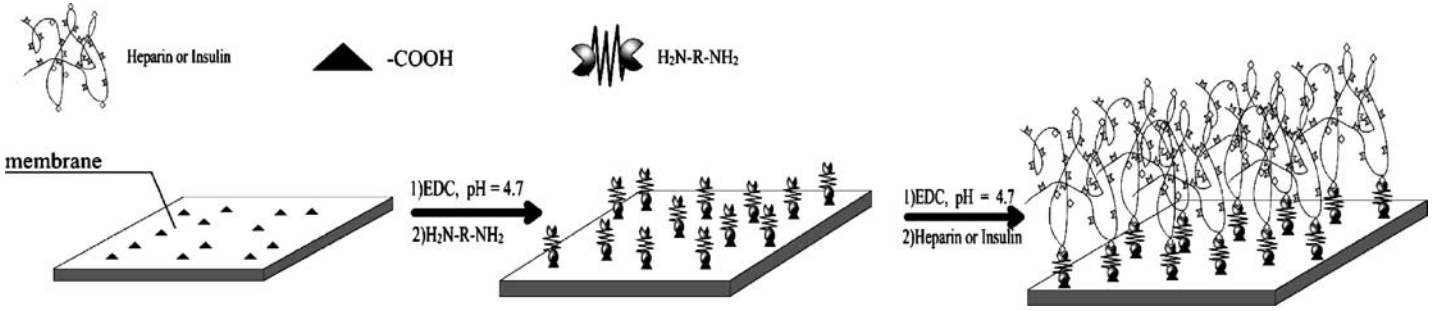

Fig. 14. Chemical scheme of the immobilization of heparin or insulin. *DMF* Dimethylformamide

We also immobilized heparin or insulin onto the PANCMA membrane; the procedure is illustrated in Fig. 14. Through the platelet- and macrophage-adhesion experiments, it was found that the immobilization of heparin or insulin improved the hemocompatibility of PANCMA membranes.

10.6 Biomimetic Modification

A potential technique for reducing protein adsorption on polymeric membranes is to mimic a biologic surface in nature, commonly named biomimetic modification. For example, the red blood cell plasma membrane, unlike synthetic polymer membranes, naturally resists protein fouling. This property may be attributed to the unique phospholipid bilayer structure of the biomembrane. Therefore, great efforts have been made to immobilize phospholipid molecules onto the polymer surface to build a biocompatible surface. To improve the physical and chemical stability, phospholipid molecules with polymerizable groups were synthesized. Researchers have synthesized many kinds of phospholipid-analogous polymers and developed various methods to immobilize them.

We have developed a PAN-based membrane containing phospholipid moieties to improve its protein resistance and hemocompatibility. Two methods were adopted to build the biomimetic surface containing phospholipid moieties. As illustrated in Figs. 15 and 16, one is copolymerizing acrylonitrile with a polymerizable monomer containing phospholipid moieties, the other is to introduce phospholipid moieties onto the acrylonitrile/HEMA copolymer (PANCHEMA) membrane surface by chemical reactions. The resultant membrane containing phospholipid moieties was denoted as a PMANCP membrane. Results from Fourier transfer infrared spectroscopy, x-ray photoelectron spectroscopy, and proton/phosphor nuclear magnetic resonance confirmed the chemical structure of the membrane containing phospholipid moieties.

Water contact angle was used to characterize the improvement of hydrophilicity by the introduction of phospholipid moieties. Static contact angles as a function of contact time on the PAN, PANCHEMA, and PMANCP membranes are shown in Fig. 17. It can be seen that the water contact angles on PAN and PANCHEMA membranes decreased slightly with time, whereas those on the PMANCP membrane decreased sharply. Furthermore, the water on the PMANCP membrane surface extended out in a few minutes. This was due to the interaction between the water and the polar group of zwitterion moieties on the membrane surface. Advancing and receding water contact angles are presented in Fig. 18. As reported by Ulbricht et al. (1998), grafting hydrophilic polymers on the PAN-based membrane surface only

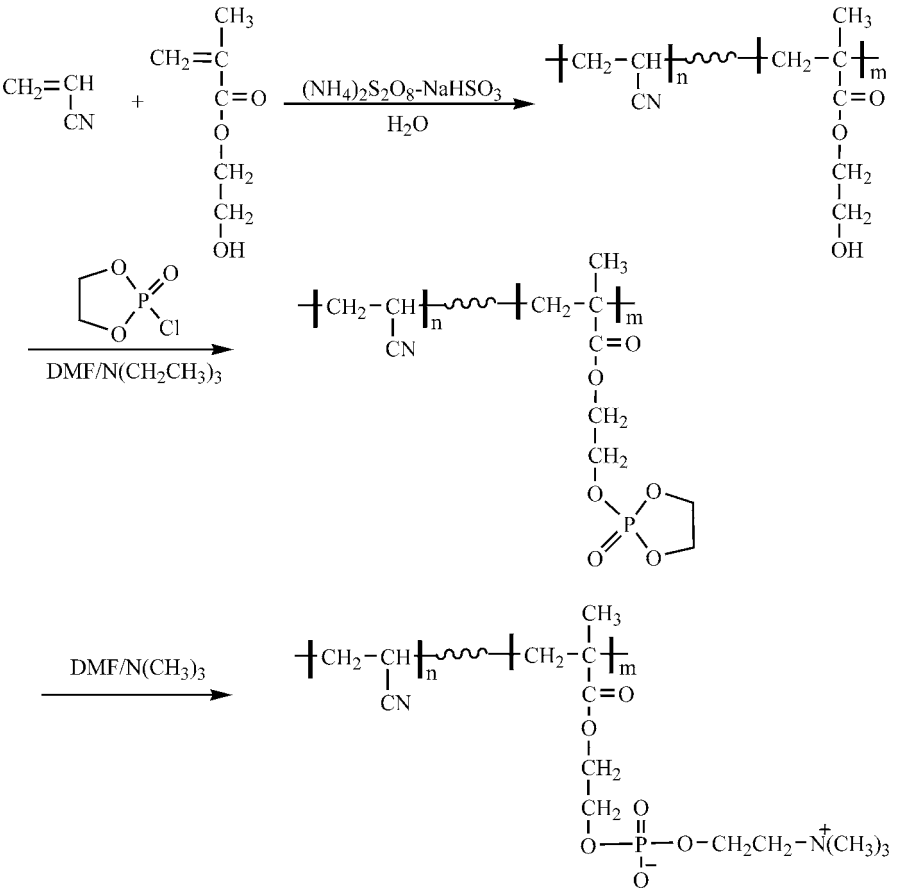

Fig. 15. Schematic representation of the synthesis of PAN containing phospholipid moieties. *THF* Tetrahydrofuran

had a slight effect on the contact angle; similar results were obtained from the measurements. However, the hydrophilicity was effectively improved by introducing the phospholipid moieties onto the PAN-based membrane, it can be seen from Fig. 18 that the dynamic contact angles on the phospholipid-moiety-modified membranes were obviously lower than on the PANCHEMA membranes.

According to the platelet-adhesion experiments, the hemocompatibility of the PAN membrane was remarkably improved by the introduction of phospholipid moieties. This was also confirmed by the static protein adsorption, which is shown in Fig. 19. It was found that the amount of BSA adsorbed on the PAN and PANCHEMA membranes increased almost linearly with the increase in the concentration of BSA. However, differing

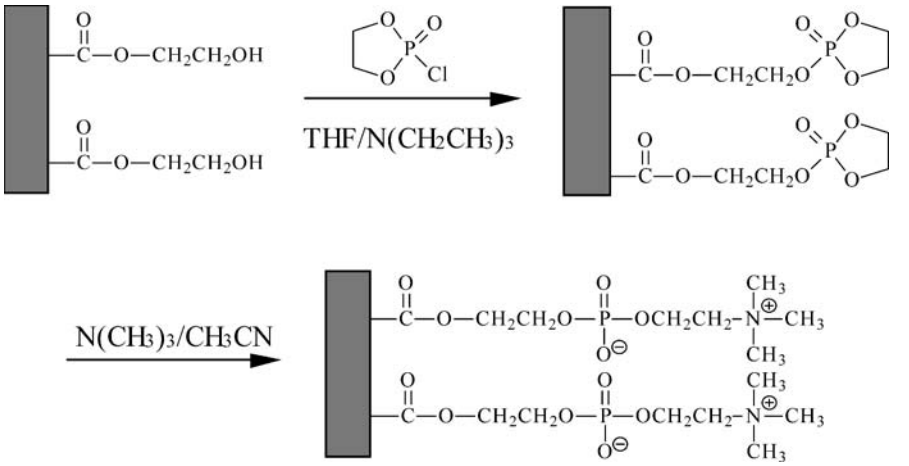

Fig. 16. Schematic representation for introducing phospholipid moieties onto the acrylonitrile/2-hydroxyethyl methacrylate (HEMA) copolymer (PANCHEMA) membrane surface

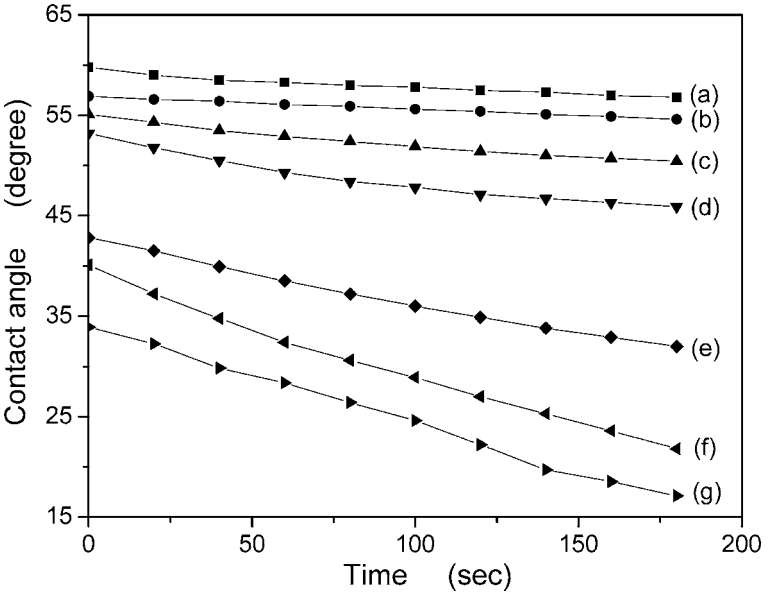

Fig. 17. Water contact angle as a function of contact time on the PAN-based membranes. The HEMA mole fraction in the PANCHEMA membrane is 0% (**a**), 6.4% (**b**), 9.3% (**c**), and 17.8% (**d**). The mole fraction of phospholipid moiety on the PANCHEMA membrane containing phospholipids (PMANCP) membrane surface is 6.09% (**e**), 9.19% (**f**), and 17.1% (**g**)

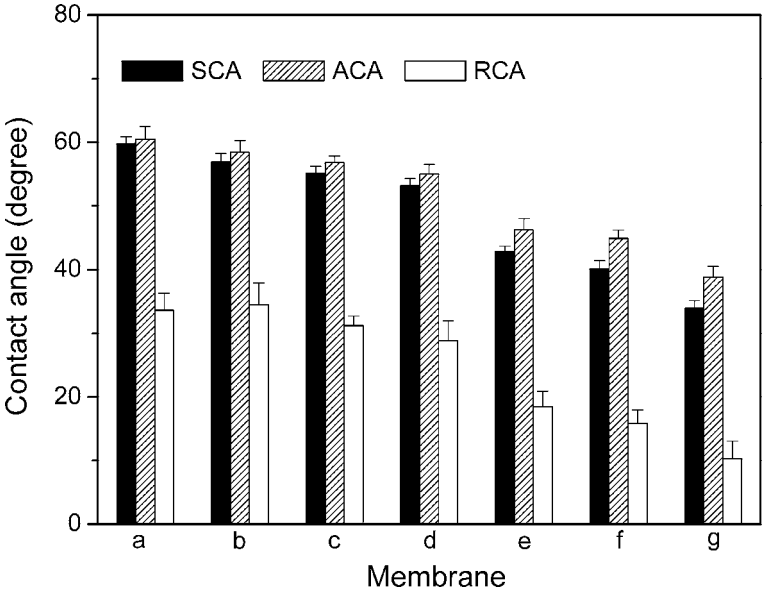

Fig. 18. Static (*SCA*, *black columns*), advancing (*ACA*, *hatched columns*), and receding (*RCA*, *white columns*) contact angles on the PAN-based membranes. The HEMA mole fraction in the PANCHEMA membrane is 0% (**a**), 6.4% (**b**), 9.3% (**c**), and 17.8% (**d**). The mole fraction of phospholipid moiety on PMANCP membrane surface is 6.09% (**e**), 9.19% (**f**), and 17.1% (**g**)

from those on the PAN and PANCHEMA, the adsorbance of BSA onto the PMANCP membranes increased slightly and stayed at a certain low level regardless of further increases in BAS concentration. All samples were immersed in the aqueous medium during the BSA adsorption measurement; in general, the relatively high level of free water fraction on the phospholipid-modified membrane surface might effectively suppress protein adsorption and platelet adhesion.

In addition to the aforementioned approaches, other methods such as blending can be used to obtain protein-resistant PAN-based membranes. To sum up, the successful development of a protein-resistant microporous membrane is an interesting issue for both water treatment membranes and blood-contacting membranes.

10.7 Conclusion

To some extent, protein resistance is very important for both antifouling of membranes during filtration and improving the hemocompatibility of

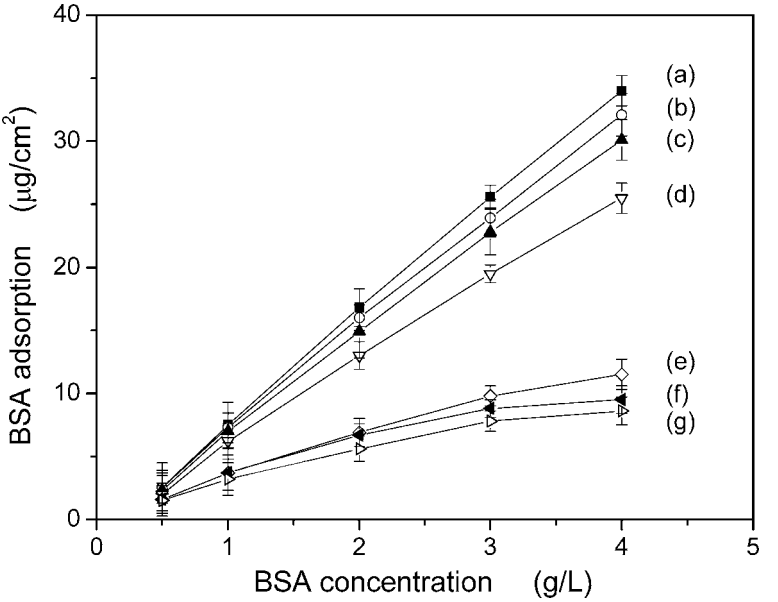

Fig. 19. BSA adsorption on PAN-based membranes. The HEMA mole fraction in the PANCHEMA membrane is 0% (**a**), 6.4% (**b**), 9.3% (**c**), and 17.8% (**d**), and the mole fraction of phospholipid moiety on PMANCP membrane surface is 6.09% (**e**), 9.19% (**f**), and 17.1% (**g**)

blood-contact membranes. The methods overviewed above, such as copolymerization, PEG tethering, physical adsorption, biomacromolecule immobilization, and biomimetic modification, provide promising opportunities for protein resistance at the surface of PAN-based membranes. Many kinds of modifiers based on different protein–membrane interactions may lead to protein resistance in the same way. Among them, hydrophilic, charged, sterically hindered, or biomimetic agents ought to receive preference. Since there are so many modification methods and each approach possesses innate relative merits, one should choose the most suitable method in terms of the given aim and the varying membrane system.

Acknowledgements. Financial support obtained from the National Natural Science Foundation of China (Grant no. 50273032) and the National Basic Research Program of China (Grant no. 2003CB15705) are gratefully acknowledged. The authors thank Dr. Fu-Qiang Nie and Dr. Rui-Qiang Kou very much for their contribution.

References

Dee KC, Puleo DA, Bizios R (2002) An Introduction to Tissue–Biomaterial Interactions. John Wiley & Sons, New York

Etheve J, Dejardin P, Boissiere M (2003) Adsorption of lysozyme on a hemodialysis sulfonated polyacrylonitrile membrane, with and without preadsorbed poly(ethyleneimine) on the external faces. Colloids Surf B 28:285–293

Godjevargova T, Konsulov V, Dimov A, Vasileva N (2000) Behavior of glucose oxidase immobilized on ultrafiltration membranes obtained by copolymerizing acrylonitrile and N-vinylimidazol. J Membr Sci 172:279–285

Groth T, Seifert B, Malsch G, Albrecht W, Paul D, Kostadinova A, Krasteva N, Altankov G (2002) Interaction of human skin fibroblasts with moderate wettable polyacrylonitrile-copolymer membranes. J Biomed Mater Res 61:290–300

Hayama M, Yamamoto K, Kohori F, Sakai K (2004) How polysulfone dialysis membranes containing polyvinylpyrrolidone achieve excellent biocompatibility? J Membr Sci 234:41–49

Huang XJ, Xu ZK, Wan LS, Wang ZG, Wang JL (2005) Novel acrylonitrile-based copolymers containing phospholipid moieties: synthesis and characterization. Macromol Biosci 5:322–330

Huang XJ, Xu ZK, Wan LS, Wang ZG, Wang JL (2005) Surface modification of polyacrylonitrile-based membranes by chemical reactions to generate phospholipid moieties. Langmuir 21:2941–2947

Klee D, Hocker H (2000) Polymers for biomedical applications: improvement of the interface compatibility. Adv Polym Sci 149:1–57

Krasteva N, Harms U, Albrecht W, Seifert B, Hopp M, Altankov G, Groth T (2002) Membranes for biohybrid liver support systems – investigations on hepatocyte attachment, morphology and growth. Biomaterials 23:2467–2478

Lin WC, Liu TY, Yang MC (2004) Hemocompatibility of polyacrylonitrile dialysis membrane immobilized with chitosan and heparin conjugate. Biomaterials 25:1947–1957

Liu TY, Lin WC, Huang LY, Chen SY, Yang MC (2005) Hemocompatibility and anaphylatoxin formation of protein-immobilizing polyacrylonitrile hemodialysis membrane. Biomaterials 26:1437–1444

Musale DA, Kulkarni SS (1996) Fouling reduction in poly(acrylonitrile-co-acrylamide) ultrafiltration membranes. J Membr Sci 111:49–56

Musale DA, Kulkarni SS (1997) Relative rates of protein transmission through poly(acrylonitrile) based ultrafiltration membranes. J Membr Sci 136:13–23

Nie FQ, Xu ZK, Huang XJ, Ye P, Wu J (2003) Acrylonitrile-based copolymer membranes containing reactive groups: Surface modification by the immobilization of poly(ethylene glycol) for improving antifouling property and biocompatibility. Langmuir 19:9889–9895

Nie FQ, Xu ZK, Ming YQ, Kou RQ, Liu ZM, Wang SY (2004) Preparation and characterization of polyacrylonitrile-based membranes: effects of internal coagulant on poly(acrylonitrile-co-maleic acid) ultrafiltration hollow fiber membranes. Desalination 160:43–50

Nie FQ, Xu ZK, Qian Y, Jian W, Wan LS (2004) Surface modification of poly(acrylonitrile-co-maleic acid) membranes by the immobilization of poly(ethylene glycol). J Membr Sci 235:147–155

Nie FQ, Xu ZK, Wan LS, Ye P, Wu H (2004) Acrylonitrile-based copolymers containing reactive groups: synthesis and preparation of ultrafiltration membranes. J Membr Sci 230:1–11

Nie FQ, Xu ZK, Ye P, Wu J, Seta P (2004) Acrylonitrile-based copolymer membranes containing reactive groups: effects of surface-immobilized poly(ethylene glycol)s on antifouling properties and blood compatibility. Polymer 45:399–407

Sun SD, Yue YL, Huang XH, Meng DY (2003) Protein adsorption on blood-contact membranes. J Membr Sci 222:3–18

Thomas M, Vakette P, Mausset A-L, Déjardin P (2000) High molecular weight kininogen adsorption on hemodialysis membranes: influence of pH and relationship with contact phase activation of blood plasma. Influence of pre–treatment with poly(ethyleneimine). Inter J Artif Organs 23:20–28

Ulbricht M, Belfort G (1996) Surface modification of ultrafiltration membranes by low temperature plasma II. Graft polymerization onto polyacrylonitrile and polysulfone. J Membr Sci 111:193–215

Ulbricht M, Richau K, Kamusewitz H (1998) Photomodification of ultrafiltration membranes – Part 11 – Chemically and morphologically defined ultrafiltration membrane surfaces prepared by heterogeneous photo-initiated graft polymerization. Colloids Surf A 138:353–366

Valette P, Thomas M, Dejardin P (1999) Adsorption of low molecular weight proteins to hemodialysis membranes: experimental results and simulations. Biomaterials 20:1621–1634

Wan LS, Xu ZK, Huang XJ, Wang ZG, Wang JL (2005) Copolymerization of acrylonitrile with N-vinyl-2-pyrrolidone to improve the hemocompatibility of polyacrylonitrile. Polymer 46:7715–7723

Xu ZK, Kou RQ, Liu ZM, Nie FQ, Xu YY (2003) Incorporating alpha-allyl glucoside into polyacrylonitrile by water-phase precipitation copolymerization to reduce protein adsorption and cell adhesion. Macromolecules 36:2441–2447

Xu ZK, Nie FQ, Qu C, Wan LS, Wu J, Yao K (2005) Tethering poly(ethylene glycol)s to improve the surface biocompatibility of poly(acrylonitrile-co-maleic acid) asymmetric membranes. Biomaterials 26:589–598

Xu ZK, Qian Y, Kou RQ, Jian W, Wang JQ (2004) First results of hemocompatible membranes fabricated from acrylonitrile copolymers containing sugar moieties. J Membr Sci 243:195–202

Yan F, Dejardin P, Mulvihill JN, Cazenave J-P, Crost T, Thomas M, Pusineri C (1992) Influence of a preadsorbed terpolymer on human platelet accumulation, fibrinogen adsorption, and ex vivo blood activation in hemodialysis hollow fibers. J Biomater Sci Polym Ed 3:389–402

11 Modulation of the Adsorption and Activity of Protein/Enzyme on the Polypropylene Microporous Membrane Surface by Surface Modification

Qian Yang, Zhi-Kang Xu, Zheng-Wei Dai

Abstract. As an excellent membrane material, polypropylene microporous membrane (PPMM), has received much consideration in recent years. PPMM has also been used widely in many fields such as water treatment, enzyme immobilization, and blood oxygenation. However, poor surface properties cumber the further applications of this material. Many efforts have been made to solve this problem, and surface modification seems to be the most efficient way. In this article we introduce some work in which surface modification was conducted to reduce nonspecific protein adsorption and to modulate the activity of immobilized enzymes on the PPMM surface. We focus on the studies of our group, although other researches are also discussed.

11.1 Surface Modifications for Reducing Nonspecific Protein Adsorption

There have been many interests in membrane processes for last decade because of they are extremely efficient, have a low energy consumption, and are easy to carry out. Nowadays, membranes are used widely, especially in biomedical applications such as dialysis, plasmapheresis, and oxygenation of blood during cardiac surgery. However, it is well known that the major obstacle to the extensive use of membrane processes in therapeutic treatment is protein fouling of polymeric membrane materials. Protein deposition on the membrane surface can cause unstable transport characteristics, and cellular interactions with artificial surface are also assumed to be mediated through adsorbed proteins (Deppisch et al. 1998). Designing a polymer surface that rejects proteins (i. e., a nonfouling surface) has been a central issue in the field of biomedical materials research (Ikada 1994; Klee and Hocker 1999; Ratner et al. 1979). The adsorption of proteins is highly complex. We do understand that these interactions are determined by the

Qian Yang, Zhi-Kang Xu, Zheng-Wei Dai: Institute of Polymer Science, Zhejiang University, Hangzhou 310027, People's Republic of China, E-mail: xuzk@ipsm.zju.edu.cn

Principles and Practice
Proteins at Solid–Liquid Interfaces
Philippe Déjardin (Ed.)
© Springer-Verlag Berlin Heidelberg 2006

hydrophobic/hydrophilic, charged/uncharged, and polar/nonpolar parts of the proteins, and by the nature of the membrane surface. The adsorbed protein film shows time-dependent conformational changes, which may cause desorption or protein exchange. Adsorption processes are described by the typical Langmuir isotherms. After a long contact time, a stationary state is reached, which corresponds to an irreversible protein adsorption (Lundstrom and Elwing 1990; Sonderquist and Walton 1980). However, in spite of extensive investigations (Guell et al. 1999; Kuberkar and Davis 2000; Mueller and Davis 1996; Tie et al. 2003), the mechanism of protein adsorption onto the membrane surface remains unsolved.

Nevertheless, The primary method of reducing protein adsorption onto polymeric materials is surface modification. There are many methods of surface modification, as outlined in Table 1 (Ratner 1995). Among them, the covalent method offers a more stable modification surface as compared to other methods (Gupta and Anjum 2003). Graft polymerization is one such method in which polymer chains are tethered to the material surface. Grafting has several advantages over other methods, including easy and controllable introduction of graft chains with a high density and exact

Table 1. Physical and chemical surface modification methods. *UV* Ultraviolet, *RF* radio frequency

Covalently attached coatings
Radiation grafting (electron accelerator and gamma)
Photografting (UV and visible sources)
Plasma (gas discharge; RF, microwave, acoustic)
Gas phase deposition
Ion beam sputtering
Chemical vapor deposition
Chemical grafting (e. g., ozone treatment + grafting)
Silanization
Biological modification (biomolecule immobilization)
Modification of the original surface
Ion beam etching (e. g., argon, xenon)
Ion beam implantation (e. g., nitrogen)
Plasma etching (e. g., nitrogen, argon, oxygen, water vapor)
Corona discharge (in air)
Electron beam treatment
Ion exchange
UV irradiation
Chemical reaction
Nonspecific oxidation (e. g., ozone)
Functional group modifications (oxidation, reduction)
Addition reactions (e. g., acetylation, chlorination)
Conversion coatings (phosphating, anodization)

location of graft chains to the surface, with the bulk properties remaining unchanged. This method is also applied in membrane surface modification to reduce protein adsorption and there are many research groups making efforts to develop membrane surface biocompatibility using this method. Hydrophilic polymers are often used for this purpose because of their wettability and biocompatibility. However, derivatives of native substances existing in the biological systems (such as phospholipid, carbohydrate, and polypeptide), which have excellent biocompatibility, are thought to be efficient for the reduction of protein deposition. Herein, the discussion will focus on these biomimetic polymer modifiers used by our group, although other polymers will also be mentioned.

11.1.1 Plasma treatment

Plasma modification of polymeric materials is an extremely useful way of tailing a polymer into a desired material by utilizing the selective chemistry and molecular structure on the surface (Kiaei et al. 1995; Lee et al. 1991; Oehr et al. 1999). It is an efficient way to produce functional groups such as hydroxyl groups, amino groups, and carboxylic groups. Plasma can also initiate polymerization reactions of monomers on a surface. Graft polymerization can be carried out by plasma treatment either directly or indirectly. For the former, monomers are exposed to the plasma environment on the objective surface. At the same time, indirect polymerization can also be initiated by functional groups produced by the plasma.

Kou et al. (2003) grafted a glycopolymer to polypropylene microporous membrane (PPMM) surface by direct plasma polymerization (Fig. 1a). A monomer containing sugar moieties, α-allyl glucoside (AG), was synthesized and grafted to PPMMs (Fig. 1b). In that case the PPMM was immersed in an AG solution of *N*,*N*-dimethylformamide for a predetermined time, and the solvent was evaporated in a vacuum oven. The coated AG monomer was then grafted chemically onto the membrane surface by N_2 plasma. Bovine serum albumin (BSA) was used as a model protein to evaluate the anti-protein-fouling characteristic of this modified PPMM. As shown in Fig. 2, increases in the AG grafting degree leads to a reduction in the amount of protein deposited to the membrane surface. This is due to the hydrophilicity and biocompatibility of the grafted AG.

Liu et al. (2003) tethered a polypeptide, poly(γ-stearyl-L-glutamate) (PSLG), to the PPMM surface by plasma treatment (Fig. 3). First, the PPMM was treated by plasma under an atmosphere of ammonia to introduce amino groups to the surface. Then, a monomer, *N*-carboxyanhydride (NCA), was subjected to ring-opening polymerization initiated by the amino groups on

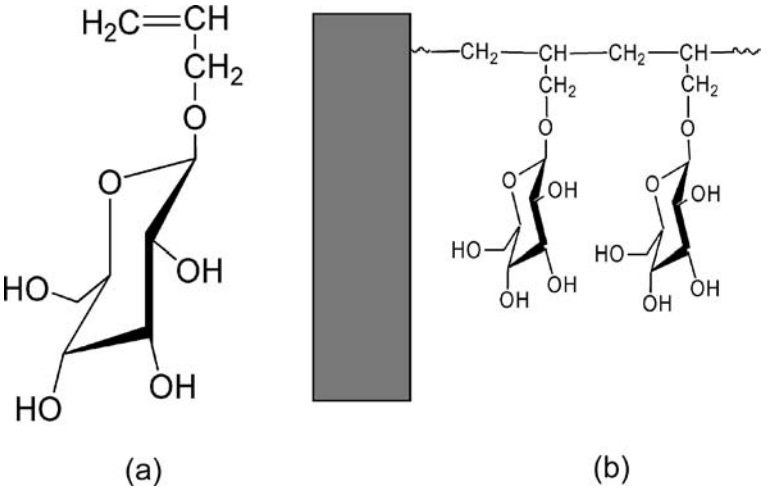

Fig. 1. Molecular structure of α-allyl glucose (AG; **a**) and poly (α-allyl glucoside) (PAG)-modified polypropylene microporous membrane (PPMM; **b**)

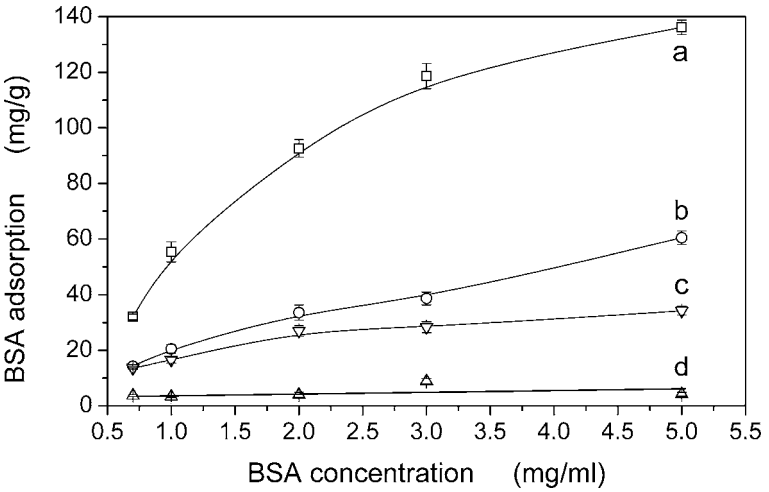

Fig. 2. a–d Effect of AG grafting degree on bovine serum albumin (BSA) adsorption (**a–d**: 0, 0.82, 1.86, 3.46 wt.%, respectively)

the membrane surface, and PSLG was grafted onto the membrane surface. There are two mechanisms of ring-opening polymerization of NCA (Fig. 3b) and the active monomer mechanism, which is initiated by hydroxyl groups, must be depressed to improve the grafting degree. Thus γ-(aminopropyl) triethanoxysilane (γ-APS) was used to eliminate the effect of hydroxyl groups by reacting with them. The results of BSA adsorption experiments are shown in Fig. 4.

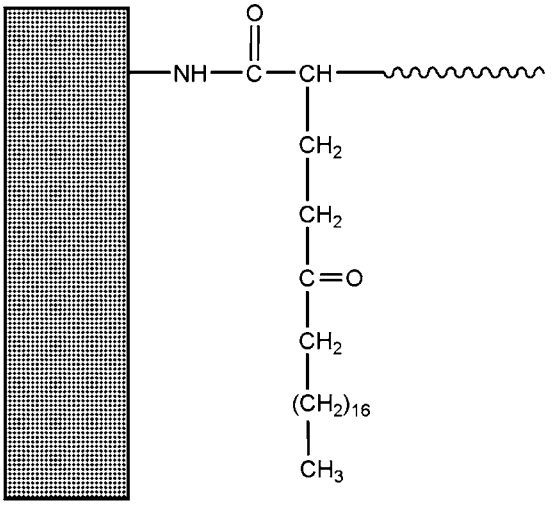

a

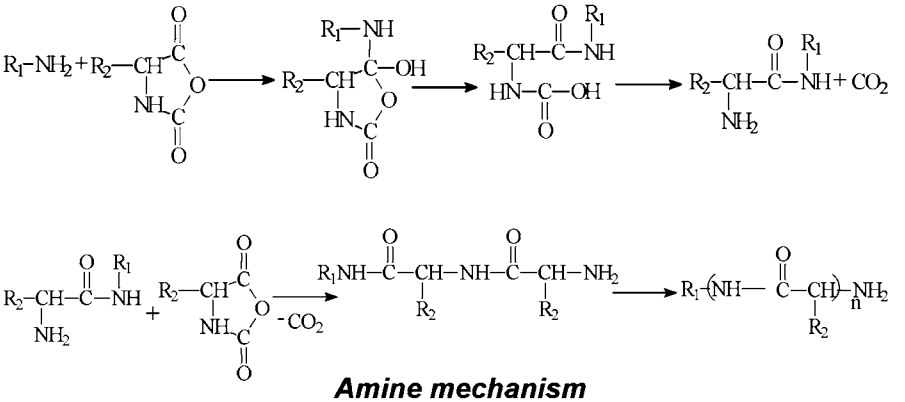

Amine mechanism

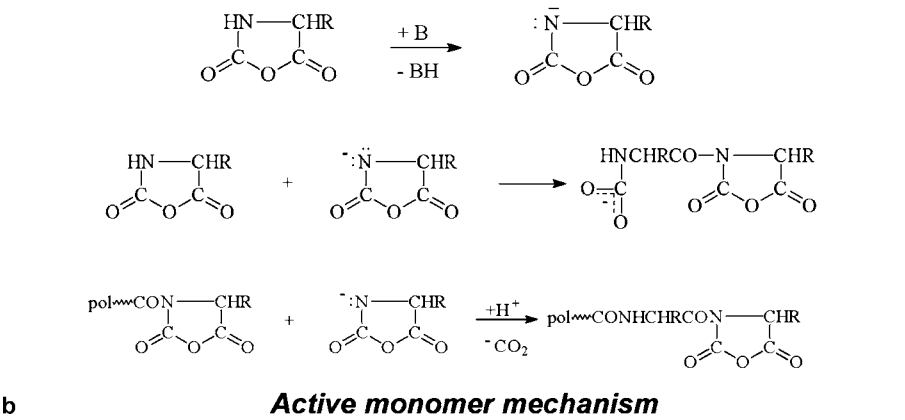

b

Active monomer mechanism

Fig. 3. Poly(γ-stearyl-L-glutamate) (PSLG)-modified PPMM (**a**) and mechanisms for the synthesis of polypeptide from *N*-carboxyanhydride (NCA) monomers (**b**)

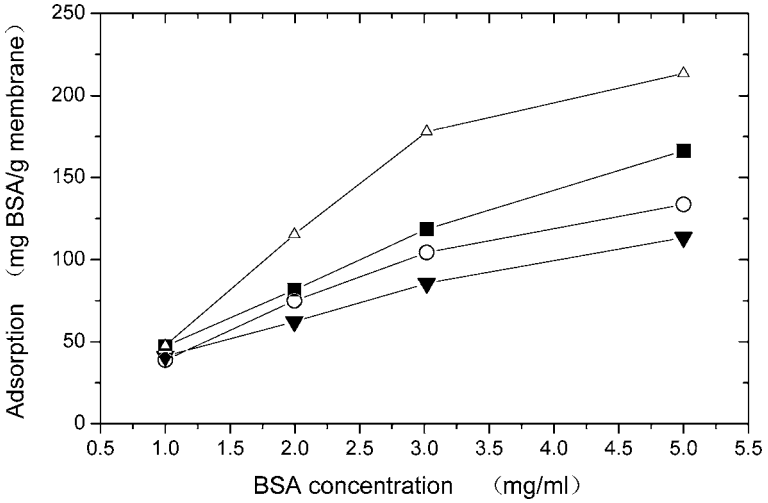

Fig. 4. BSA adsorption onto different PPMMs. ■ original membrane; ▼ NH_3-plasma-treated membrane; ○ PSLG-grafted membrane without γ-(aminopropyl) triethanoxysilane (γ-APS) treatment; △ PSLG-grafted membrane with γ-APS treatment

For the ammonia-plasma-treated membranes, BSA adsorption was reduced slowly as a result of the hydrophilic groups generated on the membrane surface. However, what surprised us was that the PSLG-γ-APS-PPMM exhibited greatly increased protein adsorption, even larger than the nascent PPMM. This could be interpreted by the conformation of PSLG on the surface. It is known that polypeptide exhibits α-helix and coil conformations under different conditions. For the poly(γ-stearyl-L-glutamic acid) with long stearyl groups, Poche et al. (1995) speculated that the grafted PSLG in solutions formed an α-helix conformation that was supported by the intramolecular hydrogen bonds, with the peptide main chains in the cores and γ-stearyl long side chains stretched outside. This molecular model of PSLG could be used to explain the BSA adsorption results. For the PSLG-PPMM, the amount of adsorbed BSA increased a little; this could be ascribed to the existence of -OH groups, which led to low polymerization degree. For the PSLG-γ-APS-PPMM, the polymerization degree of grafted chains increased, the stearyl long side chains stretched outside, thus greatly increasing the surface hydrophobicity, resulting in an increase in BSA adsorption. This characteristic was used to immobilize lipase in our further work.

11.1.2 Ultraviolet (UV) modification

UV irradiation is an effective technique for membrane surface modification. It may be the most appropriate of all surface modification techniques

because of certain features: the low cost of operation, mild reaction conditions, it is highly surface-selective, and because it alters the material surface with facile control of the chemistry (Ma et al. 2000a). Several studies have been carried out using photoinitiators (Kita et al. 1994; Richey et al. 2000; Ulbricht et al. 1998) or specially synthesized molecules with UV-sensitive end groups (Taniguchi et al. 2003; Thom et al. 2000). Figure 5 shows a typical two-step process for UV-induced polymerization (Ma et al. 2000b).

Xu and coworkers (2004) modified PPMMs using phospholipid-analogous polymers (PAPs) (Fig. 6). *N*,*N*-dimethylaminorthyl methacrylate (DMAEMA) was grafted to the membrane surface by photoinduced graft polymerization and then reacted with 2-alkyloxy-2-oxo-1,3,2-dioxaphospholanes. Five 2-alkyloxy-2-oxo-1,3,2-dioxaphospholanes, containing octyloxy, dodecyloxy, tetradecyloxy, hexadecyloxy, and octadecyloxy groups in their molecular structure, were used to fabricate the PAP-modified PPMMs. The influence of grafting degree on BSA adsorption is shown in Fig. 7. It can be seen that the adsorbed BSA on the membrane decreased with increasing grafting degree for both poly(DMAEMA)-grafted and PAP-modified membranes at the studied range. The five PAP-modified membranes had better protein resistance than the unmodified polypropylene membrane and poly(DMAEMA)-grafted membranes. Nevertheless, as the number of carbon atoms was increased from 14 to 16 and 18, BSA adsorption on the membrane surface was clearly suppressed. The reason for this was probably the mimetic characteristics of the PAP-modified membranes; the principal components of a biomembrane are lipids, proteins, and carbo-

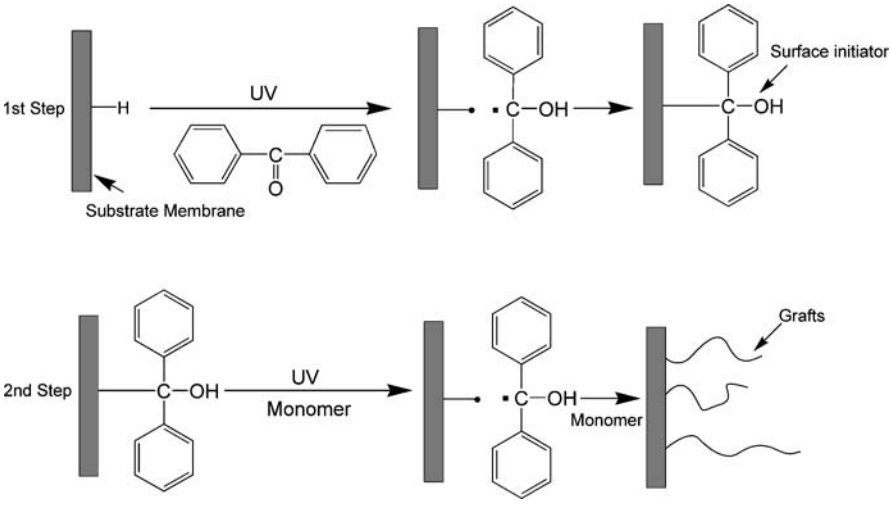

Fig. 5. Schematic diagram of a novel two-step process for photoinduced graft polymerization

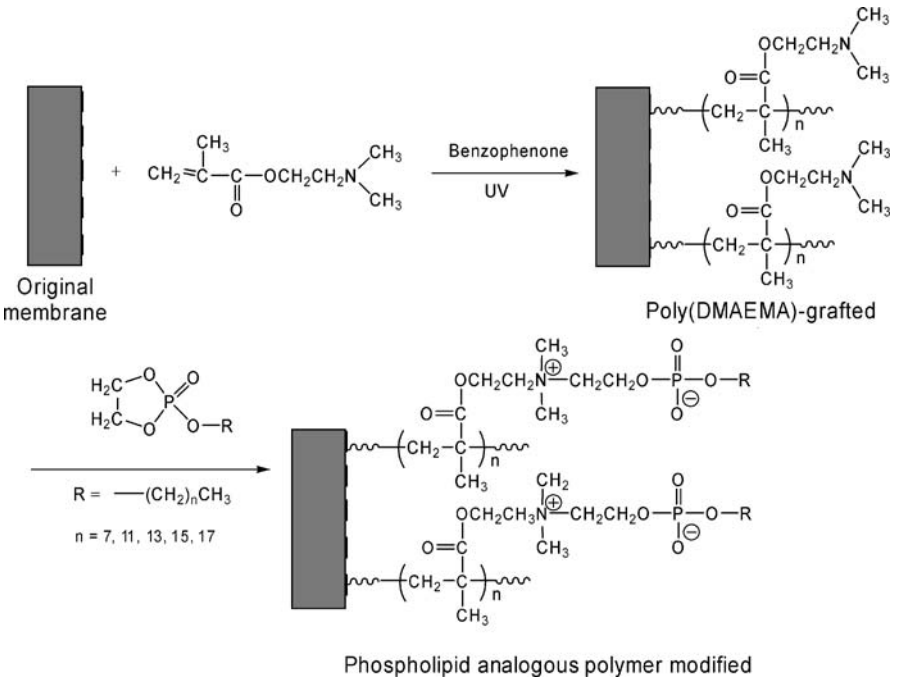

Fig. 6. Schematic representation for the fabrication of phospholipid-analogous polymer (PAP)-modified PPMMs. *DMAEMA N,N*-dimethylaminorthyl methacrylate

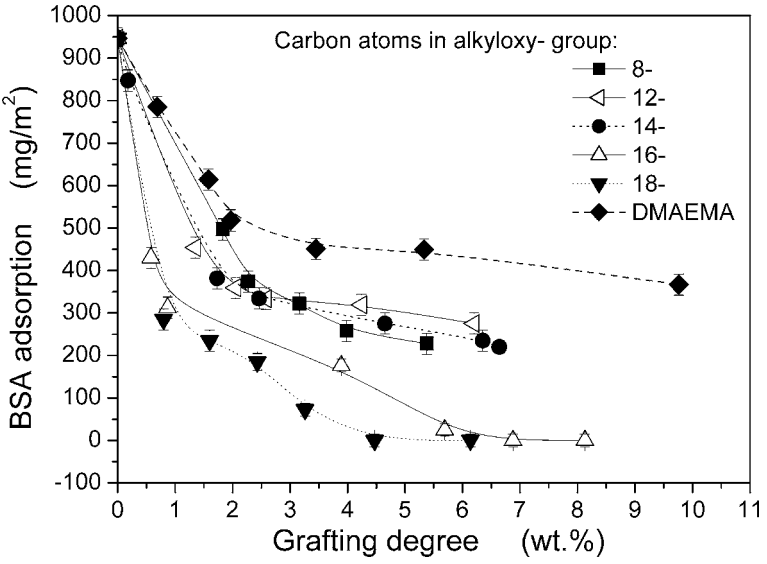

Fig. 7. BSA adsorption on poly(DMAEMA)-grafted and PAP-modified membranes

hydrates. However, the amount of proteins and carbohydrates is relatively small. Most of the lipids are phospholipids such as phosphatidylcholine, phosphatidylethanolamine, phosphatidylserine, phosphatidic acid, phosphatidylinositol, and phosphatidylglycerol. As part of their structure, these phospholipids all have two long alkyloxy groups. Two layers of phospholipid molecules are facing each other, burying the hydrophobic moieties inside the membrane. The zwitterionic species cover the membrane surface and there is a reorientation of the PAP to put the zwitterions at the surface of PAP-modified PPMMs. During the protein adsorption measurements, the PAP-modified PPMMs were immersed in BSA solution for 24 h. In that case, the membranes were in an aqueous environment and should present the zwitterions at the surface. Thus, in these conditions, the membrane surfaces were hydrophilic and were relatively similar to those of the biomembranes. The hydrophilic surfaces normally facilitate the reduction of protein adsorption on the membrane (Ma et al. 2000a; Steen et al. 2002; Wavhal and Fisher 2003; Xu et al. 2003). Furthermore, with an increase of the number of carbon atoms of the long alkyloxy groups, the impact of the original membrane surface on protein adsorption could be reduced, which leads to a decrease in protein adsorption on the PAP-modified membranes. Therefore the membranes exhibit excellent protein resistance.

N-Vinyl-2-pyrrolidone is a hydrophilic and nonionic monomer that can be easily initiated through radical, thermal, or photo irradiation (Senogles and Thomas 1975). Poly(*N*-vinyl-2-pyrrolidone) (PVP) is a polymer with great potential applications in different areas of biomedicine due to its ex-

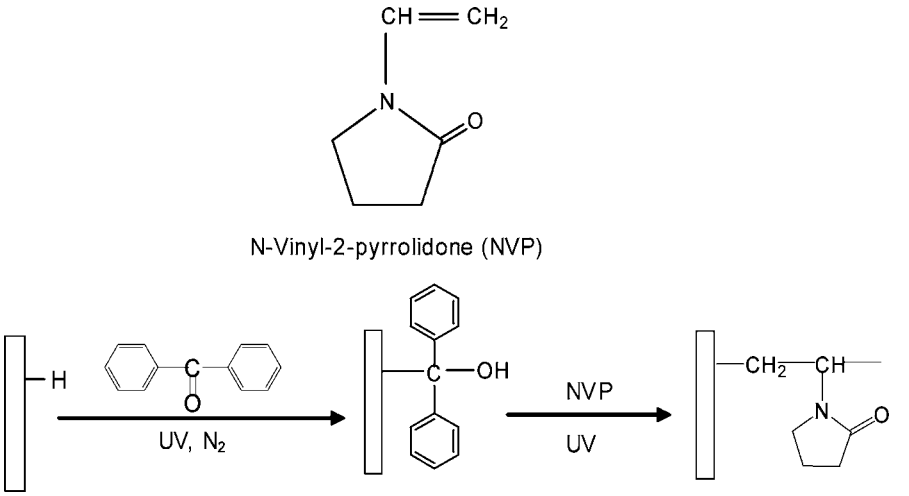

Fig. 8. Molecular structure of *N*-vinyl-2-pyrrolidone (*NVP*) and ultraviolet (UV)-induced grafting polymerization

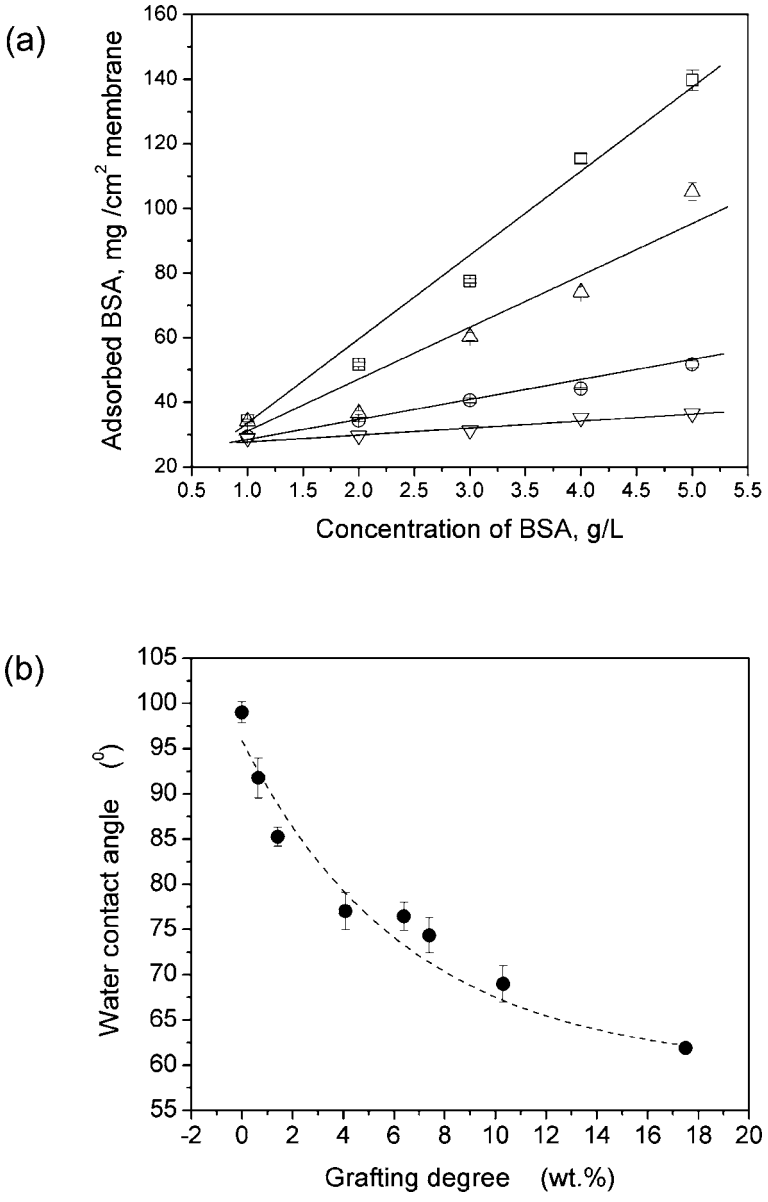

Fig. 9. **a** Effect of grafting degree (GD) on BSA adsorption in PVP-modified PPMMs. ● nascent PPMM; ○ PVP-modified PPMM GD = 1.49 wt. % and △ PVP-modified PPMM GD = 4.08 wt. %. **b** Static contact angle of PVP-modified PPMMs with different grafting degrees

cellent biocompatibility with living tissues and extremely low cytotoxicity (Wetzels and Koole 1999). Due to its outstanding performance, PVP has also been used widely as a surface-modification agent. Liu et al. (2004) used PVP as modifier to improve the surface properties of PPMMs by UV-induced graft polymerization of *N*-vinyl-2-pyrrolidone, as shown in Fig. 8. After grafting PVP to the membrane surface, as been expected, protein adsorption was markedly reduced with increasing grafting degree (Fig. 9). Usually, materials processing hydrophilic surface show relatively low non-specific adsorption for proteins or cells. Therefore, the reduction in BSA adsorption could be ascribed mainly to the improvement in hydrophilicity effected by the introduction of PVP chains on the PPMM surface.

Yang et al. (2005) grafted a novel glycopolymer containing linear sugar moieties, D-gluconamidoethyl methacrylate (GAMA) (Fig. 10), to the PPMMs by UV-induced graft polymerization and obtained a hydrophilic surface with low protein fouling and relatively high flux recovery (Table 2). After surface modification, the antifouling property was evaluated by filtrating a 1 g/L BSA solution through the membranes. Pure water flux after cleanout was also examined to confirm flux recovery. The ethanol-wetted nascent membrane showed the largest loss of flux within the measurement time, which suggests that a large amount of BSA protein had been deposited on the surface. However, the reduction in flux was suppressed by grafting of GAMA, indicating that the GAMA polymer layer effectively prevented the

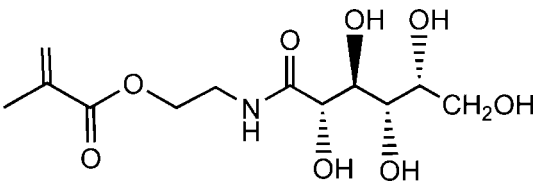

Fig. 10. Molecular structure of GAMA

Table 2. Permeation and antifouling properties of D-gluconamidoethyl methacrylate (GAMA) grafted polypropylene microporous membrane (PPMMs). J_W Flux of pure water, J_P flux of 1 g/l bovine serum albumin solution, J_R flux after cleanout, *RFR* relative flux reduction as $(1 - J_P/J_W) \times 100\%$, *FRR* flux recovery ratio as $J_R/J_W \times 100\%$

Membrane	J_W (kg/m^2 h)	J_P (kg/m^2 h)	J_R (kg/m^2 h)	RFR	FRR
Ethanol-wetted	340 ± 7	93 ± 22	219 ± 22	73	64
2.23 wt% GAMA grafted	466±26	187±24	390±26	60	84
3.5 wt% GAMA grafted	608±21	348±37	488±38	57	80
4.58 wt% GAMA grafted	729±14	452±38	646±30	38	89
5.47 wt% GAMA grafted	762±22	434±32	658±33	57	86
6.03 wt% GAMA grafted	764±28	452±25	649±35	59	85

adsorption of BSA. Moreover, the recovery flux increased significantly with increasing grafting degree, and a relatively high flux recovery ratio (> 80%) was achieved even at lower grafting degree. All of these improvements in surface properties can be ascribed to the highly hydrophilic nature of the linear sugar moieties in the grafted chains.

11.1.3 γ-Ray-induced modification

γ-Ray-induced graft polymerization has been used extensively because it is the most versatile and promising one due to its rapid formation of active sites on the substrate surface and in the material matrix. Almost all of the polymeric materials can be modified by γ-ray with different monomers and the resulting material is highly pure as no initiator or related impurities remain in the matrix. However, as a very high energy radiation, γ-rays have a tremendous penetrability such that active sites are also generated in the material bulk, which often affects the inherent bulk properties.

Table 3. Characteristics and bovine serum albumin (BSA) permeation properties of 2-hydroxyethyl methacrylate (HEMA)-grafted PPMMs with different grafting degrees (PH*n*)

Sample code	Degree of grafting[b] (wt %)	Flux (l/m^{2}h)		Resistance (10^{14}m^{-1})			Wettability[h] (cos θ)	Surface potential ζ[i] (mV)	**Adsorbed BSA[j] (μg/cm^2)**
		J_w[c]	J_s[d]	R_m[e]	R_t[f]	R_c[g]			
PP[a]		77.1	24.2	4.67	14.8	10.1	−0.32	−36.47	**104.5**
PH1	2.9	75.2	26.9	4.78	13.4	8.60	−0.15	−31.33	**83.6**
PH2	7.2	69.9	27.8	5.15	12.9	7.75	0.03	−29.10	**69.4**
PH3	12.5	68.6	28.7	5.28	12.5	7.22	0.27	−26.72	**38.1**
PH4	24.0	68.1	37.6	5.43	9.57	4.14	0.31	−11.57	**20.9**
PH5	32.2	66.3	43.6	5.64	8.25	2.61	0.44	−7.75	**26.9**
PH6	40.6	60.9	44.8	5.91	8.03	2.12	0.56	−5.22	**9.0**

[a] PPMM with exposure of γ-rays

[b] Degree of grafting (wt %) = $(w_g - w_0)/w_0 \times 100$, where w_0 and w_g are the weights of the membrane before and after the grafting reaction, respectively

[c] Deionized water flux

[d] Flux of 1 g/l BSA in 10 mM PBS of pH 7.4 at 23 ± 2 °C

[e] The membrane resistance (R_m) was calculated by the measured deionized water flux

[f] The total resistance (R_t) during the filtration of protein solution was calculated by the flux (J_s) of BSA protein solution

[g] R_c caused by BSA protein in solution was calculated by subtracting R_m from R_t

[h] The average estimated error for cosθ was ±0.04

[I] The average estimated error was ±9%

[j] Irreversible adsorptive fouling of the membrane was defined as the amount of BSA absorbed onto the surface of the membrane after chemical cleaning

Kang et al. (2001) used Co^{60} as a γ-ray source for surface modification on the PPMMs by graft polymerization of 2-hydroxyethyl methacrylate (HEMA). Through adjusting the radiation dose, modified PPMMs with different grafting degrees were prepared. Protein adsorption measurements were carried out on these membranes by filtration of BSA solution through the membranes. The results are shown in Table 3 and Fig. 11. The flux of deionized water decreased with increases in the grafting degree of polyHEMA (PHEMA). On the other hand, the flux of BSA buffer solution increased with increasing PHEMA grafting degree. Clearly, the more hydrophilic the surface (increasing cosθ value), the lower the flux decline with

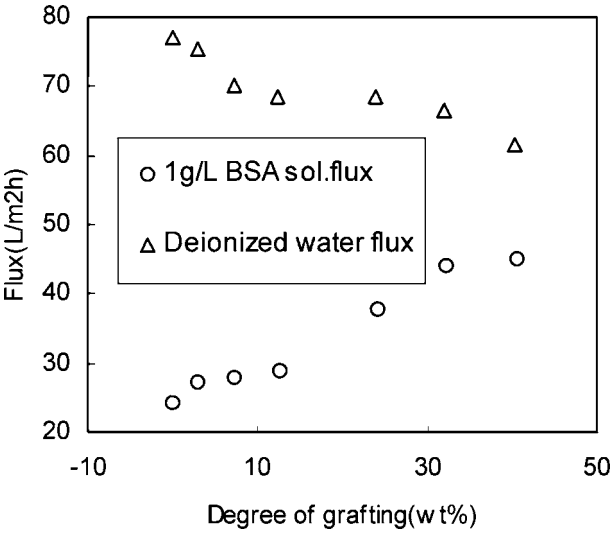

Fig. 11. Buffer flux as a function of the 2-hydroxyethyl methacrylate (HEMA) grafting degree

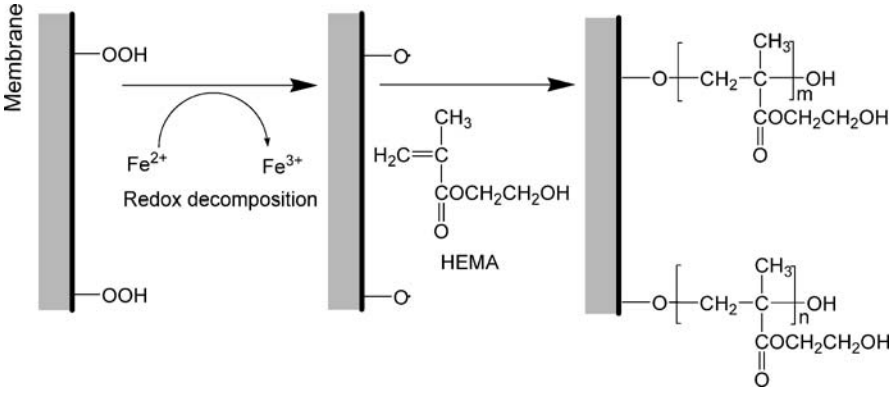

Fig. 12. Schematic illustration of ozone-induced graft polymerization

BSA buffer solution. The decrease of flux of the deionized water could be explained by narrowed or plugged pores as a result of the swelling of grafted PHEMA in a buffer solution. In the case of the permeation of BSA buffer solution, although the pores narrowed with increasing PHEMA grafting degree, the increased flux of the PHEMA-grafted membranes was due to the weakening of hydrophobic interaction between the BSA molecules and the hydrophilic membrane surface. Therefore, the flux of BSA buffer solution increased because the fouling caused by the adsorption of BSA was reduced with increasing PHEMA grafting degree.

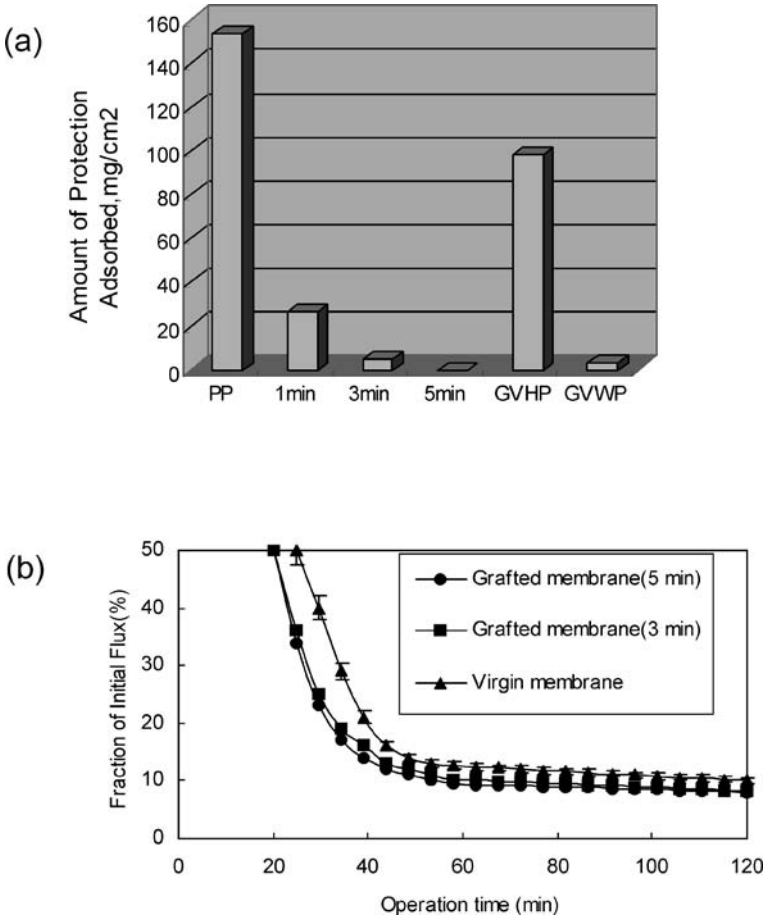

Fig. 13. a Amount of protein adsorbed per unit area of the virgin PPMM, grafted (ozone treated for 1, 3, and 5 min) and the commercial modified GVHP (hydrophobic) and GVWP (hydrophilic) membranes. **b** Fluxes for virgin and modified membranes during BSA solution permeation

11.1.4
Ozone Method

Wang et al. (2000) performed surface modification of PPMMs by using ozone to introduce peroxide onto the membrane surface. After that, graft polymerization of HEMA was carried out. The polymerization was initiated at a mild temperature by redox decomposition of the peroxide (Fig. 12). Similar to the results of Kang et al. (see previous section), these HEMA-grafted PPMMs also showed great protein resistance (see Figs. 13a,b and 14). The trend of flux decline for the modified (grafted) membrane was nearly the same as that of the unmodified (virgin) membrane. However, the flux recovery efficiency (Fig. 14), which is closely associated with the reversibility of membrane fouling layers, increased markedly with increasing ozone-treatment time by up to 5 min. It appears that membrane fouling might be the result of accumulation of protein aggregates at the membrane surface regardless of the membranes used (grafted or not), but could be reversed more easily for the grafted membranes with an appropriate time of ozonation. This can be attributed to the more hydrophilic nature of the modified membrane surfaces. Also, the steric hindrance resulting from the grafted PHEMA chains may play an important role in preventing the direct interaction between the membrane surfaces and proteins.

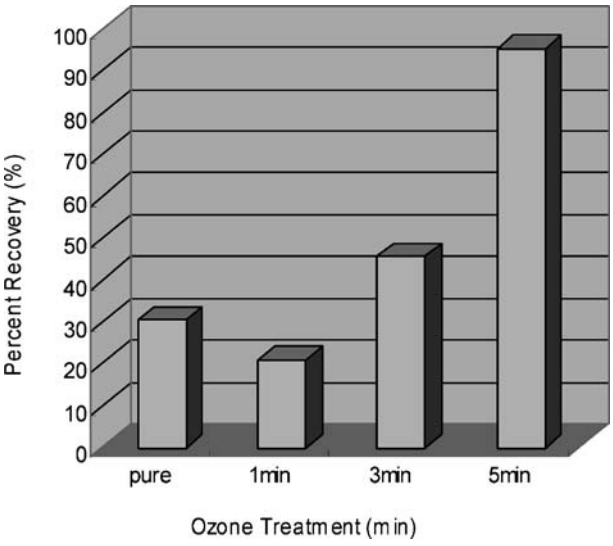

Fig. 14. Flux recovery efficiencies with water flushing at the end of operation

11.2 Surface-Modified PPMMs for Enzyme Immobilization

Catalysis is frequently a prerequisite for efficiency in organic reactions (Woltinger et al. 2001). As biocatalysts, enzymes exhibit several features that make their use advantageous compared to conventional chemical catalysts. The specific features presented by enzymes are the high level of catalytic efficiency and high degree of specificity including substrate specificity, region specificity and stereospecificity. However, conventional catalytic processes are often carried out in a homogeneous way, which frequently renders the separation of the catalyst from the reaction medium a cumbersome nuisance (Annis and Jacobsen 1999; Garber et al. 2000). Moreover, the loss of the precious enzymes in these catalysis processes becomes a great obstacle for commercial application. Therefore, efforts have been made to bind enzymes to an insoluble support/carrier.

In recent years, artificial membranes have been applied in biotechnology because of their interesting properties of high specific surface area and the possibility of combining separation with the chemical reaction (Gekas 1986). Among these membranes, the polypropylene membrane is particularly interesting due to its well-controlled porosity, chemical and thermal inertness, and high potential for comprehensive applications. However, PPMMs are pressed for polar functional groups, which are necessary for the covalent immobilization of proteins. Moreover, the poor biocompatibility of this membrane may cause nonbiospecific interactions, protein denaturation, and loss of enzyme activity (Kasemo 2002). Thus, one can envisage that it is possible to introduce a reactive and biofriendly interface on the PPMM surface for enzyme immobilization through surface modification technologies, which may reduce some of the nonspecific enzyme–support interactions, create a specific microenvironment for the enzyme, and benefit the enzyme activity (Deng 2004b). The introduction of polymer chains carrying polar and reactive groups to the PPMM surface may solve this problem easily. Tethering of polymers to the membrane surface can offer relatively high functional group density and depress the hindrance effect, which may cumber the immobilization of the enzyme. In general, the polymer carboxylic, amino, or thio groups, grafted to the membrane surface, are used for the immobilization of enzymes (Sano et al. 1993). Hydrophilic monomers, such as acrylic acid, HEMA, glycidyl methacrylate (GMA), are often used to modify the membrane surface, enhancing the hydrophilicity and biocompatibility of the membranes. However, for some enzymes, hydrophilic polymers are not always a suitable choice. In the case of lipase, the enzyme is activated in the presence of aqueous–hydrophobic interfaces. In addition, polymers that exhibit semiconductivity are preferred for the immobilization of enzymes that catalyze reactions via electron trans-

fer. Anyway, the purpose of modification is to provide the enzyme with conditions similar to those that it requires in nature.

There are three methods for immobilizing enzymes: physical adsorption/entrapment, direct grafting, and site-specific immobilization. In general, physical adsorption/entrapment offers better enzyme activity but relatively low stability. On the contrary, covalent immobilization is much more stable but often causes the enzyme to denature.

11.2.1 Physical Adsorption/Entrapment

Physical adsorption is the most convenient way to achieve enzyme immobilization, avoiding the tedious and time-consuming multistep procedure of covalent binding (Aleixo et al. 1985; Cleveland et al. 1981). Entrapment immobilizes enzymes by trapping them into porous materials (membranes). Because there is no covalent attachment, the activity of the enzymes immobilized by physical adsorption, and entrapment is easily maintained. However, loss of enzyme in applications is inevitable for the physical adsorption method, impeding the further utility of this method. At the same time, how substrates diffuse into the porous materials and how products diffuse out are the critical problems associated with the entrapment strategy.

Deng et al. (2004a,b,c) immobilized *Candida rugosa* lipase on a series of surface-modified PPMMs by adsorption and compared their effects on the enzyme activity. Three different kinds of modifiers, poly(α-allyl glucoside) (PAG), two polypeptides with short and long hydrophobic side chains, poly(γ-ethyl-L-glutamate) and poly(γ-stearyl-L-glutamate), and phospholipid-analogous polymers (PAP) containing hydrophobic octyloxy, dodecyloxy, and octadecyloxy groups (8-PAP, 12-PAP, and 18-PAP respectively), were tethered onto PPMMs (see Figs. 1, 3, and 6). Then lipases from *Candida rugosa* were immobilized on these membranes by adsorption and their activity was examined. The specific activity and the activity retention of the lipase immobilized onto the hydrophobic polypeptide- and PAP-modified membranes were both higher than those of nascent and hydrophilic PAG-modified membranes (Table 4). This can be ascribed to the large hydrophobic surface that surrounds the catalytic site of the lipase; lipase is thought to be activated in the presence of a hydrophobic interface, which can be helpful for the rearrangement of the protein conformation to yielding an "open state" of the lipase active site. There is a strong hydrophobic interaction between the long alkyl chain of PAP and polypeptides and the hydrophobic domain around the active site of lipase, which stabilizes the "open state" conformation of lipases and favors the accessibility of the

Table 4. Comparing of lipase activity as function of different modifier. *PAG* Poly (α-allyl glucoside), *PAP* phospholipids analogous polymers, *PELG* poly(γ-ethyl-L-glutamate), *PSLG* poly(γ-stearyl-L-glutamate)

Membrane/Modifier		Grafting degree (wt.%)	Water contact angle (°C)	Specific activity (U/mg protein)	Activity retention (%)
Nascent PPMM		–	118	69.9	57.5 ± 2.8
PAG		2.1	60	61.3	50.4 ± 2.7
		2.8	48	62.3	51.2 ± 2.8
		3.7	36	60.7	49.9 ± 2.9
PAP	8-PAP	10.6	53	90.1	74.1 ± 3.2
	12-PAP	10.9	92	94.3	77.5 ± 3.7
	18-PAP	10.8	96	101.2	83.2 ± 3.3
Polypeptide	PELG	3.5	113	76.4	62.8 ± 3.3
	PSLG	3.6	122	88.1	72.4 ± 3.9

active site to substrates. On the other hand, after modification with PAG, the sharp increase in hydrophilicity induces the conformational equilibrium of lipase, to some extent shifting it toward the unfavorable "closed state".

Tanioka et al. (1998) entrapped invertase in the pores of PPMMs, and these membranes were used to hydrolyze sucrose. As show in Fig. 15, they embedded invertase into the pores of PPMMs and then grafted poly(acrylic acid) (PAA) onto the membrane surface to entrap the enzyme. The invertase-entrapped PPMM was immersed in sucrose aqueous solution to hydrolyze the sucrose. The sucrose that permeated through the PAA layer on the membrane surface was hydrolyzed into fructose and glucose by invertase, and the decomposed products exited to the external solution. The hydrolyzation process of the sucrose caused a change in optical rotation, and inspection could be made using a polarimeter. Figure 16a,b shows the hydrolysis process of the invertase-immobilized PPMMs with a high (Fig. 16a) and low (Fig. 16b) PAA grafting degree, respectively, as a function of time. Arrows indicate that the membranes were removed from the sucrose solution. After this removal, hydrolysis cannot be observed at all in the case with the high grafting degree (Fig. 16a), but can still be observed in that of the low grafting degree (Fig. 16b). This indicates that invertase leakage occurred in the case of a low grafting degree, in which the PAA layer was not thick enough to prevent the invertase from spilling. However, with higher PAA grafting degree invertase could be entrapped stably in the PPMM pores and the hydrolysis processed very well.

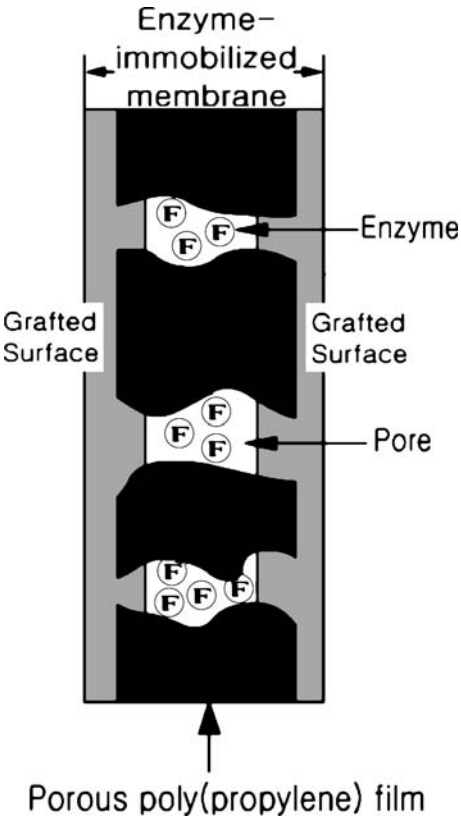

Fig. 15. Schematic representation of enzyme entrapment

11.2.2 Covalent Binding

Covalent binding means that the enzyme is immobilized by a chemical reaction between the enzyme and the support material to form covalent bonds. Although this immobilization generally enhances enzyme stability, one major disadvantage of this method is that the activity of the immobilized enzyme is often significantly decreased because the active site may be blocked, multiple point-binding may occur, or the enzyme may be denatured (Butterfield et al. 1994; Ganapathi et al. 1998; Zhuang and Butterfield 1992, 1993). As shown in Fig. 17a, the enzyme is directly immobilized, often through the ε-amino functionality of lysine residues on the protein. Because the protein often contains multiple lysine residues, which spread over the enzyme surface, different orientations of the enzyme occur, and it may thus be difficult for the active site of the enzyme to interact with the substrate.

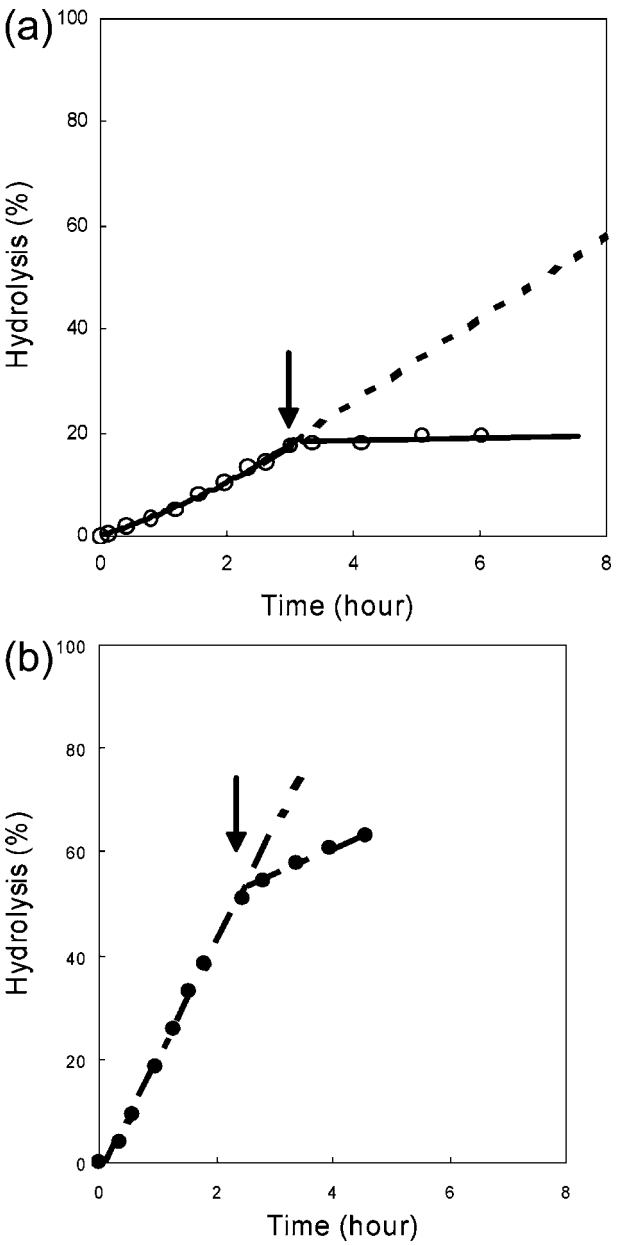

Fig. 16. Hydrolysis process of high (**a**) and low (**b**) poly(acrylic acid) grafting degree

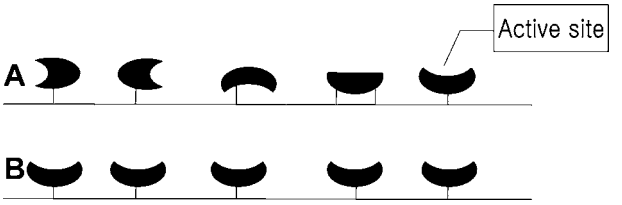

Fig. 17. Schematic representation of direct graft (**a**) and site-specific (**b**) immobilization of enzymes

Piletsky et al. (2003) functionalized PPMMs with polyaniline (PANI) and immobilized horseradish peroxidase (HRP) onto the membrane surface by both physical adsorption and covalent attachment. PANI is a semiconductive material that is stable in an oxygen atmosphere, contains amino groups, and is suitable for the covalent immobilization of biomolecules through carbodiimide or glutaric dialdehyde chemistry. Electronactive properties of PANI polymer could be envisaged as an additional advantage over conventional polymer matrices for enzyme immobilization, due to the fact that the electron-donating ability of PANI may play an important role in the enzyme catalysis of redox reactions (Malinauskas 1999). The PANI-coated PPMMs showed a high affinity for this enzyme as a result of the combination of electronstatic and hydrophobic interactions between the PANI and proteins (Bossi et al. 2002; Chen et al. 2000a, b). PANI has three oxidation states, leukoemeraldine (reduced), emeraldine, and pernigraniline (oxidized; see Fig. 18), and these different forms possess different adsorption properties to proteins. The highest and lowest bindings were achieved by reduced and oxidized PANI, respectively. HRP immobilized on the PANI-coated PPMM was shown to retain 70% of its activity after 3 months of storage at +5 °C, suggesting that this material can be used for practical application, such as in bioreactors as enzyme membranes.

Becker and coworkers (2002) presented a process involving continuous synthesis and simultaneous product release of amylase by an enzyme-immobilized membrane (see Fig. 19). PPMMs were functionalized by photoinitiated graft polymerization of GMA and the enzyme, amylosucrase, was immobilized by the reaction with epoxy groups on the membrane surface. Amylosucrases are found in many *Neisseria* species and catalyze the reaction

$$\text{sucrose} + \{1,4\text{-}\alpha\text{-D-glucosyl}\}_n \rightarrow \text{D-fructose} + \{1,4\text{-}\alpha\text{-D-glucosyl}\}_{n+1}$$

The enzyme transfers the glucose moiety of sucrose to the nonreducing end of an α-1,4-glucan chain, extending it linearly by one glucose unit and thereby releasing a fructose molecule. A sucrose solution and maltooligosaccharide (MOS) mixture containing from 3 to 6 glucose units with

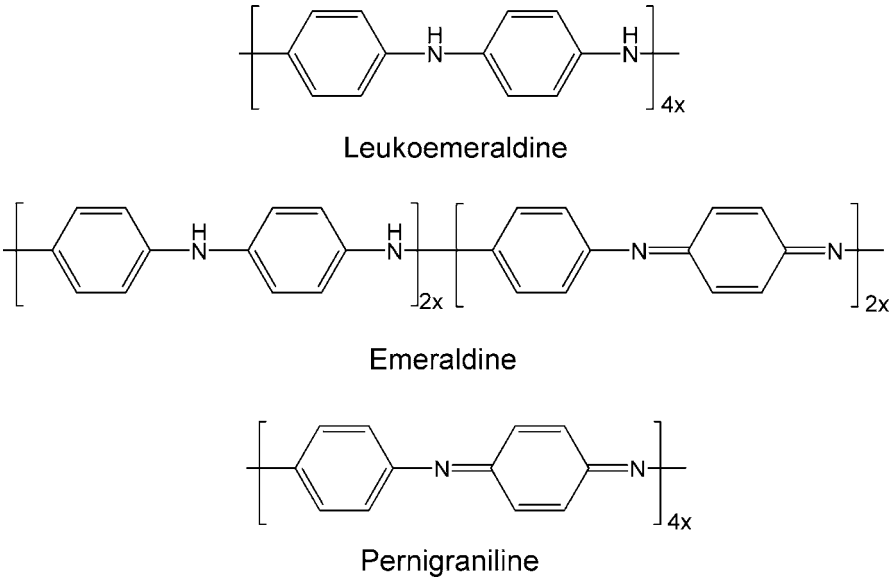

Fig. 18. Oxidation states of polyaniline

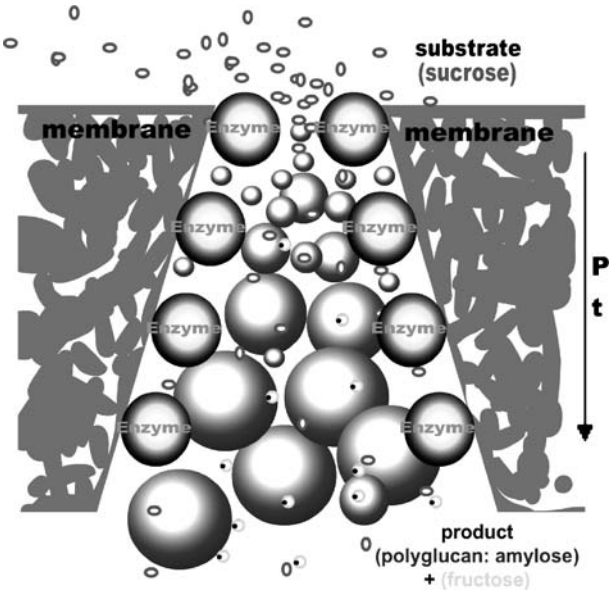

Fig. 19. Scheme of enzymatic poly- or oligoglucan synthesis within the membrane pore

α-1,4-linkage was used as a primer to filtrate through the membrane at 37 °C. The formed products (i. e., glucose coupled to the primer molecule), was characterized by high-performance liquid chromatography analysis of the filtrates at different flow rate (Fig. 20). The initial MOS mixture contained oligosaccharides with a degree of polymerization (DP, i. e., number

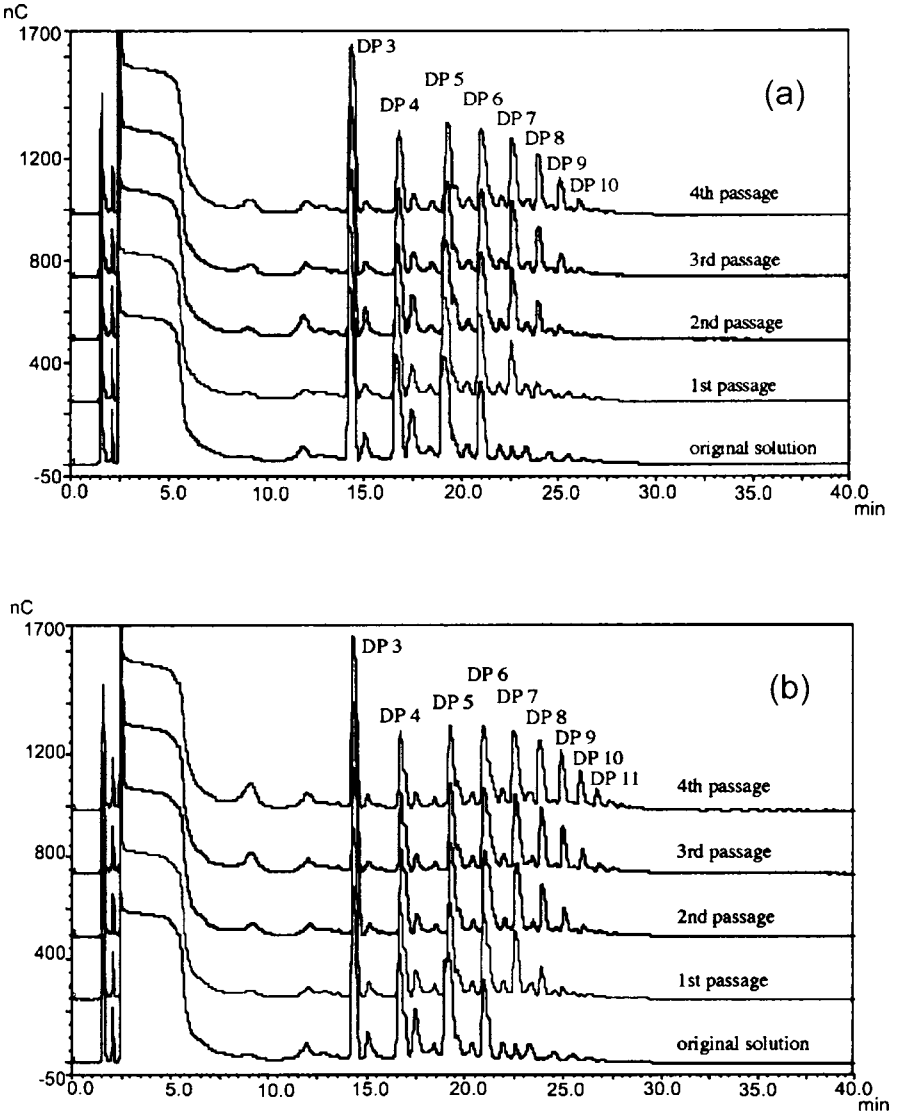

Fig. 20. Chromatograms of the filtrates with flow rate of 0.2 ml/min. (**a**) and 0.1 ml/min (**b**). *DP* Degree of polymerization

of glucose residues) of 3, 4, 5, and 6, with the DP3 oligosaccharide being most abundant followed by DP4 and DP5 oligosaccharides. At the flow rate of 0.2 ml/min the maltooligosaccharides were enlarged by one glucose unit per membrane passage and a definite shift can be seen in the oligosaccharide distribution: the DP3 peak remains almost constant, the DP4 peak is much reduced, implying that the DP4 product may be preferentially utilized by the enzyme as an acceptor for the glucose moiety (Fig. 20a). In addition, at the slower flow rate of 0.1 ml/min, more than one glucose unit is coupled to a subset of the primer molecules at each passage (Fig. 20b).

11.2.3 Site-Specific Immobilization

Compared to the two aforementioned methods, site-specific immobilization can offer both highly specific orientation and reliable stability of the immobilized enzyme (Fig. 17b). The active sites of the immobilized enzymes face away from the support surface and a consequent higher activity can be obtained (Butterfield et al. 2001). A typical site-specific process utilizes the biotin–avidin interaction to immobilize enzymes. Firstly, a single biotin moiety is incorporated onto the appropriate place (opposite the active site) of the enzymes. The biotin is recognized by avidin, which is immobilized onto the membrane surface, and the enzymes are immobilized to the membrane in a specific orientation (Fig. 21). As an advanced technique, site-specific immobilization provides a very promising way to realize simultaneously high stability and activity. Unfortunately, site-specific

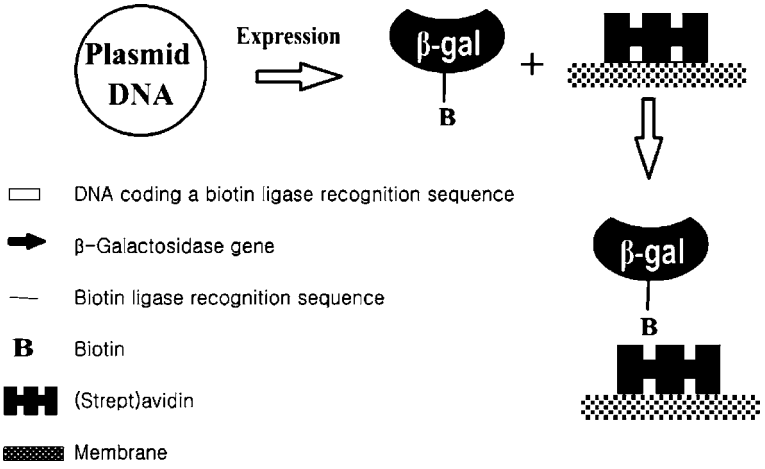

Fig. 21. Site-specific immobilization of enzyme by the biotin–avidin interaction. *β-Gal* β-Galactosidase

functionalized enzymes are not easy or readily produced and are usually very expensive. Thus, to our knowledge, no study has been carried out on PPMM with this technique. However, it is predictable that with the current rapid advances in biology this technique will receive more and more consideration in the near future.

11.3 Conclusions

The surface of a material is the phase boundary that resides between the bulk material and the outer environment. The performance of materials relies largely upon the properties of the boundaries in many applications. For biological/biomedical applications, polypropylene membranes often suffer from grievous problems such as hydrophobicity, being chemical inert, and lacking functional groups. These disadvantages cause nonspecific protein adsorption and make PPMMs incapable of enzyme immobilization. However, as we can see, graft polymerization of some polymers carrying various functional groups (such as $-OH$, $-NH_3$, and $-OOH$) to the membrane surface is an effective way to conquer these shortcomings. We can choose different modifiers to confer upon the membrane different specialties for diverse applications. Hydrophilic polymers, such as poly(ethylene glycol), polyHEMA, and PAA) are usually used to reduce nonspecific protein adsorption because that protein adsorption is mediated mainly by hydrophobic interactions between the protein and the membrane surface. Nevertheless, it is more intricate for enzyme immobilization due to the complexity of the enzyme itself. Lipase has an affinity for hydrophobic surfaces; however, enzymes that catalyze redox reactions benefit from semiconducting materials. Modifiers must be adapted to a given enzyme in order to maintain its activity.

Acknowledgements. Financial support from the National Natural Science Foundation of China (Grant no. 20474054 and 20074033) and the National Basic Research Program of China (Grant no. 2003CB15705) are gratefully acknowledged. The authors thank Dr. Zhen-Mei Liu, Dr. Hong-Tao Deng, and Dr. Rui-Qiang Kou very much for their contribution.

References

Aleixo JAG, Swaminathan B, Minnich SA, Wallshein VA (1985) Enzyme immunoassay: binding of Salmonella antigens to activated microtiter plates. J Immunoassay 6:391–407

Annis DA, Jacobsen EN (1999) Polymer-supported chiral co(salen) complexes: synthetic applications and mechanistic investigations in the hydrolytic kinetic resolution of terminal epoxides. J Am Chem Sci 121:4147–4154

Becker M, Provart N, Lehmann I, Ulbricht M, Hicke H (2002) Polymerization of glucans by enzymatically active membranes. Biotechnol Progr 18:964–968

Bossi A, Piletsky SA, Turner APF, Righetti PG (2002) Repartition effect of aromatic polyaniline coatings on the separation of bioactive peptides in capillary electrophoresis. Electrophoresis 23:203–208

Butterfield DA, Lee J, Ganapathi S, Bhattacharyya D (1994) Biofunctional membranes IV. Active site structure and stability of an immobilized enzyme, papain, on modified polysulfone membranes studies by electron paramagnetic resonance and kinetics. J Membr Sci 91:41–52

Butterfield DA, Bhattacharyya D, Daunert S, Bachas L (2001) Catalytic biofunctional membranes containing site-specifically immobilized enzyme arrays: a review. J Membr Sci 181:29–37

Chen Y, Kang ET, Neoh KG, Tan KL (2000a) Covalent immobilization of invertase onto the surface-modified polyaniline from graft copolymerization with acrylic acid. Eur Polym J 36:2095–2103

Chen Y, Kang ET, Neoh KG, Wang P, Tan KL (2000b) Surface modification of polyaniline film by grafting of poly(ethylene glycol) for reduction in protein adsorption and platelet adhesion. Synth Met 110:47–55

Cleveland PH, Wicham GM, Goldbaum MH, Ryan AF, Worthen DM (1981) Rapid and efficient immobilization of soluble and small particulate antigens for solid phase immunoassays. J Immunoassay 2:117–136

Deng HT, Xu ZK, Huang XJ, Wu J, Seta P (2004a) Adsorption and activity of *Candida rugosa* lipase on polypropylene hollow fiber membrane modified with phospholipid analogous. Langmuir 20:10168–10173

Deng HT, Xu ZK, Liu ZM, Wu J, Ye P (2004b) Adsorption immobilization of Candida rugosa lipases on polypropylene hollow fiber microfiltration membranes modified by hydrophobic polypeptides. Enzyme Microb Technol 35:437–443

Deng HT, Xu ZK, Wu J, Ye P, Liu ZM, Seta P (2004c) A comparative study on lipase immobilized polypropylene microfiltration membranes modified by sugar-containing polymer and polypeptide. J Mol Catal B Enzym 28:95–100

Deppisch R, Storr M, Buck R, Gohl H (1998) Blood material interactions at the surfaces of membranes in medical applications. Sep Purif Technol 14:241–254

Ganapathi S, Butterfield DA, Bhattacharyya D (1998) Kinetics and active fraction determination of a protease enzyme immobilized on functionalized membranes: mathematical modeling and experimental results. Biotechnol Progr 14:865–873

Garber SB, Kingsbury JS, Gray BL, Hoveyda AH (2000) Efficient and recyclable monomeric and dendritic ru-based metathesis catalysts. J Am Chem Sci 122:8168-8179

Gekas VC (1986) Artificial membranes as carriers for the immobilization of biocatalysts. Enzyme Microb Technol 8:450–460

Guell C, Czekaj P, Davis RH (1999) Microfiltration of protein mixtures and the effects of yeast on membrane fouling. J Membr Sci 155:113–122

Gupta B, Anjum N (2003) Plasma and radiation-induced graft modification of polymers for biomedical applications. Adv Polym Sci 162:35–61

Ikada Y (1994) Surface modification of polymers for medical applications. Biomaterials 15:725–726

Kang JS, Shim JK, Huh H, Lee YM (2001) Colloidal adsorption of bovine serum albumin on porous polypropylene-g-poly(2-hydroxyethyl methacrylate) membrane. Langmuir 17:4352–4359

Kasemo B (2002) Biological surface science. Surf Sci 500:656–677

Kiaei D, Hoffman AS, Horbett TA (1995) Radio-frequency gas discharge (RFGD) fluorination of polymers: protein and cell interactions at RFGD-fluorinated interfaces. Radiat Phys Chem 46:191–197

Kita H, Inada T, Tanaka K, Okamoto K (1994) Effect of photocrosslinking on permeability and permselectivity of gases through benzophenone-containing polyimide. J Membrane Sci 87:139–147

Klee D, Hocker H (1999) Polymers for biomedical applications: improvement of the interface compatibility. Adv Polym Sci 149:1–57

Kou RQ, Xu ZK, Deng HT, Liu ZM, Seta P, Xu YY (2003) Surface modification of microporous polypropylene membranes by plasma-induced graft polymerization of γ-allyl glucoside. Langmuir 19:6869–6875

Kuberkar VT, Davis RH (2000) Modeling of fouling reduction by secondary membranes. J Membrane Sci 168:243–258

Lee JH, Park JW, Lee HB (1991) Cell adhesion and growth on polymer surfaces with hydroxyl groups prepared by water vapour plasma treatment. Biomaterials 12:443–448

Liu ZM, Xu ZK, Wang JQ, Yang Q, Wu J, Seta P (2003) Surface modification of microporous polypropylene membranes by the grafting of poly(γ-stearyl-L-glutamate). Eur Polym J 39:2291–2299

Liu ZM, Xu ZK, Wang JQ, Wu J, Fu JJ (2004) Surface modification of polypropylene microfiltration membranes by graft polymerization of *N*-vinyl-2-pyrrolidone. Eur Polym J 40:2077–2087

Lundstrom I, Elwing H (1990) Simple kinetic models for protein exchange reactions on solid surfaces. J Colloid Interface Sci 136:68–80

Ma H, Bowman CN, Davis RH (2000a) Membrane fouling reduction by backpulsing and surface modification. J Membr Sci 173:191–200

Ma H, Davis RH, Bowman CN (2000b) A novel sequential photoinduced living graft polymerization. Macromolecules 33:331–335

Malinauskas A (1999) Electrocatalysis at conducting polymers. Synth Met 107:75–83

Mueller J, Davis RH (1996) Protein fouling of surface-modified polymeric microfiltration membranes. J Membr Sci 116:47–60

Oehr C, Muller M, Elkn B, Vohrer U (1999) Plasma grafting – a method to obtain monofunctional surfaces. Surf Coat Tech 116:25–35

Piletsky S, Piletska E, Bossi A, Turner N, Turner A (2003) Surface functionalization of porous polypropylene membranes with polyaniline for protein immobilization. Biotechnol Bioeng 82:86–92

Poche DS, Daly WH, Russo PS (1995) Synthesis and some solution properties of poly(γ-stearyl-L-glutamate). Macromolecules 28:6745–6763

Ratner BD, Hoffman AS, Hanson SR, Harker LA, Whiffen JD (1979) Blood-compatibility-water-content relationships for radiation-grafted hydrogels. J Polym Sci Polym Symp 66:363–375

Ratner BD (1995) Surface modification of polymers: chemical, biological and surface analytical challenges. Biosens Bioelectron 10:797–804

Richey T, Iwata H, Oowaki H, Uchida E, Matsuda S, Ikada Y(2000) Surface modification of polyethylene balloon catheters for local drug delivery. Biomaterials 21:1057–1065

Sano S, Kato K, Ikada Y (1993) Introduction of functional groups onto the surface of polyethylene for protein immobilization. Biomaterials 14:817–822

Senogles E, Thomas R (1975) Polymerization kinetics of *N*-vinyl pyrrolidone. J Polym Sci Symp 49:203–210

Sonderquist ME, Walton AG (1980) Structural change in proteins adsorbed on polymer surfaces. J Colloid Interface Sci 75:386–397

Steen ML, Jordan AC, Fisher ER (2002) Hydrophilic modification of polymeric membranes by low temperature H_2O plasma treatment. J Membr Sci 204:341–357

Taniguchi M, Pieracci J, Samsonoff WA, Belfort G (2003) UV-assisted graft polymerization of synthetic membranes: mechanistic studies. Chem Mater 15:3805–3812

Tanioka A, Yokoyama Y, Miyasaka, K (1998) Preparation and properties of enzyme-immobilized porous polypropylene films. J Colloid Interface Sci 200:185–187

Thom V, Altankov G, Groth T, Jankova K, Jonsson G, Ulbricht M (2000) Optimizing cell-surface interactions by photografting of poly(ethylene glycol). Langmuir 16:2756–2765

Tie Y, Calonder C, Van Tassel PR (2003) Protein adsorption: kinetics and history dependence. J Colloid Interface Sci 268:1–11

Ulbricht M, Richau K, Kamusewitz H (1998) Chemically and morphologically defined ultrafiltration membrane surfaces prepared by heterogeneous photo-initiated graft polymerization. Colloid Surf A 138:353–366

Wang Y, Kim JH, Choo KH, Lee YS, Lee CH (2000) Hydrophilic modification of polypropylene microfiltration membranes by ozone-induced graft polymerization. J Membr Sci 169:269–276

Wavhal DS, Fisher ER (2003) Membrane surface modification by plasma-induced polymerization of acrylamide for improved surface properties and reduced protein fouling. Langmuir 19:79–85

Wetzels GMR, Koole LH (1999) Photoimmobilisation of poly(*N*-vinylpyrrolidinone) as a means to improve haemocompatibility of polyurethane biomaterials. Biomaterials 20:1879–1887

Woltinger J, Bommarius AS, Drauz K, Wandrey C (2001) The chemzyme membrane reactor in the fine chemicals industry. Org Proc Res Dev 5:241–248

Xu ZK, Kou RQ, Liu ZM, Nie FQ, Xu YY (2003) Incorporating r-allyl glucoside into polyacrylonitrile by water-phase precipitation copolymerization to reduce protein adsorption and cell adhesion. Macromolecules 36:2441–2447

Xu ZK, Dai QW, Wu J, Huang XJ, Yang Q (2004) Covalent attachment of phospholipid analogous polymers to modify a polymeric membrane surface: a novel approach. Langmuir 20:1481–1488

Yang Q, Xu ZK, Dai ZW, Wang JL, Ulbricht M (2005) Surface modification of polypropylene microporous membranes with a novel glycopolymer. Chem Mater 17:3050–3058

Zhuang P, Butterfield DA (1992) Structural and enzymatic characterizations of papain immobilized onto vinyl alcohol/vinyl butyral copolymer membrane. J Membr Sci 66:247–257

Zhuang P, Butterfield DA (1993) Optimization of covalently coupling enzymes to polymeric membranes: EPR studies of papain. J Appl Polym Sci 47:1329–1342

12 Nonbiofouling Surfaces Generated from Phosphorylcholine-Bearing Polymers

Yasuhiko Iwasaki, Nobuo Nakabayashi, Kazuhiko Ishihara

Abstract. The preparation and characterization of nonbiofouling surfaces generated from phosphorylcholine (PC)-bearing polymers are described. It is proposed that PC groups are an optimum surface with which to create biointerfaces because the surfaces have similarities with biomembranes. Nonspecific protein adsorption is generally the first process to occur when polymers come into contact with the vital environment, and this induces unfavorable bioreactions. Due to the properties of PC surfaces, such as high hydrophilicity, water structure, and zero ζ-potential, protein adsorption is effectively reduced on the PC-bearing surface. This surface property may be important for biomedical applications. The well-defined design of PC surfaces is also introduced in this chapter. These surfaces may be micro- or nanofabricated for, for example, medical devices and sensors. Control of cell–material interactions is effective on PC-bearing surfaces due to the negligible nonspecific interactions.

12.1 Introduction

Protein adsorption is the first phenomenon that occurs when synthetic materials come into contact with a living organism. The uncontrolled protein adsorption functions as a trigger for foreign body reactions to materials from a host. For biomedical applications, control of protein adsorption becomes quite important in the preparation of synthetic materials. Many concepts have been proposed for non-protein-fouling surfaces using physicochemical, biochemical, and biological approaches. One of the most robust approaches is phosphorylcholine immobilization as a mimicker of a biomembrane (Iwasaki and Ishihara 2005). A well-known model of the

Yasuhiko Iwasaki, Nobuo Nakabayashi: Institute of Biomaterials and Bioengineering, Tokyo Medical and Dental University, 2-3-10 Kanda-surugadai, Chiyoda-ku, Tokyo 101-0062, Japan, E-mail: yasu.org@tmd.ac.jp

Kazuhiko Ishihara: Department of Materials Engineering, School of Engineering, The University of Tokyo, 7-3-1 Hongo, Bunkyo-ku, Tokyo 113-8656, Japan

Principles and Practice
Proteins at Solid–Liquid Interfaces
Philippe Déjardin (Ed.)
© Springer-Verlag Berlin Heidelberg 2006

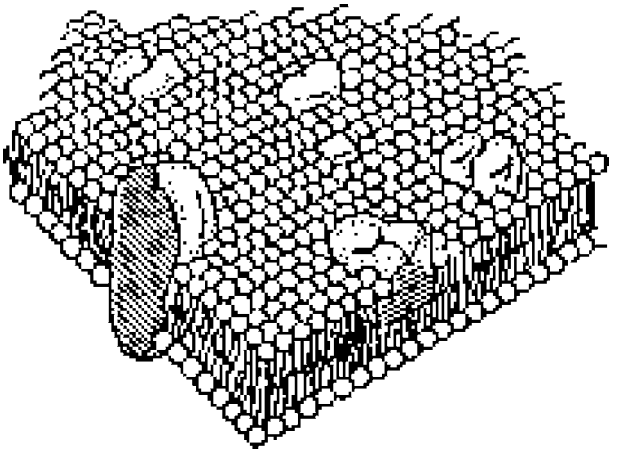

Fig. 1. Fluid-mosaic model of biomembrane

structure of a biomembrane is the fluid-mosaic model (Fig. 1; Singer and Nicolson 1972). According to this model, amphiphilic phospholipids are arranged in a bilayer structure and proteins are located in or upon it. In all cells for which lipid compositional asymmetry has been described, negatively charged phospholipids such as phosphatidylserine are found predominantly on the inner, cytoplasmic side of the membrane, whereas the neutral, zwitterionic phosphorylcholine lipids such as phosphatidylcholines are located in the outer leaflet. The phosphorylcholine surface provides an inert surface for biological reactions of proteins and glycoproteins to occur smoothly on the membrane. This fact provides very significant information in the development of nonfouling polymer surfaces.

In this chapter, a variety of methodologies for making biomimetic phosphorylcholine-bearing surfaces, including well-defined surface preparation (i. e., self-assembled monolayers, SAMs) and polymer brushes, and the surface characteristics of the surfaces are introduced. In addition, an explanation is given as to how securing protein adsorption onto the surface enables the control of cell–material interactions.

12.2 Forces Involved in Protein Adsorption

The interactions that are involved in protein adsorption to solid surfaces (Lee et al. 2001) are known to include van der Waals forces, electrostatic "double-layer" forces, solvation forces, and entropic forces (Israelachivili and McGuiggan 1988; Oscarsson 1997). The extent of protein adsorption is

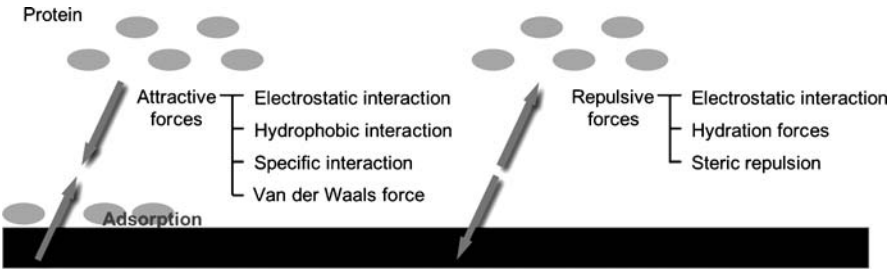

Fig. 2. Types of attractive and repulsive forces

determined by competition between attractive interactions and nonspecific repulsion (Fig. 2).

Among these forces, van der Waals and electrostatic forces are fundamental, while others are introduced by structural or conformational changes. The electrostatic attractions are not likely to play a significant role since most biomaterial surfaces are made of electrically neutral materials. In addition, the Debye length in physiological fluids is usually less than 10 Å. Specific interactions are also expected to be absent, since biomaterial surfaces do not generally possess structures that can be recognized by molecules with specific tertiary structures, such as binding sites of antibodies and enzymes. In general, specific interactions are highly attractive. For example, the free energy of the binding of dinitrophenol by its specific antibodies ranges from –35 kJ/mol to –72 kJ/mol (Bongard 1988). In the absence of such interactions, however, van der Waals forces and hydrophobic interactions are most important. Between hydrophobic surfaces, hydrophobic interactions generally operate over greater distances than does the van der Waals force (Pashley et al. 1985).

As mentioned earlier, of the repulsive interactions, electrostatic repulsion is not significant in physiological conditions such as in body fluids or blood. Repulsive hydration forces arise whenever water molecules bind to the surface containing hydrophilic groups (Israelachvili 1985). Steric repulsion can provide long-range repulsion; the long-range aspect is provided by the thickness of the grafted layer of hydrophilic molecules. Thus, it is mostly the long-range steric repulsion that effectively overcomes the attractive interactions in the physiological milieu. If the grafted layer is rather thin (i. e., if the range of the steric repulsion is rather short), the hydration repulsion becomes a significant portion of the overall repulsion. In that case it may not be easy to distinguish between the osmotic factor of the steric repulsion and the hydration forces (Israelachvili 1985).

12.3 Design of Phosphorylcholine-Bearing Surfaces

What is the most appropriate surface for controlling interactions with proteins? Although this question has been considered for a long time in relation to the creation of biomedical materials, we have not succeeded in obtaining the expected surface because most surface design is approached from a physicochemical perspective. In contrast, biomembrane surfaces may possess the most preferable characteristics for controlling complex biological interactions. Recently, use of biomembrane structures has been adopted for preparing the surfaces of biomaterials.

In an attempt to understand biocompatibility, Nakabayashi and coworkers (Kadoma et al. 1978) first synthesized a methacrylate monomer with a phosphorylcholine group, 2-methacryloyloxyethyl phosphorylcholine (MPC), to obtain new medical polymer materials to mimic biomembrane surfaces (Fig. 3). In 1982, Nakaya et al. also succeeded in synthesizing MPC (Umeda et al. 1982). However, at those times, the degree of purity and yield of MPC was insufficient to allow evaluation of their functions. Ishihara et al. (1990) then developed a new synthetic route and succeeded in producing MPC with good yield as a white powder by recrystallization. MPC, which contains the polymerizable methacrylate group, can readily be copolymerized, enabling the design of numerous polymers with a wide range of molecular architectures including random (Ishihara et al. 1990; Ueda et al. 1992), block (Kojima et al. 1991; Ma et al. 2003a, b; Li et al. 2003), graft (Ishihara et al. 1994b; Iwasaki and Akiyoshi 2004), charged (Ishihara et al. 1994a; Ito et al. 2003), and end-functional polymers (Ishihara et al. 1994b). The homopolymer of MPC [poly(MPC)] is soluble in water. The solubility of MPC polymers can easily be altered by changing the structure and fraction of the comonomers.

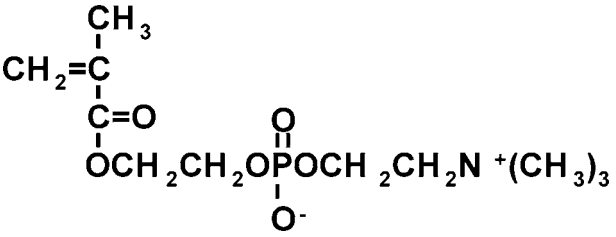

Fig. 3. Chemical structure of 2-methacryloyloxyethyl phosphorylcholine (MPC)

12.4 Mechanism of Resistance to Protein Adsorption on the MPC Polymer Surface

To reduce protein adsorption on polymer surfaces, surface modifications that induce repulsive interactions or reduce attractive interactions have been conducted. It has been known for quite some time that in general, as a surface becomes more hydrophobic, the extent of protein adsorption increases (Elwing et al. 1987; Golander and Pitt 1990; Golander et al. 1990; Lee and Lee 1993). The unusually strong attraction between proteins and hydrophobic surfaces in water has been described by a hydrophobic interaction, which arises primarily from the structural rearrangement of water molecules in the overlapping solvation zones as proteins adsorb to the surface. Thus, the hydrophobic interaction is primarily an entropic phenomenon without any specific associated bond. The orientation of water molecules adjacent to hydrophobic surfaces is entropically unfavorable. Upon adsorption of proteins to hydrophobic surfaces, the entropically unfavorable water is released in bulk, thereby reducing the total free energy. The hydrophobic interaction then results in the strong attraction of proteins toward the hydrophobic surface. To weaken the hydrophobic interaction, hydrophilic polymers [e.g., poly(2-hydroxyethyl methacrylate) (HEMA), poly(acryl amide), poly(vinylpyrrolidone)] have been applied for surface modification. While these hydrophilic polymers could relatively reduce protein adsorption, their use precludes the accurate control of protein adsorption.

Recently, it has been reported that the structure of water absorbed in the polymer materials influences protein adsorption on their surfaces. When protein molecules adsorb to a polymer surface, water molecules between the protein and the surface must be displaced, as shown in Fig. 4 (Lu et al. 1991). A repulsive solvation interaction arises whenever water molecules are associated with a surface that contains hydrophilic groups. Its strength depends on the energy necessary to disrupt the ordered water structure and ultimately dehydrate the surface. Even on a hydrophilic surface, the water structure has a major effect on protein adsorption and subsequent conformational change.

Tsuruta (1996) reported that the random networks of water molecules on the material surface are very important in explaining protein adsorption. Protein adsorption processes are considered to start with protein trapping by the random networks of water molecules on the material surface. The material surface, which cannot undergo hydrogen bonding with water, will then reduce protein adsorption. Table 1 lists the free water concentration in the hydrated polymer membrane with a 0.36 water fraction determined

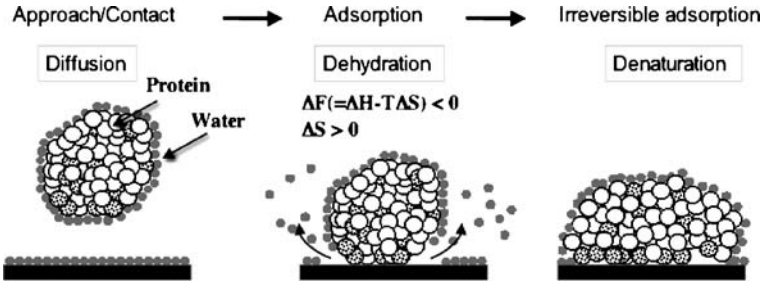

Fig. 4. Schematic description of protein adsorption on the polymer surface. Water molecules are moved from contact sites between amino acid residues and the polymer surface. A change in the conformation of the adsorbed protein then occurs and the protein binds to the surface tightly. ΔF Free energy, ΔH enthalpy, T absolute temperature, ΔS entropy

Table 1. Characteristics of hydration state of polymer. *Heq* = (weight of water in the polymer membrane)/(weight of polymer membrane saturated with water) at 25 °C, *Poly(HEMA)* poly(2-hydroxyethyl methacrylate), *PMB* poly(MPC-co-n-butyl methacrylate), Number after PMB is molar percent of MPC in the coplymer

	Poly(HEMA)	PMB	
		10	30
Heq	0.40	0.23	0.84
Free water fraction at Heq	0.34	0.25	0.84
At H = 0.36	0.28	–	0.69

with differential scanning calorimetry (Ishihara et al. 1998). The fraction of free water (not bound water) in the MPC polymer was 0.65, which was found to be significantly higher than that in poly(HEMA), which was 0.28. In addition, the structure and hydrogen bonding of water in the vicinity of poly(MPC-co-butyl methacrylate) (PMB) were analyzed in their aqueous solutions and thin films with contours of O-H stretching of the Raman and attenuated total reflection infrared (ATR-IR) spectra, respectively (Kitano et al. 2000, 2003).

Figure 5 shows the O-H stretching Raman band of water in various polymer solutions recorded in the region between 2500 and 4000/cm by using the polarization method. For the polarization geometries $X(ZZ)Y$ (parallel position, $I_{//}$) and $X(ZX)Y$ (perpendicular position, $I_{\perp}$), a polarizer plate was rotated exactly 90 °C in front of the slit, where X and Y are the directions of the laser beam and observation, respectively.

A depolarization ratio, r, is an indicator of symmetry of the vibration mode, and is expressed by $r = I_{//}/I_{\perp}$, where $I_{//}$ and $I_{\perp}$ are the intensities of the spectra observed with the polarizer oriented parallel and perpendicular to the incident laser beam, respectively. The component of the O–H

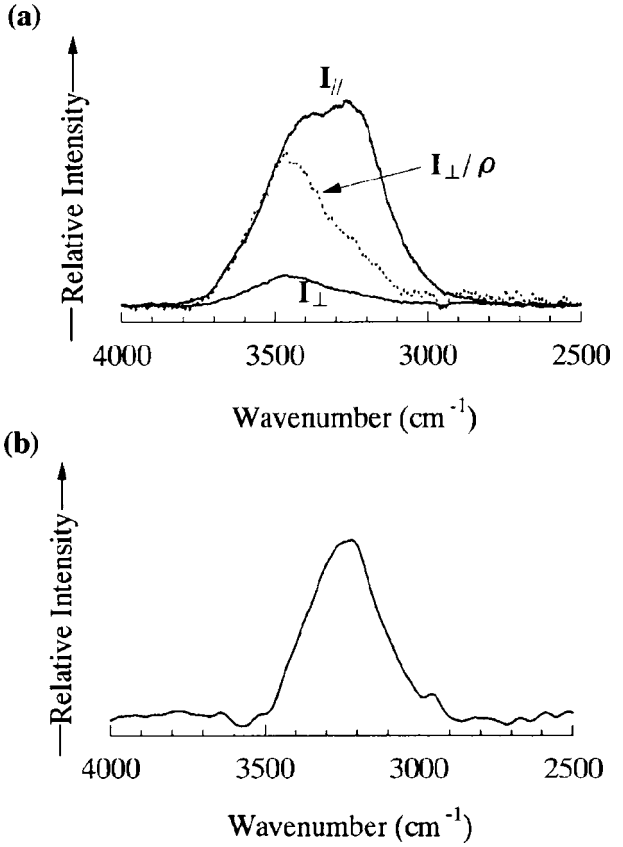

Fig. 5. Raman shifts of O–H stretching region. **a** $I_{//}$ and $I_{\perp}$ spectra of pure water at 25 °C, where $I_{//}$ and $I_{\perp}$ are the intensities of the spectra observed with the polarizer oriented parallel and perpendicular to the incident laser beam, respectively. The $I_{\perp}/\rho$ spectrum (where ρ is the depolarization ratio) is shown with a *dotted line*. **b** The collective band of water. Reprinted with permission from Kitano et al. (2000), copyright (2000) American Chemical Society

stretching band of water centered at 3250/cm was highly polarized and diminished in the spectra at the perpendicular position. The polarized O–H stretching band of water, which is called a collective band, is ascribed to an H_2O molecule executing u_1 vibrations all in phase with each other but with a vibrational amplitude varying from molecule to molecule in water clusters, which are strongly hydrogen-bonded. Theoretical calculations of a random network model, which is characterized by fluctuating defects in water–water hydrogen bonds in a distorted tetrahedral network, support the interpretation.

To clarify the effect of polymers on the structure of water, the intensity of the collective band (I_c) observed at around 3250/cm was separated from the spectra using Eq. 1 (Fig. 5):

$$I_c = I_{//} - I_{\perp}/r_{O-H} \quad (1)$$

Since the intensities of Raman spectra are not absolute, the area of I_c was normalized as Eq. 2:

$$C = \int I_c(w)dw / \int I_{\perp}(w)dw = C_x/C_w \quad (2)$$

where w is the Raman shift in cm^{-1}.

Figure 6 shows the effect of the molecular weight (M_w)of different kinds of polymers on the relative intensities of the collective bands (C) at a constant molar fraction of monomer units (p_x = 0.01 or 0.05). In the case of aqueous sodium poly(styrenesulfonate) solution, a very strong fluorescence background made the Raman spectroscopic measurements impossible. The values of C for other polymer solutions were almost constant in the region of relatively low M_w, and decreased with an increase in M_w in the region where the M_w values were larger than some critical values. In general, the whole concentration region of polymer solutions can be divided into three parts: dilute, semidilute, and concentrated. The macroscopic properties of polymer solutions in the different concentration regions are

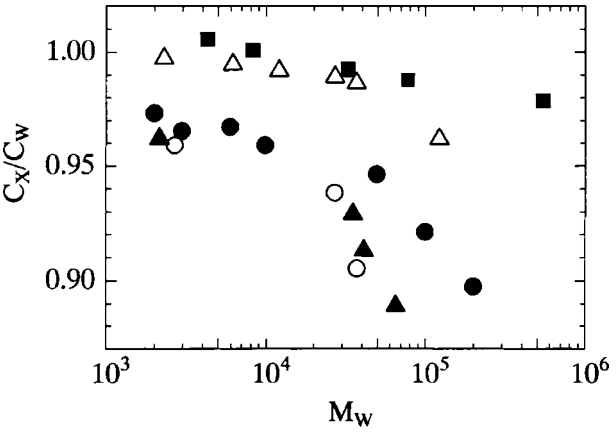

Fig. 6. Plots of values of the relative intensities of the collective bands (C) for various aqueous polymer solutions at molar fraction (p_x) = 0.01 and 25 °C versus molecular weight (M_w). Sodium poly(styrenesulfonate) (*open triangles*), poly-L-lysine hydrobromide (*open circles*), poly(2-methacryloyloxyethyl phosphorylcholine) [poly(MPC); *filled squares*], poly(*N*-vinylpyrrolidone) (*filled triangles*), and poly(ethylene glycol) (*filled circles*; p_x = 0.05). Reprinted with permission from Kitano et al. (2000), copyright (2000) American Chemical Society

significantly altered. The figure seems to show that the structure of water in a dilute polymer solution and in a semidilute polymer solution are different, as discussed below.

The *C* value for the aqueous solution of poly(MPC)s was very close to that for pure water, as shown in Fig. 6, which is in contrast with the smaller *C* value in the aqueous solution of ordinary polyelectrolytes. A similar tendency was also observed on hydrated thin polymer films. These results suggest that the PMB does not significantly disturb the hydrogen bonding between the water molecules in either the aqueous solution or the thin film systems.

The equilibrium amount of the proteins bovine serum albumin (BSA) and bovine plasma fibrinogen (BPF) adsorbed on the polymer surface was measured and represented with the free water fraction in the hydrated polymers, as shown in Fig. 7 (Ishihara 2000). The amounts of both proteins adsorbed on poly(HEMA), poly(acryl amide (AAm)-co-*n*-butyl methacrylate) (BMA), and poly(*N*-vinylpyrrolidone (VPy)-co-BMA) were larger than were those on poly(MPC-co-dodecyl methacrylate) (PMD) and PMB. It was reported that the theoretical amount of BSA and BPF adsorbed on the surface in a monolayer state were 0.9 and 1.7 μg/cm, respectively. On the surface of the MPC polymers, the amount of adsorbed proteins was less than these theoretical values.

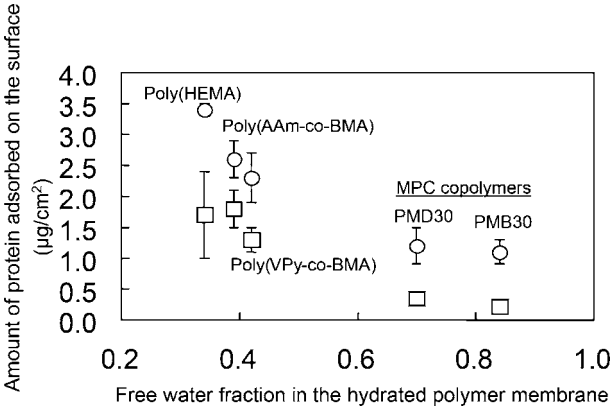

Fig. 7. Relationship between free water fraction in hydrated polymer membrane and amount of proteins adsorbed on the polymer. Concentration of bovine serum albumin (*[BSA]*) in phosphate-buffered saline (PBS) = 0.45 g/dl (*squares*); concentration of bovine plasma fibrinogen ([BPF]) = 0.30 g/dl (*circles*). *Poly(HEMA)* Poly(2-hydroxyethyl methacrylate), *Poly(AAm-co-BMA)* poly(acryl amide-co-*n*-butyl methacrylate), Poly(VPy-c-BMA) poly(*N*-vinylpyrrolidone-co-butyl methacrylate), *PMD* poly(MPC-co-dodecyl methacrylate), *PMB* poly(MPC-co-butyl methacrylate)

Electrostatic interactions between proteins and solid surfaces have also been discussed. Almost all proteins in plasma are negatively charged under physiological conditions because their isoelectric points are below pH 7.4. Therefore, plasma proteins adsorbed favorably onto positively charged surfaces. Holmlin and coworkers (2001) compared surface ability to resist nonspecific protein adsorption on zwitterionic SAMs, referring both to SAMs formed from a 1:1 mixture of positively and negatively charged thiols and thiols combined in a positively and negatively charged moiety in the same molecule. As shown in Fig. 8, the amount of adsorbed protein on zwitterionic SAMs was much less than that on positively charged or negatively charged SAMs. Moreover, single-component SAMs formed from thiols ter-

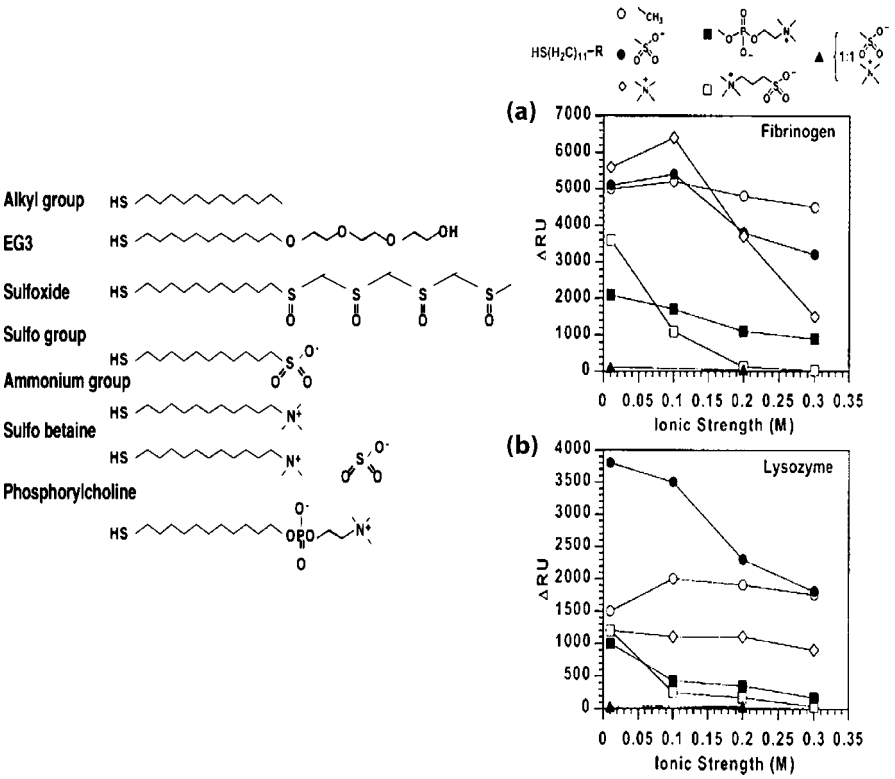

Fig. 8. Plots of the change in response unit (Δ*RU*) or irreversible adsorption of fibrinogen (**a**) and lysozyme (**b**) to different self-assembled monolayers (SAMs) as a function of the ionic strength of the buffer dissolving the protein. The buffer was 4.4 mM phosphate (pH 7.4, ionic strength 10 mM); the ionic strength was adjusted by dissolving NaCl in the appropriate concentrations. The symbols corresponding to the different functional groups presented at the SAM–buffer interface are defined above the plots. Reprinted with permission from Holmlin et al. (2001), copyright (2001) American Chemical Society

minating in groups combining a positively charged moiety and a negatively charged moiety were capable of resisting the adsorption of proteins.

Poly(ethylene oxide) (PEO) is one of the most widely used hydrophilic polymers for surface modification of biomaterials (Harris 1992). The high water solubility of PEO is the result of a good structural fit between water molecules and the polymer. Steric repulsion and molecular flexibility are believed to be the dominant factors for reduction protein adsorption on PEO-immobilized surfaces. However, surface modification with few highly dense ethylene oxide oligomers is also effective in reducing protein adsorption (Johnston et al. 2005; Wu et al. 2000). The length of such oligomers is on the order of 1 nm. These results suggest that steric repulsion is not the dominating factor in the prevention of protein adsorption by surface modification. A similar behavior can be seen on a phosphorylcholine surface. In previous literature on MPC copolymer systems, chain mobility was thought to be the dominant factor in resisting protein adsorption onto a surface. Conversely, high-density MPC polymer brushes also reduced protein adsorption. The molecular mobility of a polymer brush, which is defined by the hysteresis between the contact angles of advancing and receding water, was much lower than that of the MPC copolymer.

The surface characteristics of a phosphorylcholine polymer surface for the reduction of protein adsorption are summarized in Fig. 9. The phos-

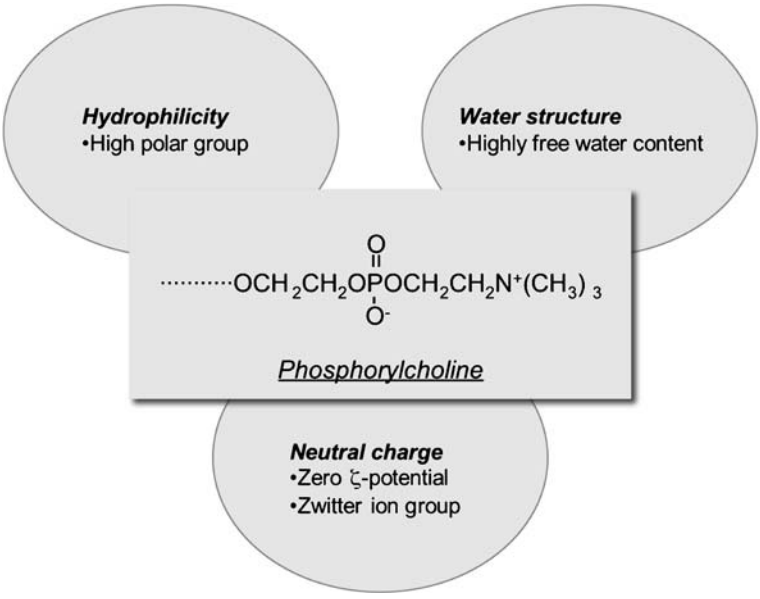

Fig. 9. Possible factors for the nonfouling property of phosphorylcholine-bearing surfaces. *ζ-potential* Charge potential

phorylcholine group is very hydrophilic, which means it is unfavorable for attracting hydrophobic interactions with proteins. Moreover, the phosphorylcholine polymer does not disintegrate the water structure around the polymer. This is a unique property of phosphorylcholine polymers in comparison with conventional hydrophilic polymers. In addition, electrostatic interactions between a phosphorylcholine polymer surface and proteins are weak because the charge potential (ζ-potential) of phosphorylcholine is neutral (Ishihara et al. 1994a). Therefore, phosphorylcholine polymer has several factors for reducing nonspecific protein adsorption. This polymer is one of the best polymer materials for making a nonbiofouling surface.

12.5 Fundamental Interactions Between MPC Polymers and Proteins

Protein adsorption on material surfaces causes serious biological reactions such as, for example, thrombus formation, immune response, and complement activation, capsulation (Brash and Horbett 1987; Horbett and Brash 1995). To understand the blood compatibility of surfaces, it is necessary not only to determine the amount of adsorbed protein but also the species

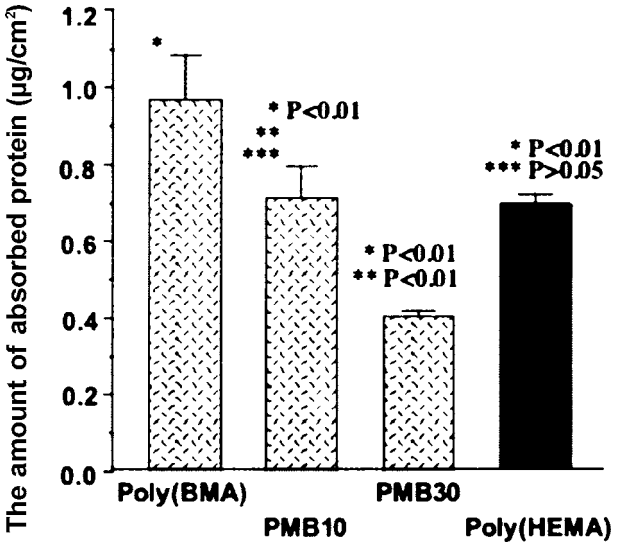

Fig. 10. Amount of protein adsorbed on polymer surfaces from human plasma. *Poly(BMA)* poly(butyl methacrylate), *Poly(HEMA)* poly(2-hydroxyethyl methacrylate), *PMB* poly(MPC-co-n-butyl methacrylate). Number after PMB is molar percent of MPC in the coplymer

of the protein. Therefore, the effects of MPC units on protein adsorption were investigated. Figure 10 shows the amount of protein adsorbed on PMB, poly(HEMA), and poly(butyl methacrylate) (BMA) after contact with plasma for 60 min (Ishihara et al. 1992). On poly(BMA), many more proteins were adsorbed than on either poly(HEMA) or PMB. The amount of proteins adsorbed on PMB decreased with increases in the ratio of the MPC composition of the polymer. The species and distribution of the protein adsorbed on PMB were also determined by gold-colloid and radiolabeled immunoassay (Ishihara et al. 1991b). From these experiments, it was clarified that the PMB could reduce plasma protein adsorption nonspecifically. Thrombus formation on conventional polymeric materials occurred through the multilayers of plasma proteins denatured by contact with the surfaces. The secondary structures of BSA and BPF adsorbed onto the PMB were evaluated by circular dichroism (CD) spectroscopy (Ishihara et al. 1991a, 1998). Figure 11 shows the CD spectra of BSA in phosphate-buffered saline (PBS) and that adsorbed on the polymer surface. For BSA in PBS, the mean molecular residual ellipticity had a large negative value at 222 nm. The CD spectrum of BSA adsorbed onto PMB was almost the same as that in PBS. The negative ellipticity at 222 nm of BSA adsorbed on the MPC polymers increased as the ratio of MPC decreased, then became almost zero for BSA adsorbed on poly(HEMA). The authors found the same tendency in the case of BPF. Calculation of the α-helix contents of BSA and BPF revealed that the PMB could effectively suppress the conformational change of proteins even when the proteins were adsorbed on the surface (Ishihara et al. 1991, 1998).

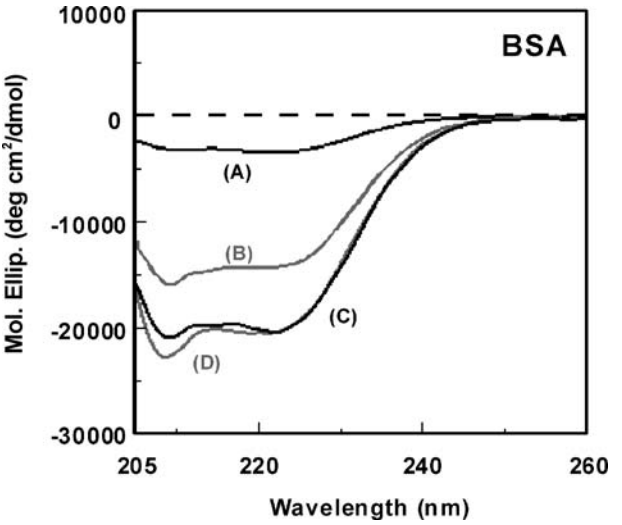

Fig. 11. Circular dichroism spectra of BSA in PBS and of that adsorbed on polymer surfaces. **A** poly(HEMA), **B** PMB10, **C** PMB30, **D** BSA/PBS. *Mol. Ellip.* Molar ellipticity

In contrast, the α-helix content of both proteins adsorbed on poly(HEMA) decreased significantly. The protein-adsorption-resistant properties of the MPC polymer have also been determined by other researchers (Campbell et al. 1994; Chang et al. 1998; Sugiyama et al. 1997).

12.6 Recent Designs of Nonfouling Phosphorylcholine Surfaces with Well-Defined Structures

MPC is one of the best monomers with which to produce biomimetic surfaces because it can be applied to a wide variety of surface modifications, as shown in Fig. 12. These methods have been applied to improve the bio/blood compatibility of numerous biomedical devices (Iwasaki and Ishihara 2005).

To better understand protein–material and cell–material interactions at the submolecular level, well-defined biomimetic surfaces have recently been produced (Fig. 13).

Alkanethiols terminating in various functional groups have been used to study the physical-organic chemistry of the adsorption of proteins to synthetic surfaces (Kohler at al. 1996; Marra et al. 1997; Tegoulia and Cooper 2000; Wang et al. 2000). It is clear that alkanethiols fixed on a gold surface create a SAM. Tegoulia and Cooper (2000) first reported that adhesion of neutrophils was effectively reduced on a SAM surface with phosphorylcholine groups. Chen et al. (2005) synthesized disulfide molecules having phosphorylcholine groups and prepared SAMs on a gold surface.

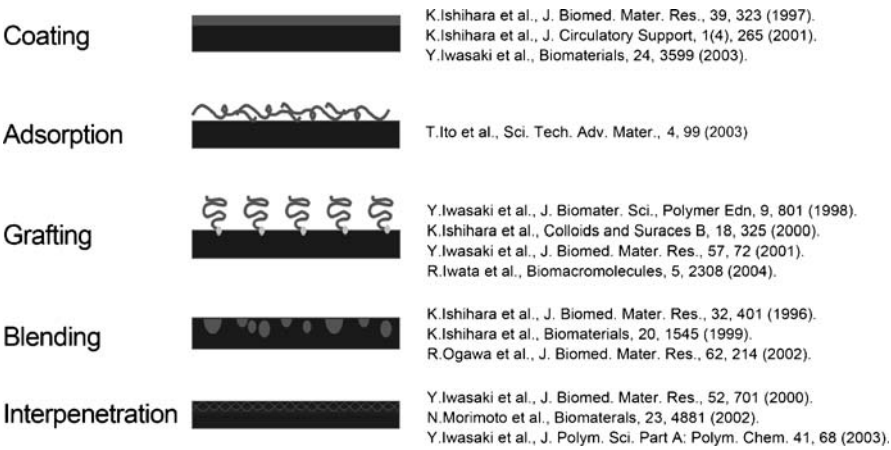

Fig. 12. Surface modifications of a polymer surface with MPC polymers

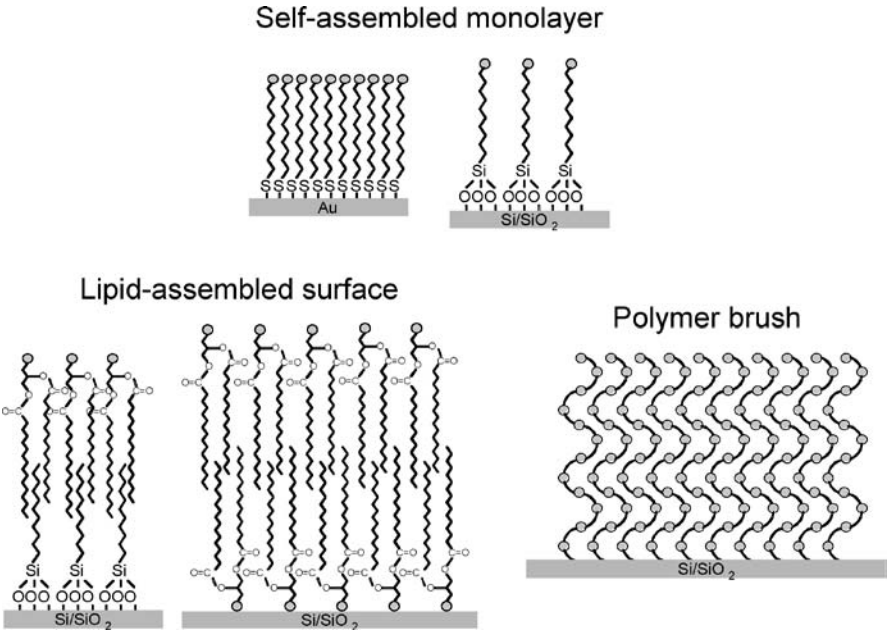

Fig. 13. Well-defined designs of phosphorylcholine-bearing surfaces

Marra et al. (1997) synthesized the phospholipid monomer 1-palmitoyl-2-[12-(acryloyloxy)dodecanoyl]-sn-glycero-3-phosphorylcholine, prepared as unilamellar vesicles, and fused them onto alkylated glass. Free-radical polymerization was performed in an aqueous solution at 70 °C. It was clear from x-ray photoelectron spectroscopy analysis that the phospholipid assembly had a closely packed monolayer formation. This formation is very stable under static conditions in water and air, as well as in an environment where there is a high shear flow. There are several procedures for the creation of biomembrane-like surfaces with polymerizable phospholipids (Conboy et al. 2003; Feng et al. 2002; Kim et al. 2004).

Surface modification using silane coupling has also been demonstrated with reagents bearing phosphorylcholine. The process was classified into two approaches. One is generated from hydroxyl-terminated monolayers on a silicon wafer (Durrani et al. 1986; Hayward et al. 1984). The other is the chemical or physical adsorption of phospholipids or phospholipid derivatives on alkylsilane monolayers (Hayward et al. 1986a, b; Marra et al. 1997; Tegoulia and Cooper 2000). Kohler et al. (1996) prepared a glass surface that reacted with 3-aminopropyl-trimethoxysilane. The carboxylated phosphatidylcholine was grafted with a coupling agent.

Matsuda and coworkers (2003a) prepared a phosphorylcholine-end-capped poly(*N*,*N*'-dimethylacrylamide) [poly(DMEAA)] and a block co-

oligomer with poly(styrene) with the aid of a photoiniferter-based quasi-living polymerization technique. The oligomer exhibits amphiphilic properties and chemisorbs on a gold surface with hydrophobic anchoring. The surface coated with the oligomers reduced plasma protein adsorption and cell adhesion. The authors also explored a surface design for producing one or two phosphorylcholine groups capped at the terminal end of a graft chain of poly(DMEAA) (Matsuda et al. 2003b).

Polymers may have more worth because of their great potential for multiple functionalities. Although preparation of a well-defined surface is normally difficult due to their structural and size distributions, well-defined MPC polymer brushes on silicon wafers have been prepared quite recently by atom transfer radical polymerization (ATRP) (Feng et al. 2004, 2005; Iwata et al. 2004). ATRP is one of the best methods for living radical polymerization because it can be applied to a wide range of monomers. An alternative process, pioneered by Wirth and Tsujii (Huang et al. 1997, 1999; Ejaz et al. 1998, 2002), to prepare well-defined polymer brushes on solid surfaces with ATRP is considerably theoretical and deals with experimental interests in the control of surface properties. Iwata et al. (2004) reported the manipulation of protein adsorption on a thin MPC polymer brush surface. First, they treated silicon wafers with 3-(2-bromoisobutyryl)propyl dimethylchlorosilane (BDCS) to form a monolayer that acts as an initiator for ATRP. Silicon-supported BDCS monolayers were soaked in a methanol/water solution containing Cu(I)Br, bipyridine, and a sacrificial initiator. After MPC was added to the solution, ATRP was allowed to progress for 18 h. The synthetic scheme for poly(MPC) brushes is shown in Fig. 14a. The M_w and thickness of the poly(MPC) brush layer on the silicon surface increased with increasing polymerization time, as shown in Fig. 14b. The dense polymer brushes were obtained by the "grafting from" system. By selective decomposition of the BDCS monolayer by ultraviolet (UV)-light-irradiation, the poly(MPC) brush region and the sizes were well controlled, resulting in fabricating micropatterned poly(MPC) brushes.

12.7 Control of Cell–Material Interactions on a Phosphorylcholine Polymer Nonfouling Surface

Cell adhesion on material surfaces depends strongly on the plasma (serum) protein adsorption onto the surface because there are many kinds of cell adhesive proteins in plasma (serum). It has already been reported that an MPC polymer can reduce the adhesion of a variety of cells such as blood cells (Hasegawa et al. 2002; Ishihara et al. 1992, 1993, 2000; Iwasaki et al. 1997, 2001), fibroblasts (Ishihara et al. 1999; Iwasaki et al. 1999), and

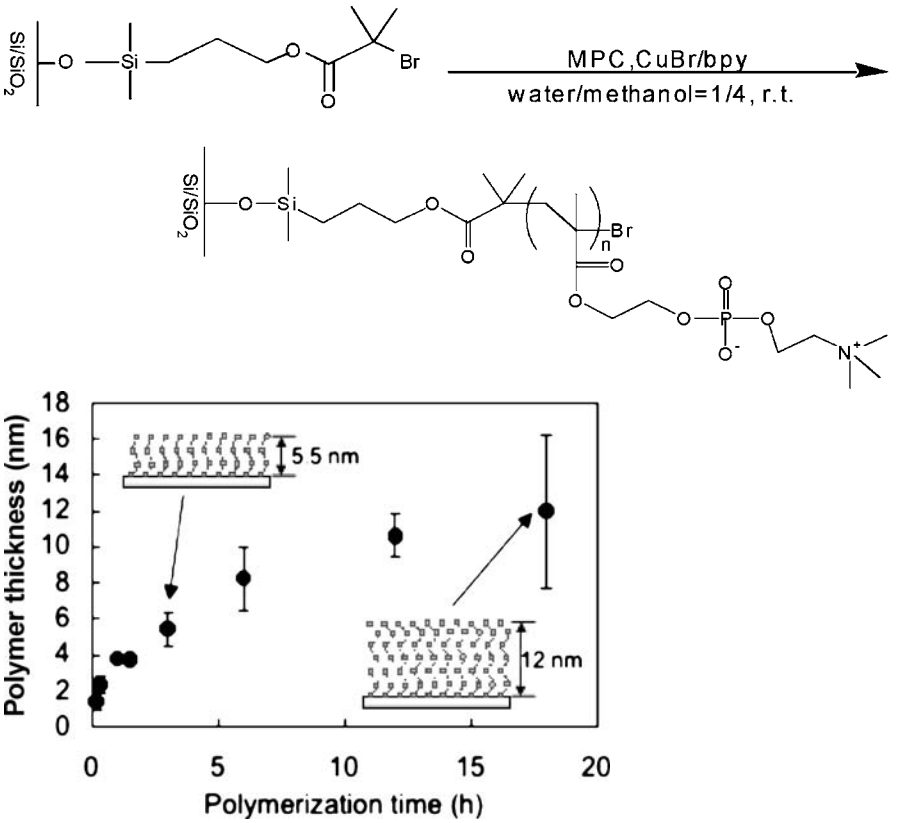

Fig. 14. **a** Synthetic route of poly(MPC) brushes on silicon wafer via atom transfer radical polymerization. **b** Thickness of silicon-sputtered poly(MPC) brushes as function of polymerization time

bacteria (Hirota et al. 2005; Patel et al. 2005). By manipulation of the surface distribution of MPC polymers or tag-immobilization to recognize a cell on MPC polymers, the cell attachment on the surface will be well controlled.

12.7.1 Cell Manipulation on a Well-Defined Phosphorylcholine Polymer Brush

Adsorption of fluorescein-isothiocyanate-labeled BSA was well controlled on a patterned graft polymer surface, as shown in Fig. 15. On an UV-irradiated region with no polymer brush, the fluorescence intensity was significantly high, indicating that a large amount of BSA was adsorbed in this region. Conversely, BSA adsorption was remarkably reduced in the

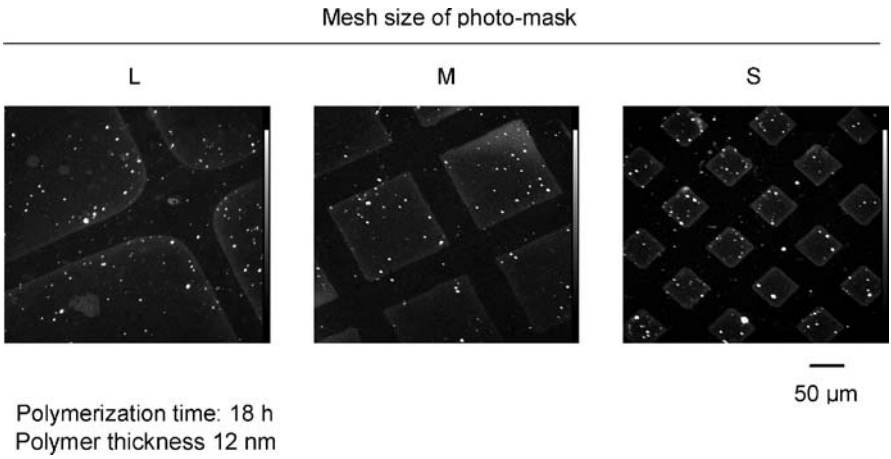

Fig. 15. Fluorescence micrographs of fluorescein isothiocyanate-labeled albumin adsorption on patterned poly(MPC) brush surface after contact with 0.45 g/dl FITC-albumin in PBS for 30 min. Reprinted with permission from Iwata et al. (2004), copyright (2004) American Chemical Society

poly(MPC) brush layer. Figure 16 shows the fibronectin adsorption pattern on the pattern surface after contact with the cell culture medium for 60 min. The adsorption pattern was determined by immunoassay. On the polymer brush prepared by polymerization for 10 min, fluorescence caused by the adsorbed fibronectin was observed to be homogeneous. The difference in fibronectin adsorption on the patterned surface was clearly related to the

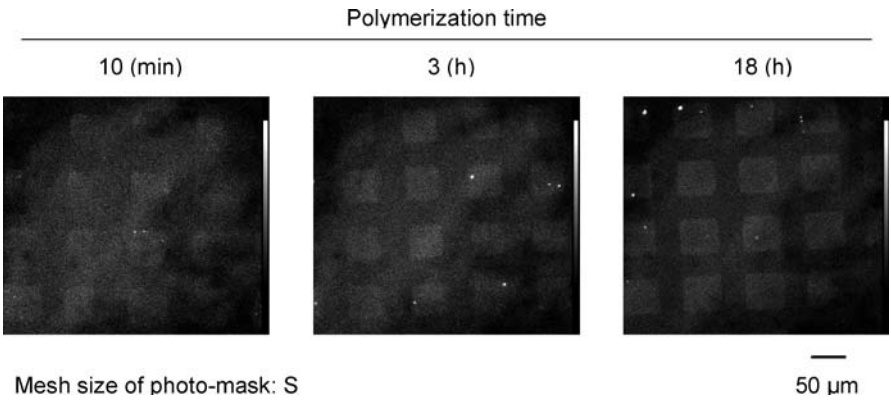

Fig. 16. Fluorescence micrographs of fibronectin adsorption on a patterned poly(MPC) brush surface after contact with cell culture medium for 30 min. Reprinted with permission from Iwata et al. (2004), copyright (2004) American Chemical Society. *L* Large, *M* medium, *S* small

time of polymerization of the polymer brushes. On the poly(MPC) brush surface, fibronectin adsorption was effectively reduced. The reduction of plasma protein adsorption on MPC polymer surfaces has been reported previously, and the mechanism is considered to be related to the structure of the polymer surface (Ishihara et al. 1998).

The study to clarify the difference in surface structure between a PMB coating and the dense poly(MPC) brush prepared in this study on the reduction of protein adsorption is still ongoing. However, it has been shown that poly(MPC) brushes just 5 nm thick prepared by the "grafting from" system can reduce protein adsorption. Although the thickness of the cast film of PMB that we made has been normally controlled on a submicron scale, the poly(MPC)-brush thickness can be controlled on the scale of a few nanometers. This is a great advantage for surface modification to improve the nonfouling properties of micro- or nanodevices.

Figure 17 presents fluorescence micrographs of fibroblasts that adhered onto the patterned surface. The effect of surface grafting of poly(MPC) by polymerization for 10 min on fibroblast adhesion was not observed and the cells adhered homogeneously to the surface. By adjusting the time of polymerization, cell adhesion was controlled and fibroblasts adhered to UV-irradiated regions that had no poly(MPC) brushes. This result is coincident with protein adsorption on the surface. Above a poly(MPC)-brush thickness of about 5 nm, protein adsorption and cell adhesion was remarkably reduced (i. e., they were able to recognize the thickness of the thin brush). The effect of the grafting density of poly(ethylene glycol) on protein adsorption has been reported by Sofia and coworker (1998). Grafting density may also be important for controlling protein adsorption on poly(MPC)-brush surfaces.

The number of adherent cells can also be controlled with a change in the surface area of the UV-irradiated region. The surface area of the pattern affected cell density. The surface areas for adherent cells on small- and medium-sized pattern surfaces were 844 ± 185 μm^2/cell and 1188 ± 240 μm^2/cell, respectively. The large-sized pattern surface had a cell density of 159 ± 34 μm^2/cell, which is significantly higher. Cell communication depends on the area of the surface where the cells are able to adhere.

To fabricate a microscale pattern on a solid surface, microcontact printing and soft lithography techniques have been applied. Whitesides and coworkers reported that microscale patterning provides a versatile method for creating novel adhesive substrates that are useful for spatially positioning mammalian cells and controlling their viability, form, and function (Brock et al. 2003; Chen et al. 1997; Singhvi et al. 1994).

Armes and coworkers have reported that the molecular architectures of MPC polymers can be easily controlled with ATRP in protic solvents (Li et al. 2003; Lobb et al. 2001; Ma et al. 2002), with the result that a wide vari-

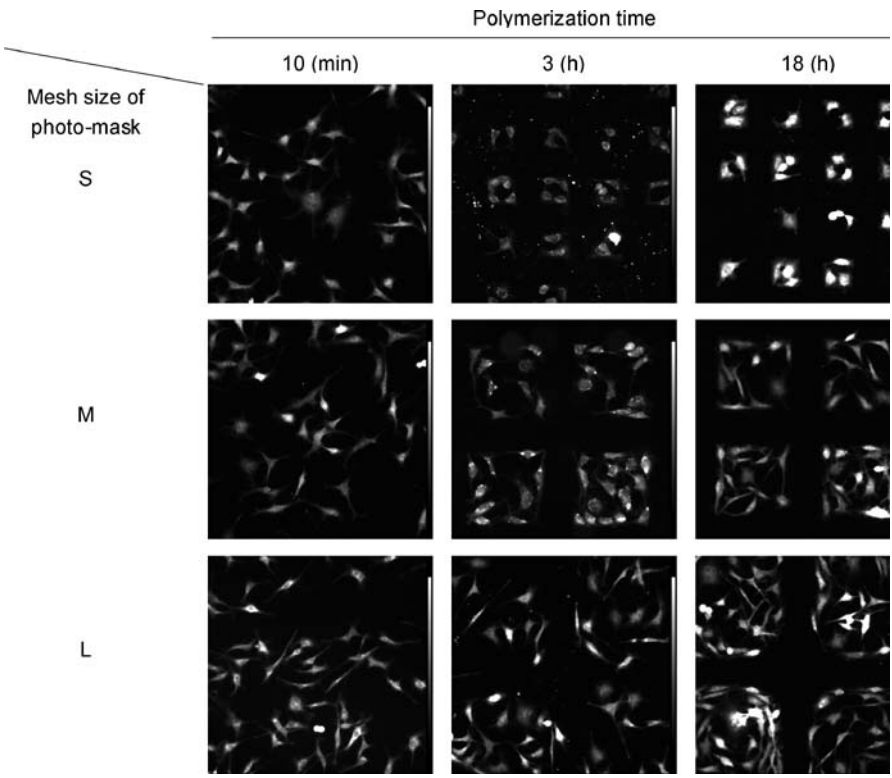

Fig. 17. Fluorescence micrographs of fibroblast adhesion on patterned poly(MPC) brush surface after incubation for 24 h. Concentration of fibroblasts, [Fibroblast] = 5.0×10^4 cells/ml. Reprinted with permission from Iwata et al. (2004), copyright (2004) American Chemical Society

ety of polymer surface designs will be possible. Surface modification with well-defined MPC polymers would be considered as one of the most robust methods with which to optimize biointerfaces on a molecular scale. Microfabrication with MPC polymers might prove to be important in separations, biosensors, and the development of biomedical materials.

12.7.2 Selective Cell Attachment to a Biomimetic Polymer Surface Through the Recognition of Cell-Surface Tags

Synthetic polymers capable of selectively recognizing proteins or cells play important roles in cell separation, biosensors, and the development of biomedical materials (Ratner 1993, 1996). In general, few synthetic poly-

mers can recognize a specific biomolecule or cell in vivo because of the complexity of the environment. In a living cell, carbohydrates on the cell surface contribute to most of the communications between the cell and its environment (Dwek 1996). Therefore, it might be possible to control cell functions with polymers, which can affect carbohydrate interactions with a cell surface. Tagging of carbohydrates on the cell membrane, as well as the polymer design, might be effective for the recognition of a specific cell.

The incorporation of unnatural carbohydrates into living cells provides an opportunity to study the specific contributions of sialic acid and its N-acyl side chains to sialic acid-dependent ligand-receptor interactions at a submolecular level. Bertozzi and coworkers have expressed unnatural functional groups (i. e., acetyl, levulinoyl, and azideacetyl groups), on living cell surfaces through the glycosylation of unnatural monosaccharides (Mahal et al. 1997; Saxon and Bertozzi 2000; Yarema and Bertozzi 2001; Yarema et al. 1998).

Iwasaki et al. (2005) reported a novel strategy for controlling selective cell attachment and detachment even in nonadhesive cells by using biomimetic polymer surface engineering and cell-surface engineering. To this end, they designed reactive biomimetic MPC polymer surfaces with hydrazide groups, which can react selectively with unnatural ketone-containing carbohydrates as a cell surface tag. Figure 18 shows a schematic representation of selective cell attachment through the recognition of a cell-surface tag. The MPC polymer surface prohibits nonspecific interaction with plasma protein, which often interferes with the specificity of the interaction of materials with a cell membrane. Hydrazide groups on the MPC polymer surface react with ketone groups on the cell surface even in cell culture medium. Surface tags on living cells can be introduced in the presence of *N*-levulinoylmannosamine (ManLev) by surface engineering (Lee et al. 1999; Lemieux et al. 1999). The chemical structures of MPC polymers to control cell attachment are shown in Fig. 19.

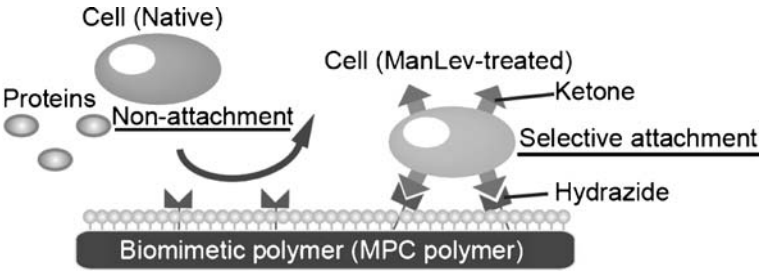

Fig. 18. Schematic representation of specific cell attachment to a nonfouling MPC polymer surface through cell-surface tags

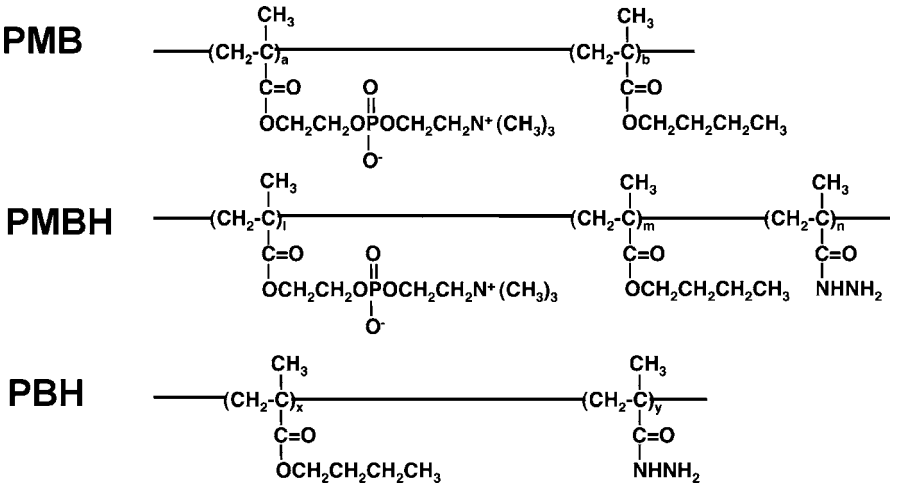

Fig. 19. Chemical structures of PMB, poly(MPC-o-BMA-co-MH) (PMBH), and poly(BMA-co-MH) (PBH)

To clarify the possibility of using a polymer surface to recognize specific cells with cell-surface tags, the coculture of ManLev-treated HL-60 cells with native HeLa cells was examined. HeLa cells are typical cancer cells that adhere nonspecifically to conventional polymer surfaces through cell-binding proteins adsorbed on the surface. Figure 20 shows phase-contrast and fluorescence microscopy images of polymer surfaces after the coculture experiment. Cell adhesion on the PMB surface was completely suppressed.

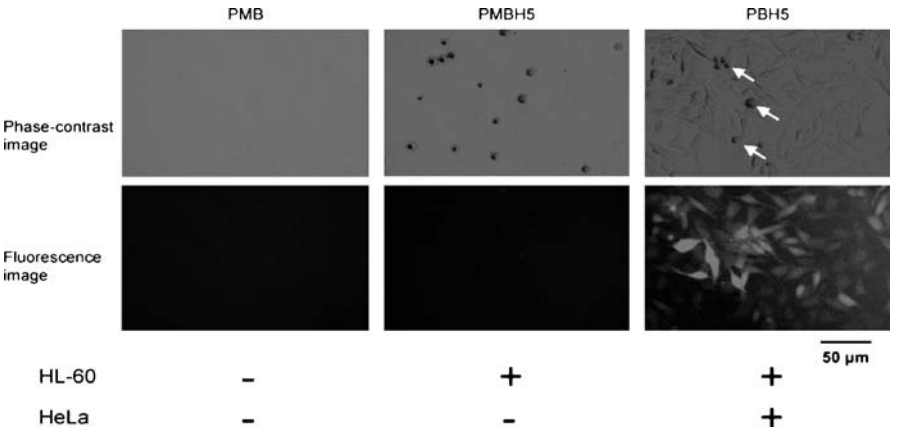

Fig. 20. Phase-contrast and fluorescence micrographs of polymer surfaces after the coculture experiment. *White arrows* indicate HL-60 cells. Reprinted with permission from Iwasaki et al. (2005), copyright (2005) American Chemical Society

In contrast, both HL-60 and HeLa cells were observed on poly(BMA-co-MH) (PBH). HL-60 cells selectively attached to poly(MPC-o-BMA-co-MH) (PMBH), while HeLa cells did not. The adhesion of HeLa to a polymer surface is closely associated with the adsorption of cell-binding proteins on the surface, such as fibronectin, fibrinogen, and vitronectin, because these proteins have an RGD binding site for the integrin of the cell membrane (Hirano et al. 1993). On PMBH, the adhesion of HeLa cells was reduced due to fibronectin resistance. It has been reported previously that MPC polymer can nonspecifically reduce plasma protein adsorption (Ishihara et al. 1998). The nonfouling property of the MPC polymer surface is quite important for achieving specific interactions with a cell.

These results indicate that cell-surface recognition by a polymer surface is evident in both single- and two-cell systems. Such recognition on an MPC polymer surface is effective in a multiple-cell system because the MPC polymer surface rejects the adhesion of cells without tags. Moreover, the control of cell attachment can be applied to a wide range of cells because the expression of unnatural carbohydrates on cell surfaces has been observed on numerous types of cells.

12.8 Conclusion

The control of protein adsorption on material surfaces is a most fundamental as well as important biomaterial-related research subject. Although surface designs have been performed to control protein–material interactions for many years, the surface structure, which can completely control the interactions, has not yet been optimized. To this end, nonfouling surfaces are required, and biomembrane-mimetic surfaces (e. g., phosphorylcholine polymers) might be one of the most suitable materials. In addition, a well-defined surface would be useful for clearly understanding protein–material interactions at the submolecular level. The study of adsorption is necessary to achieve progress with the next generation of biomaterials and thus secure a material that can control protein.

References

Bongard P (1988) Physical Basis of Cell–Cell Adhesion. CRC Press, Boca Raton, FL

Brash JL, Horbett TA (eds) (1987) Proteins at Interfaces: Physicochemical and Biochemical Studies. ACS Symposium Series 343. American Chemical Society, Washington, DC

Brash JL, Horbett TA (eds) Proteins At Interfaces II: Fundamentals and Applications. American Chemical Society, Washington, DC

Brock A, Chang E, Ho CC, LeDuc P, Jiang X, Whitesides GM, Ingber DE (2003) Geometric determinants of directional cell motility revealed using microcontact printing. Langmuir 19:1611–1617

Campbell EJ, O'Byrne V, Stratford PW, Quirk I, Vick TA, Wiles MC, Yianni YP (1994) Biocompatible surfaces using methacryloylphosphorylcholine laurylmethacrylate copolymer. ASAIO J 40:853–857

Chang PC, Lee SD, Hsiue GH (1998) Heterobifunctional membranes by plasma induced graft polymerization as an artificial organ for penetration keratoprosthesis. J Biomed Mater Res 39:380–389

Chen C, Zheng J, Li L, Jiang S (2005) Strong resistance of phosphorylcholine self-assembled monolayers to protein adsorption: insights into nonfouling properties of zwitterionic materials. J Am Chem Soc 127:14473–14478

Chen CS, Mrksich M, Huang S, Whitesides GM, Ingber DE (1997) Geometric control of cell life and death. Science 276:1425–1428

Conboy JC, Liu S, O'Brien F, Saavedra SS (2003) Planar supported bilayer polymers formed from bis-diene lipids by Langmuir-Blodgett deposition and UV irradiation. Biomacromolecules 4:841–849

Durrani AA, Hayward JA, Chapman D (1986) Biomembranes as models for polymer surfaces. II. The syntheses of reactive species for covalent coupling of phosphorylcholine to polymer surfaces. Biomaterials 7:121–125

Dwek RA (1996) Glycobiology: toward understanding the function of sugars. Chem Rev 96:683–720

Ejaz M, Yamamoto S, Ohno K, Tsujii Y, Fukuda T (1998) Controlled graft polymerization of methyl methacrylate on silicon substrate by the combined use of the Langmuir-Blodgett and atom transfer radical polymerization techniques. Macromolecules 31:5934–5936

Ejaz M, Yamamoto S, Ohno K, Tsujii Y, Fukuda T (2002) Fabrication of patterned high-density polymer graft surfaces. 1. Amplification of phase-separated morphology of organosilane blend monolayer by surface-initiated atom transfer radical polymerization. Macromolecules 35:1412–1418

Elwing H, Welin A, Askendahl A, Nilsson U, Lundstrom I (1987) A wettability gradient method for studies of macromolecular interaction at the liquid/solid interface. J Colloid Interface Sci 119:203–210

Feng J, Tseng P-Y, Faucher KM, Orban JM, Sun XL, Chaikof EL (2002) Functional reconstitution of thrombomodulin within a substrate-supported membrane-mimetic polymer film. Langmuir 18:9907–9913

Feng W, Brash J, Zhu SP (2004) Atom-transfer radical grafting polymerization of 2-methacryloyloxyethyl phosphorylcholine from silicon wafer surfaces. J Polym Sci A Polym Chem 42:2931–2942

Feng W, Zhu S, Ishihara K, Brash JL (2005) Adsorption of fibrinogen and lysozyme on silicon grafted with poly(2-methacryloyloxyethyl phosphorylcholine) via surface-initiated atom transfer radical polymerization. Langmuir 21:5980–5987

Golander CG, Lin YS, Hlady V, Andrade JD (1990) Wetting and plasma-protein adsorption studies using surfaces with a hydrophobicity gradient. Colloids Surf 49:289–302

Golander CG, Pitt WG (1990) Characterization of hydrophobicity gradients prepared by means of radio frequency plasma discharge. Biomaterials 11:32–35

Harris JM (1992) Poly(ethylene glycol) Chemistry. Plenum Press, N.Y

Hasegawa T, Iwasaki Y, Ishihara K (2002) Preparation of blood-compatible hollow fibers from a polymer alloy composed of polysulfone and 2-methacryloyloxyethyl phosphorylcholine polymer. J Biomed Mater Res 63:333–341

Hayward JA, Chapman D (1984) Biomembrane surfaces as models for polymer design: the potential for haemocompatibility. Biomaterials 5:135–142

Hayward JA, Durrani AA, Lu Y, Clayton CR, Chapman D (1986a) Biomembranes as models for polymer surfaces. IV. ESCA analyses of a phosphorylcholine surface covalently bound to hydroxylated substrates. Biomaterials 7:252–258

Hayward JA, Durrani AA, Shelton CJ, Lee DC, Chapman D (1986b) Biomembranes as models for polymer surfaces. III. Characterization of a phosphorylcholine surface covalently bound to glass. Biomaterials 7:126–131

Hirano Y, Okuno M, Hayashi T, Goto K, Nakajima A (1993) Cell-attachment activities of surface immobilized oligopeptides RGD, RGDS, RGDV, RGDT, and YIGSR toward five cell lines. J Biomater Sci Polym Ed 4:235–243

Hirota K, Murakami K, Nemoto K, Miyake Y (2005) Coating of a surface with 2-methacryloyloxyethyl phosphorylcholine (MPC) co-polymer significantly reduces retention of human pathogenic microorganisms. FEMS Microbiol Lett 248:37–45

Holmlin RE, Chen X, Chapman RG, Takayama S, Whitesides GM (2001) Zwitterionic SAMs that resist nonspecific adsorption of protein from aqueous buffer. Langmuir 17:2841–2850

Horbett TA, Brash JL (1995) Proteins at Interfaces II – Fundamentals and Applications. ACS Symposium Series 602. American Chemical Society, Washington, D.C

Huang X, Wirth MJ (1997) Surface-initiated radical polymerization on porous silica. Anal Chem 69:4577–4580

Huang X, Wirth MJ (1999) Surface initiation of living radical polymerization for growth of tethered chains of low polydispersity. Macromolecules 32:1694–1696

Ishihara K (2000) Bioinspired phospholipid polymer biomaterials for making high performance artificial organs. Sci Technol Adv Mater 1:131–138

Ishihara K, Fujita H, Yoneyama T, Iwasaki Y (2000) Antithrombogenic polymer alloy composed of 2-methacryloyloxyethyl phosphorylcholine polymer and segmented polyurethane. J Biomater Sci Polym Ed 11:1183–1195

Ishihara K, Inoue H, Kurita K, Nakabayashi N (1994a) Selective adhesion of platelets on a polyion complex composed of phospholipid polymers containing sulfonate groups and quarternary ammonium groups. J Biomed Mater Res 28:1347–1355

Ishihara K, Ishikawa E, Iwasaki Y, Nakabayashi N (1999) Inhibition of fibroblast cell adhesion on substrate by coating with 2-methacryloyloxyethyl phosphorylcholine polymers. J Biomater Sci Polym Ed 10:1047–61

Ishihara K, Nomura H, Mihara T, Kurita K, Iwasaki Y, Nakabayashi N (1998) Why do phospholipid polymers reduce protein adsorption? J Biomed Mater Res 39:323–330

Ishihara K, Oshida H, Endo Y, Ueda T, Watanabe A, Nakabayashi N (1992) Hemocompatibility of human whole blood on polymers with a phospholipid polar group and its mechanism. J Biomed Mater Res 26:1543–1552

Ishihara K, Oshida H, Endo Y, Watanabe A, Ueda T, Nakabayashi N (1993) Effects of phospholipid adsorption on nonthrombogenicity of polymer with phospholipid polar group. J Biomed Mater Res 27:1309–1314

Ishihara K, Tsuji T, Kurosaki K, Nakabayashi N (1994b) Hemocompatibility on graft copolymers composed of poly(2methacryloyloxyethyl phosphorylcholine) side chain and poly(*n*-butyl methacrylate) backbone. J Biomed Mater Res 28:225–232

Ishihara K, Ueda T, Nakabayashi N (1990) Preparation of phospholipid polymers and their properties as polymer hydrogel membrane. Polym J 22:355–360

Ishihara K, Ueda T, Saito N, Kurita K, Nakabayashi N (1991a) Suppression of protein adsorption and denaturation on polymer surface with phospholipid polar group. Seitai Zairyou (J J Soc Biomater) 9:243–249

Ishihara K, Ziats NP, Tierney BP, Nakabayashi N, Anderson JM (1991b) Protein adsorption from human plasma is reduced on phospholipid polymers. J Biomed Mater Res 25:1397–1407

Israelachvili JN (1985) Intermolecular and Surface Forces. Academic Press, New York
Israelachvili JN, McGuiggan M (1988) Forces between surfaces in liquids. Science 241:795–800
Ito T, Iwasaki Y, Narita T, Akiyoshi K, Ishihara K (2003) Controlled adhesion of human lymphocytes on electrically charged polymer surface having phosphorylcholine moiety. Sci Technol Adv Mater 4:99–104
Iwasaki Y, Akiyoshi K (2004) Design of biodegradable amphiphilic polymers: well–defined amphiphilic polyphosphates with hydrophilic graft chains via ATRP. Macromolecules 37:7637–7642
Iwasaki Y, Ishihara K (2005) Phosphorylcholine-containing polymers for biomedical applications. Anal Bioanal Chem 381:534–546
Iwasaki Y, Mikami A, Kurita K, Yui N, Ishihara K, Nakabayashi N (1997) Reduction of surface-induced platelet activation on phospholipid polymer. J Biomed Mater Res 36:508–515
Iwasaki Y, Nakabayashi N, Ishihara K (2001) Preservation of platelet function on 2-methacryloyloxyethyl phosphorylcholine-graft polymer as compared to various water-soluble graft polymers. J Biomed Mater Res 57:72–78
Iwasaki Y, Sawada S, Nakabayashi N, Khang G, Lee HB, Ishihara K (1999) The effect of the chemical structure of the phospholipid polymer on fibronectin adsorption and fibroblast adhesion on the gradient phospholipid surface. Biomaterials 20:2185–2191
Iwasaki Y, Tabata E, Kurita K, Ishihara K (2005) Selective cell attachment to a biomimetic polymer surface through the recognition of cell-surface tags. Bioconjugate Chem 16:567–575
Iwata R, Suk-In P, Hoven VP, Takahara A, Akiyoshi K, Iwasaki Y (2004) Control of nanobiointerfaces generated from well-defined biomimetic polymer brushes for protein and cell manipulations. Biomacromolecules 5:2308–2314
Johnston EE, Bryers JD, Ratner BD (2005) Plasma deposition and surface characterization of oligoglyme, dioxane, and crown ether nonfouling films. Langmuir 21:870–881
Kadoma Y, Nakabayashi N, Masuhara E, Yamauchi J (1978) Synthesis and hemolysis test of polymer containing phophorylcholine groups. Koubunshi Ronbunshu (Jpn J Polym Sci Technol) 35:423–427
Kim K, Shin K, Kim H, Kim C, Byun Y (2004) In situ photopolymerization of a polymerizable poly(ethylene glycol)-covered phospholipid monolayer on a methacryloyl-terminated substrate. Langmuir 20:5396–5402
Kitano H, Sudo K, Ichikawa K, Ide M, Ishihara K (2000) Raman spectroscopic study on the structure of water in aqueous polyelectrolyte Solutions. J Phys Chem B 104:11425–11429
Kitano H, Imai M, Mori T, Gemmei-Ide M, Yokoyama Y, Ishihara K (2003) Structure of water in the vicinity of phospholipid analogue copolymers as studied by vibrational spectroscopy. Langmuir 19:10260–10266
Kohler AS, Parks PJ, Mooradian DL, Rao GHR, Furcht LT (1996) Platelet adhesion to novel phospholipid materials: modified phosphatidylcholine covalently immobilized to silica, polypropylene, and PTFE materials. J Biomed Mater Res 32:237–242
Kojima M, Ishihara K, Watanabe A, Nakabayashi N (1991) Interaction between phospholipids and biocompatible polymers containing a phosphorylcholine moiety. Biomaterials 12:121–124
Lee JH. Baker TJ, Mahal LK, Zabner J, Bertozzi C R, Wiemer DF, Welsh MJ (1999) Engineering novel cell surface receptors for virus-mediated gene transfer. J Biol Chem 274:21878–21884
Lee JH, Lee HB (1993) A wettability gradient as a tool to study protein adsorption and cell adhesion on polymer surfaces. J Biomater Sci Polym Ed 4:467–481

Lee JH, Li T, Park K (2001) Solvation interactions for protein adsorption to biomaterials surfaces. In: Mora M (ed) Water in Biomaterials Surface Science. John Wiley & Sons, Chichester, pp 127–146

Lemieux GA, Yarema KJ, Jacobs CL, Bertozzi CR (1999) Exploiting differences in sialoside expression for selective targeting of MRI contrast reagents. J Am Chem Soc 121:4278–4279

Li Y, Armes SP, Jin X, Zhu S (2003) Direct synthesis of well-defined quaternized homopolymers and diblock copolymers via ATRP in protic media. Macromolecules 36:8268–8275

Lobb EJ, Ma IY, Billingham NC, Armes SP, Lewis AL (2001) Facile synthesis of well-defined, biocompatible phosphorylcholine-based methacrylate copolymers via atom transfer radical polymerization at 20 °C. J Am Chem Soc 123:7913–7914

Lu DR, Lee SJ, Park K (1991) Calculation of solvation interaction energies for protein adsorption on polymer surfaces. J Biomater Sci Polym Ed 3:127–147

Ma Y, Lobb EJ, Billingham NC, Armes SP, Lewis AL, Lloyd AW, Salvage J (2002) Synthesis of biocompatible polymers. 1. Homopolymerization of 2-methacryloyloxyethyl phosphorylcholine via ATRP in protic solvents: an optimization study. Macromolecules 35:9306–9314

Ma Y, Tang Y, Billingham NC, Armes SP, Lewis AL (2003a) Synthesis of biocompatible, stimuli-responsive, physical gels based on ABA triblock copolymers. Biomacromolecules 4:864–868

Ma Y, Tang Y, Billingham NC, Armes SP, Lewis AL, Lloyd AW, Salvage JP (2003b) Well-defined biocompatible block copolymers via atom transfer radical polymerization of 2-methacryloyloxyethyl phosphorylcholine in protic media. Macromolecules 36:3475–3484

Mahal LK, Yarema KJ, Bertozzi CR (1997) Engineering chemical reactivity on cell surfaces through oligosaccharide biosynthesis. Science 276:1125–1128

Matsuda T, Kaneko M, Ge S (2003a) Quasi-living surface graft polymerization with phosphorylcholine group(s) at the terminal end. Biomaterials 24:4507–4515

Matsuda T, Nagase J, Ghoda A, Hirano Y, Kidoaki S, Nakayama Y (2003b) Phosphorylcholine-endcapped oligomer and block co-oligomer and surface biological reactivity. Biomaterials 24:4517–4527

Marra KG, Winger TM, Hanson SR, Chaikof EL (1997) Cytomimetic biomaterials. 1. In-situ polymerization of phospholipids on an alkylated surface. Macromolecules 30:6483–6488

Oscarsson S (1997) Factors affecting protein interaction at sorbent interfaces. J Chromatography B699:117–131

Pashley RM, McGuiggan Pm, Ninham BW, Evans DF (1985) Attractive forces between uncharged hydrophobic surfaces: direct measurements in aqueous solution. Science 229:1088–1089

Patel JD, Iwasaki Y, Ishihara K, Anderson JM (2005) Phospholipid polymer surfaces reduce bacteria and leukocyte adhesion under dynamic flow conditions. J Biomed Mater Res A 73:359–366

Ratner BD (1993) New ideas in biomaterials science – a path to engineered biomaterials. J Biomed Mat Res 27:837–850

Ratner BD (1996) The engineering of biomaterials exhibiting recognition and specificity. J Mol Recognit 9:617–625

Saxon E, Bertozzi CR (2000) Cell surface engineering by a modified Staudinger reaction. Science 287:2007–2010

Singer SJ, Nicolson GL (1972) The fluid mosaic model of the structure of cell membranes. Science 175:723–731

Singhvi R, Kumar A, Lopez GP, Stephanolpoulos GN, Wang DI, Whitesides GM Ingber DE (1994) Engineering cell shape and function. Science 264:696–698

Sofia SJ, Premnath V, Merrill EW (1998) Poly(ethylene oxide) grafted to silicon surfaces: grafting density and protein adsorption. Macromolecules 31:5059–5070

Sugiyama K, Mitsuno S, Shiraishi K (1997) Adsorption of protein on the surface of thermosensitive poly(methyl methacrylate) microspheres modified with the N-(2-hydroxypropyl)methacrylamide and 2-(methacryloyloxy)ethyl phosphorylcholine moieties. J Polym Sci A Polym Chem 35:3349–3355

Tegoulia VA, Cooper SL (2000) Leukocyte adhesion on model surfaces under flow: effects of surface chemistry, protein adsorption, and shear rate. J Biomed Mater Res 50:291–301

Tsuruta T (1996) Contemporary topics in polymeric materials for biomedical applications. Adv Polym Sci 126:1–51

Ueda T, Oshida H, Kurita K, Ishihara K, Nakabayashi N (1992) Preparation of 2-methacryloyloxyethyl phosphory1choline copolymers with alkyl methacrylates and their blood compatibility. Polym J 24:1259–1269

Umeda T, Nakaya T, Imoto M (1982) Polymeric phospholipid analogues, 14. The convenient preparation of a vinyl monomer containing a phospholipid analogue. Macromol Chem Rapid Commun 3:457–459

Wang Y, Su TJ, Green R, Tang Y, Styrkas D, Danks TN, Bolton R, Lu JR (2000) Covalent coupling of phospholipid monolayers on the surface of ceramic materials. Chem Commun 7:587–588

Wu YJ, Timmons RB, Jen JS, Molock FE (2000) Non-fouling surfaces produced by gas phase pulsed plasma polymerization of an ultra low molecular weight ethylene oxide containing monomer. Colloids Surf B Biointerfaces 18:235–248

Yarema KJ, Mahal LK, Bruehl RE, Rodriguez EC, Bertozzi CR (1998) Metabolic delivery of ketone groups to sialic acid residues. Application to cell surface glycoform engineering. J Biol Chem 273:31168–31179

Yarema KJ, Bertozzi CR (2001) Characterizing glycosylation pathways. Genome Biol 2:REVIEWS0004

Subject Index